UNIVERSIDAD DE LA RIOJA

TESIS DOCTORAL

Título
Compuestos fotoluminiscentes de Pt(II) y Pt(II)-Pb(II): modulación de sus propiedades
Autor/es
Santiago Ruiz Abeytua
Director/es
Elena Lalinde Peña y María Teresa Moreno García
Facultad
Facultad de Ciencias, Estudios Agroalimentarios e Informática
Titulación
Departamento
Química
Curso Académico
2013-2014

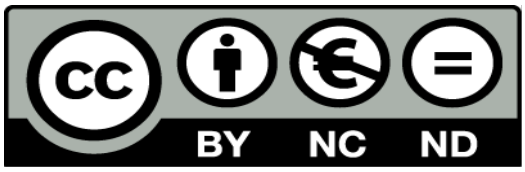

Tesis Doctoral

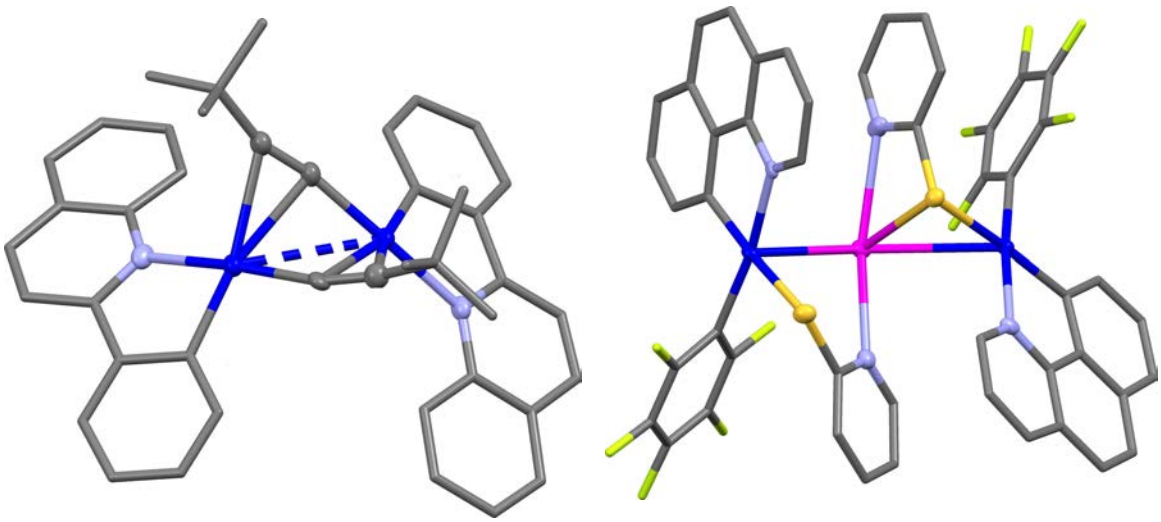

COMPUESTOS FOTOLUMINISCENTES DE Pt(II) Y Pt(II)-Pb(II): MODULACION DE SUS PROPIEDADES

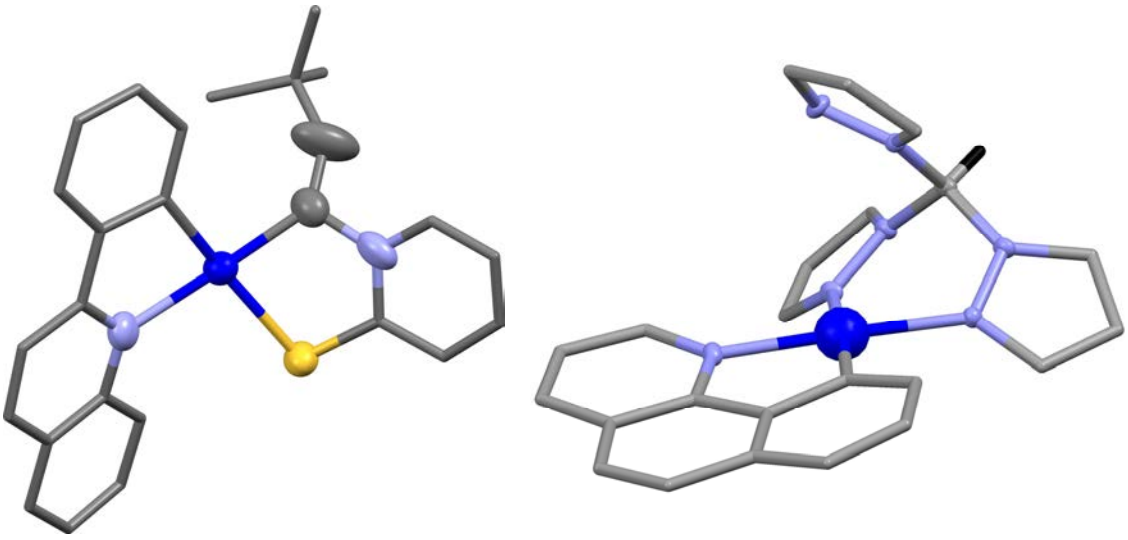

Santiago Ruiz Abeytua

COMPUESTOS FOTOLUMINISCENTES DE Pt(II) Y Pt(II)-Pb(II): MODULACION DE SUS PROPIEDADES

Memoria presentada en el Departamento de Química de la Universidad de La Rioja para optar al título de Doctor por el licenciado:

Santiago Ruiz Abeytua

Universidad de La Rioja-2014

GOBIERNO DE ESPAÑA MINISTERIO DE ECONOMIA Y COMPETITIVIDAD

UNIVERSIDAD DE LA RIOJA

CISQ CENTRO DE INVESTIGACIÓN EN SÍNTESIS QUÍMICA UNIVERSIDAD DE LA RIOJA

ELENA LALINDE PEÑA, Catedrática de Química Inorgánica de la Universidad de La Rioja.

Mª TERESA MORENO GARCÍA, Profesora Titular del Departamento de Química de la Universidad de La Rioja.

CERTIFICAN:

Que el presente trabajo de investigación titulado **"Compuestos fotoluminiscentes de Pt(II) y Pt(II)-Pb(II): modulación de sus propiedades"** ha sido realizado en el Departamento de Química-Centro de Investigación en Síntesis Química (C.I.S.Q.) de la Universidad de La Rioja bajo nuestra dirección por el Licenciado en Química Santiago Ruiz Abeytua y autorizan su presentación para que sea calificado como Tesis Doctoral.

Logroño, Septiembre de 2014

Fdo.: Prof. Elena Lalinde Peña **Fdo.: Prof. Mª Teresa Moreno García**

ÍNDICE

ABREVIATURAS Y SIGLAS

bzq	7,8-Benzoquinolato
ppy	2-Fenilpiridinato
pq	2-Fenilquinolato
pyz	Pirazina
py	Piridina
bpy	4,4'-Bipiridina
bpa	1,2-Bis(bipiridil)etano
bpe	*trans*-1,2-Bis(4-piridil)etileno
bpac	1,2-Bis(4-piridil)acetileno
tpab	1,3,5-Tris(piridin-4-yletinil)benceno
HSpy	Mercaptopiridina
pz	Pirazolato
Me	Metilo
Bu	*n-B*utilo
^{t}Bu	*tert-B*utilo
^{i}Pr	*iso*-Propilo
Ph	Fenilo
Tol	*para*-Tolilo
THF	Tetrahidrofurano
ej./i. ex.	Ejemplo/ In example
E_p^{ox}	Potencial de oxidación
E_p^{red}	Potencial de reducción
DRX /XRD	Difracción de Rayos-X/X-Ray diffraction
IR	Infrarrojo
ν	Vibración de tensión
st	Stretching
mf/vs	Muy fuerte/Very strong
f/s	Fuerte/Strong
m	Medio/Medium
d/w	**D**ébil/Weak
a/br	Ancho/Broad
h/sh	Hombro/Shoulder
TGA	*Thermogravimetric analysis*
ESI	*Electrospray ionization*
MALDI	*Matrix-assisted laser desorption ionization*
TOF	*Time of flight*
RMN/NMR	Resonancia magnética nuclear/ Nuclear magnetic resonance
COSY	*Correlation spectroscopy*
HSQC	*Heteronuclear single quantum coherence*
HMBC	*Heteronuclear multiple bond Coherence*
PGSE	Pulse Field Gradient Spin
DOSY	Diffussion Ordered Spectroscopy
Double STE	Double Stimulated Echo Pulse Sequence
δ	Desplazamiento químico en RMN
s	Singlete/Singlet
d	Doblete/Doublet
t	Triplete/Triplet
m	Multiplete/Multiplet
i-	*ipso-*
o-	*orto-*
m-	*meta-*
p-	*para-*
D	Coeficiente de Difusión
r	Radio
r_H	Radio hidrodinámico
T^a	Temperatura
UV-Vis	Ultravioleta-visible
ε	Coeficiente de absorción molar
λ_{abs}	Longitud de onda de absorción
max	Máximo/Maximum
ϕ	Rendimiento cuántico de luminiscencia
τ	Tiempo de vida de emisión
λ_{em}	Longitud de onda emisión
λ_{exc}	Longitud de onda de excitación
k_r	Constante radiativa
k_{nr}	Constante no radiativa
IL	Intraligando

MLCT	Transferencia de carga del metal al ligando	**SCF**	Self-consistent field
ILCT	Transferencia de carga intraligando	***f***	Fuerza del oscilador
LL'CT	Transferencia de carga del ligando al ligando	$\mathbf{S_n}$	Enésimo estado singlete
LC	Transferencia entrada en el ligando	$\mathbf{T_1}$	Primer estado triplete
TD-DFT	Time Dependent-Density Functional Theory	**HOMO**	High occuped molecular orbital
DFT	Density Functional Theory	**LUMO**	Low unoccuped molecular orbital
PCM	Polarizble continuum method	**HSOMO**	High single occuped molecular orbital
		LSOMO	Low single occuped molecular orbital
		NBO	Natural bond orbital

INTRODUCCIÓN

Introducción

Antecedentes

Sistemas mono y polimetálicos de Platino

En los últimos años la investigación en la química de coordinación del platino ha sufrido un notable desarrollo, debido a sus potenciales aplicaciones en fotocatálisis,[1] sensores químicos,[2] óptica no lineal,[3] dispositivos para la conversión de energía solar[4] o como emisores fosforescentes en diodos orgánicos emisores de luz (OLEDs).[5]

La disposición plano cuadrada de los complejos de Pt^{II} (d^8) es la responsable de muchos de los procesos fundamentales que influyen en la absorción, luminiscencia y otras propiedades del estado excitado[6] y, por lo tanto, de las interesantes propiedades ópticas y fotofísicas de este tipo de derivados.[7]

Un factor adicional que contribuye a las interesantes propiedades ópticas que exhiben los derivados de Pt^{II} es el hecho de que este metal, al igual que otros metales de la 3ª serie de transición, y algunos de la segunda, presenta una constante de acoplamiento espín-órbita grande, lo que provoca un rápido cruce entre sistemas (Intersystem crossing, ISC) desde un estado singlete a uno triplete.[7c] Como se observa en el diagrama de Jablonski de niveles de energía (Figura I.1), cuando una molécula se excita por absorción de luz, pasa de un estado fundamental singlete a un estado excitado singlete. Si el acoplamiento espín-órbita no es bueno, la desactivación al estado fundamental puede producirse en este momento, con emisión de luz (fluorescencia) o mediante procesos no radiativos (p. ej. relajación vibracional). Para estados excitados singlete, con importante contribución de los orbitales del metal, el cruce entre sistemas es un proceso mucho más rápido (10^{12} s^{-18}) que el de desactivación desde el estado excitado singlete (10^8 s^{-1}). Esto implica que la desactivación inicial no se produce al estado fundamental, sino a un estado intermedio triplete, y de ahí al estado fundamental singlete. Estas transiciones triplete (excitado) $\rightarrow$ singlete (fundamental), son de tipo fosforescente (con tiempos de vida relativamente largos, del orden de μs), y están

formalmente prohibidas por el espín. En compuestos puramente orgánicos, este tipo de transiciones tienen unas constantes de velocidad bajas (~10^3 s^{-1}), lo que supone que la fosforescencia es un proceso lento en comparación a los procesos mucho más rápidos de desactivación no radiante. Sin embargo, en los compuestos de Pt^{II}, la presencia del centro metálico, con su alta constante de acoplamiento espín-órbita, acelera el proceso hasta valores del orden de 10^5–10^7 s^{-1}, lo que permite la relajación a través del proceso de desactivación triplete → singlete. Este hecho hace que los derivados de Pt^{II} luminiscentes sean especialmente interesantes para ser utilizados como dopantes en OLEDs, mejorando la eficiencia respecto a un sistema puramente orgánico. Así, cuando el sistema es orgánico, los estados singlete y triplete se forman en proporción 1:3 (S:T), lo que lleva a un eficiencia del 25%, mientras que cuando se introduce un compuesto organometálico fosforescente, es posible observar emisión desde estados excitados triplete pudiendo incrementar la eficiencia del dispositivo hasta un 100%.

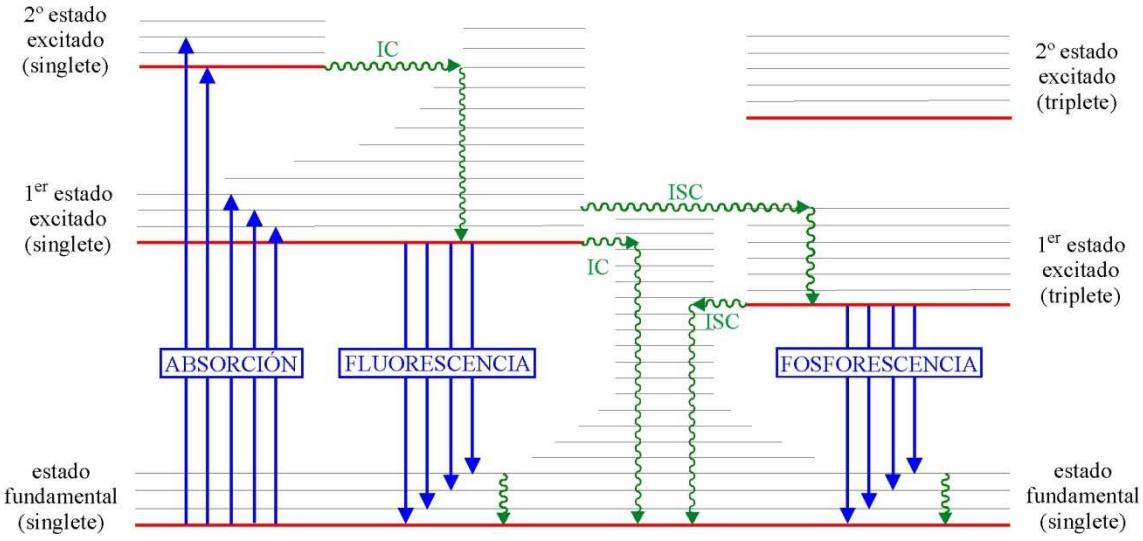

Figura I.1: Diagrama de Perrin-Jablonski de niveles de energía

Debido a estas razones, los derivados de Pt^{II} presentan características y propiedades específicas y diferentes a las de los compuestos de otros metales de transición para los que también se han descrito propiedades luminiscentes, como Cr^{III},[9] Ru^{II},[10] Os^{II},[10b,11] Rh^{III},[10b,12] Ir^{III} [10b,13](generalmente octaédricos), Cu^{I} [10b,14] (tetraédricos), o lantánidos[14-15] (índices de coordinación de 8 o 9).

Un factor fundamental tanto en las propiedades luminiscentes de los complejos de Pt^{II} como en su naturaleza son los ligandos que se coordinan al metal. Así, los

complejos de Pt^{II} con ligandos que generan un campo débil (aminas, fosfinas, halogenuros…) presentan un diagrama de orbitales moleculares como el mostrado en la Figura I.2**A**, y generalmente no son luminiscentes en disolución. Este comportamiento es consecuencia del carácter fuertemente antienlazante del orbital LUMO (fundamentalmente centrado en el metal, basado en el orbital $d_{x^2-y^2}$), ya que cuando la molécula alcanza el estado excitado y se puebla este orbital antienlazante, la geometría de la molécula sufre una gran distorsión, favoreciéndose por el principio de Frank-Condon, la desactivación no radiante (sin emisión de luz) a través de procesos como la conversión interna (IC) o el cruce entre sistemas (ISC), en lugar de hacerlo mediante una transición centrada en el metal (MC) con emisión de luz. La introducción de ligandos aromáticos conjugados (polipiridilos, ciclometalados…) y/o grupos fuertemente dadores (acetiluros, cianuros…) en el entorno metálico induce la desestabilización del orbital vacío centrado en el metal y la formación de un LUMO centrado en los ligandos, reduciendo así la probabilidad de la desactivación no radiante y permitiendo la formación de estados excitados de transferencia de carga del metal al ligando (MLCT) (Figura I.2**B**), o incluso centrados en el ligando (LC) de tipo $\pi \cdot\cdot \pi^*$ (Figura I.2**C**), lo que posibilita la desactivación con emisión de luz, en ocasiones incluso en disolución a temperatura ambiente.

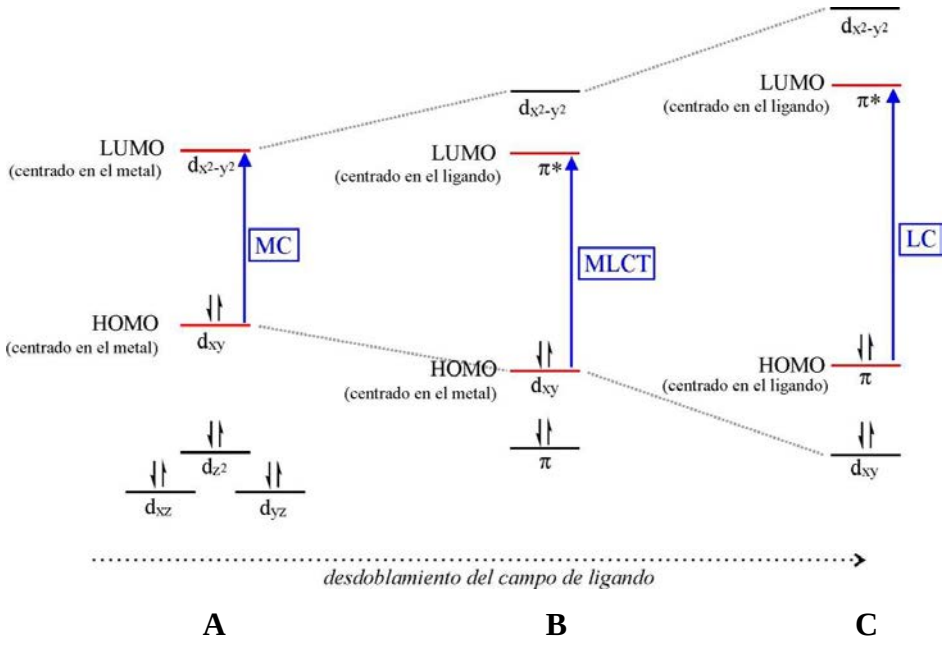

Figura I.2: Representación esquemática de las transiciones HOMO (Orbital ocupado de mayor energía)-LUMO (Orbital vacío de menor energía) en función del tipo de ligando.

En consecuencia, la introducción de ligandos aromáticos conjugados en estos derivados afecta de manera muy importante a las propiedades de este tipo de complejos.

Sin embargo, se observan diferencias notables entre el uso de ligandos de tipo polipiridilo (N^N, N^N^N)[7a,16] o ciclometalado (C^N, C^N^N, N^C^N)[2d,3a,5d,7c,16c,d,17] (Figura I.3). Así, en los compuestos de platino con ligandos ciclometalados, el átomo de carbono coordinado al centro metálico (formalmente aniónico, C^-) se comporta como fuerte σ-dador, mientras que el átomo de nitrógeno del fragmento piridilo (N:) permanece como buen π-aceptor. Esto genera un aumento del desdoblamiento del campo de ligando respecto del provocado por un ligando de tipo polipiridilo con sólo átomos N-dadores, con lo que, teniendo en cuenta lo comentado anteriormente, se favorece aún más la generación de estados excitados triplete de tipo ^{3}LC ó ^{3}MLCT. Este comportamiento favorece que muchos derivados ciclometalados de Pt(II) presenten luminiscencia incluso en disolución a temperatura ambiente.

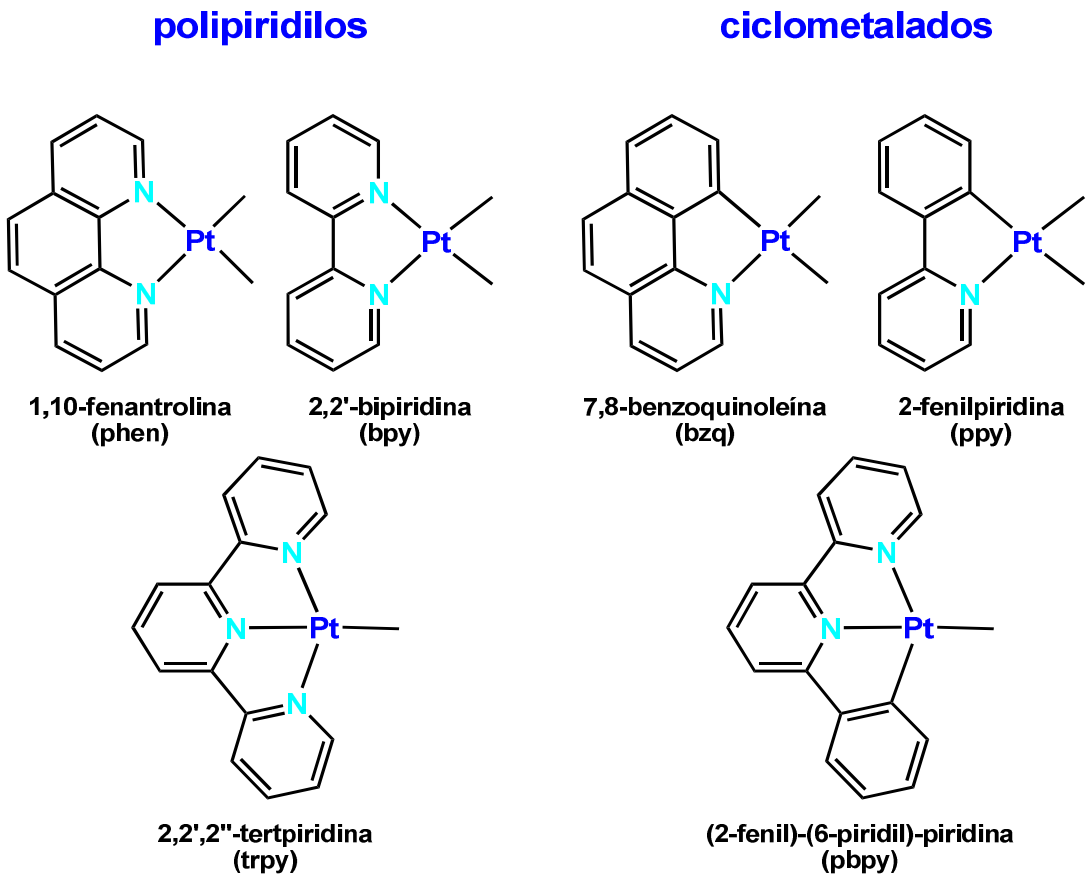

Figura I.3: Ejemplos de compuestos de Pt^{II} con ligandos polipiridilos o ciclometalados

La mayor parte de los estudios recogidos en la bibliografía de compuestos ciclometalados de Pt^{II} que exhiben propiedades luminiscentes se han centrado en complejos neutros o catiónicos. En referencia a los ligandos bidentados de tipo C^N que

se utilizan en este trabajo, se conocen derivados mononucleares de tipo bis-ciclometalado $Pt(C\hat{}N)_2$,[18] cuyos estados emisivos se atribuyen al estado ^{3}MLCT y derivados binucleares de puentes cloro $[Pt(C\hat{}N)(\mu\text{-}Cl)]_2$.[19] Estos dímeros sufren fácilmente reacciones de ruptura del sistema de puentes cloro con ligandos del tipo L^L (L^L = diaminas, diiminas, tales como etilenodiaminas, bipiridina, fenantrolina, ...) para formar derivados mononucleares $[Pt(C\hat{}N)(N\hat{}N)]^{+}$[20] o con ligandos bidentados aniónicos del tipo L^X, tales como las β-dicetonas, para dar complejos del tipo $[Pt(C\hat{}N)(O\hat{}O)]$.[21] También se han introducido ligandos monodentados generando compuestos tipo $[Pt(C\hat{}N)Cl_2]^-$,[20] $[Pt(C\hat{}N)(CO)(Cl)]$,[19a,20b,22] y $[Pt(C\hat{}N)(Cl)(CNR)]$.[23] De acuerdo con las características comentadas anteriormente, los complejos que contienen ligandos de campo débil, como los ligandos cloruro, son luminiscentes a 77 K, pero no a temperatura ambiente. Sin embargo, la incorporación de ligandos de campo fuerte como la etilenodiamina (en), 2,2'-bipiridina (bpy) o 1,10-fenantrolina (phen), permite que estos compuestos sean luminiscentes incluso en disolución a temperatura ambiente, asignándose la luminiscencia a transiciones ^{3}MLCT. En este sentido, la introducción de ligandos alquinilo, también de campo fuerte, aumenta de forma notable la eficiencia de la emisión en complejos de Pt^{II}. Además, la presencia de estos grupos insaturados introduce nuevos puntos de interés estructural, electrónico y de reactividad.

De hecho, la química de metales de transición con grupos C≡CR ha sido muy estudiada desde hace años debido a su gran diversidad estructural,[24] su interesante reactividad, que incluye la formación de clusters y agregados polinucleares,[24b,25] así como su transformación en vinilos, vinilidenos, alenilidenos o cumulenilidenos,[26] o su participación en procesos de formación y ruptura de enlaces carbono-carbono, en particular en derivados de metales del principio de las series de transición.[27]

En la Figura I.4, se recogen, de forma esquemática, algunos de los distintos modos de coordinación conocidos para los ligandos alquinilos. En general, cuando este grupo actúa como ligando puente entre centros metálicos, lo más frecuente es que conecte dos núcleos empleando los modos **IIa**[28] y **IIb**.[29] No obstante, se han descrito numerosos ejemplos en los que estos ligandos conectan tres, cuatro e incluso cinco átomos metálicos (modos de coordinación **III**,[30] **IV**[31] y **V**,[32] (respectivamente).

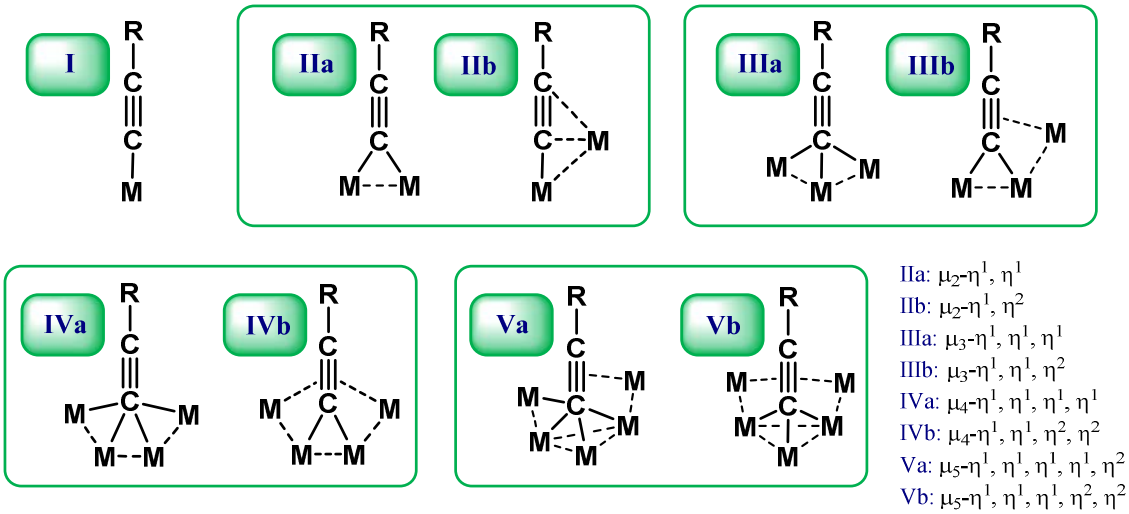

Figura I.4: Posibles modos de coordinación de los ligandos alquinilo

Además, la geometría lineal del fragmento alquinílico, así como la densidad electrónica π del triple enlace C≡C facilitan la deslocalización electrónica y los convierten en excelentes candidatos para el diseño de nuevos materiales moleculares.[33] Estos sistemas poseen un gran potencial debido a que pueden mostrar interesantes propiedades relacionadas con procesos de transferencia de carga, como procesos redox, propiedades ópticas y electrónicas e, incluso, propiedades magnéticas o de cristales líquidos.[17e,34]

Estas características han suscitado el interés de numerosos grupos de investigación por la química de los ligandos alquinilo, no sólo en el área de la química organometálica, sino también en ciencia de materiales. Este campo, se ha visto potenciado recientemente por el interesante comportamiento fotoquímico y fotofísico de algunos de estos sistemas, por lo que se ha dedicado una atención especial a sistemas que incluyen metales de capa cerrada d^{10} (Au^I, Ag^I, Cu^I, Hg^{II}) y/o subcapa cerrada d^8, $ns^2(n-1)d^{10}$ (Pt^{II}, Rh^I, Ir^I, Tl^I).[24a-c,25a,34a,34i-l,35] Este tipo de compuestos presenta una gran variedad estructural, determinada tanto por las características electrónicas y/o estéricas del metal, como por las del ligando alquinilo. De particular interés en el trabajo desarrollado en esta memoria, destacamos el avance espectacular desarrollado en el estudio de las propiedades ópticas de alquinilos de Pt^{II} en los últimos años.[7c,16a,17e,34j,k,34m,36]

Desde los primeros estudios del grupo de Lukehart de las propiedades ópticas de compuestos mononucleares de platino, que asignaba la emisión de los derivados *trans*-$Pt(C{\equiv}CR)_2(PEt_3)_2$ (R = H, Ph) a una banda de transferencia de carga desde el orbital dz^2 del platino a los orbitales π* de los grupos alquinilo,[37] son numerosos los grupos de investigación que han concentrado sus esfuerzos en el estudio de las propiedades ópticas de nuevos derivados de platino con ligandos σ-alquinilo, tanto mononucleares como de mayor nuclearidad.[25d,38]

La mayor parte de los compuestos mononucleares de platino luminiscentes descritos son derivados heterolépticos estabilizados por coligandos neutros de tipo fósforo o nitrógeno dador, siendo particularmente escasos los sistemas que contienen, simultáneamente, grupos carbonados.[38a,b] Dentro de éstos, los más estudiados son derivados con disposición *trans*-bis(alquinilo)bis(fosfina), análogos al previamente estudiado por Lukehart, de los que se muestran algunos ejemplos en la Figura I.5.[39] Estas especies presentan interesantes propiedades ópticas,[40] que parecen estar asociadas con procesos de comunicación electrónica entre los ligandos alquinilo a través del platino, con pobre o nula influencia de las fosfinas,[39b,41] convirtiéndolas en especies idóneas para el diseño de dispositivos captadores de fotones.

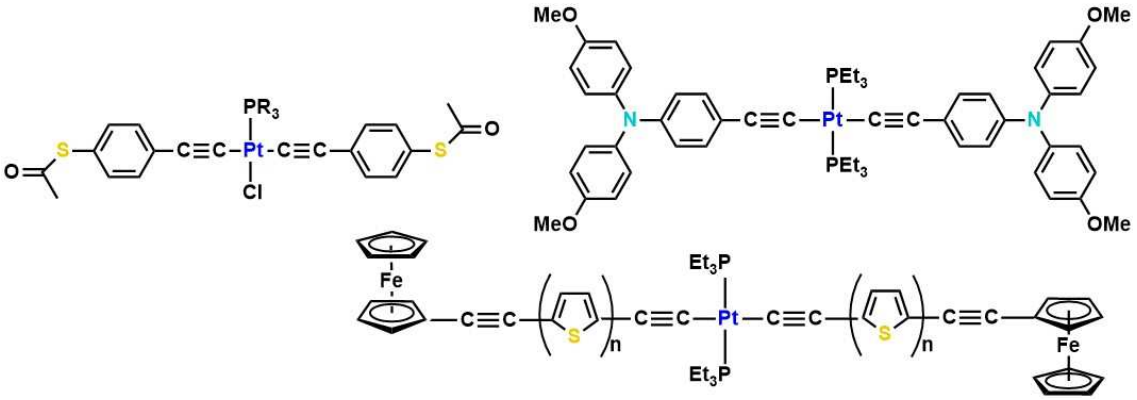

Figura I.5: Sistemas con disposición *trans*-bis(alquinilo)bis(fosfina)

La versatilidad de estos ligandos favorece la formación de derivados homopolinucleares estabilizados por interacciones entre el centro de Pt y los ligandos acetiluro.[25d] En este campo, se han descrito derivados en los que el puente alquinilo está soportado por otros grupos puente como diimina $[(C_6F_5)_2Pt(\mu\text{-}C{\equiv}CPh)(\mu\text{-napy})Pt(C_6F_5)(napy)]$,[42] difosfina, $[Pt_2(\mu\text{-dppm})_2(\mu\text{-}C{\equiv}CR)(C{\equiv}CR)_2]^+$ [R = ^{t}Bu, Ph,

C_6H_4Ph-*p*, C_6H_4Et-*p*, C_6H_4OMe-*p*; dppm = bis(difenilfosfino)metano],[43] hidruro [*cis*, *cis*-$(PPh_3)_2Pt(\mu\text{-}H)(\mu\text{-}C{\equiv}CR)Pt(C_6F_5)_2$], [*trans*-$(PPh_3)(C_6F_5)Pt(\mu\text{-}H)(\mu\text{-}C{\equiv}CR)Pt(C_6F_5)(PPh_3)$][25d,44] o alquinil fosfinas [$\{Pt(\mu\text{-}\kappa(P)\text{:}\eta^2\text{-}PPh_2C{\equiv}CR)_2(\mu\text{-}\eta^1\text{:}\eta^2\text{-}C{\equiv}CR)_2\}\{Pt(C_6F_5)_2\}_2$],[45] y también complejos en los que alquinilo actúa como único grupo puente (ejemplos representativos se recogen en la Figura I.6[25d]). Sin embargo, en estos sistemas los estudios se han centrado en aspectos estructurales y de reactividad y son muy escasos los estudios sobre sus propiedades ópticas.[42,46]

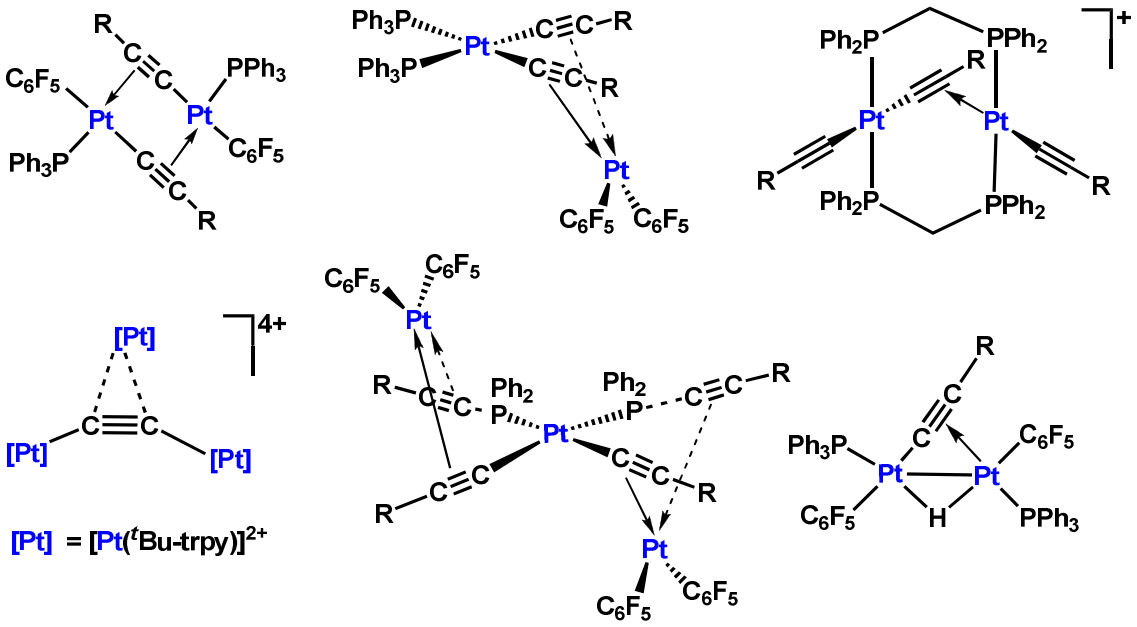

Figura I.6: Derivados homopolinucleares estabilizados mediante interacciones entre el centro de Pt y los ligandos acetiluro

En 1994, el grupo de investigación del profesor C.M. Che, publicó el primer complejo de Pt^{II} con ligandos acetiluro y un ligando aromático de tipo diimina $[Pt(phen)(C{\equiv}CPh)_2]$ (phen = 1, 10-fenantrolina).[47] Este derivado presentaba una intensa emisión en disolución a temperatura ambiente, que se asignaba a una transferencia de carga ^{3}MLCT desde el orbital 5d del platino al orbital π* de la fenantrolina. Desde entonces, han sido numerosos los estudios de especies con ligandos quelato tipo polipiridilo[7a,7c,48] o ciclometalado que contienen ligandos alquinilo[49] (algunos ejemplos con ligandos ciclometalados se recogen en la Figura I.7), dado el enorme potencial que se les presume en la construcción de OLEDs,[5d,17b,49b,50] sistemas de separación de carga

fotoinducidos,[48a] producción fotovoltaica de hidrógeno,[51] vapocromismo[52] o sensores luminiscentes.[53]

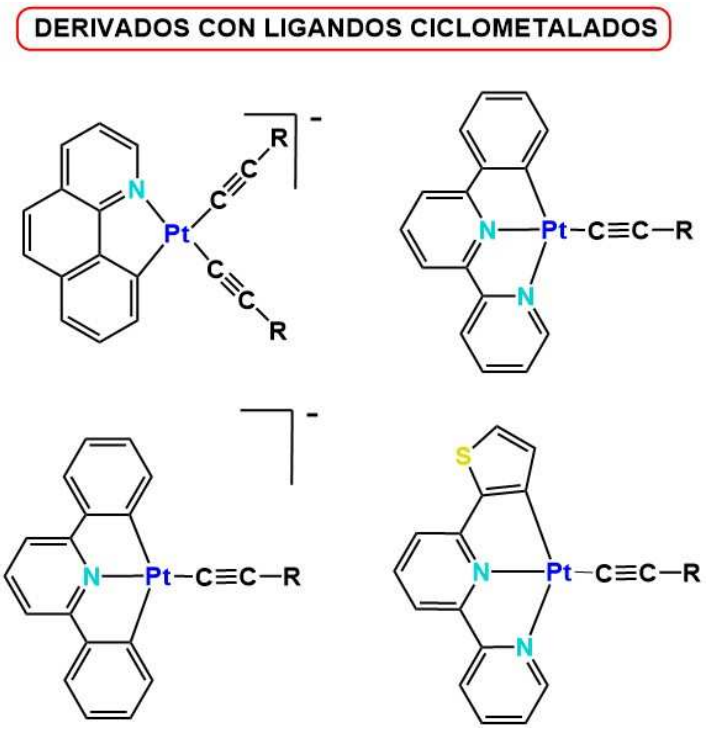

Figura I.7: Derivados cicloplatinados con ligandos acetiluro

La introducción de ligandos alquinilo en sistemas de Pt^{II} con ligandos ciclometalados permite modular las propiedades fotofísicas de los compuestos finales, e incluso, dependiendo de los sustituyentes del ligando alquinilo, modificar la naturaleza del estado emisivo [^{3}LLCT, ^{3}LC(alquinilo)]. También en estos sistemas, aparecen emisiones de tipo ^{3}MMLCT y/o excimércas $^3\pi\pi^*$ con relativa facilidad, asociadas a interacciones Pt···Pt y/o$\pi\cdot\cdot\pi$,[49f,53c,54] como se analiza posteriormente.

Sorprendentemente, y a pesar del gran número de derivados homopolinucleares de Pt^{II} estabilizados por puentes acetiluro existentes, únicamente los complejos $[Pt_2(bzq)_2(\mu\text{-}Cl)(\mu\text{-}C{\equiv}CR)]_2$ (Figura I.8a) y $[Pt(dppyH)_2(\mu\text{-}Cl)(\mu\text{-}C{\equiv}C^tBu)]$, publicados por nuestro grupo de investigación,[55] y el derivado $[Pt(C\text{^}N)(\mu\text{-}C{\equiv}CSiMe_3)]_2$,[56] representado en la Figura I.8b presentan un grupo ciclometalado C^N.

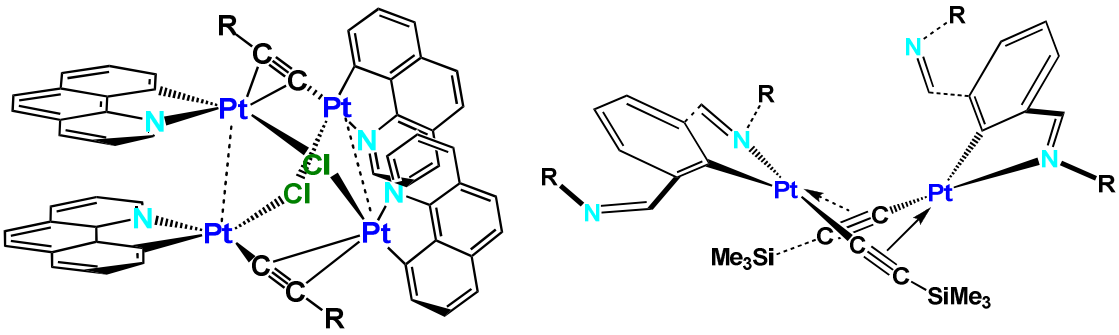

Figura I.8: Derivados cicloplatinados homopolinucleares estabilizados por puentes acetiluro

Para entender las emisiones asociadas a interacciones Pt···Pt y/o π···π debemos considerar la disposición plano cuadrada de los complejos de Pt^{II}, junto con la elección de ligandos esencialmente planos, lo que permite establecer contactos e interacciones con otras moléculas iguales (apilamiento intermolecular o agregados si se forman en estado fundamental y excímeros si se forman en el estado excitado) o con moléculas distintas (exciplejos). El apilamiento en el estado fundamental implica una interacción Pt···Pt a través de los orbitales d_{z^2} de los centros de Pt, que se encuentran perpendiculares al plano de coordinación del metal. Una separación intermolecular suficientemente pequeña permite el solapamiento de los orbitales $6p_z$ y $5d_{z^2}$, dando lugar a nuevos orbitales moleculares enlazantes (pσ, dσ) y antienlazantes (pσ*, dσ*)[57] (Figura I.9). Aunque formalmente el orden de enlace Pt–Pt es cero, porque los orbitales dσ y dσ* están completamente ocupados, la interacción neta, aunque débil, es energéticamente favorable y la molécula resultante es más estable que en los monómeros.

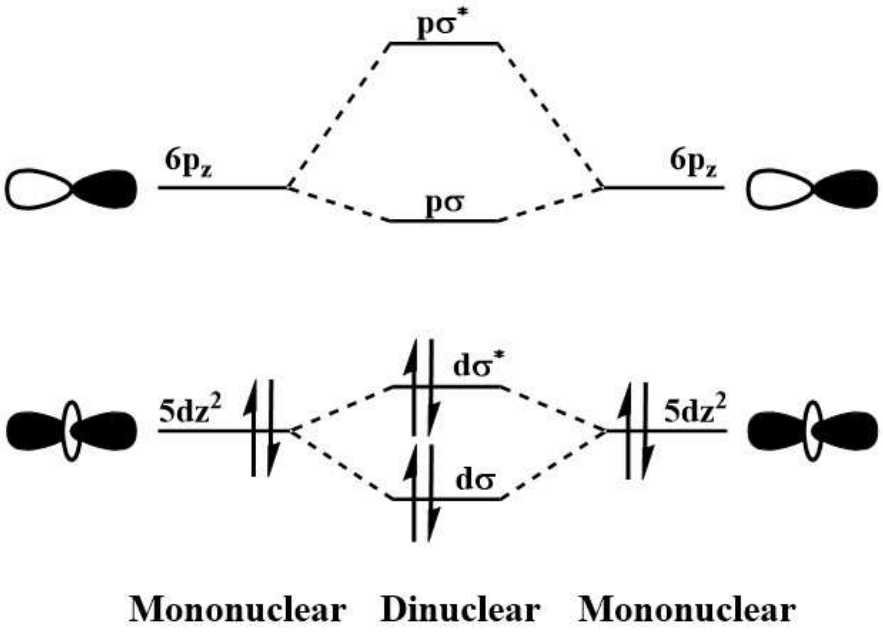

Figura I.9: Diagrama de orbitales moleculares general de un compuesto planocuadrado de Pt^{II} que presenta interacciones Pt···Pt

La tendencia de los complejos plano cuadrados a apilarse puede dar lugar a arquitecturas en cadena (1D) dirigidas por interacciones Pt···Pt. Ejemplos típicos son las sales dobles (Figura I.10), que consisten en cadenas infinitas de aniones y cationes alternados, con los átomos de Pt alineados y separados aproximadamente 3.3 Å, entre las que se pueden destacar la sal de Magnus $[Pt(NH_3)_4][PtCl_4]$[58] o sales relacionadas, $[Pt(NH_2R)_4][PtCl_4]$[59] o $[Pt(CNR)_4][PtCl_4]$,[60] así como las sales dobles con ligandos cianuro e isocianuro $[Pt(CNR)_4][Pt(CN)_4]$,[60] $[Pt(bzq)(CNR)_2][Pt(bzq)(CN)_2]$ (bzq = benzo[h]quinolato).[61]

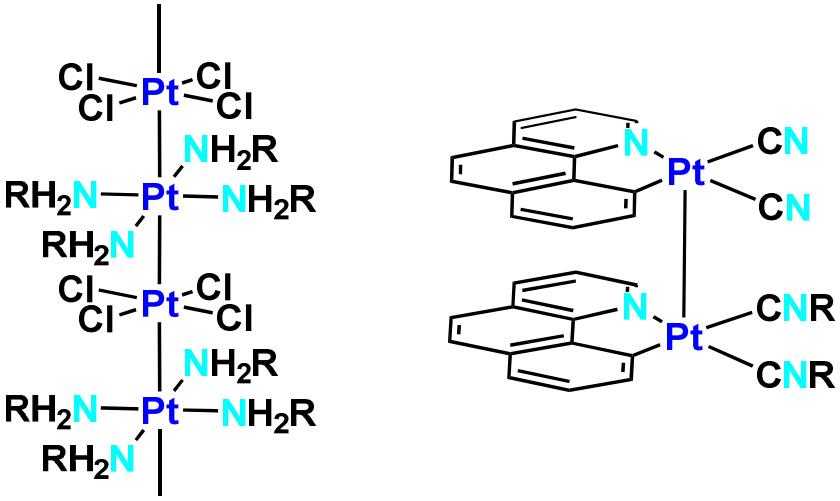

Figura I.10: Ejemplos de sales dobles con enlaces Pt-Pt

En estos casos, el empaquetamiento está controlado en su mayor parte por interacciones electrostáticas, pero existe una pequeña contribución de tipo covalente a la interacción Pt···Pt.[62] Estas estructuras de cadena lineal no sólo se han observado en sales dobles, sino también en complejos aniónicos,[63] catiónicos[53c,64] o neutros.[2a,23a,65] Algunos ejemplos ilustrativos se pueden encontrar en sales de $[Pt(CN)_4]^{2-}$,[63] $[Pt(Nttpy)Cl]^{2+}$ (Nttpy = 4'-(*p*-nicotinamida-*N*-metilfenil)2,2':6',2''-terpiridina),[66] $[Pt(tpy)(C{\equiv}C\text{-}C{\equiv}CX)]^{+}$ (tpy = 2,2':6',2''-terpiridina, X = H, C_6H_5, 4-OCH_3-C_6H_4)[53c,64b] y $[Pt(tpy)Cl]^{+}$ [64c] y en los complejos neutros $[PtCl_2(bpy)]$ (bpy = bipiridina),[65a,67] $[Pt(CN)_2(bpy)]$,[65c,68] $[Pt(bpm)Cl_2]$ (bpm = 2,2'-bipirimidina),[65b] [Pt(phen)$(CN)_2$] (phen = fenantrolina),[65b] [Pt(bpy)$(NCS)_2$],[65b] [*cis*-Pt(CN-*p*-$(C_2H_5)C_6H_4)_2(CN)_2$],[65d] [*trans*-Pt(CN-*p*-$(C_2H_5)C_6H_4)_2(CN)_2$],[65e] $[cis\text{-}Pt(CN)_2(CN^tBu)_2]$[2a,69] (Figura I.11), [*cis*-$PtCl_2(CNPh)_2$][70] y [Pt(bzq)Cl(CN^tBu)] (bzq = benzo[h]quinolato).[71]

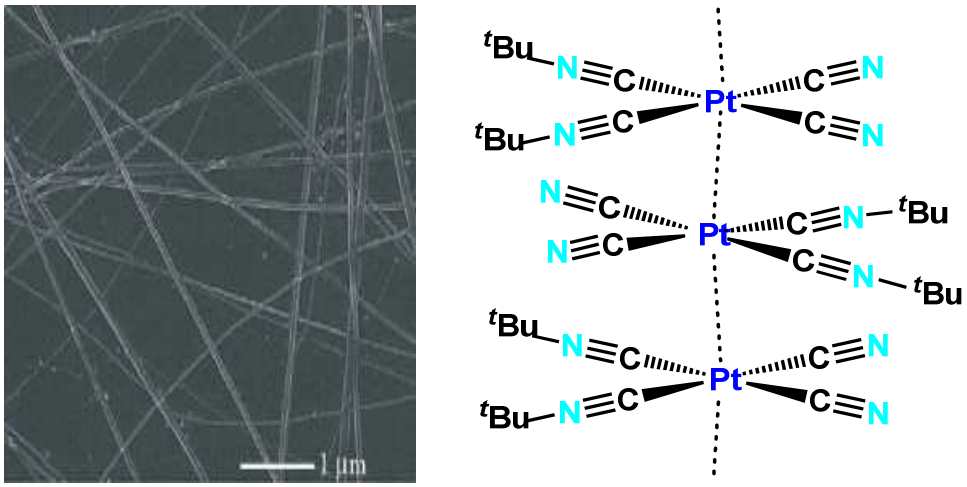

Figura I.11. A: a) Nanoestructuras y b) estructura cristalina de [*cis*-$Pt(CN)_2(CN\text{-}^tBu)_2$].

Además de esto, si los ligandos presentes en los complejos son poco voluminosos y con sistemas π conjugados como diimina, terpiridil o ligandos C,N-ciclometalados, las interacciones π···π se añaden a las Pt···Pt como las principales fuerzas que determinan la estructura supramolecular.[72] En estos casos hay una contribución importante a la estabilidad de la estructura cuando la distancia Pt···Pt es inferior a 3.5 Å[62] y la separación entre los grupos aromáticos es menor de 3.8 Å,[73] lo que conlleva también una modificación importante en las propiedades ópticas de los complejos. Así, sistemas dinucleares $[Pt_2]$ o dímeros $[Pt]_2$ con fragmentos cicloplatinados C^N que muestran interacciones Pt···Pt y/oπ··π presentan, en general, el diagrama de energías que se muestra en la Figura I.12. Como se puede observar, el

orbital ocupado de mayor energía (HOMO) está principalmente formado por el orbital antienlazante dσ∗ y el LUMO se localiza principalmente en los orbitales π*[7c] del ligando aromático conjugado.

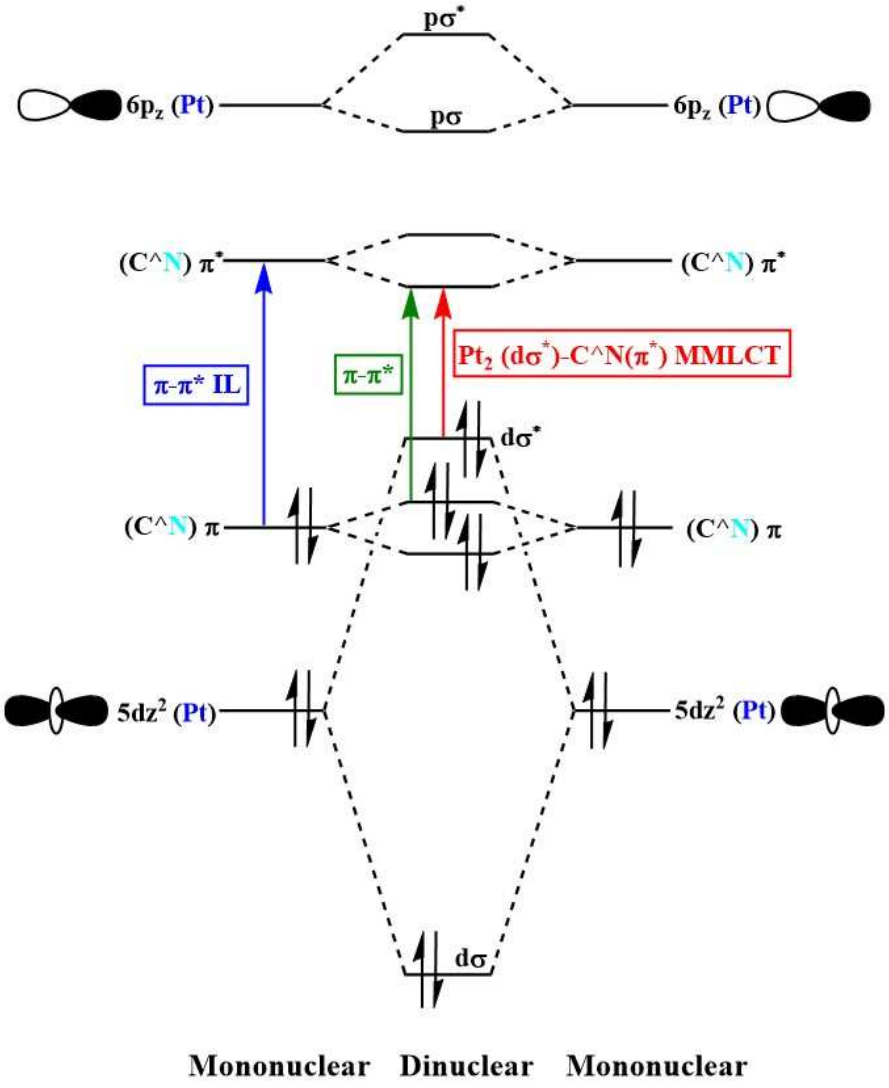

Figura I.12. Diagrama simplificado de orbitales moleculares de un complejo C^N ciclometalado de Pt^{II} (d^8) dinuclear con interacciones Pt···Pt yπ··π

Como consecuencia, estos sistemas presentan emisiones que provienen desde estados excitados de transferencia de carga metal-metal ligando ^{3}MMLCT ^{3}[dσ*(Pt)$_2$→π*(L)] y/o estados excitados exciméricos ligando-ligando (^{3}ππ*).[7b,36d,53c,74] Estas propiedades difieren de las que se observan para los complejos mononucleares aislados,[7b] ya que la emisión aparece desplazada hacia el rojo y dependen de la extensión de las interacciones intermoleculares Pt···Pt y/oπ···π.[5d,7c,71,74a-c,75]

Ambos tipos de interacciones Pt···Pt y/o π···π pueden derivar en la formación de especies de mayor nuclearidad, no sólo en estado sólido, sino también en disolución (tanto más cuanto mayor es la concentración), dando lugar tanto a la formación de agregados, en el estado fundamental,[53c,64b,76] como de excímeros o exciplejos[49f,74a,74h,77] en el estado excitado.

En disoluciones diluídas en las que las interacciones Pt···Pt y/o π···π son débiles o inexistentes, las propiedades luminiscentes debidas a estados ^{3}MMLCT se pierden fácilmente. Una estrategia para mantener fijas estas interacciones y poder obtener emisores de tipo ^{3}MMLCT estables es el uso de ligandos auxiliares que puedan actuar como puente formando así estructuras estables con distancias intermetálicas cortas (Figura I.13). Se han descrito complejos dinucleares discretos de Pt^{II} con una distancia corta Pt-Pt bien definida utilizando ligandos puente como PPi (pirofosfato, $P_2O_7^{4-}$),[78] Spy (piridin-2-tiolato),[79] amidato[80] o dppm (difenilfosfinometano).[81] Recientemente se han descrito también los complejos *anti*- y *syn*-[{Pt(d-t-bpy)(NS_2)}$_2$] (d-t-bpy = 4,4'-di*tert*-butil-2,2'-bipiridina, NS_2 = 2-mercaptobenzotiazolato, 2-mercaptoimidazolato, 2-mercaptobenzoxazolato).[82]

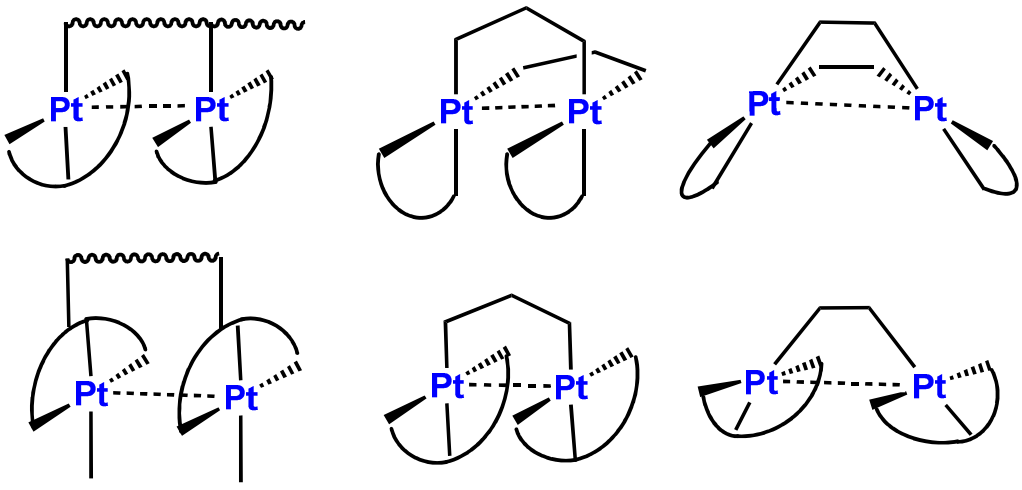

Figura I.13: Ejemplos más representativos de sistemas dinucleares ciclometalados de Pt^{II} con ligandos puente

Los complejos di y oligonucleares de Pt con débiles interacciones Pt···Pt, soportadas por ligandos puente, presentan propiedades fotoluminiscentes muy interesantes, que dependen no sólo del número (uno o dos) y del tipo de conector (rígido o flexible) entre las distintas unidades, sino también del medio (sólido, fluido) (Figura

I.13).[74f,74i,79a,83] En el caso de ligandos puente que favorecen la formación de disposiciones cara-cara, las interacciones π···π que se forman en el estado fundamental y/o en el estado excitado determinan sus propiedades ópticas.[74f,74i,79a,83a-g] En estos sistemas, la naturaleza de los estados emisivos es sensible al entorno y se ha utilizado como una herramienta interesante para modificar las características emisivas con la simple modulación de las distancias o de la orientación entre los fragmentos de Pt, con potencial interés como emisores de baja energía o sensores. La razón de este comportamiento se debe a que, en estos compuestos, el LUMO suele localizarse en los orbitales π* del ligando ciclometalado[83h-n] (o en el homólogo enlazante de los dos orbitales π*, si existe una interacción π··π),[74f,74i,79a,83a-g] mientras que el HOMO puede ser tanto un orbital dσ* centrado en el enlace metal-metal (cuando la interacción Pt···Pt es suficientemente corta), como un orbital centrado en el ligando o en el fragmento metal-ligando (d/π), en sistemas donde los Pt no interaccionan (Figura I.12). Como consecuencia, y dependiendo de la energía relativa de estos orbitales y del grado de mezcla entre ellos, la emisión puede variar desde un estado excitado fundamentalmente localizado en las unidades de platino (^{3}MLCT y/o ^{3}LC) a un estado de tipo ^{3}MMLCT (L = ligando ciclometalado). En estos últimos, el cambio más importante tras la excitación HOMO-LUMO es el fortalecimiento del enlace Pt-Pt con un acortamiento de la distancia entre los planos de coordinación del Pt.

En la actualidad está bien documentado que se puede producir un cambio en la energía de estos estados, en su grado de mezcla y, en consecuencia, en el color de las emisiones, mediante pequeñas modificaciones en el entorno electrónico de los centros de platino.

Sistemas heteropolinucleares Pt-M

Como se ha comentado anteriormente, en los complejos plano-cuadrados de Pt^{II}, el orbital d_{z^2} del metal está lleno, pudiendo actuar como base de Lewis frente a metales que actúan como ácidos, dando lugar a la formación de enlaces metal-metal de tipo dador–acceptor. Estas interacciones pueden dar lugar no sólo a simples compuestos bimetálicos sino también a complejos clusters de gran nuclearidad o polímeros. En la química del Pt^{II}, se han utilizado con éxito complejos aniónicos ricos en electrones en la

formación de clusters que contiene enlaces dador-aceptor $Pt^{II}\rightarrow M$ [M = d^{10} (Cu^{I}, Ag^{I}, Au^{I}, Cd^{II}, Hg^{II}), d^{10} ns^2 (Tl^{I}, Sn^{II} o Pb^{II})]. También se han utilizado con éxito complejos de Pt^{II} con ligandos cromóforos C^N^C-ciclometalados o C^N ciclometalados como 2-fenilpiridina (Hppy), 2-(2-tienil)piridina (Hthpy) o benzo[h]quinolina (bzq)[84] como productos de partida en la obtención de clusters con enlaces dador-aceptor $Pt^{II}\rightarrow M$,[85] ya que aumentan la capacidad electro dadora del Pt^{II}, incluso en sustratos neutros de tipo $[Pt(C^N)_2]$[85g,86] o catiónicos como $[Pt(ppy)9S3]^+$ (ppy = 2-fenilpiridinato; 9S3 = 1,4,7-tritiaciclononano).[85f] La presencia de enlaces dador-aceptor $Pt^{II}\rightarrow M$, normalmente, se traduce en un cambio en las propiedades emisoras de los complejos respecto a los complejos de Pt^{II} mononucleares (^{3}IL, ^{3}MLCT o ^{3}LML'CT).[36b,87]

En este campo, frente al elevado número de clusters con enlaces $Pt^{II}\rightarrow Ag^{I}$ descritos[85b,88] los sistemas heteropolimetálicos que incorporan fragmentos de Pt^{II} y metales $d^{10}s^2$ han resultado menos explorados a pesar de las interesantes propiedades ópticas que generan. Entre ellos el ión metálico más usado ha sido, sin duda, el Tl^{I}. Los primeros estudios de propiedades ópticas en un derivado Pt^{II}-Tl^{I} fueron publicados por Balch en el derivado $[PtTl_2(CN)_4]$.[89] Este derivado exhibe una intensa luminiscencia azul (λ_{em} = 444 nm), que se relaciona con la formación de enlaces Pt-Tl y que se atribuye, de acuerdo con el diagrama cualitativo de orbitales moleculares propuesto para este tipo de interacciones metálicas (Figura I.14) a una transición de transferencia de carga metal-metal' (MM'CT).[89-90] A partir de estos estudios pioneros, se han descrito numerosas familias de compuestos heteropolinucleares Pt^{II}–Tl^{I} que exhiben interesante propiedades fotofísicas.[85c,85i,91]

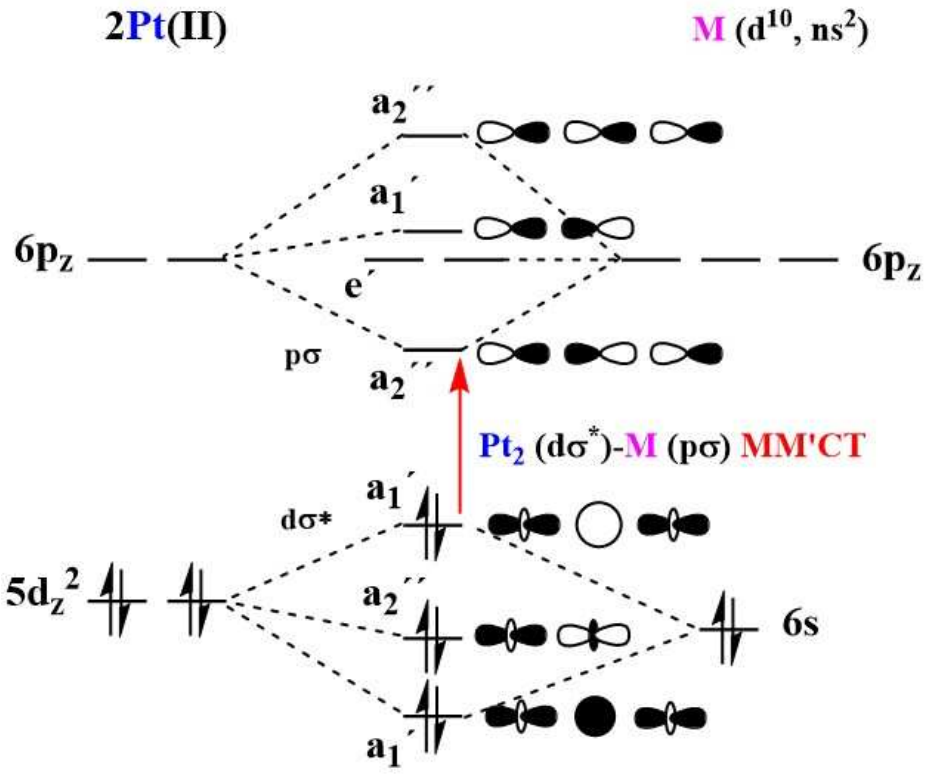

Figura I.14. Diagrama simplificado de orbitales moleculares para sistemas trinucleares $(Pt^{II})_2$-M (M = d^{10} ns^2)

En estos sistemas Pt→M el origen de la luminiscencia puede ser debido a la formación de los enlaces metal–metal, de modo que la luminiscencia se asigna a transiciones de transferencia de carga metal–metal (^{3}MM'CT), como en los complejos ciclo-[{Pt(C_6Cl_5)$_2$(μ-OH) (μ-Ag)}$_4$],[88e] [*trans-trans-trans*-Tl{Pt(C_6F_5)$_2$(CN)$_2$}],[91h] {Tl[Tl{*cis*-Pt(C_6F_5)$_2$(CN)$_2$}]}[91h] o [Tl{*cis*-Pt(C_6F_5)$_2$(CN)($PPh_2C{\equiv}CPh$)}][91h] (Figura I.15), que exhiben luminiscencia debida a transiciones Pt(5dσ*)→Ag(6pσ) o Pt(d_{z^2}) →Tl($6p_z$), respectivamente. Si el complejo de Pt^{II} inicial ya contiene grupos cromóforos en la molécula,[85c,92] la presencia de enlaces metal–metal modifica la naturaleza del estado excitado y con ello las características de la emisión. Por ejemplo, en los compuestos [(C_6F_5)$_2$(bzq)PtCd(cyclen)]ClO_4,[85d] [{Pt(bzq)(C_6X_5)$_2$}Ag(PPh_3)] (X = F, Cl)[85b] y [Cd{Pt(Bdt)(DTBbpy)}$_2$(ClO_4)(H_2O)](ClO_4) (Bdt = 1,2-bencenoditiolato y DTBbpy = 4,4′-di-tert-butil-2,2′-bipiridina),[93] los enlaces dador–aceptor Pt^{II}→M (M = Ag^{I}, Cd^{II}) disminuyen la densidad electrónica del átomo de Pt^{II}, provocando un desplazamiento de las bandas de absorción y emisión hacia el azul, que se asignan a una mezcla de transiciones ^{3}MLCT y ^{3}IL. Por el contrario, en los compuestos [PtTl(bzq)(C≡CR)$_2$] (R = Ph, C_5H_4N-2), [PtTl(C^N)(CN)$_2$] (C^N = bzq, ppy), [85c] y

[{PtTl(dppy)(CN^{t}Bu)}$_3$](PF$_6$)$_3$ (dppy = 2,6 difenilpiridinato),[94] la formación de los enlaces dador–aceptor Pt^{II}→Tl^{I} provoca una disminución de la diferencia energética HOMO-LUMO, lo que desplaza la emisión MM'LCT [d/sσ*(Pt,Tl) → π*(C^N)] hacia el rojo. Los ligandos auxiliares también juegan un papel importante, ya que modifican la densidad electrónica sobre el Pt^{II} y además pueden actuar como grupos puente, favoreciendo la formación de enlaces dativos metal–metal y manteniendo a los centros metálicos suficientemente cerca incluso en disolución.

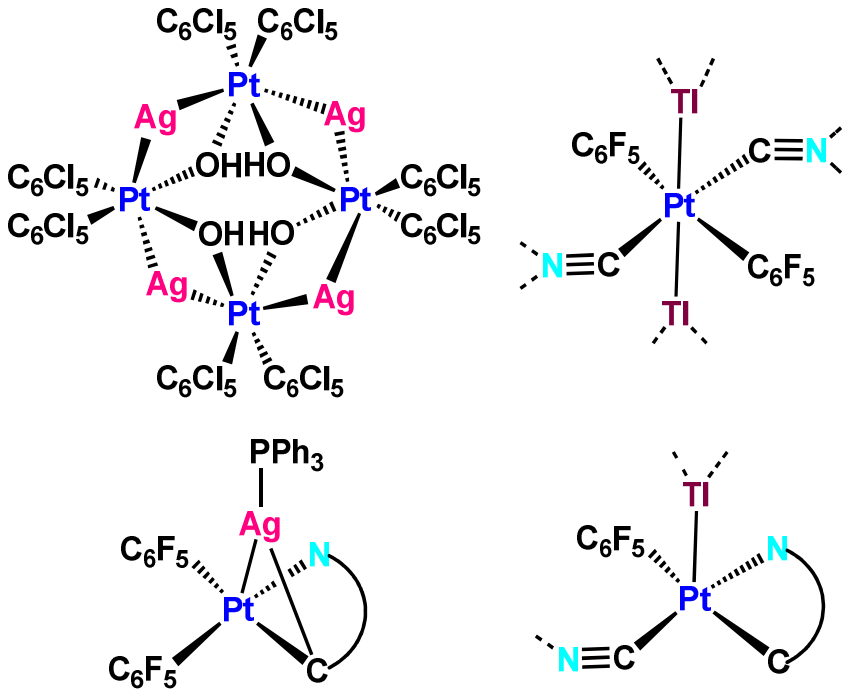

Figura I.15: Complejos polimetálicos seleccionados con enlaces Pt^{II}-M

En este área, el número de sistemas heteropolimetálicos descritos de fragmentos de Pt^{II} con el ión Pb^{II}, más duro, es mucho más pequeño,[52a,90a,91n,95] y son más escasos aún los estudios publicados de sus propiedades ópticas.[52a,95a,95e,f] A pesar de la naturaleza tóxica del plomo, su química ha atraído en los últimos años un gran interés, no sólo por su versatilidad estructural,[96] asociado con la variación en la actividad estereoquímica del par solitario, sino también por sus potenciales aplicaciones en óptica no lineal,[97] ferroeléctricas,[98] semiconductoras[99] y en materiales luminiscentes.[90a,95b,95e,100]

El análisis de un extraordinario número de estructuras cristalinas de compuestos de Pb^{II} ha permitido establecer una relación entre la actividad del par estereoquímico y la naturaleza de los ligandos auxiliares con la versatilidad estructural en torno al centro de plomo.[101] Los centros de Pb^{II} pueden adoptar entornos de coordinación *holodirigidos* o *hemidirigidos* (Figura I.16).

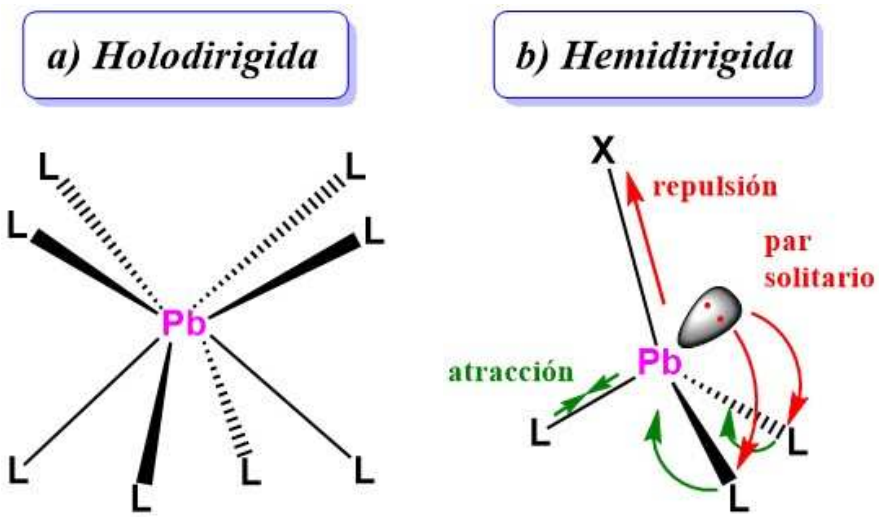

Figura I.16: Impacto estructural del par inerte en geometrías *Holo-* (**a**) y *Hemidirigidas* (**b**).

En la geometría *holodirigida* el par inerte no tiene carácter p y dota a la estructura de simetría en el entorno de coordinación del Pb^{II} (Figura I.16a). En la *hemidirigida* el orbital del par de electrones inerte tiene cierto carácter p. Este hecho origina un hueco en la esfera de coordinación del Pb, dando lugar a entornos asimétricos en los que se alargan los enlaces en la dirección del par inerte y se acortan los enlaces opuestos a este orbital (Figura I.16b). La coordinación *hemidirigida* suele aparecer en compuestos de Pb^{II} con ligandos duros y básicos, que induce una mayor mezcla de orbitales 6s y 6p, generando estructuras con bajos índices de coordinación en torno al Pb (2–5), aunque suele ser frecuente también en compuestos con números de coordinación intermedios (6–8). La coordinación *holodirigida*, sin embargo, suele ser frecuente con altos números de coordinación (9–10). En conclusión, la actividad del par de electrones depende del tipo de ligandos (duros o blandos), de su requerimiento estérico, del mayor o menor carácter p del par de electrones y de la mayor o menor transferencia de carga de los ligandos al metal.[101] Aunque existen numerosos estudios de la relación entre el par solitario y las estructuras, se tiene muy poco conocimiento de su papel en las propiedades ópticas.[101] Es de esperar que cuando el par solitario está

activo, su grado de actividad puede estar influenciado por factores externos, como vapores de disolventes dadores o fuerzas mecánicas, con cambios simultáneos en la estructura y propiedades.

Balch y colaboradores ya pusieron de manifiesto hace años que la obtención de compuestos con enlaces entre centros de Pt^{II} y Pb^{II} no es sencilla.[95b] Es decir, que a pesar de la similitud electrónica entre el Tl^{I} y el Pb^{II} ($6s^2$), la formación de enlaces polares Pt-Tl^{I} es fácil, en contraste con la formación de enlaces Pt^{II}-Pb^{II}. Así, por ejemplo, la reacción entre $K_2[Pt(CN)_4]$ y $TlNO_3$ genera el compuesto trimetálico $[PtTl_2(CN)_4]$,[91k] del que ya se ha hablado anteriormente, con dos enlaces cortos Pt-Tl (Figura I.17a) y una intensa luminiscencia azul, mientras que la reacción análoga con $Pb(NO_3)_2$ produce cristales de estequiometría $K_2Pb[Pt(CN)_4]\cdot 6H_2O$,[95b] que presentan una estructura en columnas formada por interacciones Pt··Pt [3.267(1), 3.298(1) Å], con los iones Pb^{2+} y K^{+} separados de las columnas (Figura I.17b).[95b] Este distinto comportamiento pone de manifiesto la menor tendencia del Pt^{II} a formar enlaces con el Pb^{II}, probablemente debido a su mayor carga y la consiguiente contracción del orbital $6s^2$.

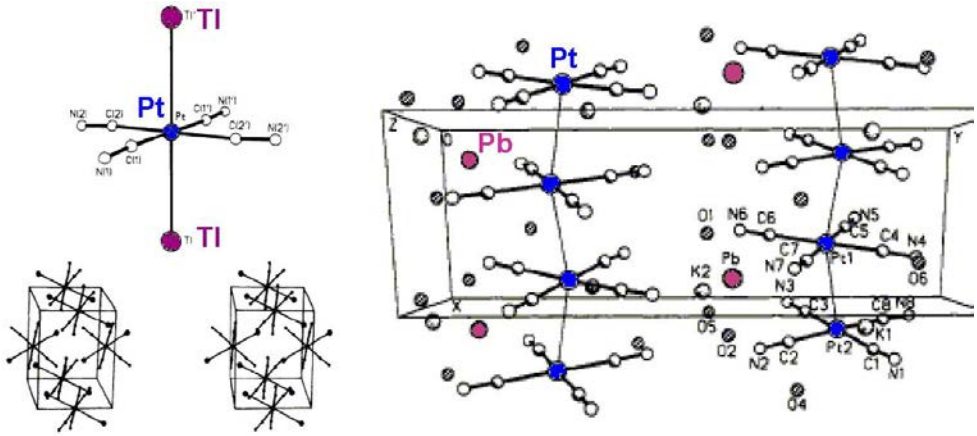

a) b)

Figura I.17: Estructuras cristalinas de los compuestos $[Tl_2Pt(CN)_4]$ (a) y $K_2Pb[Pt(CN)_4]$ (b).

Estos mismos autores han preparado los derivados bimetálicos $[Tl(crown\text{-}P_2)Pt(CN)_2]^{+}$ y $[(CH_3CO_2)Pb(crown\text{-}P_2)Pt(CN)_2]^{+}$ (crown-P_2 = 1,10-bis(difenilfosfino-metil)-1,10-diaza-4,7,13,16-tetraoxaoctadecano) (Figura I.18).[95b] Las estructuras cristalinas de estas especies revelan que las distancias Pt-Tl son inferiores [0.40 – 0.35 Å] a la distancia Pt-Pb [2.911(2), 2.958(2) Å *vs* 3.313(2) Å],[95b] a pesar de que el tamaño del ión Pb^{II} es menor que el del Tl^{I}.[102] Este hecho sugiere que el orbital $6s^2$ del Pb^{II}

presenta una interacción menos eficaz con los orbitales del platino que la que presenta el orbital $6s^2$ del Tl^I.

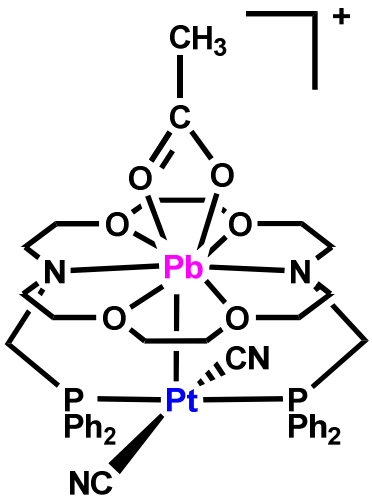

Figura I.18: Esquema del catión $[(CH_3CO_2)Pb(\textit{crown}\text{-}P_2)Pt(CN)_2]^+$

El grupo de investigación del Prof. J. Forniés publicó en 1992 el primer compuesto organometálico con enlaces Pt–Pb, $(NBu_4)_2[\{Pt(C_6F_5)_4\}_2Pb]$ (Figura I.19a), por reacción de $(NBu_4)_2[Pt(C_6F_5)_4]$ con $Pb(NO_3)_2$, que exhibe una disposición trinuclear Pt–Pb–Pt lineal. [95c] En colaboración con nuestro grupo se sintetizó posteriormente el derivado aniónico trinuclear Pt–Tl-Pt isoelectrónico de cadena lineal $(NBu_4)_3[\{Pt(C_6F_5)_4\}_2Tl]$ usando $TlNO_3$ (Figura I.19b).[91a] En contraste con el comportamiento observado en los derivados anteriores, en este caso, los enlaces Pt^{II}-Pb^{II} [2.769(2) y 2.793(2) Å] son claramente más cortos que los enlaces Pt^{II}-Tl^I [2.9777(4) y 3.0434(4) Å] y esta característica no se puede justificar por la presencia de contactos adicionales σ-F···M, ya que éstos son aproximadamente del mismo orden en ambos aniones $[\{Pt(C_6F_5)_4\}_2M]^{n-}$ (M = Pb, n = 2; M = Tl, n = 3). Estas diferencias estructurales se reflejan en las propiedades ópticas, ya que mientras el derivado $(NBu_4)_3[\{Pt(C_6F_5)_4\}_2Tl]$ exhibe una intensa luminiscencia azul (λ_{em} = 450 nm) asociada a la transición $^3[d\sigma^* \rightarrow p\sigma]$ (^{3}[MM'CT]) localizada en el cromóforo trimetálico,[91a] esta emisión en el derivado análogo con Pb^{II} $(NBu_4)_2[\{Pt(C_6F_5)_4\}_2Pb]$ aparece notablemente desplazada hacia menores energías (λ_{em} = 539 nm, ϕ = 0.43).[95a]

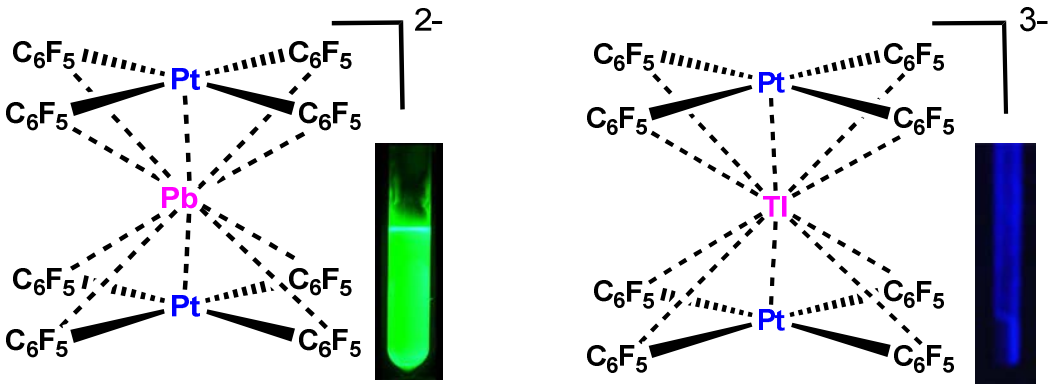

a) b)

Figura I.19: Estructura y luminiscencia en estado sólido de a) $(NBu_4)_2[\{Pt(C_6F_5)_4\}_2Pb]$ y b) $(NBu_4)_3[\{Pt(C_6F_5)_4\}_2Tl]$

Posteriormente se describieron los derivados trinucleares aniónicos $(NBu_4)[(C_6F_5)_3Pt(\mu\text{-}Pb)(\mu\text{-}X)Pt(C_6F_5)_3]$[95f] (X = Cl, I, OH) (Figura I.20a), que presentan una disposición angular Pt^{II}–Pb^{II}–Pt^{II} y el inusual cluster tetranuclear $(NBu_4)[Pb\{Pt(\mu\text{-}Cl)(C_6F_5)_2\}_3]$[95e] (Figura I.20b), en el que el plomo se enlaza a tres centros de platino. Estos compuestos exhiben intensa fosforescencia que depende no sólo del sistema Pt–Pb–Pt, sino también del grupo X que conecta los centros de Pt.

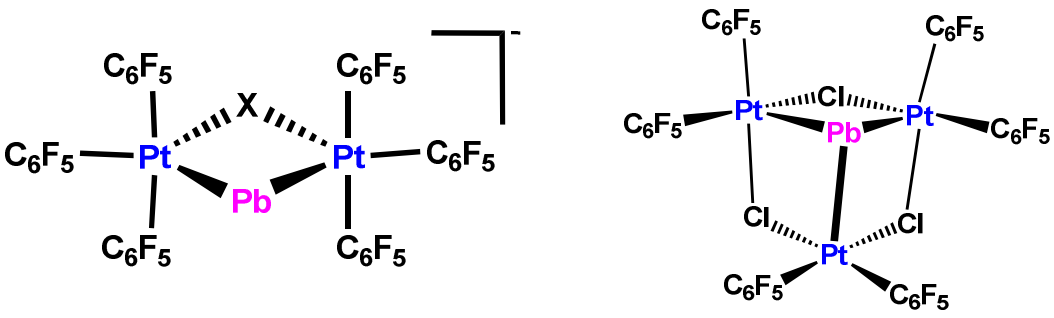

a) b)

Figura I.20: Compuestos heteropolinucleares Pt-Pb conteniendo ligandos pentafluorofenilo

Con ligandos alquinilo nuestro grupo de investigación publicó en 2008 la síntesis del compuesto trinuclear Pt^{II}–Pb^{II}–Pt^{II} aniónico $[\{Pt(C{\equiv}CTol)_4\}_2Pb(OH)_2]^{2-}$, que exhibe una disposición Pt–Pb–Pt lineal con distancias Pt^{II}–Pb^{II} muy cortas. El Pb^{II} presenta un entorno de coordinación *hemidirigido* de bipirámide trigonal con los centros de Pt^{II} y dos moléculas de H_2O definiendo las posiciones axiales y ecuatoriales, respectivamente y el par inerte $6s^2$ estereoquímicamente activo. Este compuesto muestra cambios reversibles de color y de emisión en contacto con acetona.

Desafortunadamente, la baja estabilidad de este compuesto y la falta de cristales de disoluciones de acetona no permitieron estudiar la naturaleza de este comportamiento con más detalle.[95a]

Por neutralización completa del precursor aniónico correspondiente $(NBu_4)_2[Pt(C{\equiv}CR)_4]$ con $Pb(ClO_4)_2{\cdot}3\ H_2O$ se obtienen los derivados tetranucleares romboidales $[\{Pt(C{\equiv}CR)_4\}Pb]_2$ (R = Tol, C_6H_4OMe-3, C_6H_4OMe-4), estabilizados por una combinación sinérgica de interacciones Pt^{II}–Pb^{II} y/o η^1, η^2 $Pb^{II}\cdots$alquinilo(C≡CR) (Figura I.21a).[52a] Estos clusters se aíslan como sólidos naranjas no solvatados y exhiben una intensa luminiscencia atribuída a un estado excitado de naturaleza mixta $Pt(d){\rightarrow}Pt_2Pb_2/\pi\pi^*C{\equiv}CR$ (^{3}MLCT/^{3}IL) con una notable contribución de los centros de Pb y con carácter enlazante $Pb\cdots Pb$. La importante contribución de los centros de Pb en el estado excitado y el entorno claramente *hemidirigido* del ión en los agregados está relacionado con la rápida respuesta que exhiben a estímulos externos. Así, los tres clusters exhiben un comportamiento mecanocrómico reversible muy acusado y, además, las derivados con R = Tol y C_6H_4OMe-4 muestran un comportamiento vapocrómico y vapoluminiscente selectivo reversible frente a disolventes moderadamente dadores (NCMe, THFMe-2, acetona). El análisis estructural de diversos solvatos ha permitido atribuir este comportamiento a la formación y ruptura rápida de los clusters solvatados $[Pt_2Pb_2(C{\equiv}CR)_8S_x]$ (S_x = molécula dadora volátil, $x \geq 2$), con cambios geométricos y electrónicos del core metálico Pt_2Pb_2. Estos cambios están relacionados con la variación de la actividad estereoquímica del par solitario del Pb^{II} que conlleva una modificación simultánea del estado excitado de naturaleza mixta cluster/ligando Pt_2Pb_2/C≡CR (^{3}MLCT/^{3}IL) con una fuerte contribución Pb–Pb. Los cálculos teóricos realizados (TD-DFT, NBO) sobre el ión Pb^{II} revelan una disminución gradual de la actividad electrónica del par $6s^2$ (disminución de la contribución p) al aumentar el número de moléculas de disolvente que interaccionan con el centro de Pb, lo que está de acuerdo con la formación de entornos más *holodirigidos*.

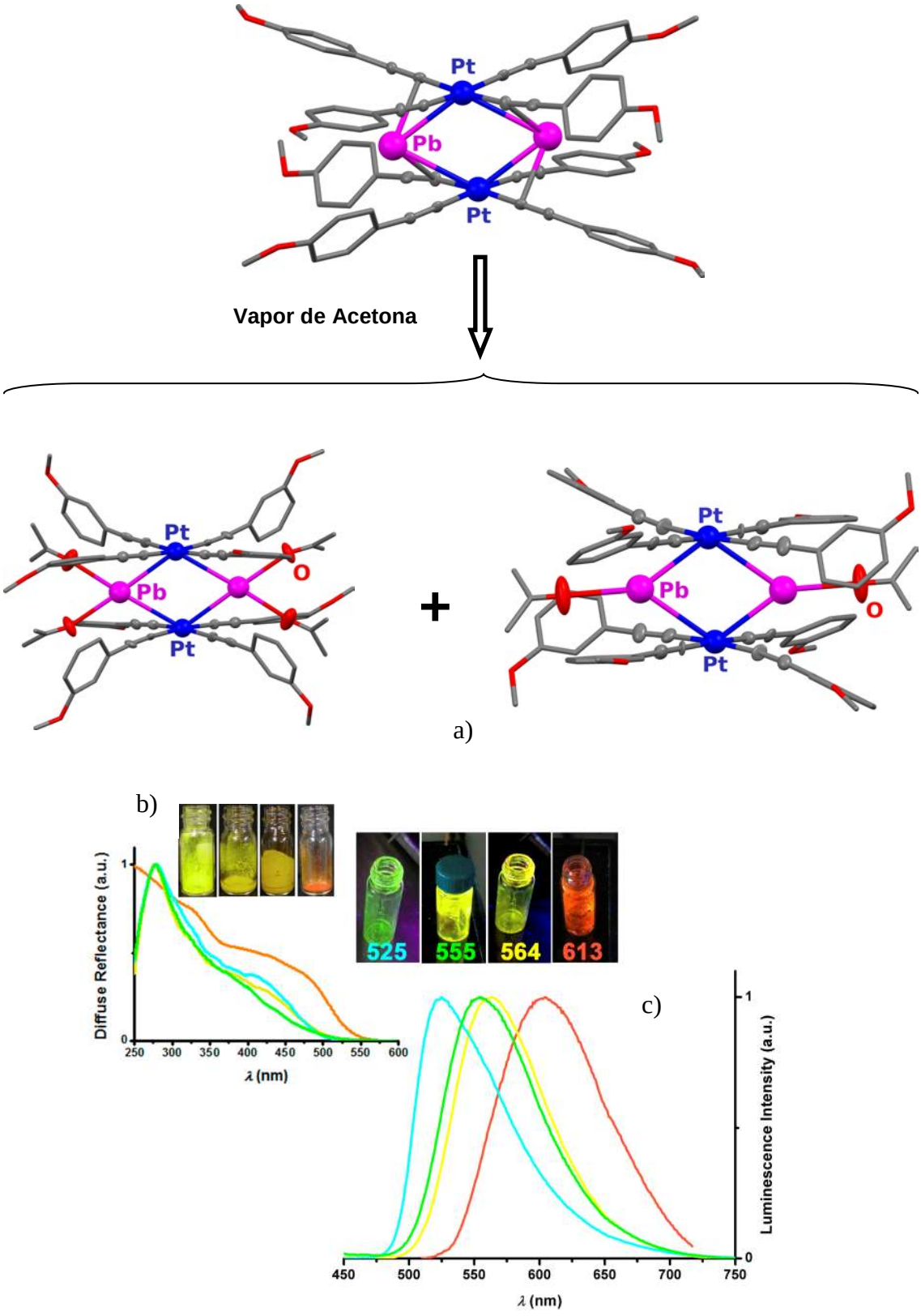

Figura I.21: a) Estructuras cristalinas del cluster $[\{Pt(C{\equiv}CC_6H_4OMe\text{-}4)_4\}Pb]_2$ y de su solvato de acetona ($[\{Pt(C{\equiv}CC_6H_4OMe\text{-}4)_4\}Pb]_2 \cdot 3$ acetona), mostrando las dos moléculas presentas en la celdilla unidad. b) Espectros de reflectancia difusa y c) de luminiscencia de $[\{Pt(C{\equiv}CC_6H_4OMe\text{-}4)_4\}Pb]_2$ (naranja) y de sus solvatos tras exposición a vapores de acetona (amarillo), THFMe-2 (verde) y CH_3CN (azul)

El derivado aniónico heteroléptico $(NBu_4)_2$[*trans*-$Pt(C{\equiv}CTol)_2(CN)_2$] se ha utilizado como unidad de construcción en la formación de un polímero de coordinación Pt^{II}-Pb^{II}. Así, por reacción con perclorato de trispirazolilborato plomo $[Pb(HBpz_3)]ClO_4$ ($[PbTp]ClO_4$) se obtiene el derivado {[*trans*-$Pt(C{\equiv}CTol)_2(CN)_2$][$(PbTp)(acetona)]_2$}$\cdot H_2O$, en el que los centros de Pb se coordinan al par solitartio de los ligandos cianuro, dando lugar a unidades trinucleares [Pb]-NC-Pt-CN-[Pb] (Figura I.22a), que forman una cadena extendida 1D por interacciones metalofílicas $Pt^{II}\cdots Pb^{II}$ muy débiles [3.62554(4) Å] entre unidades $PtPb_2$ adyacentes (Figura I.22b). Este cluster muestra un interesante comportamiento termocrómico, ya que a 298 K presenta una emisión verde a 501 nm que se desplaza hacia el azul (450 nm) al disminuir la temperatura hasta 77 K (Figura I.22c),[103] lo que de nuevo nos muestra la influencia que tienen los factores externos en las propiedades emisivas de los derivados con enlaces Pt^{II}-Pb^{II}.

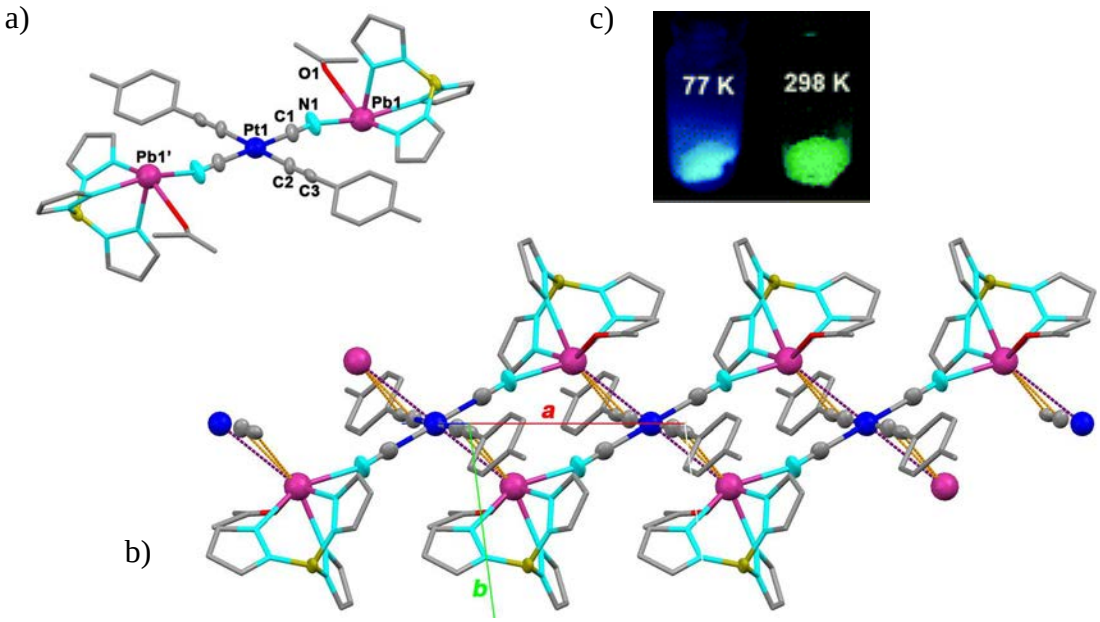

Figura I.22: Estructura a) cristalina y b) supramolecular mostrando la cadena unidimensional formada por interacciones débiles Pt-Pb y c) fotografías de luminiscencia a 298 y 77 K del derivado {[*trans*-$Pt(C{\equiv}CTol)_2(CN)_2$][$(PbTp)(acetona)]_2$}$\cdot H_2O$

Con ligandos ciclometalados y alquinilo nuestro grupo publicó en 2008 una serie de derivados trinucleares obtenidos por reacción de los sustratos (NBu_4)[$Pt(bzq)(C{\equiv}CR)_2$] con $Pb(ClO_4)_2\cdot 3\ H_2O$[95a] (Figura I.23), que representan los únicos derivados descritos heteropolimetálicos Pt–Pb con ligandos ciclometalados.[87b]

Con R = Ph se genera el derivado neutro [{Pt(bzq)(C≡CR)$_2$}$_2$Pb] en el que el centro de Pb muestra una coordinación simétrica *hemidirigida*, enlazándose a cuatro enlaces Pt–C_α, que definen el plano basal de una geometría de pirámide de base cuadrada, mientras que el vértice lo ocupa el par solitario del plomo. Con el sustituyente $C_6H_4CF_3$-4 pobremente dador, se obtienen una mezcla del correspondiente derivado neutro [{Pt(bzq)(C≡C$C_6H_4CF_3$-4)$_2$}$_2$Pb] y del aducto aniónico (NBu_4)[{Pt(bzq)(C≡C$C_6H_4CF_3$-4)$_2$}$_2$Pb(O_2ClO_2)], en el que el Pb se coordina débilmente a un grupo perclorato, presentando una octacoordinación final asimétrica. Los derivados muestran una intensa emisión en sólido a 77 K, tentativamente asignada a una transición ^{3}MLM'CT ^{3}[Pt(dz^2)/π(C≡CR)→Pt(pz)Pb(sp)/π*(C≡CR)] combinada con un cierto carácter excimérico en los derivados neutros y modificada por la presencia de contactos $Pb^{II}\cdots O$ en el derivado de perclorato.

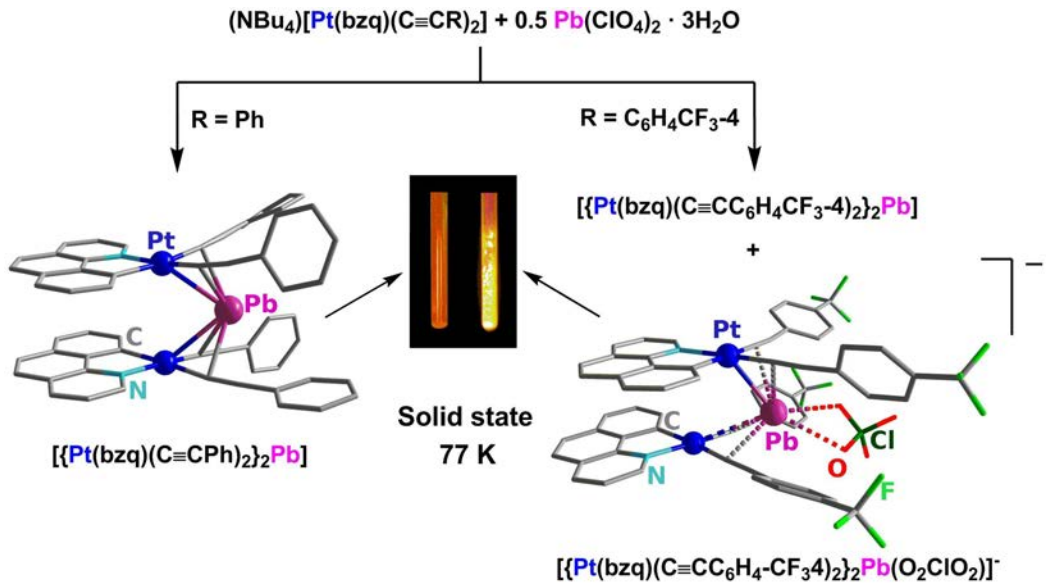

Figura I.23

La escasa representación de derivados heteropolinucleares Pt–Pb con ligandos ciclometalados nos ha impulsado a la preparación de nuevos sistemas de este tipo que permiten establecer correlaciones entre la actividad estereoquímica del par solitario del Pb y las propiedades fotoluminiscentes.

Objetivos

El trabajo descrito en esta Memoria está centrado en la síntesis, caracterización y estudio de propiedades fotofísicas de compuestos luminiscentes cicloplatinados. La Memoria se ha estructurado en 5 capítulos que se centran en el estudio de compuestos cicloplatinados luminiscentes mononucleares con ligandos nitrógeno dadores (Capítulo 1), mono y homopolinucleares con ligandos acetiluro (Capítulos 2 y 3) y heteropolinucleares con enlaces Pt-Pb (Capítulos 4 y 5).

Teniendo en cuenta los precedentes existentes en la química del Pt^{II} con grupos ciclometalados bidentados de tipo C^N y ligandos nitrogenados, cuando se comenzó el trabajo que se presenta en esta Memoria, se decidió elegir para su estudio como coligandos, los ligandos tipo escorpionato bis y tris (pirazolil) borato o metano $[H_2Bpz_2]^-$, $[HBpz_3]^-$, $[H_2Cpz_2]$, $[HCpz_3]$ y estudiar su influencia en las propiedades ópticas de los derivados sintetizados.

Así, en el Capítulo 1 se describe la síntesis y caracterización de nuevos complejos mononucleares neutros y catiónicos con ligandos auxiliares tipo escorpionato $[Pt(C^N)\{L'\}]^{n-}$ (L' = $[H_2B(pz)_2]^-$/$[HB(pz)_3]^-$, n = 0; $[H_2C(pz)_2]$/$[HC(pz)_3]$, n = 1) y tres ligandos ciclometalados [C^N= benzoquinolato (bzq), 2-fenilpiridinato (ppy) y 2-fenilquinolato (pq)]. Se han estudiado sus propiedades ópticas y electroquímicas y sus variaciones se han justificado mediante cálculos teóricos en modelos representativos.

Como se ha dicho anteriormente, la inclusión de ligandos de campo fuerte, como los grupos C≡CR, en la esfera de coordinación del Pt, favorece la formación de estados excitados centrados en los ligandos. Así, en la actualidad existe un gran número de compuestos cicloplatinados C^N con ligandos acetiluro, varios de ellos sintetizados por nuestro grupo de investigación.

Siguiendo con nuestro interés en este tipo de derivados, en el Capítulo 2 se estudia la reacción del sustrato dinuclear de puentes cloro $[Pt(pq)(\mu\text{-}Cl)]_2$ frente a LiC≡CR, variando tanto la relación Pt:LiC≡CR como el sustituyente del ligando acetiluro, obteniéndose los complejos mononucleares $[Pt(Hpq)(C{\equiv}CR)_3]^-$ (R = Ph,

C_6H_4OMe-3, $C_6H_4CF_3$-4) o los dinucleares $[Pt(pq)(\mu-\kappa C^{\alpha}:\eta^2-C\equiv CR)]_2$ (R = ^{t}Bu, Ph, C_6H_4OMe-3, $C_6H_4CF_3$-4), estabilizados mediante un sistema de doble puente σ/π alquinilo. Todos los derivados presentan interesantes propiedades luminiscentes, que se han racionalizado analizando en detalle tanto sus estructuras cristalinas como sus optimizaciones mediante cálculos teóricos.

Sorpredentemente, y a pesar del gran número de derivados de platino homodinucleares con ligandos acetiluro actuando como puente, los compuestos $[Pt(pq)(\mu-\kappa C^{\alpha}:\eta^2-C\equiv CR)]_2$ (R = ^{t}Bu, Ph, C_6H_4OMe-3, $C_6H_4CF_3$-4) estudiados en el Capítulo 2, representan uno de los pocos ejemplos de este tipo de sistemas con ligandos ciclometalados C^N. Este hecho, unido a la experiencia acumulada en nuestro grupo de investigación en la reactividad de los derivados $[Pt(\mu-\kappa C^{\alpha}:\eta^2-C\equiv CR)(C_6F_5)(PPh_3)]_2$, nos animó a estudiar la reactividad del *tert*-butil derivado $[Pt(pq)(\mu-\kappa C^{\alpha}:\eta^2-C\equiv C^tBu)]_2$ (**16**) frente a varios ligandos dadores.

Así, en la primera parte del Capítulo 3 se analizan los resultados de la reacción entre **16** y diversos ligandos nitrógeno dadores bi- o tridentados, teniendo en cuenta las propiedades luminóforas del fragmento "Pt(pq)(C≡C^{t}Bu)" y de los ligandos nitrogeno dadores. Este estudio nos ha permitido sintetizar derivados binucleares $[\{Pt(pq)(C\equiv C^tBu)\}_2(\mu\text{-L})]$ (**20**-**25**) y el compuesto trinuclear $[\{Pt(pq)(C\equiv C^tBu)\}_3(\mu\text{-L})]$ (**26**). En estos sistemas, la combinación de estudios de difracción de rayos-X, RMN{^{1}H}, IR, espectrometría de masas permite confirmar la presencia de equilibrios dinámicos en disolución entre el derivado binuclear $[\{Pt(pq)(C\equiv C^tBu)\}_2(\mu\text{-L})]$, el mononuclear $[Pt(pq)(C\equiv C^tBu)(L)]$, el ligando nitrógeno dador libre y el derivado dinuclear de partida. Se han analizado también las propiedades fotofísicas de estos complejos en estado sólido y en disolución. En la segunda parte de este capítulo, y siguiendo con el estudio de la reactividad del complejo $[Pt(pq)(\mu-\kappa C^{\alpha}:\eta^2-C\equiv C^tBu)]_2$, se analizan las reacciones de este derivado frente a 2- y 4- mercaptopiridina, obteniéndose distintas estructuras lo que influye claramente en las propiedades ópticas de los derivados obtenidos.

Como ya se ha comentado anteriormente, en las últimas décadas el estudio de sistemas heterometálicos ha sufrido un notable desarrollo, debido a que la formación de

enlaces Metal-Metal favorece la luminiscencia de estos sistemas. Además, el ión Pb^{II} posee una gran diversidad estructural asociada con la variación en la actividad del par solitario, lo que puede nos puede permitir modular las propiedades ópticas de sistemas heterometálicos que contengan Pb^{II}. A pesar de esto, el número de derivados con enlaces Pt^{II}-Pb^{II} es extremadamente bajo. Por todo ello nos propusimos sintetizar varios derivados polimetálicos cicloplatinados con enlaces Pt-Pb estabilizados por interacciones Pb-C≡C (Capítulo 4) o por un ligando puente como la 2-mercapto piridina (capítulo 5)

Así, en el Capítulo 4 se recogen las reacciones de los sustratos aniónicos $(NBu_4)[Pt(bzq)(C{\equiv}CR)_2]$ frente al derivado $[Pb(HBpz_3)]Cl$. Estas reacciones conducen a distintos tipos de derivados heteropolinucleares en función del sustituyente del alquinilo: clusters tetranucleares $[\{Pt(bzq)(C{\equiv}CR)_2\}\{Pb(HBpz_3)\}]_2$ y (R = Ph, C_6H_4OMe–3) y el derivado aniónico trinuclear $(NBu_4)[\{Pt(bzq)(C{\equiv}CC_6H_4CF_3$–$4)_2\}_2\{Pb(HBpz_3)\}]$, estabilizados mediante enlaces Pt···Pb y/o interacciones $Pb^{II}\cdots\eta^2$-alquinilo(C≡CR), de las que sólo existen las aportaciones descritas por nuestro grupo. Además, se ha realizado un estudio comparativo de sus propiedades ópticas en relación a las de los sustratos de partida.

Por su parte, en el Capítulo 5 se estudia una serie de clusters trinucleares Pt_2Pb $[\{Pt(C_6F_5)(C\hat{}N)\}_2Pb(SpyR\text{-}5)_2]$ (C^N = bzq, ppy; R = H, CF_3), obtenidos por reacción de los solvatos $[Pt(C_6F_5)(C\hat{}N)(S)]$ (C^N = bzq, S = acetona; C^N = ppy, S = dmso) con el apropiado bis(piridintiolato)plomo(II). Los clustres de bzq muestran una respuesta vapoluminiscente hacia el azul rápida y reversible cuando están en presencia de disolventes dadores, asociada a cambios en el entorno de ión Pb^{II} desde un entorno asimétrico *hemidirigido* a un entorno más simétrico y *holodirigido* tras la coordinación de la molécula dadora. Aunque los derivados con el ligando 2-fenilpiridinato (ppy) no muestran respuesta vapoluminiscente, el cluster $[\{Pt(ppy)(C_6F_5)\}Pb(SpyCF_3\text{-}5)_2]$ presenta un rico polimorfismo con distintas e interconvertibles formas de cristalización en función del disolvente y la velocidad de cristalización, en las que aparecen diferentes entornos en el Pb, con distintas separaciones Pt···Pb y diferentes emisiones. La transformación de la forma más simétrica a las más asimétricas es posible también por estímulo mecánico. Para entender las propiedades vapoluminiscentes, vapocrómicas y

mecanocrómicas se han realizado cálculos TD DFT sobre algunos de los clusters solvatados y sin solvatar.

Parte de este trabajo de investigación ha dado lugar a las siguientes publicaciones:

1) Luminescent cycloplatinated complexes containig poly(pyrazolyl)-borate and –methane ligands.
Jesús R. Berenguer, Álvaro Díez, Elena Lalinde, M. Teresa Moreno, Santiago Ruiz and Sergio Sánchez., *Organometallics* **2011**, 30, 5776-4792.

2) Solvent-induced lone pair activity tuning and vapoluminescence in a Pt_2Pb Cluster.
Jesús R. Berenguer, Elena Lalinde, Antonio Martín, M. Teresa Moreno, Santiago Ruiz, Sergio Sánchez and Hamid R. Shahsavari. *Chem. Commun*. **2013**, 49, 5067-5069

3) Synthesis, structural, and photophysical studies of phenylquinoline and phenylquinolinyl alkynyl based Pt(II) complexes
Jesús R. Berenguer, Álvaro Díez, Elena Lalinde, M. Teresa Moreno, Santiago Ruiz and Sergio Sánchez., *Organometallics* **2014**, 33, 3078-3090.

4) Photophysical responses in Pt_2Pb Clusters driven by solvent interactions and structural changes in the Pb^{II} environment
Jesús R. Berenguer, Elena Lalinde, Antonio Martín, M. Teresa Moreno, Santiago Ruiz, Sergio Sánchez and Hamid R. Shahsavari. *Inorg. Chem.* **2014**, 53, 8770-8785

5) Attach of luminescent neutral "Pt(pq)(C≡C^{t}Bu)" units to di and tri-donor connecting ligands. Solution behaviour and photophysical properties.
Elena Lalinde, M. Teresa Moreno, Santiago Ruiz and Sergio Sánchez. *Inorganics.* **2014**, Enviada

El material suplementario se incluye al término de cada capítulo. Por su parte la Bibliografía se recoge después de la discusión de cada capítulo y al final de la Introducción, y de la Parte Experimental.

Bibliografía

1. (a) Mori, K.; Ogawa, S.; Martis, M.; Yamashita, H. *J. Phys. Chem. C* **2012**, *116*, 18873; (b) Kim, J.-H.; Kim, J.-H. *J. Am. Chem. Soc.* **2012**, *134*, 17478; (c) Paw, W.; Cummings, S. D.; Mansour, M. A.; Connick, W. B.; Geiger, D. K.; Eisenberg, R. *Coord. Chem. Rev.* **1998**, *171*, 125.
2. (a) Sun, Y. H.; Ye, K. Q.; Zhang, H. Y.; Zhang, J. H.; Zhao, L.; Li, B.; Yang, G. D.; Yang, B.; Wang, Y.; Lai, S. W.; Che, C. M. *Angew. Chem., Int. Ed.* **2006**, *45*, 5610; (b) Yang, X.; Huang, Z.; Dang, J.; Ho, C.-L.; Zhou, G.; Wong, W.-Y. *Chem. Commun.* **2013**, *49*, 4406; (c) Muro, M. L.; Daws, C. A.; Castellano, F. N. *Chem. Commun.* **2008**, 6134; (d) Guerchais, V.; Fillaut, J.-L. *Coord. Chem. Rev.* **2011**, *255*, 2448; (e) Wang, A. H. J.; Nathans, J.; van Der Marel, G.; van Boom, J. H.; Rich, A. *Nature* **1978**, *276*, 471.
3. (a) Boixel, J.; Guerchais, V.; Le Bozec, H.; Jacquemin, D.; Amar, A.; Boucekkine, A.; Colombo, A.; Dragonetti, C.; Marinotto, D.; Roberto, D.; Righetto, S.; De Angelis, R. *J. Am. Chem. Soc.* **2014**, *136*, 5367; (b) Espa, D.; Pilia, L.; Makedonas, C.; Marchiò, L.; Mercuri, M. L.; Serpe, A.; Barsella, A.; Fort, A.; Mitsopoulou, C. A.; Deplano, P. *Inorg. Chem.* **2014**, *53*, 1170; (c) Dragonetti, C.; Righetto, S.; Roberto, D.; Ugo, R.; Valore, A.; Ledoux-Rak, I. *Nonlinear Optics Quantum Optics* **2012**, *43*, 197; (d) Gunder, P. *Non linear Optical Effects and Materials*; Springer: New York, 2000.
4. (a) Kwok, E. C.-H.; Chan, M.-Y.; Wong, K. M.-C.; Yam, V. W.-W. *Chem. Eur. J.* **2014**, *20*, 3142; (b) Diwan, K.; Chauhan, R.; Singh, S. K.; Singh, B.; Drew, M. G. B.; Bahadur, L.; Singh, N. *New J. Chem.* **2014**, *38*, 97; (c) Archer, S.; Weinstein, J. A. *Coord. Chem. Rev.* **2012**, *256*, 2530; (d) Hissler, M.; McGarrah, J. E.; Connick, W. B.; Geiger, D. K.; Cummings, S. D.; Eisenberg, R. *Coord. Chem. Rev.* **2000**, *208*, 115.
5. (a) Huang, L.-M.; Tu, G.-M.; Chi, Y.; Hung, W.-Y.; Song, Y.-C.; Tseng, M.-R.; Chou, P.-T.; Lee, G.-H.; Wong, K.-T.; Cheng, S.-H.; Tsai, W.-S. *J. Mater. Chem. C* **2013**, *1*, 7582; (b) Wang, Q.; Oswald, I. W. H.; Perez, M. R.; Jia, H.; Gnade, B. E.; Omary, M. A. *Adv. Funct. Mater.* **2013**, *23*, 5420; (c) Kalinowski, J.; Fattori, V.; Cocchi, M.; Williams, J. A. G. *Coord. Chem. Rev.* **2011**, *255*, 2401; (d) Williams, J.

A. G.; Develay, S.; Rochester, D. L.; Murphy, L. *Coord. Chem. Rev.* **2008**, *252*, 2596.

6. Valeur, B. *Molecular Fluorescence - Principles and Applications*; Wiley - VCH, 2002.
7. (a) Wong, K. M.-C.; Yam, V. W.-W. *Coord. Chem. Rev.* **2007**, *251*, 2477; (b) Kato, M. *Bull. Chem. Soc. Jpn.* **2007**, *80*, 287; (c) Williams, J. A. G. *Top. Curr. Chem.* **2007**, *281*, 205.
8. Yeh, A. T.; Shank, C. V.; McCusker, J. K. *Science* **2000**, *289*, 935.
9. Kane-MacGuire, N. A. P. *Top. Curr. chem.* **2007**, *280*, 37.
10. (a) Campagna, S.; Puntoriero, F.; Nastasi, F.; Bergamini, G.; Balzani, V. In *Top. Curr. Chem.* 2007; Vol. 280, p 117; (b) Visbal, R.; Gimeno, M. C. *Chem. Soc. Rev.* **2014**, *43*, 3551.
11. (a) Zhang, X.; Canton, S. E.; Smolentsev, G.; Wallentin, C.-J.; Liu, Y.; Kong, Q.; Attenkofer, K.; Stickrath, A. B.; Mara, M. W.; Chen, L. X.; Wärnmark, K.; Sundström, V. *J. Am. Chem. Soc.* **2014**, *136*, 8804; (b) Kumaresan, D.; Shankar, K.; Vaidya, S.; Schmehl, R. H. In *Top. Curr. Chem.* 2007; Vol. 281, p 101.
12. Indelli, M. T.; Chiorboli, C.; Scandola, F. In *Top. Curr. Chem.* 2007; Vol. 280, p 215.
13. (a) Flamigni, L.; Barbieri, A.; Sabatini, C.; Ventura, B.; Barigelletti, F. In *Top. Curr. Chem.* 2007; Vol. 281, p 143; (b) Lanoë, P. H.; Tong, C. M.; Harrington, R. W.; Probert, M. R.; Clegg, W.; Williams, J. A. G.; Kozhevnikov, V. N. *Chem. Commun.* **2014**, *50*, 6831.
14. Armaroli, N.; Accorsi, G.; Cardinali, F.; Listorti, A. In *Top. Curr. Chem.* 2007; Vol. 280, p 69.
15. (a) Tu, D.; Zheng, W.; Liu, Y.; Zhu, H.; Chen, X. *Coord. Chem. Rev.* **2014**, *273–274*, 13; (b) Xu, L.-J.; Xu, G.-T.; Chen, Z.-N. *Coord. Chem. Rev.* **2014**, *273–274*, 47.
16. (a) Castellano, F. N.; Pomestchenko, I. E.; Shikhova, E.; Hua, F.; Muro, M. L.; Rajapakse, N. *Coord. Chem. Rev.* **2006**, *250*, 1819; (b) Yam, V. W.-W.; Wong, K. M.-C.; Zhu, N. *Angew. Chem. Int. Ed.* **2003**, *42*, 1400; (c) McGuire Jr, R.; McGuire, M. C.; McMillin, D. R. *Coord. Chem. Rev.* **2010**, *254*, 2574; (d) McGuire, R.; Wilson, M. H.; Nash, J. J.; Fanwick, P. E.; McMillin, D. R. *Inorg. Chem.* **2008**, *47*, 2946; (e) Lazzaro, D. P.; Fanwick, P. E.; McMillin, D. R. *Inorg.*

Chem. **2012**, *51*, 10474; (f) Kwok, E. C. H.; Chan, M. Y.; Wong, K. M. C.; Yam, V. W. W. *Chem. Eur. J.* **2014**, *20*, 3142.

17. (a) Williams, J. A. G. *Chem. Soc. Rev.* **2009**, *38*, 1783; (b) Chi, Y.; Chou, P. T. *Chem. Soc. Rev.* **2010**, *39*, 638; (c) Yersin, H.; Donges, D. *Top. Curr. Chem.* **2004**, *241*, 81; (d) Lai, S. W.; Che, C. M. *Top. Curr. Chem.* **2004**, *241*, 27; (e) Muro, M. L.; Rachford, A. A.; Wang, X.; Castellano, F. N. *Top. Organomet. Chem.* **2010**, *29*, 159; (f) Ma, B.; Djurovich, P. I.; Thompson, M. E. *Coord. Chem. Rev.* **2005**, *249*, 1501; (g) Zou, T.; Liu, J.; Lum, C. T.; Ma, C.; Chan, R. C.-T.; Lok, C.-N.; Kwok, W.-M.; Che, C.-M. *Angew. Chem. Int. Ed.* **2014**, n/a; (h) Prokhorov, A. M.; Hofbeck, T.; Czerwieniec, R.; Suleymanova, A. F.; Kozhevnikov, D. N.; Yersin, H. *J. Am. Chem. Soc.* **2014**, *136*, 9637.
18. (a) Yersin, H.; Donges, D. *Top. Curr. Chem* **2001**, *214*, 81; (b) Chassot, L.; Muller, E.; Von Zelewsky, A. *Inorg. Chem.* **1984**, *23*, 4249; (c) Maestri, M.; Sandrini, D.; Balzani, V.; Chassot, L.; Jolliet, P.; von Zelewsky, A. *Chem. Phys. Lett.* **1985**, *122*, 375.
19. (a) Mdleleni, M. M.; Bridgewater, J. S.; Watts, R. J.; Ford, P. C. *Inorg. Chem.* **1995**, *34*, 2334; (b) Pregosin, P. S.; Wombacher, F.; Albinati, A.; Lianza, F. *J. Organomet. Chem.* **1991**, *418*, 249.
20. (a) Kvam, P. I.; Puzyk, M. V.; Balashev, K. P.; Songstad, J. *Acta Chem. Scand.* **1995**, *49*, 335; (b) Balashev, K. P.; Puzyk, M. V.; Kotlyar, V. S.; Kulikova, M. V. *Coord. Chem. Rev.* **1997**, *159*, 109.
21. (a) Brooks, J.; Babayan, Y.; Lamansky, S.; Djorovich, P. I.; Tsyba, I.; Bau, R.; Thompson, M. E. *Inorg. Chem.* **2002**, *41*, 3055; (b) Colombo, A.; Dragonetti, C.; Marinotto, D.; Righetto, S.; Roberto, D.; Tavazzi, S.; Escadeillas, M.; Guerchais, V.; Le Bozec, H.; Boucekkine, A.; Latouche, C. *Organometallics* **2013**, *32*, 3890; (c) Bossi, A.; Rausch, A. F.; Leitl, M. J.; Czerwieniec, R.; Whited, M. T.; Djurovich, P. I.; Yersin, H.; Thompson, M. E. *Inorg. Chem.* **2013**, *52*, 12403; (d) Xu, X.; Zhao, Y.; Dang, J.; Yang, X.; Zhou, G.; Ma, D.; Wang, L.; Wong, W.-Y.; Wu, Z.; Zhao, X. *Eur. J. Inorg. Chem.* **2012**, *2012*, 2278.
22. Yersin, H.; Donges, D.; Humbs, W.; Strasser, J.; Sitters, R.; Glasbeek, M. *Inorg. Chem.* **2002**, *41*, 4915.
23. (a) Díez, A. l.; Forniés, J.; Larraz, C.; Lalinde, E.; López, J. A.; Martín, A.; Moreno, M. T.; Sicilia, V. *Inorg. Chem.* **2010**, *49*, 3239; (b) Sicilia, V.; Fuertes, S.; Martín, A.; Palacios, A. *Organometallics* **2013**, *32*, 4092.

24. (a) Lang, H.; Köhler, K.; Blau, S. *Coord. Chem. Rev.* **1995**, *143*, 113; (b) Forniés, J.; Lalinde, E. *J. Chem. Soc., Dalton Trans.* **1996**, 2587; (c) Lang, H.; George, D. S. A.; Rheinwald, G. *Coord. Chem. Rev.* **2000**, *206–207*, 101; (d) Mingos, D. M. P.; Vilar, R.; Rais, D. *J. Organomet. Chem.* **2002**, *641*, 126; (e) Mak, T. C. W.; Zhao, L. *Chem. Asian J.* **2007**, *2*, 456; (f) Mathur, P.; Chatterjee, S.; Avasare, V. D. *Adv. Organomet. Chem.* **2008**, *55*, 201; (g) Bruce, M. I. *Chem. Rev.* **1991**, *91*, 197; (h) Mak, T. C. W.; Zhao, X.-L.; Wang, Q.-M.; Guo, G.-C. *Coord. Chem. Rev.* **2007**, *251*, 2311.

25. (a) Lotz, S.; Van Rooyen, P. H.; Meyer, R. *Adv. Organomet. Chem.* **1995**, *37*, 219; (b) Holton, J.; Lappert, M. F.; Pearce, R.; Yarrow, P. I. W. *Chem. Rev.* **1983**, *83*, 135; (c) McArdle, C. P.; Vittal, J. J.; Puddephatt, R. J. *Angew. Chem. Int. Ed.* **2000**, *39*, 3819; (d) Berenguer, J. R.; Lalinde, E.; Moreno, M. T. *Coord. Chem. Rev.* **2010**, *254*, 832.

26. (a) Bruce, M. I. *Coord. Chem. Rev.* **1997**, *166*, 91; (b) Bruce, M. I. *Chem. Rev.* **1998**, *98*, 2797; (c) Touchard, D.; Dixneuf, P. H. *Coord. Chem. Rev.* **1998**, *178-180*, 409; (d) Cadierno, V.; Gamasa, M. P.; Gimeno, J. *Coord. Chem. Rev.* **2004**, *248*, 1627; (e) Puerta, M. C.; Valerga, P. *Coord. Chem. Rev.* **1999**, *193–195*, 977; (f) Werner, H. *Coord. Chem. Rev.* **2004**, *248*, 1693; (g) Winter, R. F.; Záliš, S. *Coord. Chem. Rev.* **2004**, *248*, 1565; (h) Selegue, J. P. *Coord. Chem. Rev.* **2004**, *248*, 1543; (i) Rigaut, S.; Touchard, D.; Dixneuf, P. H. *Coord. Chem. Rev.* **2004**, *248*, 1585; (j) Bruce, M. I. *Coord. Chem. Rev.* **2004**, *248*, 1603; (k) Wakatsuki, Y. *J. Organomet. Chem.* **2004**, *689*, 4092.

27. Rosenthal, U.; Pellny, P.-M.; Kirchbauer, F. G.; Burlakov, V. V. *Acc. Chem. Res.* **2000**, *33*, 119.

28. (a) Berenguer, J. R.; Falvello, L. R.; Fornies, J.; Lalinde, E.; Tomas, M. *Organometallics* **1993**, *12*, 6; (b) Evans, W. J.; Drummond, D. K.; Hanusa, T. P.; Olofson, J. M. *J. Organomet. Chem.* **1989**, *376*, 311.

29. (a) Cao, D. H.; Stang, P. J.; Arif, A. M. *Organometallics* **1995**, *14*, 2733; (b) Janssen, M. D.; Köhler, K.; Herres, M.; Dedieu, A.; Smeets, W. J. J.; Spek, A. L.; Grove, D. M.; Lang, H.; van Koten, G. *J. Am. Chem. Soc.* **1996**, *118*, 4817; (c) Zhang, D.; McConville, D. B.; Tessier, C. A.; Youngs, W. J. *Organometallics* **1997**, *16*, 824; (d) Ara, I.; Berenguer, J. R.; Forniés, J.; Lalinde, E. *Inorg. Chim. Acta* **1997**, *264*, 199; (e) Pellny, P.-M.; Peulecke, N.; Burlakov, V. V.; Tillack, A.; Baumann, W.; Spannenberg, A.; Kempe, R.; Rosenthal, U. *Angew. Chem. Int. Ed.*

1997, *36*, 2615; (f) Pin, C.-W.; Peng, J.-J.; Shiu, C.-W.; Chi, Y.; Peng, S.-M.; Lee, G.-H. *Organometallics* **1998**, *17*, 438; (g) Ara, I.; Berenguer, J. R.; Eguizábal, E.; Forniés, J.; Lalinde, E.; Martín, A.; Martínez, F. *Organometallics* **1998**, *17*, 4578; (h) Falvello, L. R.; Forniés, J.; Martín, A.; Gómez, J.; Lalinde, E.; Moreno, M. T.; Sacristán, J. *Inorg. Chem.* **1999**, *38*, 3116.

30. (a) Ara, I.; Fornies, J.; Lalinde, E.; Moreno, M. T.; Tomas, M. *J. Chem. Soc., Dalton Trans.* **1994**, 2735; (b) Janssen, M. D.; Donkervoort, J. G.; van Berlekom, S. B.; Spek, A. L.; Grove, D. M.; van Koten, G. *Inorg. Chem.* **1996**, *35*, 4752; (c) Díez, J.; Gamasa, M. P.; Gimeno, J.; Aguirre, A.; García-Granda, S. *Organometallics* **1997**, *16*, 3684; (d) Yam, V. W.-W.; Fung, W. K.-M.; Cheung, K.-K. *Organometallics* **1998**, *17*, 3293; (e) Ara, I.; Fornies, J.; Lalinde, E.; Moreno, M. T.; Tomas, M. *J. Chem. Soc., Dalton Trans.* **1995**, 2397; (f) Yam, V. W.-W.; Choi, S. W.-K.; Chan, C.-L.; Cheung, K.-K. *Chem. Commun.* **1996**, 2067.
31. (a) Wei, Q.-H.; Yin, G.-Q.; Zhang, L.-Y.; Shi, L.-X.; Mao, Z.-W.; Chen, Z.-N. *Inorg. Chem.* **2004**, *43*, 3484; (b) Akita, M.; Hirakawa, H.; Sakaki, K.; Moro-oka, Y. *Organometallics* **1995**, *14*, 2775; (c) Chi, Y.; Wu, C. H.; Peng, S. M.; Lee, G. H. *Organometallics* **1991**, *10*, 1676.
32. (a) Adams, C. J.; Bruce, M. I.; Horn, E.; Skelton, B. W.; Tiekink, E. R. T.; White, A. H. *Journal of the Chemical Society, Dalton Transactions* **1993**, 3313; (b) Akita, M.; Hirakawa, H.; Tanaka, M.; Moro-oka, Y. *J. Organomet. Chem.* **1995**, *485*, C14.
33. (a) Akita, M.; Koike, T. *Dalton Trans.* **2008**, 3523; (b) Szafert, S.; Gladysz, J. A. *Chem. Rev.* **2006**, *106*, PR1; (c) *J. Organomet. Chem.* **1999**, 578 (número especal: "Carbon-rich Organometallics; (d) H. F. Bunz, U.; Rubin, Y.; Tobe, Y. *Chem. Soc. Rev.* **1999**, *28*, 107; (e) Manners, I. *Angew. Chem. Int. Ed.* **1996**, *35*, 1602.
34. (a) Yam, V. W.-W.; Lo, K. K. W.; Wong, K. M.-C. *J. Organomet. Chem.* **1999**, *578*, 3; (b) Shelton, A. H.; Price, R. S.; Brokmann, L.; Dettlaff, B.; Schanze, K. S. *ACS Appl. Mater. Interfaces* **2013**, *5*, 7867; (c) Wang, D.; Zou, L.-y.; Huang, S.; Feng, J.-k.; Ren, A.-m. *Dyes and Pigments* **2014**, *105*, 75; (d) Powell, C. E.; Humphrey, M. G. *Coord. Chem. Rev.* **2004**, *248*, 725; (e) Long, N. J.; Williams, C. K. *Angew. Chem., Int. Ed.* **2003**, *42*, 2586; (f) Bruce, M. I.; Low, P. J. *Adv. Organomet. Chem.* **2004**, *Volume 50*, 179; (g) Rosenthal, U. *Angew. Chem., Int. Ed. Engl.* **2003**, *42*, 1794; (h) Szafert, S.; Gladysz, J. A. *Chem. Rev.* **2003**, *103*, 4175; (i) Yam, V. W.-W.; Lo, K.-W. *Chem. Soc. Rev.* **1999**, *28*, 323; (j) Yam, V. W.-W. *Acc. Chem. Res.* **2002**, *35*, 555; (k) Yam, V. W. W.; Lo, W. Y.; Lam, C. H.; Fung,

W. K. M.; Wong, K. M. C.; Lau, V. C. Y.; Zhu, N. *Coord. Chem. Rev.* **2003**, *245*, 39; (l) Yam, V. W.-W. *J. Organomet. Chem.* **2004**, *689*, 1393; (m) Evans, R. C.; Douglas, P.; Winscom, C. J. *Coord. Chem. Rev.* **2006**, *250*, 2093.

35. (a) Puddephatt, R. J. *Coord. Chem. Rev.* **2001**, *216-217*, 313; (b) Mingos, D. M. P.; Vilar, R.; Rais, D. *J. Organomet. Chem.* **2002**, *641*, 126; (c) Lang, H.; del Villar, A. *J. Organomet. Chem.* **2003**, *670*, 45; (d) Lang, H.; Stein, T. *J. Organomet. Chem.* **2002**, *641*, 41; (e) Gimeno, A.; Cuenca, A. B.; Suárez-Pantiga, S.; De Arellano, C. R.; Medio-Simõn, M.; Asensio, G. *Chem. Eur. J.* **2014**, *20*, 683.
36. (a) Wong, W.-Y. *Dalton Trans.* **2007**, 4495; (b) Chen, Z. N.; Zhao, N.; Fan, Y.; Ni, J. *Coord. Chem. Rev.* **2009**, *253*, 1; (c) Wong, M. C.; Yam, V. W. W. *Molecular Design and Applications of Photofunctional Polymers and Materials.* ; RSC Polymer Chemistry Series No.2,: Cambridge, UK, 2012; (d) Lu, W.; Mi, B. X.; Chan, M. C. W.; Hui, Z.; Che, C. M.; Zhu, N.; Lee, S. T. *J. Am. Chem. Soc.* **2004**, *126*, 4958; (e) Yersin, H. *Highly Efficient OLEDs with Phosphorescent materials*; Wiley-VCH: Weinheim, Germany, 2008.
37. (a) Baralt, E.; Boudreaux, E. A.; Demas, J. N.; Lenhert, P. G.; Lukehart, C. M.; McPhail, A. T.; McPhail, D. R.; Myers, J. B.; Sacksteder, L.; True, W. R. *Organometallics* **1989**, *8*, 2417; (b) Sacksteder, L.; Baralt, E.; DeGraff, B. A.; Lukehart, C. M.; Demas, J. N. *Inorg. Chem.* **1991**, *30*, 2468.
38. (a) Osakada, K. In *Comprehensive Organometallic Chemistry III*; Mingos, D. M. P., Crabtree, R. H., Eds.; Elsevier: Oxford, 2007, p 445; (b) Anderson, G. K. In *Comprehensive Organometallic Chemistry II*; Abel, E. W., Stone, F. G. A., Wilkinson, G., Eds.; Elsevier: Oxford, 1995, p 431; (c) Lüning, A.; Schur, J.; Hamel, L.; Ott, I.; Klein, A. *Organometallics* **2013**, *32*, 3662.
39. (a) Wong, W.-Y.; Lu, G.-L.; Ng, K.-F.; Choi, K.-H.; Lin, Z. *J. Chem. Soc., Dalton Trans.* **2001**, 3250; (b) Schull, T. L.; Kushmerick, J. G.; Patterson, C. H.; George, C.; Moore, M. H.; Pollack, S. K.; Shashidhar, R. *J. Am. Chem. Soc.* **2003**, *125*, 3202; (c) Harriman, A.; Hissler, M.; Trompette, O.; Ziessel, R. *J. Am. Chem. Soc.* **1999**, *121*, 2516.
40. Choi, C. L.; Chen, Y. F.; Yip, C.; Phillips, D. L.; Yam, V. W. W. *Organometallics* **2000**, *19*, 3192.
41. Jones, S. C.; Coropceanu, V.; Barlow, S.; Kinnibrugh, T.; Timofeeva, T.; Brédas, J.-L.; Marder, S. R. *J. Am. Chem. Soc.* **2004**, *126*, 11782.

42. Casas, J. M.; Diosdado, B. E.; Forniés, J.; Martín, A.; Rueda, A. J.; Orpen, A. G. *Inorg. Chem.* **2008**, *47*, 8767.
43. Lam, W. H.; Yam, V. W.-W. *Inorg. Chem.* **2010**, *49*, 10930.
44. Berenguer, J. R.; Bernechea, M.; Lalinde, E. *Organometallics* **2007**, *26*, 1161.
45. (a) Ara, I.; Falvello, L. R.; Fernández, S.; Forniés, J.; Lalinde, E.; Martín, A.; Moreno, M. T. *Organometallics* **1997**, *16*, 5923; (b) García, A.; Lalinde, E.; Moreno, M. T. *Eur. J. Inorg. Chem.* **2007**, *2007*, 3553.
46. Wong, K. M.-C.; Lam, W. H.; Zhou, Z.-Y.; Yam, V. W.-W. *Chem. Eur. J.* **2008**, *14*, 10928.
47. Chan, C. W.; Cheng, L. K.; Che, C. M. *Coord. Chem. Rev.* **1994**, *132*, 87.
48. (a) McGarrah, J. E.; Kim, Y. J.; Hissler, M.; Eisenberg, R. *Inorg. Chem.* **2001**, *40*, 4510; (b) Tam, A. Y.-Y.; Lam, W. H.; Wong, K. M.-C.; Zhu, N.; Yam, V. W.-W. *Chem. Eur. J.* **2008**, *14*, 4562; (c) James, S. L.; Younus, M.; Raithby, P. R.; Lewis, J. *J. Organomet. Chem.* **1997**, *543*, 233; (d) McGarrah, J. E.; Eisenberg, R. *Inorg. Chem.* **2003**, *42*, 4355; (e) Ji, S.; Wu, W.; Zhao, J.; Guo, H.; Wu, W. *Eur. J. Inorg. Chem.* **2012**, *2012*, 3183; (f) Sun, H.; Guo, H.; Wu, W.; Liu, X.; Zhao, J. *Dalton Trans.* **2011**, *40*, 7834; (g) Wong, K. M.-C.; Yam, V. W.-W. *Acc. Chem. Res.* **2011**, *44*, 424.
49. (a) Savel, P.; Latouche, C.; Roisnel, T.; Akdas-Kilig, H.; Boucekkine, A.; Fillaut, J.-L. *Dalton Trans.* **2013**, *42*, 16773; (b) Liu, R.; Chang, J.; Xiao, Q.; Li, Y.; Chen, H.; Zhu, H. *Dyes and Pigments* **2011**, *88*, 88; (c) Wu, W.; Huang, D.; Yi, X.; Zhao, J. *Dyes and Pigments* **2013**, *96*, 220; (d) Shao, P.; Li, Y.; Yi, J.; Pritchett, T. M.; Sun, W. *Inorg. Chem.* **2010**, *49*, 4507; (e) Fernández, S.; Forniés, J.; Gil, B.; Gómez, J.; Lalinde, E. *Dalton Trans.* **2003**, 822; (f) Berenguer, J. R.; Lalinde, E.; Torroba, J. *Inorg. Chem.* **2007**, *46*, 9919; (g) Lu, W.; Mi, B. X.; Chan, M. C. W.; Hui, Z.; Zhu, N.; Lee, S. T.; Che, C. M. *Chem. Commun.* **2002**, 206.
50. Chan, S. C.; Chan, M. C. W.; Wang, Y.; Che, C. M.; Cheung, K. K.; Zhu, N. *Chem. Eur. J.* **2001**, *7*, 4180.
51. (a) Zhang, D.; Wu, L.-Z.; Zhou, L.; Han, X.; Yang, Q.-Z.; Zhang, L.-P.; Tung, C.-H. *J. Am. Chem. Soc.* **2004**, *126*, 3440; (b) Du, P.; Schneider, J.; Jarosz, P.; Eisenberg, R. *J. Am. Chem. Soc.* **2006**, *128*, 7726.
52. (a) Berenguer, J. R.; Fernández, J.; Gil, B.; Lalinde, E.; Sánchez, S. *Chem. Eur. J.* **2014**, *20*, 2574; (b) Lu, W.; Chan, M. C. W.; Zhu, N.; Che, C.-M.; He, Z.; Wong, K.-Y. *Chem. Eur. J.* **2003**, *9*, 6155.

53. (a) Tang, W.-S.; Lu, X.-X.; Wong, K. M.-C.; Yam, V. W.-W. *J. Mater. Chem.* **2005**, *15*, 2714; (b) Chung, C. Y.-S.; Yam, V. W.-W. *Chem. Eur. J.* **2013**, *19*, 13182; (c) Yam, V. W.-W.; Chan, K. H.-Y.; Wong, K. M.-C.; Zhu, N. *Chem. Eur. J.* **2005**, *11*, 4535; (d) Wong, K. M.-C.; Tang, W.-S.; Lu, X.-X.; Zhu, N.; Yam, V. W.-W. *Inorg. Chem.* **2005**, *44*, 1492.
54. Yam, V. W. W.; Tang, R. P. L.; Wong, K. M. C.; Lu, X. X.; Cheung, K. K.; Zhu, N. *Chem. Eur. J.* **2002**, *8*, 4066.
55. Berenguer, J. R.; Díez, Á.; García, A.; Lalinde, E.; Moreno, M. T.; Sánchez, S.; Torroba, J. *Organometallics* **2011**, *30*, 1646.
56. Hoogervorst, W. J.; Elsevier, C. J.; Lutz, M.; Spek, A. L. *Organometallics* **2001**, *20*, 4437.
57. Roundhill, D. M.; Gray, H. B.; Che, C. M. *Acc. Chem. Res.* **1989**, *22*, 55.
58. Atoji, M.; Richardson, J. W.; Rundle, R. E. *J. Am. Chem. Soc.* **1957**, *79*, 3017.
59. Bremi, J.; Brovelli, D.; Caseri, W.; Hähner, G.; Smith, P.; Tervoort, T. *Chem. Mater.* **1999**, *11*, 977.
60. (a) Drew, S. M.; Janzen, D. E.; Buss, C. E.; MacEwan, D. I.; Dublin, K. M.; Mann, K. R. *J. Am. Chem. Soc.* **2001**, *123*, 8414; (b) Drew, S. M.; Janzen, D. E.; Mann, K. R. *Anal. Chem.* **2002**, *74*, 2547.
61. Forniés, J.; Fuertes, S.; Larraz, C.; Martín, A.; Sicilia, V.; Tsipis, A. C. *Organometallics* **2012**, *31*, 2729.
62. Doerrer, L. H. *Dalton Trans.* **2010**, *39*, 3543.
63. Gliemann, G.; Yersin, H. *Struture and Bonding*; Springer-Verlag: Berlin-Heilderberg, 1985.
64. (a) Wadas, T. J.; Wang, Q. M.; Kim, K. Y.; Flaschenreim, C.; Blanton, T. N.; Eisenberg, R. *J. Am. Chem. Soc.* **2004**, *126*, 16841; (b) Yam, V. W. W.; Wong, K. M. C.; Zhu, N. *J. Am. Chem. Soc.* **2002**, *124*, 6506; (c) Bailey, J. A.; Hill, M. G.; Marsh, R. E.; Miskowski, V. M.; Schaefer, W. P.; Gray, H. B. *Inorg. Chem.* **1995**, *34*, 4591.
65. (a) Connick, W. B.; Henling, L. M.; Marsh, R. E.; Gray, H. B. *Inorg. Chem.* **1996**, *35*, 6261; (b) Connick, W. B.; Marsh, R. E.; Schaefer, W. P.; Gray, H. B. *Inorg. Chem.* **1997**, *36*, 913; (c) Kato, M.; Kosuge, C.; Morii, K.; Ahn, J. S.; Kitagawa, H.; Mitani, T.; Matsushita, M.; Kato, T.; Yano, S.; Kimura, M. *Inorg. Chem.* **1999**, *38*,

1638; (d) Buss, C. E.; Mann, K. R. *J. Am. Chem. Soc.* **2002**, *124*, 1031; (e) Dylla, A. G.; Janzen, D. E.; Pomije, M. K.; Mann, K. R. *Organometallics* **2007**, *26*, 6243.

66. (a) Wadas, T. J.; Wang, Q.-M.; Kim, Y.-j.; Flaschenreim, C.; Blanton, T. N.; Eisenberg, R. *J. Am. Chem. Soc.* **2004**, *126*, 16841; (b) Han, A.; Du, P.; Sun, Z.; Wu, H.; Jia, H.; Zhang, R.; Liang, Z.; Cao, R.; Eisenberg, R. *Inorg. Chem.* **2014**, *53*, 3338.
67. Osborn, R. S.; Rogers, D. *J. Chem. Soc., Dalton Trans.* **1974**, 1002.
68. Connick, W. B.; Henling, L. M.; Marsh, R. E. *Acta Crystallogr., Sect. B* **1996**, *52*, 817.
69. Sun, Y.; Ye, K.; Zhang, H.; Zhang, J.; Zhao, L.; Li, B.; Yang, G.; Yang, B.; Wang, Y.; Lai, S.-W.; Che, C.-M. *Angew. Chem.* **2006**, *118*, 5738.
70. Jovanocic, B.; Manojlovic-Muir, L.; Muir, K. W. *J. Chem. Soc., Dalton Trans.* **1972**, 1178.
71. Díez, Á.; Forniés, J.; Larraz, C.; Lalinde, E.; López, J. A.; Martín, A.; Moreno, M. T.; Sicilia, V. *Inorg. Chem.* **2010**, *49*, 3239.
72. (a) Eryazici, I.; Moorefield, C. N.; Newkome, G. R. *Chem. Rev.* **2008**, *108*, 1834; (b) Moussa, J.; Man-Chung Wong, K.; Chamoreau, L.-M.; Amouri, H.; Wing-Wah Yam, V. *Dalton Trans.* **2007**, 3526; (c) Leung, S. Y.-L.; Tam, A. Y.-Y.; Tao, C.-H.; Chow, H. S.; Yam, V. W.-W. *J. Am. Chem. Soc.* **2011**, *134*, 1047.
73. Janiak, C.; Temizdemir, S.; Scharmann, T. G.; Schmalstieg, A.; Demtschuk, J. *Z. Anorg. Allg. Chem.* **2000**, *626*, 2053.
74. (a) Kui, S. C. F.; Chui, S. S. Y.; Che, C. M.; Zhu, N. *J. Am. Chem. Soc.* **2006**, *128*, 8297; (b) Díez, Á.; Forniés, J.; Fuertes, S.; Lalinde, E.; Larraz, C.; López, J. A.; Martín, A.; Moreno, M. T.; Sicilia, V. *Organometallics* **2009**, *28*, 1705; (c) Anderson, B. M.; Hurst, S. K. *Eur. J. Inorg. Chem.* **2009**, *21*, 3041; (d) Utsuno, M.; Yutaka, T.; Murata, M.; Kurihara, M.; Tamai, N.; Nishihara, H. *Inorg. Chem.* **2007**, *46*, 11291; (e) Poater, A.; Moradell, S.; Pinilla, E.; Poater, J.; Sola, M.; Martinez, M. A.; Llobet, A. *Dalton Trans.* **2006**, 1188; (f) Ding, J.; Pan, D.; Tung, C.-H.; Wu, L.-Z. *Inorg. Chem.* **2008**, *47*, 5099; (g) Lai, S.-W.; Lam, H. W.; Lu, W.; Cheung, K.-K.; Che, C.-M. *Organometallics* **2002**, *21*, 226; (h) Lu, W.; Chan, M. C. W.; Cheung, K. K.; Che, C. M. *Organometallics* **2001**, *20*, 2477; (i) Lu, W.; Chan, M. C. W.; Zhu, N.; Che, C. M.; Li, C.; Hui, Z. *J. Am. Chem. Soc.* **2004**, *126*, 7639; (j) Lai, S. W.; Chan, M. C. W.; Cheung, K. K.; Che, C. M. *Organometallics* **1999**, *18*,

3327; (k) Lai, S. W.; Chan, M. C. W.; Cheung, K. K.; Peng, S. M.; Che, C. M. *Organometallics* **1999**, *18*, 3991.

75. Forniés, J.; Fuertes, S.; López, J. A.; Martín, A.; Sicilia, V. *Inorg. Chem.* **2008**, *47*, 7166.
76. Po, C.; Tam, A. Y.-Y.; Wong, K. M.-C.; Yam, V. W.-W. *J. Am. Chem. Soc.* **2011**, *133*, 12136.
77. (a) Ionkin, A. S.; Marshall, W. J.; Wang, Y. *Organometallics* **2005**, *24*, 619; (b) Farley, S. J.; Rochester, D. L.; Thompson, A. L.; Howard, J. A. K.; Williams, J. A. G. *Inorg. Chem.* **2005**, *44*, 9690; (c) Laskar, I. R.; Hsu, S.-F.; Chen, T.-M. *Polyhedron* **2005**, *24*, 881.
78. Marino, N.; Fazen, C. H.; Blakemore, J. D.; Incarvito, C. D.; Hazari, N.; Doyle, R. P. *Inorg. Chem.* **2011**, *50*, 2507.
79. (a) Aoki, R.; Kobayashi, A.; Chang, H.-C.; Kato, M. *Bull. Chem. Soc. Jpn.* **2011**, *84*, 218; (b) Umakoshi, K.; Kinoshita, I.; Ichamura, A.; Ooi, S. *Inorg. Chem.* **1987**, *26*, 3551; (c) Kato, M.; Omura, A.; Tashikawa, A.; Kishi, S.; Sugimoto, Y. *Angew. Chem., Int. Ed.* **2002**, *41*, 3183; (d) Tzeng, B. C.; Fu, W. F.; Che, C. M.; Chao, H. Y.; Cheung, K. K.; Peng, S. M. *J. Chem. Soc., Dalton Trans.* **1999**, 1017.
80. (a) Liu, F.; Chen, W.; Wang, D. *Dalton Trans.* **2006**, 3445; (b) Chen, W.; Matsumoto, K. *Inorg. Chim. Acta* **2003**, *342*, 88.
81. Yam, V. W.-W.; Yu, K.-L.; Wong, K. M.-C.; Cheung, K.-K. *Organometallics* **2001**, *20*, 721.
82. Tzeng, B.-C.; Chiu, T.-H.; Lin, S.-Y.; Yang, C.-M.; Chang, T.-Y.; Huang, C.-H.; Chang, A. H.-H.; Lee, G.-H. *Cryst. Growth. Des.* **2009**, *9*, 5356.
83. (a) Guo, Z.; Chan, M. C. W. *Chem. Eur. J.* **2009**, *15*, 12585; (b) Lai, S.-W.; Chan, M. C.-W.; Cheung, T. C.; Peng, S. M.; Che, C.-M. *Inorg. Chem.* **1999**, *38*, 4046; (c) Koo, C. K.; Wong, K. L.; Lau, K. C.; Wong, W. Y.; Lam, M. H. W. *Chem. Eur. J.* **2009**, *15*, 7689; (d) Sun, W.; Zhu, H.; Barron, P. M. *Chem. Matter.* **2006**, *18*, 2602; (e) Kui, S. C. F.; Sham, I. H. T.; Cheung, C. C. C.; Ma, C.-W.; Yan, B.; Zhu, N.; Che, C.-M.; Fu, W.-F. *Chem. Eur. J.* **2007**, *13*, 417; (f) Shao, P.; Sun, W. *Inorg. Chem.* **2007**, *46*, 8603; (g) Sicilia, V.; Forniés, J.; Casas, J. M.; Martín, A.; López, J. A.; Larraz, C.; Borja, P.; Ovejero, C.; Tordera, D.; Bolink, H. *Inorg. Chem.* **2012**, *51*, 3427; (h) Ma, B.; Li, J.; Djurovich, P. I.; Yousufuddin, M.; Bau, R.; Thompson, M. E. *J. Am. Chem. Soc.* **2005**, *127*, 28; (i) Koo, C. K.; Ho, Y. M.; Chow, C. F.; Lam, M. H. W.; Lau, T. C.; Wong, W. Y. *Inorg. Chem.* **2007**, *46*, 3603; (j)

Rachford, A. A.; Castellano, F. N. *Inorg. Chem.* **2009**, *48*, 10865; (k) Saito, K.; Nakao, Y.; Sakaki, S. *Inorg. Chem.* **2008**, *47*, 4329; (l) Chakraborty, A.; Deaton, J. C.; Haefele, A.; Castellano, F. N. *Organometallics* **2013**, *32*, 3819; (m) Lockard, J. V.; Rachford, A. A.; Smolentsev, G.; Stickrath, A. B.; Wang, X.; Zhang, X.; Atenkoffer, K.; Jennings, G.; Soldatov, A.; Rheingold, A. L.; Castellano, F. N.; Chen, L. X. *J. Phys. Chem. A* **2010**, *114*, 12780; (n) Cho, S.; Mara, M. W.; Wang, X.; Lockard, J. V.; Rachford, A. A.; Castellano, F. N.; Chen, L. X. *J. Phys. Chem. A* **2011**, *115*, 3990.

84. Pyykko, P.; Desclaux, J. P. *Acc. Chem. Res.* **1979**, *12*, 276.
85. (a) Fuertes, S.; Woodall, C. H.; Raithby, P. R.; Sicilia, V. *Organometallics* **2012**, *31*, 4228; (b) Forniés, J.; Ibáñez, S.; Martín, A.; Sanz, M.; Berenguer, J. R.; Lalinde, E.; Torroba, J. *Organometallics* **2006**, *25*, 4331; (c) Forniés, J.; Fuertes, S.; Martín, A.; Sicilia, V.; Gil, B.; Lalinde, E. *Dalton Trans.* **2009**, 2224; (d) Forniés, J.; Ibáñez, S.; Martín, A.; Gil, B.; Lalinde, E.; Moreno, M. T. *Organometallics* **2004**, *23*, 3963; (e) Jamali, S.; Mazloomi, Z.; Nabavizadeh, S. M.; Milić, D.; Kia, R.; Rashidi, M. *Inorg. Chem.* **2010**, *49*, 2721; (f) Janzen, D. E.; Mehne, L. F.; VanDerveer, D. G.; Grant, G. J. *Inorg. Chem.* **2005**, *44*, 8182; (g) Yamaguchi, T.; Yamazaki, F.; Ito, T. *J. Am. Chem. Soc.* **2001**, *123*, 743; (h) Martín, A.; Belío, Ú.; Fuertes, S.; Sicilia, V. *Eur. J. Inorg. Chem.* **2013**, 2231; (i) Belío, Ú.; Fuertes, S.; Martín, A. *Inorg. Chem.* **2013**, *52*, 5627.
86. (a) Yamaguchi, T.; Yamazaki, F.; Ito, T. *J. Am. Chem. Soc.* **1999**, *121*, 7405; (b) Oberbeckmann-Winter, N.; Morise, X.; Braunstein, P.; Welter, R. *Inorg. Chem.* **2005**, *44*, 1391.
87. (a) Wong, K. M.-C.; Hui, C.-K.; Yu, K.-L.; Yam, V. W.-W. *Coord. Chem. Rev.* **2002**, *229*, 123; (b) Díez, Á.; Lalinde, E.; Moreno, M. T. *Coord. Chem. Rev.* **2011**, *255*, 2426.
88. (a) Forniés, J.; Martín, A. In *Metal Clusters in Chemistry*; Braunstein, P., Oro, L. A., Raithby, P. R., Eds.; Wiley-VCH: Verlag: Weinheim, Germany, 1999; Vol. 1, p 417; (b) Gil, B.; Forniés, J.; Gómez, J.; Lalinde, E.; Martín, A.; Moreno, M. T. *Inorg. Chem.* **2006**, *45*, 7788; (c) Yin, G.-Q.; Wei, Q.-H.; Zhang, L.-Y.; Chen, Z.-N. *Organometallics* **2006**, *25*, 580; (d) Lang, H.; del Villar, A.; Stein, T.; Zoufalá, P.; Rüffer, T.; Rheinwald, G. *J. Organomet. Chem.* **2007**, *692*, 5203; (e) Falvello, L. R.; Forniés, J.; Lalinde, E.; Menjón, B.; García Monforte, M. A.; Moreno, M. T.; Tomás, M. *Chem. Commun.* **2007**, 3838.

89. Maliarik, M.; Nagle, J. K.; Ilyukhin, A.; Murashova, E.; Mink, J.; Skripkin, M.; Glaser, J.; Kovacs, M.; Horváth, A. *Inorg. Chem.* **2007**, *46*, 4642.
90. (a) Catalano, V. J.; Bennett, B. L.; Noll, B. C. *Chem. Commun.* **2000**, 1413; (b) Dolg, M.; Pyykkö, P.; Runember, N. *Inorg. Chem.* **1996**, *35*, 7450.
91. (a) Falvello, L. R.; Forniés, J.; Garde, R.; García, A.; Lalinde, E.; Moreno, M. T.; Steiner, A.; Tomás, M.; Usón, I. *Inorg. Chem.* **2006**, *45*, 2543; (b) Ara, I.; Berenguer, J. R.; Forniés, J.; Gómez, J.; Lalinde, E.; Martín, A.; Merino, R. *Inorg. Chem.* **1997**, *36*, 6461; (c) Berenguer, J. R.; Forniés, J.; Gómez, J.; Lalinde, E.; Moreno, M. T. *Organometallics* **2001**, *20*, 4847; (d) Charmant, J. P. H.; Forniés, J.; Gómez, J.; Lalinde, E.; Merino, R. I.; Moreno, M. T.; Orpen, A. G. *Organometallics* **2003**, *22*, 652; (e) Berenguer, J. R.; Forniés, J.; Gil, B.; Lalinde, E. *Chem. Eur. J.* **2006**, *12*, 785; (f) Díez, Á.; Fernández, J.; Lalinde, E.; Moreno, M. T.; Sánchez, S. *Inorg. Chem.* **2010**, *49*, 11606; (g) Díez, A.; Forniés, J.; Gómez, J.; Lalinde, E.; Martín, A.; Moreno, M. T.; Sánchez, S. *Dalton Trans.* **2007**, 3653; (h) Forniés, J.; García, A.; Lalinde, E.; Moreno, M. T. *Inorg. Chem.* **2008**, *47*, 3651; (i) Usón, R.; Forniés, J.; Tomás, M.; Garde, R. *Inorg. Chem.* **1997**, *36*, 1383; (j) Wu, G.; Wang, D. *J. Cluster Sci.* **2007**, *18*, 406; (k) Nagle, J. K.; Balch, A. L.; Olmstead, M. M. *J. Am. Chem. Soc.* **1988**, *110*, 319; (l) Stork, J. R.; Olmstead, M. M.; Balch, A. L. *J. Am. Chem. Soc.* **2005**, *127*, 6512; (m) Stork, J. R.; Olmstead, M. M.; Fettinger, J. C.; Balch, A. L. *Inorg. Chem.* **2006**, *45*, 849; (n) Balch, A. L.; Rowley, S. P. *J. Am. Chem. Soc.* **1990**, *112*, 6139; (o) Renn, O.; Lippert, B.; Mutikainen, I. *Inorg. Chim. Acta* **1993**, *208*, 219; (p) Oberbeckmann-Winter, N.; Braunstein, P.; Welter, R. *Organometallics* **2004**, *23*, 6311; (q) Song, H. B.; Zhang, Z. Z.; Hui, H.; Che, C. M.; Mak, T. C. W. *Inorg. Chem.* **2002**, *41*, 3146; (r) Quadrelli, E. A.; Davies, J. E.; Johnson, B. F. G.; Feeder, N. *Chem. Commun.* **2000**, 1031; (s) Chen, W.; Liu, F.; Xu, D.; Matsumoto, K.; Kishi, S.; Kato, M. *Inorg. Chem.* **2006**, *45*, 5552.
92. (a) Berenguer, J. R.; Fernández, J.; Gil, B.; Lalinde, E.; Sánchez, S. *Inorg. Chem.* **2010**, *49*, 4232; (b) Elbjeirami, O.; Rawashdeh-Omary, M.; Omary, M. *Res. Chem. Intermed.* **2011**, *37*, 691; (c) Forniés, J.; Ibáñez, S.; Lalinde, E.; Martín, A.; Moreno, M. T.; Tsipis, A. C. *Dalton Trans.* **2012**, 3439.
93. Honda, H.; Matsumoto, T.; Sakamoto, M.; Kobayashi, A.; Chang, H.-C.; Kato, M. *Inorg. Chem.* **2013**, *52*, 4324.
94. Belio, U.; Fuertes, S.; Martin, A. *Dalton Trans.* **2014**, *43*, 10828.

95. (a) Berenguer, J. R.; Díez, A.; Fernández, J.; Forniés, J.; García, A.; Gil, B.; Lalinde, E.; Moreno, M. T. *Inorg. Chem.* **2008**, *47*, 7703; (b) Balch, A. L.; Fung, E. Y.; Nagle, J. K.; Olmstead, M. M.; Rowley, S. P. *Inorg. Chem.* **1993**, *32*, 3295; (c) Usón, R.; Forniés, J.; Falvello, L. R.; Usón, M. A.; Usón, I. *Inorg. Chem.* **1992**, *31*, 3697; (d) Albano, V. G.; Castellari, C.; Monari, M.; De Felice, V.; Ferrara, M. L.; Ruffo, F. *Organometallics* **1995**, *14*, 4213; (e) Ara, I.; Falvello, L. R.; Forniés, J.; Gómez-Cordón, J.; Lalinde, E.; Merino, R. I.; Usón, I. *J. Organomet. Chem.* **2002**, *663*, 284; (f) Casas, J. M.; Forniés, J.; Martín, A.; Orera, V. M.; Orpen, A. G.; Rueda, A. *Inorg. Chem.* **1995**, *34*, 6514; (g) Heitmann, D.; Pape, T.; Hepp, A.; Mück-Lichtenfeld; S. Grimme; Ekkehardt-Hahn, F. *J. Am. Chem. Soc.* **2011**, *133*, 11118; (h) Braunschweig, H.; Damme, A.; Dewhurst, R. D.; Hupp, F.; Jiménez-Halla, J. O. C.; Radacki, K. *Chem. Commun.* **2012**, *48*, 10410.

96. (a) Parr, J. *Comprehensive Coordination Chemistry II*; (Ed: G.F.R. Parkin), Elsevier Pergamon: Boston, 2004; Vol. 3, pp 545-608; (b) Weidenbruch, M. In *Comprehensive Organometallic Chemistry III*, *Vol. 3*; Mingos, D. M. P., Crabtree, R. H., Eds.; Elsevier: Oxford, 2007, p 885.

97. Tang, G.; Liu, C.; Luo, L.; Chen, W. *J. Lumin.* **2010**, *130*, 821.

98. Newnham, R. E. *MRS Bull.* **1997**, *22*, 20.

99. C. B. Murray; S. Sun; W. Gaschler; H. Doyle; T. A. Betley; C. R. Kagan *IBM J. Res. Dev.* **2001**, *45*, 47.

100. (a) Zhao, S.-P.; Ren, X.-M. *Dalton Trans.* **2011**, *40*, 8261; (b) Wang, S.; Garzón, G.; King, C.; Wang, J. C.; Fackler Jr, J. P. *Inorg. Chem.* **1989**, *28*, 4623; (c) Catalano, V. J.; Bennett, B. L.; Malwitz, M. A.; Yson, R. L.; Kar, H. M.; Muratidis, S.; Horner, S. J. *Comments Inorg. Chem.* **2003**, *24*, 39.

101. (a) Shimoni-Liuny, L.; Glusker, J. P.; Bock, C. W. *Inorg. Chem.* **1998**, *37*, 1853; (b) Davidovich, R. L.; Stavila, V.; Marinin, D. V.; Voit, E. I.; Whitmire, K. H. *Coord. Chem. Rev.* **2009**, *253*, 1316; (c) Davidovich, R. L.; Stavila, V.; Whitmire, K. H. *Coord. Chem. Rev.* **2010**, *254*, 2193; (d) Gourlaouen, C.; Gérard, H.; Piquemal, J.-P.; Parisel, O. *Chem. Eur. J.* **2008**, *14*, 2730; (e) Greer, B. J.; Michaelis, V. K.; Katz, M. J.; Leznoff, D. B.; Schreckenbach, G.; Kroeker, S. *Chem. Eur. J.* **2011**, *17*, 3609.

102. Shannon, R. D. *Acta Cryst.* **1976**, *A32*, 751.

103. Berenguer, J. R.; Fernández, J.; Lalinde, E.; Sánchez, S. *Chem. Commun.* **2012**, *48*, 6384.

CAPÍTULO 1

Complejos cicloplatinados con ligandos tipo escorpionato

Complejos cicloplatinados con ligandos tipo escorpionato

Desde la síntesis de los primeros ligandos polipirazolil borato por Trofimenko en los años 60,[1] y su extensión a los ligandos polipirazolilalcanos,[2] su interés en la química de coordinación, organometálica, bioinorgánica y supramolecular ha sido impresionante. El nombre genérico de escorpionatos hace alusión a la posibilidad de cambiar su modo de coordinación (de bidentado a tridentado) (Figura 1.1). La química de estos ligandos se recoge extensivamente en los textos monográficos Scorpionates[1a] (publicados por S. Trofimenko) y Scorpionates II (publicado por C. Pettinari).[1b] Se han descrito tres generaciones de ligandos de este tipo y su estabilidad química y estructural y su versatilidad espacial y electrónica han hecho posible su coordinación a una gran variedad de iones metálicos. Además, los derivados con ligandos escorpionato han jugado un papel importante en numerosas aplicaciones como activación de enlaces C–H,[3] procesos catalíticos,[4] modelos de reacciones enzimáticas,[5] extracción de metales[1,6] y aplicaciones biomédicas. [5a,7]

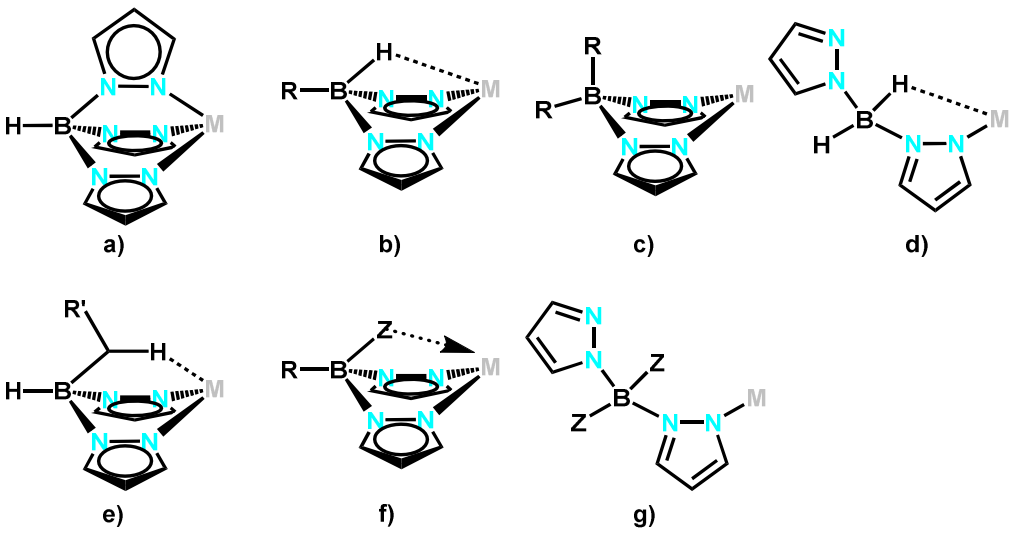

Figura 1.1: Modos de coordinación seleccionados de los ligandos bis y tris(pirazolil)boratos

Sin embargo, se conocen muy pocos estudios de la influencia de estos ligandos en las propiedades fotofísicas de complejos metálicos,[8] y en particular en complejos planocuadrados cicloplatinados.[8d,9] Hasta donde nosotros sabemos, los únicos derivados

de Pt^{II} descritos contienen ligandos basados en la fenilpiridina y ligandos bis(pirazolil)borato (Figura 1.2) y exhiben luminiscencia tanto en estado sólido como en disolución a temperatura ambiente.[8d,9]

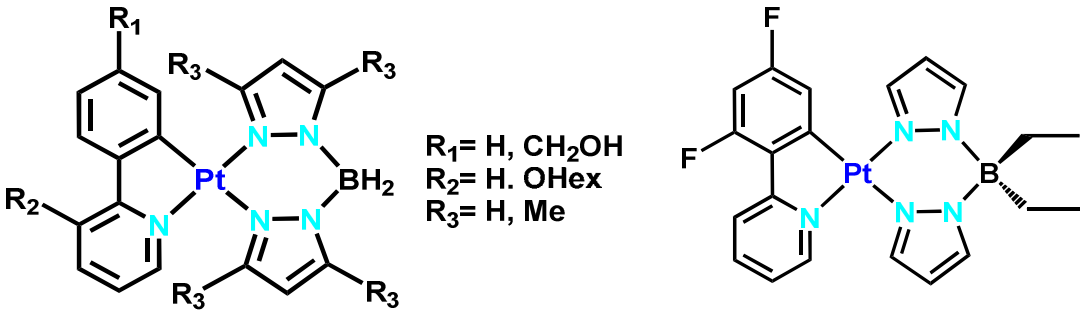

Figura 1.2: Derivados cicloplatinados con ligandos tipo escorpionato

Así, en este capítulo nos propusimos preparar varias series de complejos cicloplatinados neutros y catiónicos de tipo $[Pt(C\hat{}N)\{L'\}]^n$ con tres grupos ciclometalados distintos [C^N = 7,8-benzoquinolato (bzq), 2-fenilpiridinato (ppy) y 2-fenilquinolato (pq)] y ligandos polipirazolilborato o metano [L' = $[H_2B(pz)_2]^-$/ $[HB(pz)_3]^-$, n = 0 ; $[H_2C(pz)_2]$ /$[HC(pz)_3]$, n = 1]. Los compuestos sintetizados han mostrado unas interesantes propiedades fotoelectrónicas (UV–vis y luminiscencia), y electroquímicas que se han estudiado con detalle. Finalmente, se ha analizado la naturaleza de las absorciones y la emisión en estos compuestos mediante cálculos teóricos DFT y TD–DFT.

1.1 Síntesis

Este trabajo se inicia con la preparación de la sal potásica de los ligandos bis y tris(pirazolil)borato $[H_2B(pz)_2]^-$ y $[HB(pz)_3]^-$[10] y la del tris(pirazolil)metano $[HC(pz)_3]$[11] siguiendo los métodos descritos en la bibliografía, mientras que, el ligando bis(pirazolil)metano $[H_2C(pz)_2]$ se obtiene siguiendo un método que implica modificación del propuesto por el Prof Reger para el tris(pirazolil)metano[11] (Ver Parte Experimental).

La síntesis de los complejos de platino se ha llevado a cabo siguiendo rutas bien establecidas y se resume en los Esquemas 1.1 y 1.2. En primer lugar se estudiaron las

reacciones de los derivados dinucleares simétricos de platino con puentes cloro $[Pt(C\hat{}N)(\mu\text{-}Cl)]_2$ frente a $K[H_2B(pz)_2]$, $[H_2C(pz)_2]$ y $[HC(pz)_3]$. Las rutas sintéticas para la obtención de compuestos cicloplatinados catiónicos o neutros con ligandos bis(pirazolil)borato o poli(pirazolil)metano se recogen en el Esquema 1.1

Según se describe la parte experimental (Esquema 1.1i), el tratamiento de una suspensión coloreada de los derivados dinucleares simétricos de platino con puentes cloro $[Pt(C\hat{}N)(\mu\text{-}Cl)]_2$ con 2 equivalentes de $K[H_2B(pz)_2]$ en acetona, proporciona tras un tiempo de reacción (30-60 min) y posterior extracción en CH_2Cl_2 la serie de compuestos bis(pirazolil)borato $[Pt(C\hat{}N)\{H_2B(pz)_2\}]$ (C^N = bzq **1**, ppy **2** y pq **3**) de colores amarillo (**1, 2**) y naranja (**3**), en rendimientos de moderados a buenos (43%–79%). Debemos indicar que en el curso de la preparación de esta memoria se ha descrito la síntesis del derivado **2** a partir de $(NBu_4)[Pt(ppy)Cl(Hppy)]$.[8d]

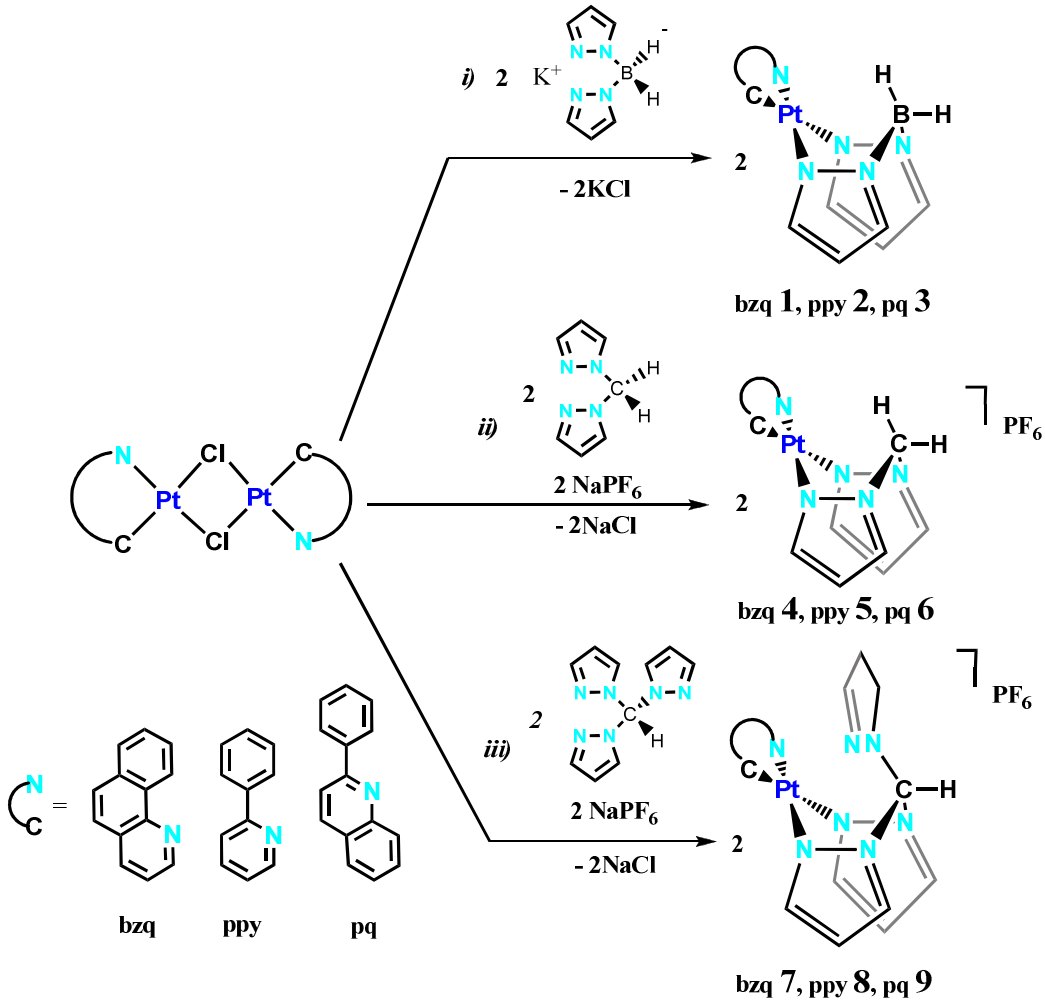

Esquema 1.1

Tratamientos similares de los sustratos $[Pt(C^N)(\mu\text{-}Cl)]_2$ con los ligandos neutros bis(pirazolil)metano $[H_2C(pz)_2]$ o tris(pirazolil)metano $[HC(pz)_3]$ en acetona, en presencia de 2 equivalentes de $NaPF_6$, (Esquema 1.1ii/iii) nos permiten obtener las series de derivados catiónicos ciclometalados de Pt(II) bis(pirazolil)metano $[Pt(C^N)\{H_2C(pz)_2\}]PF_6$ (C^N = bzq **4**, ppy **5** y pq **6**) y tris(pirazolil)metano $[Pt(C^N)\{HC(pz)_3\}]PF_6$ (C^N = bzq **7**, ppy **8** y pq **9**) de colores amarillo (**4**, **5**, **7**, **8**) y naranja (**6**, **9**) con buenos rendimientos (70 – 75%).

Tras diversos ensayos las reacciones de los sustratos $[Pt(C^N)(\mu\text{-}Cl)]_2$ con 2 equivalentes de $K[HB(pz)_3]$ se optimizaron y los mejores resultados se obtuvieron empleando atmósfera inerte y acetona destilada (Esquema 1.2). Únicamente la reacción del sustrato $[Pt(pq)(\mu\text{-}Cl)]_2$ con 2 equivalentes de $K[HB(pz)_3]$ evoluciona de forma análoga a lo descrito con los otros ligandos, dando lugar al derivado $[Pt(pq)\{HB(pz)_3\}]$ (**10**) en forma de sólido naranja con un rendimiento del 77% (Esquema 1.2i). Sin embargo, la reacción de $[Pt(bzq)(\mu\text{-}Cl)]_2$ con $K[HB(pz)_3]$ no produce el derivado buscado. En este sistema (ver parte experimental), se produce la ruptura del enlace B-N,[12] y la formación de mezclas en las que se detectan fundamentalmente los isómeros *cis* y *trans* $[Pt(bzq)(\mu\text{-}pz)]_2$, previamente descritos[13] y de las que se obtienen cristales de *trans*-$[Pt(bzq)(\mu\text{-}pz)]_2$ (**11**), adecuados para un estudio de difracción de Rayos X, por lenta cristalización en CH_2Cl_2/hexano (Esquema 1.2ii). Por último, la reacción del derivado $[Pt(ppy)(\mu\text{-}Cl)]_2$ con $K[HB(pz)_3]$, produce un sólido amarillo en escaso rendimiento, que se identifica como una mezcla del compuesto mononuclear buscado $[Pt(ppy)\{HB(pz)_3\}]$ (**12**) y de los derivados dinucleares *cis* y *trans*-$[Pt(ppy)(\mu\text{-}pz)]_2$, previamente descritos en la bibliografía,[13-14] en relación ~1:1 (Esquema 1.2ii). El tratamiento de este sólido con tolueno permite separar una fracción que se identifica como *cis* y *trans*-$[Pt(ppy)(\mu\text{-}pz)]_2$ y otra segunda fracción minoritaria (~5%) del producto $[Pt(ppy)\{HB(pz)_3\}]$ (**12**).

Es de destacar que, aunque son muy raras, existen precedentes de roturas de enlaces B–N en ligandos poli(pirazolil)borato para dar grupos pirazolato y/o pirazol,[32,33] aunque no en la química del Pt.

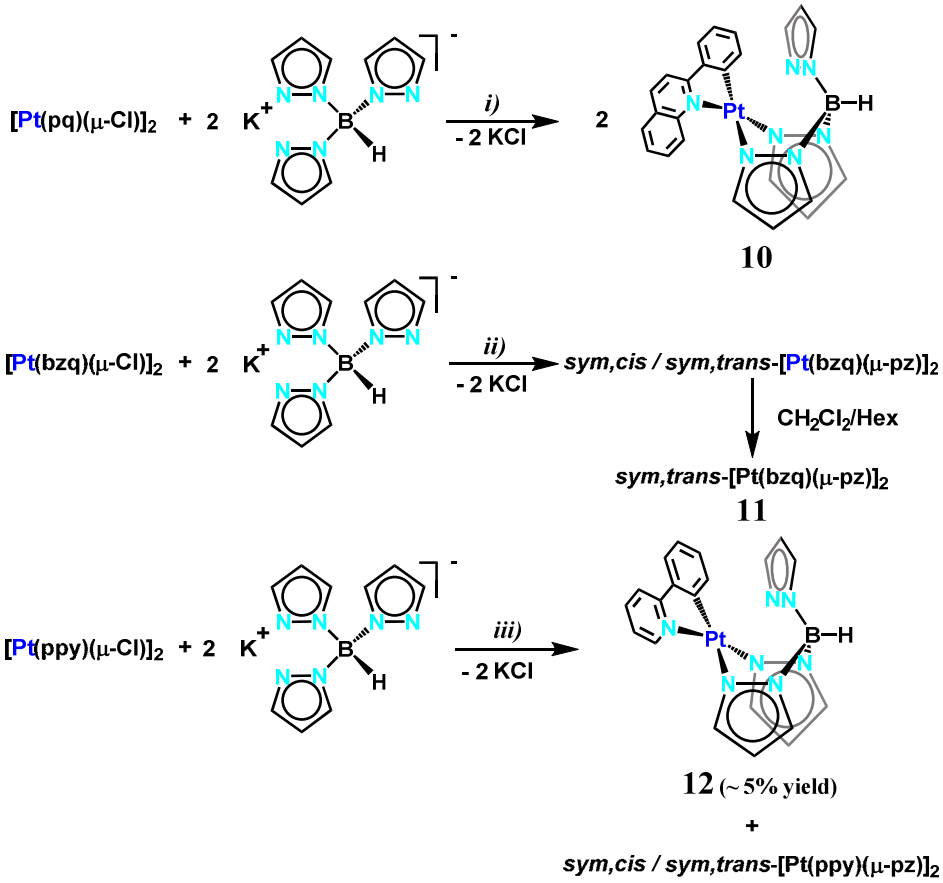

Esquema 1.2

1.2 Caracterización de los compuestos 1-10

Todos los complejos mononucleares son estables al aire a temperatura ambiente y su caracterización se basa en datos analíticos (C, H, N), métodos espectroscópicos [IR (**1**–**10**), espectroscopía de masas, RMN de ^{1}H (**1**–**10**), y ^{13}C{^{1}H} (**1**–**6**, **9** y **10**)], y cuando ha sido posible, mediante difracción de Rayos X de monocristal (**1**, **3**, **6**–**9** y **11**).

1.2.1 Caracterización espectroscópica

Los espectros de masas MALDI-TOF (+) de los derivados neutros **1**–**3** y **10** exhiben como pico padre el pico molecular $[M]^+$ o el pico molecular con pérdida de un hidrógeno $[M\text{-}H]^+$ mientras que los de los complejos catiónicos bis y tris(pirazolil)metano muestran el esperado catión molecular $[M\text{-}PF_6]^+$ (100%). Los espectros IR de los complejos de pirazolilborato (**1**–**3**, **10**) muestran una señal intensa

asignable a la vibración de tensión ν(B-H), [2407 (**1**), 2412 (**2**), 2431 (**3**) y 2419 (**10**) cm^{-1}] de acuerdo con la señal descrita por Trofimenko.[10]

Los espectros de RMN de ^{1}H y $^{13}C\{^{1}H\}$ muestran de forma inequívoca la presencia de los ligandos ciclometalados. Las asignaciones (ver Experimental) se han llevado a cabo teniendo en cuenta las espectros de los ligandos, la presencia y valores de las constantes de acoplamiento y los espectros de correlación COSY ^{1}H-^{1}H y HSQC ^{1}H-^{13}C registrados para los compuestos **1** – **10** (^{1}H-^{1}H) y **1** – **3** y **10** (^{1}H-^{13}C).

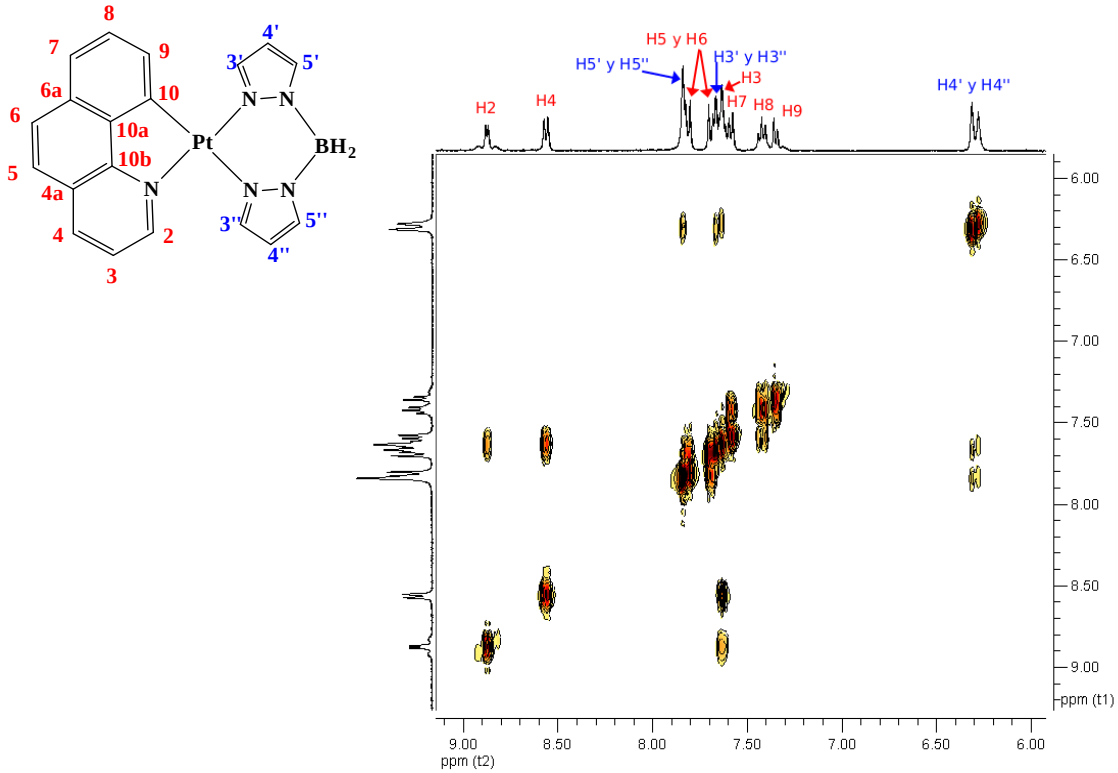

Figura 1.3: Espectro de Correlación ^{1}H-^{1}H para el compuesto **1** en CD_3COCD_3

En los espectros de RMN de ^{1}H de los derivados con *bzq* (**1, 4 y 7**) (ver Tabla A1.1 y Figura 1.3 para **1**) se observan dos señales doblete características a campo bajo. La primera localizada a δ 9.01 (**1**), 9.08 (**4**) y 9.04 (**7**), con una constante de acoplamiento a ^{195}Pt $^{3}J_{Pt\text{-}H}$ de 32.9 (**1**), 41.0 (**4**) y 39.9 (**7**) Hz se asigna al protón H^2 y la segunda a δ 7.48 (**1**), 7.45 (**4**) y 7.36 (**7**) con acoplamiento Pt–H con un valor $^{3}J_{Pt\text{-}H}$ de 37.8 (**1**), 34.7 (**4**) y 33.8 (**7**) Hz se asigna al protón H^9. En relación a las señales del ligando Hbzq libre (δ H^2 9.29; H^9 7.79) se observa un desplazamiento de las mismas a frecuencias más bajas. Las diferencias encontradas entre los distintos derivados, tanto en el desplazamiento como en las constantes de acoplamiento, nos muestran la

influencia que tiene el átomo al que se unen los grupos pirazolato en el pirazolil derivado así como el número de éstos. Además de las señales debidas a los protones aromáticos de la bzq, se observan como señales características de los grupos bis(pirazolil)borato o metano dos tripletes a campo alto [δ 6.45 y 6.41 (**1**) 6.88 y 6.87 (**4**)] asignados a los protones 4' y 4'' de los grupos pirazolato. En el derivado de tris(pirazolil)metano (**7**) se observa un único triplete a δ 7.06, correspondiente a los protones $H^{4'}$ y $H^{4''}$ coordinados y un singlete ancho a campo alto (δ 6.23) asignado al protón $H^{4'''}$ del pirazolato libre. El resto de señales se asignaron siguiendo la conectividad escalar en los espectros COSY ^{1}H-^{1}H y HSQC (ver Figura 1.3 para **1**).

Para analizar los posibles procesos de agregación en **7** en disoluciones concentradas, se llevó a cabo un estudio de RMN de ^{1}H a temperatura variable en CD_3CN. Los espectros de ^{1}H son idénticos en concentraciones diluidas y concentradas, por lo que se llevó a cabo un estudio en una disolución 10^{-3}M. A 243 K, el espectro muestra señales intensas y bien resueltas para las resonancias del ligando bzq y los 3 grupos pirazolato no equivalentes, por lo que se excluye la presencia de agregación, que daría, posiblemente, señales más anchas. A 298 K, las señales de la bzq no se desplazan, mientras que las de los grupos pirazolato aparecen como señales anchas, sugiriendo que estos anillos pueden estar implicados en un proceso dinámico lento en la escala de tiempo del RMN.

En los espectros de RMN de $^{13}C\{^{1}H\}$ a 25 ºC de **1** ($CDCl_3$) y **4** (CD_3COCD_3) se observan las resonancias esperadas para los ligandos bzq y $[H_2B(pz)_2]^-$. Algunas de las señales han sido asignadas tentativamente con ayuda de las constantes de acoplamiento $^{n}J_{Pt\text{-}C}$ y del correspondiente espectro de correlación HSQC. En la Tabla A1.1 se recoge una selección de las señales más características. A frecuencias altas resuena el carbono metalado C^{10} [δ 157.5 (**1**) y 154.4 (**4**)]. Como señales del ligando bzq más características se asignan, además, la señal del carbono contiguo al nitrógeno del ligando bzq (C^2) con satélites de platino [δ $C^2/^2J_{Pt\text{-}C}$ 148.3/26.7 Hz (**1**), 154.3/23.8 Hz (**4**)] y la señal del carbono unido al carbono ortometalado C^9, también con acoplamiento al centro de platino [δ $C^9/^2J_{Pt\text{-}C}$ 131.7/64.6 Hz (**1**), 135.2/65.1 Hz (**4**)]. Por otra parte, las señales asociadas a los C cuaternarios (4a, 6a, 10, 10a y 10b) se han asignado por similitud con los datos registrados en la base de datos sdbs (http://riodb01.ibase.aist.go.jp/sdbs/cgi-

bin/direct_frame_top.cgi). La asignación de las señales de carbono de los grupos pirazolato se ha realizado teniendo en cuenta las diferencias en las constantes de acoplamiento, ya que las $^{3}J_{Pt\text{-}C}$ son mayores en el grupo pirazolato en posición *trans* al nitrógeno del grupo ciclometalado [δ C$^{3'}$/$^{2}J_{Pt\text{-}C}$ 142.0/79.1 Hz (**1**), 150.2/68.3 Hz (**4**); C$^{4'}$/$^{3}J_{Pt\text{-}C}$ 105.7/50.5 Hz (**1**), 114.1/49.7 Hz (**4**)], que los del pirazolato en *cis* [δ C$^{3''}$/$^{2}J_{Pt\text{-}C}$ 140.0/24.3 Hz (**1**), 149.0/19.0 Hz (**4**); C$^{4''}$/$^{3}J_{Pt\text{-}C}$ 105.7/18.2 Hz (**1**), 113.9/16.0 Hz (**4**)].

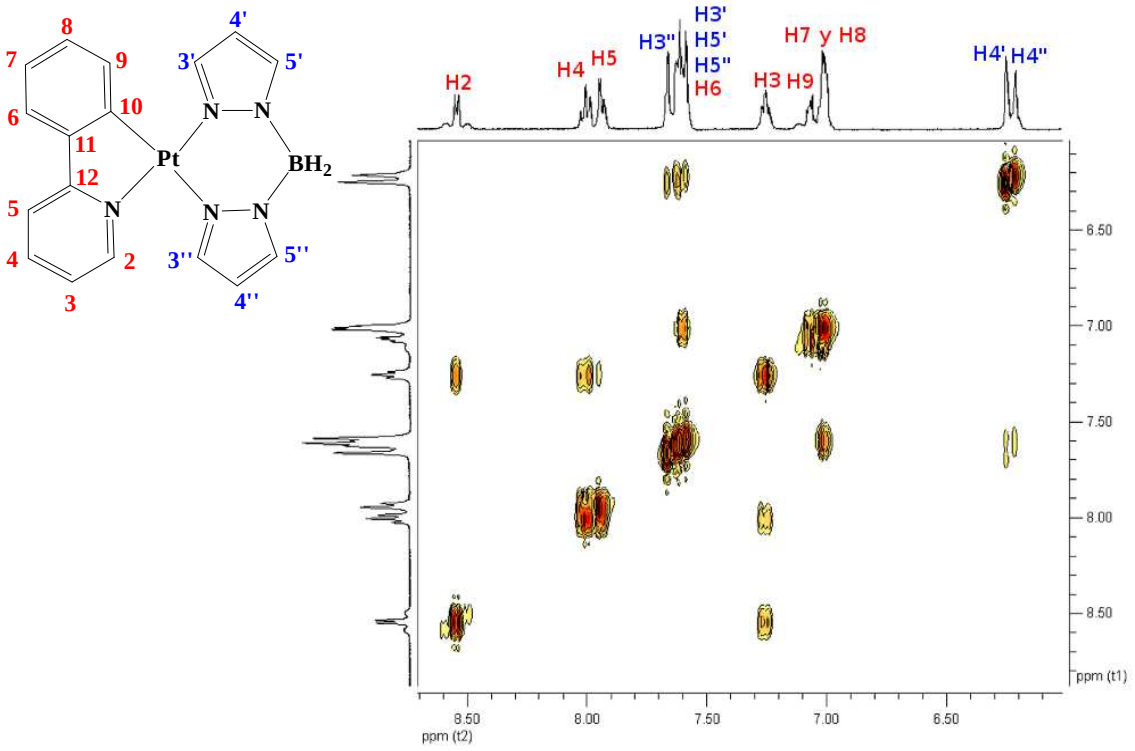

Figura 1.4: Espectro de Correlación ^{1}H-^{1}H para el compuesto **2** en CD_3COCD_3

En los espectros de RMN de ^{1}H de los derivados de *fenilpiridina* (**2, 5 y 8**) (Tabla A1.2 y Figura 1.4 para **2**) se observa, una señal doblete característica a campo bajo [δ 8.68 (**2**), 8.74 (**5**) y 8.66 (**8**)], asignada al protón H^{2}, en la que es visible el acoplamiento a ^{195}Pt [$^{3}J_{Pt\text{-}H}$ de 37.0 (**2**), 37.7 (**5**), y 35.1 (**8**) Hz]. Los hidrógenos H$^{4'/4''}$ de los grupos pirazolato resuenan como dos tripletes característicos a frecuencias bajas [δ 6.36, 6.39 (**2**), 6.81, 6.83 (**5**)] ó como un triplete ancho (δ 6.99) con otra señal a 6.34 debida a H$^{4'''}$ para el derivado **8**.

Los espectros de RMN de ^{13}C{^{1}H} de estos derivados muestran las once resonancias esperadas para el ligando fenilpiridinato (ppy) y las señales de $[H_2B(pz)_2]^-$,

$[H_2C(pz)_2]$ y $[HC(pz)_3]$. La señal del carbono ortometalado (C^{10}) aparece desplazada aprox. 10 ppm a campo más bajo con relación a los derivados de bzq (δ 168.6 **2**, 167.8 **5**) en cada caso. Es de destacar el menor valor de las constantes $^2J_{Pt\text{-}C}$ del H^2 en los compuestos de ppy [$^2J_{Pt\text{-}C}$ = 19.7 (**2**) y 20.2 Hz (**8**)] frente a los de bzq (26.7 y 23.8 Hz **1** y **4**), lo que nos confirma una menor retrodonación de densidad electrónica del Pt al ligando ciclometalado 2-fenilpiridina (ppy), comparada con el ligando bzq, que influirá en las propiedades ópticas de estos compuestos. En la Tabla A1.2 se recogen las señales de carbono más características.

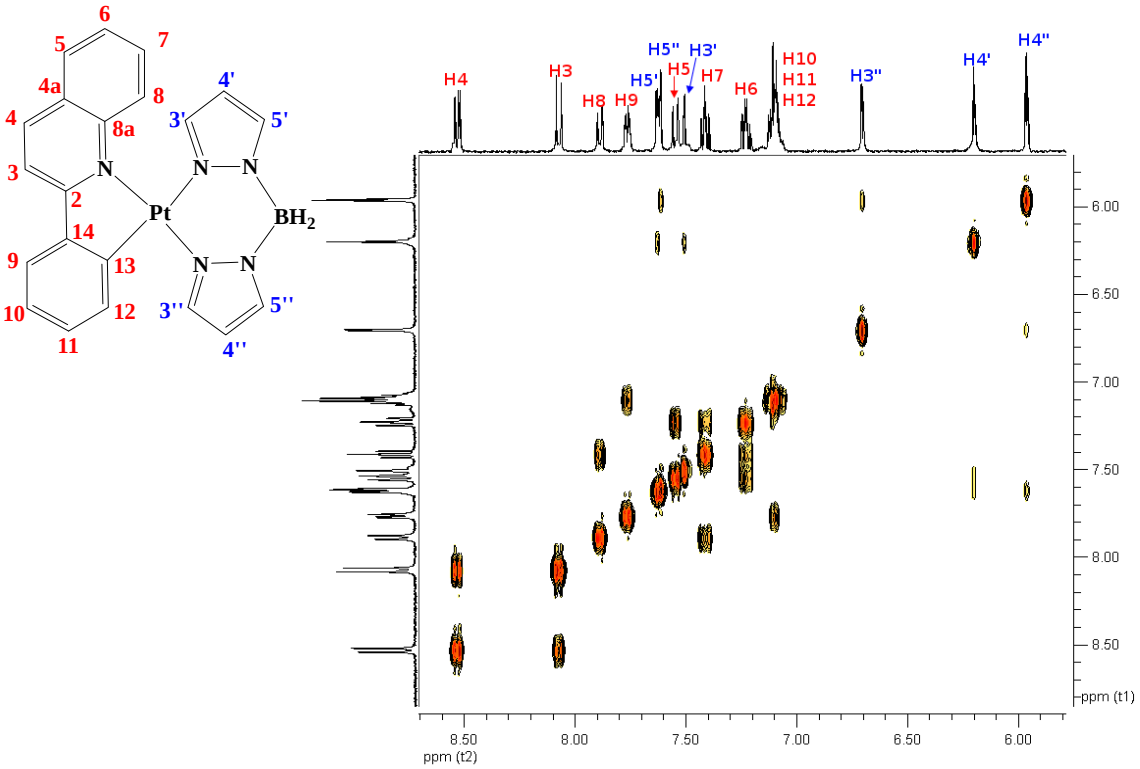

Figura 1.5: Espectro de Correlación ^1H-^1H para el compuesto **3** en CD_3COCD_3

El análisis de los espectros de RMN de ^1H (Tabla A1.3, Figura 1.5 para **3**) de los derivados de *fenilquinolato* (pq) (**3**, **6** y **9**) nos muestra dos señales a campo bajo [δ 8.53/8.07 (**3**), 8.79/8.32 (**6**), 8.72/8.23 (**9**)] que se atribuyen a los hidrógenos H^4 y H^3 del ligando pq. El hidrógeno en posición α u *orto* al carbono ortometalado (H^{12}) aparece como un doblete a δ 7.10 (**3**), 7.20 (**6**) y 7.26 (**9**), con acoplamiento a platino en el caso de **6** ($^2J_{Pt\text{-}C}$ = 32.0 Hz). Este hidrógeno es equivalente, en posición, al H^9 en los ligandos bzq y ppy. De nuevo, los protones $H^{4'}$ y $H^{4''}$ de los grupos pirazolato aparecen como tripletes a campo alto, siguiendo el mismo esquema de los derivados anteriores.

En los espectros RMN de $^{13}C\{^1H\}$ son llamativas las señales del carbono C^{12} (*orto* al carbono metalado), del C^9 y del C^3 del ligando ciclometalado, que aparecen todas ellas en orden de mayor a menor frecuencia y con satélites de platino (ver Tabla A1.3).

La presencia de los grupos $H_2B(pz)_2$ en **1**–**3** se observa muy bien en los espectros de RMN de protón, donde aparece una señal triplete muy ancha 1:1:1 para **1** y **2** ($^1J_{B-H}$ = 143.3–161.2 Hz) en el rango 3.88–3.97, asignada a los hidrógenos del grupo BH_2, ensanchada debido a la naturaleza cuadrupolar del ^{11}B, que no se resuelve bien, en el compuesto **3**, por lo que aparece como singlete ancho. Asimismo, la presencia de los grupos [$H_2C(pz)_2$] se observa en los espectros de RMN de $^{13}C\{^1H\}$ de los compuestos **4** y **5** como una señal singlete localizada a δ 68.6 y a 64.6 respectivamente, con un acoplamiento $^3J_{Pt-C}$ de 28.0 y 26.7 Hz, respectivamente, y en los protones de los derivados **4**–**6**, ya que la señal de los H del CH_2 aparece en la zona de aromáticos como un sistema AB [δ 7.35 (**4**), 7.29 (**5**), 7.43 (**6**)] con constantes de acoplamiento J_{H-H} de 14.7 (**4**), 14.4 (**5**) y 15.7 Hz (**6**). Asimismo, en los derivados con el ligando [$HC(pz)_3$] el hidrógeno del grupo C*H*, se observa en el espectro de protón de **7**–**9** como una señal singlete situada a campo bajo [δ 9.45 (**7**), 9.40 (**8**), 9.53(**9**)] y en el de $^{13}C\{^1H\}$ de **9** una señal característica del carbono a δ 80.7.

1.2.2 Caracterización mediante Difracción de Rayos X de monocristal

Con objeto de confirmar la estructura de los derivados estudiados, así como la disposición espacial de los anillos ciclometalados y de los grupos poli(pirazolil)borato o metano se llevó a cabo un estudio estructural por difracción de Rayos X sobre monocristal de los derivados **1**, **3**, **6**, **7**–**9** y del derivado [Pt(bzq)(μ-pz)]$_2$ (**11**). Una revisión de la *Cambridge Data Base* de Febrero de 2014 nos indica que se han determinado previamente por difracción de Rayos X las estructuras cristalinas de los compuestos [Pt(ppy){$H_2B(3,5\text{-}Me_2pz_2)$}][8d] y [Pt(dfppy){$Et_2B(pz)_2$}] (dfppy = 6,8-difluoro-fenilpiridinato)[9]relacionadas con el compuesto **2**.

Se obtuvieron monocristales amarillos (**1**, **7**, **8**, **11**) o naranjas (**3**, **6**, **9**) adecuados para el estudio por difracción de Rayos X mediante lenta difusión de hexano (**1**, **3**, **11**),

EtOH (**6**, **8**, **9**) o *i*-PrOH (**7**) sobre disoluciones de acetona (**1**), CH_2Cl_2 (**3**, **6**, **11**) o acetonitrilo (**7**, **8**, **9**) a temperatura ambiente. La estructura molecular de los derivados neutros **1** y **3** y de los catiónicos (**6**$^+$–**9**$^+$) se muestra en las Figuras 1.6 y 1.7 y las distancias y ángulos de enlace más relevantes se recogen en las Tabla 1.1–1.2.

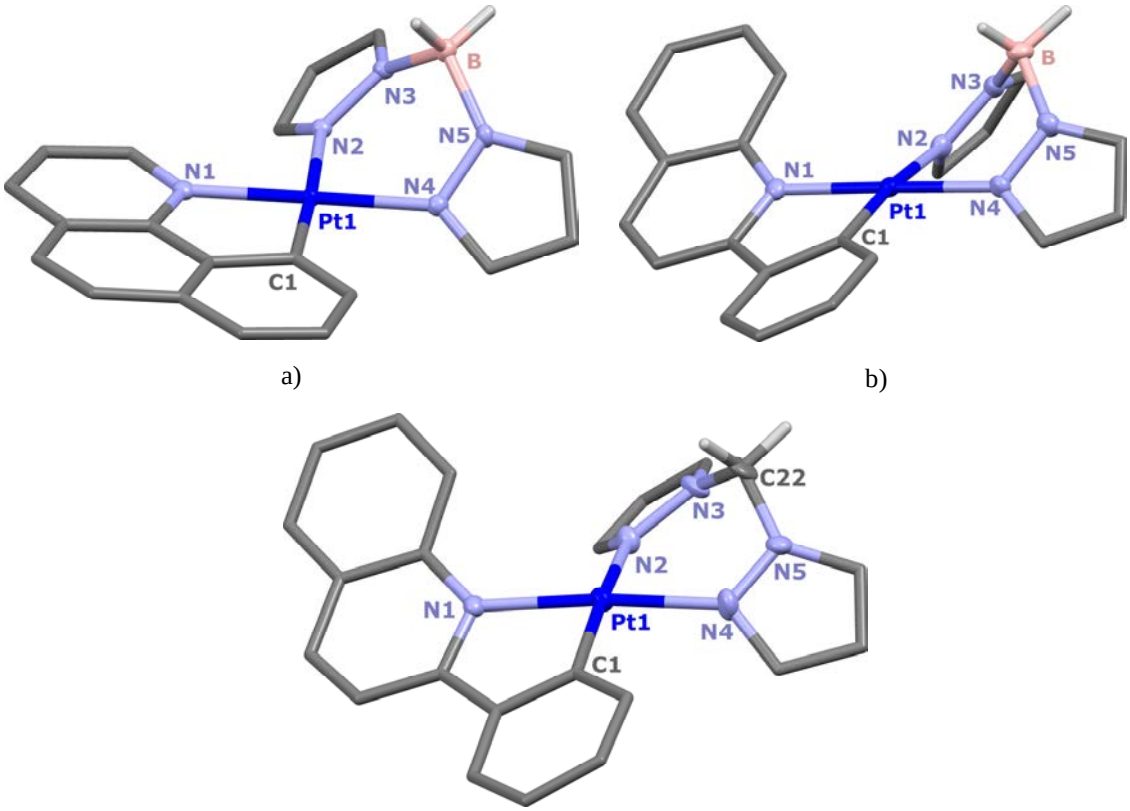

Figura 1.6: Estructura cristalina de los derivados neutros a) [Pt(bzq){$H_2B(pz)_2$}] (**1**), b) [Pt(pq){$H_2B(pz)_2$}] (**3**) y del catión c) [Pt(pq){$H_2C(pz)_2$}]$^+$ (**6**)

Tabla 1.1: Distancias [Å] y ángulos [º] para los derivados **1**, **3** y **6**

1		**3**		**6**	
Pt-N(1)	2.028(2)	Pt-N(1)	2.040(4)	Pt-N(1)	2.046(7)
Pt-N(2)	2.098(2)	Pt-N(2)	2.098(5)	Pt-N(2)	2.104(8)
Pt-N(4)	2.024(2)	Pt-N(4)	2.008(4)	Pt-N(4)	2.025(7)
Pt-C(1)	2.007(3)	Pt-C(1)	1.993(6)	Pt-C(1)	1.99(1)
B-N(3)	1.551(4)	B-N(3)	1.563(7)	C(22)-N(3)	1.43(1)
B-N(5)	1.555(4)	B-N(5)	1.565(7)	C(22)-N(5)	1.46(1)
B-H	0.9700	B-H	0.9700	C(22)-H	0.9700
N(1)-Pt-C(1)	81.6(1)	N(1)-Pt-C(1)	80.8(2)	N(1)-Pt-C(1)	80.4(3)
N(2)-Pt-N(4)	87.12(9)	N(2)-Pt-N(4)	84.6(2)	N(2)-Pt-N(4)	85.1(3)
N(1)-Pt-N(2)	95.75(9)	N(1)-Pt-N(2)	98.3(2)	N(1)-Pt-N(2)	98.4(3)
C(1)-Pt-N(4)	95.5(1)	C(1)-Pt-N(4)	96.3(2)	C(1)-Pt-N(4)	95.4(4)
N(3)-B-N(5)	107.4(2)	N(3)-B-N(5)	104.2(4)	N(3)-C(22)-N(5)	110.1(8)
H-B-H	108.5	H-B-H	108.9	H-C(22)-H	108.2

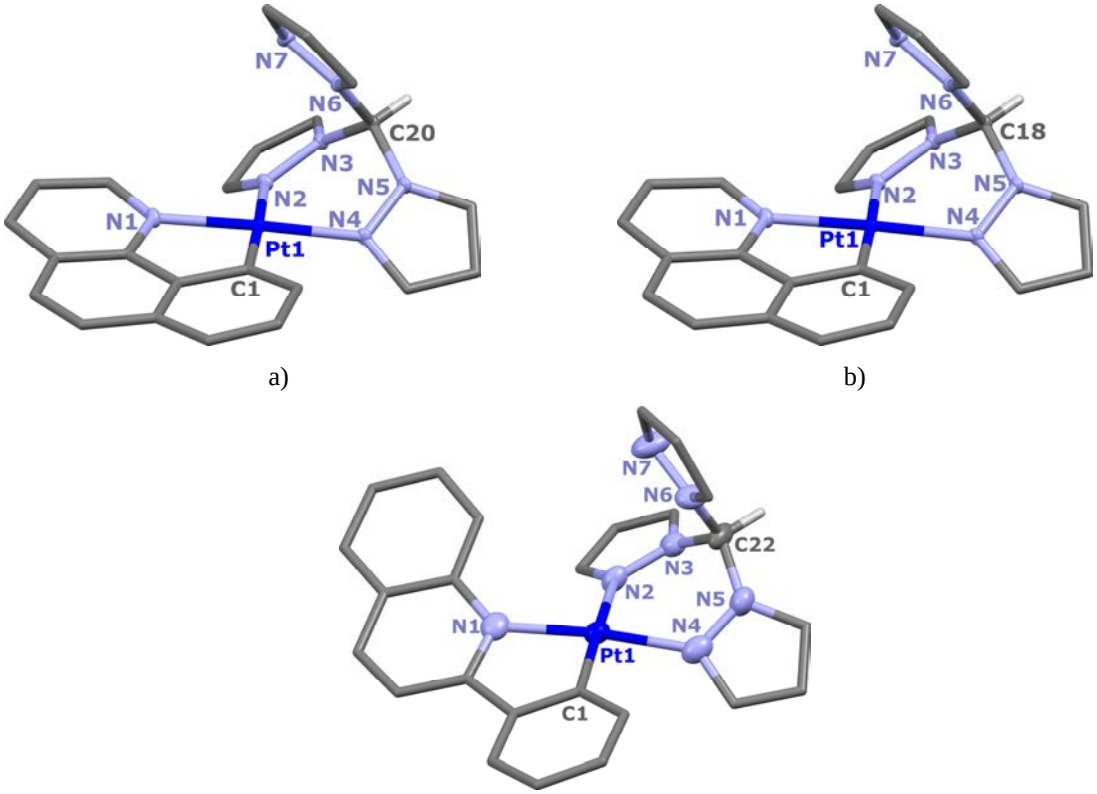

Figura 1.7: Estructura molecular de los cationes a) $[Pt(bzq)\{HC(pz)_3\}]^+$ ($\mathbf{7}^+$), b) $[Pt(ppy)\{HC(pz)_3\}]^+$ ($\mathbf{8}^+$) y c) $[Pt(pq)\{HC(pz)_3\}]^+$ ($\mathbf{9}^+$)

Tabla 1.2: Distancias [Å] y ángulos [º] para los derivados **7**, **8** y **9**

7		**8**		**9**	
Pt-N(1)	2.019(2)	Pt-N(1)	2.015(3)	Pt-N(1)	2.030(8)
Pt-N(2)	2.095(2)	Pt-N(2)	2.107(3)	Pt-N(2)	2.130(7)
Pt-N(4)	2.035(2)	Pt-N(4)	2.032(3)	Pt-N(4)	2.011(8)
Pt-C(1)	2.010(3)	Pt-C(1)	1.991(3)	Pt-C(1)	1.979(9)
C(20)-N(3)	1.446(3)	C(18)-N(3)	1.450(4)	C(22)-N(3)	1.44(1)
C(20)-N(5)	1.448(3)	C(18)-N(5)	1.450(4)	C(22)-N(5)	1.46(1)
C(20)-N(6)	1.455(3)	C(18)-N(6)	1.454(4)	C(22)-N(6)	1.46(1)
C(20)-H	0.91(3)	C(18)-H	0.9800	C(22)-H	0.9800
N(1)-Pt-C(1)	82.0(1)	N(1)-Pt-C(1)	81.0(1)	N(1)-Pt-C(1)	79.8 (3)
N(2)-Pt-N(4)	85.73(8)	N(2)-Pt-N(4)	84.9(1)	N(2)-Pt-N(4)	84.4(3)
N(1)-Pt-N(2)	96.02(9)	N(1)-Pt-N(2)	97.7(1)	N(1)-Pt-N(2)	100.3(3)
C(1)-Pt-N(4)	96.16(9)	C(1)-Pt-N(4)	96.5(1)	C(1)-Pt-N(4)	95.2(3)
N(3)-C(20)-N(5)	110.5(2)	N(3)-C(18)-N(5)	110.2(3)	N(3)-C(22)-N(5)	110.3(7)
H-C(20)-N(6)	114.1(2)	H-C(18)-N(6)	109.2	H-C(22)-N(6)	108.8

En estos complejos, el átomo de platino presenta un entorno pseudo planocuadrado formado por los dos átomos de nitrógeno de los grupos pirazolato y los átomos de carbono y nitrógeno coordinados del ligando ciclometalado. Los parámetros geométricos son similares a los encontrados en los escasos ejemplos descritos de

derivados de Pt con ligandos ciclometalados y escorpionato, (2-fenilpiridina)dihidrobis (3,5-dimetilpirazolil)borato platino(II)[8d] y 2-(2,4-diflurofenilpiridina)dietilbis(pirazolil) boratoplatino(II).[9] La naturaleza de los átomos de carbono y de nitrógeno del ligando ciclometalado quedó perfectamente establecida después del refinamiento de la estructura, con distancias Pt-C(1) [1.991(3)–2.010(3) Å], ligeramente más cortas que las Pt-N(1) [2.015(3)–2.046(7) Å].

Como es de esperar, el C ortometalado C(1) ejerce mayor influencia *trans* que el átomo de nitrógeno N(1) del ligando ciclometalado, como se deduce del análisis de las distancias Pt-N(2) [2.095(2)–2.130(7) Å], que son claramente más largas que las distancias Pt-N(4) [2.008(4)–2.035(2) Å]. Si analizamos la distancia Pt-N(2) en los complejos **7**–**9** observamos que sigue la serie 2.130(7) Å **9** > 2.107(3) **8** >2.095(2) **7**, lo que sugiere que la influencia *trans* del C_{sp^2} del ligando metalado en estos derivados es ligeramente mayor en el 2-fenilquinolinato (pq) que en el 2-fenilpiridinato (ppy) y a su vez que en el benzoquinolinato (bzq).

La desviación del entorno planocuadrado que sufre el átomo metálico se observa claramente tanto en el ángulo de mordedura N(1)-Pt-C(1) [79.8(3)º–82.0(1)º], que es similar al encontrado en derivados de Pt(II) con ligandos ciclometalados similares,[8d,9,15] como en el ligero desplazamiento que sufre el centro de platino respecto a su plano de coordinación PtN_3C (0.031 **1**, 0.077 **3**, 0.133 $\mathbf{6}^+$, 0.029 $\mathbf{7}^+$, 0.033 $\mathbf{8}^+$, 0.087 Å $\mathbf{9}^+$).

Los ligandos ciclometalados muestran diferentes disposiciones, presentando distintos ángulos dihedrales entre el plano formado por el ligando ciclometalado y el plano de coordinación del Pt. Así, mientras en **1** y $\mathbf{7}^+$ el ligando benzoquinolato (bzq) se sitúa prácticamente en el plano de coordinación del Pt (PtN_3C), en los derivados **3**, $\mathbf{6}^+$ y $\mathbf{9}^+$ el grupo fenilquinolato (pq) está muy aleteado formando ángulos dihedrales de 21.6º (**3**), 19.1º ($\mathbf{6}^+$) y 21.2º ($\mathbf{9}^+$) y en el derivado $\mathbf{8}^+$ el ligando 2-fenilpiridinato (ppy) exhibe un ángulo intermedio de 16.7º. En todos los complejos estudiados el ciclo de seis miembros PtN_4Y (Y = B, C) adopta una conformación tipo barca, típica en las estructuras de los derivados que se forman con este tipo de ligandos.[1b,8d,9,16] También se observa que en los derivados catiónicos $\mathbf{7}^+$ – $\mathbf{9}^+$ el ligando pirazolato libre exhibe una orientación *endo* en relación al centro de Pt, similar a lo observado en complejos relacionados publicados anteriormente por Ma[9] y Slugovc[8d]. El átomo de hidrógeno del

enlace Y-H (Y = B, C) está lo suficientemente lejos del centro de platino (Pt···H 3.210 **1**, 3.110 **3**, 2.982 Å $\mathbf{6}^{+}$) como para descartar un interacción agóstica Pt···H (Pt-H < 2.5 Å) del átomo de H orientado de forma *sym*.

El análisis del empaquetamiento de estas moléculas (Figuras A1.1–A1.6) indica algunos hechos significativos:

Los derivados neutros **1** (Figura A1.1) y **3** (Figura A1.2) y el catiónico **7** (Figura A1.3) se organizan en dímeros cabeza–cola, cola–cabeza a través de interacciones intermoleculares π···π entre los ligandos ciclometalados, con distancias de 3.298 **1**, 3.249 **3**, 3.399 Å **7**. Sin embargo, queremos destacar que no se ha observado influencia de estas interacciones en las propiedades ópticas. Por otra parte, las entidades catiónicas de los complejos **6** (Figura A1.4), **8** (Figura A1.5) y **9** (Figura A1.6) no muestran interacciones π···π entre los correspondientes ligandos ciclometalados, posiblemente debido a la presencia de los aniones PF_6^-, y en el caso de **8** y **9** debido, en parte, al voluminoso grupo pirazolato libre.

En la Figura 1.8 se muestra la estructura molecular del derivado $[Pt(bzq)(\mu\text{-}pz)]_2$. Las distancias y ángulos de enlace más relevantes se recogen en la Tabla 1.3. Este derivado de pirazolato puente $[Pt(bzq)(\mu\text{-}pz)]_2$ consiste en dos fragmentos "Pt(bzq)" unidos a través de dos ligandos pirazolato *exo*-bidentados.

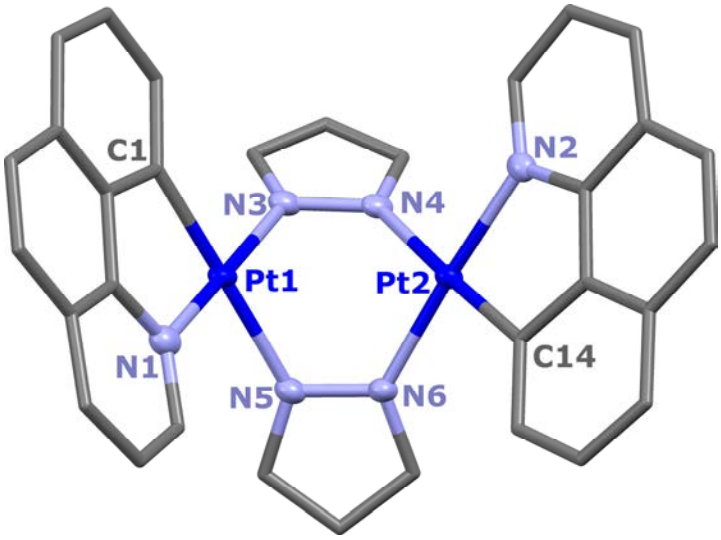

Figura 1.8: Estructura molecular del derivado $[Pt(bzq)\{\mu\text{-}pz\}]_2$

Tabla 1.3: Distancias [Å] y ángulos [º] para el derivado $[Pt(bzq)\{\mu\text{-}pz\}]_2$ (**11**)

Distancias [Å]		**Ángulos [º]**	
Pt(1)-N(1)	2.014(3)	N(1)-Pt(1)-C(1)	82.12(14)
Pt(1)-C(1)	1.994(3)	N(1)-Pt(1)-N(5)	94.18(12)
Pt(1)-N(3)	2.029(3)	N(3)-Pt(1)-N(5)	88.28(11)
Pt(1)-N(5)	2.065(3)	N(3)-Pt(1)-C(1)	95.30(13)
Pt(2)-N(2)	2.027(3)	N(2)-Pt(2)-C(14)	82.14(13)
Pt(2)-C(14)	1.989(3)	N(2)-Pt(2)-N(4)	95.72(11)
Pt(2)-N(6)	2.005(3)	N(6)-Pt(2)-N(4)	87.90(11)
Pt(2)-N(4)	2.080(3)	N(6)-Pt(2)-C(14)	94.24(13)
Pt(1)-Pt(2)	3.319		

Este complejo adopta una estructura en forma de mariposa, con el ciclo de 6 miembros "Pt_2N_4" central en conformación tipo bote con los dos platinos en los vértices del bote, similar a la encontrada en derivados relacionados de Pt^{II} con puentes pirazolato. Como se observa en la Figura 1.8, la molécula adopta una conformación *trans*, al igual que en los derivados $[Pt(ppy)\{\mu\text{-}pz\}]_2$,[14b] $[Pt(ppy)\{\mu\text{-}dmpz\}]_2$,[14b] $[Pt\{(2,4\text{-}F_2C_6H_2)py\}_2\{\mu\text{-}3\text{-}Me,5\text{-}^tBupz\}]$[9] y $[Pt(thpy)\{\mu\text{-}pz\}]_2$[13] [Hdmpz = 3,5-$(CH_3)_2$pz; thpy = tienilpiridina] y a diferencia de la conformación *cis* encontrada, por ejemplo, en $[Pt\{2,4\text{–}F_2C_6H_8)py\}\{\mu\text{-}R_2pz\}]_2$.[17]

Los dos átomos de platino presentan un entorno planocuadrado distorsionado formado por los dos átomos de N de los grupos pirazolato y los átomos de C y N coordinados del grupo ciclometalado. Los dos anillos pirazolato son prácticamente planos, formando un ángulo dihedral de 82.47º entre los planos creados por cada uno de ellos mostrando diferentes distancias Pt–N, lo que refleja la diferente influencia *trans* del C metalado y del N piridínico de los ligandos bzq. Las distancias Pt-N_{pz} más cortas las tienen los átomos de N *trans* a N(bzq) [Pt(1)-N(3) 2.029(3) Å, Pt(2)-N(6) 2.005(3) Å], mientras que las distancias Pt-N más largas las tienen el N_{pz} *trans* al C metalado [Pt(1)-N(5) 2.065(3) Å, Pt(2)-N(4) 2.080(3) Å]. Al igual que en los otros derivados de bzq (**1** y **7**) los anillos ciclometalados son prácticamente coplanares con el plano del platino y forman un ángulo dihedral de 82.47º entre ellos. Los centros de Pt están separados (3.319 Å) con una distancia comparable a la encontrada en los derivados $[PtCl(PPh_2Me)(\mu\text{-}dmpz)]_2$ (3.170 Å)[18] $[Pt(thpy)(\mu\text{-}pz)]_2$ (3.432 Å),[13] $[Pt(ppy)(\mu\text{-}pz)]_2$ (3.298 Å),[14b] $[Pt(ppy)(\mu\text{-}dmpz)]_2$ (3.196 Å),[14b] y $[Pt\{(2,4\text{-}F_2C_6H_2)py\}(\mu\text{-}R_2pz)]_2$ (2.8343-3.3763 Å).[17] Thomposon y col ha publicado que tanto la distancia Pt···Pt, como

el ángulo entre los fragmentos de platino parecen disminuir a medida que se colocan sustituyentes voluminosos en posición 3 y 5 en los ligandos pirazolato puente.[17]

Como se observa en la Figura 1.9, la estructura supramolecular de este derivado está basada en la formación de cadenas unidimensionales giradas creadas por dímeros. Estos dímeros se forman por interacciones π···π entre dos bzq de distintas moléculas con una distancia entre planos de 3.345 Å (Figura 1.9 en azul), que se refuerza por interacciones secundarias de tipo T entre los protones del anillo central de la bzq con el C y el N ciclometalado del otro ligando bzq (2.832, 2.741 Å) (Figura 1.9 en rojo). Estos dímeros se unen entre sí a través de interacciones intermoleculares π···π entre ligandos bzq de distintos dímeros (3.355 Å) (Figura 1.9 en verde) y de interacciones no clásicas entre $H_{pz}\cdots C_{pz}$ (2.889 Å) y $H_{pz}\cdots C_{ciclometalado}$ (2.813 Å) (Figura 1.9 en violeta) que provocan un giro en la cadena. Estas cadenas se unen mediante interacciones secundarias $H_{bzq}\cdots N_{bzq}/C_{bzq}$ (2.741 Å/ 2.830–2.630 Å), $C_{pz}\cdots C_{bzq}$ (3.132 Å), $H_{pz}\cdots C_{pz}$ (2.813 Å) y $C_{pz}\cdots C_{pz}$ (2.888 Å).

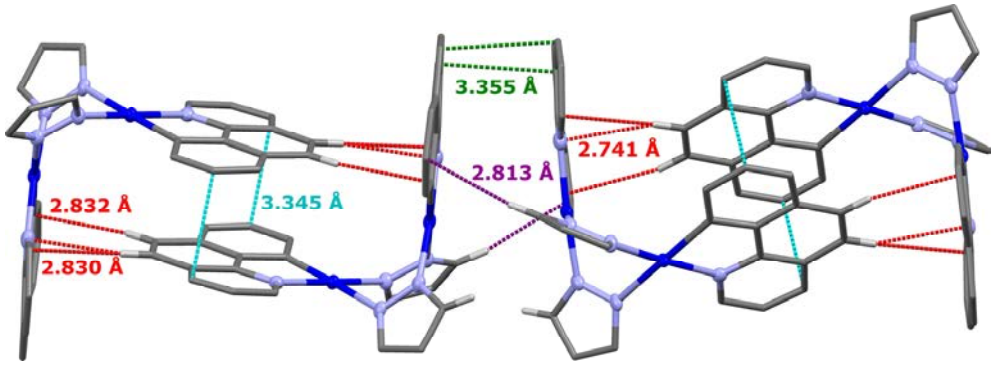

Figura 1.9: Formación de dímeros y principales interacciones intermoleculares en $[Pt(bzq)(\mu\text{-}pz)]_2$ (interacciones π···π dentro del dímero en azul y entre dímeros en verde, interacciones T dentro del dímero en rojo y entre dímeros en violeta)

1.3 Propiedades ópticas de los derivados 1–10

1.3.1 Espectros de Absorción

Se ha realizado un estudio de los espectros de absorción UV-visible de todos los compuestos en CH_3CN 5 x 10^{-5} M, en el que todos son solubles, y en los casos en los que la solubilidad lo ha permitido, se ha realizado un estudio en disolventes de distinta

polaridad (tolueno y CH_2Cl_2). Con objeto de asignar adecuadamente las bandas de absorción se han realizado los espectros de los ligandos $K[H_2B(pz)_2]$, $[H_2C(pz)_2]$, $[HC(pz)_3]$ y $K[HB(pz)_3]$, así como los de los ligandos ciclometalados protonados Hbzq, Hppy, Hpq en CH_3CN (5×10^{-5} M) y los datos se recogen en la Tabla A1.4. Así mismo los datos obtenidos para los derivados **1**–**10** en disolución se recogen en la Tabla 1.4.

Tabla 1.4: Datos de absorción UV-visible de los compuestos **1**-**10** en disolución 5×10^{-5} M en los disolventes indicados y en estado sólido (Medidas de Reflectancia difusa)

Compuesto	λ_{abs}/nm (10^3 ε $M^{-1}cm^{-1}$)
$[Pt(bzq)\{H_2B(pz)_2\}]$ **1**	279 (24.7), 317 (13.6), 333 (11.0), 368 (7.2), 423 (3.2) **Tolueno** 241 (61.0), 264 (53.6), 310 (13.4), 328 (10.2), 358 (5.7), 413 (2.6) **CH_2Cl_2** 195 (75.2), 210 (62.6), 250 (42.8), 306 (13.8), 324 (11.0), 353 (5.4), 405 (2.4) **CH_3CN** 256, 310, 365, 424, 465_h **sólido**
$[Pt(ppy)\{H_2B(pz)_2\}]$ **2**	287 (16.5), 317 (10.5), 332 (9.3), 356 (7.5), 403 (2.1) **Tolueno** 228 (46.8), 254 (25.6), 283 (14,3), 314 (6.4), 328 (6.4), 348 (5.7), 392 (0.7) **CH_2Cl_2** 199 (46.7), 212 (39.6), 227_h (22.6), 253 (26.9), 281_h (14.9), 313 (6.9), 325 (7.0), 341 (5.7), 389 (1.5) **CH_3CN** 250, 280, 318, 353, 400, 450_d, 485_d **sólido**
$[Pt(pq)\{H_2B(pz)_2\}]$ **3**	285 (26.3), 297 (32.8), 358 (13.8), 384 (10.6), 397 (10.8), 440 (4.6) **Tolueno** 228 (18.4), 257 (23.8), 292 (21.0), 356 (8.4), 386 (6.2), 430 (1.7) **CH_2Cl_2** 199 (32.0), 222 (26.8), 255 (24.8), 290 (20.6), 352 (81.2), 383 (6.4), 425 (2.2) **CH_3CN** 230, 258, 293, 362, 390, 435, 515_d **sólido**
$[Pt(bzq)\{H_2C(pz)_2\}]PF_6$ **4**	238 (31.2), 305 (15.3), 316_h (11.5), 344 (1.2), 389 (1.1), 406 (1.3) **CH_2Cl_2** 223 (50.0), 238 (58.4), 267 (45.4), 270 (41.4), 292_h (12.9), 300 (13.9), 339 (3.3), 389 (2.2) **CH_3CN** 245, 302, 345, 390, 403, 460_d **sólido**
$[Pt(ppy)\{H_2C(pz)_2\}]PF_6$ **5**	238 (28.6), 253 (33.2), 274 (39.2), 314 (10.6), 327 (10.8), 364 (2.9), 383 (2.2) **CH_2Cl_2** 223(50.0), 241 (54.7), 267 (44.9), 270 (43.5), 313 (7.6), 324 (8.6), 361 (2.9), 377 (2.4) **CH_3CN** 276, 327, 365, 381, 446_d, 478_d **sólido**
$[Pt(pq)\{H_2C(pz)_2\}]PF_6$ **6**	245 (25.4), 279 (32.4), 288_h (28.9), 341_h (10.0), 352 (13.4), 366_h (8.55), 403 (3.2) **CH_2Cl_2** 226 (23.0), 279 (29.2), 339_h (11.5), 350 (14.8), 366_h (9.2), 401(4.2) **CH_3CN** 248, 279, 288, 342_h, 352, 366, 404, 501_d, 534_d **sólido**
$[Pt(bzq)\{HC(pz)_3\}]PF_6$ **7**	229 (20.0), 274 (13.5), 290 (12.7), 302 (14.7), 324_h (7.5), 341 (3.7), 389 (2.2) **CH_3CN** 281, 345_h, 386, 405, 438_h **sólido**
$[Pt(ppy)\{HC(pz)_3\}]PF_6$ **8**	229 (20.0), 275 (14.6), 313 (6.2), 324 (6.8), 358 (1.8), 377_h (1.4) **CH_3CN** 258, 328, 366, 386, 445_d, 465_d **sólido**
$[Pt(pq)\{HC(pz)_3\}]PF_6$ **9**	238 (28.3), 281 (29.9), 336_h (8.8), 351 (12.8), 365_h (8.6), 402 (3.4) **CH_2Cl_2** 229 (17.6), 279 (20.0), 336_h (6.0), 350 (8.4), 368_h (5.6), 402 (2.2) **CH_3CN** 237, 285, 356, 371_h, 410 **sólido**
$[Pt(pq)\{HB(pz)_3\}]$ **10**	230 (24.0), 256 (30.7), 284_h (22.8), 292 (25.8), 342_h (8.2), 355 (11.1), 379 (7.9), 429 (2.4) **CH_2Cl_2** 223 (50.4), 242 (57.2), 266 (48.4), 289 (27.9), 341_h (9.0), 352 (11.5), 379 (8.5), 420 (3.5) **CH_3CN** 232_h, 278, 348, 398, 440_h, 497_d, 530_d **sólido**

Fundamentalmente, los ligandos poli(pirazolil)borato o metano muestran bandas intensas en el rango 223–270 nm, mientras que los ligandos C^NH (ppyH, bzqH, pqH) muestran además de bandas intensas en la zona 225–275 nm, bandas de menor intensidad en la región 292-345 (Hbzq), 296 (Hppy) y 284-336 (Hpq).

Los derivados **1–10** exhiben varias absorciones intensas en la zona de alta energía (región en CH_3CN: 229–330 nm), que pueden ser atribuidas a transiciones intraligando ^{1}IL ($\pi\pi^*$) centradas en los ligandos ciclometalados (L) y poli(pirazolil)borato o metano (L'), quizás algo perturbadas por la coordinación al metal. Las absorciones en la región comprendida entre 330-370 nm están muy mezcladas, según se deriva del estudio teórico TD-DFT en **1**, **7** y **9** (ver Sección 1.5, Tabla A1.7 para asignaciones detalladas) y se atribuyen a transiciones intraligando y/o de transferencia de carga metal-ligando y ligando–ligando (^{1}ILCT, ^{1}MLCT, ^{1}ML'CT y ^{1}L'LCT).

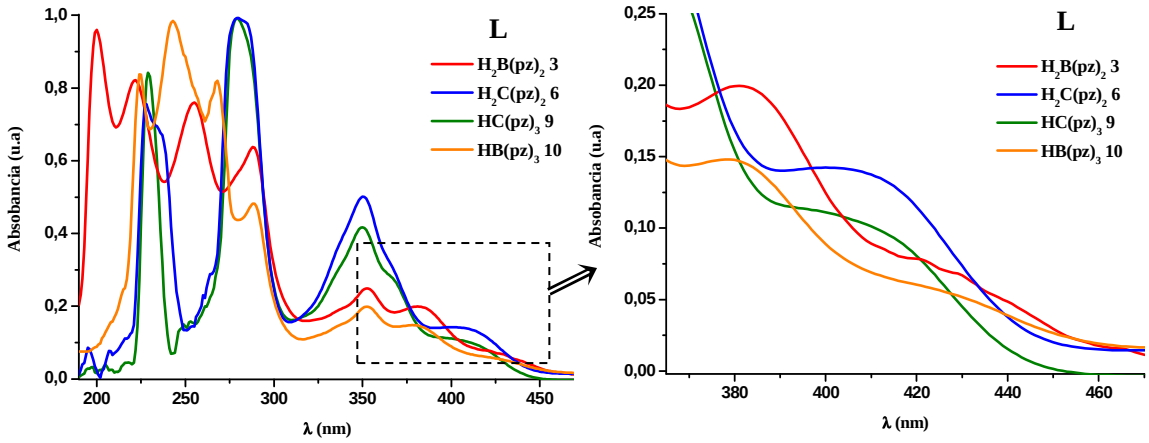

a) b)

Figura 1.10: a) Espectros de absorción normalizados de los compuestos [Pt(pq)L_2] **3**, **6**, **9** y **10** en CH_3CN b) Zona ampliada de baja energía de los espectros de absorción para la serie de compuestos **3**, **6**, **9** y **10**

Además, todos ellos muestran una banda de absorción de menor energía e intensidad ($\varepsilon = 1.4–4.2 \times 10^3$ $M^{-1}cm^{-1}$) que de acuerdo a estudios previos, puede ser adscrita a una mezcla de transiciones ^{1}IL/^{1}MLCT. Esta banda de baja energía muestra cierta dependencia con el coligando poli(pirazolil)borato o metano (L') y con el ligando ciclometalado (L) (Figura 1.10). Así, si se comparan los espectros en CH_3CN de estos

compuestos manteniendo fijo el ligando ciclometalado y variando el ligando nitrogenado, se observa en todos los casos la misma secuencia [**bzq**: 405 (**1**), 389 (**4**), 389 (**7**) nm; **ppy** 389 (**2**), 377 (**5**), 377 (**8**) nm; **pq** 425 (**3**), 401 (**6**), 402 (**9**) nm (CH_3CN)] con valores más desplazados hacia el rojo para los derivados neutros de bis(pirazolil)borato $[H_2B(pz)_2]^-$ (**1**, **2** y **3**) y prácticamente iguales en los derivados catiónicos de $H_2C(pz)_2$ y $HC(pz)_3$ (**4** y **7**; **5** y **8**; **6** y **9**). El derivado **10**, único ejemplo con el ligando tris(pirazolil)borato $[HB(pz)_3]^-$, también muestra un desplazamiento hacia el rojo en relación a los de carbono [425 nm (**10**) *vs* 401 (**6**), 402 nm (**9**)] e igual al derivado **3** con $[H_2B(pz)_2]^-$ (425 nm). El desplazamiento hacia el azul en los derivados catiónicos en relación a los neutros análogos se puede explicar considerando una mayor contribución de la transición intraligando ^{1}IL [$\pi\rightarrow\pi^*$(C^N)], junto con menor carácter ^{1}MLCT en las bandas de baja energía, como se deduce también de los cálculos DFT (Sección 1.5)

Como puede verse en la Figura 1.11a, las bandas de baja energía también están influenciadas por la variación del ligando ciclometalado. Para todas las series de compuestos con el mismo ligando ciclometalado se observa un comportamiento bastante similar. En general, se observa un notable desplazamiento a mayores longitudes de onda en los derivados de 2-fenilquinoleína (pq), localizándose a menores λ los derivados de benzoquinoleína (bzq) y finalmente a mayores energías los de 2-fenilpiridina (ppy) [425 (**3**) › 405 (**1**) › 389 (**2**); 401 (**6**) › 389 (**4**) › 377 (**5**); 402 (**9**) › 389 (**7**) › 377 nm (**8**)]. El desplazamiento hacia el rojo de los compuestos de pq en relación a los de bzq y a los de ppy está de acuerdo con la mayor deslocalización electrónica del grupo bzq en relación al grupo ppy y a la mayor capacidad π-aceptora del ligando pq.

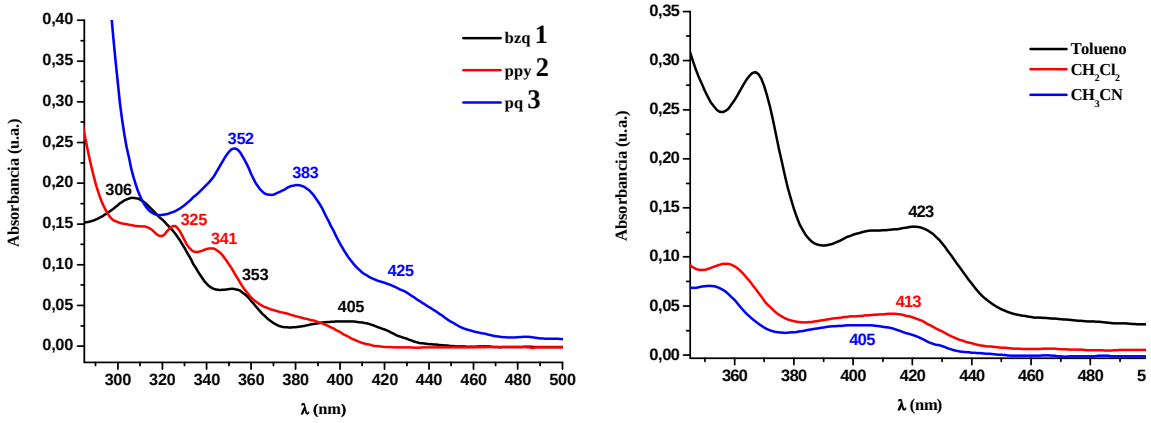

a) b)

Figura 1.11: Zona de baja energía de los espectros de absorción de a) los compuestos **1**, **2** y **3** y b) **1** en disoluciones 5 x 10^{-5} M de diferentes disolventes, mostrando solvatocromismo negativo

Como se indica en la Figura 1.11b, estas bandas de baja energía experimentan un desplazamiento solvatocrómico negativo, ya que se desplazan hacia el rojo al disminuir la polaridad de los disolventes [CH_3CN, CH_2Cl_2, tolueno; por ejemplo (**1**): 405, 413, 423 nm; (**2**): 389, 392, 403 nm; (**3**) 425, 430, 440 nm], lo que indica que el estado fundamental es más polar que el estado excitado,[19] sugiriendo una cierta componente de transferencia de carga para estas transiciones. Los cálculos teóricos llevados a cabo (Ver Sección 1.5) sugieren una considerable mezcla de orbitales para estas transiciones fundamentalmente ^{1}ILCT/^{1}MLCT/^{1}ML'CT en el complejo neutro **1**, que contiene el grupo $[H_2B(pz)_2]^-$. Sin embargo en la serie de compuestos catiónicos con el ligando $HC(pz)_3$ (**7–9**) esta transición es de naturaleza principalmente ^{1}ILCT combinado con cierto carácter de transferencia de carga del Pt a ambos ligandos (^{1}MLCT/^{1}ML'CT para **9** o al ligando tris(pirazolil)metano (^{1}ML'CT) en **7** y **8**.

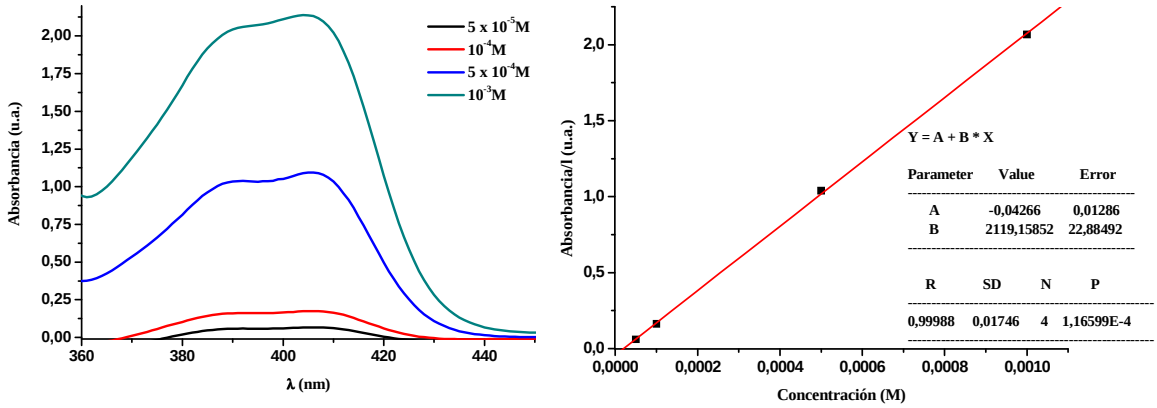

a) b)

Figura 1.12 a) Expansión de la región de baja energía de los espectros de absorción de UV-visible del complejo **4** en CH_2Cl_2 a 298 K a diferentes concentraciones. b) Representación del ajuste lineal de la absorbancia a 392 nm frente a la concentración

Como es de esperar estas bandas de baja energía a ~400 nm siguen en todos los compuestos la ley de Lambert-Beer en el rango de concentraciones 5 x 10^{-5} M a 10^{-3} M, lo que nos permite excluir la existencia de procesos de agregación en el estado fundamental (Figura 1.12).

Además, debemos señalar que algunos derivados muestran bandas de intensidad muy débil ($\varepsilon < 50\ \mu^{-1}cm^{-1}$) a muy baja energía [462 (**1**), 445, 478 (**2**), 502, 537 (**3**), 459 (**4**), 443, 475 (**5**), 493, 532 (**6**), 494, 531 nm (**9**)] en disoluciones muy concentradas (10^{-2} - 10^{-3} M, CH_2Cl_2) (Figura A1.7 para **3**). Para estudiar el efecto de la concentración de la disolución sobre la intensidad de estas bandas, se registraron los espectros de absorción UV-visible del compuesto **3** en el rango de concentraciones 10^{-2}–10^{-3} M, encontrándose que estas bandas (502, 537 nm) no obedecen la ley de Lambert-Beer en ese rango de concentración. Aunque no se puede excluir la existencia de procesos de oligomerización en el estado fundamental a altas concentraciones, estas bandas son tentativamente atribuidas a la población directa de estados triplete de carácter mixto ILCT/MLCT/ML'CT/LL'CT, facilitado por el acoplamiento spín-órbita asociado al ión Pt^{II}. Este tipo de transiciones se encuentran formalmente prohibidas por las reglas de selección, por lo que su observación en los espectros de absorción no es frecuente. Sin embargo, se han observado previamente a energías similares y con muy baja intensidad en algunos compuestos de Pt con ligandos ciclometalados.[20]

Los espectros de absorción en estado sólido se obtuvieron usando la transformación Kubelka-Munk a partir de los espectros de Reflectancia Difusa en el estado sólido. Todos ellos muestran bandas similares a las encontradas en disolución, incluidas las bandas de baja energía observadas en disoluciones concentradas (10^{-2} M) y a energías muy parecidas (Figura 1.13). Esto indica que las posibles interacciones $\pi\cdot\cdot\pi$ entre monómeros afectan muy poco a los máximos de absorción.

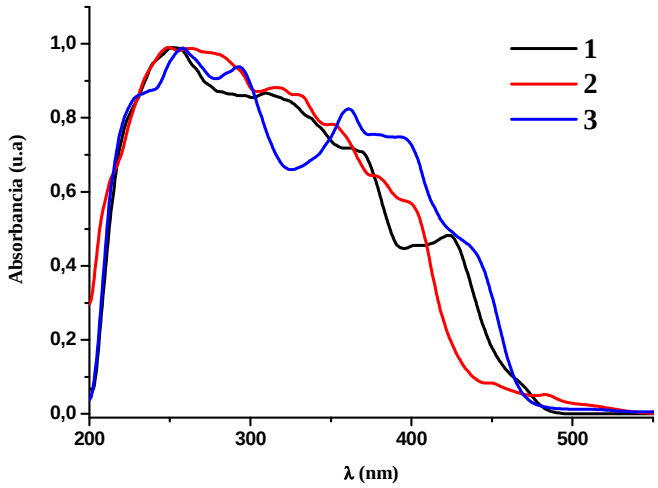

Figura 1.13: Espectros de Absorción normalizados calculados de sus espectros de Reflectancia difusa de **1**, **2** y **3** en estado sólido

1.3.2 Espectros de Emisión

Los compuestos **1–10** son en general luminiscentes tanto a Tª ambiente como a baja Tª en estado de matriz rígida (77 K, sólido y vidrio congelado). En la Tabla 1.5 se recogen los datos extraídos de los estudios de luminiscencia en estado sólido a 298 K y a 77 K y en las Tablas 1.6 y A1.5 se encuentran los datos obtenidos a 298 K y 77 K en disolución de CH_3CN y otros disolvente, respectivamente.

Estado Sólido

En estado sólido a temperatura ambiente (298 K) todos los compuestos (excepto los derivados **4** y **10**) exhiben luminiscencia (Tabla 1.5, Figuras 1.14–1.15), mostrando una banda ancha estructurada con espaciados vibrónicos de ~1200-1300 cm^{-1},

característicos de los ligandos ciclometalados, lo que indica su participación en el estado emisivo.

Tabla 1.5**:** Datos de emisión y tiempos de vida media de los derivados **1**–**10** en estado sólido a 298 y 77 K

Compuesto	T[a] (K)	λ_{em}/nm (λ_{exc}/nm)	τ/μs
[Pt(bzq){$H_2B(pz)_2$}]	298	519_{max}, 560, 590 (330-470)	11.4 (519); 12.3 (590)
1	77	520_{max}, 560, 600 (340-460)	11.4 (87%); 66.5 (13%) (520)
[Pt(ppy){$H_2B(pz)_2$}]	298	490, 520_{max}, 560, 590_{sh} (310-410)	8.0 (490)
2	77	490, 524_{max}, 560, 590_{sh} (330-450)	9.5 (490); 9.2 (560)
[Pt(pq){$H_2B(pz)_2$}]	298	580, 610_{max}, 670_{sh} (400-450)	8.8(580)
3	77	580_{max}, 610, 660_{sh} (340-510)	9.8(580)
[Pt(bzq){$H_2C(pz)_2$}]$^+$	298	No presenta emisión	
4	77	500_{max}, 537, 570, 612_{sh} (350-460)	308 (500/570)
[Pt(ppy){$H_2C(pz)_2$}]$^+$	298	511, 530_{max}, 580_h (345-450)	10.2(530)
5	77	507, 543_{max}, 580 [a] (310-450)	11.3(507)
[Pt(pq){$H_2C(pz)_2$}]$^+$	298	560, 591_{max} [b] (350-440)	8.6(560/645)
6	77	555, 594_{max} [b] (350-440)	14.7(555)
[Pt(bzq){$HC(pz)_3$}]$^+$	298	514, 552_{max}, 590[b] (370-450)	9.5(514); 12.4(550)
7	77	505_{max}, 546, 590 (370-450)	192 (64%), 18.7 (36%) (505)
[Pt(ppy){$HC(pz)_3$}]$^+$	298	503, 528_{max}, 566_h (330-390)	9.5(503)
8	77	505_{max}, 540, 575, 610 (370-440)	11.3(505)
[Pt(pq){$HC(pz)_3$}]$^+$	298	557, 592_{max}, 630_h (370-440)	8.7(592)
9	77	590_{max}, 630, 670_h (370-440)	12.3(590)
[Pt(pq){$HB(pz)_3$}]	298	No presenta emisión	
10	77	604[b] (390-550)	11.1(604/665)

a) cola hasta 650 nm, b) cola hasta 750 nm

La variación del ligando ciclometalado produce un evidente impacto en los máximos de emisión y se observa la misma secuencia en las distintas series. Así, en las series $[Pt(C\wedge N)L_2]^{n+}$ [n = 0, L_2= $\{H_2B(pz)_2\}^-$ **1**–**3**; n = 1, L_2 =$\{H_2C(pz)_2\}$ **4**–**6**; $\{HC(pz)_3\}$ **7**–**9**] los máximos de emisión en estado sólido a 298 K se desplazan siempre hacia el rojo siguiendo el orden: ppy < bzq < pq [490 nm (**2**), 519 (**1**), 580 nm (**3**) (Figura 1.14a); 511 (**5**), 560 nm (**6**), 503 (**8**), 514 (**7**), 557 nm (**9**)], de acuerdo con una conjugación más extendida del ligando ciclometalado.

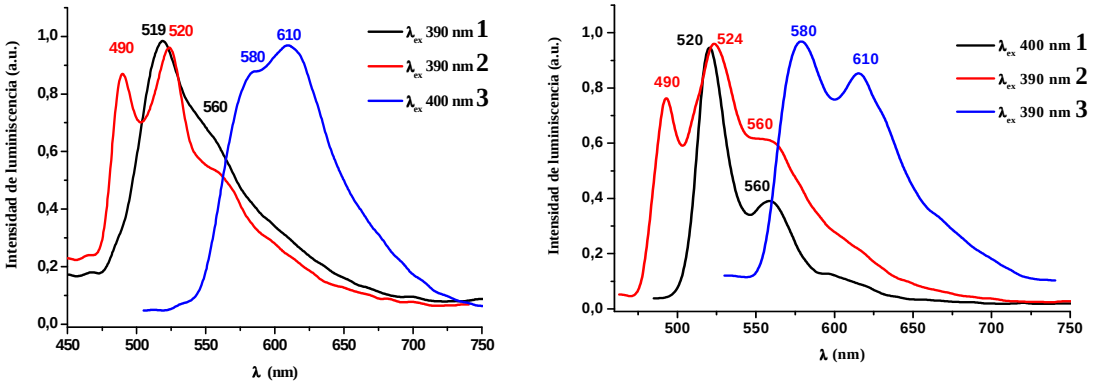

(a) (b)

Figura 1.14: Espectros de emisión de los compuestos **1**, **2** y **3** a) en estado sólido a 298 K y b) en estado sólido a 77 K (λ_{ex} 390–400 nm)

La correlación en los máximos de la emisión con los cambios de los ligandos poli(pirazolil)borato o metano es algo menos clara. Así, en los derivados con benzoquinolato (bzq) (**1**, **4** y **7**) y con fenilquinolato (pq) (**3**, **6** y **9**) el máximo aparece a energías más altas en los derivados catiónicos, con los grupos poli(pirazolil)metano, que en los neutros con el grupo bis(pirazolil)borato [500 nm (**4**), 514 (**7**) *vs* 519 nm (**1**); 560 (**6**), 557 (**9**) *vs* 580 nm (**3**)] (Figura 1.15a para la serie con pq). Este comportamiento es coherente con la previsible estabilización del HOMO basado en una mezcla Pt/C^N y el consiguiente incremento del gap HOMO–LUMO al aumentar la carga en el centro de platino y, en consecuencia con un carácter de transferencia de carga Metal–Ligando (ortometalado) en el estado excitado (^{3}MLCT). Sin embargo, como puede apreciarse en la Figura 1.15b, en los derivados con la fenilpiridina (ppy **2**, **5** y **8**) la emisión aparece a energías más altas en el derivado neutro que en los catiónicos [490 nm (**2**) *vs* 511 (**5**) y 503 nm (**8**)], lo que puede sugerir una cierta contribución de los ligandos bis y tris (pirazolil)metano en las transiciones (cierto carácter ^{3}ML'CT), que más adelante se confirman con ayuda de la optimización del estado triplete en el compuesto **8** (Sección 1.5).

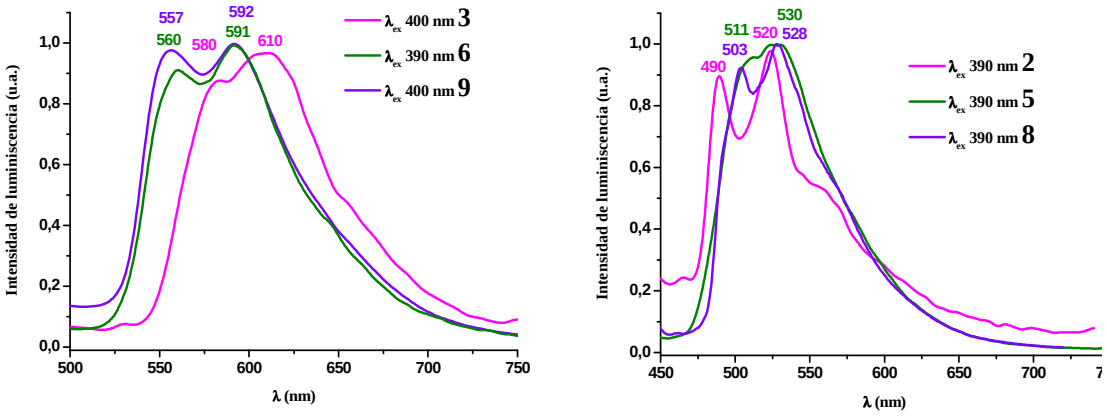

a) b)

Figura 1.15: Espectros de emisión de los compuestos a) **3**, **6** y **9** (serie de pq) en estado sólido a 298 K y b) **2**, **5** y **8** (serie de ppy) en estado sólido a 298 K (λ_{ex} 390–400 nm)

Al disminuir la Tª (77 K), estas emisiones aumentan su intensidad de manera considerable observándose, en general, la misma regularidad en los máximos de emisión al variar el ligando ciclometalado o los ligandos poli(pirazolil)borato o metano comentada anteriormente. El derivado neutro [Pt(pq){HB(pz)$_3$}] (**10**) muestra a 77 K, al igual que su homólogo catiónico con {HC(pz)$_3$} (**9**), una banda ancha asimétrica, aunque como es de esperar, desplazada al rojo respecto al complejo **9** (604 **10** *vs* 590 nm **9**).

En general la forma estructurada de las bandas, típica de monómeros, y los largos tiempos de vidas medias (8.0 – 11.4 μs 298 K; 9.5 – 308 μs 77 K), característicos de estado triplete, indican que las emisiones provienen presumiblemente de transiciones con mezcla de contribuciones intraligando y Metal – ligando ortometalado ^{3}ILCT/^{3}MLCT, aunque como ya hemos señalado en los derivados **2**, **5** y **8** con el ligando 2-fenilpiridinato, que es el menos aceptor, no se puede descartar una cierta contribución de los coligandos poli(pirazolil)borato o metano (^{3}ML'CT). Sin embargo, los derivados de bzq en estado sólido a 77 K muestran valores de vidas medias muy elevados [**1**: 66.5 (13%), 11.4 μs (87%); **4**: 308 μs; **7**: 192 (64%); 18.7 μs (36%)] comparados con lo observado en los derivados de ppy y pq, lo que sugiere que la componente ^{3}ILCT es particularmente remarcable en los derivados de benzoquinoleína. Este comportamiento ya ha sido previamente observado en complejos catiónicos ciclometalados de Pt(II) con ligandos bis(difenilfosfino)alcano donde los derivados con

el grupo benzoquinolato presentan valores más elevados de vidas medias en relación con los derivados de otros grupos heterocíclicos.[15d,21] Este hecho ha sido atribuido a una menor diferencia energética en el estado excitado singlete–triplete en los compuestos con el ligando bzq, lo que conduce a cruces intersistémicos más efectivos y a mayores valores de vida media.[15d,21b]

Disolución y vidrios congelados

Todos los derivados son emisivos en disolución a 298 K y en vidrios congelados a 77 K. Debido a que **7** y **8** son sólo solubles en CH_3CN, con fines comparativos, se han llevado a cabo las medidas de todos los compuestos en este disolvente. Además, los espectros de los derivados **1**–**6, 9, 10** se han registrado en CH_2Cl_2 y los de **1** y **2** en tolueno. Los datos en CH_3CN se recogen en la Tabla 1.6 y en el resto de disolventes en la Tabla A1.5.

Al igual que en estado sólido las propiedades ópticas en disolución muestran una fuerte dependencia con la naturaleza del ligando ciclometalado y en algunos casos, aunque en menor medida, con la de los grupos poli(pirazolil)borato o metano. A continuación se realizará un estudio detallado de las propiedades emisivas de estos derivados en disolución en función de sus distintos ligandos.

Tabla 1.6: Datos de emisión de todos los derivados (**1–10**) en disolución de CH_3CN a 298 y 77 K

Compuesto	Concentración /M (T^a/K)	λ_{em}/nm (λ_{exc}/nm)
[Pt(bzq){$H_2B(pz)_2$}] **1**	10^{-3} (298)	485_{max}, 520, 550 (385–450)
	10^{-4} (298)	350, 365, 380, 485_{max}, 500, 550_h (280)
		485_{max}, 500, 550_h (330-410)
	5×10^{-5} (298)[a]	350, 365, 380, 485_{max}, 500, 550_{sh} (280)
		485_{max}, 500, 550_h (330-410)
	5×10^{-5} (77)[b]	480_{max}, 515, 560 (285-420)
[Pt(ppy){$H_2B(pz)_2$}] **2**	10^{-3} (298)	480_{max}, 510, 560, 600_h (360–450)
	5×10^{-5} (298)[a]	430, 480_{max}, 510, 545, 590_h (280–330)
		480_{max}, 515, 545, 600 (350–380)
	5×10^{-5} (77)[b]	480_{max}, 520, 550 (280–400)
[Pt(pq){$H_2B(pz)_2$}] **3**	10^{-3} (298)	590_{max}, 660_h (420–450)
	5×10^{-5} (298)	447, 590_{max} (350–380)
		590_{max}, 660_h (420)
	10^{-3} (77)	580_{max}, 610, 660_h (330–440)
	5×10^{-5} (77)	560_{max}, 600, 655_h (350–430)
[Pt(bzq){$H_2C(pz)_2$}]$^+$ **4**	10^{-3} (298)	474, 493[c] (362, 421)
	10^{-4} (298)	350, 365_{max}, 480_a (280)
		365_{max}, 480_a (330–350)
	5×10^{-5} (298)[a]	350, 365_{max}, 480_a (280)
		365_{max}, 480_a (330–350)
	10^{-3} (77)	500_{max}, 535, 566, 620_h (330–400)
	5×10^{-5} (77)	478_{max}, 512, 550, 600_h (300–400)
[Pt(ppy){$H_2C(pz)_2$}]$^+$ **5**	10^{-3} (298)	479_{max}, 512, 546, 586_h (390)
	5×10^{-5} (298)[a]	479_{max}, 512, 546, 586 (290–380)
	5×10^{-5} (77)	487_{max}, 522, 554[c] (330–380)
[Pt(pq){$H_2C(pz)_2$}]$^+$ **6**	10^{-3} (298)	565_{max}, 591[c] (440)
	5×10^{-5} (298)[a]	560_{max}, 590 [c] (345–400)
	10^{-3} (77)	563_{max}, 605, 646_h[c] (355–420)
	5×10^{-5} (77)[a]	556_{max}, 598, 650_h[c] (355–420)
[Pt(bzq){$HC(pz)_3$}]$^+$ **7**	10^{-3} (298)	440_{max}, 480_h, 520_h (360)
		480_{max}, 520_h (425)
	10^{-4} (298)	349_{max}, 365, 383 (270– 330)
		440_{br} (360)
	5×10^{-5} (298)[a]	349_{max}, 365, 383 (270–330)
		440_{br} (360)
	10^{-3} (77)	496, 535, 612_{max}, 660_h (360–430)
	5×10^{-5} (77)	485_{max}, 520, 560, 620 (340–400)
[Pt(ppy)$HC(pz)_3$]$^+$ **8**	10^{-3} (298)	477_{max}, 511_{max}, 530, 560_h (350–390)
	5×10^{-5} (298)	340 (280)
		428, 478_{max}, 512, 535, 560_h (330)
		478_{max}, 512, 535, 560 (360–380)
	5×10^{-5} (77)[d]	480_{max}, 520, 550, 590_h (330–380)
[Pt(pq){$HC(pz)_3$}]$^+$ **9**	10^{-3} (298)	562, 592_{max}, 640_h (440)
	5×10^{-5} (298)	561, 590_{max}, 640_h (350–390)
	5×10^{-5} (77)[b]	561_{max}, 597, 640 (350–420)
[Pt(pq){$HB(pz)_3$}] **10**	10^{-3} (298)	590_{max}[c] (444)
	5×10^{-5} (298)[a]	590_{max}[c] (350–420)
	5×10^{-5} (77)[b]	560_{max}, 602, 652 (355–430)

a) Idéntico espectro a 10^{-4} M, b) Idéntico espectro a 10^{-3} y 10^{-4} M, c) Cola hasta 650 nm.

En disoluciones diluidas (5 x 10^{-5} M) desoxigenadas de CH_3CN los compuestos de la serie **[Pt(bzq)(L_2)]$^{n+}$** [n = 0, L_2 = {$H_2B(pz)_2$}$^-$ **1**; n = 1, L_2 = {$H_2C(pz)_2$}**4**; {$HC(pz)_3$}**7**] muestran un interesante comportamiento a 298 K. **1** y **4** exhiben dos emisiones estructuradas claramente diferentes: una de alta energía centrada a ~350 nm, obtenida por excitación a altas energías (λ_{ex}< 330 nm) y otra de baja energía en el rango 485-566 nm, obtenida por excitación a λ_{ex} > 350 nm, cuyos espectros de excitación reproducen los espectros de absorción en la región de baja energía (Figura 1.16a para **1**). La banda estructurada de alta energía claramente se origina de un estado excitado permitido de espín (fluorescencia) $^1\pi\pi^*$ centrado en el ligando bzq. Esta asignación se lleva a cabo teniendo en cuenta el pequeño desplazamiento de Stokes entre los espectros de excitación y de emisión, la similitud con el espectro del ligando libre (Hbzq = 349, 366 y 385 nm) y la comparación con sistemas de bzq relacionados, en los que esta emisión dual es rara, pero no inusual.[20b,20d] Al igual que en los espectros de absorción, la emisión fosforescente de baja energía en el derivado catiónico experimenta un ligero desplazamiento hipsocrómico en relación al neutro (485 **1** *vs* 480 nm **4**), por lo que se asigna a un estado excitado centrado en el ligando ciclometalado ^{3}ILCT, con cierto carácter de transferencia de carga ^{3}MLCT. De acuerdo con esta asignación, al registrar el espectro sin desoxigenar previamente la disolución, la banda de baja energía decrece considerablemente en intensidad confirmando así que se debe a fosforescencia, que se desactiva en presencia de O_2 molecular,[22] mientras que la banda de alta energía no se modifica (Figura 1.16b). Al registrar estas emisiones en función del tiempo de retraso desde la excitación, se ha encontrado un similar *decay* para la fluorescencia y la fosforescencia (Figura 1.16c), lo que sugiere que la señal de alta energía se trata de una *fluorescencia retardada*, que tiene lugar cuando se observa la emisión desde un estado singlete en equilibrio térmico con un estado triplete, y en consecuencia, con un tiempo de vida media más largo. Este tipo de emisión tiene precedentes en la química del platino.[20d,23] La comparación entre **1** y **4** indica que la presencia de fluorescencia es más determinante en el compuesto **4** que en el **1** en las mismas condiciones de ausencia de O_2 (Figuras 1.16a y d).

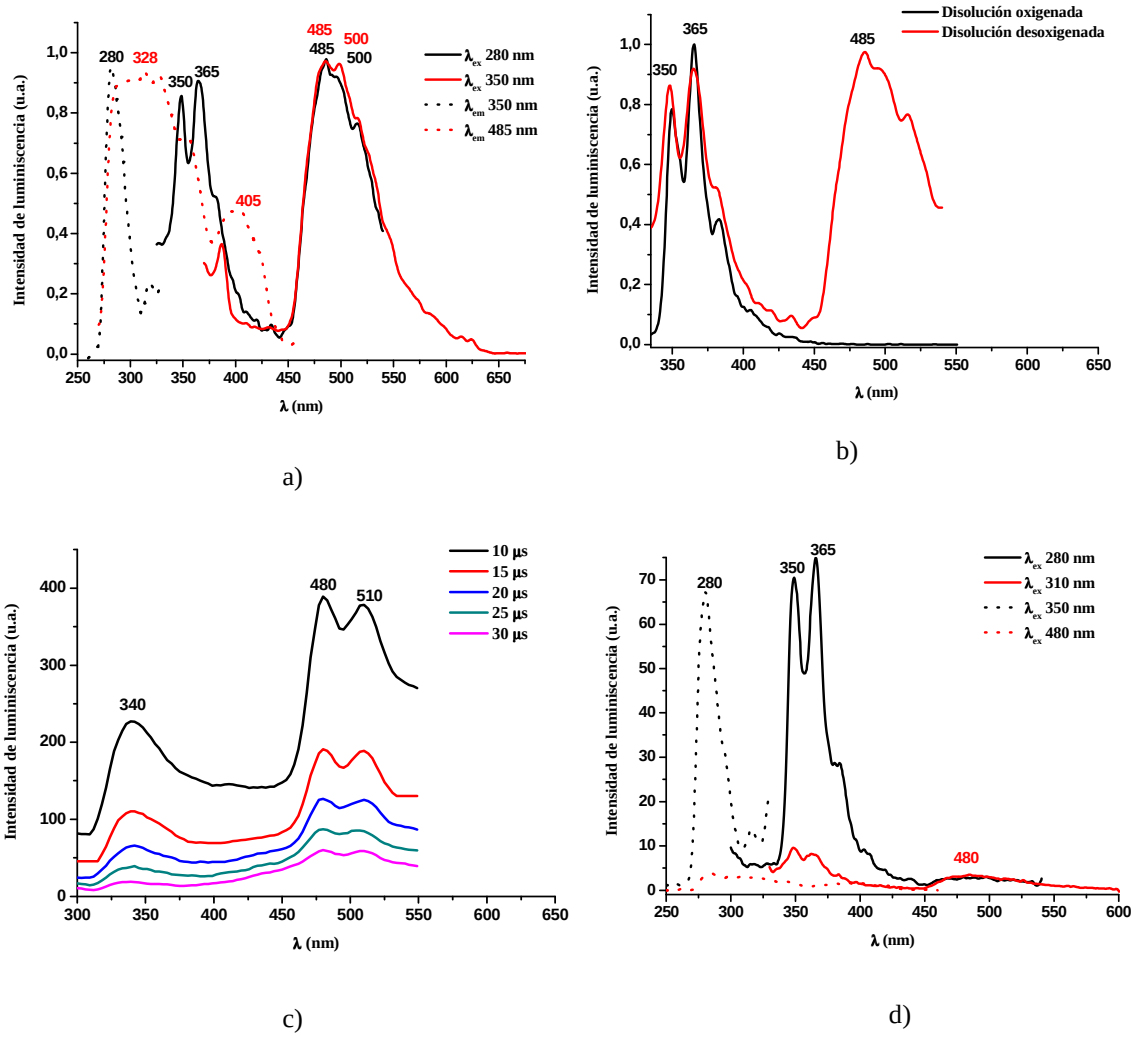

Figura 1.16: Espectros de excitación (líneas punteadas) y emisión (líneas continuas) normalizados de **1** en CH_3CN (5 x 10^{-5} M) a 298 K, a) desoxigenado, b) sin desoxigenar, c) resuelto en el tiempo, (λ_{ex} 285 nm) d) Espectros de excitación y emisión normalizados de **4** en CH_3CN (5 x 10^{-5}M) a 298 K

Curiosamente el compuesto catiónico **7** con el ligando [$HC(pz)_3$] no muestra fosforescencia de baja energía en disoluciones desoxigenadas diluidas de CH_3CN (5 x 10^{-5} M), probablemente debido a la presencia del átomo de N del grupo pirazolato libre, que puede interactuar con el centro de platino desactivando el estado excitado triplete ^{3}MLCT. Así, este compuesto exhibe la banda estructurada de fluorescencia de alta energía (~350 nm) por excitación a λ_{ex}< 330 nm, mientras que con λ_{ex}> 350 nm presenta una banda ancha no estructurada a ~440 nm, cuyo espectro de excitación (relacionado con un pico a 360 nm) varía del obtenido recogiendo en la banda de alta energía, lo que sugiere un estado emisivo diferente (Figura 1.17). Al aumentar la concentración (10^{-4} y 10^{-3} M) esta emisión se favorece en relación a la fluorescencia, que desaparece a 10^{-3} M, por lo que se asigna tentativamente a un excímero de

fluorescencia.[24] Una emisión similar ha sido observada previamente en el derivado $[Pt(bzq)(NCMe)_2](ClO_4)$.[20d]

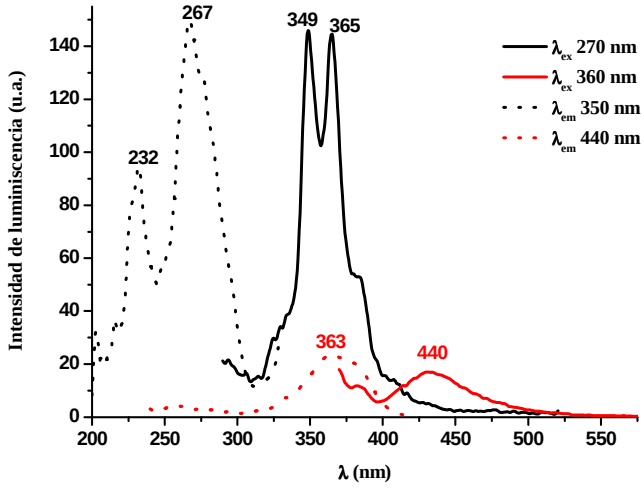

Figura 1.17: Espectros de excitación y emisión sin normalizar de **7** en CH_3CN (5×10^{-5} M) a 298 K

El efecto del disolvente se estudió en **1** (Ver Tablas 1.6 y A1.5), observándose prácticamente el mismo comportamiento en CH_3CN y en CH_2Cl_2, modificándose batocrómicamente el máximo de la emisión de fosforescencia (485 CH_3CN *vs* 487 nm en CH_2Cl_2), mientras que en tolueno, disolvente menos polar, se pierde la fluorescencia, observándose únicamente la banda ^{3}ILCT/^{3}MLCT, notablemente desplazada a 491 nm. Este resultado parece indicar que al disminuir la polaridad del disolvente se estabiliza el estado triplete ^{3}ILCT/^{3}MLCT en relación al estado singlete y el equilibrio entre ambos estados se dificulta desapareciendo la fluorescencia con retardo.

En la serie **$[Pt(ppy)(L_2)]^{n+}$** [n = 0, L_2 = $\{H_2B(pz)_2\}^-$ **2**; n = 1, L_2 =$\{H_2C(pz)_2\}$ **5**; $\{HC(pz)_3\}$ **8**], también los dos primeros compuestos **2** y **5** muestran un comportamiento en CH_3CN diferente al tercero (**8**). No obstante, en esta serie, los derivados **2** y **5** no muestran fluorescencia. Así **2** y **5** exhiben una emisión estructurada muy similar en la zona verde-azulada (480 **2**; 479 nm **5**) con un espaciamiento vibrónico claro (~1300 cm^{-1}), por lo que se asigna a fosforescencia fundamentalmente ^{3}ILCT, mezclado con algo de ^{3}MLCT. El efecto del disolvente se estudió con detalle en el compuesto **2**, observándose el mismo comportamiento con máximos de emisión ligeramente desplazados al rojo al disminuir la polaridad del disolvente, igual que en la serie anterior (480 CH_3CN, 485 CH_2Cl_2 y 487 nm Tolueno) (Figura 1.18) (Tablas 1.6 y A1.5).

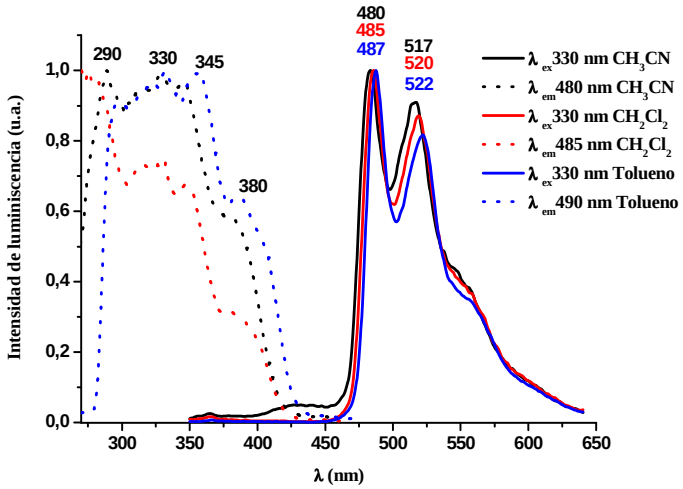

Figura 1.18: Espectros de excitación y emisión de **2** en CH_3CN, CH_2Cl_2 y Tolueno (5 x 10^{-5}M) a 298 K

El compuesto catiónico **8** con el ligando [$HC(pz)_3$] en disolución de CH_3CN (5 x 10^{-5} M) muestra a 298 K un comportamiento distinto, a pesar de que todas las disoluciones se han desoxigenado de igual forma. Por excitación a λ_{ex} 280 nm se observa la banda de fluorescencia del ligando ciclometalado $^1(\pi\pi^*)$, mientras que excitando a 360 nm se observa la banda estructurada de fosforescencia (^{3}ILCT/^{3}MLCT) y una banda ancha no estructurada a 428 nm, asignada al igual que en **7**, a excímero de fluorescencia, relacionada con un máximo de excitación a 377 nm (Figura 1.19). Probablemente, la presencia del pirazol libre y su proximidad con el centro de platino podría estar relacionado con la aparición de esta emisión.

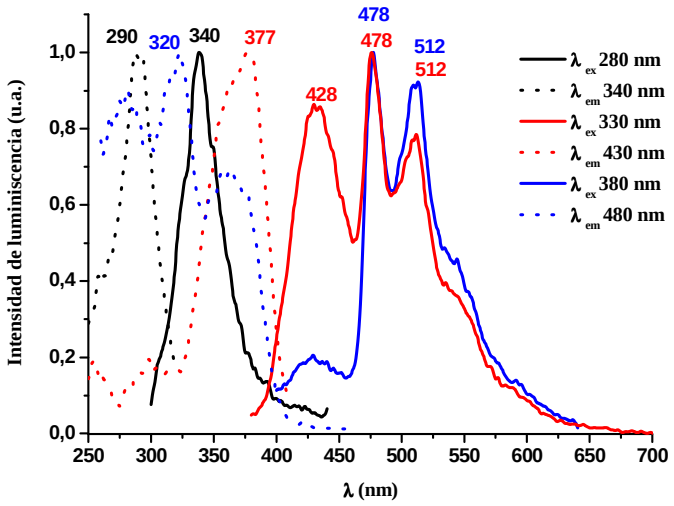

Figura 1.19: Espectros de excitación y emisión de **8** en CH_3CN 5 x 10^{-5} M a 298 K

Debido a la baja energía del grupo 2-fenilquinolato los compuestos con este ligando **[Pt(pq)(L_2)]$^{n+}$** [n = 0, L_2 = {$H_2B(pz)_2$}$^-$ **3**, {$HB(pz)_3$}$^-$ **10**, n = 1, L_2 ={$H_2C(pz)_2$} **6**, {$HC(pz)_3$} **9**] en CH_3CN 5 x 10^{-5} M no muestran fluorescencia estructurada de alta energía (Tablas 1.6 y A1.5). Todos ellos exhiben una banda ancha con máximos en ~590 nm **3**, 560, 590 **6**, 561, 590 **9** y ~590 nm **10** (Figura 1.20 para **6**). Los máximos de estas emisiones están claramente desplazados al rojo, respecto a los observados en los derivados homólogos con los grupos bzq y ppy, al igual que en los espectros en sólido, lo que está de acuerdo con la mayor extensión de la conjugación en el ligando pq. La emisión en los derivados catiónicos **6** y **9** está más estructurada que en los derivados neutros **3** y **10** y se encuentra desplazada a energías más altas. Este hecho está de acuerdo con un marcado carácter de transferencia de carga ^{3}MLCT en éstos últimos. Adicionalmente, el derivado **3** muestra, junto con la banda de baja energía de ~590 nm, otra banda ancha centrada a 447 nm por excitación a λ_{ex}< 400 nm, asignada al excímero de la fluorescencia, que sin embargo, no se observa en CH_2Cl_2 y tolueno a esa concentración (Figura 1.21).

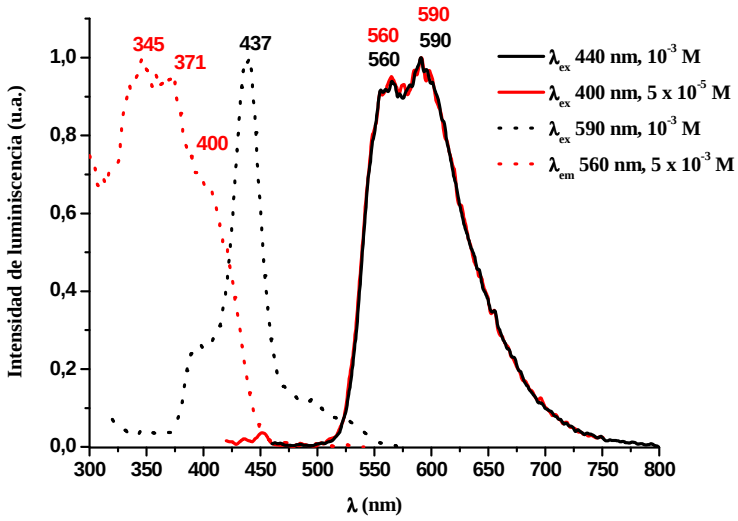

Figura 1.20: Espectros de excitación y emisión de **6** en CH_3CN 5 x 10^{-5} M y 10^{-3} M a 298 K

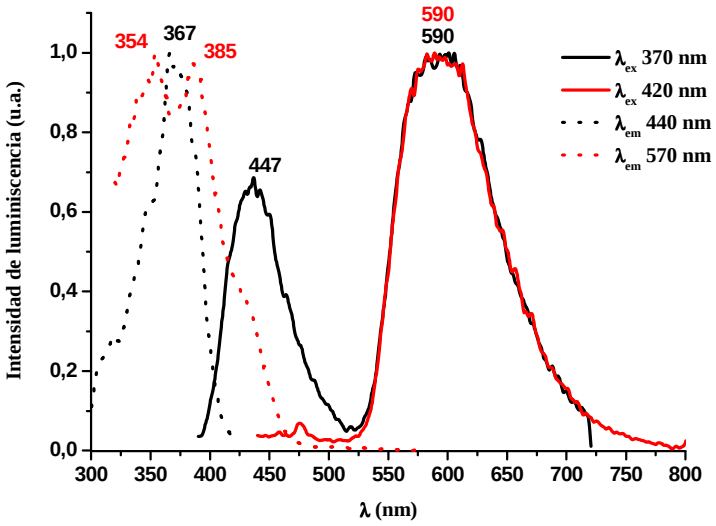

Figura 1.21: Espectros de excitación y emisión de **3** en CH_3CN 5 x 10^{-5} M a 298 K

En todos estos compuestos se analizó el efecto de la concentración a 298 K (Ver Tablas 1.6 y A1.5). La característica más llamativa es que en aquellos casos en los que se observa fluorescencia en disoluciones diluidas, en disoluciones más concentradas (10^{-3} M), en los disolventes estudiados, desaparecen estas bandas de fluorescencia, manteniéndose únicamente las bandas de fosforescencia. Debemos indicar que en muchos casos todavía se observan las bandas de fluorescencia a concentraciones de 10^{-4} M, por lo que se requiere alcanzar la concentración de 10^{-3} M para que éstas desaparezcan. En general, los perfiles de emisión asociados a la banda ^{3}ILCT/^{3}MLCT son similares a los obtenidos en disoluciones diluidas, y no se observan bandas de baja energía asociadas a agregados π···π o Pt···Pt. Como se muestra en las Figura 1.22 un hecho llamativo al aumentar la concentración es que las excitaciones cambian claramente respecto a las observadas en concentraciones diluidas, observándose dos máximos de excitación muy claros a 10^{-3} M (ej: 385, 430 nm **1**; 362, 421 nm **4**). No conocemos las razones por las que se producen cambios en el aspecto de excitación, pero podría ser debido a la presencia de diferentes especies que absorben energía al aumentar la concentración.

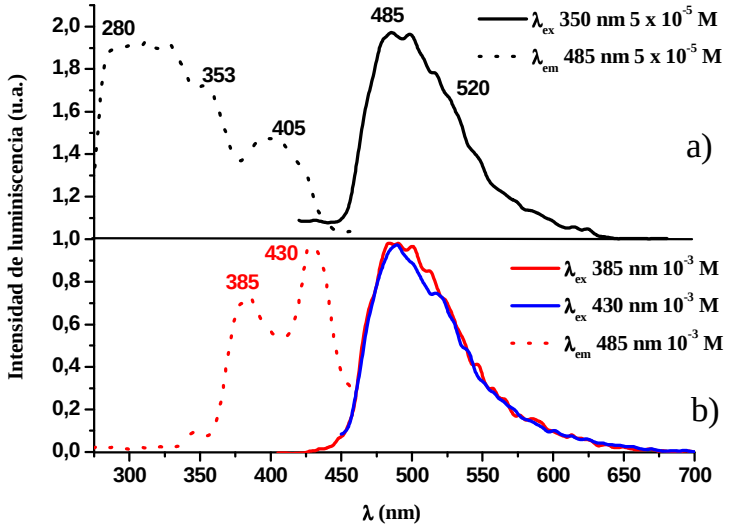

Figura 1.22: Espectros de excitación y de emisión de **1** en CH_3CN a) 5 x 10^{-5} M y b) 10^{-3} M a 298 K

Cuando las disoluciones diluidas se congelan (77 K) las emisiones de fluorescencia $^1(\pi\pi^*)$ y de excímero de fluorescencia (~430 nm) desaparecen, lo que indica una caída efectiva a los estados emisivos de baja energía. Los dos primeros complejos de bzq **[Pt(bzq)(L$_2$)]$^{n+}$** [n = 0, **1**; n = 1, **4**] y todos los de pq **[Pt(pq)(L$_2$)]$^{n+}$** [n = 0, **3**, **10**; n = 1, **6**, **9**] muestran en disoluciones diluidas de CH_3CN (5 x 10^{-5} M) una banda claramente estructurada ^{3}ILCT/^{3}MLCT (Figura 1.23a para **1**) desplazada al azul respecto a las observadas a 298 K, mientras que en los derivados de la serie de ppy [Pt(ppy)(L$_2$)]$^{n+}$ [n = 0, 2; n = 1, 5 y 8] el máximo no cambia (**2**) o se desplaza ligeramente hacia el rojo (**5**, **8**). (Figura 1.23b para **5**). Comportamientos similares se observan en al realizar el estudio en otros disolventes (Ver Tabla A1.5).

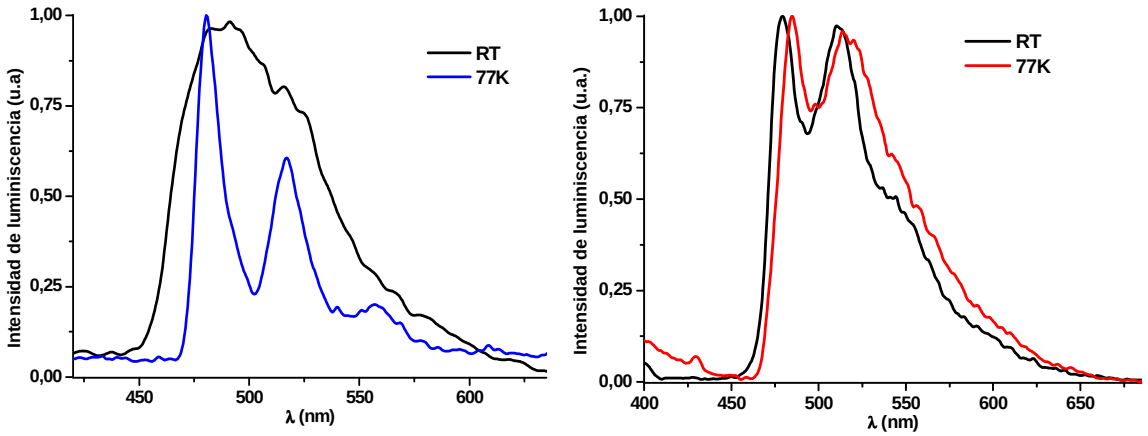

a) b)

Figura 1.23: Espectros de emisión a 298 K y 77 K de disoluciones (CH_3CN 5 x 10^{-5} M) de a) **1** y b) **5**

Sin embargo, el análogo con el ligando tris(pirazolil)metano $\{HC(pz)_3\}^+$ (**7**) muestra de nuevo un comportamiento algo distinto, ya que además de la banda estructurada centrada a 485 nm, muestra la presencia de una banda adicional ancha no estructurada de baja energía a 560 nm, que podría estar asociada con la formación de excímeros en la matriz rígida (Figura 1.24a). De acuerdo con esta asignación, los perfiles de excitación obtenidos recogiendo a 485 nm y 560 nm son muy parecidos. Como se observa en la Figura 1.24b al aumentar la concentración hasta 10^{-3} M, además de una banda estructurada con máximo a 496 nm aparece un banda ancha centrada en torno a 620 nm. El espectro de excitación de esta nueva banda es diferente al obtenido a 490 y 560 nm, lo que sugiere que la banda de baja energía se origina desde un estado emisivo diferente, seguramente debido a procesos de agregación en estado fundamental favorecidos por la presencia de interacciones π···π entre los fragmento "Pt(bzq)" de los cationes $\mathbf{7}^+$.

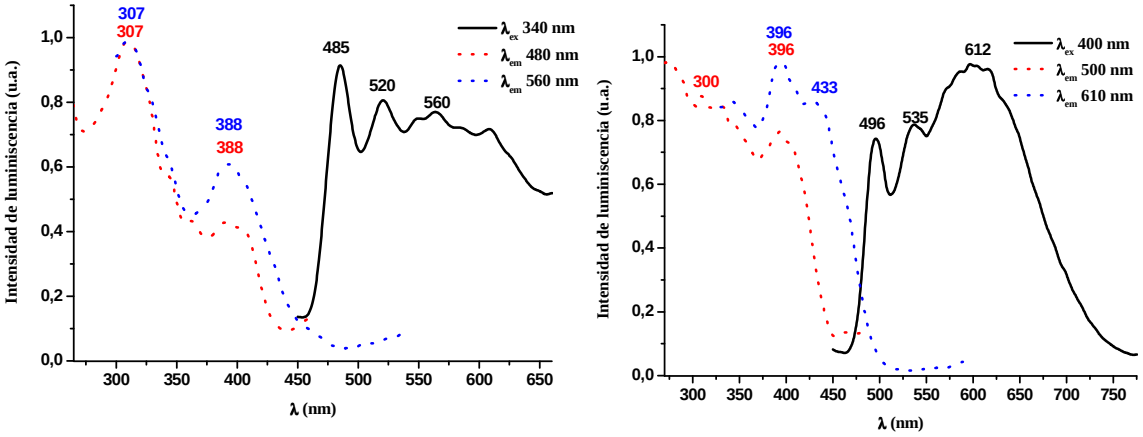

a) b)

Figura 1.24: Espectros de excitación y de emisión de **7** en CH_3CN a 77 K a) 5 x 10^{-5} M, b) 10^{-3} M

La aparición de excímeros (o agregados, en el estado fundamental) en los vidrios congelados a 77 K y no a 298 K es un hecho bastante normal e indica que la constante de asociación será demasiado pequeña como para observarse a temperatura ambiente.

El análisis de los vidrios obtenidos de disoluciones 10^{-3} M revela que en el derivado de bzq **1** y en los de ppy **2**, **5** y **8** la banda no se modifica, mientras que en los de pq **(3**, **6**, **9** y **10)** se observa un ligero desplazamiento hacia el rojo al aumentar la concentración (Ver Tabla A1.5). En el caso de [Pt(bzq){$H_2C(pz)_2$}] (**4**) aparece una banda estructurada, desplazada hacia el rojo cuyos máximos coinciden con los observados en sólido a 77 K, por lo que no se puede descartar la presencia de sólido en el vidrio.

Como se ha puesto de manifiesto en esta discusión, en las series con los ligandos ciclometalados bzq y ppy los compuestos con ligandos disustituidos $[H_2B(pz)_2]^-$ y $[H_2C(pz)_2]$ tienen un comportamiento en disolución a 298 K similar, independientemente de la carga, pero distinto a los compuestos con el ligando trisustituido $[HC(pz)_3]$. Probablemente, la presencia de pirazol libre y su proximidad al centro de Pt podría estar relacionado con estas diferencias. En la serie de pq, los máximos en disolución a 298 K aparecen a energías más altas en los derivados catiónicos que en los neutros, lo que está de acuerdo con una mayor contribución ^{3}MLCT de las emisiones.

1.4 Propiedades electroquímicas

Se han estudiado las propiedades electroquímicas de los complejos **1**–**10**, mediante voltametría cíclica obteniéndose los datos de potenciales de oxidación y reducción en CH_3CN que se muestran en la Tabla 1.7.

Tabla 1.7: Datos electroquímicos de los derivados **1**–**10** en CH_3CN[a]

Complejo	E_p^{red} (V)	E_p^{ox} (V)
[Pt(bzq){$H_2B(pz)_2$}] **1**	-1.70	+1.38[b]
[Pt(ppy){$H_2B(pz)_2$}] **2**	-1.90	+1.49[b]
[Pt(pq){$H_2B(pz)_2$}] **3**	-1.50	+1.49[b]
[Pt(bzq){$H_2C(pz)_2$}]PF_6 **4**	-1.54	+1.68
[Pt(ppy){$H_2C(pz)_2$}]PF_6 **5**	-1.73	+1.90
[Pt(pq){$H_2C(pz)_2$}]PF_6 **6**	-1.33	
[Pt(bzq){$HC(pz)_3$}]PF_6 **7**	-1.52	
[Pt(ppy){$HC(pz)_3$}]PF_6 **8**	-1.72	
[Pt(pq){$HC(pz)_3$}]PF_6 **9**	-1.32	
[Pt(bzq){$HB(pz)_3$}] **10**	-1.48	+0.90

[a] Todas las medidas se han realizado en disoluciones 0.1M en NBu_4PF_6 a 25ºC, con una velocidad de escaneado de 100 mVs^{-1} y usando un electrodo de Ag/AgCl como referencia.[b] Junto con otras pequeñas bandas irreversibles [1.10, 1.64 V(**1**); 1.00, 1.82 V (**2**); 1.00, 1.70 V(**3**)]

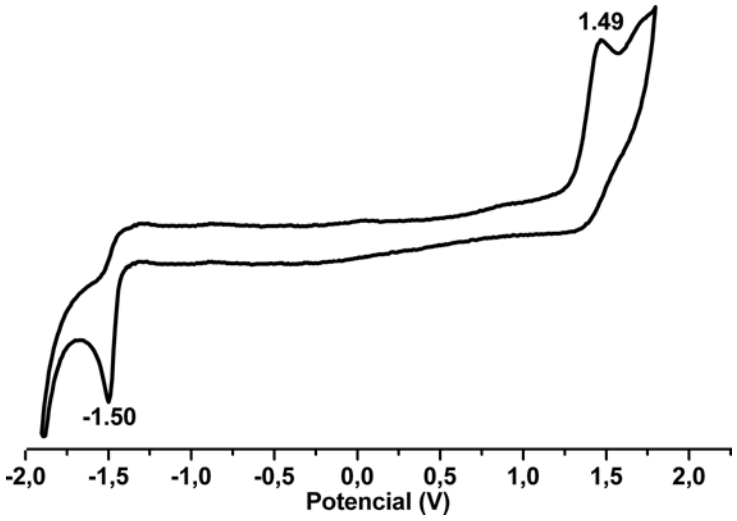

Figura 1.25. Voltamograma de [Pt(pq){$H_2B(pz)_2$}] (**3**) con velocidad de barrido de 100 mV/s

La mayoría de los complejos descritos muestran una banda de reducción irreversible entre -1.32 y -1.90 V y una oxidación irreversible entre +0.90 y +1.90 V (excepto **6**–**9**), junto con otras ondas de menor intensidad observadas en el ciclo de vuelta, probablemente debidas a subproductos generados electroquímicamente (Figura 1.25 para **1**). Generalmente, en los productos ciclometalados la reducción se localiza en

el ligando C^N, mientras que la oxidación se produce en el centro de Pt(II).[15c,25] Este comportamiento electroquímico está de acuerdo con un LUMO basado en el ligando ciclometalado y un HOMO con cierto carácter metálico, como se observa en los cálculos teóricos DFT (Ver Sección 1.5).

En general, en todas las series, el potencial de reducción irreversible está fuertemente influenciado por el ligando ciclometalado. Así, los derivados con el ligando **pq** presentan mayores potenciales de reducción (-1.50 **3**, -1.33 **6**, -1.32 **9**, -1.48 **10** V), mientras que los complejos con el ligando **ppy** son los más difíciles de reducir (-1.90 **2**, -1.73 **5**, -1.72 **8** V) y los de **bzq** presentan valores intermedios (-1.70 **1**, -1.54 **4**, -1.52 **7** V). Esto está de acuerdo con la distinta conjugación de los ligandos C^N. Así, a mayor conjugación π de un ligando ciclometalado, es más fácil la reducción debido a una mayor estabilización de la carga negativa en los orbitales π más deslocalizados. Esta secuencia está de acuerdo con la dependencia observada en las bandas de absorción de más baja energía y en los máximos de emisión en estado sólido a 298 K con el ligando ciclometalado.

Como es de esperar, los derivados catiónicos son más fáciles de reducir que sus correspondientes derivados neutros (**bzq**: -1.70 **1**, -1.54 **4**, -1.52 **7** V; **ppy**: -1.90 **2**, -1.73 **5**, -1.72 **8** V; **pq**: -1.50 **3**, -1.33 **6**, -1.32 **9**, -1.48 **10** V). Sin embargo, como se observa en la Tabla 1.7 los complejos con la misma carga y el mismo ligando ciclometalado, presentan potenciales de reducción similares (por ejemplo: -1.73 **5** *vs* -1.72 **8**; -1.50 **3** *vs* -1.48 **10** V), lo que parece sugerir una pequeña influencia de los ligandos pirazolilborato o metano en los potenciales de reducción, de acuerdo con los resultados de las emisiones.

El análisis de las bandas de oxidación irreversible, nos indica que, como es de esperar, los derivados catiónicos (**4**, **5**) son más difíciles de oxidar que los neutros (**1**–**3** y **10**), y probablemente por esta razón, no se observan bandas de oxidación en la ventana estudiada para la mayor parte de los derivados catiónicos.

1.5 Cálculos teóricos TD-DFT

Para comprender mejor la naturaleza de las absorciones y las emisiones de estos derivados en CH_3CN, se llevó a cabo un estudio teórico mediante Density Functional Theory (DFT) y Time Dependent-Density Functional Theory (TD-DFT). El estudio se centró en algunos de los derivados caracterizados por difracción de Rayos X tanto neutros (**1**) cómo catiónicos (**7**, **8** y **9**), usando el método B3LYP con la base LanL2DZ para el Pt y la base 6-31G(d,p) para los átomos de los ligandos. Las estructuras optimizadas S_0 y T_1 se muestran en las Figuras del Apéndice 1 (Figuras A1.8-A1.11) junto con los principales parámetros geométricos (Tabla A1.6), que como se puede observar, son muy parecidos a los valores experimentales.

1.5.1 Optimización Singlete

Los espectros de absorción en disolución de CH_3CN para **1**, **7**, **8** y **9** se resolvieron utilizando el modelo continuo polarizable, en el que el disolvente se simula como un continuo de constante dieléctrica uniforme ε. Los correspondientes orbitales moleculares (diagramas de densidad electrónica) que están implicados en los principales estados excitados se muestran en el Apéndice 1 (Figuras A1.12-A1.15). En la Figura 1.26 se muestran los orbitales frontera HOMO y LUMO de **1**, **7**, **8** y **9** y su composición relativa en términos de los fragmentos principales se muestra en la Tabla 1.8.

Tabla 1.8: Composición (%) de los orbitales moleculares frontera en el estado fundamental para **7**, **8** y **9** en CH_3CN

	1			**7**			**8**			**9**		
O.M.	**pz**	**Pt**	**bzq**	**pz**	**Pt**	**bzq**	**pz**	**Pt**	**ppy**	**pz**	**Pt**	**pq**
L +4	52	26	22	19	51	30	25	50	25	17	48	36
L +3	40	36	24	89	2	10	96	2	2	94	2	4
L +2	6	6	88	16	3	81	6	1	93	1	2	97
L +1	1	3	95	70	3	27	85	3	11	86	4	11
LUMO	1	3	95	18	4	77	27	6	67	9	4	87
HOMO	8	29	63	2	14	84	5	23	73	1	19	80
H -1	39	45	17	1	9	89	4	8	88	6	21	73
H -2	6	91	4	8	86	6	17	79	5	1	11	88
H -3	52	13	35	9	38	54	96	3	1	7	81	12
H-4	60	5	35	22	54	24	29	56	15	98	1	1
H-5	72	2	26	95	2	3	82	15	2	18	51	31

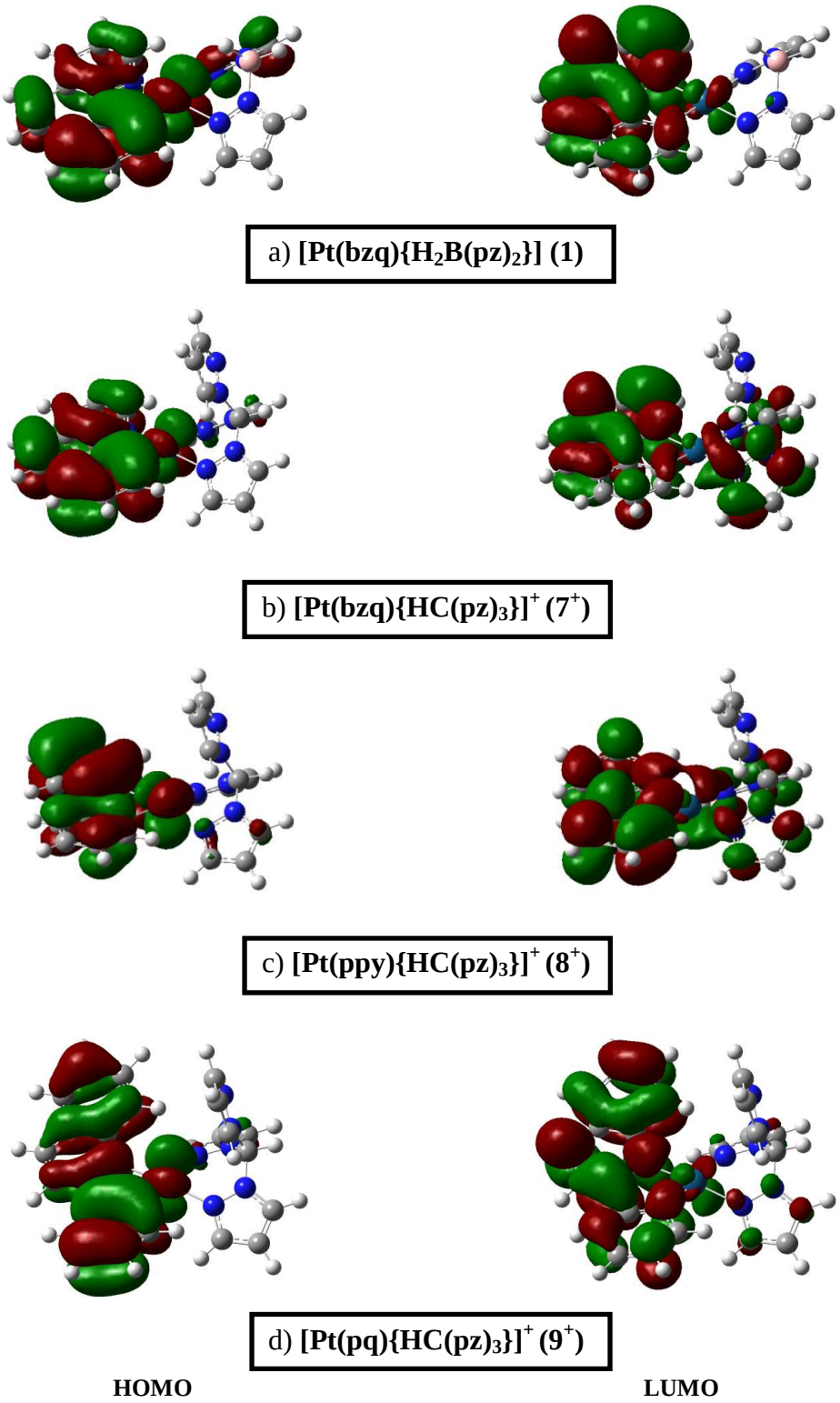

Figura 1.26: Dibujos de los orbitales frontera HOMO – LUMO obtenidos por DFT para a) **1**, b)**7**$^{+}$, c) **8**$^{+}$ y d) **9**$^{+}$

El análisis de estos orbitales frontera (Ver Tabla 1.8) nos indica:

1) Los orbitales moleculares de más alta energía ocupados (HOMO) tienen carácter fundamentalmente π^* [dπ(Pt)- π^*(ciclometalado)], con una configuración similar en todos los casos, centrados en el ligando ciclometalado (63 % bzq **1**, 84% bzq **7**, 73% ppy **8**, 80% pq **9**) y en el Pt (29% **1**,14% **7**, 23% **8**, 19% **9**). La contribución del ligando pirazolato es muy escasa, siguiendo el orden 8% **1**, 5% **8**, 2% **7**, 1% **9**. La comparación de los dos compuestos de bzq (**1** y **7**) indica que en el derivado de bis(pirazolil)borato neutro **1**, la composición del Pt aumenta a costa principalmente de la contribución de la bzq, que disminuye (Pt 29% **1**, 14% **7**, bzq 63% **1**, 84% **7**).

Comparando los derivados de tris(pirazolil)metano se observa una disminución de la contribución del ligando ciclometalado en el sentido bzq > pq > ppy (C^N = 84% **7**, 80% **9**, 73% **8**) y una disminución de la contribución del Pt en el sentido contrario ppy > pq > bzq (Pt = 23% **8**, 19% **9**, 14% **7**).

2) Sin embargo, mientras el HOMO-1 sigue estando localizado principalmente en el ligando ciclometalado en **7**–**9** (89% **7**, 88% **8**, 73% **9**), la participación del ligando bzq en **1** es claramente minoritaria (17%), repartiéndose entre el ligando bis(pirazolil)borato (39%) y el Pt (45%), que aumentan notablemente.

3) Con respecto a los HOMO-2, sólo el ligando ppy se mantiene como mayoritario en el derivado **9** (88%), disminuyendo drásticamente su contribución en el resto de los derivados (4% **1**, 6% **7**, 5% **8**), aumentando claramente la contribución del Pt (91% **1**, 86% **7**, 79% **8**) y algo la de los grupos pirazolato en **7** y **8** (8% y 17%, respectivamente).

4) Los orbitales no ocupados de más baja energía (LUMO) están dominados fundamentalmente por el ligando ciclometalado. En el derivado **1**, tanto el LUMO como el LUMO+1 están principalmente compuestos del ligando bzq con una pequeña contribución del Pt (bzq 95%, Pt 3%).

5) Sin embargo para los derivados catiónicos de tris(pirazolil)metano (**7**, **8** y **9**) los orbitales LUMO están centrados fundamentalmente en el ligando ciclometalado con

una mayor contribución de los grupos pirazolato de **9** a **8** [9% (**9**), 18% (**7**), 27% (**8**)] y las composiciones de los LUMO+1 se invierten claramente, estando ahora centrados en los grupos pirazolato en el orden (86% **9**, 85% **8** y 70% **7**) con una menor contribución del ligando ciclometalado (11% **9**, 11% **8**, 27% **7**). Sin embargo, el LUMO+2 vuelve a estar dominado por el ligando ciclometalado en todos ellos (97%, **9**, 93% **8**, 88% **1**, 81% **7**).

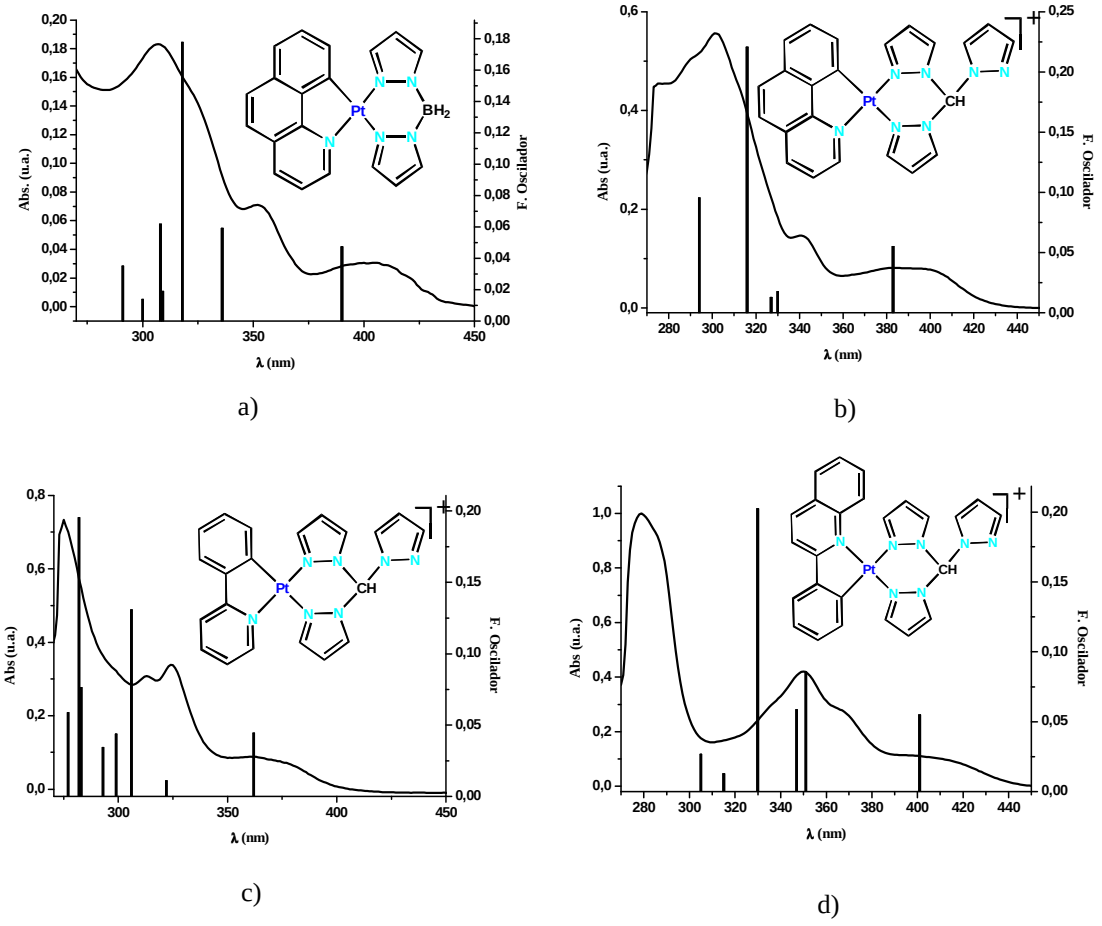

Figura 1.27: Espectros de absorción calculados (dibujados en barras) en CH_3CN y espectros experimentales UV-vis en CH_3CN de a) **1**, b) **7**, c) **8** y d) **9**

La Tabla A1.7 muestra los estados excitados calculados en disolución de CH_3CN (los primeros singletes) con la fortaleza del oscilador, las transiciones con sus principales contribuciones y las posibles asignaciones. En la Figura 1.27 se muestran las transiciones permitidas seleccionadas como barras incluidas dentro de los espectros de absorción experimentales obtenidos en CH_3CN para los derivados estudiados. Como se observa en la Tabla A1.7, las absorciones de más baja energía permitidas por el dipolo están a 390 **1**, 383 **7**, 362 **8** y 402 nm **9** respectivamente, y reproduce, aunque un poco

desplazado hacia el azul, la tendencia observada en los espectros experimentales (405 **1**, 389 **7**, 377 **8** y 402 nm **9**). En todos los derivados, la principal contribución a esta banda es la transición HOMO→ LUMO (91% **7** y **8**, 90% **1** y **9**). Considerando la naturaleza del HOMO y del LUMO, comentados anteriormente, la absorción de más baja energía en el derivado **1** se atribuye principalmente a transiciones ^{1}ILCT (L = bzq) con una importante contribución de ^{1}MLCT (Pt→bzq), mientras que en los derivados catiónicos **7**–**9**, la transición ^{1}ILCT se combina con transferencias de carga del platino a ambos ligandos en **9** [^{1}MLCT/^{1}ML'CT; L = C^N, L' = $HC(pz)_3$] o al ligando tris(pirazolil)metano (^{1}ML'CT) en **7** y **8**. Un análisis pormenorizado de la composición de los orbitales frontera, nos permite observar que en la transición de más baja energía la contribución ^{1}ML'CT sigue la secuencia **8** > **7** > **9** y que la contribución ^{1}ILCT lo hace en sentido opuesto (**9** > **7** >**8**). Esto nos indica que la contribución Metal–Ligando tris(pirazolil)metano aumenta al disminuir la contribución Metal→Ligando ciclometalado (ppy < bzq < pq). La Tabla A1.7 nos indica que para el resto de transiciones de más alta energía (λ < 300 nm) hay una considerable mezcla de orbitales.

1.5.2 Optimización Triplete

La geometría optimizada del estado triplete de más baja energía T_1 es muy similar a la observada en estado fundamental en todos los derivados estudiados (**1**, **7**, **8** y **9**) (Tabla A1.6). Las bandas de emisión fosforescente calculadas para **1**, **7**, **8** y **9** (Tabla 1.9) basadas en la optimización triplete no restringida U-B3LYP siguen la misma tendencia observada experimentalmente aunque con máximos ligeramente desplazados hacia el rojo respecto a los obtenidos de disoluciones diluidas (5×10^{-5} M) de CH_3CN a temperatura ambiente, excepto en el derivado **7** que al no presentar propiedades emisivas en estas condiciones se compara con los datos obtenidos a 77 K.

Tabla 1.9: Máximos calculados de emisión fosforescente para **1**, **7**$^+$–**9**$^+$ con el método TD–DFT/PCM (CH_3CN) (en paréntesis se muestra la primera transición triplete con geometría S_0), junto con los valores obtenidos experimentalmente en disoluciones de CH_3CN (5×10^{-5} M) a 298 K

Comp.	Configuración (| CI coef. |)	Calculado (nm)	Asignación	λ_{em} Experimental (nm)
1	95→94 (0.64) 95→93 (0.32) 96→94 (0.30)	612 (464)	^{3}ILCT/^{3}MLCT	485
7$^+$	112→111 (0.66) 112→110 (0.33) 113→111 (0.29)	620 (461)	^{3}ILCT/^{3}MLCT	485[a]
8$^+$	106→105 (0.75)	590 (449)	^{3}ILCT/^{3}MLCT	478
9$^+$	119→118 (0.77) 119→117 (0.21)	720 (514)	^{3}ILCT/^{3}MLCT/^{3}ML'CT	561

a) en vidrio congelado a 77 K

Los diagramas de transición de un electrón para las emisiones de baja energía de **1**, **7**, **8** y **9**, basados en cálculos TD-DFT optimizados para disoluciones de CH_3CN, se muestran en la Figura 1.28 etiquetando los orbitales respecto al estado fundamental S_0, para una mejor comprensión.

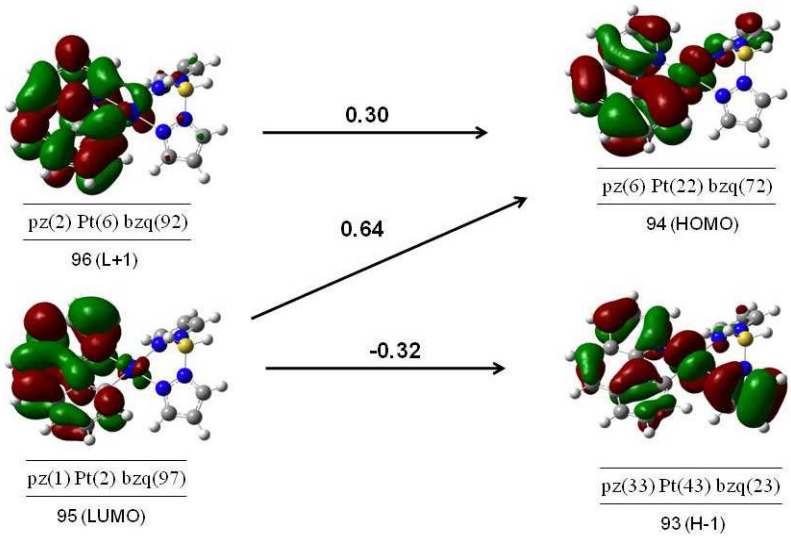

a) **[Pt(bzq){$H_2B(pz)_2$}] (1)**

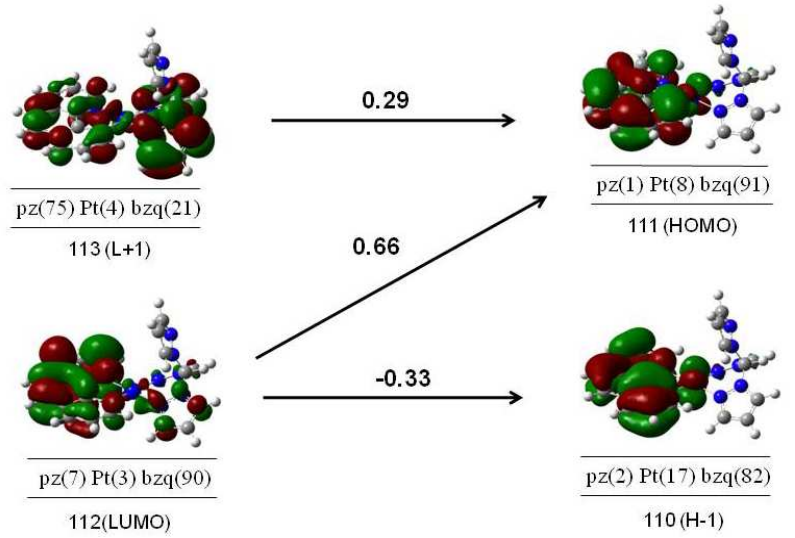

b) **[Pt(bzq){HC(pz)$_3$}]$^+$ (7$^+$)**

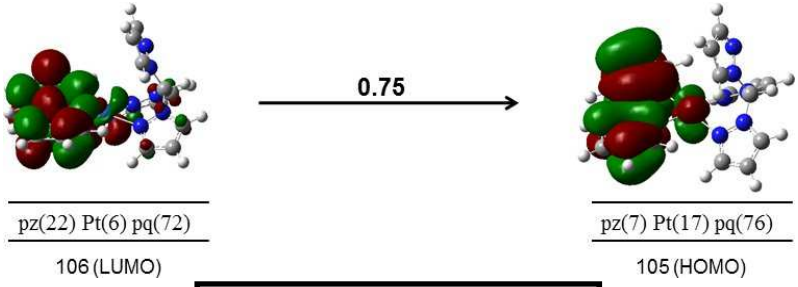

c) **[Pt(ppy){HC(pz)$_3$}]$^+$ (8$^+$)**

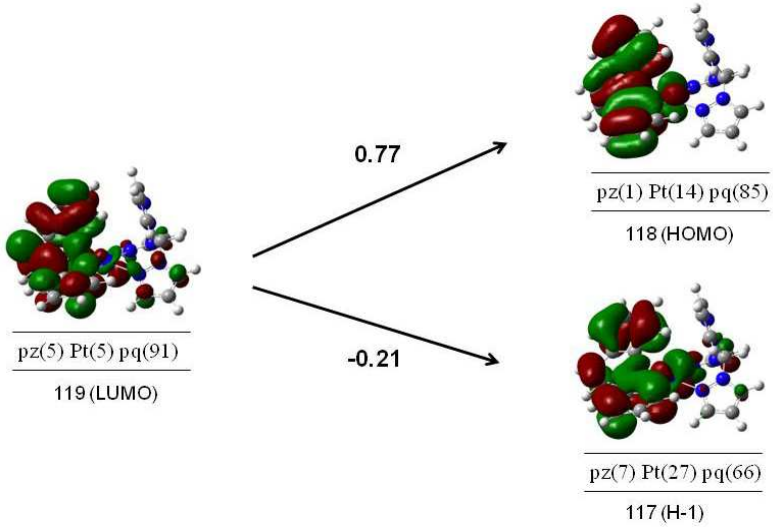

d) **[Pt(pq){HC(pz)$_3$}]$^+$ (9$^+$)**

Figura 1.28: Transiciones de un electrón con |Coeficientes CI|> 0.20 de acuerdo con los cálculos teóricos TD-DFT para las emisiones en CH_3CN de a) **1** a 612 nm, b) **7**$^+$ a 620 nm c) **8**$^+$ a 590 nm d) **9**$^+$ a 720 nm. Los orbitales (composición en %) se referencian respecto a S_0

El análisis de este estudio indica que el triplete de más baja energía está formado principalmente por la transición del HSOMO (LUMO en notación S_0) al LSOMO (HOMO en notación S_0), junto con otras transiciones de menor importancia. En el complejo neutro **1** el orbital LSOMO está localizado principalmente en el ligando ciclometalado bzq (72%) con una pequeña contribución tanto del Pt (22%) como del ligando bis(pirazolil)borato (6%), mientras que el HSOMO está centrado en el ligando bzq (97%). Esto nos permite asignar esta emisión a una transición intraligando ^{3}ILCT perturbada por el metal (transferencia de carga metal–ligando ^{3}MLCT). En el caso de los derivados catiónicos **7**–**9** el orbital LSOMO está localizado en el ligando C^N (91% **7**, 76% **8**, 85% **9**) con una menor contribución del átomo de Pt (8% **7**, 17% **8**, 14% **9**) y una pequeña contribución del ligando tris(pirazolil)metano (1% **7**, **9**, 7% **9**). El orbital HSOMO está formado principalmente por el C^N (90% **7**, 72% **8**, 91% **9**) con alguna contribución del ligando tris(pirazolil)metano, en contraste con lo observado en el derivado neutro **1** donde apenas contribuye, y que sigue el orden **9** < **7** < **8** (5% **9**, 7% **7**, 22% **8**). En vista de estos resultados, se puede proponer que la emisión fosforescente de los derivados catiónicos se puede asignar a una transición ^{3}ILCT mezclada con ^{3}ML'CT (más importante en el derivado **8**) y con una ligera contribución de ^{3}MLCT en **9**.

1.6 Resumen

En resumen, se ha abordado la preparación de tres series de derivados ciclometalados neutros [Pt(C^N){$H_2B(pz)_2$}] (**1**-**3**) y catiónicos [Pt(C^N){$H_2C(pz)_2$}]$^+$ (**4**-**6**), [Pt(C^N){$HC(pz)_3$}]$^+$ (**7**-**9**) (C^N = bzq, ppy, pq), que contienen ligandos poli(pirazolil)-borato y metano como ligandos auxiliares, mediante reacciones de ruptura de puentes y sustitución de Cl^- en los precursores [Pt(C^N)(μ-Cl)]$_2$ por el correspondiente ligando. El complejo neutro [Pt(pq){$HB(pz)_3$}] **10** se prepara siguiendo la misma metodología, mientras que los derivados relacionados de *bzq* y *ppy* son inaccesibles por esta ruta, debido a que se forman sistemas binucleares de puentes pirazolato [Pt(C^N)(μ-pz)]$_2$ (mezcla de *cis* y *trans*), implicando rotura de enlaces B-N.

Las propiedades fotofísicas se pueden modular tanto por los ligandos ciclometalados (L) como por los ligandos chelato (L'). La absorción y la emisión se desplazan al rojo siguiendo el orden (*pq* < *bzq* < *ppy*) y se asocian a transiciones mixtas IL/MLCT. Los derivados catiónicos se desplazan al azul con respecto a los análogos neutros (**1**-**3**, **10**), de acuerdo con una mayor contribución de los estados IL y una disminución del carácter MLCT. Estas tendencias se correlacionan con los datos de oxidación/reducción obtenidos mediante voltametría cíclica.

Este estudio revela que en disoluciones diluidas a 298 K los derivados que contienen el ligando plano *bzq* (**1**, **4**, **7**) y algunos de los derivados con el grupo tris(pirazolil)metano [$HC(pz)_3$] muestran además de la emisión ^{3}IL/^{3}MLCT, fluorescencia y/o excímero de fluorescencia. El registro de estas emisiones en función del tiempo de retraso desde la excitación sugiere que se trata de una *fluorescencia retardada*. Esta conclusión es coherente con el estudio de dependencia de la emisión con el disolvente que se ha realizado en el compuesto **1**, que indica que en el disolvente menos polar usado (tolueno) la fluorescencia desaparece, mientras que la emisión ^{3}ILCT/^{3}MLCT se estabiliza. En los vidrios congelados sólo se observa la emisión de fosforescencia. En general no se observan emisiones de baja energía debidas a excímeros o agregados, incluso en disoluciones concentradas ni a 298 K ni a 77 K, probablemente debido al impedimento estérico de los ligandos quelato voluminosos. Únicamente se observa una emisión excimérica en el complejo catiónico de [$HC(pz)_3$]

(**7**) en vidrios congelados diluidos y agregados a mayores longitudes de onda en vidrios concentrados.

Los cálculos DFT llevados a cabo en los derivados neutros **1** y catiónicos **7**-**9** indican que la absorción de mas baja energía es de naturaleza ^{1}ILCT/^{1}MLCT en **1 y** en la serie [HC(pz)$_3$] (**7**-**9**) esta transición se asigna principalmente a ^{1}ILCT combinada con ^{1}MLCT/^{1}ML'CT para **9** o ML'CT para **7** y **8**. Los cálculos TD-DFT de la optimización del estado triplete de más baja energía responsable de la fosforescencia de estos complejos, indican que mientras en el derivado neutro **1** esta emisión tiene un origen ^{3}ILCT con mezcla de carácter ^{3}MLCT, en los derivados catiónicos **7**-**9**, ésta proviene de una transición ^{3}ILCT mezclada con ^{3}ML'CT (especialmente en **8**) y con algo de carácter ^{3}MLCT en **9**.

1.7 Bibliografía

1. (a) Trofimenko, S. *In Scorpionates: The Coordination Chemistry of Polypyrazolyl Borate Ligands*; Ed. Imperial College Press, 1999; (b) Pettinari, C. *In Scorpionates II: Chelating Borate Ligands*; Ed. Imperial College Press, 2008.
2. Pettinari, C.; Pettinari, R. *Coord. Chem. Rev.* **2005**, *249*, 525.
3. (a) Tellers, D. M.; Bergman, R. G. *J. Am. Chem. Soc.* **2001**, *123*, 11508; (b) Tellers, D. M.; Bergman, R. G. *J. Am. Chem. Soc.* **2000**, *122*, 954; (c) Gutiérrez-Puebla, E.; Monge, A.; Paneque, M.; Poveda, M. L.; Salazar, V.; Carmona, E. *J. Am. Chem. Soc.* **1998**, *121*, 248; (d) Wiley, J. S.; Heinekey, D. M. *Inorg. Chem.* **2002**, *41*, 4961; (e) Tellers, D. M.; Bergman, R. G. *Organometallics* **2001**, *20*, 4819; (f) Vetter, A. J.; Jones, W. D. *Polyhedron* **2004**, *23*, 413; (g) Rangan, K.; Fianchini, M.; Singh, S.; Rasika Dias, H. V. *Inorg. Chim. Acta* **2009**, *362*, 4347; (h) Wick, D. D.; Jones, W. D. *Inorg. Chim. Acta* **2009**, *362*, 4416.
4. (a) Dehestani, A.; Wu, A.; Hayoun, R.; Kaminsky, W.; Mayer, J. M. *Inorg. Chim. Acta* **2009**, *362*, 4534; (b) Chisholm, M. H. *Inorg. Chim. Acta* **2009**, *362*, 4284; (c) Engelman, K. L.; White, P. S.; Templeton, J. L. *Inorg. Chim. Acta* **2009**, *362*, 4461; (d) Handy, S. T.; Ivanow, A. *Inorg. Chim. Acta* **2009**, *362*, 4468; (e) Martín, C.; Muñoz-Molina, J. M.; Locati, A.; Alvarez, E.; Maseras, F.; Belderrain, T. R.; Pérez, P. J. *Organometallics* **2010**, *29*, 3481.
5. (a) Kitajima, N.; Tolman, W. B. *Prog. Inorg. Chem.* **1995**, *43*, 419; (b) Cecchi, P.; Bovio, B.; Lobbia, G. G.; Pettinari, C.; Leonesi, D. *Polyhedron* **1995**, *14*, 2441.
6. (a) Trofimenko, S. *Chem. Rev.* **1993**, *93*, 943; (b) Trofimenko, S. *Prog. Inorg. Chem.* **1986**, *34*, 115; (c) Kitano, T.; Sohrin, Y.; Hata, Y.; Kawakami, H.; Hori, T.; Ueda, K. *J. Chem. Soc., Dalton Trans.* **2001**, 3564; (d) Kitano, T.; Sohrin, Y.; Hata, Y.; Mukai, H.; Wada, H.; Ueda, K. *Polyhedron* **2004**, *23*, 283.
7. Garcia, R.; Paulo, A.; Santos, I. *Inorg. Chim. Acta* **2009**, *362*, 4315.
8. (a) Huang, L.; Seward, K. J.; Sullivan, B. P.; Jones, W. E.; Mecholsky, J. J.; Dressick, W. J. *Inorg. Chim. Acta* **2000**, *310*, 227; (b) Li, J.; Djurovich, P. I.; Alleyne, B. D.; Tsyba, I.; Ho, N. N.; Bau, R.; Thompson, M. E. *Polyhedron* **2004**, *23*, 419; (c) Carvalho, A.; Domingos, Â.; Isolani, P. C.; Marques, N.; Pires de Matos, A.; Vicentini, G. *Polyhedron* **2000**, *19*, 1707; (d) Niedermair, F.; Waich, K.; Kappaun, S.; Mayr, T.; Trimmel, G.; Mereiter, K.; Slugovc, C. *Inorg. Chim. Acta* **2007**, *360*, 2767.

9. Ma, B.; Li, J.; Djurovich, P. I.; Yousufuddin, M.; Bau, R.; Thompson, M. E. *J. Am. Chem. Soc.* **2005**, *127*, 28.
10. Trofimenko, S. *J. Am. Chem. Soc.* **1967**, *89*, 3170.
11. Reger, D. L.; Grattan, T. C.; Brown, K. J.; Little, C. A.; Lamba, J. J. S.; Rheingold, A. L.; Sommer, R. D. *J. Organomet. Chem.* **2000**, *607*, 120.
12. (a) White, J. M.; Ng, V. W. L.; Clarke, D. C.; Smith, P. D.; Taylor, M. K.; Young, C. G. *Inorg. Chim. Acta* **2009**, *362*, 4570 and references therein; (b) Carmona, E.; Cingolani, A.; Marchetti, F.; Pettinari, C.; Pettinari, R.; Skelton, B. W.; White, A. H. *Organometallics* **2003**, *22*, 2820.
13. Lai, S. W.; Chan, M. C. W.; Cheung, K. K.; Peng, S. M.; Che, C. M. *Organometallics* **1999**, *18*, 3991.
14. (a) Rachford, A. A.; Castellano, F. N. *Inorg. Chem.* **2009**, *48*, 10865; (b) Ghavale, N.; Wadawale, A.; Dey, S.; Jain, V. K. *J. Organomet. Chem.* **2010**, *695*, 1237.
15. (a) Díez, Á.; Forniés, J.; García, A.; Lalinde, E.; Moreno, M. T. *Inorg. Chem.* **2005**, *44*, 2443; (b) Jolliet, P.; Gionini, M.; von Zelewsky, A.; Bernardinelly, G.; Stoeckli-Evans, H. *Inorg. Chem.* **1996**, *35*, 4883; (c) Brooks, J.; Babayan, Y.; Lamansky, S.; Djorovich, P. I.; Tsyba, I.; Bau, R.; Thompson, M. E. *Inorg. Chem.* **2002**, *41*, 3055; (d) De Priest, J.; Zheng, G. Y.; Goswami, N.; Eichhorn, D. M.; Woods, C.; Rillema, D. P. *Inorg. Chem.* **2000**, *39*, 1955; (e) Hoogervorst, W. J.; Elsevier, C. J.; Lutz, M.; Spek, A. L. *Organometallics* **2001**, *20*, 4437; (f) Fernández, S.; Forniés, J.; Gil, B.; Gómez, J.; Lalinde, E. *Dalton Trans.* **2003**, 822.
16. (a) Thomas, C. M.; Peters, J. C. *Organometallics* **2005**, *24*, 5858; (b) Ruiz, J.; Florenciano, F.; Rodríguez, V.; de Haro, C.; López, G.; Pérez, J. *Eur. J. Inorg. Chem.* **2002**, *2002*, 2736.
17. Goel, A. B.; Goel, S.; Vanderveer, D. *Inorg. Chim. Acta* **1984**, *82*, L9.
18. Jain, V. K.; Kannan, S.; Tiekink, E. R. T. *J. Chem. Soc., Dalton Trans.* **1993**, 3625.
19. (a) Wadas, T. J.; Chakraborty, S.; Lachicotte, R. J.; Wang, Q. M.; Eisenberg, R. *Inorg. Chem.* **2005**, *44*, 2628; (b) Reichardt, C. *Solvent and solvent effects in organic chemistry; 2*; ed. VCH: Weinhein, 1988.
20. (a) Lai, S. W.; Chan, M. C. W.; Wang, Y.; Lam, H. W.; Peng, C. Y. *J. Organomet. Chem.* **2001**, *617-618*, 133; (b) Díez, Á.; Forniés, J.; Fuertes, S.; Lalinde, E.; Larraz, C.; López, J. A.; Martín, A.; Moreno, M. T.; Sicilia, V. *Organometallics* **2009**, *28*, 1705; (c) Berenguer, J. R.; Lalinde, E.; Torroba, J. *Inorg. Chem.* **2007**, *46*, 9919; (d) Díez, Á.; Forniés, J.; Larraz, C.; Lalinde, E.; López, J. A.; Martín, A.;

Moreno, M. T.; Sicilia, V. *Inorg. Chem.* **2010**, *49*, 3239; (e) Yam, V. W. W.; Tang, R. P. L.; Wong, K. M. C.; Lu, X. X.; Cheung, K. K.; Zhu, N. *Chem. Eur. J.* **2002**, *8*, 4066; (f) Develay, S.; Blackburn, O.; Thompson, A. L.; Williams, J. A. G. *Inorg. Chem.* **2008**, *47*, 11129.

21. (a) De Priest, J.; Zheng, G. Y.; Woods, C.; Rillema, D. P.; Mikirova, N. A.; Zandler, M. E. *Inorg. Chim. Acta* **1997**, *264*, 287; (b) Zheng, G. Y.; Rillema, D. P.; DePriest, J.; Woods, C. *Inorg. Chem.* **1998**, *37*, 3588.
22. (a) Turro, N. J. *Modern Molecular Photochemistry*; The Benjamin/Cummings Publishing Company: California, 1978; (b) Valeur, B. *Molecular Fluorescence - Principles and Applications*; Wiley - VCH, 2002.
23. Bellows, D.; Aly, S. M.; Gros, C. P.; El Ojaimi, M.; Barbe, J. M.; Guilard, R.; Harvey, P. D. *Inorg. Chem.* **2009**, *48*, 7613.
24. Yamaji, M.; Tsukada, H.; Nishimura, J.; Shizuka, H.; Tobita, S. *Chem. Phys. Lett.* **2002**, *357*, 137.
25. (a) Qiu, D.; Wu, J.; Xie, Z.; Cheng, Y.; Wang, L. *J. Organomet. Chem.* **2009**, *694*, 737; (b) Kulikova, M. V.; Balashev, K. P.; Kvam, P. I.; Songstad, J. *Russ. J. Gen. Chem.* **2000**, *70*, 166; (c) Clark, M. L.; Diring, S.; Retailleau, P.; McMillin, D. R.; Ziessel, R. *Chem. Eur. J.* **2008**, *14*, 7168.

1.8 Apéndice

Tabla A1.1: Datos característicos de RMN de ^{1}H (CD_3COCD_3) y de $^{13}C\{^{1}H\}$[a] (δ en ppm y *J* en Hz) de los compuestos que contienen el grupo benzoquinolato (**1**, **4** y **7**)

	^{1}H				
	bzq				pz
	H^2 ($^{3}J_{Pt-H}$)	H^4	H^8	H^9 ($^{3}J_{Pt-H}$)	$H^{4'/4''}$
1	9.01 (32.9)	8.70	7.56	7.48 (37.8)	6.45/6.41
4	9.08 (41.0)	8.82	7.64	7.45 (34.7)	6.88/6.87
7	9.04 (39.9)	8.77	7.57	7.36 (33.8)	7.06[b]

	$^{13}C\{^{1}H\}$						
	bzq			pz			
	C^{10}	C^2 $^{2}J_{Pt-C}$	C^9 $^{2}J_{Pt-C}$	$C^{3'}$ $^{2}J_{Pt-C}$	$C^{4'}$ $^{3}J_{Pt-C}$	$C^{3''}$ $^{2}J_{Pt-C}$	$C^{4''}$ $^{3}J_{Pt-C}$
1	157.5	148.3 (26.7)	131.7 (64.6)	142.0 (79.1)	105.7 (50.15)	140.0 (24.3)	105.7 (18.2)
4	154.4	154.3 (23.8)	135.2 (65.1)	150.2 (68.3)	114.1 (49.7)	149.0 (19.0)	113.9 (16.0)

a) **1** en $CDCl_3$, **4** en CD_3COCD_3, **7** no es suficientemente soluble

b) El protón $H^{4'''}$ del grupo pirazolato sin coordinar aparece como un singlete a 6.23 ppm

Tabla A1.2: Datos espectroscópicos de RMN de ^{1}H y de $^{13}C\{^{1}H\}$ (CD_3COCD_3) (δ en ppm y *J* en Hz) de los compuestos que contienen el grupo fenilpiridinato (**2**, **5** y **8**)

	^{1}H			
	ppy			pz
	H^2 ($^{3}J_{Pt-H}$)	H^4	H^9 ($^{3}J_{Pt-H}$)	$H^{4'/4''}$
2	8.68 (37.0)	8.15	7.20 (35.6)	6.36/6.39
5	8.74 (37.7)	8.22[a]	7.83 (-)	6.81/6.83
8	8.66 (35.1)	8.20	7.73 (-)	6.99[b]

	$^{13}C\{^{1}H\}$[c]						
	ppy			pz			
	C^{10}	C^2 $^{2}J_{Pt-C}$	C^9 $^{2}J_{Pt-C}$	$C^{3'}$ $^{2}J_{Pt-C}$	$C^{4'}$ $^{3}J_{Pt-C}$	$C^{3''}$ $^{2}J_{Pt-C}$	$C^{4''}$ $^{3}J_{Pt-C}$
2	168.6	150.5 (19.7)	134.5 (58.4)	142.8 (80.4)	106.5 (51.4)	141.3 (24.5)	106.5 (18.1)
5	167.8	150.9 (20.2)	133.7 (56.3)	146.1 (68.7)	110.0 (48.6)	144.8 (15.1)	109.8 (16.2)

a) Solapado con H^5

b) El protón $H^{4'''}$ del grupo pirazolato sin coordinar aparece como un singlete a 6.34 ppm

c) **8** No es suficientemente soluble como para registrar el espectro de $^{13}C\{^{1}H\}$

Tabla A1.3: Datos más característicos de RMN de ^{1}H y de $^{13}C\{^{1}H\}$ (CD_3COCD_3) (δ en ppm y *J* en Hz) de los compuestos que contienen el grupo fenilquinolato (**3**, **6**, **9** y **10**)

	^{1}H		
	pq		pz
	H^{4}/H^{3}	H^{12} ($^{3}J_{Pt-H}$)	$H^{4'/4''}$
3	8.53/8.07	7.10 (-)	6.20/5.96
6	8.79/8.32	7.20 (32.0)	6.79/6.57
9	8.72/8.23	7.26[a](-)	7.02[b]
10	8.50/8.02	7.10 [a]	6.34/6.02[c]

	$^{13}C\{^{1}H\}$						
	pq			pz			
	C^{12} $^{2}J_{Pt-C}$	C^{9} $^{3}J_{Pt-C}$	C^{3} $^{3}J_{Pt-C}$	$C^{3'}$ $^{2}J_{Pt-C}$	$C^{4'}$ $^{3}J_{Pt-C}$	$C^{3''}$ $^{2}J_{Pt-C}$	$C^{4''}$ $^{3}J_{Pt-C}$
	134.8	126.5	117.9	142.8	106.2	142.3	105.9
	(58.5)	(35.7)	(44.4)	(83.0)	(52.5)	(29.6)	(20.2)
6	134.1	127.0	118.1	146.3	109.7	145.8	109.3
	(57.6)	(27.6)	(47.7)	(73.9)	(51.4)	(-)	(-)
9	133.0	126.1	117.2	147.8	109.6	d)	108.3[e]
	(53.0)	(35.8)	(48.1)	(61.8)	(44.7)		(-)
10	d)	130.7	122.0	d)	110.2	d)	110.2

a) Solapado con otras señales del ligando pq

b) El protón $H^{4'''}$ del grupo pirazolato sin coordinar aparece como un singlete a 6.63 ppm

c) Otra señal a 6.76 ppm debida al $H^{4'''}$ libre

d) No se puede asignar inequívocamente

e) Solapado con otras señales

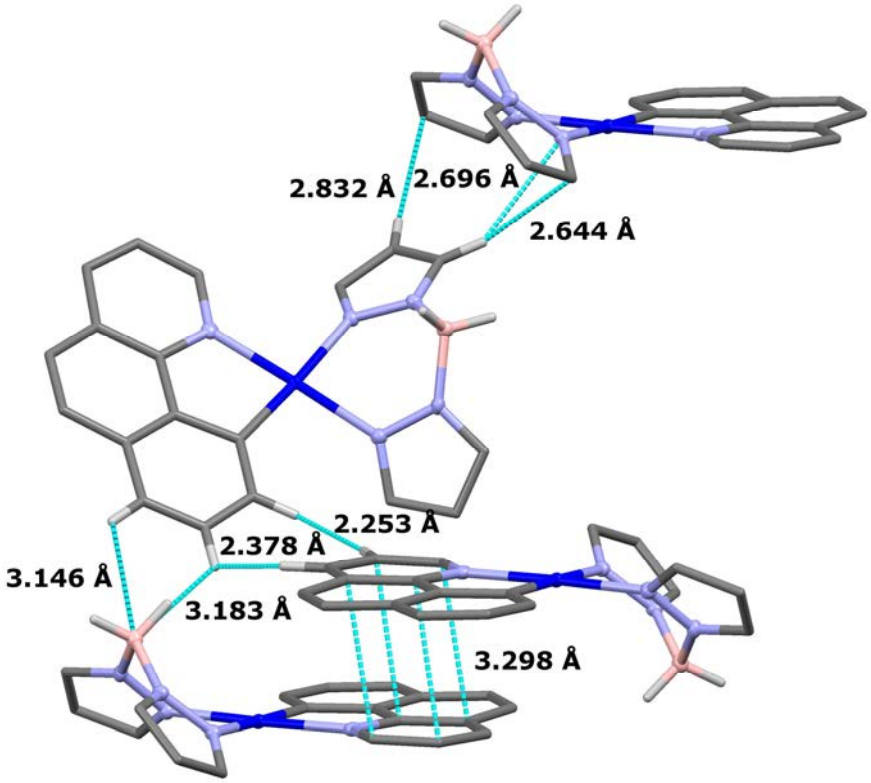

Figura A1.1: Estructura supramolecular del derivado **1** mostrando las principales interacciones intermoleculares π(bzq)···π (bzq) (3.298 Å), $B_{BH_2}\cdots H_{bzq}$, (3.146, 3.183 Å), $H_{bzq}\cdots H_{bzq}$ (2.253, 2.378 Å), $H_{pz}\cdots N_{pz}$ (2.696 Å) y $H_{pz}\cdots C_{pz}$ (2.644, 2.832 Å)

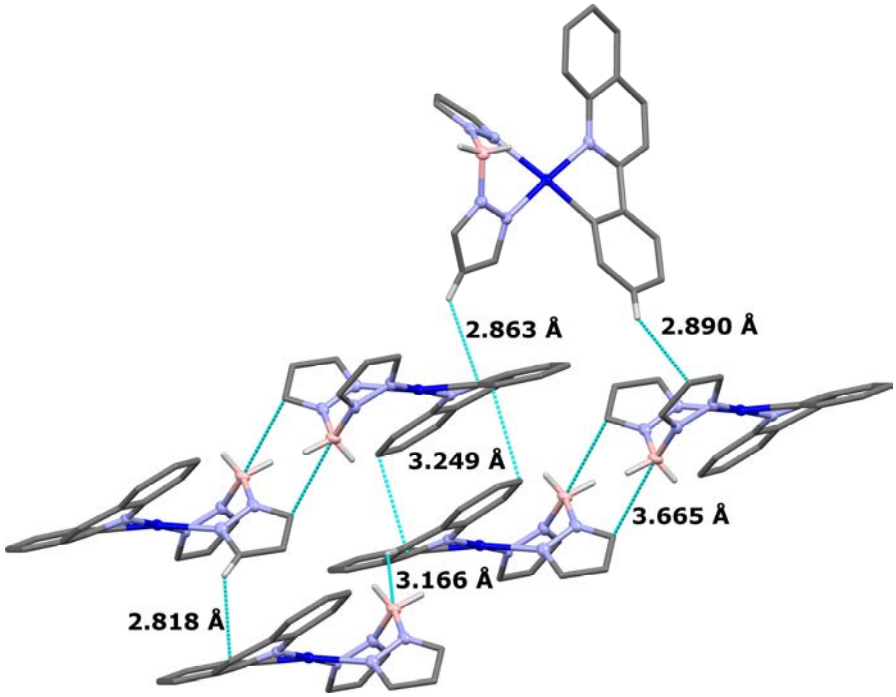

Figura A1.2: Estructura supramolecular del derivado **3** mostrando las principales interacciones intermoleculares π(bzq)··· π(bzq) (3.249 Å), $B\cdots H_{pq}$ (3.166 Å), $B\cdots C_{pz}$ (3.665 Å), $H_{pz}\cdots C_{pq}$ (2.818, 2.863 Å), $H_{pq}\cdots C_{pz}$ (2.890 Å)

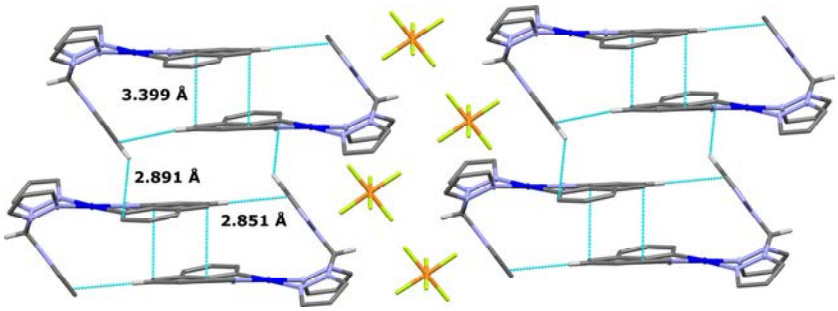

a)

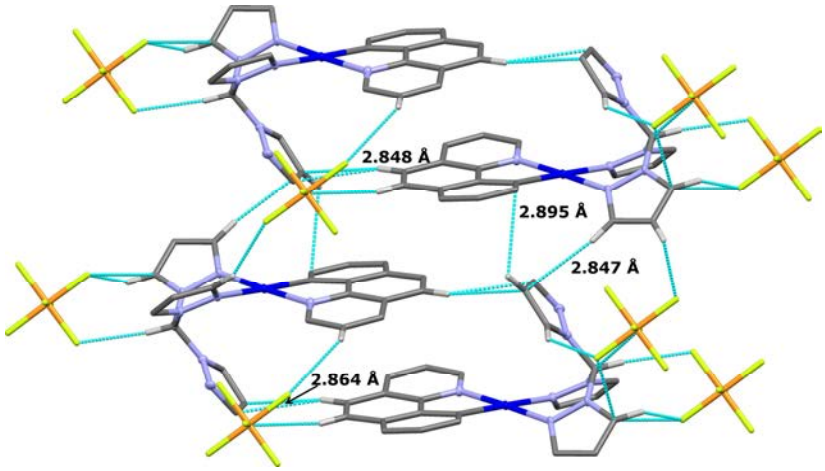

b)

Figura A1.3: Estructura supramolecular de **7** a) disposición de los dímeros en las cadenas mostrando las interacciones $\pi\cdot\cdot\pi$ entre los anillos ciclometalados (3.399 Å), con contribución de interacciones $H_{bzq}\cdot\cdot\cdot C_{pz\ libre}$ (2.851 Å) e interaccionan entre estos dímeros a través de contactos $\pi\cdot\cdot\pi$ bzq) (2.891 Å), b) interacciones entre los cationes y el anión PF_6^-

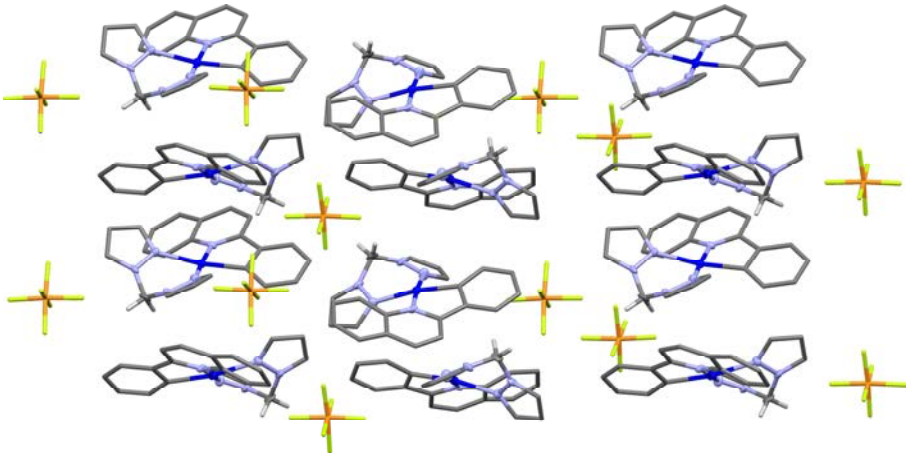

a)

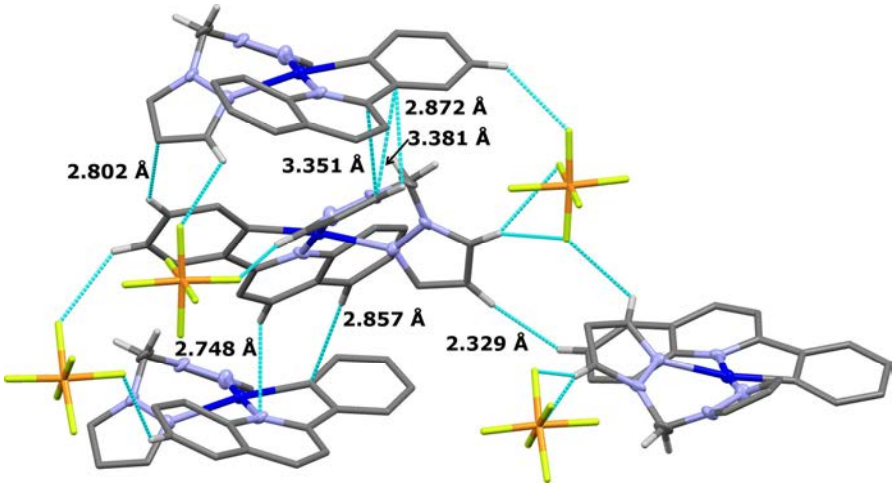

b)

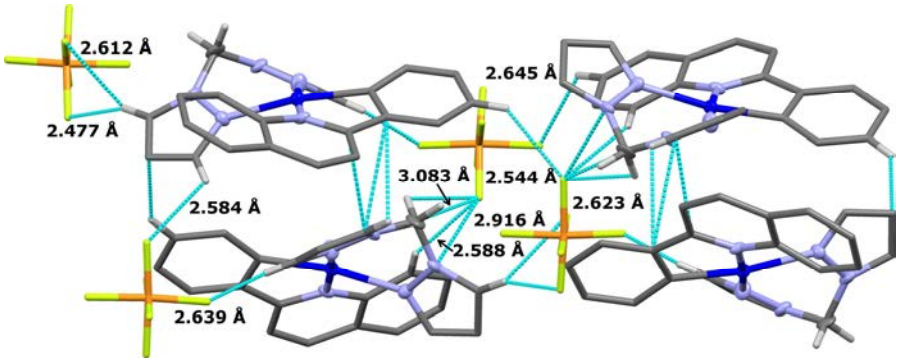

c)

Figura A1.4: Estructura supramolecular de [Pt(pq){$H_2C(pz)_2$}]PF_6 **6** a) disposición de las moléculas, b) y c) e interacciones entre los cationes y los aniones PF_6^- [$F_{PF_6}\cdots C_{C\text{-}H}$ (3.083 Å), $H_{C\text{-}H}$ (2.623 Å), H_{pq} (2.645–2.544 Å), N_{pz} (2.916 Å) y H_{pz} (2.639, 2.612, 2.584 y 2.477 Å), $H_{pz}\cdots H_{pq}$ (2.329 Å), $pq\cdots C_{pz}$ (3.381, 3.351 Å), $pq\cdots H_{pz}$ (2.872 Å), $H_{pq}\cdots C_{pz}$ (2.802 Å), $H_{pq}\cdots N_{pz}$ (2.748 Å), y $C_{pq}\cdots C_{pq}$ entre moléculas (2.857 Å)]

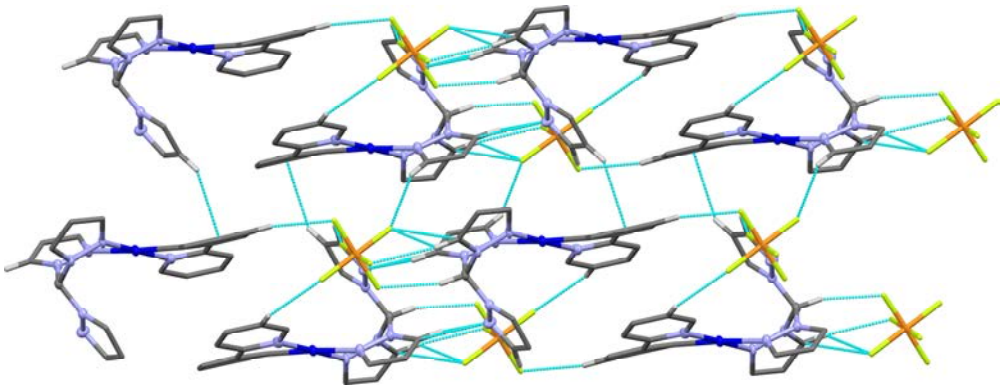

Figura A1.5: Estructura supramolecular de **8** mostrando las principales interacciones entre los cationes de $[Pt(ppy)\{HC(pz)_3\}]^+$ y los aniones PF_6^-

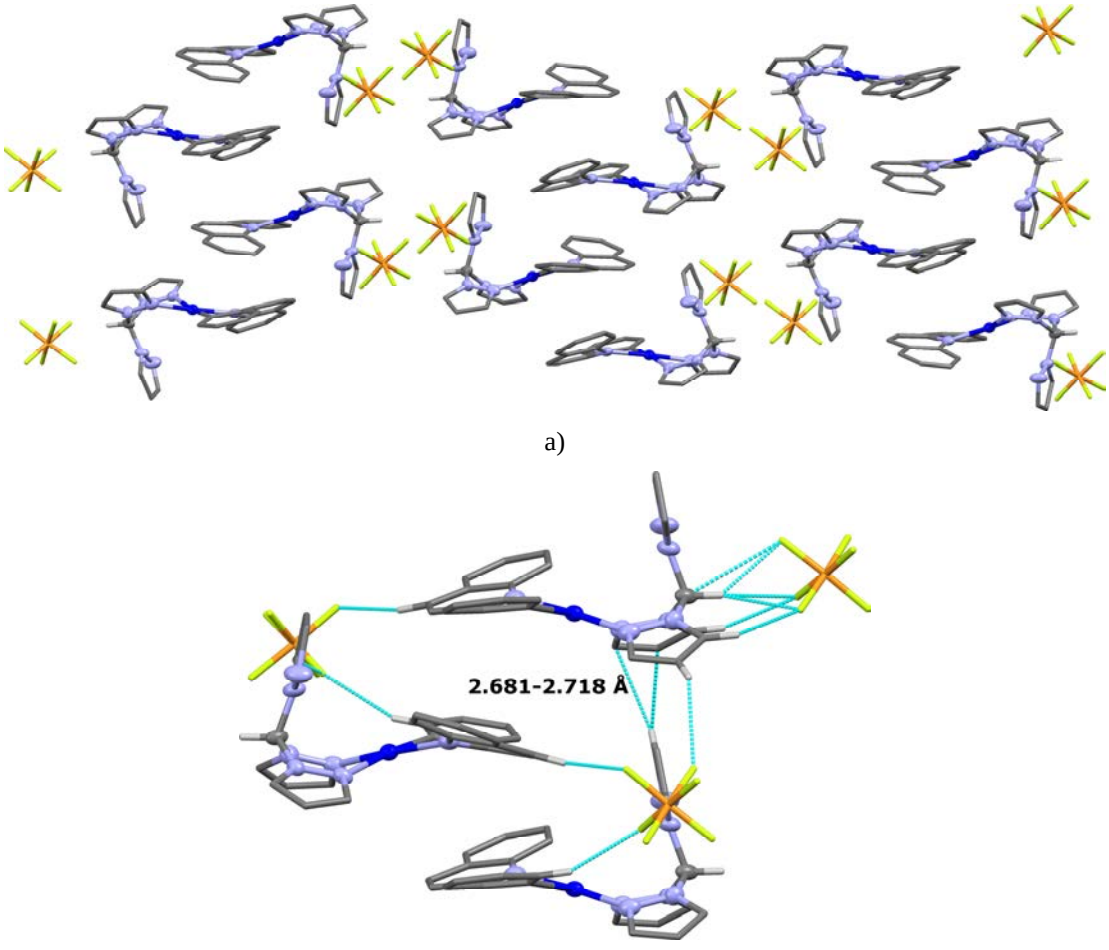

a)

b)

Figura A1.6: Estructura supramolecular de **9**. a) Disposición entre los cationes $[Pt(ppy)\{HC(pz)_3\}]^+$ con los aniones PF_6^- y b) principales interacciones [H_{C-H}, $H_{pz\ libre\ y\ coordinado}$ y H_{pq} (2.345–3.157 Å). $H_{pz\ libre}$ y un enlace C-C del anillo pirazolato coordinado *trans* a Carbono (2.681–2.718 Å)]

Tabla A1.4: Datos de Absorción UV-visible de los ligandos en disoluciones de CH_3CN $5x10^{-5}$ M a 298K

Ligando	λ_{abs}/nm (10^3 ε $M^{-1}cm^{-1}$)
Hbzq	231 (34.2), 272 (12.3), 292 (4.5), 329 (1.5)
Hppy	240 (7.7), 275 (8.5), 296_{sh} (1.5)
Hpq	225 (13.7), 238 (11.5), 273 (6.0), 284 (5.5) 322 (4.7), 336 (3.1)
$KH_2B(pz)_2$	223 (37.1), 248 (44.5), 266 (36.6), 270 (32.3)
$H_2C(pz)_2$	223 (39.1), 247 (44.8), 266 (36.3), 270 (12.2)
$HC(pz)_3$	223 (40.2), 247 (44.3), 266 (35.9), 270 (31.7)
$KHB(pz)_3$	223 (35.0), 247 (44.3), 266 (39.0), 270 (37.4), 283 (9.0)

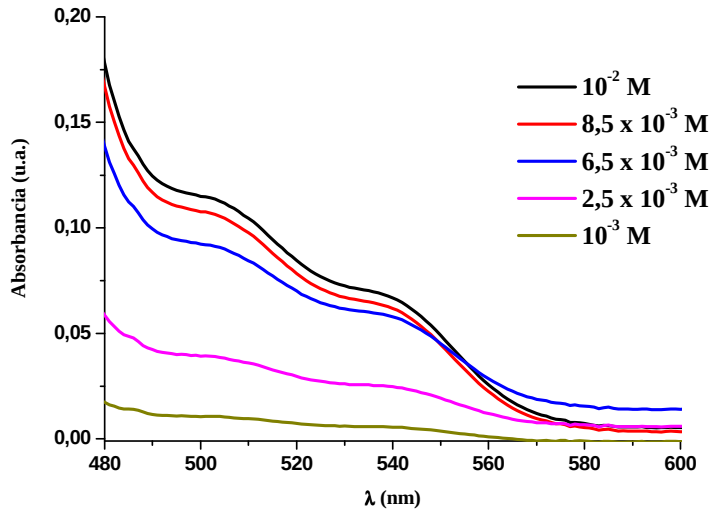

Figura A1.7: Ampliación de la zona de muy baja energía de los espectros UV-visible del compuesto **3** en CH_2Cl_2 en el rango de concentraciones 10^{-3}–10^{-2} M

Tabla A1.5: Datos de emisión de todos los derivados (**1**–**6**, **9** y **10**) en distintos disolventes a 298 y 77 K

Compuesto	Concentración/M (T°/K)	λ_{em}/nm (λ_{exc}/nm)
[Pt(bzq){$H_2B(pz)_2$}] **1**	CH_2Cl_2 10^{-3} (298)	490_{max}, 524, 560 (387–435)
	CH_2Cl_2 10^{-4} (298)	350, 375, 400_{sh}, 490_{max}, 524, 560_{sh} (280–300)
		490_{max}, 524, 560_{sh} (320–420)
	CH_2Cl_2 5×10^{-5} (298)	350_{max}, 367_{max}, 400_{sh}, 487, 520, 570_{sh} (280–320)
		487_{max}, 520, 570 (360–420)
	Tolueno 10^{-3} (298)	493_{max}, 524, 540 (390, 440)
	Tolueno 10^{-4} (298)	491_{max}, 522, 570 (370–420)
	Tolueno 5×10^{-5} (298)[a]	491_{max}, 522, 570 (370–420)
	CH_2Cl_2 10^{-3} (77)	500, 520_{max}, 560, 600 (330–420)
	CH_2Cl_2 10^{-4} (77)	500_{max}, 535, 600 (320–420)
	CH_2Cl_2 5×10^{-5} (77)	482_{max}, 520, 560 (310–420)
	Tolueno 5×10^{-5} (77)[b]	490_{max}, 530, 570 (340–430)
[Pt(ppy)$H_2B(pz)_2$] **2**	CH_2Cl_2 10^{-3} (298)	485_{max}, 520, 550, 600_{sh} (405)
	CH_2Cl_2 5×10^{-5} (298)	485_{max}, 520, 550, 600_{sh} (330–400)
	Tolueno 10^{-3} (298)	487_{max}, 522, 555, 600_{sh} (420)
	Tolueno 5×10^{-5} (298)[a]	487_{max}, 522, 555 (330–400)
	CH_2Cl_2 10^{-3} (77)	485_{max}, 520, 550, 630 (330–400)
	CH_2Cl_2 5×10^{-5} (77)	480_{max}, 520, 550 (330–400)
	Tolueno 5×10^{-5} (77)[b]	485_{max}, 520, 545, 600_{sh} (330–420)
[Pt(pq){$H_2B(pz)_2$}] **3**	CH_2Cl_2 10^{-3} (298)	$580–608_{max}$, 650_{sh} (455)
	CH_2Cl_2 5×10^{-5} (298)	$578–611_{max}$, 650_{sh} (320–420)
	CH_2Cl_2 5×10^{-5} (77)[a]	565_{max}, 607, 650_{sh} (350–440)
[Pt(bzq){$H_2C(pz)_2$}]$^+$ **4**	CH_2Cl_2 10^{-3} (298)	440_{max}, 490, 520_{sh} (365)
		490_{max}, 520_{sh} (425)
	CH_2Cl_2 5×10^{-5} (298)[a]	350, 365_{max}, 480 (275)
		365_{max}, 480 (330-350)
		480 (400)
	CH_2Cl_2 10^{-3} (77)	495_{max}, 532, 572 (320-390)
	CH_2Cl_2 10^{-4} (77)	495_{max}, 530, 570_{sh} (320-390)
	CH_2Cl_2 5×10^{-5} (77)	495_{max}, 520 (320-390)
[Pt(ppy)$H_2C(pz)_2$]$^+$ **5**	CH_2Cl_2 10^{-4} (298)[b]	480_{max}, 515, 543, 590_{sh} (350, 395)
	CH_2Cl_2 5×10^{-5} (298)	350, 364, 391_{sh}, 481_{max}, 515, 548, 589_{sh} (310–320)
		481_{max}, 515, 548, 589 (360–380)
	CH_2Cl_2 5×10^{-5} (77)[c]	481_{max}, 517, 545 (330–380)
[Pt(pq){$H_2C(pz)_2$}]$^+$ **6**	CH_2Cl_2 10^{-3} (298)	562, 594_{max}, 640_{sh} (440)
	CH_2Cl_2 5×10^{-5} (298)[b]	481, 516, 563_{max} (305–330)
		563_{max}, 595, 640_{sh} (350–400)
	CH_2Cl_2 5×10^{-5} (77)[c]	562_{max}, 602, 640_{sh} (350–430)
[Pt(pq){$HC(pz)_3$}]$^+$ **9**	CH_2Cl_2 10^{-3} (298)	560, 590_{max}, 642_{sh} (400–440)
	CH_2Cl_2 5×10^{-5} (298)	560_{max}, 602, 640_{sh} (350–420)
	CH_2Cl_2 5×10^{-5} (77)[c]	548_{max}, 590, 640 (340–440)
[Pt(pq){$HB(pz)_3$}] **10**	CH_2Cl_2 10^{-3} (298)	574-604[d] (456)
	CH_2Cl_2 5×10^{-5} (298)[b]	574-604[d] (360–430)
	CH_2Cl_2 5×10^{-5} (77)[c]	570_{max}, 610, 650_{sh} (340–430)

a) idéntico espectro a 10^{-4} M, b) idéntico espectro a 10^{-3} y 10^{-4} M

Tabla A1.6: Comparación de las distancias y ángulos de enlace de las estructuras experimentales y las estructuras optimizadas (S_0 y T_1) mediante cálculos DFT de **1**, **7, 8** y **9**

	1		
	Rayos X	**S_0**	**T_1**
Pt-N(1)	2.028(2)	2.06949	2.06964
Pt-N(2)	2.098(2)	2.17292	2.1595
Pt-N(4)	2.024(2)	2.04158	2.05379
Pt-C(1)	2.007(3)	2.01606	1.99650
B-N(5)	1.555(4)	1.56850	1.56829
B-N(3)	1.551(4)	1.56479	1.56411
B-H	0.9700	1.20499,1.20511	1.20514, 1.20463
N(1)-Pt-C(1)	81.62(10)	81.27159	80.72218
N(2)-Pt-N(4)	87.12(9)	85.47468	85.47409
N(1)-Pt-N(2)	95.75(9)	96.84431	97.11616
C(1)-Pt-N(4)	95.46(10)	96.40512	96.68666
N(3)-B-N(5)	107.4(2)	105.69545	105.58868
	7		
	Rayos X	**S_0**	**T_1**
Pt-N(1)	2.019(2)	2.05716	2.04681
Pt-N(2)	2.095(2)	2.21059	2.19417
Pt-N(4)	2.035(2)	2.06082	2.07373
Pt-C(1)	2.010(3)	2.01494	2.00821
C^a-N(5)	1.448(3)	1.44986	1.44911
C^a -N(3)	1.446(3)	1.45441	1.45443
C^a-N(6)	1.455(3)	1.44678	1.44690
C^a -H	0.91(3)	1.09449	1.09450
N(1)-Pt-C(1)	82.04(10)	81.40122	80.84369
N(2)-Pt-N(4)	85.73(8)	83.11196	83.22004
N(1)-Pt-N(2)	96.02(9)	98.53611	98.31278
C(1)-Pt-N(4)	96.16(9)	96.92804	97.58468
N(3)- C^a-N(5)	110.19(19)	110.98270	110.95036
H- C^a-N(6)	114.1(18)	110.85439	110.88547
	8		
	Rayos X	**S_0**	**T_1**
Pt-N(1)	2.015(3)	2.04775	2.02102
Pt-N(2)	2.107(3)	2.23934	2.22593
Pt-N(4)	2.032(3)	2.06315	2.07292
Pt-C(1)	1.991(3)	2.00252	1.97217
C^a-N(5)	1.450(4)	1.45158	1.45058
C^a -N(3)	1.450(4)	1.45242	1.45184
C^a-N(6)	1.454(4)	1.44582	1.44674
C^a -H	0.980	1.09436	1.09440
N(1)-Pt-C(1)	80.98(13)	80.59257	81.53331
N(2)-Pt-N(4)	84.86(10)	82.44711	82.77901
N(1)-Pt-N(2)	97.65(11)	99.63834	98.78317
C(1)-Pt-N(4)	96.50(12)	93.31704	96.92999
N(3)- C^a-N(5)	110.2(3)	110.89129	110.99654
H- C^a-N(6)	109.2	110.71197	110.76979
	9		
	Rayos X	**S_0**	**T_1**
Pt-N(1)	2.030(8)	2.06832	2.00425
Pt-N(2)	2.130(7)	2.22847	2.21760
Pt-N(4)	2.011(8)	2.06986	2.08259
Pt-C(1)	1.979(9)	1.99724	1.99364
C^a-N(5)	1.458(12)	1.45402	1.45315
C^a -N(3)	1.440(11)	1.44572	1.44571
C^a-N(6)	1.461(11)	1.44582	1.44674
C^a -H	0.980	1.09436	1.09440

N(1)-Pt-C(1)	79.8(3)	80.219	80.724
N(2)-Pt-N(4)	84.4(3)	81.93	82.77
N(1)-Pt-N(2)	100.3(3)	101.305	99.486
C(1)-Pt-N(4)	95.2(3)	96.112	96.778
N(3)- C^a-N(5)	110.3(7)	110.818	111.169
H- C^a-N(6)	108.8	110.71197	110.76979

C^a = CCH

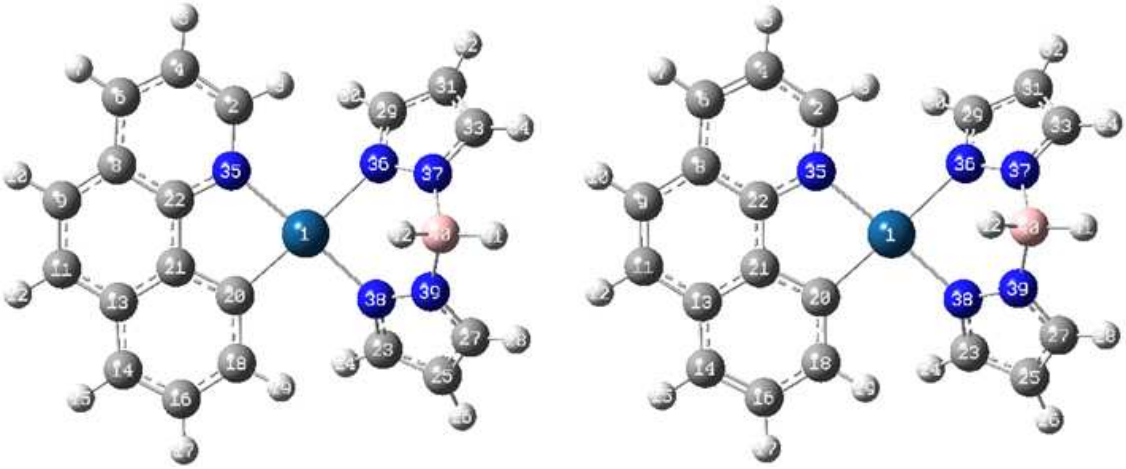

a) b)

Figure A1.8: a) Estructura optimizada mediante cálculos TD-DFT para el estado fundamental S_0 de **1**, b) Estructura optimizada mediante cálculos DFT para el estado triplete (T_1) de **1**

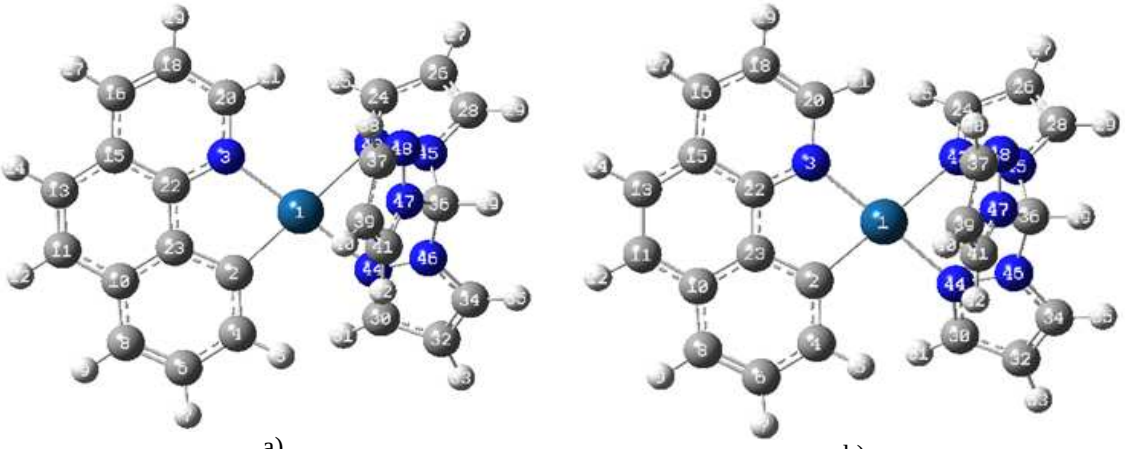

a) b)

Figure A1.9: a) Estructura optimizada mediante cálculos TD-DFT para el estado fundamental S_0 de **7**, b) Estructura optimizada mediante cálculos DFT para el estado triplete (T_1) de **7**

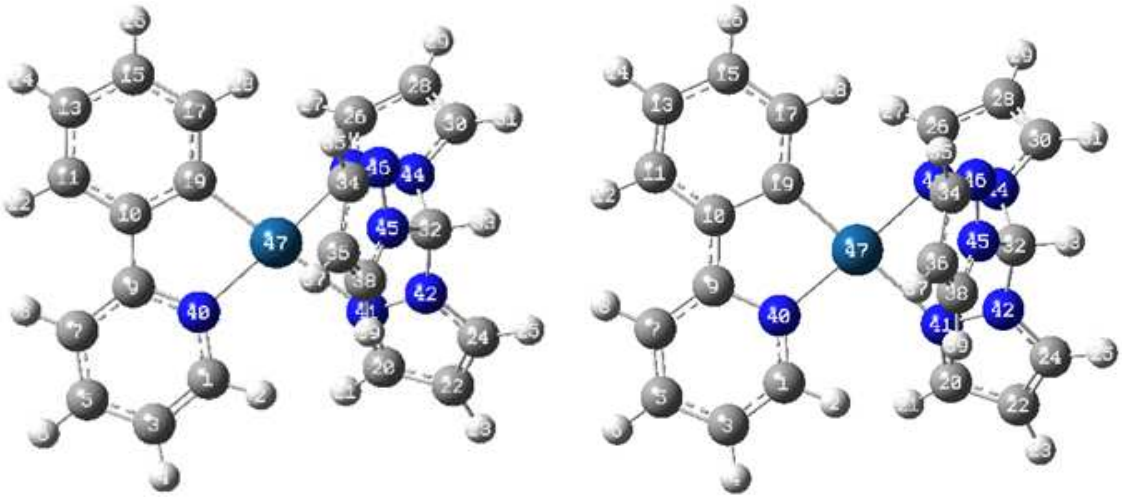

a) b)

Figure A1.10: a) Estructura optimizada mediante cálculos TD-DFT para el estado fundamental S_0 de **8**, b) Estructura optimizada mediante cálculos DFT para el estado triplete (T_1) de **8**

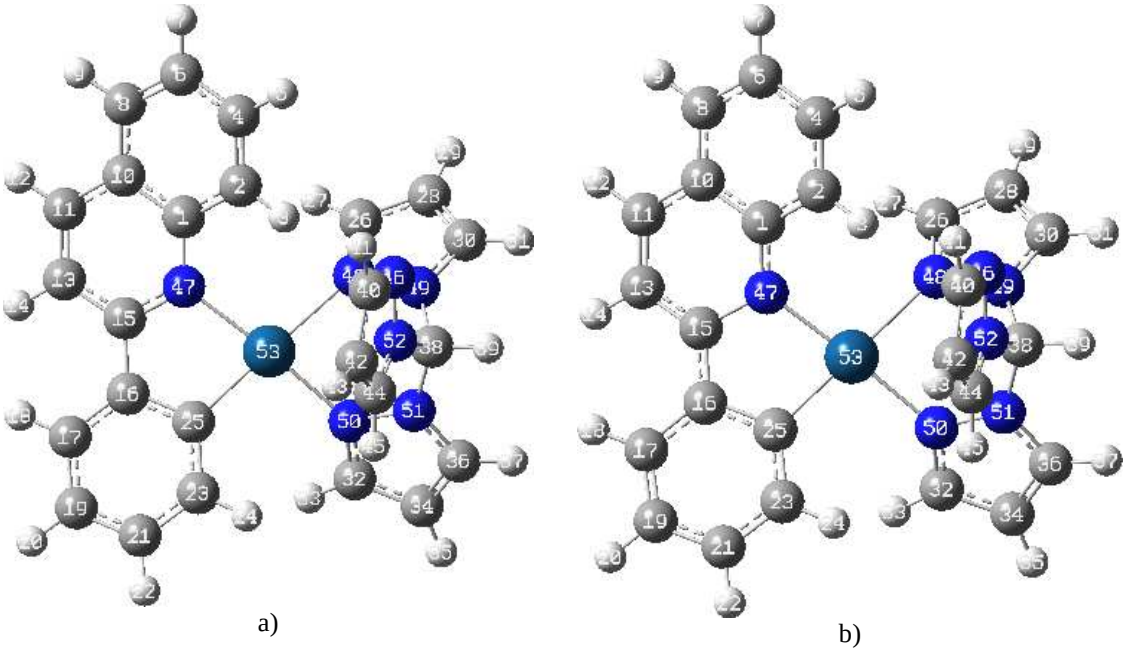

a) b)

Figure A1.11: a) Estructura optimizada mediante cálculos TD-DFT para el estado fundamental S_0 de **9**, b) Estructura optimizada mediante cálculos DFT para el estado triplete (T_1) de **9**

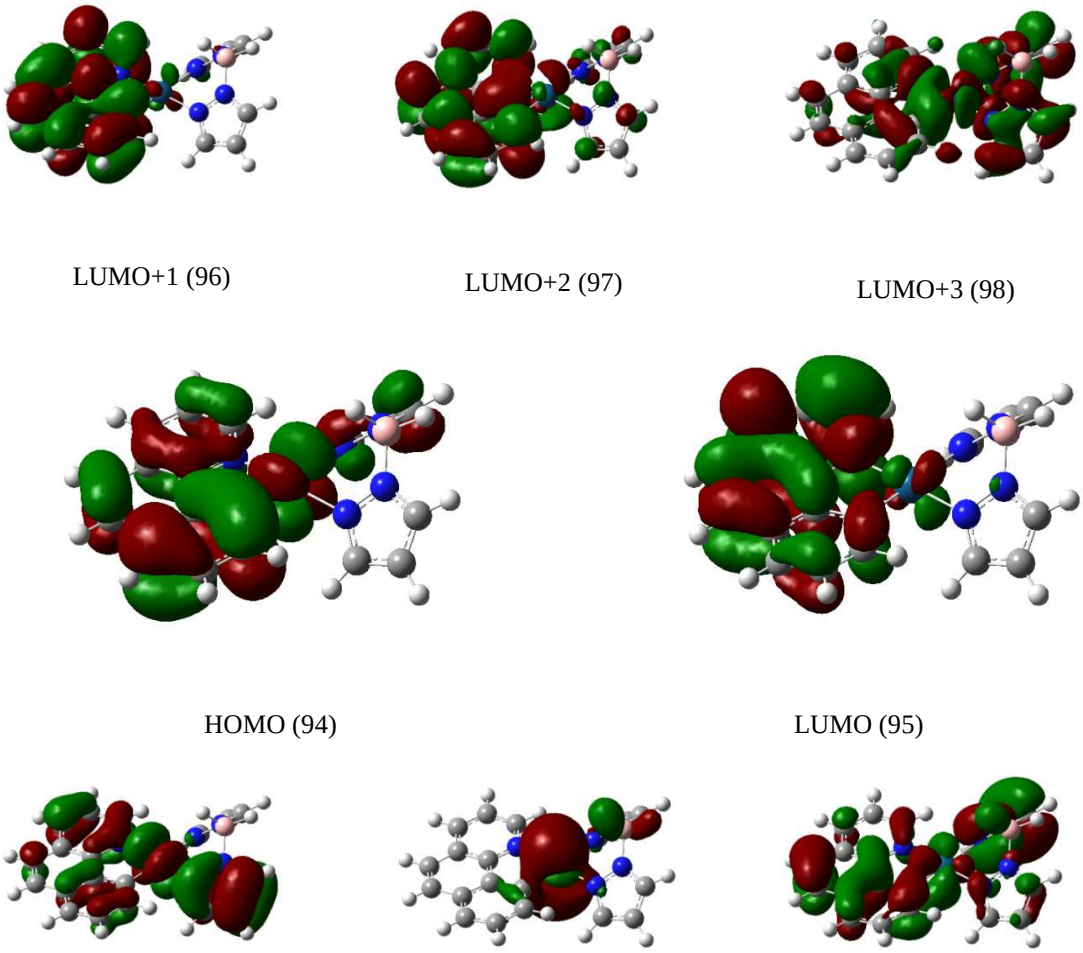

LUMO+1 (96) LUMO+2 (97) LUMO+3 (98)

HOMO (94) LUMO (95)

HOMO-1 (93) HOMO-2 (92) HOMO-3 (91)

Figura A1.12: Orbitales frontera representativos implicados en la absorción de **1** en CH_3CN

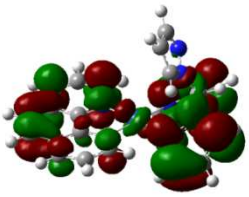

LUMO+1 (113)

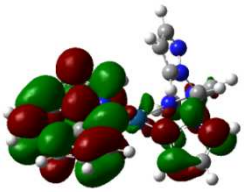

LUMO+2 (114)

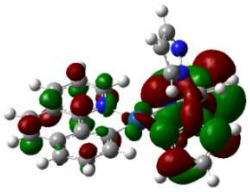

LUMO+3 (115)

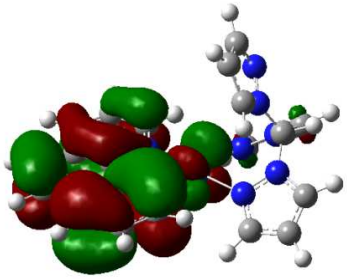

HOMO (111)

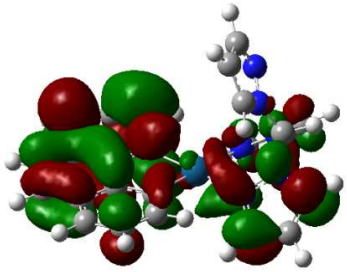

LUMO (112)

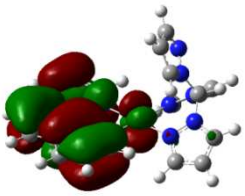

HOMO-1 (110)

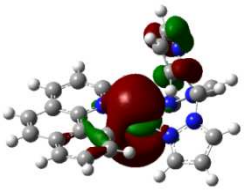

HOMO-2 (109)

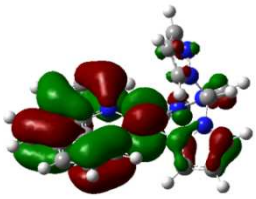

HOMO-3 (108)

Figure A1.13: Orbitales frontera representativos implicados en la absorción de **7** en CH_3CN

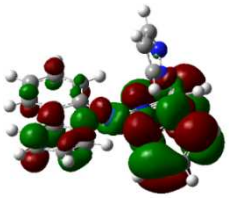

LUMO+1 (107)

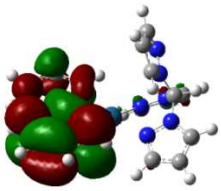

LUMO+2 (108)

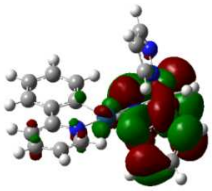

LUMO+3 (109)

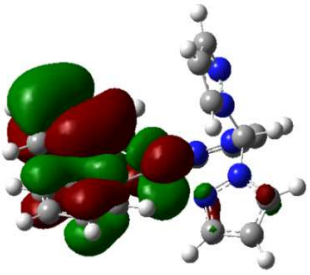

HOMO (105)

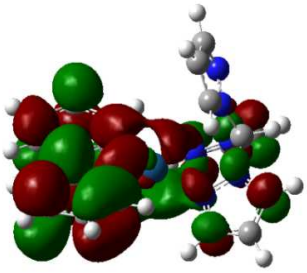

LUMO (106)

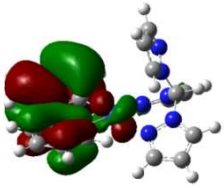

HOMO-1 (104)

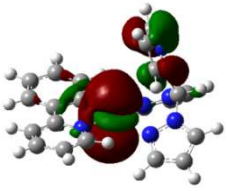

HOMO-2 (103)

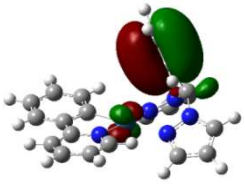

HOMO-3 (102)

Figure A1.14: Orbitales frontera representativos implicados en la absorción de **8** en CH_3CN

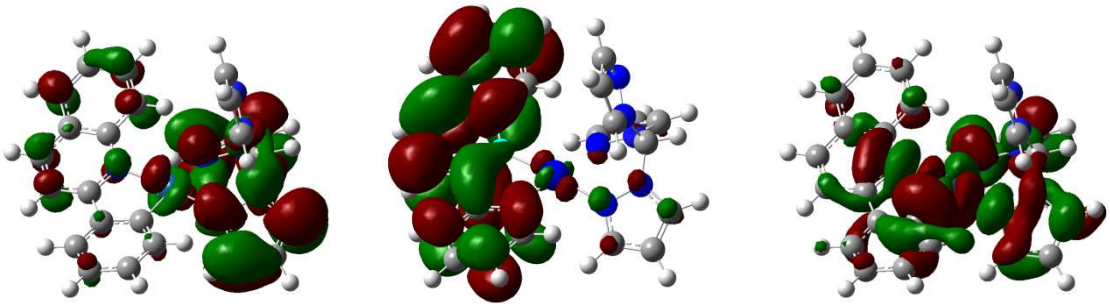

LUMO+1 (120) LUMO+2 (121) LUMO+3 (122)

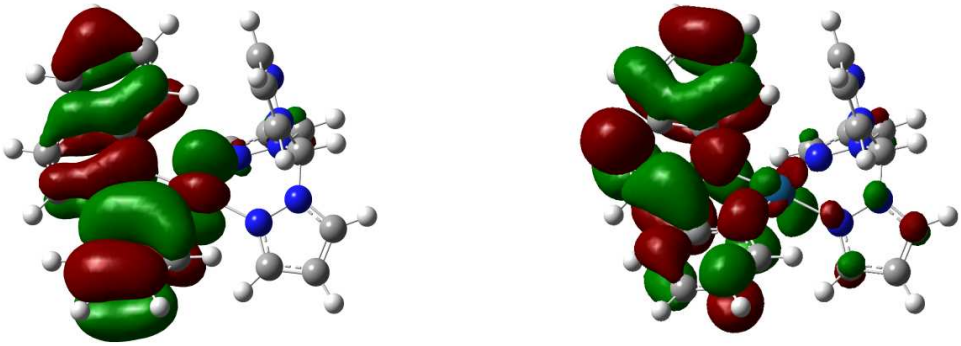

HOMO (118) LUMO (119)

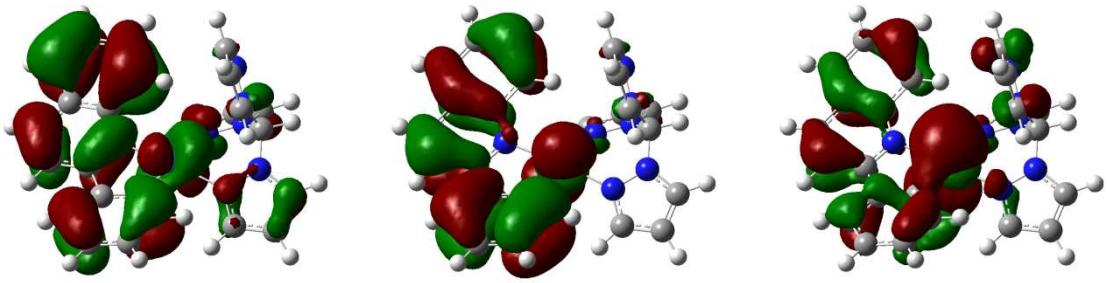

HOMO-1 (117) HOMO-2 (116) HOMO-3 (115)

Figure A1.15: Orbitales frontera representativos implicados en la absorción de **9** en CH_3CN

Tabla A1.7: Estados seleccionados singlete (S_0) de más baja energía calculados mediante DFT/CPCM (CH_3CN) con los orbitales implicados, las energías de excitación verticales y las posibles asignaciones para **1**, $\mathbf{7}^+$, $\mathbf{8}^+$ y $\mathbf{9}^+$

Estado	λ_{exc} (calc.)/nm	f [a]	Transición (Porcentaje de contribución)	Asignación (L=C^N; L'= N^N)
			1	
S_1	389.7	0.0474	HOMO->LUMO (90%)	ILCT/MLCT
S_2	338.7	0.0062	H-2->LUMO (93%)	MLCT
S_3	335.7	0.0592	H-1->LUMO (65%), HOMO->L+1 (18%), H-2->LUMO (5%)	MLCT/L'LCT
S_4	318.4	0.1777	H-3->LUMO (22%), H-1->LUMO (16%), HOMO->L+1 (52%)	ILCT/MLCT
S_5	308.8	0.0191	H-3->LUMO (67%), HOMO->L+1 (-12%), H-5-> LUMO (3%), H-4->LUMO (5%)	L'LCT/ILCT/ MLCT
S_6	308.4	0.0617	H-4->LUMO (33%), H-1->L+1 (38%), H-5->LUMO (3%), H-1->LUMO (3%), HOMO->L+1 (4%), HOMO->L+2 (2%),	L'LCT/ILCT/ MLCT
S_7	300.5	0.0138	H-4->LUMO (-10%), H-2->L+1 (67%), H-1->L+1 (9%)	MLCT
S_8	290.8	0.0351	H-5->LUMO (-11%), H-4->LUMO (35%), H-2->L+1 (26%), H-1->L+1 (-17%)	MLCT/L'LCT/ ILCT
			$\mathbf{7}^+$	
S_1	383.3	0.055	HOMO->LUMO (91%),	ILCT/ML'CT
S_2	330.3	0.0176	H-2->LUMO (-22%), H-1->LUMO (55%), HOMO->L+1 (-15%)	ILCT/LL'CT
S_3	327.1	0.0128	H-2->LUMO (74%), H-1->LUMO (12%), HOMO->L+1 (-9%)	MLCT/ML'CT/IL'CT
S_4	315.6	0.2208	H-1->LUMO (17%), HOMO->L+1 (61%), HOMO->L+2 (-4%)	LL'CT/ILCT/ ML'CT
S_5	293.6	0.0955	H-5->LUMO (48%), H-1->L+1 (-10%), HOMO->L+2 (-14%), H-3->LUMO (-8%)	L'LCT/ILCT/IL'CT
			$\mathbf{8}^+$	
S_1	362.2	0.0445	HOMO->LUMO (91%)	ILCT/ML'CT
S_2	321.7	0.0111	H-2->LUMO (95%)	MLCT/IL'CT /ML'CT
S_3	306.3	0.1308	H-1->LUMO (79%)	ILCT/LL'CT
S_4	298.8	0.0437	H-3->LUMO (59%), HOMO->L+1 (26%), HOMO->L+2 (10%)	L'LCT/IL'CT
S_5	292.7	0.0343	HOMO->L+1 (-15%), HOMO->L+2 (44%), HOMO->L+4 (29%)	ILCT/MLCT
S_6	282.9	0.0763	H-2->L+4 (-12%), HOMO->L+1 (21%), HOMO->L+4 (28%), H-3->LUMO (-9%)	LL'CT/ILCT
S_7	282.2	0.1953	H-3->LUMO (-18%), HOMO->L+1 (17%), HOMO->L+2 (32%), HOMO->L+4 (-14%), H-1->LUMO (5%)	ILCT/L'LCT/MLCT
S_8	277.3	0.0588	H-2->L+2 (17%), H-2->L+4 (42%), HOMO->L+1 (8%), HOMO->L+4 (7%)	MLCT/IL'CT
			$\mathbf{9}^+$	
S_1	401.6	0.0549	HOMO->LUMO (90%)	ILCT/MLCT/ML'CT
S_2	351.3	0.0857	H-3->LUMO (-15%), H-2->LUMO (-15%), H-1->LUMO (61%)	ILCT/MLCT
S_3	346.7	0.0578	H-3->LUMO (49%), H-2->LUMO (19%), H-1->LUMO (27%)	MLCT/ILCT
S_4	329.8	0.2023	H-3->LUMO (-29%), H-2->LUMO (53%), HOMO->L+2 (7%)	ILCT/ML'CT
S_5	315.2	0.0129	H-5->LUMO (85%)	MLCT/ILCT/L'LCT/ IL'CT
S_6	305.4	0.027	HOMO->L+1 (47%), HOMO->L+3 (24%),	L'LCT/ML'CT/ILCT

S_7	299.9	0.0552	HOMO->L+2 (6%), HOMO->L+4 (7%) HOMO->L+1 (42%), HOMO->L+2 (-10%), HOMO->L+3 (-25%)	L’LCT/ML’CT/ILCT

a) Fuerza del oscilador

CHAPTER 2

Phenylquinoline and phenylquinolinyl alkynyl based Pt^{II} complexes

Phenylquinoline and phenylquinolinyl alkynyl based Pt^{II} complexes

As commented previously in the Introduction, in contrast with the wide body of knowledge acquired on σ-alkynyl cycloplatinated complexes,[1] the chemistry of related polymetallic systems stabilized by alkynyl bridging ligands remains in its infancy.[2] In particular, as far as we know, only two C^N bimetallic complexes connected by μ–C≡CR have been described,[3] but with special focus on their structural and reactivity characteristics. Notably, several series of discrete binuclear cyclometalated complexes bearing single or double bridging ligands have been spectroscopically characterized, showing that the linkers can control the degree of metal-metal contact spacing. The linkers used so far, in most cases, are bidentate organic anions,[4] diphosphines,[4a,5] pyridine-thiolate[6] or pyrazolate ligands[5b,7] In particular, pyrazolate-bridged binuclear Pt(II) complexes have been extensively studied,[5b,7] showing that the increases steric bulk in 3 and 5 positions of the μ-pyrazolate enhanced Pt···Pt separation (stabilizing the Pt···Pt σ and destabilizing the σ* bonding orbitals), shifting systematically the emissions to lower energies.

Several years ago, our group reported the first examples of anionic cycloplatinated complexes with monodeprotonated 7,8-benzoquinolinyl $(NBu_4)[Pt(bzq)(C{\equiv}CR)_2]$[8] and the dideprotonated 2,6-diphenylpiridinyl $(NBu_4)[Pt(dppy)(C{\equiv}CR)]$[1v] groups, by using $[Pt(bzq)(\mu\text{-}Cl)]_2$ or [Pt(dppy)(dmso)] as precursors, respectively. The synthesis of these complexes required the use of appropriate LiC≡CR as alkynylating agent and subsequent precipitation of the *in situ* formal anionic species with tetrabutylamonium. By contrast, treatment of the binuclear $[Pt(C^N)(\mu\text{-}Cl)]_2$ precursors with HC≡CR in the presence of NaOMe (or HC≡CR/NEt_3/CuI) evolves with formation of the binuclear $[\{Pt(dppyH)\}4_2(\mu\text{-}Cl)(\mu\text{-}C{\equiv}C^tBu)]$ or unusual tetranuclear clusters $[Pt_2(bzq)_2(\mu\text{-}Cl)(\mu\text{-}C{\equiv}CR)_2]_2$ (R = ^{t}Bu, Ph, $C_6H_4CF_3$-4), depending on the nature of the cyclometalating ligand.[9] Aiming to expand the family of anionic precursors of the type bis(alkynyl)cycloplatinate systems $[Pt(C^N)(C{\equiv}CR)_2]^-$, we decided to study the reactions of the phenylquinolinyl derivative $[Pt(pq)(\mu\text{-}Cl)]_2$ with LiC≡CR which are described in this Chapter. We have discovered

that these reactions evolve with formation of unusual mononuclear anionic tris(alkynyl) complexes $(NBu_4)[Pt(Hpq-\kappa N)(C{\equiv}CR)_3]$ (R = Tol **13**, C_6H_4OMe-3 **14,** $C_6H_4CF_3$-4 **15**), containing the N-coordinated Hpq ligand, or binuclear cyclometalated derivatives $[Pt(pq)(\mu{-}\kappa C^{\alpha}{:}\eta^2\text{-}C{\equiv}CR)]_2$ (R = ^{t}Bu, **16**, Tol **17**, C_6H_4OMe-3 **18**, $C_6H_4CF_3$-4 **19**) stabilized by a double σ/π alkynyl bridging system, depending on the substituents in the alkynyl group and the reaction conditions. We report bellow the synthesis, characterization, electronic absorption and luminescence of both families of compounds. We have investigated how the systematic variation of alkynyl ligand affects to the photophysical properties of these complexes and a theoretical understanding of the geometries, electronic structures and phosphorescence spectra based on the study on complexes **14**$^-$, **16** and **17**.

2.1 Synthesis and characterization

Following the strategy described for the $[Pt(bzq)(C{\equiv}CR)_2]^-$ derivatives, treatment of the insoluble $[Pt(pq)(\mu\text{-}Cl)]_2$ with an excess of LiC≡CR (1:8) and subsequent extraction with deoxygenated ^{i}PrOH or mixed ^{i}PrOH/H_2O, ^{i}PrOH/CH_2Cl_2 in presence of NBu_4Br (see the Experimental Section) leads, in the case of aromatic substituents, to the formation of the anionic species $(NBu_4)[Pt(Hpq-\kappa N)(C{\equiv}CR)_3]$ (R = Tol **13**, C_6H_4OMe-3 **14**, $C_6H_4CF_3$-4 **15**) (30-58%) (Scheme 2.1a). By using 5 equiv. of LiC≡CR and the same solvents in the extraction step, the derivatives **13**–**15** were also obtained as main products. However, the reactions with the *ter*-butylethynyl LiC≡C^{t}Bu, either 1:8 or 1:5 molar ratio, gave the neutral derivative $[Pt(pq)(\mu{-}\kappa C^{\alpha}{:}\eta^2\text{-}C{\equiv}C^tBu)]_2$ (**16**), whose synthesis was optimized by using 3 equiv. of LiC≡C^{t}Bu. In fact, when the reactions of $[Pt(pq)(\mu\text{-}Cl)]_2$ with LiC≡CR (R = Tol, C_6H_4OMe-3, $C_6H_4CF_3$-4) were performed using a 1:3 molar ratio, the related binuclear complexes $[Pt(pq)(\mu{-}\kappa C^{\alpha}{:}\eta^2\text{-}C{\equiv}CR)]_2$ (**17**–**19**) were synthesized (54-87%) (Scheme 2.1b).

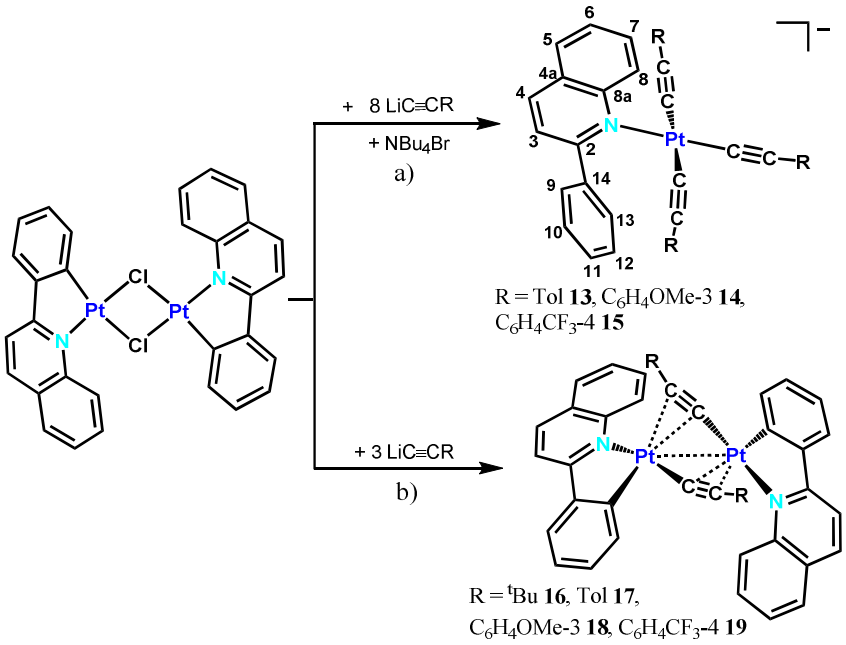

Scheme 2.1

The formation of **13**–**15** involves formally the rupture of a Pt-C ortometalated bond, the protonation of the pq ligand and the formation of three Pt-alkynyl bonds. Probably, the reaction takes place first with N-dissociation of the pq-κ*CN* ligand in the presence of excess C≡CR to give the dianionic species "[Pt(pq-κ*C*)(C≡CR)$_3$]$^{2-}$". The N-dissociation of C^N ligands to give monocoordinated κ^1*C* ligands is not a common fact, but has been observed in reactions of some C^N cycloplatinated complexes with phosphines[10] or tht.[11] The doubly charged complex would be probably unstable evolving through easy protonation by the solvent (H_2O/^{i}PrOH) to less charged κ*N* -coordinated anionic species "[Pt(Hpq-κ*N*)(C≡CR)$_3$]$^-$", which are finally precipitated as tetrabutylammonium complexes **13**–**15**. It is well known that hemilability of the ligands is relevant in view of their utility in homogeneous catalysis.[12] To avoid the protonation of the pq, we tried to extract with CH_2Cl_2 in the reaction 1:8, obtaining in these conditions mixtures of the anionic mononuclear **13**–**15** species and the corresponding neutral binuclear derivatives **17**–**19**.

All complexes **13**–**19** were obtained as orange solids in moderate (**13**–**15**) or high yields (**16**–**19**) and satisfactory mass spectra, elemental analysis, IR and NMR [^{1}H, ^{13}C{^{1}H}, ^{195}Pt{^{1}H}] spectra were obtained for each newly synthesized Pt(II) complex. The molecular structures of **14**, **16** and **17** were confirmed by X-ray crystallography.

Complexes **13**–**15** give the negative ion $[Pt(C{\equiv}CR)_3]^-$, together with the ion $[Pt(pq)(C{\equiv}CR)_2]^-$ (100%) in their MALDI(-), and their conductivity measurements in acetone confirm their behaviour as 1:1 electrolites. The IR spectra of **13**–**15** show two ν(C≡C) intense absorptions (2110-2112 and 2073-2085 cm^{-1} ranges) in the typical range for terminal σ-coordinated alkynyl ligands. The latter values lie at the low end reported for terminal alkynyl ligands, suggesting that in these anionic systems the Pt atom is probably good π-back donor toward the π* orbital of the alkynyl ligands, which weakens the corresponding C≡C bonds.

The NMR data (labelling in Scheme 2.1) unambiguously reveal the presence of the Hpq ligand and two inequivalent alkynyl groups. The ^1H NMR spectra, assigned on the basis of 2D ^1H-^1H and ^1H-^{13}C COSY experiments, show 11 signals corresponding to all nonequivalent hydrogens of the Hpq ligand (Figure 2.1). Notably, the H^{13} resonance appears at low field (δ 10.49-10.60), considerably shifted to high frequencies in comparison with the free ligand (δ 8.17), likely due to the anisotropic deshielding provoked by its close proximity to the C(25)≡C(26) acetylenic fragment.[13] The next resonance (δ 8.65-8.53) appears with platinum satellites ($J_{195Pt\text{-}H}$ = 39.1-44.6 Hz) being assigned to the H^8 proton. This signal is also downfield shifted in relation to the free ligand (δ 8.16), presumably by the close proximity of the proton H^8 to the Pt center in a pseudoaxial position, even in solution, suffering a certain anisotropic deshielding associated with the Pt dz^2 electron density.[14] In the high-field region, two different very close methyl resonances in **13** and **14** (δ CH_3 2.28, 2.27 **13**, OCH_3 3.79, 3.74 **14**) in a relation of 6:3 confirm the presence of two distinct alkynyl groups (C≡CR *trans* to N and C≡CR *trans* to C≡CR). $^{13}C\{^1H\}$ NMR spectra of **14** and **15** show the expected resonances for the Hpq ligand, in addition to those of the NBu_4^+ cation and two C≡CR different groups (acetylenic C only seen in **15**), although the assignments are uncertain because no satellites are observed. By comparison with related systems[8,15] and in base to the lower *trans* influence of the N atom, the C atoms which appear at high field (δ 100.7, 101.5) are tentatively assigned to the C^α and C^β *trans* to the N atom of the Hpq, whereas the downfield signals (δ 106.8, 111.3) are assigned to the C^α and C^β *trans* to C≡CR. The $^{195}Pt\{^1H\}$ NMR of the most soluble and stable complex **15** at low temperature (253 K) shows a broad singlet signal at δ -3845.

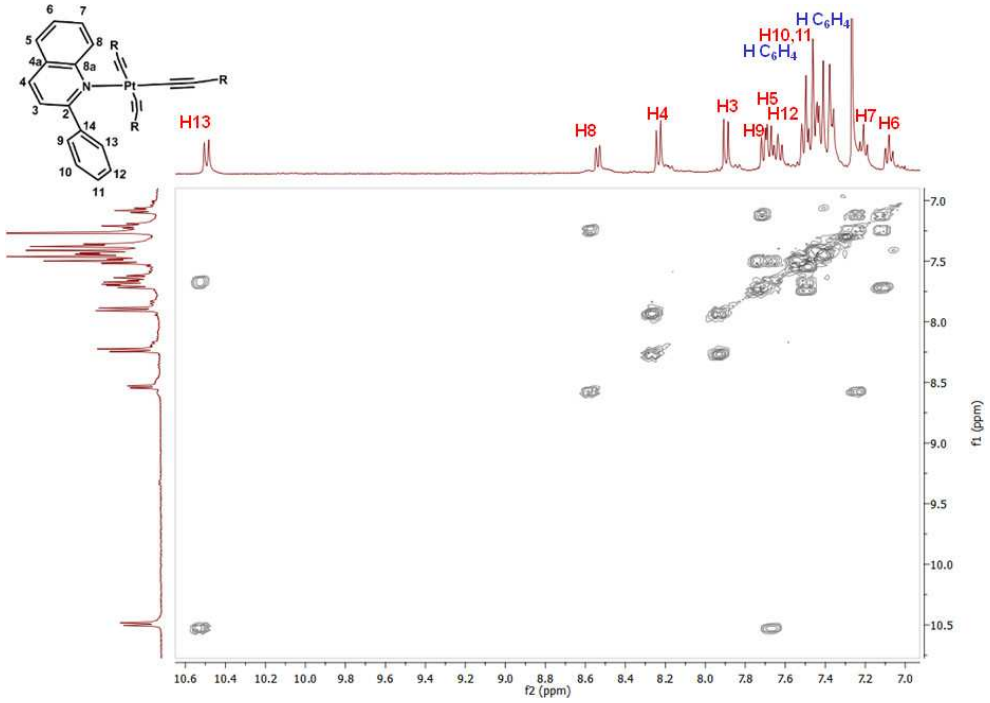

Figure 2.1: Selected region of the ^{1}H-^{1}H COSY of complex (NBu$_4$)[Pt(Hpq-κN)(C≡CC$_6$H$_4$-CF$_3$-4)$_3$] (**15**)

The molecular structure of the anion of complex **14**·CH_2Cl_2 (Figure 2.2, Table 2.1) confirmed the presence of three C≡CC$_6$H$_4$OMe-3 groups and a nonchelated 2-phenylquinoline ligand N-coordinated to the Pt center. It is worth mention that, as far as we know, only one X-ray structure based on tris(alkynyl)platinate "Pt(C≡CR)$_3$" fragments has been described.[16] The pendant phenyl ring of the Hpq group is twisted by 46.5º with respect to the quinoline fragment, which is oriented at 78.0º to the plane formed by the Pt(C≡CR)$_3^-$ fragment, being almost perpendicular to it. The steric bulk of the ligand makes the presence of π···π intermolecular interactions difficults. The symmetrical Pt-C(alkynyl) mutually *trans* distances [Pt-C(25) 1.995(6), Pt-C(34) 2.008(6) Å] are relatively longer than the Pt-C distance *trans* to the N atom [Pt-C(16) 1.966(6) Å], in agreement to the smaller *trans* influence of the N atom in relation to the acetylenic carbon. The C(25)-C(26)-C(27) alkynyl fragment is slightly distorted from the linearity [Pt-C$^{\alpha}$-C$^{\beta}$/C$^{\alpha}$-C$^{\beta}$-C$^{\gamma}$ 172.8(5)º/172.4(7)º], presumably due to the occurrence of a close H···C≡C *intramolecular* interaction with the *ortho*-H(13) phenyl pendant of the Hpq [H(13)-C(15) 2.519 Å]. It is worth noting that there are precedents for the presence of weak C-H···π(alkyne) contacts in the crystal structures of alkynyl complexes, but they are usually *intermolecular* solvent C-H···π(alkyne) interactions.[15,17]

In fact, the crystallization CH_2Cl_2 solvent also establishes a weaker contact (2.681 Å) with the same alkynyl unit (Figure 2.2). Furthermore, the coordination of the Hpq ligand places the H(8) proton of the quinoline in a pseudoaxial position above the platinum coordination plane, with a deviation of Pt-H(8) of ~14º from the normal to this plane. The Pt(1)-H(8) (2.642 Å), Pt(1)-C(8) (3.175 Å) and the angle Pt(1)-H(8)-C(8) (117.09º) fall in the lowest range of the Pt···H bonding interactions reported in the literature.[14a,b,18]

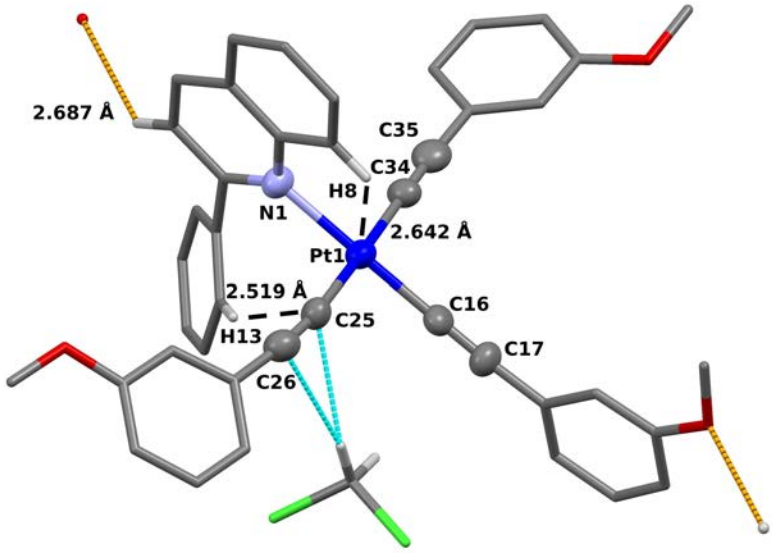

Figure 2.2: View of the molecular structure of the anion in the complex $(NBu_4)[Pt(Hpq\text{-}\kappa N)(C{\equiv}CC_6H_4OMe\text{-}3)_3]\cdot CH_2Cl_2$ (**14**·CH_2Cl_2)

Table 2.1: Selected bond lengths[**Å**] and angles[º] for $(NBu_4)[Pt(Hpq\text{-}\kappa N)(C{\equiv}CC_6H_4OMe\text{-}3)_3]\cdot CH_2Cl_2$ (**14**·CH_2Cl_2)

14·CH_2Cl_2			
Pt(1) -N(1)	2.133(4)	Pt(1) -C(25)	1.995(6)
Pt(1) -C(16)	1.966(6)	Pt(1) -C(34)	2.008(6)
C(16)-C(17)	1.176(8)	C(25)-C(26)	1.221(9)
C(34)-C(35)	1.198(9)		
C(25)-Pt(1)-C(16)	91.9(2)	N(1)-Pt(1)-C(34)	90.6(2)
C(25)-Pt(1)-N(1)	87.9(2)	C(34)-Pt(1)-C(16)	89.6(2)
Pt(1)-C(16)-C(17)	178.6(5)	C(16)-C(17)-C(18)	175.2(6)
Pt(1)-C(25)-C(26)	172.8(5)	C(25)-C(26)-C(27)	172.4(7)
Pt(1)-C(34)-C(35)	178.3(5)	C(34)-C(35)-C(36)	174.9(7)

Supramolecular packing of the crystal structure (Figures 2.2 and 2.3a) reveals the presence of a contact between the oxygen atom of the methoxy group (*trans* to Hpq) and the quinolinyl unit [O···H(Hpq) 2.687 Å] of a neighboring anion, giving rise to

extended chains, together with weak noncovalent interactions with the solvent (CH_2Cl_2) and the NBu_4^+ cation (Figure 2.3b).

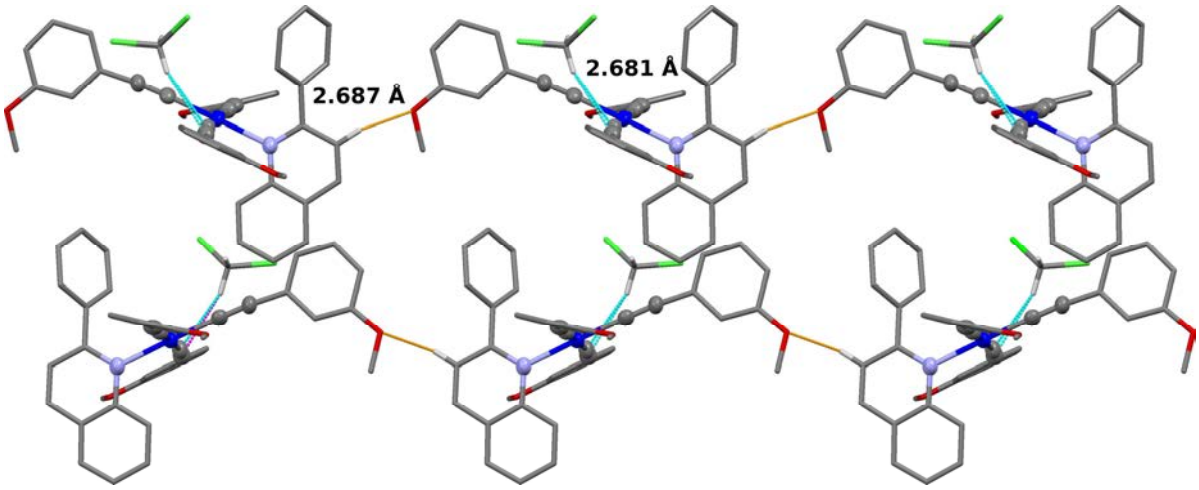

a)

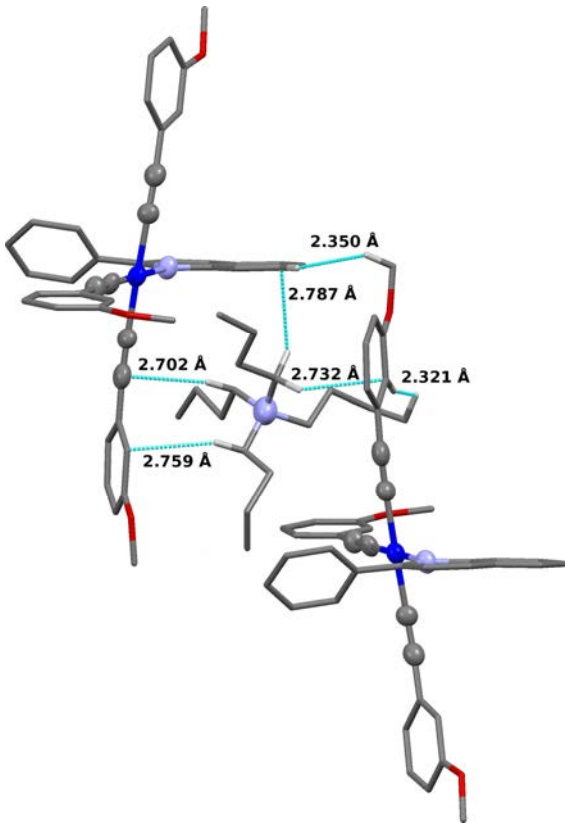

b)

Figure 2.3: Packing of the complex $(NBu_4)[Pt(Hpq\text{-}\kappa N)(C{\equiv}CC_6H_4OMe\text{-}3)_3]\cdot CH_2Cl_2$ (**14**$\cdot CH_2Cl_2$) showing a) the disposition of the chains (c axis) and b) the weak non-covalent interactions (shorter than 2.800 Å) $C/H_{Ph}\cdots H_{NBu_4}$ (2.321, 2.732, 2.759 Å), $C_{pq}\cdots H_{NBu_4}$ (2.787 Å), $C_{C\equiv C}\cdots H_{NBu_4}$ (2.702 Å) (a axis)

The symmetric binuclear complexes **16**–**19** are stabilized by a double alkynyl bridging system. As it is indicated in the Introduction, although binuclear diplatinum derivatives of this type are well known,[2a,3,19] systems containing cyclometalated ligands are rare.[3] The structure of complexes **16** and **17** (Figure 2.5 and Table 2.2, see below) and spectroscopic data of all of them confirmed that the reactions takes place selectively to give derivatives that adopt a *transoidal* disposition, as those previously described,[3] with the N of the pq ligand *trans* to the σ-alkynyl ligand and the C cyclometalated atom *trans* to the η^2-alkynyl ligand. The MALDI(+) mass spectra show the peaks corresponding to their respective molecular ion, as well as the corresponding to the loss of one alkynyl ligand. All complexes show two characteristic ν(C≡C) bands (or one broad) at 2040-1993 cm^{-1} range in the typical region of η^2-alkynyl C≡CR bridging groups[2a,3,19] The corresponding NMR spectra (^1H, $^{13}C\{^1H\}$ and ^{19}F) reveal the presence of only one set of pq signals and one type of alkynyl ligand (see Experimental Section).

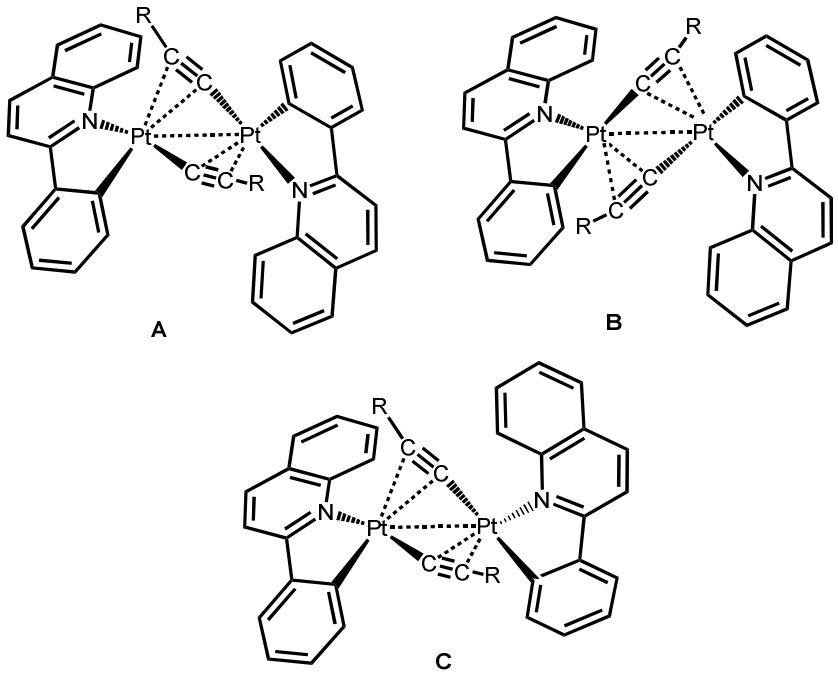

Scheme 2.2

Of the three possible isomers for this disposition μ–κC^{α}:η^2 (Scheme 2.2), only the *transoidal* isomers **A** and **B** are consistent with this pattern, because **C** should give two different sets of cyclometalated and alkynyl signals. The selective formation of **A** (confirmed by X-ray) is in accordance with that which would be expected taking into account the great *trans* influence of the σ-alkynyl carbon and the C cyclometalated.

Thus, in **A** the σ-C≡CR is *trans* to the N of less *trans* influence, whereas in **B** is located *trans* to the cyclometalated carbon.

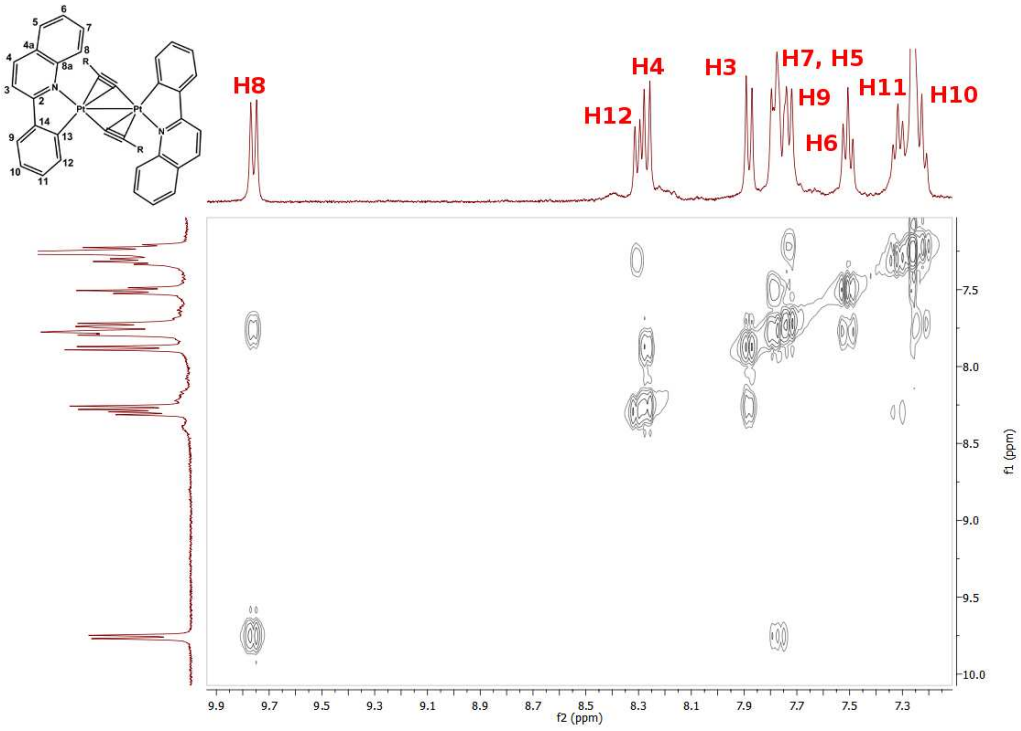

Figure 2.4: Selected region of the ^{1}H-^{1}H COSY of complex [Pt(pq)(μ–κC$^{\alpha}$:η^{2}-C≡C^{t}Bu)]$_2$ (**16**)

The most characteristic signals in their ^{1}H NMR (See Figure 2.4 for **16**) spectra correspond to H^{8} (δ 9.30-9.76 range) and H^{12} (8.44-8.30), this latter with characteristic $^{3}J^{1}_{\text{H-}^{195}\text{Pt}}$ coupling constants (72.1-82.1 Hz) (Figure 2.4). The singlet resonance at δ 0.96 (^{t}Bu **16**), 2.04 (CH_3, **17**) and 3.40 (OCH_3, **18**) in their ^{1}H NMR spectra and δ -63.0 (CF_3 **19**) in the ^{19}F NMR spectrum prove the chemical equivalence of the alkynyl ligands in each molecule. In the ^{13}C{^{1}H} NMR spectra the metalate C^{13} carbon is found at δ 147.9-145.6, although unfortunately platinum satellites are not observed. The C$^{\alpha}$ and C$^{\beta}$ alkynyl carbons exhibit only platinum satellites in **19**, allowing the assignment of the downfield signal (δ 101.7, $J_{\text{Pt-C}}$ ~ 410 Hz **19**) at the C$^{\beta}$ and the highfield signal (δ 97.1, $J_{\text{Pt-C}}$ ~ 1460 Hz **19**) at the C$^{\alpha}$ atom. The ^{195}Pt{^{1}H} NMR spectra showed one broad signal (δ -3626 **16;** -3596 **17**; -3598 **18**), confirming the equivalence of both Pt centers. The broadening of the signal is probably due to the substantial quadrupole moment for ^{14}N combined with its coupling and relaxation characteristics.[20] Examination of the chemical shift data reveals a slight upfield for the compound with the more σ-donor

substituent in the alkynyl fragment (**16**). As expected, due to the neutral charge and the withdrawing characteristics of the phenylquinolinyl cyclometalate ligand, the Pt resonance in these bimetallic complexes occurs notably deshielded with respect to the anionic mononuclear derivative **15** (δ -3845) and to other anionic complexes such as the homoleptic $(NBu_4)_2[Pt(C{\equiv}CTol)_4]$ complex (δ CD_2Cl_2 -4187).[21]

The molecular structures of **16** and **17**·$3CH_2Cl_2$ (Figure 2.5, Table 2.2) reveal a butterfly-type structure with a double alkynyl ($\mu-\kappa C^{\alpha}:\eta^2$) bridge between both platinum fragments "Pt(pq)". In accordance with the spectroscopic data, the σ-coordinated C^{α} alkynyl carbon is located *trans* to the cycloplatinate N atoms and the η^2-C≡CR *trans* to the cycloplatinate C atoms. In the tolylacetylide derivative **17**, the platinum η^2-linkages are symmetric within experimental error [Pt-C^{α}/C^{β} 2.391(6), 2.373(6)/2.386(6), 2.356(6) Å], whereas in **16** they are asymmetric [Pt-C^{α}/C^{β} 2.361(6), 2.382(6)/2.431(6), 2.440(6) Å], with the Pt-C^{α} distance being perceptibly shorter than the corresponding Pt-C^{β}. Accordingly, in complex **16** the Pt···Pt separation is shorter [3.0936(3) **16** *vs* 3.2109(3) Å **17**] and the Pt-C^{α}-Pt angle is more acute (90.2º, 91.2º **16** *vs* 94.9º, 95.4º **17**), features that are key to rationalize their photophysical properties. The C≡C distances and the distortion from the linearity of the Pt-C^{α}-C^{β} units [angles at C^{α} 164.4(5), 167.6(5)º **16**, 167.5(5), 169.4(5)º **17** and C^{β} 161.1(6), 162.6(5)º **16**, 161.3(6), 165.3(6)º **17**] are comparable to those reported in related diplatinum complexes.[2b,3,19] The dihedral angle between the best platinum coordination planes (65.7º **16**, 56.0º **17**) resembles to those of related complexes with great steric demands, which also show a puckered diplatinacycle.[3a] However, less puckered (45-49.3º)[3b,19a,19c] or even planar[19d] structures with longer Pt···Pt separations (3.22-3.65 Å) have been previously observed in other [Pt](μ-$\kappa C^{\alpha}:\eta^2$C≡CR)$_2$[Pt] complexes, thus confirming that this type of geometry strongly depends on the steric demands of coligands. The structural details concerning the "Pt(pq)" metallocycle are similar to those observed in other complexes containing it.[22] The phenylquinolinyl (pq) ligand is fluttered, forming dihedral angles of 17.9º, 25.5º (**16**) or 10.55º, 11.57º (**17**) with the Pt coordination planes.

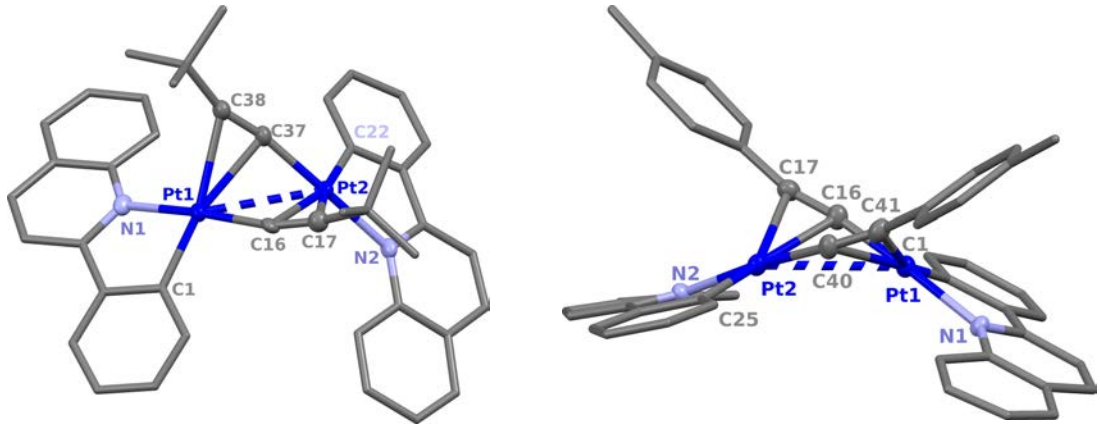

a) b)

Figure 2.5: Molecular structures of a) [Pt(pq)(μ–κC$^{\alpha}$:η^2-C≡C^{t}Bu)]$_2$ (**16**) and b) [Pt(pq)(μ–κC$^{\alpha}$:η^2-C≡CTol)]$_2$·3CH$_2$Cl$_2$ (**17**·3CH$_2$Cl$_2$)

Table 2.2: Selected bond lengths [Å] and angles [°] for [Pt(pq)(μ–κC$^{\alpha}$:η^2-C≡C^{t}Bu)]$_2$ (**16**) and [Pt(pq)(μ–κC$^{\alpha}$:η^2-C≡CTol)]$_2$·3CH$_2$Cl$_2$ (**17**·3CH$_2$Cl$_2$)

16		**17**·3CH$_2$Cl$_2$	
Pt(1)-C(1)	1.969(6)	Pt(1)-C(1)	1.983(6)
Pt(1)-N(1)	2.119(5)	Pt(1)-N(1)	2.110(5)
Pt(1)-C(16)	1.952(6)	Pt(1)-C(16)	1.952(6)
Pt(1)-C(38)	2.440(6)	Pt(1)-C(41)	2.386(6)
Pt(1)-C(37)	2.382(6)	Pt(1)-C(40)	2.391(6)
C(16)-C(17)	1.218(8)	C(16)-C(17)	1.219(8)
Pt(1)-Pt(2)	3.0936(3)	Pt(1)-Pt(2)	3.2109(3)
Pt(2)-C(22)	1.990(6)	Pt(2)-C(25)	1.999(6)
Pt(2)-N(2)	2.103(5)	Pt(2)-N(2)	2.090(5)
Pt(2)-C(37)	1.964(6)	Pt(2)-C(40)	1.951(6)
Pt(2)-C(17)	2.431(6)	Pt(2)-C(17)	2.356(6)
Pt(2)-C(16)	2.361(6)	Pt(2)-C(16)	2.373(6)
C(37)-C(38)	1.214(8)	C(40)-C(41)	1.238(8)
N(1)-Pt(1)-C(1)	80.7(2)	N(1)-Pt(1)-C(1)	80.3(2)
Pt(1)-C(16)-C(17)	167.6(5)	Pt(1)-C(16)-C(17)	169.4(5)
C(16)-C(17)-C(18)	161.1(6)	C(16)-C(17)-C(18)	165.3(6)
N(2)-Pt(2)-C(22)	80.1(2)	N(2)-Pt(2)-C(25)	80.7(2)
Pt(2)-C(37)-C(38)	164.4(5)	Pt(2)-C(40)-C(41)	167.5(5)
C(37)-C(38)-C(39)	162.6(6)	C(40)-C(41)-C(42)	161.3(6)

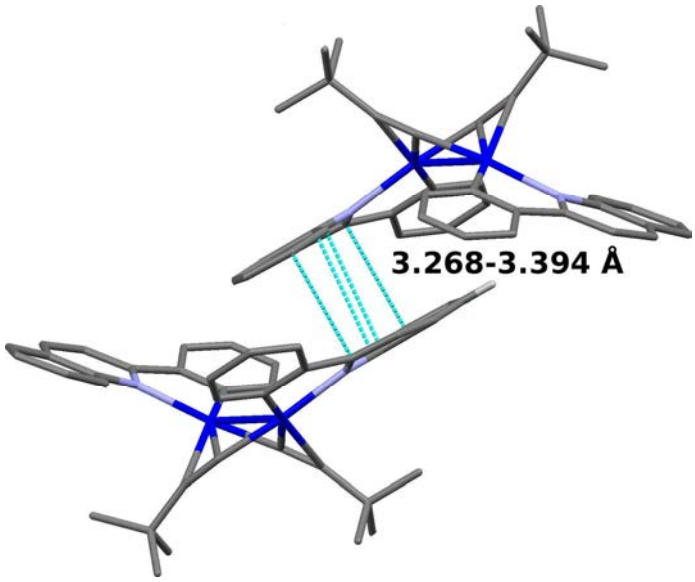

Figure 2.6: Packing of [Pt(pq)(μ–κC^{α}:η^2–C≡C^{t}Bu)]$_2$ (**16**) showing the π···π interactions between quinoline rings (3.268-3.394 Å)

The crystal packing of **16** shows that the molecules are arranged as head-to-tail dimers through moderate intermolecular π···π interactions between pq ligands (3.268 Å) (Figure 2.6). The packing of **17** shows zig-zag chains stabilized by nonparalell π····π (pq····pq) interactions (3.288 Å), which interacts mutually through weak secondary C≡C···$H_{CH_2Cl_2}$, $Cl_{CH_2Cl_2}$···C_{pq}, $H_{CH_2Cl_2}$···C_{pq/C_6H_4}, $Cl_{CH_2Cl_2}$···H_{pq}, C_{pq}···H_{pq} and H_{CH_3}···C_{pq} interactions (Figure 2.7)

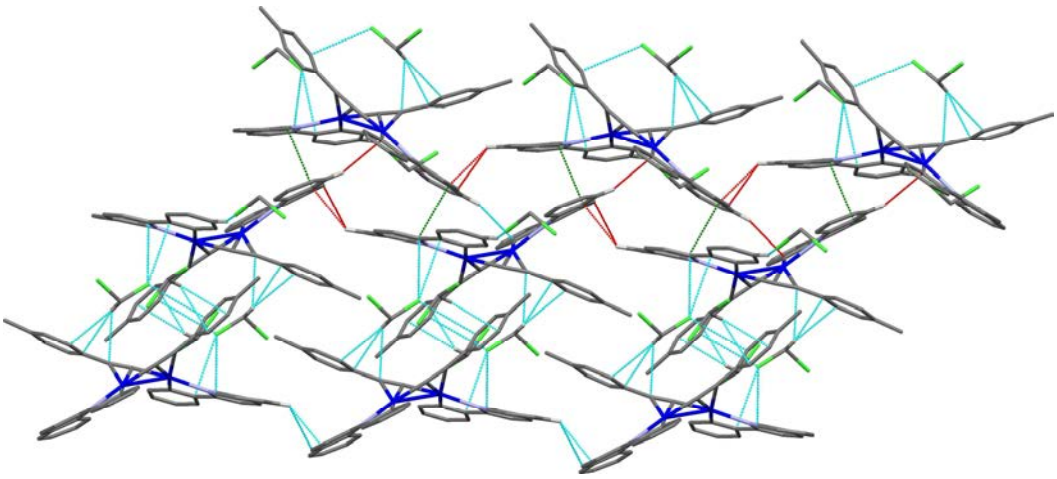

Figure 2.7: Packing of [Pt(pq)(μ–κC^{α}:η^2–C≡CTol)]$_2$·CH_2Cl_2 (**17**·CH_2Cl_2) showing the zig-zag chains supported by non-linear π···π interactions (pq····pq 3.288 Å, green lines) and weak interactions C_{pq}···H_{pq} (2.771-2.900 Å red). These chains interact with other chains via $C_{Ph/pq/CC\equiv R}$····solvent (blue) [C≡C···H_{CH2Cl2} (2.786 Å), $Cl_{CH_2Cl_2}$···C_{pq} (3.384-3.420 Å), $H_{CH_2Cl_2}$···C_{pq/C_6H_4} (2.874-2.770 Å), $Cl_{CH_2Cl_2}$···H_{pq} (2.929 Å)

2.2 Photophysical properties

2.2.1 Absorption spectroscopy

To facilitate comparison, all absorption spectra data are summarized in Table 2.3. The anionic mononuclear complexes **13**–**15** in CH_2Cl_2 5 x 10^{-5} M at 298 K (Figure 2.8a) show in CH_2Cl_2 high-energy bands (230-360 nm), which are likely of mixed configuration including ^{1}IL transitions in the Hpq and C≡CR groups. They also display a characteristic low energy band in the 423-436 nm range (ε 8.3-5.5 x 10^3 $M^{-1}cm^{-1}$), which is absent in the related homoleptic $(NBu_4)_2[Pt(C{\equiv}CR)_4]$ derivatives (see Figure 2.8b, as illustration) being, therefore, related with the coordination of the Hpq ligand. This band is sensitive to the alkynyl substituent being systematically red-shifted in accordance with the σ electron-donating ability of the substituent on the alkynyl ligand [**15** ($C_6H_4CF_3$-4) 423 nm < **14** (C_6H_4OMe-3) 430 nm < **13** ($C_6H_4CH_3$-4) 436 nm]. This behavior is opposite to that previously observed for us in the homoleptic complexes and consistent with a ligand-to-ligand ^{1}L'LCT (C≡CR→Hpq) charge-transfer transition.

Table 2.3: Absorption data for compounds $(NBu_4)[Pt(Hpq\text{-}\kappa N)(C{\equiv}CR)_3]$ (**13**–**15**) and $[Pt(pq)(\mu\text{-}\kappa C^{\alpha}{:}\eta^2\text{-}C{\equiv}CR)]_2$ (**16**–**19**) at 298 K (5 x 10^{-5} M CH_2Cl_2 Solutions and solid state[a])

Compound	λ_{abs}/nm (10^3 ε $M^{-1}cm^{-1}$)
$(NBu_4)[Pt(Hpq\text{-}\kappa N)(C{\equiv}CTol)_3]$ **13**	231 (30.0), 265 (42.1), 279 (46.5), 306 (35.6), 353 (12.1), 436 (5.8) **CH_2Cl_2** 251, 334, 378, 442, 550_{sh}, tail to 570 **solid**
$(NBu_4)[Pt(Hpq\text{-}\kappa N)(C{\equiv}CC_6H_4OMe\text{-}3)_3]$ **14**	232 (34.8), 279 (36.7), 307 (31.3), 360 (7.7), 430 (5.5) **CH_2Cl_2** 258, 281, 328, 365, 435, 498sh**,** tail to 570 **solid**
$(NBu_4)[Pt(Hpq\text{-}\kappa N)(C{\equiv}CC_6H_4CF_3\text{-}4)_3]$ **15**	231 (27.6), 264_{sh} (32.2), 281_{sh} (36.8), 304 (41.7), 332 (28.6), 359 (10.2), 423 (8.3) **CH_2Cl_2** 260, 345, 371, 430, 540_{sh}, tail to 565 **solid**
$[Pt(pq)(\mu\text{-}\kappa C^{\alpha}{:}\eta^2\text{-}C{\equiv}C^tBu)]_2$ **16**	233 (33.2), 257 (34.5), 277 (36.2), 336 (10.5), 352 (11.2), 436 (8.7) **CH_2Cl_2** 294, 340, 430, tail to 520 **solid**
$[Pt(pq)(\mu\text{-}\kappa C^{\alpha}{:}\eta^2\text{-}C{\equiv}CTol)]_2$ **17**	284 (60.8), 302 (56.5), 339 (24.2), 355 (25.9), 410 (29.9) **CH_2Cl_2** 290, 342, 370, 407, 443_{sh}, tail to 570 **solid**
$[Pt(pq)(\mu\text{-}\kappa C^{\alpha}{:}\eta^2\text{-}C{\equiv}CC_6H_4OMe\text{-}3)]_2$ **18**	284 (54.7), 298 (55.5), 336 (18.8), 355 (19.8), 406 (21.1) **CH_2Cl_2** 290, 331, 400, 437_{sh}, 536, tail to 700 **solid**
$[Pt(pq)(\mu\text{-}\kappa C^{\alpha}{:}\eta^2\text{-}C{\equiv}CC_6H_4CF_3\text{-}4)]_2$ **19**	252 (49.3), 278 (47.2), 336 (17.3), 353 (17.8), 397 (12.5) **CH_2Cl_2** 290, 313, 348, 398, 430_{sh}, tail to 520 **solid**

a) Diffuse Reflectance

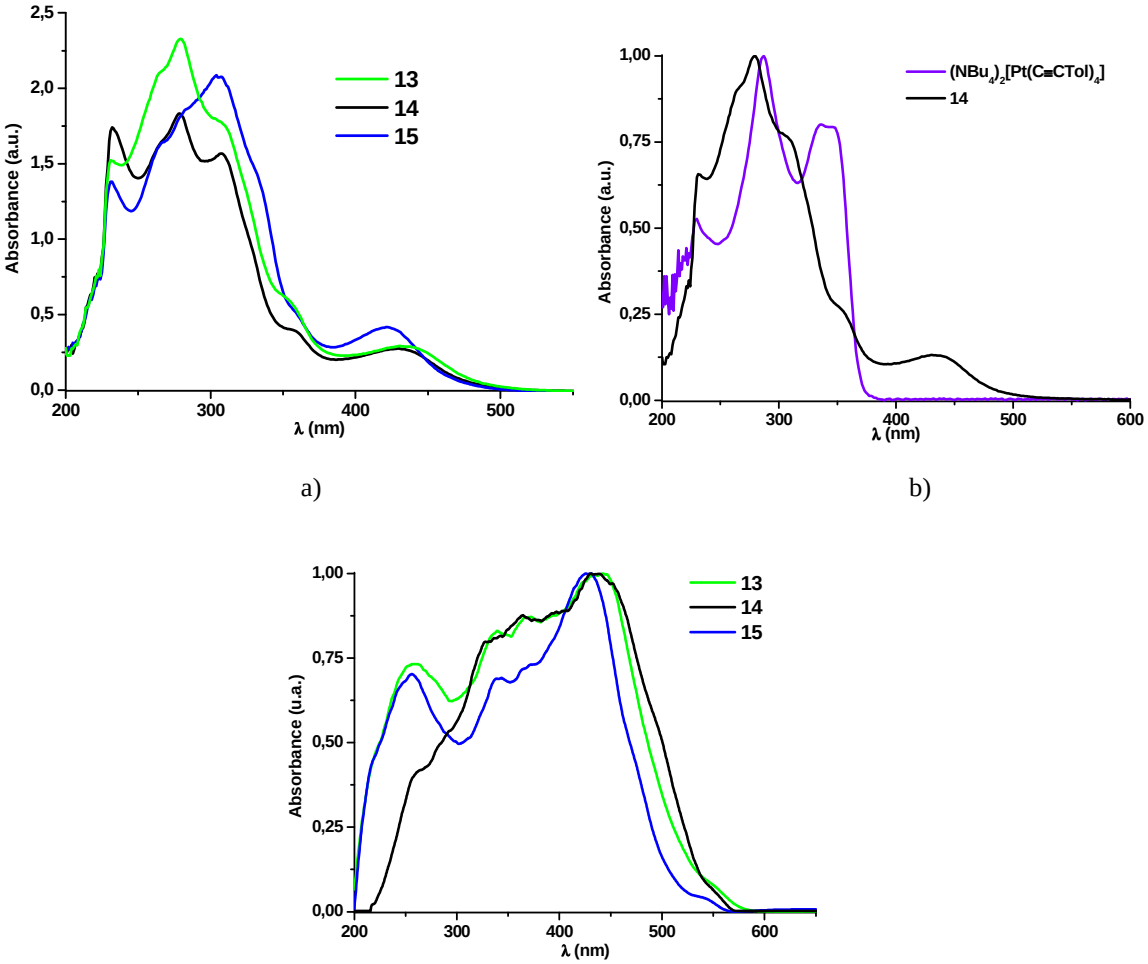

Figure 2.8: UV-vis spectra of complexes a) **13**–**15** in CH_2Cl_2 (5 x 10^{-5} M) b) $(NBu_4)[Pt(C{\equiv}CTol)_3(Hpq)]$ (**14**) and $(NBu_4)_2[Pt(C{\equiv}CTol)_4]$ in CH_2Cl_2 (5 x 10^{-5} M) and c) **13**–**15** in solid state, calculated from their reflectance spectra

In the solid state, the bands are more intense (see Figure 2.8c) (with low energy tails to *ca* 570 nm) following similar energy dependence. According to time-dependent TD-DFT calculations (see below) on complex **14**, the low-energy band is assigned to mixed ligand (C≡CR)-to-ligand (Hpq) and metal-to-ligand (Hpq) ^{1}L'LCT/^{1}MLCT charge transfer with remarkable ^{1}L'LCT contribution.

The cyclometalated complexes **16**–**19** (Figure 2.9a) contain high-energy bands (λ < 340 nm), which are dominated by spin-allowed intraligand ^{1}IL (pq/C≡CR) transitions. This region is similar for **17** and **18** and red shifted in relation to **16** and **19**, suggesting a remarkable contribution of the electron donor aryl substituent. The

moderately structured band around 355 nm remains fairly constant for all complexes (**16**–**19**), being attributed to intraligand ^{1}IL charge-transfer transition of the pq ligand. However, the low-energy band is also affected by the nature of the alkynyl bridging ligand. Thus, while the *ter*butylalkynyl has its absorption maxima at 436 nm, in the aryl derivatives this band is remarkably blue shifted and follow the trend (**19** 397 < **18** 406 < **17** 410 nm) in agreement with the participation of the C≡CR ligand in the HOMO. According to this behavior and to TD-DFT calculations (**16**, **17**) this band is assigned in **16** to as mixture of a metal-metal/alkynyl to phenylquinolinyl (^{1}MML'LCT) with intraligad pq (^{1}IL) character. By contrast in **17** the transition can be mainly ascribed to alkynyl to phenylquinolinyl ^{1}L'LCT with minor contribution of ^{1}MMLCT character and presumably in **18** and **19** it could be ascribed to ^{1}L'LCT mixed with some ^{1}MLCT of noninteracting Pt moieties.

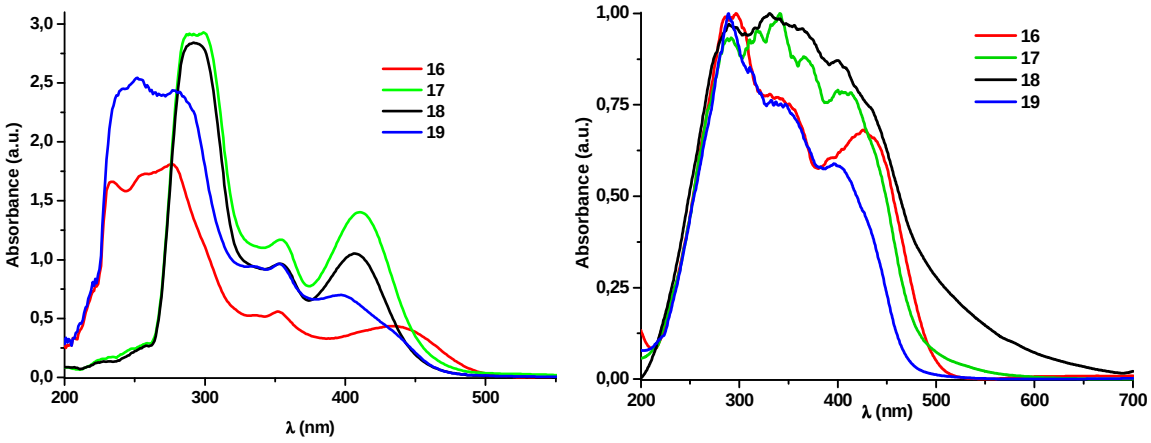

Figure 2.9: UV-vis spectra of **16**–**19** in a) CH_2Cl_2 (5 x 10^{-5} M) b) solid state calculated from their reflectance spectra

In the solid state the cyclometalated complexes **16**–**19** show intense absorptions at around 400 nm (430 nm for **16**) and tails extending to longer wavelengths 520-570 nm (Figure 2.9b). The shape, broad profile and the long tail to 700 nm of **18** is consistent with its brown color.

2.2.2 Emission Spectroscopy

All emission spectral data are summarized in Table 2.4.

Table 2.4: Photophysical data for complexes $(NBu_4)[Pt(Hpq\text{-}\kappa N)(C{\equiv}CR)_3]$ (**13**–**15**) and $[Pt(pq)(\mu\text{–}\kappa C^{\alpha}\text{:}\eta^2\text{-}C{\equiv}CR)]_2$ (**16**–**19**) in solid state and in CH_2Cl_2 solutions

Compound	Medium (T^a/K)	λ_{em}/nm (λ_{exc}/nm)	τ/μs	ϕ(%)
13	Solid (298)	592[b] (365-550)	0.5	4.8
	Solid (77)	590_{max}, 626, 664_{sh} (365-540)	10.3	
	5×10^{-5} M (77)[a]	570[b] (365-440)		
14	Solid (298)	615[b] (365-560)	0.5	2.7
	Solid (77)	598_{max}, 635 (365-450)	7.3	
	5×10^{-5} M (77)[a]	548_{max}, 578, 622_{sh} (350-440)		
15	Solid (298)	588[b] (365-550)	1.7	7.2
	Solid (77)	586_{max}, 628, 662_{sh} (365-440)	11.4	
	5×10^{-5} M (298)[c]	570[b] (365-440)		
	5×10^{-5} M (77)	542_{max}, 582 (365-440)		
16	Solid (298)	578[b] (365-500)	12.5	4.5
	Solid (77)	594[b] (365-500)	22.2	
	5×10^{-5} M (298)[c]	570 (420)		
	5×10^{-5} M (77)	562_{max}, 600 (365-450)		
17	Solid (77)[a]	562_{max}, 592 (365-470)	17.3	
	5×10^{-5} M (298)[c]	570[b] (420)		
	5×10^{-5} M (77)[a]	562_{max}, 602, 660_{sh} (350-430)		
18	Solid (77)[a]	562_{max}, 602, 660_{sh} (350-470)	9.4	
	5×10^{-5} M (298)[c]	580[b] (420)		
	5×10^{-5} M (77)	558_{max}, 600, 640_{sh} (365-420)		
19	Solid (77)[a]	560_{max}, 596, 654_{sh} (355-450)	20.0	
	5×10^{-5} M (298)[c]	580[b] (420)		
	5×10^{-5} M (77)	556_{max}, 592, 640_{sh} (365-445)		

a) Non emissive in CH_2Cl_2 at each concentration at 298 K. b) Tail to 750 nm. c) Extremely weak

Mononuclear complexes **13**–**15** exhibit luminescence in rigid media (solid and glasses). The three complexes display a slightly structured emission band in glassy CH_2Cl_2 (77 K) with peak maxima following the energy trend **15** ($C_6H_4CF_3$-4) 542 nm > **14** (C_6H_4OMe-3) 548 nm > **13** ($C_6H_4CH_3$-4) 570 nm, which resemble the absorption maxima (Figure 2.10). In solid state at 298 K they show an unstructured broad band (ϕ 2.7-7.2 %), which is affected by the alkynyl substituent in different form to that seen in glassy solution (**15** 588 > **13** 592 > **14** 615 nm Figure 2.11a). Upon cooling at 77 K, the emissions are more intense and the profiles become structured and slightly blue-shift (**15** 586 > **13** 590 > **14** 598 nm), especially in **14** (Figure 2.11b). According to DFT calculations in gas phase (see below), and the measured lifetimes typical of ^{3}CT parentage (see Table 2.4), the emission is attributed to admixture alkynyl-metal to phenylquinoline ^{3}[(L'+M)LCT] transition, which is in accordance with the tendency

observed in glassy solution. The remarkable red shift observed in complex **14** (C_6H_4OMe-3) containing the *meta*-methoxy group in relation to **13** could be tentatively attributed to the occurrence of *intramolecular* secondary contacts between the oxygen and the quinoline unit as observed by XRD, which could stabilize the accepting orbital (LUMO) located on the Hpq group.

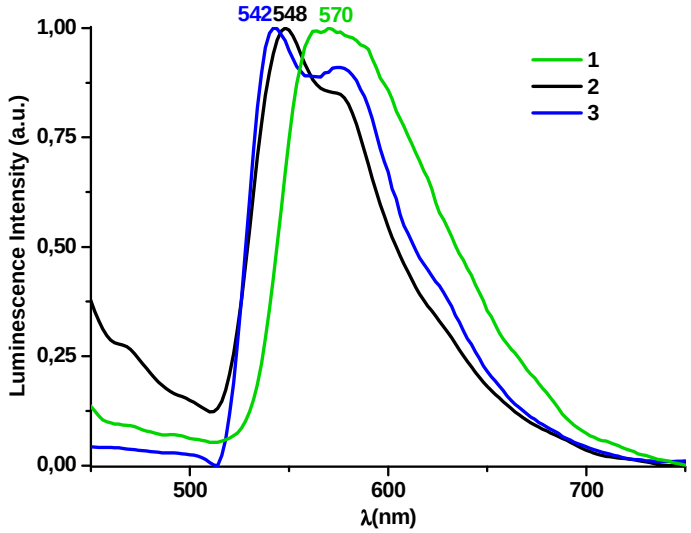

Figure 2.10: Normalized emission spectra of complexes **13**–**15** in CH_2Cl_2 5 x 10^{-5} M at 77 K (λ_{exc} 385-400 nm)

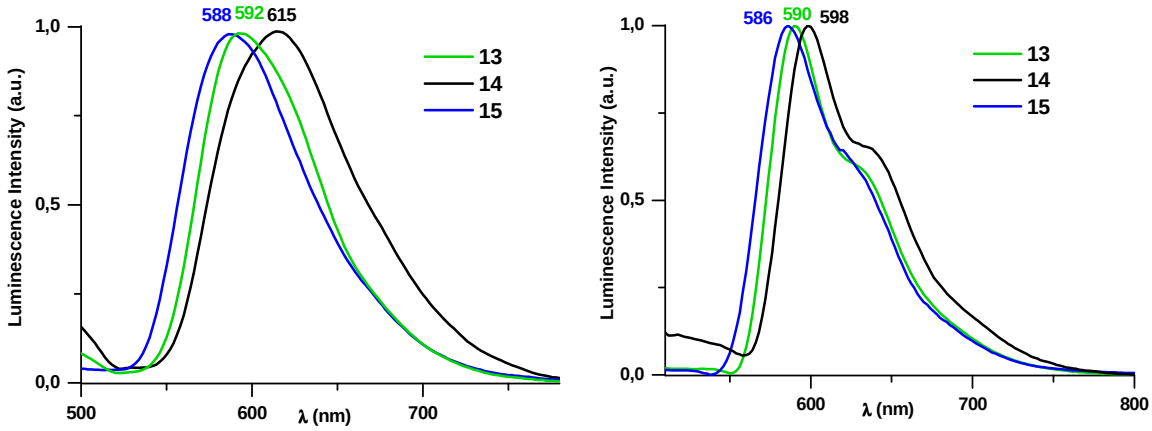

a) b)

Figure 2.11: Normalized emission spectra of complexes (NBu_4)[Pt(Hpq-κN)$(C{\equiv}CR)_3$] (**13**–**15**) in the solid state a) at 298 K b) at 77 K (λ_{exc} 430-460 nm)

Concerning the bimetallic complexes it is noteworthy that, to the best of our knowledge, this series of complexes (**16**–**19**) represent the first report on cyclometalated platinum complexes stabilized by double alkynyl ligands in which luminescent

properties have been studied. Only the ^{t}Bu-alkynyl complex **16** is emissive in solid state at room temperature, exhibiting a moderate orange structureless emission at 578 nm (Φ 4.5%, τ 12.5 μs). Upon cooling at 77K, the emission is enhanced and red shifted to 595 nm (τ 22.2 μs) (red line, Figure 2.12), this being in line with a transition involving metal-metal contribution. According to the optimized T_1, the electron distribution in the emissive state is mainly confined to orbitals of the central metallacycle $Pt_2(C{\equiv}C)_2$, having Pt···Pt bonding character, and the phenyl rings of the pq. We ascribed it as a metal-metal/alkynyl to phenylquinolinyl ^{3}[(MM+L')LCT] transition with somewhat of intraligad pq (^{3}IL) character, a behavior which is in agreement with the very short Pt···Pt found in the crystal structure of **16** [3.0936(3) Å].

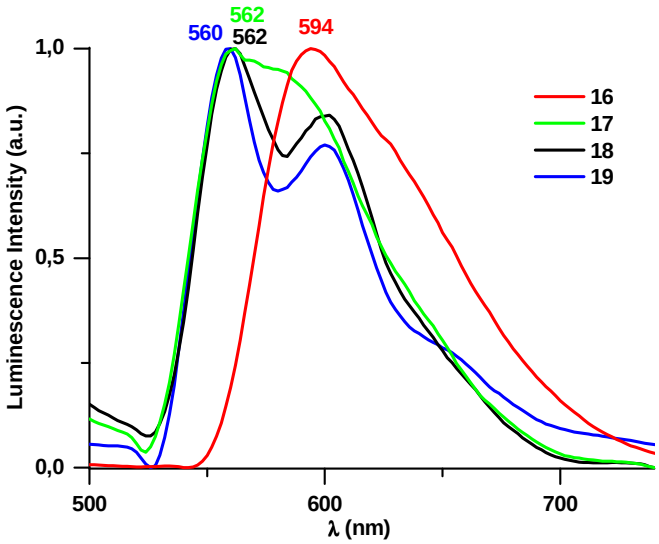

Figure 2.12: Normalized emission spectra of the complexes $[Pt(pq)(\mu{-}\kappa C^{\alpha}{:}\eta^{2}\text{-}C{\equiv}CR)]_2$ (**16-19**) in the solid state at 77 K (λ_{exc} 400 nm)

The arylalkynyl derivatives are only emissive at 77 K and, as it is illustrated in Figure 2.12, their emissions differ from that of **16**. Curiously, complexes **18** and **19** bearing the lower electron donor alkynyl bridging ligands exhibit a structured band (**18**/**19** λ_{max} 562/560 nm, τ 9.4/20 μs), which resembles to that observed for related diplatinum complexes not perturbed by metal-metal interactions.[4a,5b,5e,7a,b,7d,23] In the case of **17** the emission is rather broad with minimal structuration (λ_{max} 562 nm, τ 17.3 μs). We suggest that whereas in **18** and **19** the emission could be originated from admixture ^{3}[(L'+M)LCT] ^{3}[Pt(d)/π(C≡CR)→π*(pq)] excited state, likely due to little-

to-no metal-metal interaction, in **17** a mixture of both contributions ^{3}L'LCT and ^{3}MMLCT (minor character) could be invoked. This behavior is also consistent with the fact that, although the Pt···Pt distance in **17** [3.2109(3) Å] is longer than in **16**, it is short enough to have somewhat of an influence on the emission. The lack of emission of **17**–**19** in solid state at 298 K is consistent with the increase of contribution of ^{3}L'LCT to the excited states, which likely provides a path for rapid nonradiative deactivation decay, as it has been previously suggested in other systems.[1f,24]

The emissions in fluid CH_2Cl_2 (5 x 10^{-5} M) for all **16**–**19** complexes are very weak, showing a broad unstructured band at *ca* 570-580 nm. Interestingly, upon lowering the temperature at 77 K, the emission is enhanced, slightly blue shifted and becomes well-structured for *all* complexes (see Figure 2.13a). The emission maxima shifts slightly to the red from 556 nm in **19** (R = $C_6H_4CF_3$) to 562 nm (R = Tol, ^{t}Bu), in keeping with a metal perturbed ^{3}L'LCT ^{3}[Pt(d)/π(C≡CR)→π*(pq)] nature for the excited state. This fact suggests that, in the rigidification process all complexes form presumably diplatinacycles having a longer Pt···Pt separation to that found for **17** by XRD (> 3.2 Å). A number of platinum binuclear complexes exhibiting a controllable range of Pt···Pt distances and, as consequence, different photophysical properties have been reported.[5b,7] The behavior of complexes **16**–**19** has been also examined in a less polar solvent as toluene. In fluid solution no emission is detected and upon frozen only a minor shift in its maxima were observed (Figure 2.13b). In toluene, **16** has its emission maximum wavelength at 568 nm, while for **17**–**19** they were at 554 **17**, 550 **18**, 548 nm **19**. The red shift observed for **17**–**19** in the more polar solvent (CH_2Cl_2) suggest that the triplet excited state is probably more polar than the ground state and it is stabilized, thus suggesting a predominant charge transfer character [alkynyl to pq charge transfer (^{3}L'LCT)].

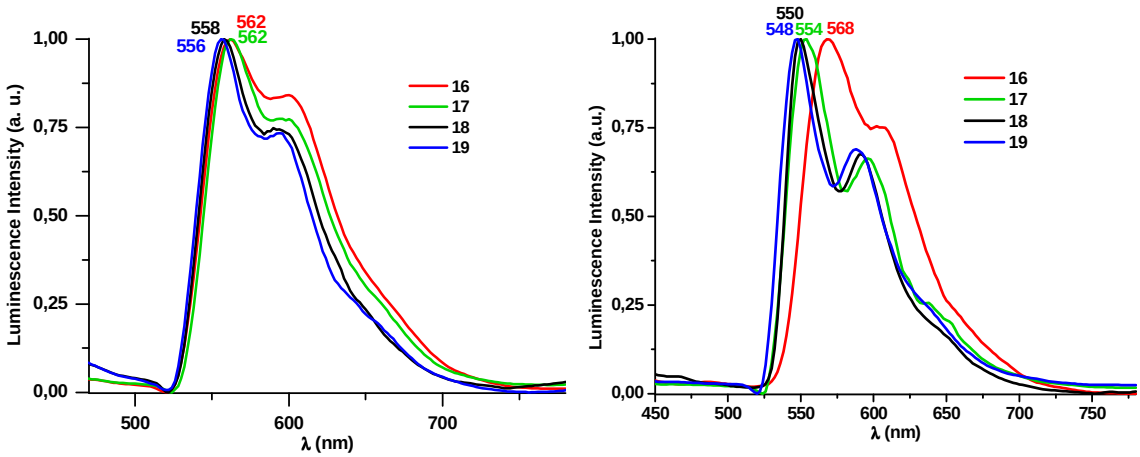

a) b)

Figure 2.13: Normalized emission spectra of the complexes a) [Pt(pq)(μ–κC^{α}:η^2-C≡CR)]$_2$ (**16**–**19**) in CH_2Cl_2 5 x 10^{-5} M at 77 K (λ_{exc} 400 nm). b) **16**–**19** in toluene 5 x10^{-5} M 77 K (λ_{ex} 400 nm)

2.3 Theoretical calculations

To gain further insight into the nature of the absorption and emission characteristics of these complexes, a theoretical analysis based on a DFT (TD-DFT) approach was performed on complexes characterized by X-ray diffraction (**14**$^-$, **16** and **17**). The structural optimization of S_0 and T_1 states were performed at the LandL2Dz(Pt)/6-31G** (ligand atoms) level.

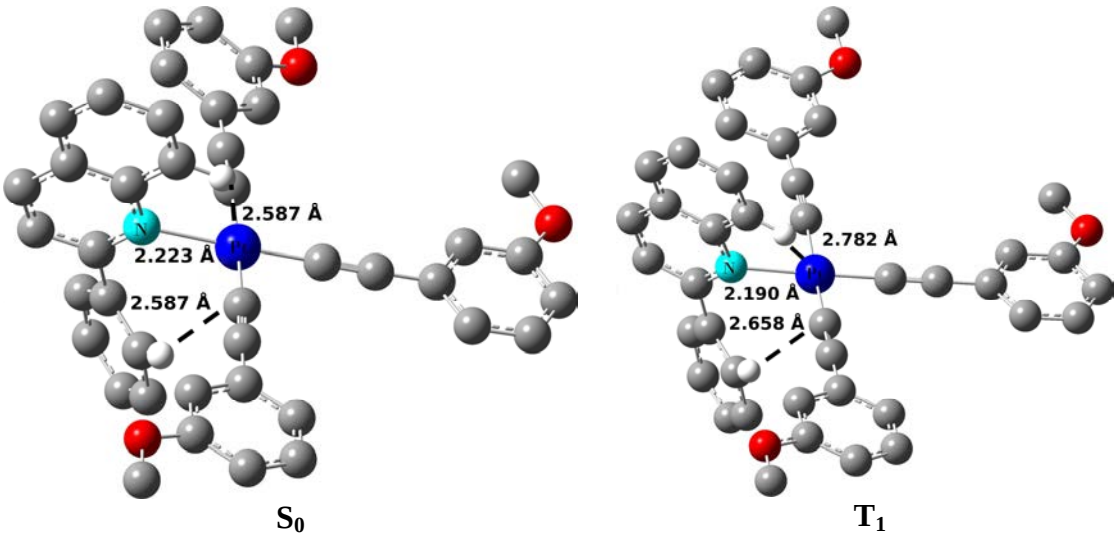

Figure 2.14: Optimized structures of S_0 and T_1 states of **14**$^-$

The calculated structures in the ground state agree in reasonable way with the data obtained from the X-ray diffraction studies. Thus, in **14**$^-$ the dihedral angle between the quinoline and the phenyl ring (49.2^o) and the *intramolecular* Pt··H(8) and H(13)··C(25)≡ (2.587 Å) are similar to those of the X-ray (Figure 2.14 and Table A2.1) and the details of the three alkynyl units are identical in the calculated structure.

For **16** and **17** the calculations confirm the bent geometry (dihedral angles calculated/X-ray 64.4º/65.7º **16**; 49.7º/56.0º **17**) and reproduce the distinct geometrical details of the central $Pt_2(C{\equiv}C)_2$ cores (∠ Pt-C$^\alpha$-Pt cal./X-ray 89.4º/av. 90.7º **16**; 96.2º/av. 95.2º **17**), being the alkynyl bridging coordination relatively symmetrical in **17** and clearly asymmetrical in **16** (Figure 2.15a). Notwithstanding, in both complexes the η^2 Pt···($C^\alpha{\equiv}C^\beta$) bond lengths [Δ (calc-X-ray) 0.16-0.3 **16**; 0.13-0.2 Å **17**] and Pt···Pt distances [calculated 3.195 **16**; 3.352 Å **17** *vs* X-ray 3.0936(3) **16**; 3.2109(3) Å **17**] are somewhat overestimated.

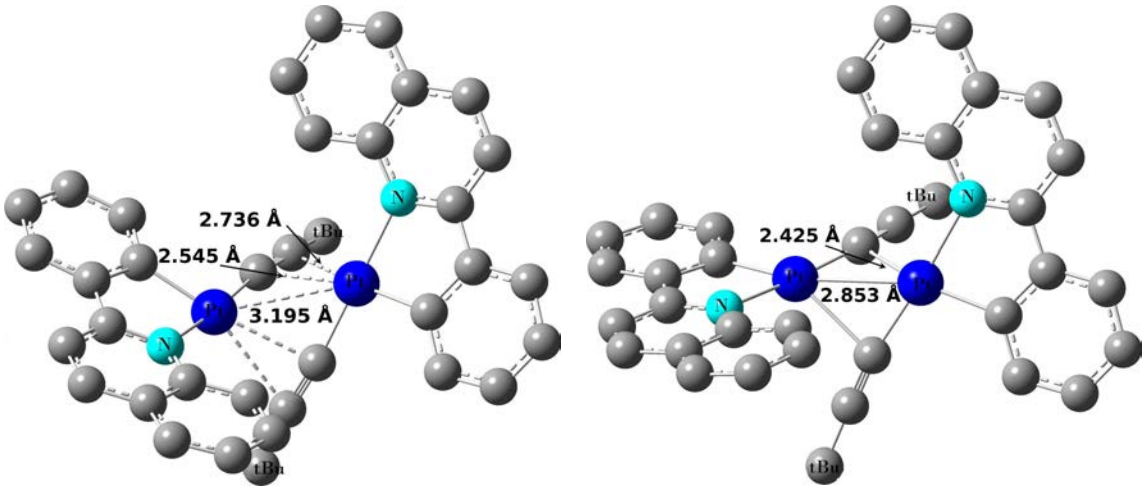

S$_0$ **T$_1$**

Figure 2.15: Optimized structures of S_0 and T_1 states of **16**

Selected low lying singlet-singlet transitions obtained in CH_2Cl_2 for the mononuclear (**14**) and both bimetallic (**16**, **17**) complexes are listed in Table A2.3. According to the orbital composition (Figure A2.1), in the case of the anionic complex **14**$^-$, the highest occupied HOMOs (HOMO-3 to HOMO) are mainly centered on the alkynyl ligands (> 70%), with some Pt character, though the distribution of the electronic density of the alkynyl groups in these orbitals differs. Thus, whereas the HOMO is mainly located on both mutually *trans* C≡CR ligands, the HOMO-1 is located

on the C≡CR ligand *trans* to Hpq and the HOMO-2 is contributed from all three alkynyl groups. The LUMO and LUMO+1, which are close in energy, are located in the Hpq ligand. For this complex, the lowest energy singlet transition calculated in CH_2Cl_2 (437 nm) arises primarily from HOMO-2 to LUMO, therefore supporting a mixed ^{1}L'LCT/^{1}MLCT transition with a remarkable ligand (alkynyl) to ligand (Hpq) character for the experimental band located at 430 nm.

Table 2.5: Composition of frontier molecular orbitals in the ground-state for **14**, **16** and **17**

	14				**16**			**17**		
MO	**Pt**	**Hpq**	**C≡CR *trans* to Hpq**	**C≡CR**	**Pt**	**pq**	**C≡C**	**Pt**	**pq**	**C≡CTol**
LUMO+6	3	32	50	15	5	93	2	37	47	16
LUMO+5	3	2	3	92	29	62	10	7	5	88
LUMO+4	2	82	0	16	36	45	19	12	65	23
LUMO+3	1	91	0	8	0	99	0	0	99	1
LUMO+2	10	21	12	57	4	94	2	12	62	26
LUMO+1	0	100	0	0	4	95	1	3	95	2
LUMO	1	99	0	0	5	92	3	5	91	4
HOMO	25	0	2	73	52	38	10	30	12	58
HOMO-1	21	1	73	5	46	23	31	24	9	67
HOMO-2	28	1	33	38	58	14	28	48	41	11
HOMO-3	14	2	29	56	45	40	16	39	57	4
HOMO-4	53	5	18	25	41	20	39	62	18	20
HOMO-5	25	1	8	66	46	40	14	49	32	19
HOMO-6	5	4	1	91	23	48	30	16	72	12

The analysis of the bimetallic cyclometalated complexes **16** and **17** reveals differences in their frontiers orbitals (Table 2.5, Figures A2.2 and A2.3), in the low lying transitions (Table A2.3) and consequently in their assignments. Figure 2.16 shows a view of the main frontier orbitals and selected allowed transitions (showed as bars) together with experimental absorption spectra in CH_2Cl_2. In **16** the HOMO is delocalized over the dimetalacycle core $Pt_2(C{\equiv}C)_2$ (Pt 52%, C≡C 10%) exhibiting metal-metal dσ* character and the phenyl ring of both cyclometalated ligands (38%), whereas the LUMO is essentially localized on the cyclometalated pq ligands. The HOMO-1 is similar but with a higher contribution of the dimetalacycle $Pt_2(C{\equiv}C)_2$ (Pt 46%, C≡C 31%, see Figure A2.2) and lower contribution of the pq ligands. The lowest-energy band is primarily due to a HOMO→LUMO transition and can be assigned as admixture of a metal-metal/alkynyl to pq ligand (^{1}MML'LCT) with intraligand ^{1}IL (L = pq) character. As can be seen in Figure 2.16, the calculated value (446 nm) is in line with the experimental observation (436 nm CH_2Cl_2). Substitution of the alkyl substituent (^{t}Bu) by a low lying aryl group ($C_6H_4CH_3$-4) in **17** modifies notably the

contribution of the ligands to the HOMO and HOMO-1. They are composed of orbitals of the dimetalacycle $Pt_2(C{\equiv}C)_2$ but conjugated in this case with the aryl alkynyl substituents. The Pt contribution decreases in relation to **16** (HOMO Pt 30%, C≡CTol 58%; HOMO-1 Pt 24 %, C≡CTol 67%) and that of pq ligands is negligible. The orbital with metal-metal dσ* character similar to the HOMO in **16** is now the HOMO-2 (Pt 48%, C≡C 11%, 41% pq). The LUMO and LUMO+1 are centered (as in **16**) on the cyclometalated pq ligand.

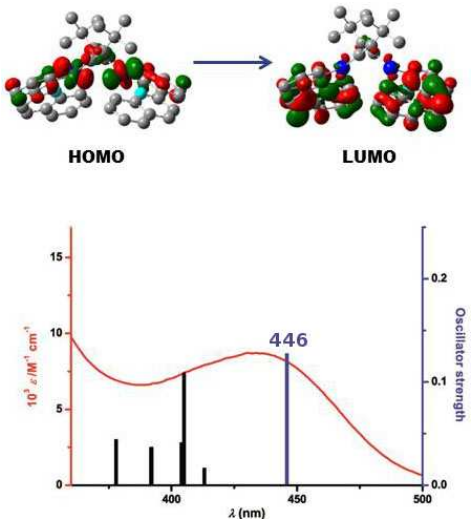

a)

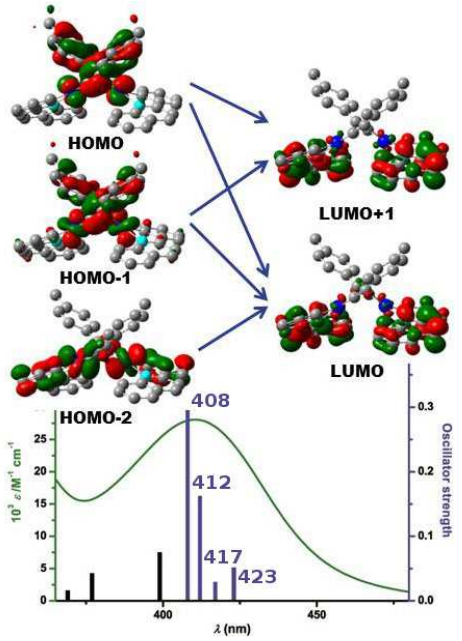

b)

Figure 2.16: View of the main frontier orbitals for a) **16** and b) **17** obtained by TD-DFT. Calculated absorption bars in CH_2Cl_2 and experimental UV-vis in CH_2Cl_2 (5 x 10^{-5} M) at 298 K

As can be seen in Figure 2.16b, the low energy band possess a complex set of electronic absorptions (S_1-S_4 408-423 nm), which are primarily associated with HOMO, HOMO-1 and HOMO-2→LUMO/LUMO+1 transitions. The absorptions derived from HOMO and HOMO-1 (S_1-S_3) are primarily of alkynyl to phenylquinolyl charge transfer ^{1}L'LCT nature, whereas the S_4 (408 nm) absorption, which contains the HOMO-2, has ^{1}MML'LCT character. In agreement with this, the low energy feature composed of several bands, could tentatively ascribed as an admixture of ^{1}L'LCT with minor contribution of ^{1}MML'LCT character. Therefore, the remarkable blue-shift from **16** to **17** (calculated 446 nm **16** to 408-423 nm **17**) could be mainly attributed to a higher metal-metal contribution in **16**.

In order to have a further insight on the emission properties of these complexes, the triplet states (T_1) of **14** and **16** were optimized. For the anionic complex **14**, the main variation in relation to the S_0 (Figure 2.14) is a slight lengthening of the H(8)···C_α (by 0.071 Å) and H(13)···Pt (by 0.195 Å)*intramolecular* contacts and a slight flattening of the Hpq (dihedral angle between phenyl and quinoline decreases from 45.24º S_0 to 35.45º in T_1). Its excitation takes place with minimal changes in the frontiers orbitals. The LSOMO is essentially analogous to the HOMO in the ground state, being located on the Pt and in the two mutually *trans* C≡CR ligand, whereas the HSOMO is almost identical to the LUMO, being centered in the Hpq (Figure 2.17, Table 2.6). Thus, the emission has a pronounced alkynyl-metal to phenylquinoline charge transfer character ^{3}[(L'+M)LCT state]. The calculated phosphorescence as the energy difference between the lowest optimized the T_1 and the ground state at the optimized triplet geometry (702 nm) is red-shifted in relation to the experimental value of 615 nm due to insufficient description of the charge transfer transitions using DFT calculations.

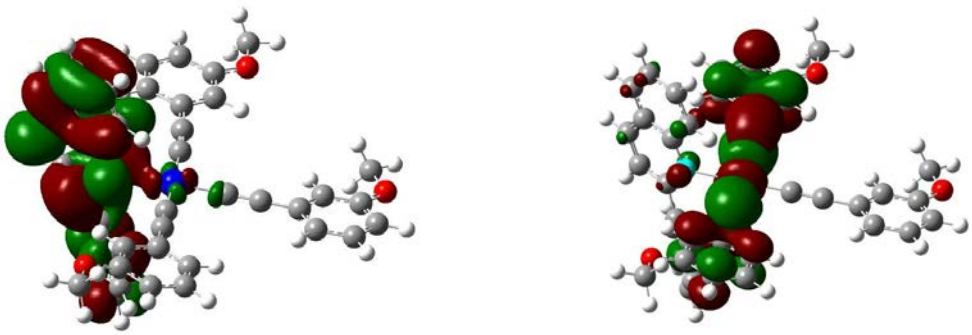

HSOMO (Hpq 97%) **LSOMO (Pt 30%/C≡CR 66%)**

Figure 2.17: Contour plots of the HSOMO and LSOMO calculated for the optimized state T_1 of **14**

Table 2.6: Composition of frontier molecular orbitals in the first triple-state for **14** and **16**

	14				**16**					
MO	**Pt**	**Hpq**	**C≡C *trans* to pq**	**C≡CR**	**Pt(1)**	**Pq(1)**	**C≡CR(1)**	**Pt(2)**	**Pq(2)**	**C≡CR(2)**
HSOMO	1	97	1	1	19	20	11	19	20	11
LSOMO	30	4	0	66	23	6	21	23	6	21

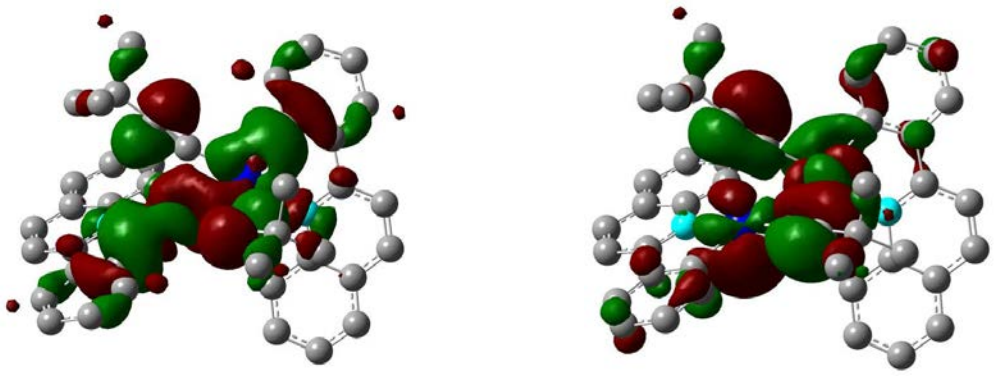

HSOMO (Pt 38%/pq 40%/C≡CR 22%) **LSOMO (Pt 46%/pq 12%/C≡CR 42%)**

Figure 2.18: Selected frontier Molecular Orbitals for complex **16** in T_1.

The calculated optimized geometry at the lowest triplet excited state (T_1) for complex **16** shows remarkable differences respect to the ground state geometry S_0 (Table A2.2 and Figure 2.15). Thus, upon excitation and subsequent relaxation, the Pt···Pt bonding distance is shortening [2.852 Å *vs* 3.195 Å in S_0] and the coordination binding mode of the alkynyl ligands changes from asymmetric σ/π-C≡C^{t}Bu to a symmetrical η^1-C≡C^{t}Bu fashion with concomitant modification in the $C^{\alpha}PtC^{\alpha}$ (~70.4º S_0 to 81.2º T_1) and $PtC^{\alpha}Pt$ (~89.4º S_0 to 80.6º T_1) angles. This is accompanied by a notable tetrahedral distortion at the Pt coordination environments [the dihedral angle of the Pt(C^N) planes with the $PtC^{\alpha}C^{\alpha}$ increases from ~ 6º in S_0 to 38.4º in T_1]. As is shown in Figure 2.18, the single occupied molecular orbitals visually identify the emission within the dimetallacycle $Pt_2(C{\equiv}C)_2$ with alkynyl to pq charge transfer ^{3}[(MM+L')LCT] with minor ^{3}IL (pq) contribution. Thus, the LSOMO and HSOMO have remarkable contribution of Pt and alkynyl orbitals [$Pt_2(C{\equiv}C)_2$ 88% LSOMO; 60% HSOMO]. It is worth noting that the contribution of the phenylquinolinyl ligand in the HSOMO decreases notably from the LUMO in the S_0 (from 92% to 40%). The calculated phosphorescence as the energy difference between the S_0 and T_1 states (674 nm) is also red-shifted in relation to the experimental value of 578 nm obtained in the emission in solid state at 298 K.

We would to remark that in most of the di or oligonuclear cycloplatinate complexes stabilized by different conectors and weak intramolecular Pt···Pt interactions, the LUMO is located on the π^* orbitals of the cyclometalated ligands[7a,7c,d,7f-i] (or on the bonding counterpart of the two π^* orbitals if π–stacking interacts are involved),[4a,4f,5b,5d-h,6] whereas the HOMO is either a weekly $d\sigma^*$ metal–metal countered orbital (when Pt···Pt is short enough) or a ligand or mixed metal–ligand orbital (d/π) in systems where Pt do not interact. Depending on the relative energies of these orbitals and the degree of mix between them, emissions are usually ascribed to ^{3}MMLCT, ^{3}MLCT and/or ^{3}LC (L = cyclometalated ligand) and, actually, it is now well documented that interplay between them can be caused by the changes in the environment. In most of the reported systems the connectors between Pt units have also a remarkable impact on the interplay or crossover of these excited states. We note that for a ^{3}MMLCT excited state the most remarkable change upon excitation HOMO-LUMO is a strengthening of Pt(II)-Pt(II) bonding with a concomitant shortening between the platinum coordination planes.

In contrast to this behavior and as shown by the theoretical studies on diplatinum complexes **16** and **17**, the utilization of two alkynyl as unique bridging groups introduces a remarkable change in the nature of the HOMO, not only because the favorable Pt(dπ)/π(C≡C) electronic interaction within the $Pt_2(C{\equiv}C)_2$ core as found in **16**, but also due to the possible delocalization through the substituents as is seen in **17**. Optimization of the T_1 excited state of **17** suggests that upon excitation not only a shortening of the Pt···Pt distance takes place but also a change in the alkynyl bonding fashion from asymmetric (μ-σ/πC≡C^{t}Bu) to a symmetrical (μ-η^{1}C≡C^{t}Bu).

2.4 Summary

In summary, Chapter 2 details the reactions of the phenylquinolinyl derivative $[Pt(pq)(\mu\text{-}Cl)]_2$ with LiC≡CR. Depending on the substituents in the alkynyl group and the reaction conditions two different series of alkynyl Pt(II) complexes have been obtained. We have investigated the phosphorescent characteristics of two very different series of alkynyl Pt(II) complexes.

On one hand, unusual tris(alkynyl) monoanionic $(NBu_4)[Pt(C{\equiv}CR)_3(Hpq)]$ (**13-15**) complexes containing the *N*-coordinated phenylquinoline (Hpq) ligand were generated by using excess of *arylethynyl* lithium. Their formation involves a rare de-orthometalation process which, to our knowledge, has no precedent in the chemistry of σ-alkynyl/cyclometalated complexes. These complexes display yellow-orange emissions in rigid media which are ascribed, on the basis of DFT calculations, to a mixed alkynyl-metal to phenylquinoline ^{3}[(L'+M)LCT] excited estate. The energy of this emission is perturbed in the solid state for **2** by the presence of *intermolecular* $O_{methoxy}\cdots H_{Hpq}$ contacts, as supported by X-ray.

By the other hand, cyclometalated binuclear $[Pt(pq)(\mu{-}\kappa C^{\alpha}{:}\eta^2 C{\equiv}CR)]_2$ (**16-19**) complexes, featuring a double σ/π alkynyl bridging ligand system, have been successfully prepared employing a more adequate stoichiometry of the alkynylating agent. The X-ray diffraction studies of **16** (R = ^{t}Bu) and **17** (R = Tol) reveal the formation of butterfly structures with short Pt···Pt separations (shorter in **16**) stabilized by η^2-C≡CR asymmetrical (**16**) or symmetrical (**17**) linkages, which seem to play a major role in their photophysical behavior.

Their emissions are clearly influenced by the nature of substituents on the alkynyl ligands and correlate with the observed intramolecular Pt···Pt distances. For the complex **16** with an alkyl substituent (^{t}Bu) and featuring a short Pt···Pt distance, the emission is located within the dimetallacycle core $Pt_2(C{\equiv}C)_2$ with some alkynyl to pq charge transfer ^{3}[(MM+L')LCT] excited state. However in **17**, with the tolyl substituent and a longer Pt···Pt distance, the emission mainly arises from a ^{3}L'LCT excited state with minor contribution of ^{3}MMLCT character. Intriguingly, the emissions profiles of

18 and **19** in solid state (77 K) and those of all complexes in glasses are characteristic of a *monomer-like* ^{3}[(L'+M)LCT] excited state with a negligible contribution of the Pt···Pt interaction. We attributed this behavior to the formation of bent $Pt_2(C{\equiv}C)_2$ cores with longer Pt···Pt distances to those found for **16** and **17** in solid state (> 3.2 Å) and in the fast frozen process. Although the generation of planar $Pt_2(C{\equiv}C)_2$ cores with long metal-metal separation could not be completely excluded, it is seems less likely due to geometrical constraints of the pq ligands.

In contrast to the behavior described in the Introduction for di and oligonuclear cycloplatinate derivatives stabilized by other types of bridging ligands and weak Pt···Pt interactions, the theoretical studies on diplatinum complexes **16** and **17** indicate that the utilization of two alkynyls as unique bridging groups introduces a remarkable change in the nature of the HOMO, not only because the favorable Pt(dπ)/π(C≡C) electronic interaction within the $Pt_2(C{\equiv}C)_2$ core as found in **16**, but also due to the possible delocalization through the substituents as is seen in **17**. Optimization of the T_1 excited state of **17** suggests that upon excitation not only a shortening of the Pt···Pt distance takes place but also a change in the alkynyl bonding fashion from asymmetric (μ-σ/πC≡C^{t}Bu) to a symmetrical (μ-η^{1}C≡C^{t}Bu).

2.5 References

1. (a) Muro, M. L.; Rachford, A. A.; Wang, X.; Castellano, F. N. *Top. Organomet. Chem.* **2010**, *29*, 159; (b) Williams, J. A. G. *Top. Curr. Chem.* **2007**, *281*, 205; (c) Zhou, G.-J.; Wong, W.-Y. *Chem. Soc. Rev.* **2011**, *40*, 2541; (d) Lu, W.; Mi, B. X.; Chan, M. C. W.; Hui, Z.; Che, C. M.; Zhu, N.; Lee, S. T. *J. Am. Chem. Soc.* **2004**, *126*, 4958; (e) Guerchais, V.; Fillaut, J.-L. *Coord. Chem. Rev.* **2011**, *255*, 2448; (f) Yang, Q.-Z.; Wu, L.-Z.; Zhang, H.; Chen, B.; Wu, Z.-X.; Zhang, L.-P.; Tung, C.-H. *Inorg. Chem.* **2004**, *43*, 5195; (g) Fillaut, J.-L.; Akdas-Kilig, H.; Dean, E.; Latouche, C.; Boucekkine, A. *Inorg. Chem.* **2013**, *52*, 4890; (h) Schneider, J.; Du, P.; Jarosz, P.; Lazarides, T.; Wang, X.; Brennessel, W. W.; Eisenberg, R. *Inorg. Chem.* **2009**, *48*, 4306; (i) Harris, C. F.; Vezzu, D. A. K.; Bartolotti, L.; Boyle, P. D.; Huo, S. *Inorg. Chem.* **2013**, *52*, 11711; (j) Zhang, Y.; Clavadetscher, J.; Bachmann, M.; Blacque, O.; Venkatesan, K. *Inorg. Chem.* **2014**, *53*, 756; (k) Zhang, Y.; Garg, J. A.; Michelin, C.; Fox, T.; Blacque, O.; Venkatesan, K. *Inorg. Chem.* **2011**, *50*, 1220; (l) Shao, P.; Li, Y.; Yi, J.; Pritchett, T. M.; Sun, W. *Inorg. Chem.* **2010**, *49*, 4507; (m) Chen, Y.; Li, K.; Lu, W.; Chui, S. S. Y.; Ma, C. W.; Che, C. M. *Angew. Chem. Int. Ed.* **2009**, *48*, 9909; (n) Qiu, D.; Zhao, Q.; Wang, H.; Feng, Y.; Bao, X.; Guo, Y.; Huang, Q. *Inorg. Chim. Acta* **2012**, *392*, 261; (o) Ravindranathan, D.; Vezzu, D. A. K.; Bartolotti, L.; Boyle, P. D.; Huo, S. *Inorg. Chem.* **2010**, *49*, 8922; (p) Liu, R.; Chang, J.; Xiao, Q.; Li, Y.; Chen, H.; Zhu, H. *Dyes and Pigments* **2011**, *88*, 88; (q) Yam, V. W.-W.; Chan, K. H.-Y.; Wong, K. M.-C.; Zhu, N. *Chem. Eur. J.* **2005**, *11*, 4535; (r) Moriuchi, T.; Sakamoto, Y.; Noguchi, S.; Fujiwara, T.; Akine, S.; Nabeshima, T.; Hirao, T. *Dalton Trans.* **2012**, *41*, 8524; (s) Lu, W.; Mi, B. X.; Chan, M. C. W.; Hui, Z.; Zhu, N.; Lee, S. T.; Che, C. M. *Chem. Commun.* **2002**, 206; (t) Lu, W.; Law, Y.-C.; Han, J.; Chui, S. S.-Y.; Ma, D.-L.; Zhu, N.; Che, C.-M. *Chem. Asian J.* **2008**, *3*, 59; (u) Clark, M. L.; Diring, S.; Retailleau, P.; McMillin, D. R.; Ziessel, R. *Chem. Eur. J.* **2008**, *14*, 7168; (v) Berenguer, J. R.; Lalinde, E.; Torroba, J. *Inorg. Chem.* **2007**, *46*, 9919.
2. (a) Díez, Á.; Lalinde, E.; Moreno, M. T. *Coord. Chem. Rev.* **2011**, *255*, 2426; (b) Berenguer, J. R.; Lalinde, E.; Moreno, M. T. *Coord. Chem. Rev.* **2010**, *254*, 832;

(c) Lam, E. S. H.; Tam, A. Y.-Y.; Lam, W. H.; Wong, K. M.-C.; Zhu, N.; Yam, V. W.-W. *Dalton Trans.* **2012**, *41*, 8773.

3. (a) Hoogervorst, W. J.; Elsevier, C. J.; Lutz, M.; Spek, A. L. *Organometallics* **2001**, *20*, 4437; (b) Casas, J. M.; Forniés, J.; Fuertes, S.; Martín, A.; Sicilia, V. *Organometallics* **2007**, *26*, 1674.
4. (a) Ding, J.; Pan, D.; Tung, C.-H.; Wu, L.-Z. *Inorg. Chem.* **2008**, *47*, 5099; (b) Hu, J.; Lin, R.; Yip, J. H. K.; Wong, K.-Y.; Ma, D.-L.; Vittal, J. J. *Organometallics* **2007**, *26*, 6533; (c) Jude, H.; Krause Bauer, J. A.; Connick, W. B. *Inorg. Chem.* **2005**, *44*, 1211; (d) Ma, B.; Djurovich, P. I.; Yousufuddin, M.; Bau, R.; Thompson, M. E. *J. Phys. Chem. C* **2008**, *112*, 8022; (e) Tzeng, B. C.; Chiu, T. H.; Lin, S. Y.; Yang, C. M.; Chang, T. Y.; Huang, C. H.; Chang, A. H. H.; Lee, G. H. *Cryst. Growth. Des.* **2009**, *9*, 5356; (f) Guo, Z.; Chan, M. C. W. *Chem. Eur. J.* **2009**, *15*, 12585.
5. (a) Lu, W.; Chan, M. C. W.; Cheung, K. K.; Che, C. M. *Organometallics* **2001**, *20*, 2477; (b) Lai, S.-W.; Chan, M. C.-W.; Cheung, T. C.; Peng, S. M.; Che, C.-M. *Inorg. Chem.* **1999**, *38*, 4046; (c) Kui, S. C. F.; Chui, S. S. Y.; Che, C. M.; Zhu, N. *J. Am. Chem. Soc.* **2006**, *128*, 8297; (d) Koo, C. K.; Wong, K. L.; Lau, K. C.; Wong, W. Y.; Lam, M. H. W. *Chem. Eur. J.* **2009**, *15*, 7689; (e) Sun, W.; Zhu, H.; Barron, P. M. *Chem. Matter.* **2006**, *18*, 2602; (f) Lu, W.; Chan, M. C. W.; Zhu, N.; Che, C. M.; Li, C.; Hui, Z. *J. Am. Chem. Soc.* **2004**, *126*, 7639; (g) Kui, S. C. F.; Sham, I. H. T.; Cheung, C. C. C.; Ma, C.-W.; Yan, B.; Zhu, N.; Che, C.-M.; Fu, W.-F. *Chem. Eur. J.* **2007**, *13*, 417; (h) Shao, P.; Sun, W. *Inorg. Chem.* **2007**, *46*, 8603.
6. (a) Aoki, R.; Kobayashi, A.; Chang, H.-C.; Kato, M. *Bull. Chem. Soc. Jpn.* **2011**, *84*, 218; (b) Sicilia, V.; Forniés, J.; Casas, J. M.; Martín, A.; López, J. A.; Larraz, C.; Borja, P.; Ovejero, C.; Tordera, D.; Bolink, H. *Inorg. Chem.* **2012**, *51*, 3427.
7. (a) Ma, B.; Li, J.; Djurovich, P. I.; Yousufuddin, M.; Bau, R.; Thompson, M. E. *J. Am. Chem. Soc.* **2005**, *127*, 28; (b) Lai, S. W.; Chan, M. C. W.; Cheung, K. K.; Peng, S. M.; Che, C. M. *Organometallics* **1999**, *18*, 3991; (c) Koo, C. K.; Ho, Y. M.; Chow, C. F.; Lam, M. H. W.; Lau, T. C.; Wong, W. Y. *Inorg. Chem.* **2007**, *46*, 3603; (d) Rachford, A. A.; Castellano, F. N. *Inorg. Chem.* **2009**, *48*, 10865; (e) Saito, K.; Nakao, Y.; Umakoshi, K.; Sakaki, S. *Inorg. Chem.* **2010**, *49*, 8977; (f) Saito, K.; Nakao, Y.; Sakaki, S. *Inorg. Chem.* **2008**, *47*, 4329; (g) Chakraborty, A.; Deaton, J. C.; Haefele, A.; Castellano, F. N. *Organometallics* **2013**, *32*, 3819;

(h) Lockard, J. V.; Rachford, A. A.; Smolentsev, G.; Stickrath, A. B.; Wang, X.; Zhang, X.; Atenkoffer, K.; Jennings, G.; Soldatov, A.; Rheingold, A. L.; Castellano, F. N.; Chen, L. X. *J. Phys. Chem. A* **2010**, *114*, 12780; (i) Cho, S.; Mara, M. W.; Wang, X.; Lockard, J. V.; Rachford, A. A.; Castellano, F. N.; Chen, L. X. *J. Phys. Chem. A* **2011**, *115*, 3990.

8. Fernández, S.; Forniés, J.; Gil, B.; Gómez, J.; Lalinde, E. *Dalton Trans.* **2003**, 822.
9. Berenguer, J. R.; Díez, Á.; García, A.; Lalinde, E.; Moreno, M. T.; Sánchez, S.; Torroba, J. *Organometallics* **2011**, *30*, 1646.
10. (a) Golbon Haghighi, M.; Rashidi, M.; Nabavizadeh, S. M.; Jamali, S.; Puddephatt, R. J. *Dalton Trans.* **2010**, *39*, 11396; (b) Jamali, S.; Nabavizadeh, S. M.; Rashidi, M. *Inorg. Chem.* **2008**, *47*, 5441; (c) Nabavizadeh, S. M.; Haghighi, M. G.; Esmaeilbeig, A. R.; Raoof, F.; Mandegani, Z.; Jamali, S.; Rashidi, M.; Puddephatt, R. J. *Organometallics* **2010**, *29*, 4893.
11. Sicilia, V.; Fuertes, S.; Martín, A.; Palacios, A. *Organometallics* **2013**, *32*, 4092.
12. Zhang, W.-H.; Chien, S. W.; Hor, T. S. A. *Coord. Chem. Rev.* **2011**, *255*, 1991.
13. Günter, H. *NMR spectroscopy : basic principles, concepts and applications in chemistry, 2nd ed, ;* Chichester : John Wiley & Sons, 1994.
14. (a) Berenguer, J. R.; Lalinde, E.; Moreno, M. T.; Sánchez, S.; Torroba, J. *Inorg. Chem.* **2012**, *51*, 11665; (b) Baya, M.; Belío, Ú.; Martín, A. *Inorg. Chem.* **2013**, *53*, 189; (c) Casas, J. M.; Falvello, L. R.; Forniés, J.; Martín, A.; Welch, A. J. *Inorg. Chem.* **1996**, *35*, 6009; (d) Albinati, A.; Lianza, F.; Pregosin, P. S.; Mueller, B. *Inorg. Chem.* **1994**, *33*, 2522.
15. Benito, J.; Berenguer, J. R.; Forniés, J.; Gil, B.; Gómez, J.; Lalinde, E. *Dalton Trans.* **2003**, 4331.
16. Tanaka, S.; Yoshida, T.; Adachi, T.; Yoshida, T.; Onitsuka, K.; Sonogashira, K. *Chem. Lett.* **1994**, 877.
17. (a) Berenguer, J. R.; Fernández, J.; Lalinde, E.; Sánchez, S. *Organometallics* **2013**, *32*, 835; (b) Müller, T. E.; Mingos, D. M. P.; Williams, D. J. *J. Chem. Soc., Chem. Commun.* **1994**, 1787; (c) Müller, T. E.; Choi, W. K.; Mingos, D. M. P.; Murphy, D.; Williams, D. J.; Yam, V. W. W. *J. Organomet. Chem.* **1994**, *484*, 209; (d) Alder, M. J.; Flower, R. K.; Pritchard, R. G. *J. Organomet. Chem.* **2001**, *629*, 153.

18. (a) Martín, A. *J. Chem. Educ.* **1999**, *76*, 578; (b) Brammer, L. *Dalton Trans.* **2003**, 3145.

19. (a) Forniés, J.; Gómez-Saso, M. A.; Lalinde, E.; Martínez, F.; Moreno, M. T. *Organometallics* **1992**, *11*, 2873; (b) Ara, I.; Falvello, L. R.; Fernández, S.; Forniés, J.; Lalinde, E.; Martín, A.; Moreno, M. T. *Organometallics* **1997**, *16*, 5923; (c) Berenguer, J. R.; Forniés, J.; Lalinde, E.; Martín, A.; Serrano, B. *J. Chem. Soc., Dalton Trans.* **2001**, 2926; (d) Berenguer, J. R.; Forniés, J.; Martínez, F.; Cubero, J. C.; Lalinde, E.; Moreno, M. T.; Welch, A. J. *Polyhedron* **1993**, *12*, 1797.

20. Pregosin, P. S.; Wombacher, F.; Albinati, A.; Lianza, F. *J. Organomet. Chem.* **1991**, *418*, 249.

21. Berenguer, J. R.; Fernández, J.; Gil, B.; Lalinde, E.; Sánchez, S. *Inorg. Chem.* **2010**, *49*, 4232.

22. (a) Berenguer, J. R.; Díez, A.; Lalinde, E.; Moreno, M. T.; Ruiz, S.; Sánchez, S. *Organometallics* **2011**, *30*, 5776; (b) De Priest, J.; Zheng, G. Y.; Goswami, N.; Eichhorn, D. M.; Woods, C.; Rillema, D. P. *Inorg. Chem.* **2000**, *39*, 1955; (c) Velusamy, M.; Chen, C.-H.; Wen, Y. S.; Lin, J. T.; Lin, C.-C.; Lai, C.-H.; Chou, P.-T. *Organometallics* **2010**, *29*, 3912.

23. Wang, K.-W.; Chen, J.-L.; Cheng, Y.-M.; Chung, M.-W.; Hsieh, C.-C.; Lee, G.-H.; Chou, P.-T.; Chen, K.; Chi, Y. *Inorg. Chem.* **2010**, *49*, 1372.

24. (a) Lanoë, P.-H.; Fillaut, J.-L.; Guerchais, V.; Le Bozec, H.; Williams, J. A. G. *Eur. J. Inorg. Chem.* **2011**, *2011*, 1255; (b) Tang, W.-S.; Lu, X.-X.; Wong, K. M.-C.; Yam, V. W.-W. *J. Mater. Chem.* **2005**, *15*, 2714.

2.6 Appendix

Table A2.1: DFT optimized geometries for ground state and triplet state of complex **14**

14			
	X-Ray	**S_0**	**T_1**
Pt(1) -N(1)	2.133(4)	2.223	2.190
Pt(1) -C(16)	1.966(6)	2.022	1.976
C(16)-C(17)	1.176(8)	1.230	1.224
C(34)-C(35)	1.198(9)	1.225	1.237
Pt(1) -C(25)	1.995(6)	1.942	1.986
Pt(1) -C(34)	2.008(6)	2.017	1.970
C(25)-C(26)	1.221(9)	1.229	1.238
Pt(1)-C(16)-C(17)	178.6(5)	179.57	179.45
Pt(1)-C(25)-C(26)	172.8(5)	177.42	178.56
Pt(1)-C(34)-C(35)	178.3(5)	177.49	175.70
C(16)-C(17)-C(18)	175.2(6)	178.56	179.27
C(25)-C(26)-C(27)	172.4(7)	178.45	178.98
C(34)-C(35)-C(36)	174.9(7)	179.67	175.61

Table A2.2: DFT optimized geometries for ground state and triplet state of complexes **16** and **17**

16			
	X-Ray	**S_0**	**T_1**
Pt(1)-C(1)	1.969(6)	1.987	2.042
Pt(1)-N(1)	2.119(5)	2.160	2.193
Pt(1)-C(16)	1.952(6)	1.960	1.949
Pt(1)-C(38)	2.440(6)	2.736	3.060
Pt(1)-C(37)	2.382(6)	2.545	2.425
C(16)-C(17)	1.218(8)	1.235	1.243
Pt(1)-Pt(2)	3.0936(3)	3.195	2.852
Pt(2)-C(22)	1.990(6)	1.987	2.042
Pt(2)-N(2)	2.103(5)	2.160	2.193
Pt(2)-C(37)	1.964(6)	1.961	1.949
Pt(2)-C(17)	2.431(6)	2.736	3.060
Pt(2)-C(16)	2.361(6)	2.545	2.425
C(37)-C(38)	1.214(8)	1.235	1.243
N(1)-Pt(1)-C(1)	80.7(2)	79.91	78.56
Pt(1)-C(16)-C(17)	167.6(5)	172.21	170.26
C(16)-C(17)-C(18)	161.1(6)	168.58	178.82
N(2)-Pt(2)-C(22)	80.1(2)	79.89	78.56
Pt(2)-C(37)-C(38)	164.4(5)	172.25	170.26
C(37)-C(38)-C(39)	162.6(6)	168.65	178.82
17			
	X-Ray	**S_0**	
Pt(1)-C(1)	1.983(6)	1.992	
Pt(1)-N(1)	2.110(5)	2.159	
Pt(1)-C(16)	1.952(6)	1.955	
Pt(1)-C(41)	2.386(6)	2.589	
Pt(1)-C(40)	2.391(6)	2.522	
C(16)-C(17)	1.219(8)	1.240	
Pt(1)-Pt(2)	3.2109(3)	3.352	
Pt(2)-C(25)	1.999(6)	1.992	
Pt(2)-N(2)	2.090(5)	2.159	
Pt(2)-C(40)	1.951(6)	1.955	
Pt(2)-C(17)	2.356(6)	2.591	
Pt(2)-C(16)	2.373(6)	2.522	
C(40)-C(41)	1.238(8)	1.240	
N(1)-Pt(1)-C(1)	80.3(2)	79.87	
Pt(1)-C(16)-C(17)	169.4(5)	171.78	
C(16)-C(17)-C(18)	165.3(6)	168.99	
N(2)-Pt(2)-C(25)	80.7(2)	79.88	

Pt(2)-C(40)-C(41)	167.5(5)	171.64
C(40)-C(41)-C(42)	161.3(6)	168.85

Table A2.3: Selected vertical excitation energies singlets (S_0) computed by TD-DFT/CPCM with the orbitals involved for complexes **14**, **16** and **17**

State	λ_{exc} (calc.)/nm	f [a]	Transition (Percentage Contribution)
			14$^-$
S_1	436.9	0.0211	HOMO-2->LUMO (98%)
S_2	400.7	0.0107	H-4->LUMO (43%), H-3->LUMO (56%)
S_3	359.1	0.0805	HOMO->L+1 (98%)
S_4	352.2	0.764	HOMO->L+2 (92%)
S_5	350.6	0.0239	H-5->LUMO (94%)
S_6	335.1	0.0104	H-2->L+1 (19%), H-2->L+2 (69%)
S_7	329.7	0.3384	H-1->L+1 (51%), H-1->L+2 (38%)
S_8	325.6	0.0785	H-1->L+1 (45%), H-1->L+2 (52%)
S_9	305.6	0.3839	HOMO->L+3 (95%)
			16
S_1	446.5	0.1271	HOMO->LUMO (90%)
S_2	413.3	0.0163	H-1->LUMO (57%), HOMO->L+1 (21%), H-3->L+1 (6%), H-2->LUMO (7%)
S_3	405.1	0.1086	H-1->L+1 (79%), H-4->LUMO (6%)
S_4	404.6	0.0407	H-3->L+1 (14%), H-2->LUMO (60%), H-1->LUMO (16%)
S_5	392.2	0.0363	H-2->L+1 (75%), H-4->LUMO (6%), H-1->L+1 (9%)
S_6	377.6	0.0439	H-4->LUMO (82%)
S_7	347.4	0.0449	HOMO->L+2 (55%), HOMO->L+4 (29%)
S_8	342.9	0.0392	H-5->LUMO (74%)
S_9	342.4	0.0135	H-6->LUMO (83%)
S_{10}	333.4	0.1566	H-6->L+1 (77%)
			17
S_1	423.2	0.0505	H-1->LUMO (67%), HOMO->L+1 (25%)
S_2	417.3	0.0284	H-1->LUMO (27%), HOMO->L+1 (56%), H-3->LUMO (9%)
S_3	412.1	0.1614	H-1->L+1 (88%)
S_4	407.8	0.2955	H-2->LUMO (74%), HOMO->LUMO (15%), H-3->L+1 (5%)
S_5	399.9	0.074	H-3->LUMO (20%), H-2->L+1 (62%), HOMO->L+1 (11%)
S_6	377.0	0.0416	H-4->LUMO (15%), H-3->L+1 (66%), H-2->LUMO (10%)
S_7	368.7	0.0154	H-4->L+1 (82%)
S_8	341.2	0.021	H-6->LUMO (15%), H-1->L+2 (65%)
S_9	339.7	0.0931	HOMO->L+2 (73%), H-5->LUMO (5%), H-2->L+2 (5%)
S_{10}	335.1	0.1338	H-5->LUMO (67%), H-9->L+1 (6%), H-4->LUMO (5%)
S_{11}	334.9	0.0186	H-6->LUMO (66%), H-1->L+2 (15%)

a) Oscillator Strength

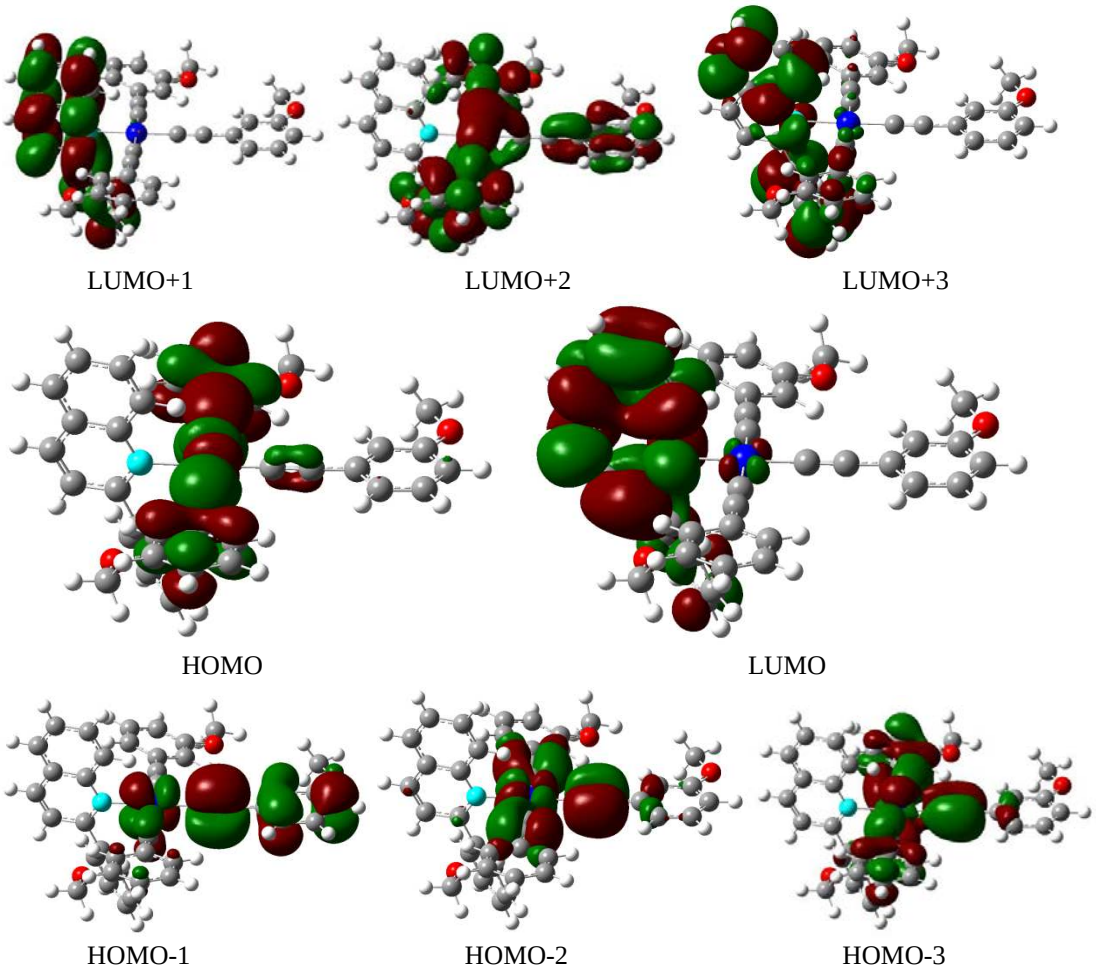

Figure A2.1: Selected frontier Molecular Orbitals for complex **14**

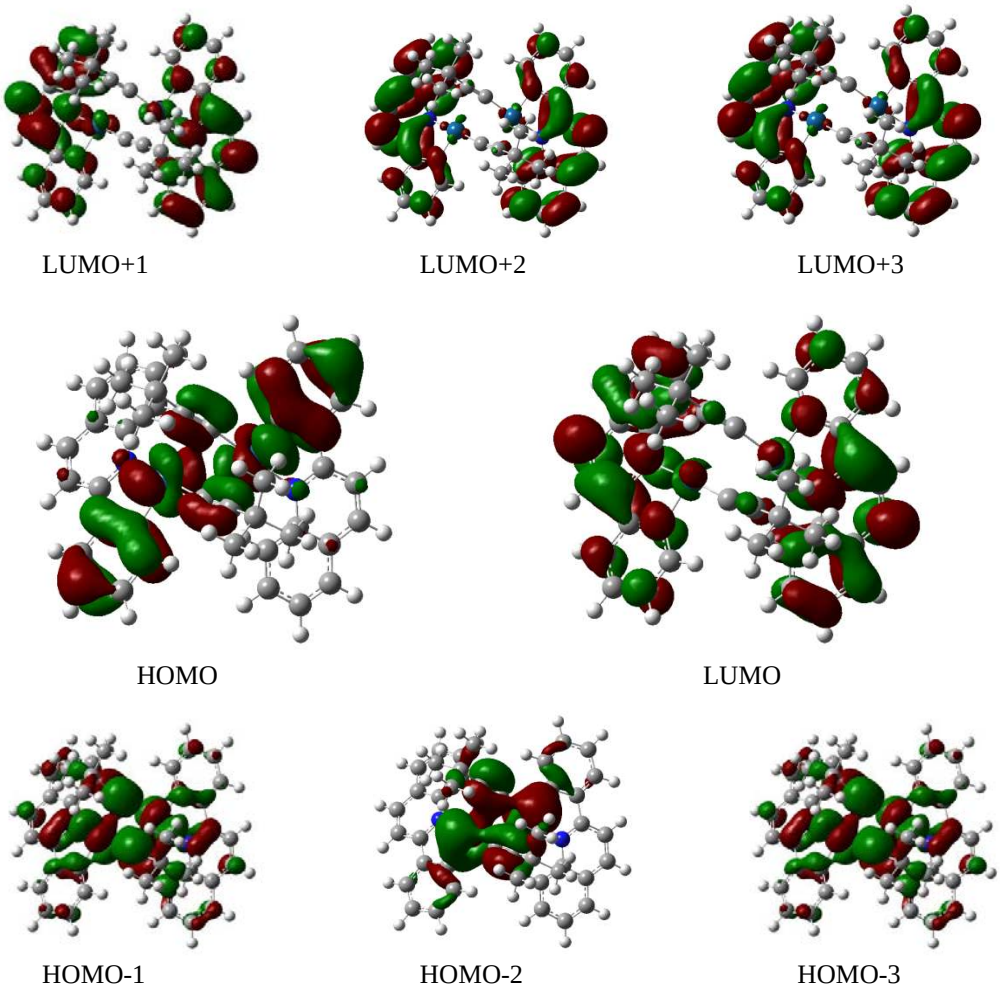

Figure A2.2: Selected frontier Molecular Orbitals for complex **16**

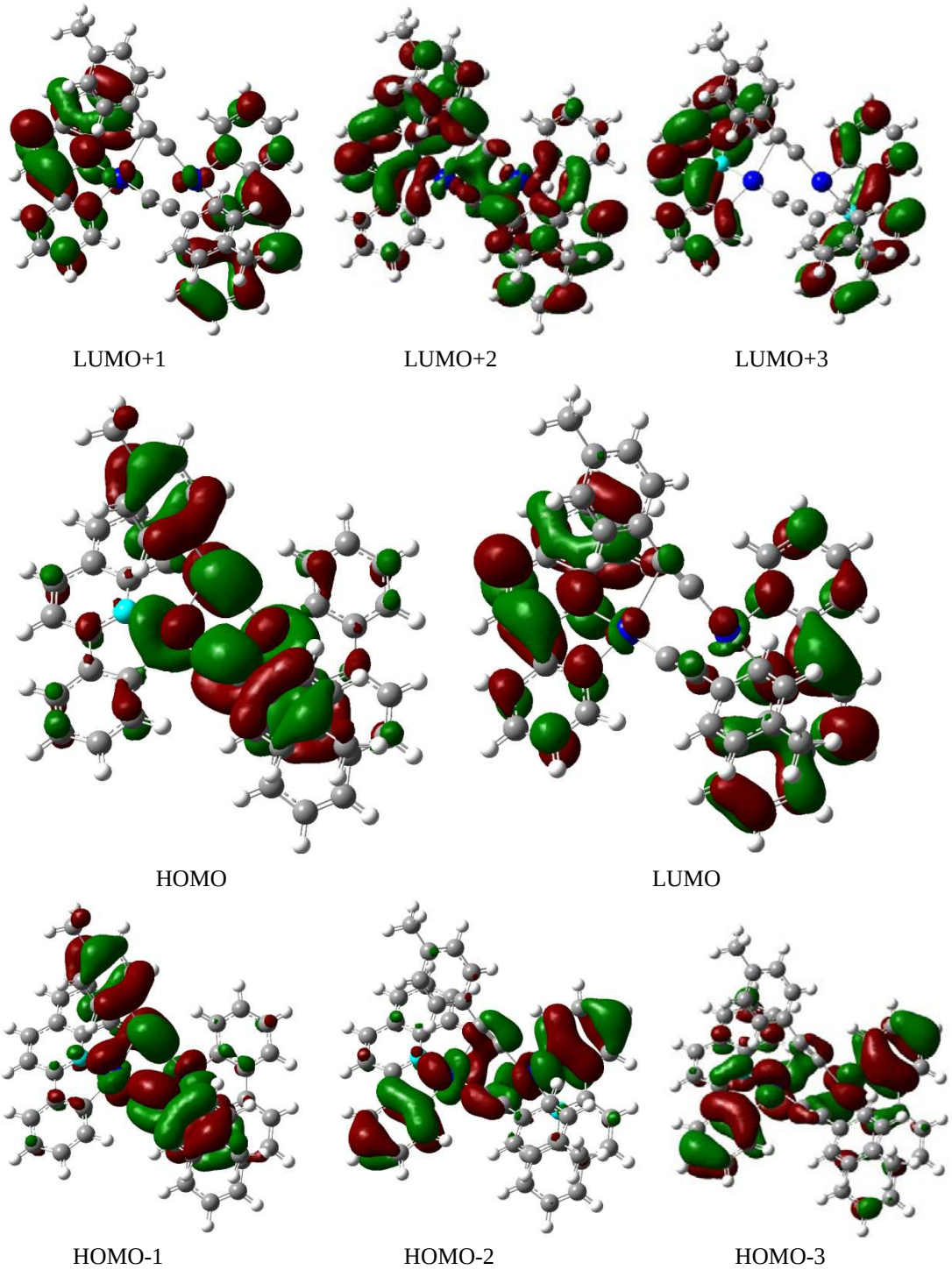

Figure A2.3: Selected frontier Molecular Orbitals for complex **17**

CHAPTER 3

Reactivity of [Pt(pq)(μ–κC^{α}:η^2-C≡C^{t}Bu)]$_2$ toward donor ligands. Solution behavior and photophysical properties

Reactivity of [Pt(pq)(μ–κC^{α}:η^2-C≡C^{t}Bu)]$_2$ toward donor ligands. Solution behavior and photophysical properties

3.1 Reactivity of [Pt(pq)(μ–κC^{α}:η^2-C≡C^{t}Bu)]$_2$ toward di and tri *N*-donor connecting ligands

The interest of alkynyl platinum(II) complexes stems from their rich structural diversity,[1] their interesting chemical reactivity[1a] and more recently from their increasing potential in material science.[2] In this field, light-emitting complexes have attracted a great deal of attention owing to their use in optoelectronic devices, chemosensors, photovoltaic cells and photocatalysis.

By using the triple bond of the alkynyl ligand, a good number of di- and triplatinum complexes in which the Pt(II) centers are stabilized by double bridging alkynyl systems with different conformations have been reported.[3] However, the reactivity of these systems has been scarcely explored. It has been reported that binuclear Pt derivatives such us [*trans*-Pt(μ–κC^{α}:η^2-C≡CR)(C_6F_5)L]$_2$ or cycloplatinate complexes [Pt(C^P)(μ–κC^{α}:η^2-C≡CR)]$_2$ undergo bridge-splitting with classical donor ligands to give mononuclear σ-alkynyl Pt(II) complexes.[3a,3f,g,3j]

By other hand, since the discovery in 1990 by Fujita of the first example of a rationally designed metallacycle, the molecular square [{Pd(en)(μ-4,4'-bpy)}$_4$](NO_3)$_8$, prepared by self–assembly of [Pd(en)(ONO_2)$_2$] (en = ethylenediamine) with the linear linker 4,4'-bipyridine (4,4'-bpy),[4] there has been increasing interest in using linear, angular, triangular or flexible linkers with bidentate or tridentate binding nitrogen units to produce fascinating metal-mediated molecular architectures, including many macrocycles and cages. Several reviews have thoroughly covered this amazing field in the last years.[5] The inherent stability and rather low reactivity of the Pt^{II} in contrast with other metals [*i.e* Pd(II)] has been the main attractive and value for the use of Pt^{II} units for metallamacrocycles.[6] Furthermore, the attractive photophysical properties of Pt^{II}

complexes, such as low-energy, tunability and long-lived excited states have prompted their incorporation into metallacyles.[7] The combination of the luminescent Pt^{II} units in the corners with luminophore N-groups that can act as linkers can be exploited in highly emissive metallacycles.[8] Comparatively, platinum binuclear derivatives bridged by dinitrogen donor ligands are less represented,[9] and particularly with cycloplatinated fragments are scarce.[9a-e]

In this work, we study the reactivity of the *ter*-butyl derivative [Pt(pq)(μ−κC$^{\alpha}$:η^2-C≡C^{t}Bu)]$_2$ (**16**) towards bidentate and tridentate nitrogen linkers, assuming that both, the "Pt(pq)(C≡C^{t}Bu)" fragment and the linkers, are luminophores. This study has allowed us to synthesize a series of platinum(II) binuclear derivatives [{Pt(pq)(C≡C^{t}Bu)}$_2$(μ-L)] bridged by ***N*-*N***-donor ligands [L = pyrazine (pyz) **20a,** 4,4'-bipyridine (bpy) **21a**, 1,2-bis(bipyridyl)ethane (bpa) **22a,** *trans*-1,2-bis(4-pyridyl)ethylene (bpe) **23a** and di(4-pyridyl)acetylene (bpac) **24a**], and the trinuclear branched derivative [{Pt(pq)(C≡C^{t}Bu)}$_3$(μ-L)] (**25a**) containing the rigid conjugated pyridyl alkynyl ligand [μ-1,3,5-tris(pyridine-4-ylethynyl)benzene]. A combination of crystallography (**21a** and **23a**), NMR, IR and mass spectrometry provides a complete picture of the equilibrium stablished in solution between derivatives with N-donor bridging ligands (**20a**-**24a**), mononuclear complexes with terminal N-ligands [Pt(pq)(C≡C^{t}Bu)(L−κ***N***)] (**20b**-**24b**) and the precursor (**16**). Furthermore, we discuss the photophysical properties of these complexes in solid state and in solution and the theoretical calculations on **21a**.

3.1.1 Synthesis and characterization

As illustrated in Scheme 3.1, the synthesis of new diplatinum derivatives [{Pt(pq)(C≡C^{t}Bu)}$_2$(μ-L)] (L = pyz **20a**, bpy **21a**, bpa **22a**, bpe **23a**, bpac **24a**) was achieved by bridged-cleavage reaction in CH_2Cl_2 of [Pt(pq)(μ−κC$^{\alpha}$:η^2-C≡C^{t}Bu)]$_2$ (**16**) with the corresponding dinitrogen donor ligand. Complexes **21a**, **22a** and **24a** were obtained as orange solids in moderate or high yields by reaction of the starting material with one equivalent of the ligand, whereas for **20a** and **23a** two equivalents of ligand were added to obtain the complexes pure in solid state. A particularly reliable indicator of the final reaction is the lack of bridging ν(C≡C) band in the IR spectra of the final

solid (see below). By other hand, the branched trinuclear platinum complex [{Pt(pq)(C≡C^{t}Bu)}$_3$(μ-tpab)] (**25a**) was obtained using the same strategy but with a **16**:ligand molar ratio of 3:2.

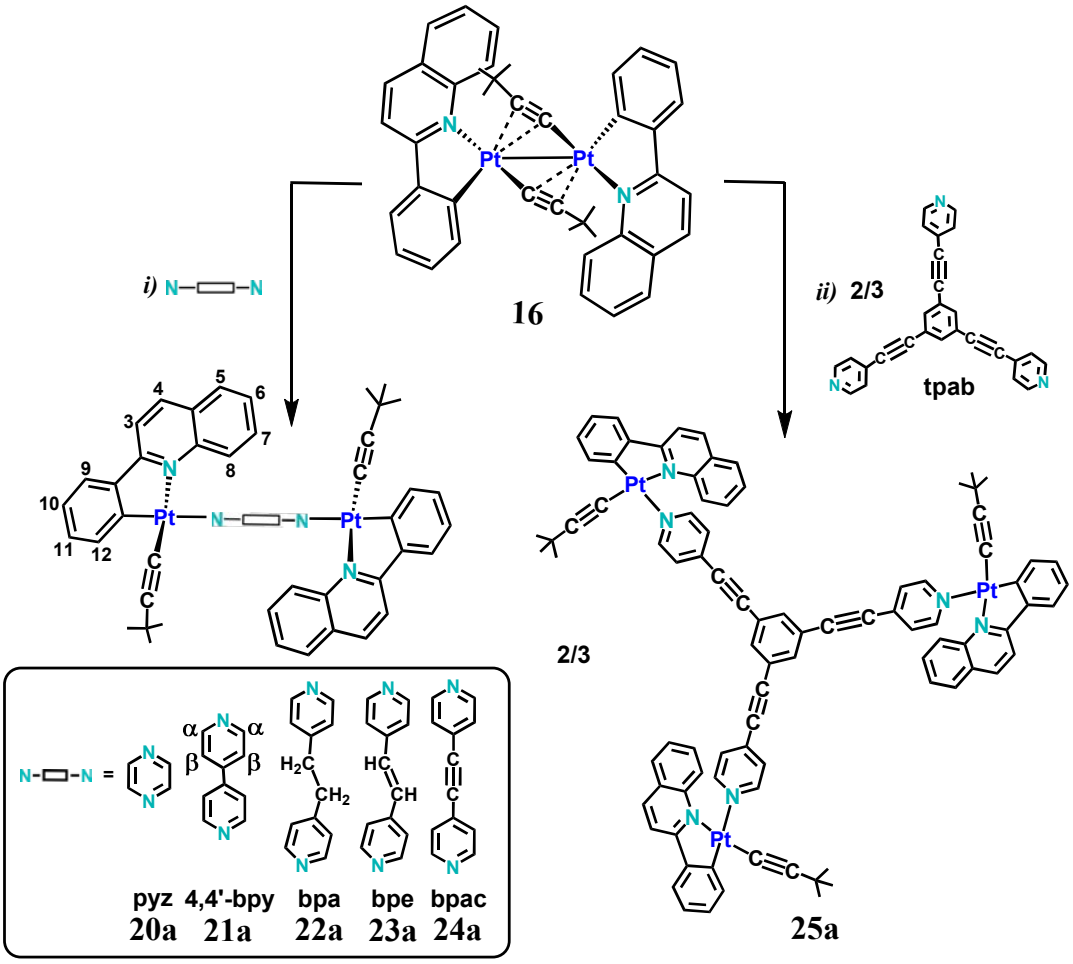

Scheme 3.1

A combination of crystallography (**21a** and **23a**), IR spectra, mass spectrometry and elemental analysis support the formulation proposed in the Scheme 3.1. ^{1}H NMR spectroscopy completes the picture in solution. The IR spectra of these complexes show one ν(C≡C) intense absorption (2114-2118 cm^{-1}) in the typical range for terminal σ-coordinated alkynyl ligands, thus confirming the cleavage of the alkynyl bridging (μ–C≡C^{t}Bu)$_2$ system. Furthermore, complexes **24a** and **25a** show one additional band at higher frequency (2223 **24a**, 2212 cm^{-1} **25a**), assigned to the ν(C≡C) stretch of the inner ethynyl entity of the 4-pyridylacetylene groups in the bpac and the tpab ligands. Because of the weak coordinative bonds, ESI is used as a soft ionization method. Analysis of the complexes in CH_2Cl_2 in the positive ion mode (exact mass) gave the

corresponding molecular peak for each complex (See Figure 3.1 for **25a**) and the fragmentation peak [Pt(pq)(C≡C^{t}Bu)L]$^+$ or [Pt$_2$(pq)$_2$(C≡C^{t}Bu)$_2$L]$^+$ (**25a**) by loss of the fragment [Pt(pq)(C≡C^{t}Bu)]. The cleavage occurs at the Pt-N covalent bond, indicating that this is the weakest link in this series of derivatives. In these complexes, there are common peaks associated with the starting material: the intact doubly σ-π alkynyl bridging molecular ion ([{Pt(pq)(C≡C^{t}Bu)}$_2$]$^+$, *m/z* 961), the loss of an alkynyl group ([Pt$_2$(pq)$_2$(C≡C^{t}Bu)]$^+$, *m/z* 879) and the cleavage ([Pt(pq)(C≡C^{t}Bu)]$^+$, *m/z* 481). In good qualitative agreement with the observations in the NMR spectra in solution (see below) these peaks are very intense in the mass spectra.

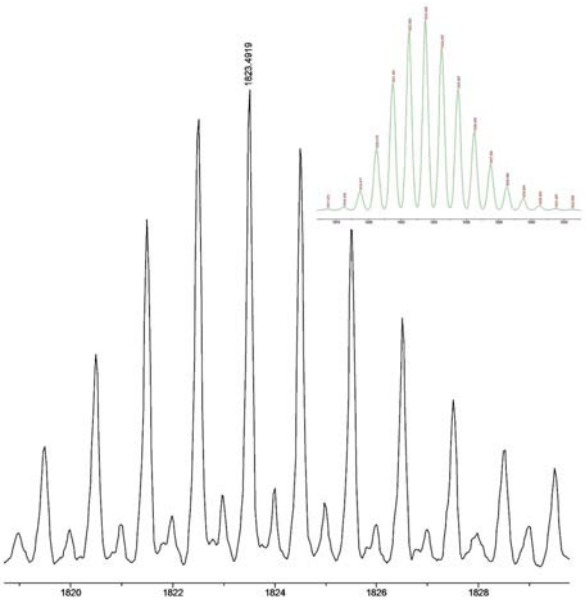

Figure 3.1: Experimental isotope pattern and predicted isotopic distribution (green) in the electrospray mass spectrum of **25a**, showing the peak [Pt$_3$(pq)$_3$(C≡C^{t}Bu)$_3$(tpab)]$^+$

Single crystals suitable for X-ray analysis were grown by slow diffusing of *n*-hexane into a $CHCl_3$ solution at -30ºC of **21a** and **23a**, respectively. The structures of [{Pt(pq)(μ–C≡C^{t}Bu)}$_2$(μ-4,4'-bpy)]·2$CHCl_3$·C_6H_{14} (**21a**·2$CHCl_3$·C_6H_{14}) and [{Pt(pq)(μ–C≡C^{t}Bu)}$_2$(μ-bpe)]·4$CHCl_3$ (**23a**·4$CHCl_3$) were confirmed by X–ray crystallography (Figures 3.2, 3.3 and A3.1; Tables 3.1 and A3.1). The asymmetric unit of **21a** contains only one molecule, whereas in **23a** the asymmetric unit is formed by one independent molecule together with two half molecules, which are completed by application of the symmetry elements. The conformation and metrical parameters of the three molecules are comparable, therefore, only the data for one of them are included in

Table 3.1. The complexes are binuclear with a 4,4'-bpy (**2a**) or bpe (**4a**) group bridging the Pt(II) centers, which complete their distorted square planar environment with a bidentate pq ligand and one terminal alkynyl group. In both complexes the N-pyridine bridging group is *trans* to the cyclometalated carbon, thus confirming that the reactions take place with retention of the geometry in the precursor, and the Pt units adopt an *anti* configuration.

Table 3.1: Selected bond lengths and angles for [{Pt(pq)(C≡C^{t}Bu)}$_2$(μ-4,4'-bpy)]·2CHCl$_3$·C$_6$H$_{14}$ (**21a**·2CHCl$_3$·C$_6$H$_{14}$ and [{Pt(pq)(C≡C^t*Bu*)}$_2$(μ-bpe)]·4CHCl$_3$ (**23a**·4CHCl$_3$) (independent molecule)

21a·2CHCl$_3$·hexane		**23a**·4CHCl$_3$	
Pt(1)-C(1)	1.994(5)	Pt(1)-C(1)	1.972(9)
Pt(1)-N(1)	2.115(4)	Pt(1)-N(1)	2.096(7)
Pt(1)-C(16)	1.967(5)	Pt(1)-C(16)	1.949(9)
Pt(1)-N(2)	2.113(4)	Pt(1)-N(2)	2.130(7)
C(16)-C(17)	1.197(7)	C(16)-C(17)	1.209(12)
Pt(2)-C(32)	1.980(5)	Pt(2)-C(34)	1.979(8)
Pt(2)-N(3)	2.127(4)	Pt(2)-N(3)	2.136(7)
Pt(2)-C(47)	1.961(5)	Pt(2)-C(49)	1.956(9)
Pt(2)-N(4)	2.125(4)	Pt(2)-N(4)	2.145(7)
C(47)-C(48)	1.209(7)	C(49)-C(50)	1.195(12)
		C(27)-C(28)	1.290(9)
N(1)-Pt(1)-C(1)	80.9(2)	N(1)-Pt(1)-C(1)	80.3(3)
C(16)-Pt(1)-C(1)	91.7(2)	C(16)-Pt(1)-C(1)	92.1(4)
C(16)-Pt(1)-N(2)	88.50(19)	C(16)-Pt(1)-N(2)	87.8(3)
N(1)-Pt(1)-N(2)	98.56(16)	N(1)-Pt(1)-N(2)	99.4(3)
Pt(1)-C(16)-C(17)	175.2(5)	Pt(1)-C(16)-C(17)	176.3(9)
C(16)-C(17)-C(18)	176.6(8)	C(16)-C(17)-C(18)	175.4(11)
N(3)-Pt(2)-C(32)	80.6(2)	N(3)-Pt(2)-C(34)	80.9(3)
C(47)-Pt(2)-C(32)	95.8(2)	C(49)-Pt(2)-C(34)	93.0(4)
C(47)-Pt(2)-N(4)	81.36(19)	C(49)-Pt(2)-N(4)	83.9(3)
N(3)-Pt(2)-N(4)	101.96(16)	N(3)-Pt(2)-N(4)	102.0(3)
Pt(2)-C(47)-C(48)	167.6(5)	Pt(2)-C(49)-C(50)	174.7(9)
C(47)-C(48)-C(49)	172.7(6)	C(49)-C(50)-C(51)	174.6(11)
		C(24)-C(27)-C(28)	121.4(14)
		C(27)-C(28)-C(31)	126.5(14)

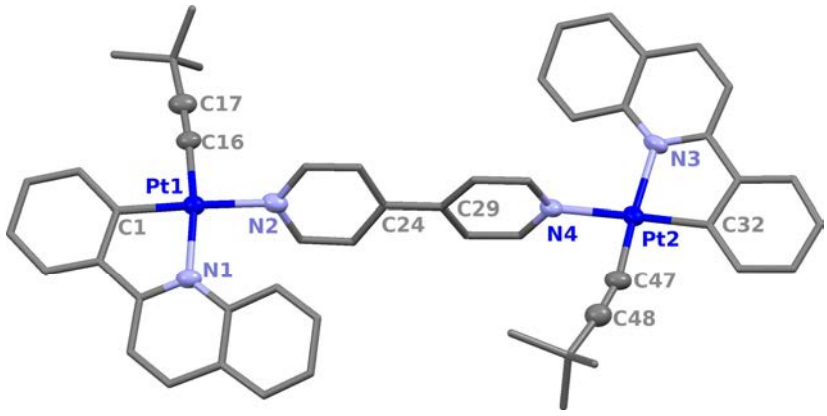

Figure 3.2: View of the molecular structure of the complex [{Pt(pq)(C≡C^{t}Bu)}$_2$(μ-4,4'-bpy)]·2CHCl$_3$·C$_6$H$_{14}$ (**21a**·2CHCl$_3$·C$_6$H$_{14}$)

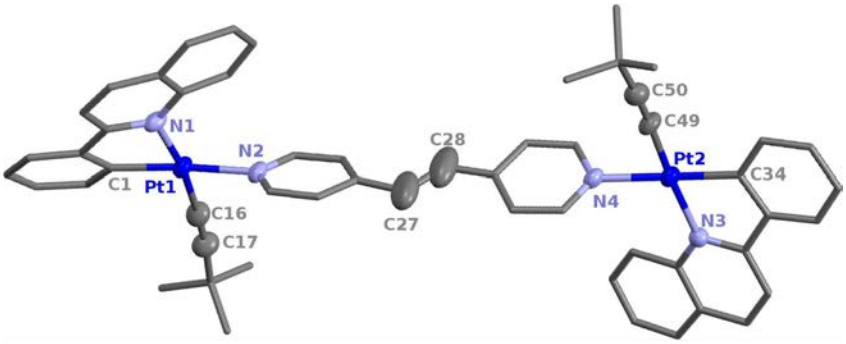

Figure 3.3: View of the independent molecule in the asymmetric unit in the molecular structure of the complex [{Pt(pq)(C≡C^{t}Bu)}$_2$(μ-bpe)]·4CHCl$_3$ (**23a**·4CHCl$_3$)

In **21a**, the two pyridyl rings form a dihedral angle between them of 16.45º (**21a**), whereas in the bpe-complex (**23a**) is of 24.0º in the complete molecule. However, due to symmetry, both rings are coplanar in the other molecules of **23a**. The bpy and bpe groups form dihedral angles with each platinum coordination plane of 67.47º, 82.18º (**21a**) and 60.36-80.41º (**23a**), respectively. These complexes show a greater variability in the angles than that observed for the related binuclear complexes with the tridentate cyclometalating pip$_2$NCN$^-$ ligand [{Pt(pip$_2$NCN)}$_2$(μ-NN)]$^{2+}$ [NN = bpy 86º, bpe 85.2º, pi$_2$NCNH = 1,3-bis(piperidylmethyl)benzene)],[9a,b] but the Pt-N (bpy or bpe) distances [2.113(4), 2.125(4) Å **21a**, 2.114(7)-2.145(7) Å **23a**] are comparable. The details of the central C=C fragment in the three molecules of **23a** [range C-C 1.240(19) - 1.334(17) Å] and those of the terminal alkynyl units in both complexes are not unusual (see Table A3.1). The phenylquinolynilyl (pq) ligand is fluttered, forming dihedral angles of 13.33, 13.97 (**21a**) and 19.82, 9.97, 20.02, 10.04º (**23a**) with the Pt coordination planes, which is consistent with other complexes containing the "Pt(pq)" metallacycle (**16**–**19**, See Chapter 2).

The crystal packing of **21a** shows that the molecules are arranged forming dimers through moderate intermolecular π···π (pq···pq) interactions (3.271, 3.336 Å, Figure A3.2a), which interacts through secondary interactions with the crystallization solvents ($CHCl_3$, *n*-hexane) and with other dimers ($H_{py}\cdots\pi_{C\equiv C}/C_{pq}$) (Figures A3.2b). However, the supramolecular structure of **23a** (Figure A3.3) does not show π···π interactions.

The ^{1}H NMR spectra of **20a-25a** in $CDCl_3$ at room temperature immediately after dissolving the corresponding solid brute or the crystalline material, are consistent with the presence of four different molecules in solution. The resonances are associated with the presence of the new diplatinum complex (species **a**), with the starting material (**16**), the free ligand and, also the corresponding mononuclear complex with the dinucleating ligand acting as monodentate terminal group [Pt(pq)(C≡C^{t}Bu)(L−κ*N*)], (hereafter denoted as species **b**). Complete experimental data obtained for all systems are summarized in the Experimental Section (labelling is shown in Scheme 3.1).

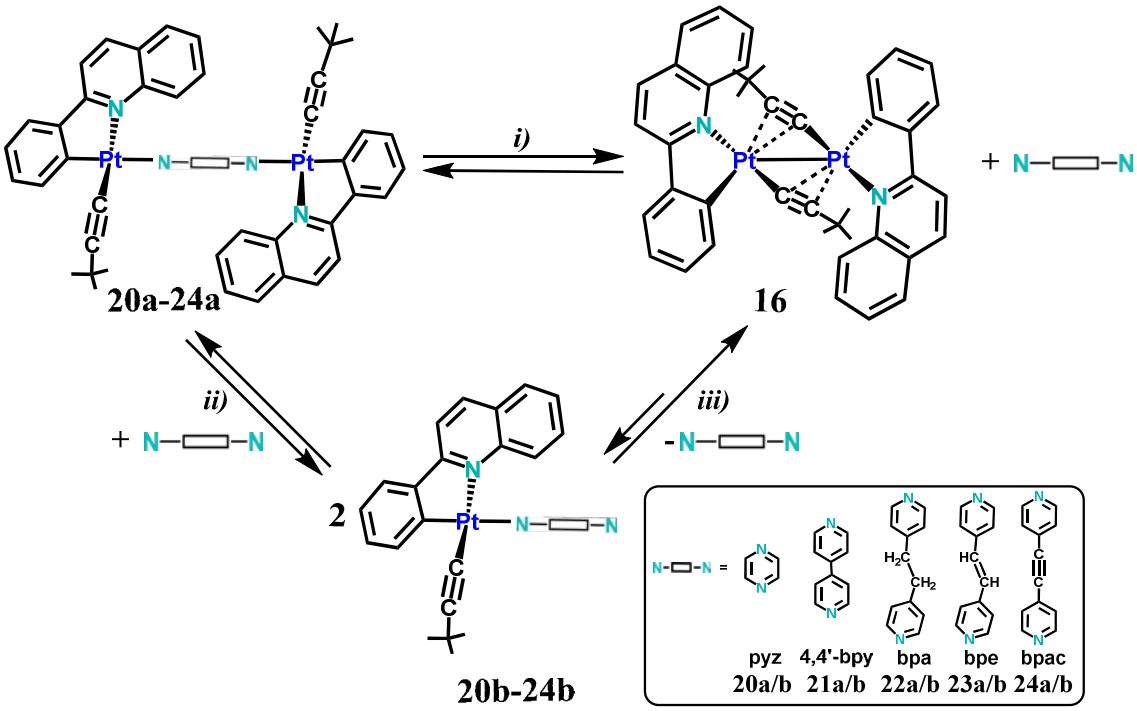

Scheme 3.2

As illustration, and for clarity, we only discuss the 4,4'-bpy complex (**21a**). The ^{1}H NMR spectra of the microcrystalline **21a** complex (B), the starting material **16** (C)

and a mixture **16**:4,4'-bpy in 1:4 molar ratio (A) are presented in Figure 3.4. It should be noted that the coordination of the pyridine N atoms to the Pt center is supported by the well-known coordination-induced shifts of the α-H_{py} protons to downfield in relation to the free ligand (δ 8.75), which has been ascribed to the loss of electron density upon pyridine ring coordination. As seen in Figure 3.4B, only one signal appears at δ 9.00 (d), which is assigned to the bridging species **21a**, whereas the two expected different resonances located at 8.96 (d), 8.79 (d) correspond to the terminal species **21b**. This later signal (δ 8.79) lies close to that of the free bpy (δ 8.75), being therefore ascribed to the two α-H_{py} protons of the uncoordinated pyridine ring in **21b**. A particularly reliable indicator of the presence of starting material (**16**) is the signal H^8 of the pq ligand, very deshielded (δ 9.75) in relation to the others. Fortunately, in all systems under study, the pyridine protons (pyrazine for **20a**) and the H^8_{pq} signal of the **16** are sufficiently separated from the other signals, so they can be used to establish the approximate ratios from their integrations. Due to remarkable overlapping (or even coincidence for pq signals) an accurate assignment for the rest of signals to individual complexes is not possible. These spectra are consistent with partial dissociation of the N-bridging ligand at room temperature in $CDCl_3$, which could be driven by the *trans* labilizing effect of the C-cyclometalate atom on the N-donor ligand and the stability of the σ/π-C≡C^{t}Bu bridging system in the precursor **16**. A reasonable equilibrium (slow on the NMR scale) between the commented species is proposed in Scheme 3.2.

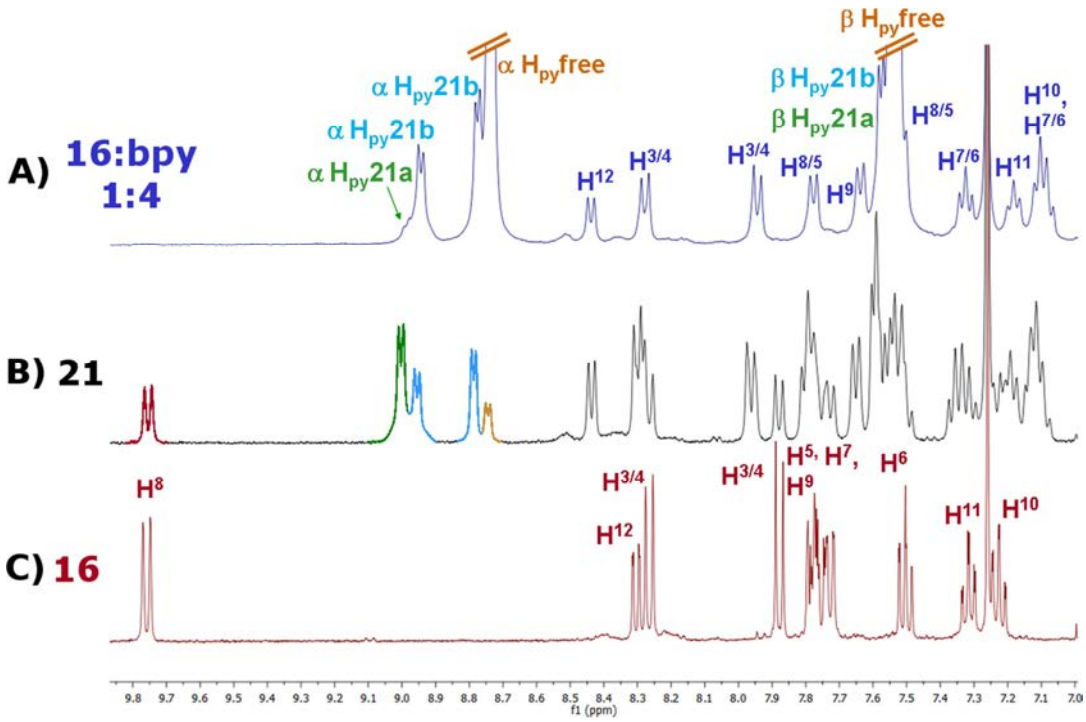

Figure 3.4: ^{1}H NMR spectra ($CDCl_3$, 400 MHz, 298 K, aromatic region) of: A) aliquot of a reaction mixture **16**/4,4'-bpy in a 1:4 molar ratio; B) microcrystalline sample of [{Pt(pq)(C≡C^{t}Bu)}$_2$(μ-4,4'-bpy)] (**21a**); C) [Pt(pq)(μ–κC$^{\alpha}$:η^{2}-C≡C^{t}Bu)]$_2$ (**16**)

From a comparison of the analysis of the ^{1}H NMR spectra of these five bimetallic assemblies, we conclude that the experimental approximate ratio determined for the four species depend on the N-donor ligand: (**a:16:b:*N*-*N*)**, ≈ 1:13.1:6.2:8.9 *pyz*, 1:0.8:1.3:0.2 *bpy*, 1:0.4:0.9:0.1 *bpa*, 1:0.5:0.9:0.1 *bpe*, 1:0.9:1.4:0.2 *bpac*). The higher proportion of the bimetallic species (**a**) in solution was found with the more flexible and donor ligands (bpa, bpe), whereas the lowest was with the short and rigid pyrazine ligand being the order: bpa ≈ bpe > bpac ≈ bpy >> pyz. For complex **25**, signals due to coordinated and free α-H pyridine protons are also observed together with that of the H^{8} (pq) proton of **16**. However, in this system the possible occurrence of stepwise decoordination of the cyclometalating Pt units cannot be excluded.

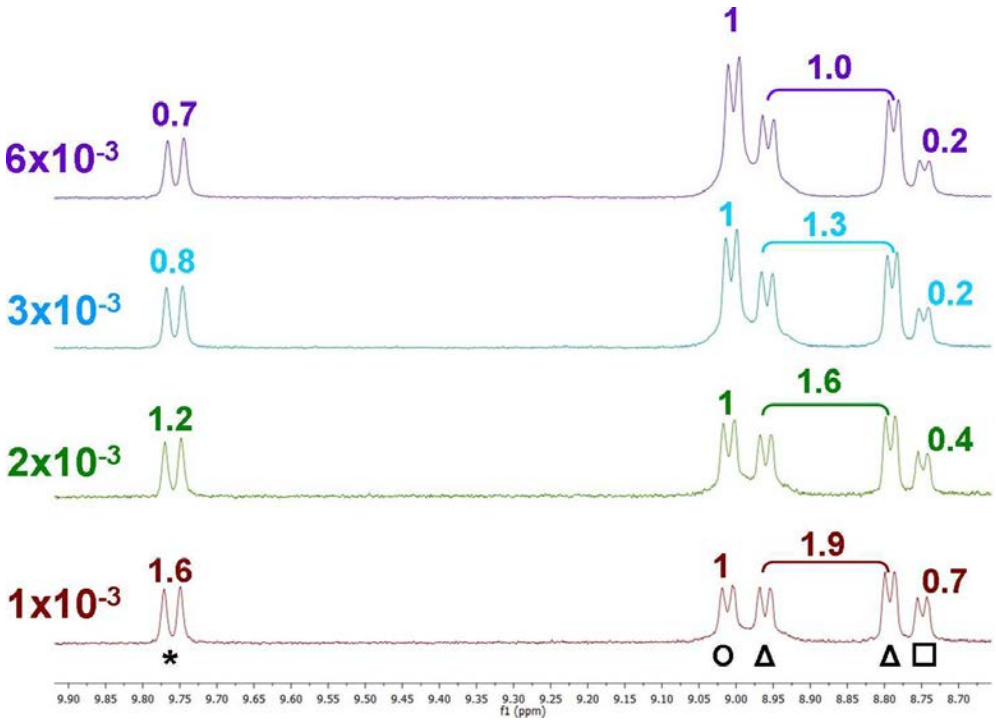

Figure 3.5: ^{1}H NMR spectra at 298 K of **21a** at different concentrations (mol/l). Selected resonances: **16** (*), **21a** (O), **21b** (Δ), free bpy (□)

Equilibria can be influenced significantly by changing concentration, temperature or solvent. Therefore, an examination of these parameters is important to get a more complete picture of the complexes under study. As representative example, we discuss in detail only the results of the 4,4'-bpy system (**21**). The influence of the concentration was confirmed by recording the ^{1}H NMR spectra of **21a** at different concentrations in $CDCl_3$. As shown in Figure 3.5, dilution of a solution from a 6 x 10^{-3} to 1 x 10^{-3} M causes a progressive shift of the equilibria (i) and (ii) to the right, increasing the presence of **16**, **21b** and free 4,4'-bpy with concomitant decreasing of **21a**. By contrast, upon lowering the temperature to 218 K (Figure A3.4) the concentration of **21a** increases, whereas those of **16**, **21b** and free bpy decrease (**21a:16:21b:*N-N*** ratio, 298 K ≈ 1:0.8:1.3:0.2 to 218 K 1:0.4:0.8:0.1 for a solution 3x10^{-3} M in $CDCl_3$). These results clearly confirm that the three complexes and the free ligand are involved in dynamic equilibrium. By using CD_3COCD_3 as solvent for **21a** the final ratio found was **a:16:b:*N-N*** ≈1:2.2:2.4:1.2 (Figure A3.5). Therefore, in this solvent not only the equilibria (i and ii) are shifted to the right in more extension to that observed in $CDCl_3$, but also the formation of **16** and bpy (equilibrium i) was favored in relation to **21b** (ii). As was expected, the bimetallic (**a**)/mononuclear (**b**) ratio was also

influenced by the concentration of the dinucleating ***N-N*** ligand. Thus, the ^{1}H NMR spectra recorded for solutions formed by a mixing of **16**/L (L **21**-**24**) 1:4 in $CDCl_3$ (established by UV-vis, see below) show mainly the signals associated to the mononuclear species (**b**), together with the free ligand in excess and small amount of the bimetallic species (**a**) (**a:16:b:*N-N*** ratio ≈1:0:8:14, bpy system, Figure 3.4A). No signals associated to the starting material (**16**) are observed, indicating that the equilibria drawn in Scheme 3.2 are essentially shifted in counterclockwise in presence of excess of ligand. In the case of the pyrazine system, a large excess of ligand is required to eliminate completely the presence of the precursor (**16:**pyz ≈1:20), what is in good agreement with the greater amount of starting material observed when the solid **20a** is dissolved. It is worth noting that from these solutions only the binuclear complexes **20a**-**24a** and mixtures **20a**-**24a**/**20b**-**24b** could be isolated. Despite many attempts we never got crystals of any of the mononuclear complexes. However, the proton spectra obtained under these conditions (ratio **16**:***N-N*** 1:4 for ligands **21**-**24** or 1:20 for **20**) have allowed us to carry out a reasonable assignment of the signals of the mononuclear complexes **20b**-**24b** (2D ^{1}H-^{1}H spectra). As the resonances of the starting material, the free ligands and the mononuclear complexes **20b**-**24b** were known, it has been also possible to identify and to assign with rather reliability some characteristic signals observed for the solids **20a**-**24a** in $CDCl_3$ solution (see Experimental Section).

3.1.2 Photophysical properties

To facilitate comparison, all absorption and emission spectral data are summarized in Tables 3.2 and 3.3.

Absorption spectroscopy

In the solid state, the diffuse reflectance of the polymetallic assemblies are characterized by a low energy and distinctive feature in the range 500-540 nm (with shoulder in **21a** and **23a**), which is absent in the precursor (Figure 3.6). According to TD-DFT in gas phase for **21a** (see below), this band is assigned to charge transfer from the Pt(pq)(C≡C^{t}Bu) units to the central ***N-N*** linker ^{1}[(M+L+L')L''CT].

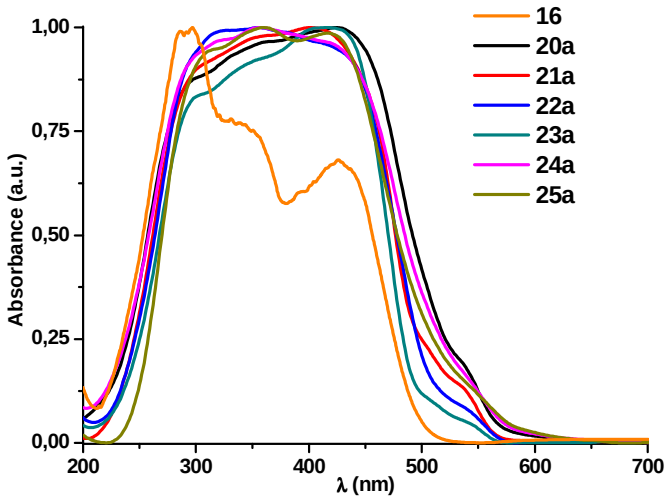

Figure 3.6: Normalized absorption spectra calculated from their reflectance spectra of **20a-25a**

Table 3.2: Absorption data for [{Pt(pq)(C≡C^{t}Bu)}$_2$(L)]· (**20-24**) and [{Pt(pq)(C≡C^{t}Bu)}$_3$(μ-tpab (**25**) at 298 K (5 x 10^{-5} M CH_2Cl_2 Solutions[a] and solid state[b])

Compound	λ_{abs}/nm (10^3 ε $M^{-1}cm^{-1}$)
[{Pt(pq)(C≡C^{t}Bu)}$_2$(μ-pyz)] **20**	242 (65.3), 276 (62.4), 304 (55.9), 353 (40.1), 408 (20.6) **CH_2Cl_2** 300, 330, 365, 390, 430, 530 **solid**
[{Pt(pq)(C≡C^{t}Bu)}$_2$(μ-bpy)] **21**	243 (63.8), 270 (59.6), 341 (17.7), 354 (18.7), 410 (13.3) **CH_2Cl_2** 305, 330, 355, 400, 500, 530 **solid**
[{Pt(pq)(C≡C^{t}Bu)}$_2$(μ-bpa)] **22**	218 (67.3), 257 (65.1), 299 (42.5), 337 (20.6), 355 (20.2), 413 (17.7) **CH_2Cl_2** 300, 320, 350, 415, 525 **solid**
[{Pt(pq)(C≡C^{t}Bu)}$_2$(μ-bpe)]· **23**	242 (63.3), 276 (63.9), 314 (58.3), 355 (29.9), 412 (20.7) **CH_2Cl_2** 305, 345, 400, 425, 505, 535 **solid**
[{Pt(pq)(C≡C^{t}Bu)}$_2$(μ-bpac)] **24**	243 (63.3), 278 (62.2), 325(60.4), 355 (33.2), 415 (20.8) **CH_2Cl_2** 305, 320, 360, 390, 420, 540 **solid**
[{Pt(pq)(C≡C^{t}Bu)}$_3$(μ-tpab)] **25**	245 (80.1), 289 (79.0), 308(71.7), 329$_{sh}$ (43.9), 355 (35), 408 (6.0) **CH_2Cl_2** 310, 360, 420, 545 tail to 630 **solid**

a) Data extracted from mixtures 1:4 (**21-25**) and 1:14 (**20**) (see text), b) Diffuse reflectance

As mentioned above, the ^{1}H NMR spectra of all complexes **20a-25a** in $CDCl_3$ solution are consistent with partial dissociation of the bridging ligand, establishing an equilibrium of the bimetallic complex (**a**) with starting material (**16**), the monometallic species (**b**) and the free ligand according to Scheme 3.2. Therefore, the obtained spectra are examined taken into account this behavior. The spectra of freshly prepared CH_2Cl_2 solutions of solid **20a-25a** show high energy features (240-330 nm) due to the

intraligand transitions (pq, C≡CR and ***N-N***-donor ligand). As is shown in Figure 3.7a for the 4,4'-bpy system, the intensity of these high energy bands exceeds of that of the starting material (**16**), as expected for the occurrence of overlapping pyridyl ligand-centered transitions in this region (see Table A3.2 for absorption of the free ligands). The moderately structured band at 355 nm (**20**-**24**) coincides with that observed in the starting material **16**, being attributed to ^{1}IL (pq) charge transfer. However, the low-energy absorption (408-413 nm) appears remarkably blue-shifted in relation to the lowest manifold in the precursor, supporting cleavage of the double-alkynyl bridging system.

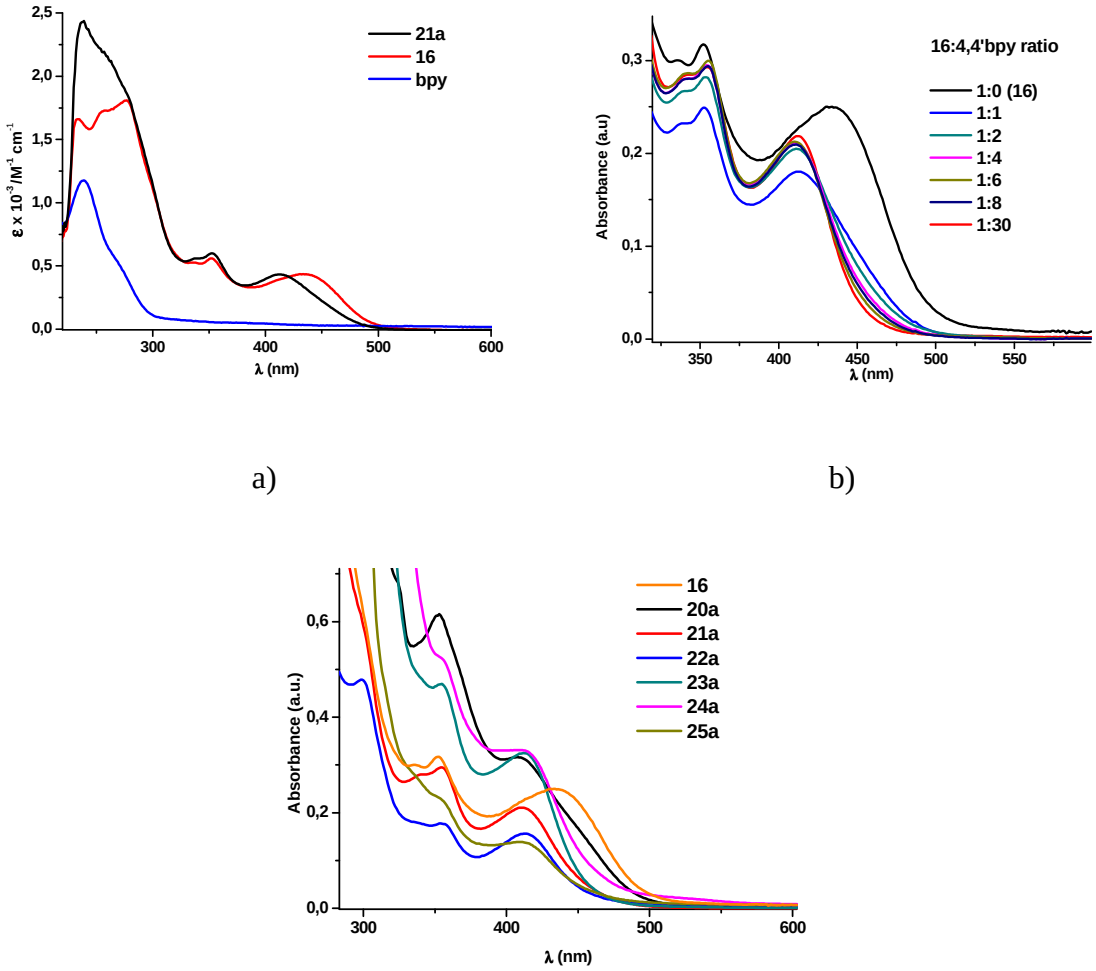

a) b)

c)

Figure 3.7: a) Absorption spectra of **21a**, [Pt(pq)(μ–κC$^{\alpha}$:η^{2}-C≡C^{t}Bu)]$_2$ (**16**) and free 4,4'-bpy in CH_2Cl_2. b) Normalized absorption spectra in CH_2Cl_2 of [Pt(pq)(μ–κC$^{\alpha}$:η^{2}-C≡C^{t}Bu)]$_2$ (**16**) and successive additions of 1, 2, 4, 6, 8 and 30 equiv of 4,4'-bpy. c) Low energy region of the absorption spectra of solids **20a**-**25a** and **16** in CH_2Cl_2

In accordance with the NMR spectra commented before, the progressive addition of the corresponding ***N*-*N***-donor ligand essentially causes the disappearance of **16**. By way of illustration, Figure 3.7b shows the spectra of the precursor (**16**), together with the changes observed upon successive addition of 4,4'-bpy. As it is observed, the maximum of the band is shifted to 410 nm with only 1 equiv of ligand, but the band shows a long tail in the region where **16** still absorbs, thus confirming its presence. Upon addition of ca. 4 equiv. of ligand, the red-side of band decreases considerably, in accordance with the essentially disappearance of **16**. The band changes relatively little with additional equivalents of ligand, though upon addition of more ligand (6 to 30 equiv.) a small decreasing of the tail is still observed. We attribute, tentatively, this latter change to a complete disappearance of bimetallic species (**a**) in solution, leaving mononuclear **b** complexes as the predominant metallic components. The fact that the stepwise addition of ligand takes place keeping the low energy maximum at 410 nm (with minor changes in the tail) suggests that the absorption profiles and electronic structures of bimetallic (species **a**) and mononuclear complexes (species **b**) are likely rather similar. A similar behavior has been previously observed in related systems.[9a] In the case of the pyz-system, the low energy absorption band shows a gradual change and we determine a relation of ca. 1:14 as the point where the precursor essentially disappears, what is also in agreement with a greater dissociation of the *N*-ligand in the assembly. As is shown in Figure 3.7c, the ancillary ***N*-*N*** ditopic ligand has little influence in the low energy manifold. On the basis of previous spectroscopic investigations in phenylquinolyl and alkynyl platinum complexes (See Chapter 2), the low energy absorption band is tentatively ascribed to admixture of platina/alkynyl to cyclometalate (pq) charge transfer [d(Pt)/C≡C→π*(pq)] ^{1}[(M+L')LCT]. This assignment is in agreement with the slight blue shift observed for the less electron donating pyrazine ligand (408 nm) and the slightly red shift seen for the most electron donating 1,2-bis(4-pyridyl)ethane (bpa, 413 nm). However, due to the low lying nature of some of the π* diimine ligands, contribution from platina-alkynyl to N-donor ligand charge transfer ^{1}[Pt(C≡C)→π*(N-donor)] could be also plausible. This contribution is apparent in the bpac system (**24**), which displays enhanced absorption in the low energy tail (line rose).

Emission spectroscopy

Qualitatively, the emissions of these complexes are much more intense in all media that those observed for the starting material (Table 3.3). The emission profiles are excitation-wavelength independent, indicating that aggregates are not responsible for the observed spectra.

Solid State

The emission spectra of **20a-25a** in solid state at room and at 77 K are shown in Figure 3.8. At room temperature, the bands are unstructured and maximize in the range 590-615 nm, whereas at low temperature the profiles become structured and slightly blue shifted. The decays for these solids were adequately modeled by a single exponential function (τ 0.3-11.4 μs 298 K; 7.6-39.2 μs 77 K) in the range of microseconds, revealing their triplet parentage. In the bpe-bridged binuclear compound **23a**, the highly structured emission profile at low temperature, with peak maxima at 588, 648 and 702 nm, the observed vibronic spacing (close to that observed for the free ligand), and also the long lifetime (39.2 μs) are consistent with a predominantly bpe-centered ^{3}IL $^3(\pi\pi)^*$ excited state. However, the emission profiles of **20a** (pyz) and **21a** (bpy) are similar (590 nm 298 K; 572, 610 77 K **20a**, 574, 612 nm 77 K **21a**) and compares to those seen for typical phenylquinolyl platinum complexes [*i.e.* [Pt(pq){$H_2B(pz)_2$}] (**3**) λ_{em} = 580, 610 nm; See Chapter 1], what is consistent with emission from a ^{3}MLCT excited state likely mixed with alkynyl to pq charge transfer contribution (^{3}MLCT/^{3}L'LCT). For the remaining complexes (**22a**, **24a** and **25a**), the low temperature profiles are also similar to those of **20a** and **21a**, but the maxima are slightly red shifted in the **25a**(tpac) > **24a**(bpa) > **24a**(bpac), pointing to some contribution of the central *N*-linker ligand.

Table 3.3: Photophysical data for complexes [{Pt(pq)(C≡C^{t}Bu)}$_2$(L)]· (**20a-24a)** and [{Pt(pq)(C≡C^{t}Bu)}$_3$(μ-tpab (**25a**) (solid state) and for mixtures **16**:L (1:4) (CH_2Cl_2, 1x 10^{-5} M)

Compound	Medium (T[a]/K)	λ_{em}/nm (λ_{exc}/nm)	τ/μs	ϕ(%)
20	Solid (298)	590_{max} [a] (365-550)	8.0	13.8
	Solid (77)	572_{max}, 610, 660_{sh} (365-540)	14.0	
	5 x 10^{-5} M (298)	595_{max} [a] (350-420)		
	5 x 10^{-5} M (77)	570_{max}, 610, 660_{sh} (365-450)		
21	Solid (298)	590[a] (365-530)	9.9	13.1
	Solid (77)	574_{max}, 612, 650 (365-530)	12.2	
	5 x 10^{-5} M (298)	590[a] (365-410)		
	5 x 10^{-5} M (77)	570_{max}, 625, 660_{sh} (365-430)		
22	Solid (RT)	610[a] (365-540)	9.9	9.4
	Solid (77)	588_{max}, 625 (365-550)	7.7	
	5*10^{-5} M (RT)	595 (365-420)		
	5*10^{-5} M (77K)	570_{max}, 610, 660_{sh} (365-460)		
23	Solid (298)	605[a] (365-540)	10.4	4.9
	Solid (77)	588_{max}, 648, 702 (365-540)	39.2	
	5 x 10^{-5} M (77)[b]	578_{max}, 620, 650_{sh} (365-440)	13.8	
24	Solid (298)	596[a] (365-540)	11.4	6.8
	Solid (77)	596[a] (365-540)	15.2	
	5 x 10^{-5} M (298)	595 (365-420)	9.2	
	5 x 10^{-5} M (77)	576_{max}, 613, 660_{sh} (365-440)	14.4	
25	Solid (298)	615[a] (365-500)	8.8	1.1
	Solid (77)	598[a] (365-480)	7.6	
	5 x 10^{-5} M (298)	595 (365-415)		
	5 x 10^{-5} M (77)	570_{max}, 612, 670_{sh} (365-480)		

a) Tail to 800 nm. b) Non emissive at 298 K.

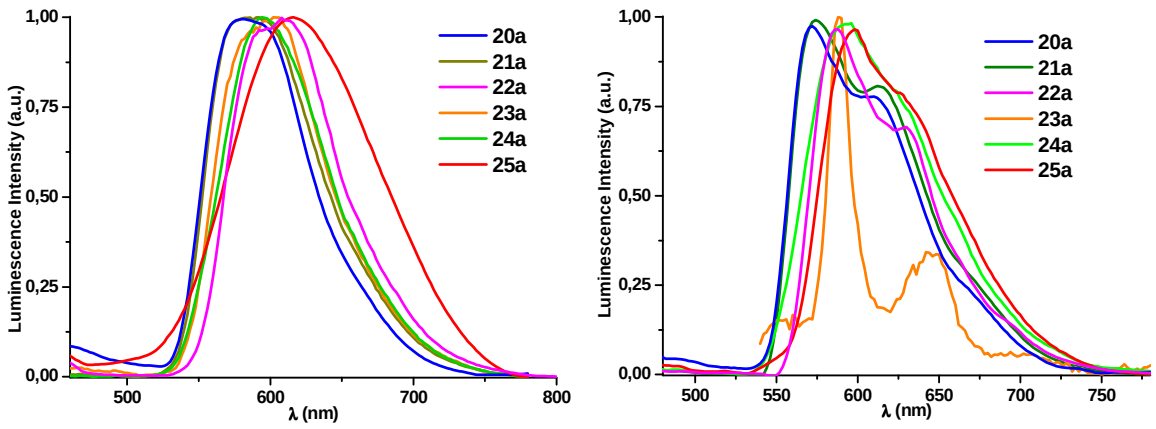

a) b)

Figure 3.8: Normalized emission spectra of complexes **20a-25a** in solid state a) at 298 K, b) at 77 K (λ_{exc} 400 nm)

Solution

Due to the occurrence of the dissociation process commented above, the study of the emissions in solution was carried out using CH_2Cl_2 solutions with a **16**:L proportion

of 1:4 (data are listed in Table 3.3). Under these conditions, the predominant species in solution is the mononuclear complex (for **21b**-**24b**) or mixtures with the corresponding binuclear complex in the case of systems with pyrazine and the trinucleating 1,3,5-tris(pyridine-4-ylethynyl)benzene ligand (**20** and **25**). As has been noted before, both species afford similar low energy absorption features.

Not unexpectedly, the bpe complex (**23b**) is not emissive in fluid, probably due to easy nonradiative relaxation by forming a twisted triplet state (^{3}p).[9a,10] The remaining complexes display a rather similar intense broad emission centered around 595 nm with negligible influence of the *N*-donor auxiliary ligand, suggesting a similar emissive state (Figure 3.9a, Table 3.3). Upon cooling at 77 K, the emission shifts remarkably to higher energies exhibiting structured profiles (Figure 3.9b) with minimal variations in λ_{max} (range 570-576 nm). At 77 K, the bpe complex **23b** is also emissive (line orange) exhibiting similar structured profile with a peak maximum at 578 nm, pointing to a similar emissive state. In fact, lifetime measurements for two representative complexes with ligands bpe and bpac in glass state are also similar (see Table 3.3). The emission is mainly attributed to mononuclear complexes and it is ascribed to admixture of ^{3}MLCT and alkynyl to pq charge transfer (^{3}MLCT/^{3}L'LCT). Further support is obtained from the excitation spectra in fluid solution, which resemble the corresponding absorption spectra in these conditions.

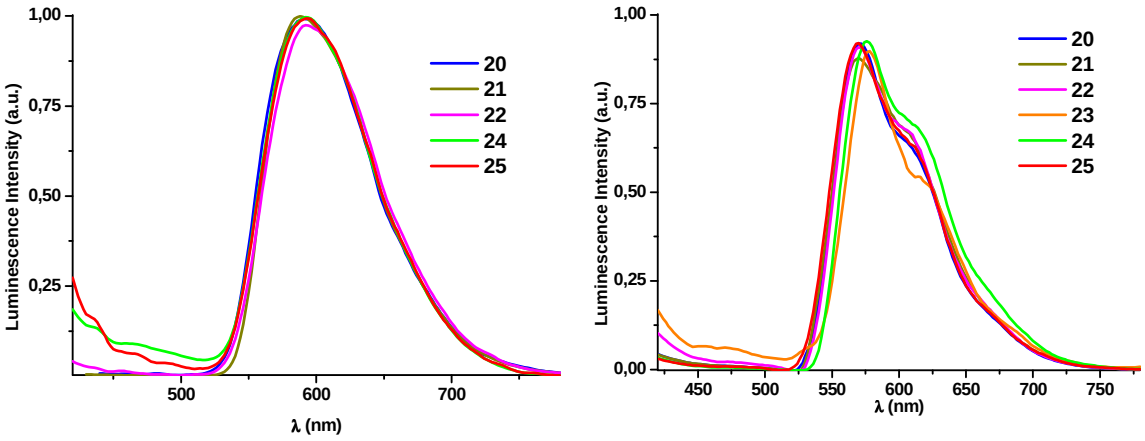

Figure 3.9: Emission spectra of mixtures (see text) of **16**:**L** (1:4 ratio) in CH_2Cl_2 (5 x 10^{-5} M) at a) 298 K and b) 77 K

Identical profiles, but with reduced intensity, are obtained from solution of binuclear **20a**-**22a** and **24a** solids (or by using **16**/L 1:1 molar ratio) likely due to similar luminescence response of the species **a** and **b** (both present in solution), which are clearly more emissive than the starting material. As illustration, the different spectra obtained for the **16**/bpy system in different molar ratio are shown in Figure A3.6. Interestingly, in contrast to the nonemissive behavior of the mononuclear complex **23b**, a diluted solution (5 x 10^{-5} M) of the bpe binuclear complex **23a** displays an unstructured band located at 600 nm upon excitation at 420 nm, which is related to the presence of the more rigid **23a** in solution. In glass, the band is only slightly structured and blue shift (565 max, 600sh nm).

3.1.3 Theoretical calculations

To shed some light, TD-DFT and DFT calculations have been carried out for the species **21a**. The optimization in the ground state agrees well with the experimental structure (see Table A3.4 for details), the most remarkable difference being the lengthening of the Pt-N(pyridyl) distances. The distribution of the frontier molecular orbitals in the ground state and the corresponding partial molecular orbital composition (percentages), together with selected low-lying transitions in vacuum and in CH_2Cl_2 solution are provided in Tables 3.4, A3.5-A3.7. Some selected orbitals are shown in Figure 3.10. The HOMO and HOMO-1 have similar contribution from each one of the Pt and alkynyl units [ie, HOMO Pt (32%) and C≡C^{t}Bu (61%) on fragment 1; HOMO-1 Pt (35%) and C≡C^{t}Bu (57%) on fragment 2] whereas the HOMO-2 and HOMO-3, are of similar energy and located on the unit 1 Pt(pq)C≡C^{t}Bu. The HOMO-4 is centered in fragment 2 [Pt (30%), pq (55%) and C≡C^{t}Bu (13%)]. The LUMO is mainly centered on the bipyridine ligand (94%) but the two following low lying virtual orbitals LUMO+1 and LUMO +2 are, however, localized on the low lying pq goups (LUMO+1 93%; LUMO+2 93%). The lowest energy absorption calculated in phase gas at 494 nm (Table A3.5) compares to that seen in the experimental solid reflectance spectrum at 530 nm. This band arises mainly from the HOMO-4 to LUMO transition and can be described to charge transfer from the Pt(pq)(C≡C^{t}Bu) units of the fragment 2 to the central ***N-N*** linker ^{1}[(M+L+L')L''CT]. The two following excitations calculated around 482 nm are of more complex configuration with significant charge transfer from HOMO and

HOMO-1 to LUMO+1 and LUMO +2. These absorptions are mainly ascribed to platinum-alkynyl to cyclometalated ^{1}[(M+L')LCT] and could be correlated with the experimental feature located at 500 nm.

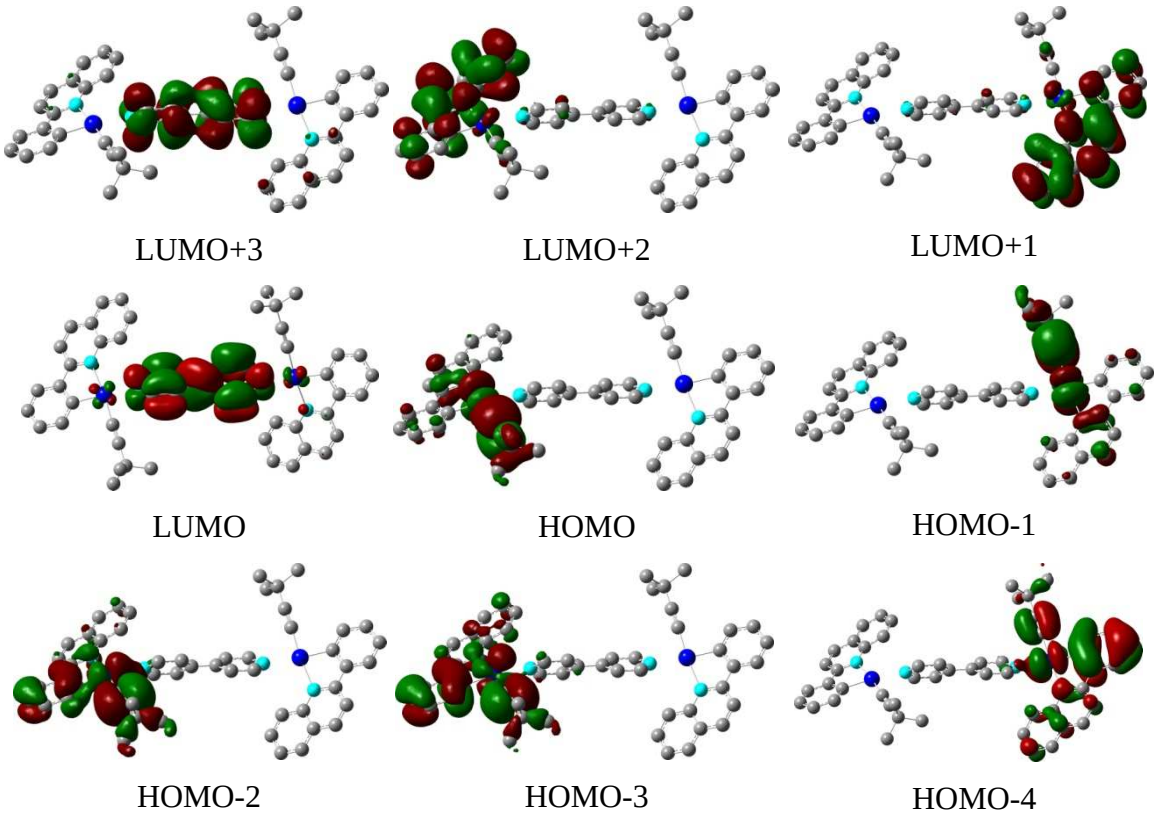

Figure 3.10: Molecular orbital plots for the computed S_0 state of complex **21a**

Table 3.4: Composition of frontier molecular orbitals in the ground-state for **21a**

MO	Energy	Pt(1)	pq(1)	C≡C^{t}Bu(1)	bpy	Pt(2)	pq(2)	C≡C^{t}Bu(2)
L+4	-1.08	0	5	0	79	1	14	0
L+3	-1.24	0	2	0	93	1	4	0
L+2	-1.96	3	93	1	2	0	1	0
L+1	-2.04	0	1	0	2	3	93	1
LUMO	-2.53	1	2	0	94	1	2	0
HOMO	-5.20	32	7	61	0	0	0	0
H-1	-5.39	0	0	0	0	35	8	57
H-2	-5.43	24	27	48	1	0	0	0
H-3	-5.49	27	43	28	2	0	0	0
H-4	-5.60	0	0	0	1	30	55	13

By taken the consideration of the solvent (CH_2Cl_2) there is an obvious blue shift in the lowest singlet excitations in agreement with its charge transfer nature (Table A3.6). Interestingly, the transition which involves charge transfer to the central bpy linker (HOMO-4 to LUMO) is now at higher energy (S_4, calculated at 419 nm). The

three lower energy singlets (S_1, S_2 and S_3) are close in energy (435, 431 and 428 nm) and are mainly composed of excitations involving HOMO-3 → LUMO to LUMO+2 transitions. Therefore, the experimental band located in solution at 410 nm could be ascribed as an admixture of platinum-alkynyl to pq charge transfer ^{1}[(M+L)L''CT] with some contribution of platinum-alkynyl to the central bpy linker ^{1}[(M+L+L')L''CT] (L = pq, L' = C≡C^{t}Bu, L''= bpy).

To clarify the emission character of **21a**, its triplet state geometry in gas phase was optimized (Table A3.4). The calculated emission using ΔSCF method at 584 nm is in accordance with the experimental value (590 nm). The excitation takes place with clear changes in the frontier orbitals respect to the ground state. The LSOMO is now located on the pq (59%), Pt (26%) and the alkynyl ligand (16%) on fragment 1, whereas the HSOMO is mainly centered in the pq(1) (92%) (Figure 3.11). In agreement, the localization of the spin density lies on one of the pq ligands and the platinum/alkynyl group of one fragment of the molecule (Figure A3.7). Thus, the emission has a mixed platinum/alkynyl to phenylquinolyl charge transfer character ^{3}[(M+L')LCT] with some minor ^{3}IL(pq) contribution, supporting the negligible influence of the N-donor linker.

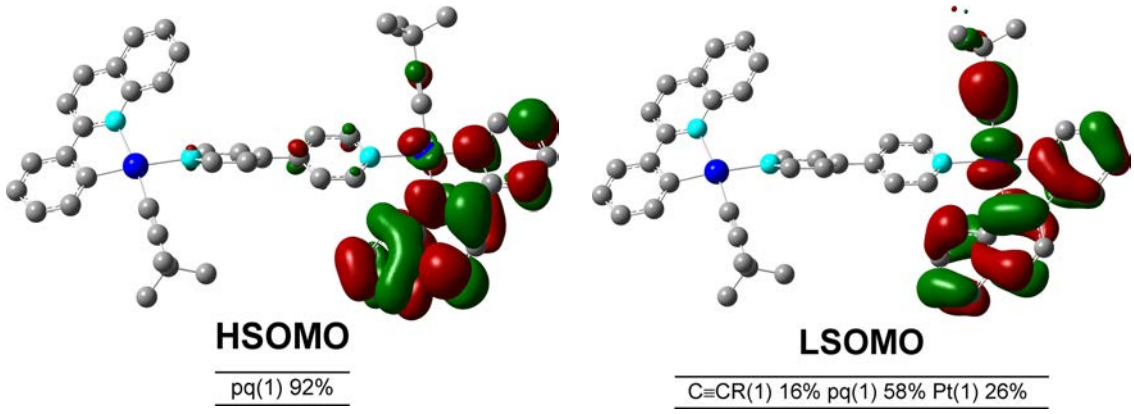

Figure 3.11: Molecular orbital plots for the computed T_1 state of complex **21a**

3.2 Reactivity of $[Pt(pq)(\mu-\kappa C^{\alpha}:\eta^{2}\text{-}C\equiv C^{t}Bu)]_2$ toward mercaptopyridines

As it has been described in Section 3.1, the reactivity of binuclear platinum derivatives stabilized by a double bridging system has been scarcely explored. In this field, our research group has explored the reactivity of the systems [*trans*-Pt(μ-C≡CR)(PPh_3)(C_6F_5)]$_2$ (R = ^{t}Bu, Ph, $SiMe_3$, CPh_2OH, CMe_2OH) towards thiols (HSPh and HSTol) with very interesting results, which depend of the substituent of the alkynyl ligand.[11] Thus, this reactivity has generated *bis*(thiolate) complexes, a vinyl thioether group bridging both Pt centers, a bridging buten-yl ligand, terminal vinyl ligand, thioplatinacyclopropane systems and cicloaddition [2+2] reactions giving diplatinum complexes bridged by a mixed thiolate/cyclobutenediylidene bridging system (Scheme 3.3).[11]

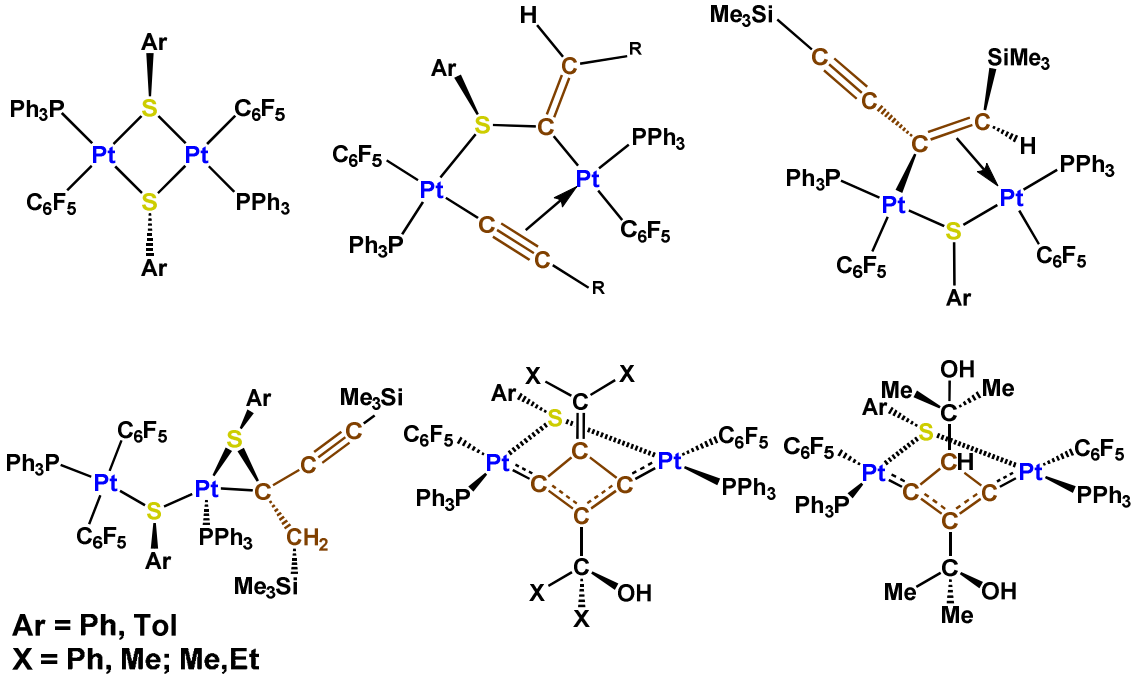

Scheme 3.3

By other hand, the research group has studied the reactivity of these systems towards molecules having two donor atoms and an acidic proton such as the 2 and 4-mercaptopyridine ligands. Mercaptopyridines are an interesting type of ambidentate ligand due to the presence in the same molecule of a soft (S) and a hard (N) basic center, which can act as terminal monodentate, or bidentate (chelate or bridging).[12]

Futhermore these ligands show a great versatility due to their mesomeric and tautomeric forms (thiol, thione or zwitterion) (Scheme 3.4).[12a,13] In function of the coordination mode, the H atom bonded to N or S can participate in molecular recognition processes by weak H bond interactions, favoring the obtention of polymetallic systems such as coordination polymers or MOFs (metal organic frameworks).[12c,13-14] These molecules are also easily deprotonated to form anionic pyridinthiolate ligands, of great interest by their structural richness,[15] and their interesting chemical, electrochemical behaviour,[12d,16] and photophysical properties.[17]

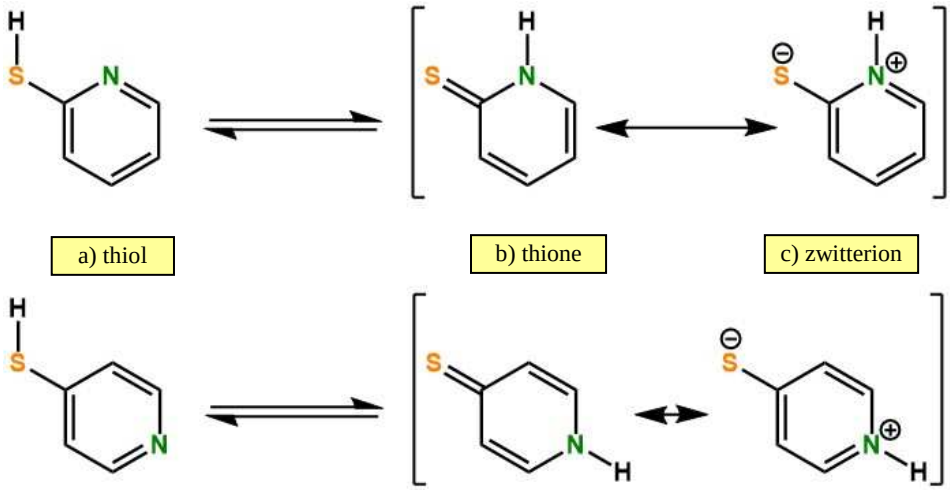

Scheme 3.4

The reactions of [*trans*-Pt(μ-C≡CR)(PPh$_3$)(C$_6$F$_5$)]$_2$ with 2-HSpy and 4-HSpy evolve with bridge-splitting to form the mononuclear Pt derivatives with the corresponding mercaptopyridine coordinated through the S center. However, these systems are not stable and evolve with subsequent *intra* or *intermolecular* hydroamination or hydrothiolation processes, respectively, as confirmed by X-Ray on the final complexes (Scheme 3.5). Thus, the complexes containing 2-HSpy generate, through an *intramolecular* hydroamination process of the C≡CR fragment, cyclic complexes of addition of different nature depending on the R substituent. However, the 4-HSpy *tert*-butylderivative system undergoes a formal *intermolecular* hydrothiolation process on the alkynyl group, generating a binuclear cyclic complex, which contain two pyridyl-vinyl-thioether bridging both Pt centers.

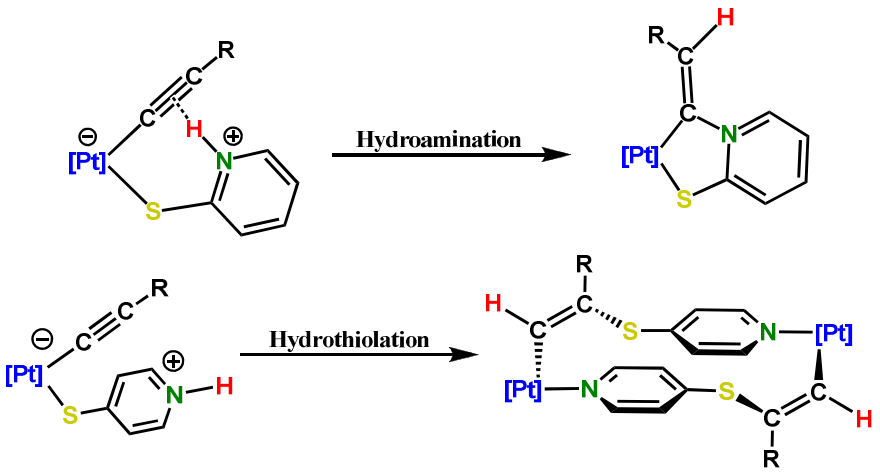

Scheme 3.5

Following our interest in the reactivity of binuclear Pt complexes stabilized by a double alkynyl bridging system, in the second part of this Chapter, we discuss the reactions of [Pt(pq)(μ–κC^{α}:η^2-C≡C^{t}Bu)]$_2$ (**16**) with 2- and 4- thiolpyridine ligands. The final reactions outcome follow the premises state above. As expected, the position of the sulphur atom in the pyiridine ring determines the geometry of the obtained complexes, which, also affects to their optical properties.

3.2.1 Synthesis and characterization

Scheme 3.6 summarizes the results of the reactions of [Pt(pq)(μ–κC^{α}:η^2-C≡C^{t}Bu)]$_2$ (**16**) with 2-HSpy and 4-HSpy. The reaction with 2 equiv. of pyridine-2-thiol (2-HSpy) in CH_2Cl_2 at 298 K afforded [Pt(pq){(κ*C*:κ*S*-2-SC_5H_4N-C=CH^{t}Bu}] (**26**) as a red solid, in moderate yield (64%). However, the reaction with 2 equiv. of 4-HSpy in acetone proceeded with formation of the cyclic bimetallic species ([Pt(pq){μ-Z-κ*C*:κ*N*-C=CH(^{t}Bu)-4-SC_5H_4N}]$_2$ (**27**) as an orange solid, which contain two pyridyl-vinyl thioether bridging both Pt centres. The results of these reactions are similar to those previously found by our group and commented before.[11a]

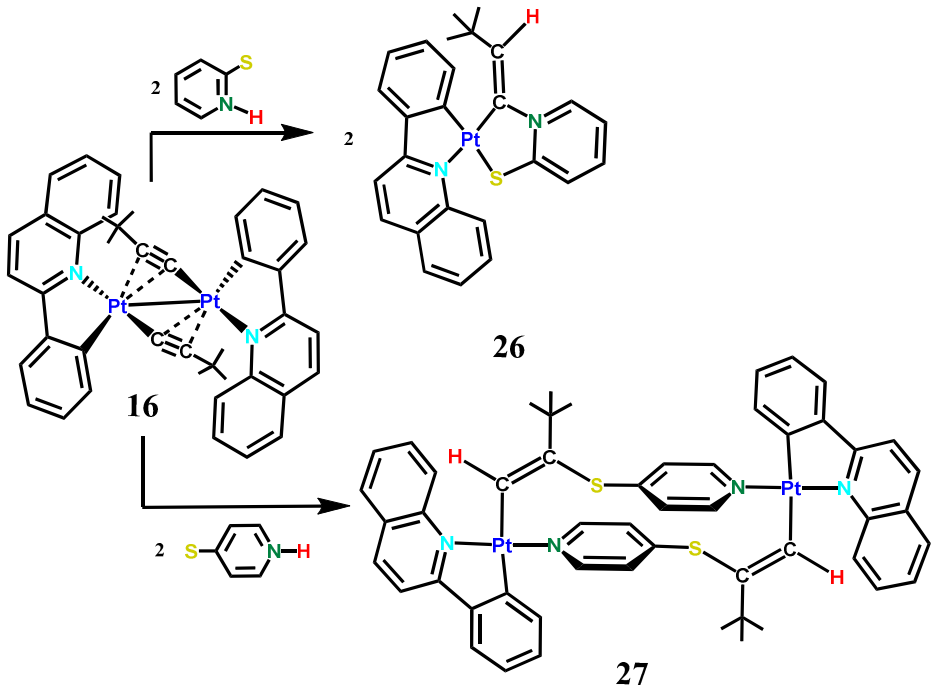

Scheme 3.6

Single-crystal X-ray analyses of **26** (Figure 3.12, Table 3.5) confirmed the geometry of the structure depicted in Scheme 3.6. Compound **26** crystallizes as a solid solution from both geometries (*Z* and *E*), which was modelled in a 70:30 molar ratio, showing a positional disorder in the *tert*-butyl group and in the C$^{\beta}$ vinylic fragment. It should be noted that the presence of a solid solution in molecular solids is not a common feature, but is a phenomenon well documented in the literature.[18] The formation of **26** formally implies the *intramolecular* addition of the N-H bond of the mercaptopyridine ligand through the C$^{\alpha}$≡C$^{\beta}$ triple bond of the alkynyl fragment, giving rise a new vinylthione C(NC$_5$H$_4$S-2)=CH^{t}Bu molecule acting as a chelatig κ*C*,*S* ligand.

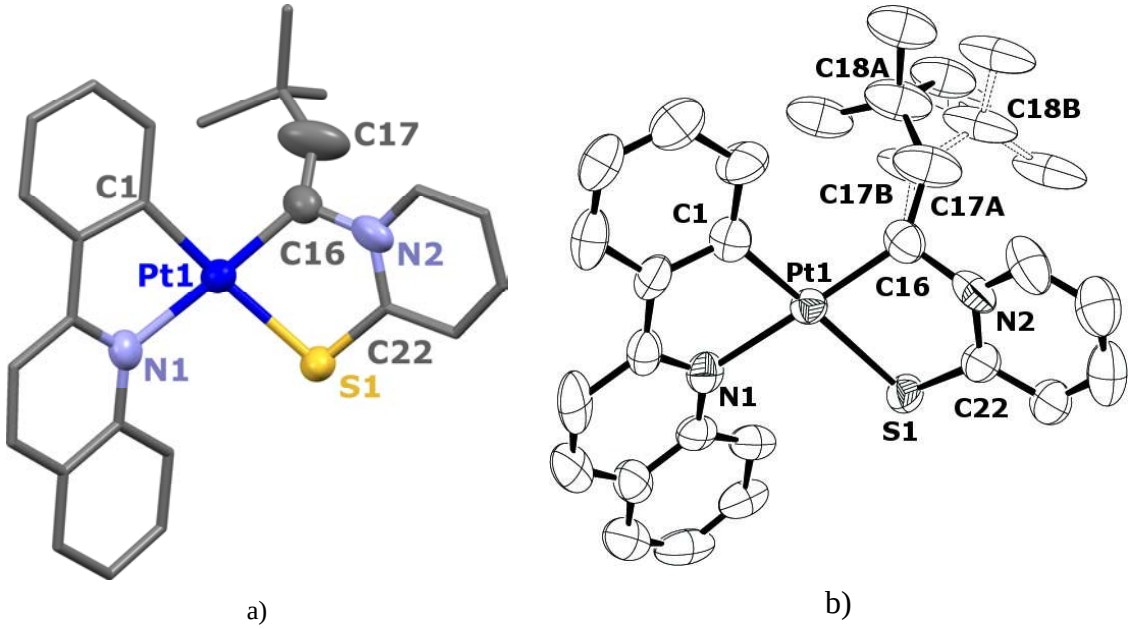

a) b)

Figure 3.12:a) Molecular structure of the majority isomer (*Z*) of [Pt(pq){(κC:κS-2-SC$_5$H$_4$N-C=CH^{t}Bu}]. (**26**) and b) ORTEP view showing the two isomers modeled in a 70:30 molar ratio with all atoms superimposed except the C=CH^{t}Bu fragment

Table 3.5: Selected bond lengths [**Å**] and angles [º] for **26**

26			
Pt(1) -N(1)	2.123(9)	Pt(1) -C(1)	1.999(11)
Pt(1) -C(16)	1.972(11)	Pt(1) –S(1)	2.385(3)
C(16)-C(17A)	1.31(2)	C(16)-C(17B)	1.45(5)
N(2)-C(16)	1.484(15)	N(2)-C(22)	1.338(13)
C(22)-S(1)	1.712(12)		
C(1)-Pt(1)-N(1)	80.4(4)	C(16)-Pt(1)-S(1)	80.9(3)
C(16)-C(17A)-C(18A)	143(2)	C(16)-C(17B)-C(18B)	134(5)
Pt(1)-C(16)-N(2)	111.8(7)	Pt(1)-S(1)-C(22)	94.9(4)
C(16)-N(2)-C(22)	116.3(9)		

The structure shows a *ter*-butylvinyl group with vinylic C$^\alpha$=C$^\beta$ distances C(16)-C(17A) [1.31(2) (*Z*), 1.45(5) (*E*) Å] and bent angles at C$^\alpha$ [135.4(15)º (*Z*), 123(2)º (*E*)] and at C$^\beta$ [143(2)º (*Z*), 134(5)º (*E*)] different in the geometries ***Z*** and ***E***. Although these parameters are in the range of sp^2 carbon atoms,[19] they are distorted from optimal values, probably, due to the steric strain of the new chelate ligand. The metalaheterocycle formed is non planar with a dihedral angle between the planes formed by C(16)-Pt(1)-S(1) and C(16)-N(2)-C(22)-S(1) of 44.84º. The short S(1)-C(22) [1.712(12) Å, r_C C(sp^2) + r_SS(sp^3)= 1.80 Å[19]] distance could indicate a certain delocalization in the polycylic system with an intermediate situation between the mesomeric forms pyridinthiolate (**A**) and pyridinthione (**B**) shown in Scheme 3.7. The

C(16)-N(2) bond length [1.484(15) Å] is typicall for a N-C(sp^3) single bond in N-alkyl pyridinium compounds, that is 1.484 (9) in average.[20]

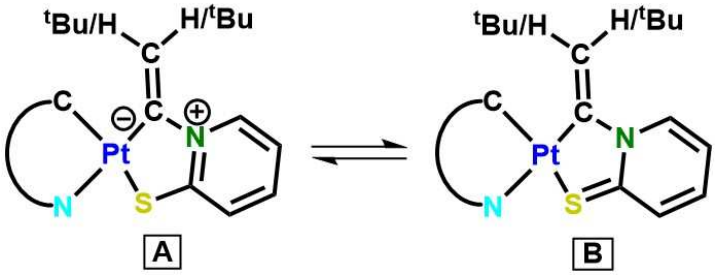

Scheme 3.7

The S(1)-Pt(1) is long [2.385(3) Å], although in the range of the Pt(Spy)$^-$ derivatives (2.228-2.43 Å range),[16e,17d,21] reflecting the strong *trans* influence of the metalated C(1) carbon of the pq. The C-C distances in the pyridinic ring [1.32(2)-1.354(18) Å] are in agreement with a high aromatic nature for the ring, suggesting a remarkable contribution of the zwitterionic resonance form (**A**). The platinum exhibits a slightly distorted square-planar environment with Pt-N(1) [2.123(9) Å] and Pt-C(1) [1.999(11) Å] distances and a chelate bite N(1)-Pt-C(1) angle [80.4(4)º], comparable to those reported for the starting material (**16**). Both heterocycles (the platinaheterocycle formed by the Pt and the mercaptopyridine and the ring formed by the chelate pq ligand and the Pt) are not planar, forming an angle between them of 33.88º. Furthermore, the pq ligand is fluttered, forming a dihedral angle of 11.95º with the Pt coordination plane. The crystal packing (Figure 3.13) shows that the molecules are arranged as head-to-tail dimers through *intermolecular* π(pq)$^{\cdots}$π(pq) interactions (3.225, 3.323 Å) (blue) and S$^{\cdots}$H$_{pq}$ weak interactions (2.994 Å) (green). These dimers connect with others through secondary C$_{Ph}$$^{\cdots}C_{Spy}$ (3.376 Å) (orange) and C$_{pq}$$^{\cdots}H_{pq}$ (2.789 Å) (pink) T interactions.

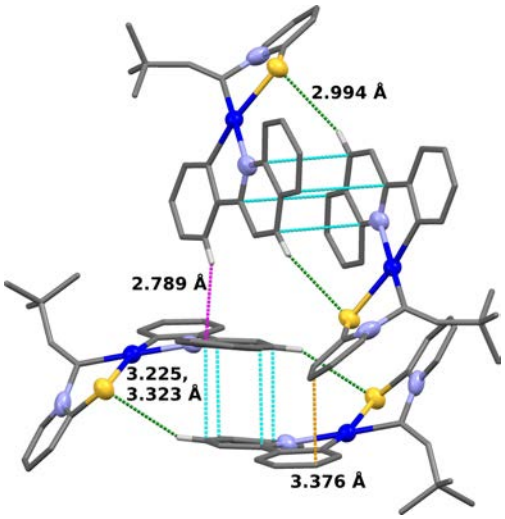

Figure 3.13: Packing of the molecular structure of [Pt(pq){(κ*C*:κ*S*-2-SC_5H_4N-C=CH^{t}Bu}] (**26**)

The spectroscopic data of **26** are in agreement with the structure. Thus, the IR spectrum shows the absence of ν(C≡C) absorptions and a band at 1602 cm^{-1} in the alkene region. The ^{1}H NMR spectrum of the as-obtained solid displays the characteristic signals for the phenylquinolinyl ligand and the presence of only one pyridinic fragment. The vinylic proton (*transoidal* to Pt in the *Z* conformation) appears as a singlet at δ 5.76 with a platinum coupling constant of 106.2 Hz (Figure 3.14 up). For the pq ligand, the most characteristics signals correspond to H^8 (δ 8.63) and H^{12} (δ 7.93) protons, this latter with a J_{Pt-H} (66.2 Hz) similar to that observed in the starting material **16** (72 Hz). Both signals appear shifted to highfield with respect to those observed in **16** (δ H^8 9.76, H^{12} 8.30). As noted above, the crystal has been modeled as a solid solution of the conformations *Z* and *E*, respectively. In agreement with this, the ^{1}H NMR spectrum of crystals obtained in the same conditions shows the expected two vinylic singlet resonances (in a 55:45 ratio) due to the isomers *Z* (δ 5.76) and *E* (δ 6.04), being the $^3J_{Pt-H}$ coupling constant in the isomer *E* of 58.3 Hz, as expected, smaller than for the *Z* isomer (105 Hz) (Figure 3.14 down). Additionally, the signals of the pq appear duplicated, being the most clear again the H^8 and H^{12} signals. Thus, together with the corresponding signals of the *Z* isomer (δ H^8 8.63, H^{12} 7.93) also appear the resonances of the *E* isomer (δ H^8 8.74, H^{12} 7.98), deshielded in the relation to the *Z*, and with a smaller $^3J_{Pt-H}$ in the *ortho* proton H^{12} (55.8 Hz *E vs* 66.2 Hz *Z*).

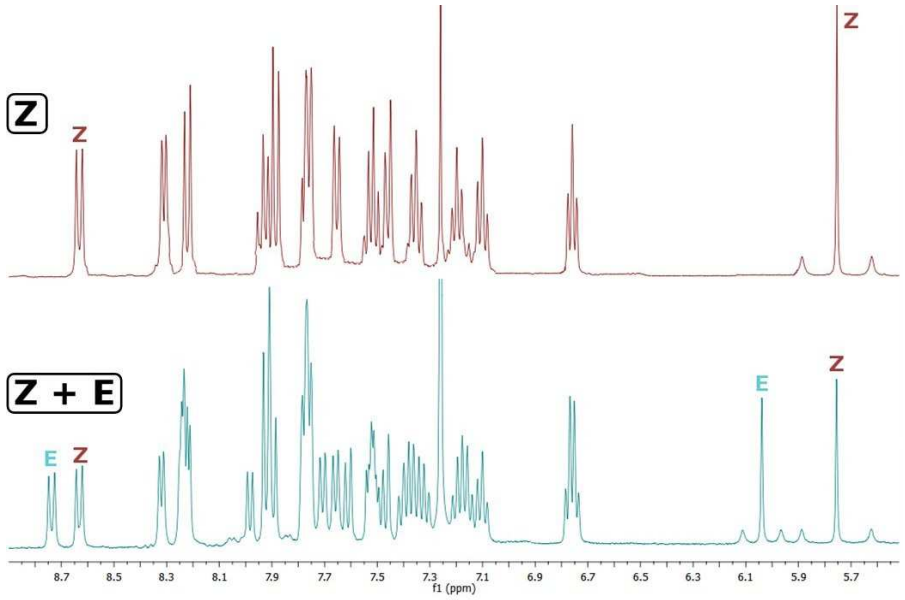

Figure 3.14: Comparative ^{1}H NMR spectra of the mixture 55:45 *Z*:*E* and the pure *Z* isomer of **26**

The corresponding $^{13}C\{^1H\}$ NMR resonances of **26$_Z$** (as-obtained solid) were assigned on the basis of two-dimensional C-H correlation experiments (HSQC and HMBC). As expected, only one set of signals due to pq, Spy and vinylic fragment are observed. The vinylic C$^{\alpha}$ (δ 150.4) and C$^{\beta}$ (δ 144.6) appear slightly shielded respect to those observed in [Pt{(κ*C*:κ*S*-2-SC$_5$H$_4$N-C=CH^{t}Bu}(C$_6$F$_5$)(PPh$_3$)] (C$^{\alpha}$ 166.6, C$^{\beta}$ 149.8 ppm).[11a] The C$^{\beta}$, clearly assigned by the cross peak with the CH$_3$ of the ^{t}Bu groups in the HMBC spectrum, presents the corresponding Pt-C coupling ($^2J_{Pt-C}$ = 92.4 Hz) significantly greater than that observed in [Pt{(κ*C*:κ*S*-2-SC$_5$H$_4$N-C=CH^{t}Bu}(C$_6$F$_5$)(PPh$_3$)] ($^2J_{Pt-C}$ = 55 Hz).[11a] This fact indicates the presence of a stronger Pt-C$^{\alpha}$ bond in the cycloplatinated derivative surely due to the lower *trans* influence of N atom in relation to the C atom of the C$_6$F$_5$ ring.

The formation of **26** could be rationalized according to the mechanism proposed in the Scheme 3.8. In the first step (*i*) the cleavage of the double alkynyl bridging ligand, and coordination of the mercaptopyridine ligand through the soft S atom would lead to the formation of the mononuclear complex **A**. In this intermediate (**A**) the 2-HSpy ligand would coordinate in an intermediate situation between the two mesomeric forms (pyrindinthiolate and pyridinthiona) and the N-H proton could be located close to the triple bond acting as H acceptor. In a subsequent step a fast hydroammination process (step *ii*) could take place giving rise to the final formation of the

platinaheterocycle mononuclear complex **26**. This mechanism is supported by the isolation of the stable mononuclear adducts [Pt(C≡CR)(C_6F_5)(PPh_3)(κ*S*-SC_5H_4NH-2)] [R = ^{t}Bu (X-Ray), $SiMe_3$, CPh_2OH, CMe_2OH, Ph] described in the PhD Thesis Memory of Dr. Sepúlveda,[11a] which evolve in solution to form the complexes [Pt{(κ*C*:κ*S*-2-SC_5H_4N-C=CHR}(C_6F_5)(PPh_3)].

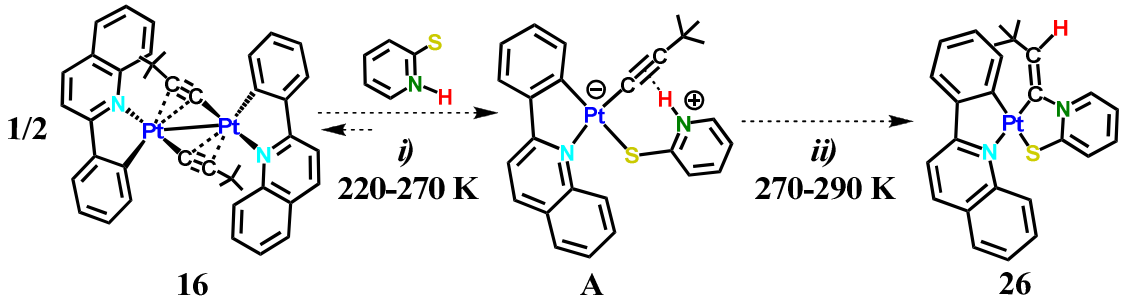

Scheme 3.8

To confirm the proposed mechanism, the reaction was monitored by variable-temperature ^{1}H NMR spectroscopy (Figure 3.15). At low temperature (< 270 K), the spectra exhibit two signals at δ 15.5 and 14.5, assigned to the pyridinic H in the intermediate coordinated species and in the free ligand, respectively. This suggests the occurence of a dynamic equilibrium between the starting materials (**16** + HSpy) and the intermediate **A** complex. Upon increasing the temperature, both signals decrease. At 270 K the resonance due to the free ligand is not observed and the vinylic proton of the final complex **26** begin to grow. At this temperature the resonance at δ 15.5, due to the intermediate **A** complex, is still observed but at 290 K the complex has evolved completely.

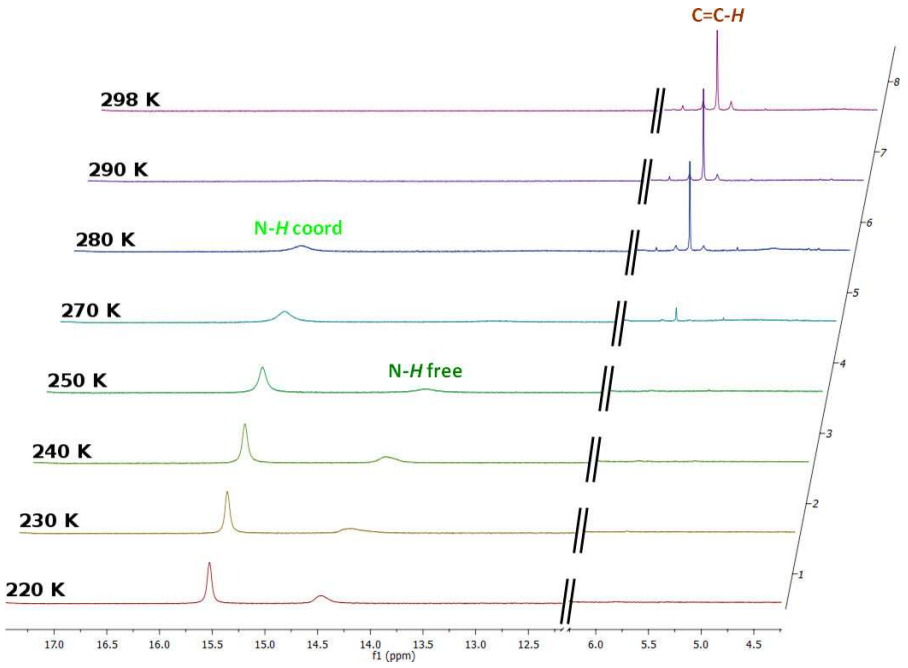

Figure 3.15: Variable temperature ^{1}H NMR in $CDCl_3$ in the N-H and vinylic H regions of **26**

As an extension of our investigation we studied the thermal and photochemical *Z*/*E* isomerization of **26**. Thermal treatment (50ºC, 12h) under ambient light of the solid **26** or a solution of **26** in CH_2Cl_2 produce a conversion of 46% and 53%, respectively. However, a CH_2Cl_2 solution protected from the light at 50ºC for 3h produced, only, a 5% of conversion, thus, suggesting that the isomerisation process does not take place thermally. We decided to study the isomerization process under photolytic conditions. Unfortunately the UV-vis absorption spectra of the *Z* isomer and *Z*/*E* mixture (see below), are essentially identical precluding us to follow the isomerization process by UV-vis. Their spectra, in CH_2Cl_2 solution (5 x 10^{-5} M-10^{-3} M), display two low-energy bands at 400 and 480 nm, respectively (Figure 3.18a, Table 3.6 and A3.8). Therefore, we irradiated above 360 nm a 10^{-3} M solution of compound **26** in CH_2Cl_2 using a tube of pyrex protected with a filter of an aqueous solution of $NaVO_3$ 0.4 M and 5% in NaOH, which absorb wavelength < 360 nm (16 W lamp). The photoisomerization process was followed by ^{1}H NMR until the photostationary state (PSS) was reached. The irradiated mixture took 30 min to reach the maxima conversion and the final equilibrated ratio at the PSS was 55%(*Z*)/45%(*E*) (Figure 3.16). This study indicates that the isomerization process takes place mainly under photolytic conditions.

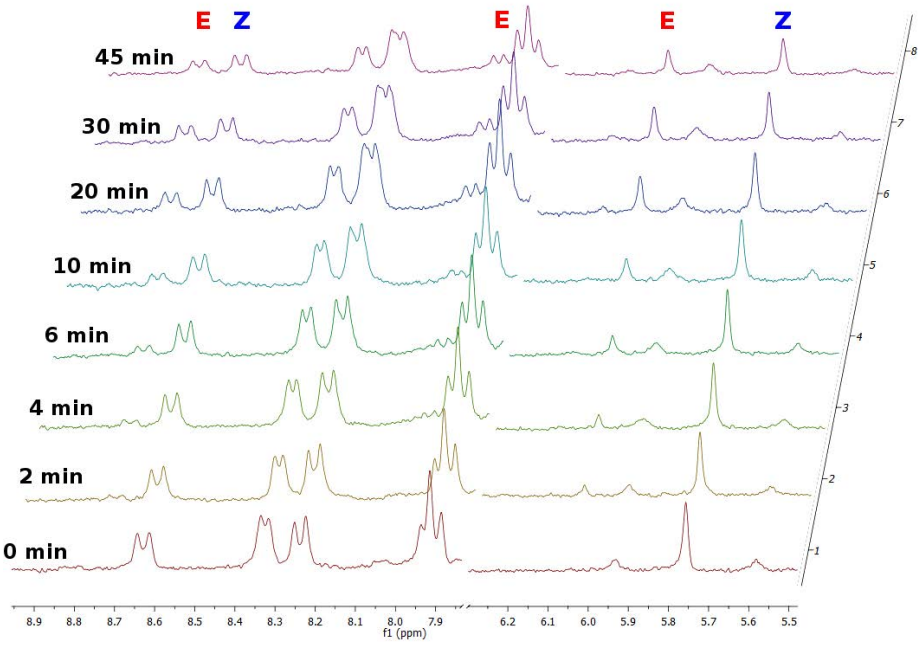

Figure 3.16: H^8-$H^{12}{}_{pq}$ region and vinylic H region of the ^1H NMR spectra of a solution of **26** (CH_2Cl_2, 10^{-3} M) under different irradiation times

As it has been described, the reaction of [Pt(pq)(μ−κC^{α}:η^2-C≡C^{t}Bu)]$_2$ (**16**) with 4-HSpy proceeded, under mild conditions, with formation of an orange solid identified as the dinuclear complex [Pt(pq){μ-Z-κC:κN-C=CH(^{t}Bu)-4-SC_5H_4N}]$_2$ (**27**) (Scheme 3.6). The electrospray mass spectrum (ESI+) of this solid showed two peaks (m/z = 880 and 1183). A closer inspection of the peak at m/z 1183 revealed a peak pattern which compare well with the predicted isotopic distribution (Figure 3.17). The ^1H NMR spectrum of **27** indicated a single product with the signals of only a set of the pq ligand and one pyridyl-vinyl-thioether group in wich both halves of the pyridine ring are inequivalent. The characteristic H^8 signal of the pq ligand, appears (δ 8.48) at similar position to that seen in **26** The vinylic H appears at 6.58 ppm with a platinum coupling constant of 143.8 Hz. This value agrees with the formulation proposed in Scheme 3.6 with the vinylic proton attached to the C^{α} carbon atom, in contrast to the C^{β} carbon in **26** (δ_H 5.76, $^3J_{Pt\text{-}H}$ 105.5 Hz). Both, the chemical shift and the coupling constant compare to those observed in related vinyl platinum complexes.[22] For this complex we propose the formulation drawn in Scheme 3.6. A cyclic diplatinum complex with a double pyridyl-vinyl-thioether bridging system between both platinum centers, similar to that formed by reaction of [Pt(μ-C≡C^{t}Bu)(C_6F_5)(PPh_3)]$_2$ with NC_5H_4SH-4 whose

structure has been confirmed by X-ray crystallography.[11a] Unfortunatelly numerous attemps to crystallize this solid resulted unsuccessful.

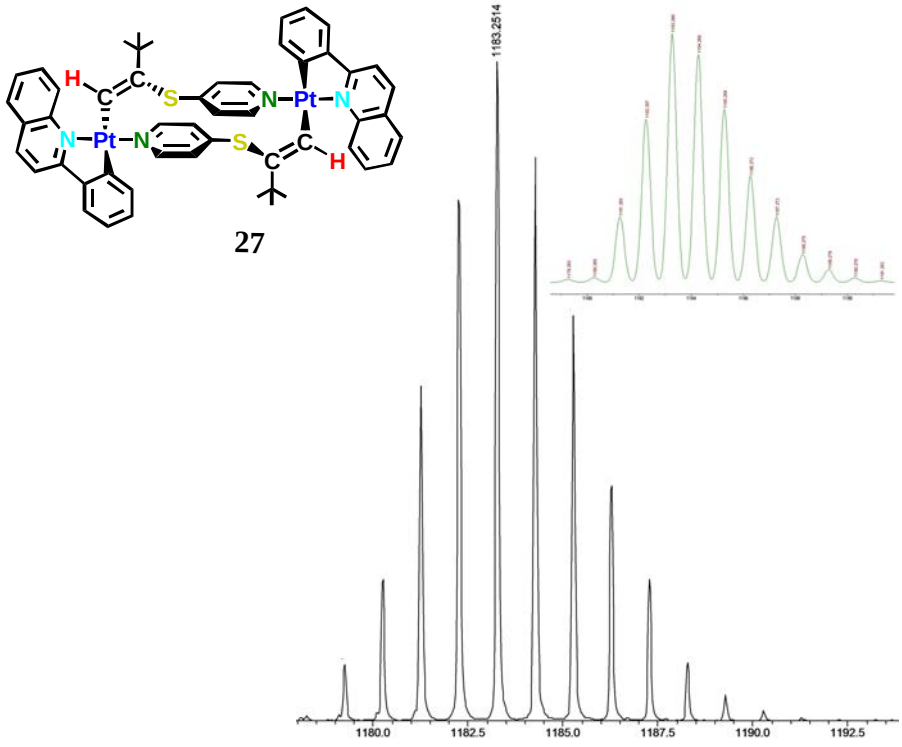

27

Figure 3.17: Experimental isotope pattern and predicted isotopic distribution (green) in the electrospray mass spectrum of **27** showing the peak [{Pt(pq)(C=CH^{t}Bu)(SC$_5$H$_4$N)}$_2$ + H]$^+$

Due to the low solubility of the 4-HSpy ligand in chlorinated solvents and of the complex **27** in donor solvents such as acetone, we could not be able to carry out a variable-temperature ^{1}H NMR spectroscopy study to investigate the mechanism of its formation. Investigations in our research group[11a] allow us to propose the mechanism of formation collected in Scheme 3.9. In a first step (*i*) the cleavage of the alkynyl bridging system and coordination of the 4-HSpy through S atom to the Pt center, could evolve to form the mononuclear complex **A**. Isomerization of the intermediate **A** complex driven by intermolecular SH···C≡C bonding interactions, followed by an hydrothiolation process would led to the final species **27**, likely through the binuclear H-bonding species **B** depicted in Scheme 3.9.

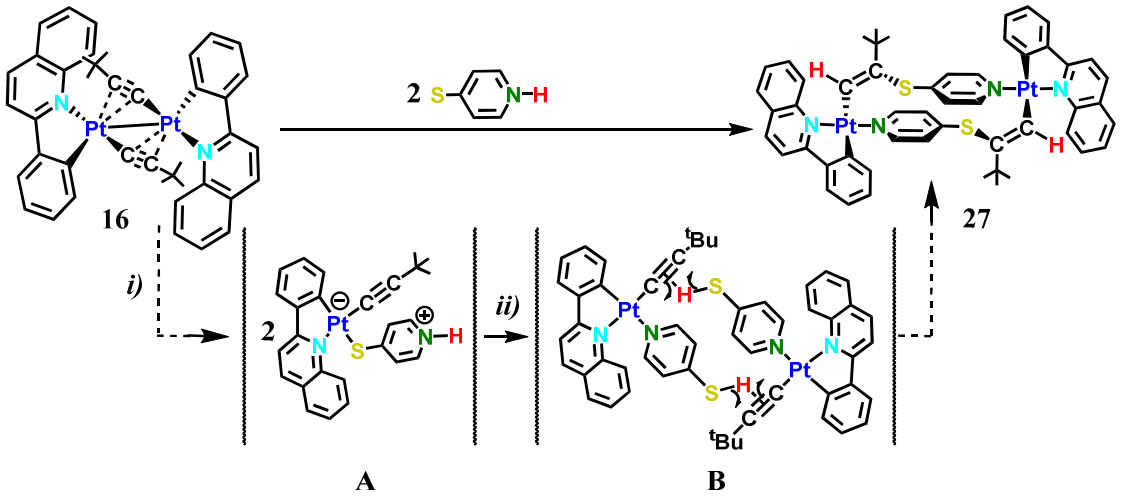

Scheme 3.9

3.2.2 Photophysical properties

To facilitate comparison, all absorption and emission spectra data are summarized in Table 3.6

Absorption spectroscopy.

As it has been commented above, the absorption spectrum of the isomer **26$_Z$** is identical to that of the equilibrated mixture *Z*:*E* 55:45 (Figure 3.18a). For this reason, we will only refer to that of **26$_Z$**, whose data are collected in Table 3.6. Both complexes (**26** and **27**) display intense bands in the UV region < 320 nm, with molar absorptions ε in the range 16.900-60.000 $M^{-1}cm^{-1}$, corresponding to $^1\pi$-π^* transitions associated to the ligands (Figure 3.18). The moderately structured band at ~ 350 nm resembles to that observed in the starting material (**16**) being attributed to ^{1}IL (pq) charge transfer. In the visible region (390-500 nm), somewhat weaker (ε < 8000 $M^{-1}cm^{-1}$) and distinct bands to those observed in the starting material appear. In **26** the lowest energy band located at 480 nm is substantially red shifted compared to that of the starting material (436 nm, **16**) (Figure 3.18a). This red shift is likely associated to the formation of the 5-membered platina-diheterocycle. The band displays a distinctic red shift with decreasing solvent polarity [473 (CH_3CN), 480 (CH_2Cl_2), 487 (THF)], (Table A3.8), a behavior typical of a negative solvatochromic effect (Figure 3.18b). This solvent dependence is consistent with a charge-transfer transition where the excited state is less polar than the

ground state. Similar solvatochromism has been also reported for [*cis*-Pt(N-N)X_2] (X = S,S; C≡CR) having electron rich atoms (S, C_{sp}) coordinated to the Pt centres.[23] In this complex **26$_Z$**, the presence of electron rich S and C atoms are expected to lead to a HOMO that will span the chelating cycle (*C*,*S*) with the Pt and phenyl ring of the pq. Therefore, the lowest energy band could be tentatively attributed to charge-transfer transitions from the heterocyclic ring-to- cyclometalated pq ligand ^{1}L'LCT or heterocycle/metal-to-pq ^{1}ML'LCT. In the case of **27**, the visible region bands (397, 429 nm) are of lower ε and occur slightly blue-shifted compared to the starting precursor (436 nm **16**), being tentatively ascribed to typical ^{1}LC/^{1}MLCT located on the Pt units (Figure 3.18c).

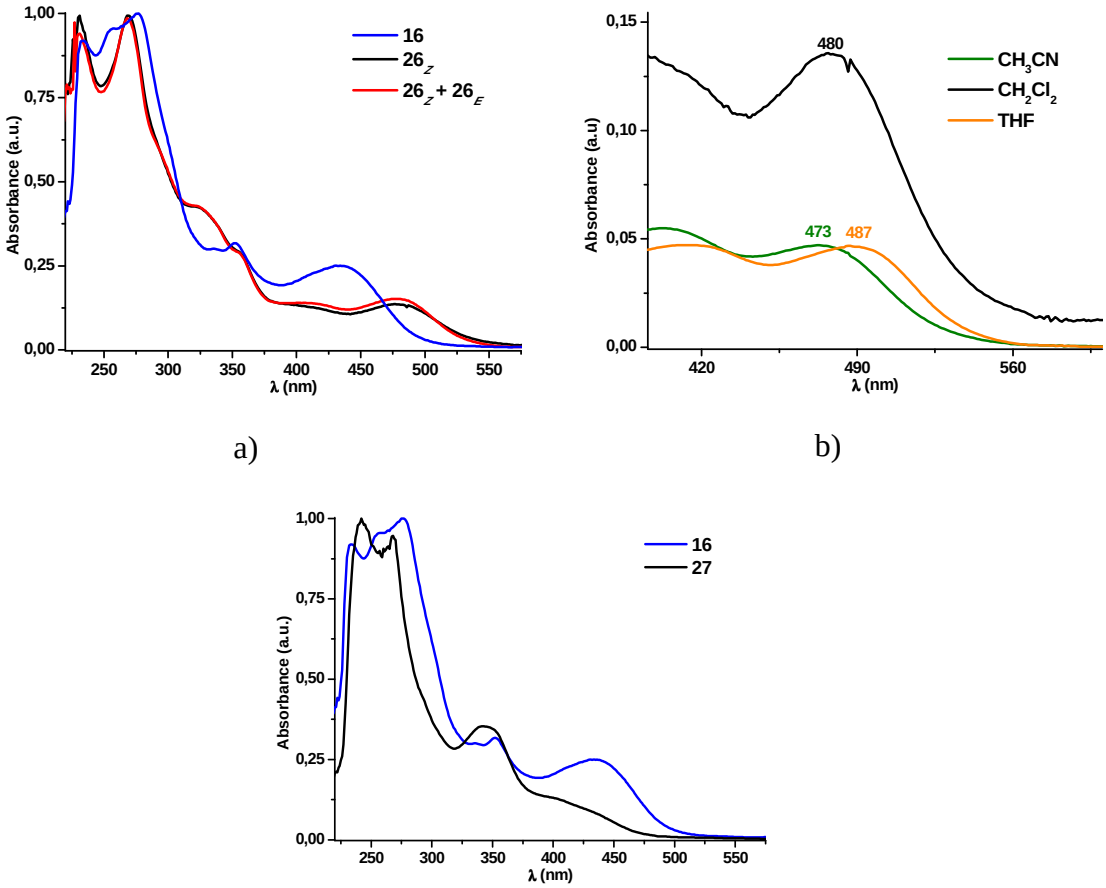

Figure 3.18: UV-vis absorption spectra in CH_2Cl_2 (5×10^{-5} M) of a) **16**, **26$_Z$** and mixture **26$_Z$**: **26$_E$** (55:45), b) **26$_Z$** in different solvent and c) **27**

Tabla 3.6: Photophysical data for **26** and **27** in solid state and CH_2Cl_2 solution at 298 and 77K

Comp.		λ_{abs}/nm (10^3 ε/$M^{-1}cm^{-1}$)	λ_{em}/nm (λ_{exc}/nm) [ϕ/%]	τ/μs
26_Z	Solid (298 K)	280, 320, 345, 395, 420, 475, 535_{sh} [a]	670 [b] (400-620) [6.1]	10.52
	Solid (77 K)		670 [b] (400-570)	10.94
	$5*10^{-5}$M (298 K)	231 (38.8), 268 (38.8), 320 (16.9), 354 (11.7), 402 (5.5), 480 (5.6)	600 [b] (365-520)	
	$5*10^{-5}$M (77 K)		550, 595, 630_{sh} [b] (365-480)	
27	Solid (298 K)	296, 331, 356, 398, 435 [a]	602 [b] (365-500) [4.8]	9.03
	Solid (77 K)		578_{max}, 611, 685_{sh} (365-480)	10.8
	$5*10^{-5}$M (298 K)	242 (60.5), 268 (57.2), 344 (21.4), 397 (8.1), 429 (5.7)	585 [b] (365-415)	
	$5*10^{-5}$M (77 K)		555_{max}, 585 (365-440)	

a) Diffuse Reflectance, b) Tail to 820 nm

However, in the solid state, the diffuse reflectance spectra of **26** and **27** show intense absorptions red-shifted in both cases in relation to the starting material **16** [475, 535_{sh} (**26**); 435 (**27**)] (Figure 3.19). The different behaviour of **27** in solid state in relation to CH_2Cl_2 solution could be related with the more rigidity of the molecule in solid state.

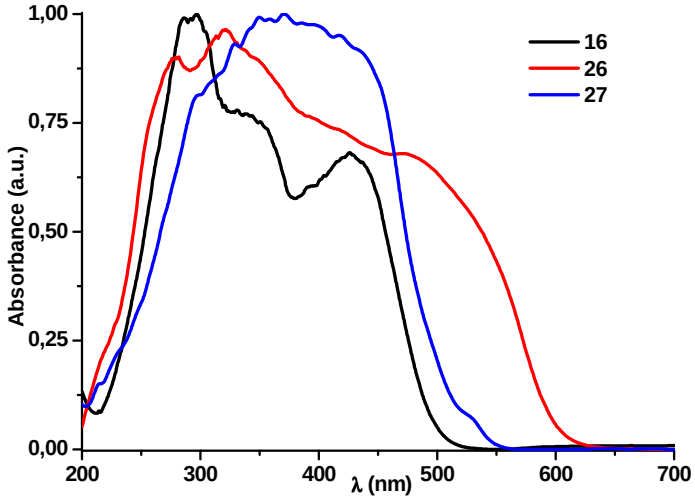

Figure 3.19: Absorption spectra calculated from their reflectance spectra in solid state of complexes **16**, **26** and **27** (diluted in SiO_2)

Emission spectroscopy

Qualitatively, the emissions of these complexes are much more intense in all media that those observed for the starting material. The emission profiles are not

dependent on the excitation-wavelength, indicating that aggregates are not responsible for the observed spectra.

Complexes **26** and **27** are luminescent in solid state and in degassed solutions at 298 K and 77 K and the emission data are compiled in Table 3.6. Complex **26** shows in solid state at 298 K a broad asymmetric band centered at 670 nm, with a quantum yield of 6.1% and a long lifetime (10.5 μs) indicative of the triplet parentage (Figure 3.20a). At 77 K, the emission spectra do not change significantly. The emission in CH_2Cl_2 solution (5 x 10^{-5} M) is blue-shifted respect to the solid, showing a broad unstructured band at 600 nm, which becomes structured (550, 595, 630_{sh}) and enhanced at 77 K (Figure 3.20b). In solution the excitation spectrum resembles the absorption spectrum suggesting that the absorving species are mononuclear complexes. We suggest that the emission could be originated from admixture ^{3}[(M+L')LCT] ^{3}[Pt(d)/heterocycle→ π*(bzq)] excited state. The remarkable red-shifted observed in the solid state and smaller Stokes shift (1.532 cm^{-1} solid *vs* 3.658 cm^{-1} solution) suggest the influence of the close π···π ligand-type (pq-pq) interactions in the emissive state. The emission in solid can be ascribed to platinum heterocycle-to-ligand (pq)/ligand (pq) charge transfer ^{3}[(M+L')LLCT].

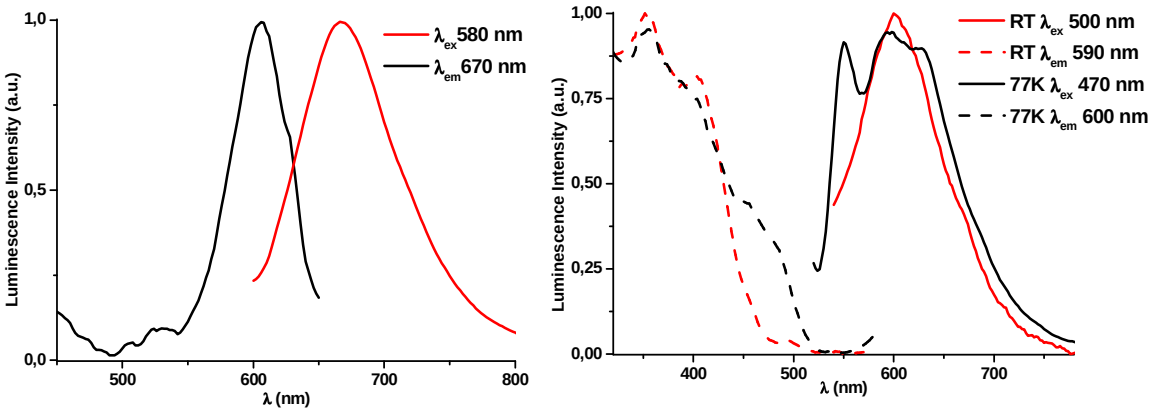

Figure 3.20: Normalized excitations (dotted lines) and emission (solid lines) spectra of **26** in a) solid state at 298 K and b) CH_2Cl_2 5 x 10^{-5} M solution at 298 and 77K

Complex **27** exhibits in the solid state at 298 K a broad asymmetric band at 602 nm (Φ 4.8 %) with a lifetime of 9.0 μs. At 77 K, the spectrum becomes vibronically

resolved and is blue-shifted (λ_{max} 578 nm) (Figure 3.21a). In CH_2Cl_2 solution at 298 K the emission is only slightly blue-shift respect to solid (585 nm) suggesting similar emissive state. Upon cooling at 77 K, the emission becomes also vibronically resolved and slightly blue-shifted (λ_{max} 555, 585 nm) (Figure 3.21b). The profile of the emission band in glassy solution is somewhat different to that observed for **26** pointing to a different contributions in the emissive state. In this complex the emission is tentatively ascribed to admixture ^{3}MLCT/^{3}LC. However, further theoretical studies are required to shed light into the behaviour of both complexes, **26** and **27**.

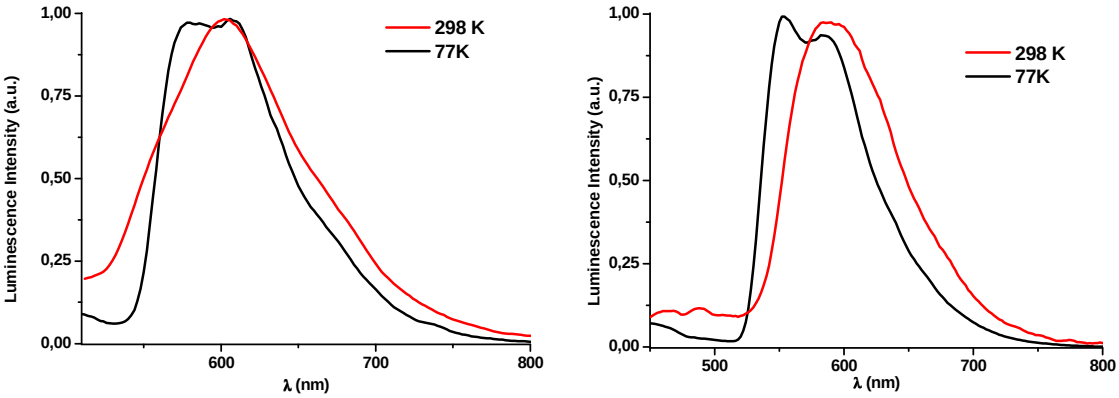

a) b)

Figure 3.21: Normalized emission spectra of **27** a) in solid state at 298 K and 77 K (λ_{exc} 450 nm), and b) in CH_2Cl_2 solution (5 x 10^{-5} M) at 298 K and 77 K (λ_{exc} 430 nm)

3.3 Summary

In Summary, this Chapter present the result of the reactions of [Pt(pq)(μ−κC$^{\alpha}$:η^2-C≡C^{t}Bu)]$_2$ (**16**) toward different donor ligands.

The first part of the Chapter focuses on the bridge-splitting reactions of **16** with bidentate *N*-donor ligands of different lengths and flexibility and one N-tridentate ligand to form binuclear [{Pt(pq)(C≡C^{t}Bu)}$_2$(μ-L)] (**20a-24a)** and trinuclear [{Pt(pq)(C≡C^{t}Bu)}$_3$(μ-L)] (**25a**) derivatives. The structures of **21a** and **23a** have been confirmed by X-ray crystallography. Probably due to the *trans* labilizing effect of the *C*-cyclometalating atom and the high stability of **16**, these complexes rearrange in solution giving rise to a dynamic equilibrium between the diplatinum complexes (**20a-24a**), the mononuclear species [Pt(pq)(C≡C^{t}Bu)(L-κ*N*)] (**20b-24b**), the precursor (**16**) and the free ligand (L), as confirmed by ^{1}H NMR experiments. The equilibrium is affected by the concentration, temperature and solvent polarity. The higher proportion of the bimetallic species (**a**) in solution was found with the more flexible and donor ligands (bpa, bpe), in concentrated solutions, at low temperatures and with less polar solvents.

TD-DFT calculations on **21a** allow to assign the low-energy absorption band in solid state to Pt(pq)(C≡C^{t}Bu) to ***N-N*** linker charge transfer (500-540 nm) ^{1}[(M+L+L')L''CT], whereas in CH_2Cl_2 solution the low energy band (408-413 nm) is ascribed mainly to admixture of platina/cyclometalate (pq) to *N*-donor ligand charge transfer ^{1}[d(Pt)/π(pq)→π*(*N*-donor)] ^{1}[(M+L)L''CT], although some platina/alkynyl to cyclometalate (pq) contribution ^{1}[d(Pt)/C≡C→π*(pq)] cannot be discarded. These assemblies show a stronger luminescence than the starting material (**16**). The emission properties of the bpe-dimer **23a** in solid state are consistent with a predominantly bpe-centered ^{3}IL ^{3}(ππ*) excited state, whereas **20a** and **21a** exhibit emission from an admixture platina/alkynyl to cyclometalated (pq) charge transfer ^{3}[(M+L')LCT], supported by DFT calculations on **21a** and in the remaining complexes some additional contribution of the central *N*-linker can be invoked. The emission in solution of the binuclear species (**a**) (predominant in mixtures **16**:L 1:1) and the mononuclear species (**b**) (predominant in mixtures **16**:L 1:4) is rather similar, suggesting a similar excited state for both types of species, attributed in all complexes to ^{3}[(M+L')LCT].

Experimental data and theoretical calculations suggest that the excitation of the molecule seems to introduce a remarkable change in the nature of the HOMO-LUMO/SOMO-1-SOMO, rising the energy of the π* diimine-based orbitals above the cyclometalated-based orbitals.

On the other hand, the second part of this Chapter is centered on the reactivity of **16** with 2- and 4- thiolpyridine. The position of the sulfur atom in the pyridine ring determines the geometry of the obtained complexes. The reaction with 2-thiolpyridine give the mononuclear complex [Pt(pq){(κ*C*:κ*S*-2-SC_5H_4N-C=CH^{t}Bu}] (**26**) with a vinylthione molecule. Its structure has been confirmed by X-Ray diffraction, observing the presence of a solid solution from both geometries (*Z* and *E*) in the ^{t}Bu residue of the alkynyl fragment. The formation of this complex implies the intramolecular addition of the N-H bond of the mercaptopyridine ligand through the $C^{\alpha}\equiv C^{\beta}$ triple bond of the alkynyl fragment, giving rise a new vinylthione C(NC_5H_4S-2)=CH^{t}Bu molecule acting as a chelatig κ*C,S* ligand, forming an unsual platinaheterocyle of five members. The mechanism of its formation has been proposed by a variable temperature ^{1}H NMR study.

The thermal and photochemical *Z/E* isomerization of this compound (**26**) has been studied. This study permits to discard the thermal isomerization and to reach the photostationary state in the photoisomerization process after ~ 30 minutes of irradiation at λ > 360 nm with a 55/45 (*Z/E*) ratio.

The reaction with 4-thiolpyridine proceeds with formation of the cyclic bimetallic species Pt(pq){μ-*Z*-κ*C*:κ*N*-C=CH(^{t}Bu)-4-SC_5H_4N}]$_2$ (**27**), which contains a pyridyl-vinyl-thioether bridging system between the two platinum centers, probably formed by an hydrothiolation process of the alkynyl fragment.

In **26** the lowest energy absorption band is substantially red shifted compared to that of the starting material and is associated with an heterocyclic ring-to-cyclometalated pq ligand ^{1}L'LCT or heterocycle/metal-to-pq ^{1}ML'LCT transition. However in **27** the lowest-energy band is slightly blue-shifted, being tentatively ascribed to typical ^{1}LC/^{1}MLCT located in the Pt units.

Both complexes show more intense emission than the precursor **16**. Complex **26** shows different emission in solid state or in solution. Thus, in the solid state it displays a broad asymmetric band, considerably red-shifted in relation to **16**, whereas in CH_2Cl_2 solution the emission is blue-shifted respect to the solid. This suggests that the emission in the solid can be influenced by the close π···π ligand-type (pq-pq) interactions and ascribed to platinum heterocycle-to-ligand (pq)/ligand (pq) charge transfer ^{3}[(M+L')LLCT], whereas in solution these π···π (pq-pq) interactions are loosed. Thus, the emission in solution is adscribed to an admixture ^{3}[(M+L')LCT] ^{3}[Pt(d)/heterocycle→ π*(bzq)] excited state.

Complex **27** exhibits in the solid state a broad asymmetric band that suffers a slightly blue-shift in CH_2Cl_2 solution, pointing to an admixture ^{3}MLCT/^{3}LC contribution.

3.4 References

1. (a) Berenguer, J. R.; Lalinde, E.; Moreno, M. T. *Coord. Chem. Rev.* **2010**, *254*, 832; (b) Lang, H.; George, D. S. A.; Rheinwald, G. *Coord. Chem. Rev.* **2000**, *206-207*, 101; (c) Lang, H.; Köhler, K.; Blau, S. *Coord. Chem. Rev.* **1995**, *143*, 113; (d) Forniés, J.; Lalinde, E. *J. Chem. Soc., Dalton Trans.* **1996**, 2587.
2. (a) Wong, K. M.-C.; Yam, V. W.-W. *Acc. Chem. Res.* **2011**, *44*, 424; (b) Yam, V. W.-W. *Acc. Chem. Res.* **2002**, *35*, 555; (c) Hissler, M.; McGarrah, J. E.; Connick, W. B.; Geiger, D. K.; Cummings, S. D.; Eisenberg, R. *Coord. Chem. Rev.* **2000**, *208*, 115; (d) Yam, V. W.-W. *J. Organomet. Chem.* **2004**, *689*, 1393; (e) Wong, W.-Y. *Dalton Trans.* **2007**, 4495; (f) Chen, Z. N.; Zhao, N.; Fan, Y.; Ni, J. *Coord. Chem. Rev.* **2009**, *253*, 1; (g) Castellano, F. N.; Pomestchenko, I. E.; Shikhova, E.; Hua, F.; Muro, M. L.; Rajapakse, N. *Coord. Chem. Rev.* **2006**, *250*, 1819; (h) Wong, K. M.-C.; Yam, V. W.-W. *Coord. Chem. Rev.* **2007**, *251*, 2477.
3. (a) Berenguer, J. R.; Forniés, J.; Lalinde, E.; Martín, A.; Serrano, B. *J. Chem. Soc., Dalton Trans.* **2001**, 2926; (b) Ara, I.; Falvello, L. R.; Fernández, S.; Forniés, J.; Lalinde, E.; Martín, A.; Moreno, M. T. *Organometallics* **1997**, *16*, 5923; (c) García, A.; Lalinde, E.; Moreno, M. T. *Eur. J. Inorg. Chem.* **2007**, *2007*, 3553; (d) Forniés, J.; Gómez-Saso, M. A.; Lalinde, E.; Martínez, F.; Moreno, M. T. *Organometallics* **1992**, *11*, 2873; (e) Falvello, L. R.; Forniés, J.; Gómez, J.; Lalinde, E.; Martín, A.; Martínez, F.; Moreno, M. T. *J. Chem. Soc., Dalton Trans.* **2001**, 2132; (f) Berenguer, J. R.; Forniés, J.; Martínez, F.; Cubero, J. C.; Lalinde, E.; Moreno, M. T.; Welch, A. J. *Polyhedron* **1993**, *12*, 1797; (g) Falvello, L. R.; Forniés, J.; Martín, A.; Gómez, J.; Lalinde, E.; Moreno, M. T.; Sacristán, J. *Inorg. Chem.* **1999**, *38*, 3116; (h) Aullón, G.; Álvarez, S. *Organometallics* **2002**, *21*, 2627; (i) Hoogervorst, W. J.; Elsevier, C. J.; Lutz, M.; Spek, A. L. *Organometallics* **2001**, *20*, 4437; (j) Casas, J. M.; Forniés, J.; Fuertes, S.; Martín, A.; Sicilia, V. *Organometallics* **2007**, *26*, 1674; (k) Forniés, J.; Lalinde, E.; Martín, A.; Moreno, M. T. *J. Chem. Soc., Dalton Trans.* **1994**, 135; (l) Berenguer, J. R.; Forniés, J.; Lalinde, E.; Martínez, F. *J. Organomet. Chem.* **1994**, *470*, C15.
4. Fujita, M.; Yazaki, J.; Ogura, K. *J. Am. Chem. Soc.* **1990**, *112*, 5645.
5. (a) Zangrando, E.; Casanova, M.; Alessio, E. *Chem. Rev.* **2008**, *108*, 4979; (b) Fujita, M. *Chem. Soc. Rev.* **1998**, *27*, 417; (c) Caulder, D. L.; Raymond, K. N. *Acc.*

Chem. Res. **1999**, *32*, 975; (d) Leininger, S.; Olenyuk, B.; Stang, P. J. *Chem. Rev.* **2000**, *100*, 853; (e) Navarro, J. A. R.; Lippert, B. *Coord. Chem. Rev.* **2001**, *222*, 219; (f) Fujita, M.; Tominaga, M.; Hori, A.; Therrien, B. *Acc. Chem. Res.* **2005**, *38*, 369; (g) Nitschke, J. R. *Acc. Chem. Res.* **2006**, *40*, 103; (h) Schmidt, A.; Casini, A.; Kühn, F. E. *Coord. Chem. Rev.* **2014**, *275*, 19.

6. Kaiser, A.; Bäuerie, P. *Top. Curr. Chem.* **2005**, *249*, 127.
7. (a) Pollock, J. B.; Schneider, G. L.; Cook, T. R.; Davies, A. S.; Stang, P. J. *J. Am. Chem. Soc.* **2013**, *135*, 13676; (b) Pollock, J. B.; Cook, T. R.; Stang, P. J. *J. Am. Chem. Soc.* **2012**, *134*, 10607; (c) Chen, J.-S.; Zhao, G.-J.; Cook, T. R.; Han, K.-L.; Stang, P. J. *J. Am. Chem. Soc.* **2013**, *135*, 6694; (d) Chen, J.-S.; Zhao, G.-J.; Cook, T. R.; Sun, X.-F.; Yang, S.-Q.; Zhang, M.-X.; Han, K.-L.; Stang, P. J. *J. Phys. Chem. A* **2012**, *116*, 9911; (e) Zhao, G.-J.; Yu, F.; Zhang, M.-X.; Northrop, B. H.; Yang, H.; Han, K.-L.; Stang, P. J. *J. Phys. Chem. A* **2011**, *115*, 6390.
8. Allendorf, M. D.; Bauer, C. A.; Bhakta, R. K.; Houk, R. J. T. *Chem. Soc. Rev.* **2009**, *38*, 1330.
9. (a) Jude, H.; Krause Bauer, J. A.; Connick, W. B. *Inorg. Chem.* **2005**, *44*, 1211; (b) Jude, H.; Krause Bauer, J. A.; Connick, W. B. *Inorg. Chem.* **2004**, *43*, 725; (c) Shi, L.-L.; Liao, Y.; Yang, G.-C.; Su, Z.-M.; Zhao, S.-S. *Inorg. Chem.* **2008**, *47*, 2347; (d) Jude, H.; Krause Bauer, J. A.; Connick, W. B. *Inorg. Chem.* **2002**, *41*, 2275; (e) Fuertes, S.; Woodall, C. H.; Raithby, P. R.; Sicilia, V. *Organometallics* **2012**, *31*, 4228; (f) Zhao, F.; Xu, X.; Khoo, Soo B.; Hor, T. S. A. *Eur. J. Inorg. Chem.* **2004**, *2004*, 69; (g) Rao, Y.-L.; Wang, S. *Inorg. Chem.* **2009**, *48*, 7698; (h) Meijer, M. D.; de Wolf, E.; Lutz, M.; Spek, A. L.; van Klink, G. P. M.; van Koten, G. *Organometallics* **2001**, *20*, 4198.
10. (a) Dattelbaum, D. M.; Itokazu, M. K.; Murakami Iha, N. Y.; Meyer, T. J. *J. Phys. Chem. A* **2003**, *107*, 4092; (b) Schanze, K. S.; Lucia, L. A.; Cooper, M.; Walters, K. A.; Ji, H.-F.; Sabina, O. *J. Phys. Chem. A* **1998**, *102*, 5577; (c) Saltiel, J.; Marchand, G. R.; Kirkor-Kaminska, E.; Smothers, W. K.; Mueller, W. B.; Charlton, J. L. *J. Am. Chem. Soc.* **1984**, *106*, 3144.
11. (a) Sepúlveda, Á. E., Tesis Doctoral, Universidad de La Rioja, 2012; (b) Berenguer, J. R.; Forniés, J.; Lalinde, E.; Martínez, F.; Sánchez, L.; Serrano, B. *Organometallics* **1998**, *17*, 1640.
12. (a) Anjali, K. S.; Vittal, J. J.; Dean, P. A. W. *Inorg. Chim. Acta* **2003**, *351*, 79; (b) Han, Y.-F.; Lin, Y.-J.; Jia, W.-G.; Jin, G.-X. *Dalton Trans.* **2009**, 2077; (c) Cheng,

J.-K.; Chen, Y.-B.; Wu, L.; Zhang, J.; Wen, Y.-H.; Li, Z.-J.; Yao, Y.-G. *Inorg. Chem.* **2005**, *44*, 3386; (d) Zhang, P.-C.; Wang, H.; Liu, S.; Guo, X.-Q.; Hou, X.-F. *J. Organomet. Chem.* **2008**, *693*, 2903.

13. Bianketti, S.; Blake, A. J.; Wilson, C.; Hubberstey, P.; Champness, N. R.; Schroder, M. *CrystEngComm* **2009**, *11*, 763.
14. (a) Räisänen, M. T.; Runeberg, N.; Klinga, M.; Nieger, M.; Bolte, M.; Pyykkö, P.; Leskelä, M.; Repo, T. *Inorg. Chem.* **2007**, *46*, 9954; (b) Wang, J.; Zhang, Y.-H.; Li, H.-X.; Lin, Z.-J.; Tong, M.-L. *Cryst. Growth Des.* **2007**, *7*, 2352; (c) Shibahara, S.; Kitagawa, H.; Ozawa, Y.; Toriumi, K.; Kubo, T.; Nakasuji, K. *Inorg. Chem.* **2007**, *46*, 1162.
15. (a) El-khateeb, M.; Damer, K.; Görls, H.; Weigand, W. *J. Organomet. Chem.* **2007**, *692*, 2227; (b) Zhang, X.-M.; Fang, R.-Q.; Wu, H.-S. *J. Am. Chem. Soc.* **2005**, *127*, 7670; (c) Neo, K. E.; Huynh, H. V.; Koh, L. L.; Henderson, W.; Hor, T. S. A. *Dalton Trans.* **2007**, 5701; (d) Wang, H.; Zhong, R.; Guo, X.-Q.; Feng, X.-Y.; Hou, X.-F. *Eur. J. Inorg. Chem.* **2010**, *2010*, 174; (e) Su, W.; Hong, M.; Weng, J.; Cao, R.; Lu, S. *Angew. Chem. Int. Ed.* **2000**, *39*, 2911.
16. (a) Hamaguchi, T.; Ujimoto, K.; Ando, I. *Inorg. Chem.* **2007**, *46*, 10455; (b) Nunes, F. S.; Bonifácio, L. D. S.; Araki, K.; Toma, H. E. *Inorg. Chem.* **2005**, *45*, 94; (c) Martínez-Salvador, S.; Menjón, B.; Forniés, J.; Martín, A.; Usón, I. *Angew. Chem. Int. Ed.* **2010**, *49*, 4286; (d) Tzeng, B.-C.; Chiu, T.-H.; Lin, S.-Y.; Yang, C.-M.; Chang, T.-Y.; Huang, C.-H.; Chang, A. H.-H.; Lee, G.-H. *Cryst. Growth. Des.* **2009**, *9*, 5356; (e) Ma, B.; Djurovich, P. I.; Garon, S.; Alleyne, B.; Thompson, M. E. *Adv. Funct. Mater.* **2006**, *16*, 2438.
17. (a) Ohba, T.; Kobayashi, A.; Chang, H.-C.; Kato, M. *Dalton Trans.* **2013**, *42*, 5514; (b) Ohba, T.; Kobayashi, A.; Chang, H.-C.; Kouyama, T.; Kato, T.; Kato, M. *Dalton Trans.* **2014**, *43*, 7514; (c) Kato, M.; Omura, A.; Tashikawa, A.; Kishi, S.; Sugimoto, Y. *Angew. Chem., Int. Ed.* **2002**, *41*, 3183; (d) Tzeng, B. C.; Chiu, T. H.; Lin, S. Y.; Yang, C. M.; Chang, T. Y.; Huang, C. H.; Chang, A. H. H.; Lee, G. H. *Cryst. Growth. Des.* **2009**, *9*, 5356; (e) Tzeng, B. C.; Fu, W. F.; Che, C. M.; Chao, H. Y.; Cheung, K. K.; Peng, S. M. *J. Chem. Soc., Dalton Trans.* **1999**, 1017; (f) Aoki, R.; Kobayashi, A.; Chang, H.-C.; Kato, M. *Bull. Chem. Soc. Jpn.* **2011**, *84*, 218; (g) Koshiyama, T.; Omura, A.; Kato, M. *Chem. Lett.* **2004**, *33*, 1386.
18. (a) Bernechea, M.; Berenguer, J. R.; Lalinde, E.; Torroba, J. *Organometallics* **2009**, *28*, 312; (b) Hill, A. F.; Rae, A. D.; Schultz, M.; Willis, A. C. *Organometallics*

2007, *26*, 1325; (c) Huang, J.; Chen, S.; Guzei, I. A.; Yu, L. *J. Am. Chem. Soc.* **2006**, *128*, 11985; (d) Pidcock, E.; DeBeer, S.; Obias, H. V.; Hedman, B.; Hodgson, K. O.; Karlin, K. D.; Solomon, E. I. *J. Am. Chem. Soc.* **1999**, *121*, 1870; (e) Wang, L.-S.; Fettinger, J. C.; Poli, R. *J. Am. Chem. Soc.* **1997**, *119*, 4453; (f) Freedman, D. A.; Janzen, D. E.; Vreeland, J. L.; Tully, H. M.; Mann, K. R. *Inorg. Chem.* **2002**, *41*, 3820; (g) Härkönen, A. U.; Ahlgrén, M.; Pakkanen, T. A.; Pursiainen, J. *Organometallics* **1997**, *16*, 689; (h) Argazzi, R.; Bergamini, P.; Costa, E.; Gee, V.; Hogg, J. K.; Martín, A.; Orpen, A. G.; Pringle, P. G. *Organometallics* **1996**, *15*, 5591; (i) Capdevila, M.; Carrasco, Y.; Clegg, W.; A. Coxall, R.; Gonzalez-Duarte, P.; Lledos, A.; Antonio Ramirez, J.; Ramirez, A. *J. Chem. Soc., Dalton Trans.* **1999**, 3103; (j) Radu, N. S.; Hollander, F. J.; Tilley, T. D.; Rheingold, A. L. *Chem. Commun.* **1996**, 2459.

19. M.Winter *Web Elements* ^{TM}*, the periodic table on the www copyright 1993-2009, , The Universirty of Sheffield and webelements LTD. UK, (www.webelements.com)* 3-September-2014.
20. Allen, F. H.; Kennard, O.; Watson, D. G.; Brammer, L.; Orpen, A. G.; Taylor, R. *J. Chem. Soc., Perkin Trans. II* **1987**, 51.
21. Chuchuryukin, A. V.; Chase, P. A.; Mills, A. M.; Lutz, M.; Spek, A. L.; van Klink, G. P. M.; van Koten, G. *Inorg. Chem.* **2006**, *45*, 2045.
22. (a) Benedetti, M.; Lamacchia, V.; Antonucci, D.; Papadia, P.; Pacifico, C.; Natile, G.; Fanizzi, F. P. *Dalton Trans.* **2014**, *43*, 8826; (b) Carlisle, S.; Matta, A.; Valles, H.; Bracken, J. B.; Miranda, M.; Yoo, J.; Hahn, C. *Organometallics* **2011**, *30*, 6446; (c) Hahn, C.; Miranda, M.; Chittineni, N. P. B.; Pinion, T. A.; Perez, R. *Organometallics* **2014**, *33*, 3040.
23. (a) Wadas, T. J.; Chakraborty, S.; Lachicotte, R. J.; Wang, Q. M.; Eisenberg, R. *Inorg. Chem.* **2005**, *44*, 2628; (b) Tarran, W. A.; Freeman, G. R.; Murphy, L.; Benham, A. M.; Kataky, R.; Williams, J. A. G. *Inorg. Chem.* **2014**, *53*, 5738; (c) Zuleta, J. A.; Burberry, M. S.; Eisenberg, R. *Coord. Chem. Rev.* **1990**, *97*, 47.

3.4 Appendix

Table A3.1: Selected bond lengths and angles for complex [{Pt(pq)(C≡C^{t}Bu)}$_2$(μ-bpe)]·4CHCl$_3$, (**23a**)·4CHCl$_3$

23a			
Pt(1)-C(1)	1.972(9)	Pt(3)-C(55)	1.988(9)
Pt(1)-N(1)	2.096(7)	Pt(3)-N(5)	2.091(7)
Pt(1)-C(16)	1.949(9)	Pt(3)-C(70)	1.959(9)
Pt(1)-N(2)	2.130(7)	Pt(3)-N(6)	2.114(7)
C(16)-C(17)	1.209(12)	C(70)-C(71)	1.195(12)
Pt(2)-C(34)	1.979(8)	Pt(4)-C(82)	1.993(9)
Pt(2)-N(3)	2.136(7)	Pt(4)-N(7)	2.146(7)
Pt(2)-C(49)	1.956(9)	Pt(4)-C(97)	1.954(9)
Pt(2)-N(4)	2.145(7)	Pt(4)-N(8)	2.125(7)
C(49)-C(50)	1.195(12)	C(97)-C(98)	1.205(12)
C(27)-C(28)	1.290(9)	C(81)-C(81)#1	1.334(17)
		C(108)-C(108)#2	1.240(19)
N(1)-Pt(1)-C(1)	80.3(3)	N(5)-Pt(3)-C(55)	79.4(3)
C(16)-Pt(1)-C(1)	92.1(4)	C(70)-Pt(3)-C(55)	94.9(4)
C(16)-Pt(1)-N(2)	87.8(3)	C(70)-Pt(3)-N(6)	86.0(3)
N(1)-Pt(1)-N(2)	99.4(3)	N(5)-Pt(3)-N(6)	99.2(3)
Pt(1)-C(16)-C(17)	176.3(9)	Pt(3)-C(70)-C(71)	177.4(8)
C(16)-C(17)-C(18)	175.4(11)	C(70)-C(71)-C(72)	175.9(10)
N(3)-Pt(2)-C(34)	80.9(3)	N(7)-Pt(4)-C(82)	79.7(4)
C(49)-Pt(2)-C(34)	93.0(4)	C(97)-Pt(4)-C(82)	92.2(4)
C(49)-Pt(2)-N(4)	83.9(3)	C(97)-Pt(4)-N(8)	86.6(3)
N(3)-Pt(2)-N(4)	102.0(3)	N(7)-Pt(4)-N(8)	101.1(3)
Pt(2)-C(49)-C(50)	174.7(9)	Pt(4)-C(97)-C(98)	173.1(8)
C(49)-C(50)-C(51)	174.6(11)	C(97)-C(98)-C(99)	173.7(11)
C(24)-C(27)-C(28)	121.4(14)	C(78)-C(81)-C(81)#1	123.6(10)
C(27)-C(28)-C(31)	126.5(14)	C(105)-C(108)-C(108)#2	124.2(15)

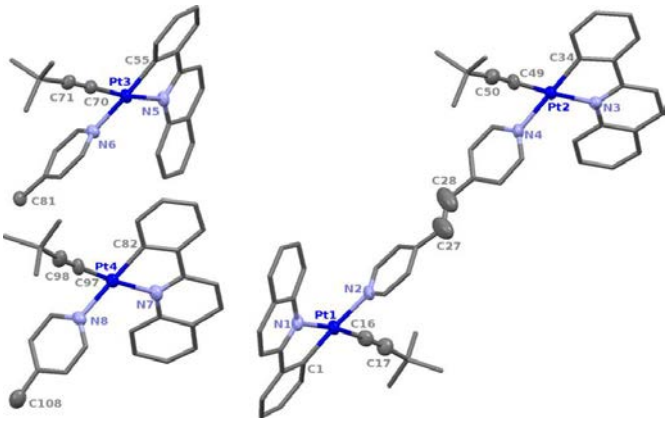

Figure A3.1: View of the asymmetric unit in the molecular structure of [{Pt(pq)(μ–C≡C^{t}Bu)}$_2$(μ-bpe)]·4CHCl$_3$ (**23a**·4CHCl$_3$)

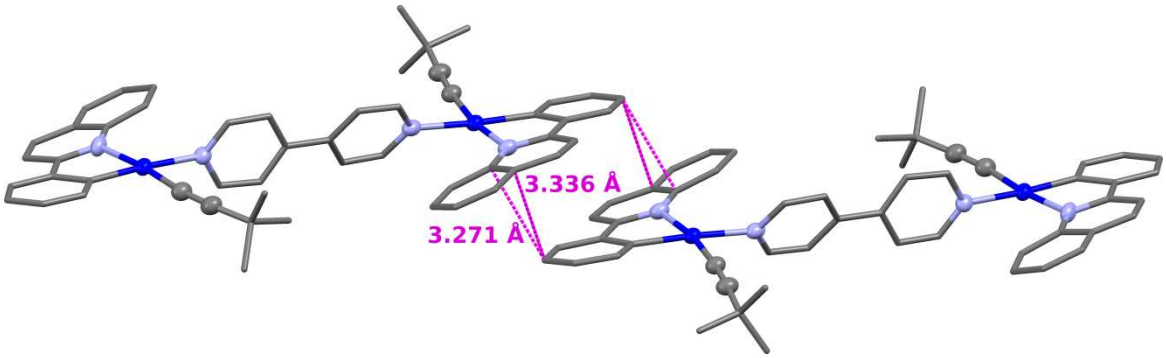

a)

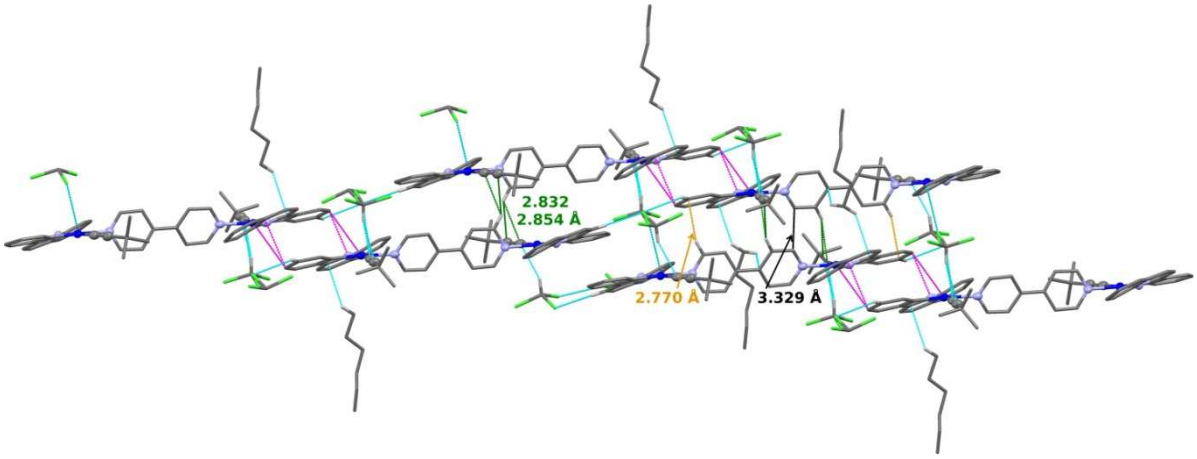

b)

Figure A3.2: Packing of the complex [{Pt(pq)(μ–C≡C^{t}Bu)}$_2$(μ-4,4'-bpy)]·2CHCl$_3$·C$_6$H$_{14}$ (**21a**·2CHCl$_3$·C$_6$H$_{14}$) showing a) the disposition of the dimers and b) the interactions through secondary interactions with the crystallization solvents (CHCl$_3$, *n*-hexane) and with other dimers (H$_{py}$···π$_{C≡C}$/C$_{pq}$)

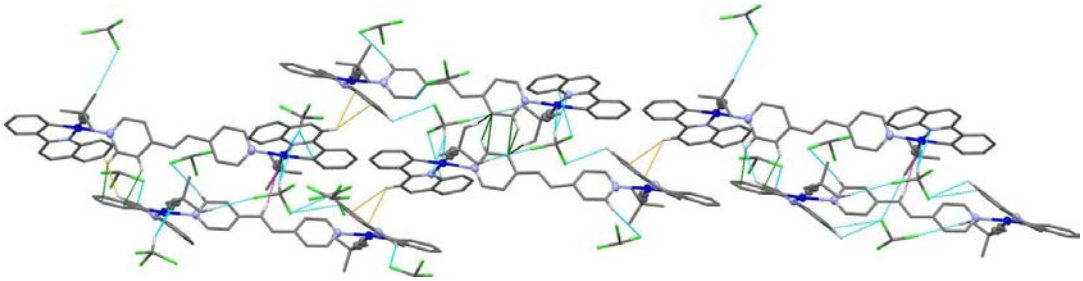

Figure A3.3: Packing of [{Pt(pq)(μ–C≡C^{t}Bu)}$_2$(μ-bpe)]·4CHCl$_3$ (**23a**·4CHCl$_3$) showing the interactions through secondary contacts between the molecules [C-H$_{py}$···C-H$_{py}$ (C···C 3.353 Å, C···H 2.897 Å, C-C-H 53.42º) (green), H$_{py}$···C$_{pq}$ (2.735 Å) (green), C$_{py}$···H^{t}Bu (2.881 Å) (black), H$_{pq}$···C$_{pq}$ (2.856, 2.885 Å) (orange) C$_{C≡C}$···H$_{C=C}$ (2.872 Å) (violet)] and between the crystallization solvents and the molecules (blue) (Cl···C^{t}Bu 3.430 Å, Cl···H^{t}Bu 2.940 Å, Cl···H$_{pq}$ 2.892–2.949 Å, Cl···C$_{pq}$ 3.376, 3.426 Å, Cl···H$_{py}$ 2.933 Å, Cl···C$_{py}$ 3.403 Å, HCHCl$_3$···C$_{C=C}$ 2.458–2.824 Å, HCHCl$_3$···Pt 2.737, 2.888 Å, H CHCl$_3$···C$_{pq}$ 2.896 Å, HCHCl$_3$···N$_{pq}$ 2.724 Å)

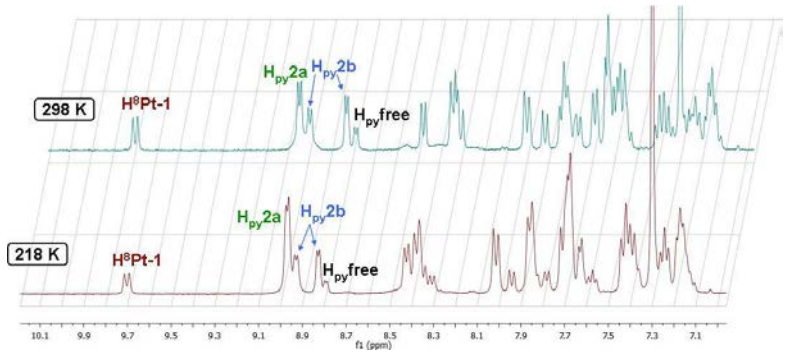

Figure A3.4: ^{1}H NMR spectra at 298 K and at 218 K of a sample of recently dissolved solid **21a**

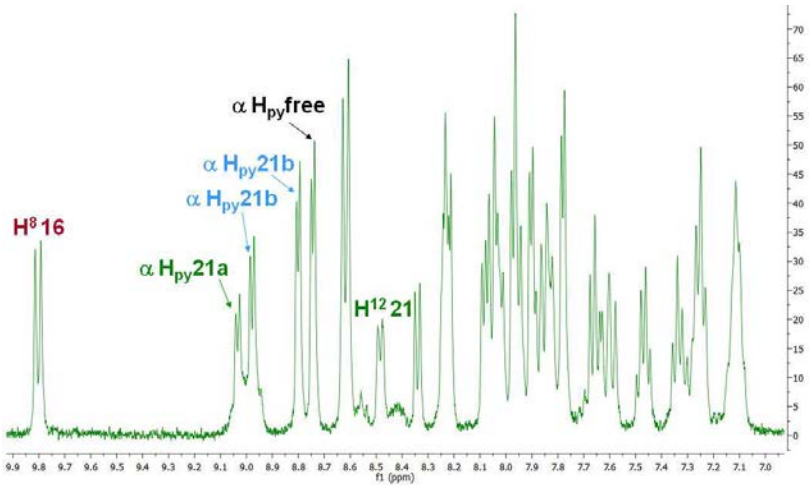

Figure A3.5: ^{1}H NMR spectra at 298 K in CD_3COCD_3 of a sample of recently dissolved solid **21a**

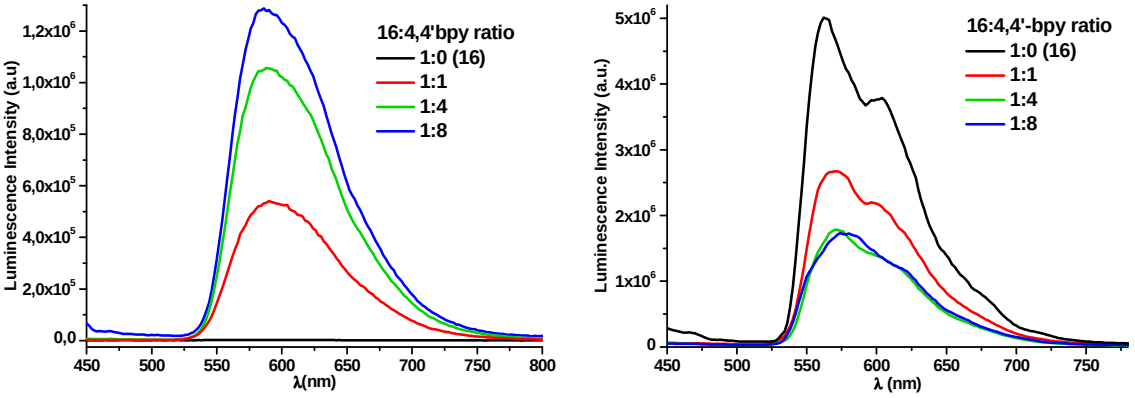

a) b)

Figure A3.6: Comparative emission spectra in CH_2Cl_2 5 x 10^{-5} M of the starting material and successive additions of 1, 4 and 8 equiv. of the 4,4'-bpy a) at 298 K, b) at 77 K

Table A3.2: Absorption data for the ligands at 298 K (5 x 10^{-5} M CH_2Cl_2 Solutions)

Compound	λ_{abs}/nm (10^3 ε $M^{-1}cm^{-1}$)
pyz	219 (20.9), 261 (11.4), 315 (3.5)
bpy	214 (21.3), 239 (23.5), 269 (10.6), tail to 300 nm
bpa	218 (11.3), 256 (7.3), 265 (4.6), 298 (1)
bpe	219 (24.9), 288 (48.6), 298 (47.3), 313 (28.0)
bpac	218 (19.9), 262 (16.7), 276 (20.7), 285 (17.6), 292 (17.4), 322 (5.0)
tpab	218 (37.9), 269 (48.2), 284 (67.8), 302 (66.7), 327 (11.2)

Table A3.3: Photophysical Data for the ligands in dichloromethane solutions

Compound	Medium (T^a/K)	λ_{em}/nm (λ_{exc}/nm)
pyz	5*10^{-5} M (298)	360_{max}, 450_{sh} (300)
	5*10^{-5} M (77K)	375_{max}, 390, 480_{sh} (250-270)
4,4'-bipy	5*10^{-5} M (298)	365 (230-300)[a)]
	5*10^{-5} M (77K)	400_{max}, 430, 460, 490_{sh} (250-270)
bpa	5*10^{-5} M (298)	380 (300), 380, 575 (340), 575 (365)[a)]
	5*10^{-5} M (77K)	490_{max}, 520, 560_{sh} (300-365)
bpe	5*10^{-5} M (298)	400 (280-300)
	5*10^{-5} M (77K)	400 (300)
bpac	5*10^{-5} M (298)	380_{max}, (300-320), 420 (365)[a)]
	5*10^{-5} M (77K)	410_{max}, 510, (365)[a)]
tpab	5*10^{-5} M (298)	350_{max}, 360, 380_{sh} (270-300) 380 (330) 420 (365)
	5*10^{-5} M (77K)	405 (230-365)

a) Weak

Table A3.4: DFT optimized geometries for ground state of complex **21a**

	21a		
	X-Ray	**S_0**	**T_1**
Pt(1)-C(1)	1.994(5)	1.99156	1.99066
Pt(1)-N(1)	2.115(4)	2.18658	2.18541
Pt(1)-C(16)	1.967(5)	1.95948	1.95941
Pt(1)-N(2)	2.113(4)	2.23148	2.23056
C(16)-C(17)	1.197(7)	1.22337	1.22336
Pt(2)-C(32)	1.980(5)	1.99088	1.99972
Pt(2)-N(3)	2.127(4)	2.18572	2.05012
Pt(2)-C(47)	1.961(5)	1.95953	1.96122
Pt(2)-N(4)	2.125(4)	2.23261	2.24171
C(47)-C(48)	1.209(7)	1.22337	1.22968
N(1)-Pt(1)-C(1)	80.9(2)	76.65	79.65
C(16)-Pt(1)-C(1)	91.7(2)	94.03	94.00
C(16)-Pt(1)-N(2)	88.50(19)	84.40	84.55
N(1)-Pt(1)-N(2)	98.56(16)	101.82	101.68
Pt(1)-C(16)-C(17)	175.2(5)	177.81	177.91
C(16)-C(17)-C(18)	176.6(8)	179.36	179.23
N(3)-Pt(2)-C(32)	80.6(2)	79.64	81.37
C(47)-Pt(2)-C(32)	95.8(2)	94.04	94.05
C(47)-Pt(2)-N(4)	81.36(19)	84.61	87.44
N(3)-Pt(2)-N(4)	101.96(16)	101.61	97.48
Pt(2)-C(47)-C(48)	167.6(5)	177.74	178.14
C(47)-C(48)-C(49)	172.7(6)	179.41	178.96

Table A3.5: Selected vertical excitation energies singlets (S_0) computed by TD-DFT in gas phase with the orbitals involved for complex **21a** (*f^a>0.01)*

State	**λ_{exc} (calc.)/nm**	***f^a***	**Transition (Percentage Contribution)**
S_1	494.3	0.1217	H-4->LUMO (93%)
S_2	482.8	0.0929	H-1->L+1 (52%), H-1->L+2 (14%), HOMO->L+2 (14%)
S_3	481.7	0.0178	H-5->LUMO (14%), HOMO->L+1 (17%), HOMO->L+2 (46%), H-1->L+1 (9%)
S_4	459.3	0.0277	H-6->LUMO (93%)
S_5	450.8	0.0107	H-2->L+1 (24%), H-2->L+2 (68%)
S_6	436.2	0.0201	H-5->L+1 (21%), H-5->L+2 (25%), H-4->L+1 (36%)
S_7	435.1	0.0855	H-5->L+1 (25%), H-4->L+2 (47%)

a) Oscillator Strength

Table A3.6: Selected vertical excitation energies singlets (S_0) computed by TD-DFT in CH_2Cl_2 with the orbitals involved for complex **21a** (f^a>0.01)

State	λ_{exc} (calc.)/nm	f^a	Transition (Percentage Contribution)
S_1	434.6	0.0153	H-2->LUMO (41%), HOMO->L+1 (25%), HOMO->L+2 (20%)
S_2	430.8	0.0114	H-2->LUMO (49%), HOMO->L+1 (19%), HOMO->L+2 (15%)
S_3	428.3	0.0113	H-3->LUMO (36%), H-1->L+1 (19%), H-1->L+2 (22%), H-5->LUMO (7%)
S_4	419.0	0.2736	H-4->LUMO (62%), H-5->L+1 (6%)
S_5	414.7	0.0179	H-5->LUMO (56%), H-4->L+1 (9%)
S_6	406.7	0.0155	H-2->L+1 (45%), H-2->L+2 (39%), H-4->LUMO (5%)
S_7	404.3	0.0143	H-3->L+1 (37%), H-3->L+2 (47%), H-5->LUMO (6%),
S_8	396.6	0.0869	H-5->L+1 (11%), H-4->LUMO (12%), H-4->L+1 (26%), H-4->L+2 (28%)
S_9	394.1	0.0829	H-5->LUMO (14%), H-5->L+1 (21%), H-5->L+2 (30%), H-4->L+2 (12%), H-4->L+1 (9%)
S_{10}	378.8	0.0196	H-6->LUMO (69%), H-6->L+1 (21%), H-6->L+2 (6%)
S_{11}	376.3	0.0133	H-7->LUMO (70%), H-7->L+1 (17%), H-7->L+2 (9%),

a) Oscillator Strength

Table A3.7: Composition of frontier molecular orbitals in the first triple-state for **21a**

	C≡C(1)	C≡C(2)	pq(1)	pq(2)	Pt(1)	Pt(2)	bpy
HSOMO	1	0	92	0	4	0	3
LSOMO	16	0	59	0	26	0	0

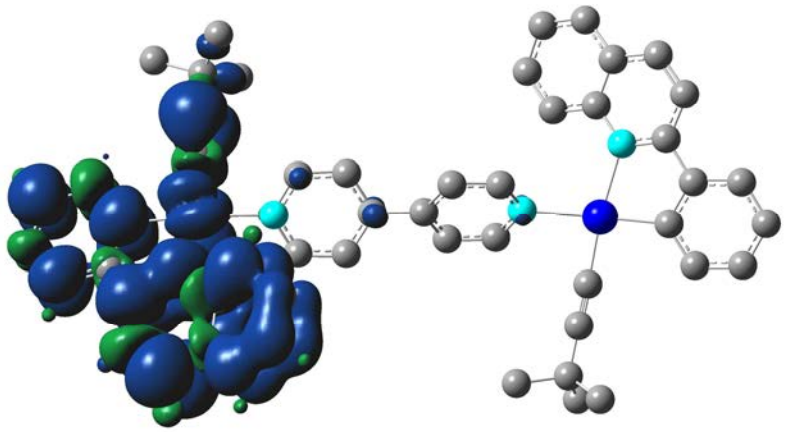

Figure A3.7: Spin density plot for the computed T_1 state of **21a**

Table A3.8: Absorption data of 10^{-3} M (CH_2Cl_2) and 5 x 10^{-5} M (CH_3CN, CH_2Cl_2 and THF) solution of **26** at 298 K

Conc. (M)	λ_{abs}/nm (10^3 ε $M^{-1}cm^{-1}$)
10^{-3}	233 (27.1), 267 (31.9), 320 (13.6), 352 (9.4), 399 (3.9), 480 (4.1) **CH_2Cl_2**
5 x 10^{-5}	212 (42.9), 265 (26.0), 318 (11.0), 351 (7.1), 402 (3.5), 473 (3.0) **CH_3CN** 231 (38.8), 268 (38.8), 320 (16.9), 354 (11.7), 402 (5.5), 480 (5.6) **CH_2Cl_2** 236 (63.0), 266 (32.7), 326 (11.8), 356 (7.1), 414 (3.1), 487 (3.1) **THF**

CAPÍTULO 4

Reactividad de $(NBu_4)[Pt(bzq)(C{\equiv}CR)_2]$ frente a $[Pb(HBpz_3)]^+$

Reactividad de $(NBu_4)[Pt(bzq)(C{\equiv}CR)_2]$ frente a $[Pb(HBpz_3)]^+$

Nuestro grupo de investigación ha descrito las reacciones de los sustratos homolépticos $[Pt(C{\equiv}CR)_4]^{2-}$ tanto con iones Pb^{2+},[1] como con fragmentos PbX^+ (X = Cl, I).[2] Estas reacciones dan lugar a cúmulos tetranucleares estabilizados por enlaces Pb···C$^{\alpha}$ y Pt···Pb. Se ha observado que los agregados que contienen las unidades "PbX^+" presentan una estabilidad muy superior a los clusters $[\{Pt(C{\equiv}CR)_4\}Pb]_2$, tanto en disolución como en estado sólido, lo que indica que la presencia de coligandos en el plomo aumenta la estabilidad de los compuestos sintetizados.

Este hecho ya se había puesto de manifiesto en sistemas heteropolinucleares Pt^{II}–Cd^{II} con ligandos alquinilo obtenidos a partir de sustratos homolépticos $[Pt(C{\equiv}CR)_4]^{2-}$ y mixtos $[Pt(C_6F_5)_2(C{\equiv}CR)_2]^{2-}$. El empleo de coligandos nitrógeno dadores coordinados al átomo de Cd monodentados (py, $NC_5H_4CH_3$-4, $NC_5H_4CF_3$-4, Hpz), bidentados (bpy, dmbpy, phen) o tridentados (trpy) contribuye a la estabilidad de los compuestos generados, al reducir la carga del centro de Cd^{II}.[3] Además, estos coligandos permiten modular las propiedades luminiscentes de los materiales de dos formas distintas: a) originando transiciones de transferencia de carga hacia los ligandos N dadores y b) modificando las propiedades electrónicas del Cd^{II} y por tanto la naturaleza de la interacción con el fragmento aniónico.

Por otro lado y como se recoge también en la Introducción, la neutralización de los sustratos ciclometalados que contienen ligando alquinilo $[Pt(bzq)(C{\equiv}CR)_2]^-$ con $Pb(ClO_4)_2{\cdot}3H_2O$ transcurre con la formación de derivados trinucleares de distinta naturaleza dependiendo del sustituyente del ligando alquinilo.[4] Así, con R = Ph se genera el derivado neutro $[\{Pt(bzq)(C{\equiv}CR)_2\}_2Pb]$, en el que el centro de Pb muestra una coordinación simética *hemidirigida*, mientras que con R = $C_6H_4CF_3$-4 el anión ClO_4^- compite por la coordinación al Pb^{II}, generándose una mezcla del correspondiente derivado neutro y del aducto aniónico $(NBu_4)[\{Pt(bzq)(C{\equiv}CC_6H_4CF_3\text{-}4)_2\}_2\{Pb(O_2ClO_2)\}]$. Teniendo en cuenta la facilidad con la que el ligando ClO_4^- se coordina al Pb^{II}, en este capítulo nos planteamos el empleo de ligandos auxiliares

coordinados al centro de plomo. En concreto, nos propusimos ensayar la reactividad de algunos de los sustratos $(NBu_4)[Pt(bzq)(C{\equiv}CR)_2]$, previamente preparados por nuestro grupo de investigación,[5] frente al derivado $[Pb(HBpz_3)]Cl$, publicado por Reger en 1992.[6] Este estudio no sólo nos proporciona la posibilidad de preparar sistemas heteropolinucleares $Pt^{II} – Pb^{II}$ que pueden presentar interacciones η^2–alquinilo$\cdots Pb^{II}$, de los que se conocen muy pocos ejemplos, sino que ofrece el interés adicional de estudiar sus propiedades ópticas, con especial énfasis en la influencia del coligando sobre la luminiscencia.

4.1 Síntesis y caracterización

Se han examinado las reacciones de neutralización de los compuestos $(NBu_4)[Pt(bzq)(C{\equiv}CR)_2]$ (R = Ph, C_6H_4OMe-3 y $C_6H_4CF_3$-4),[5,7] frente al derivado $[Pb(HBpz_3)]Cl$ en presencia de $NaPF_6$ en exceso, que actúa como abstractor de cloruros.

Como se observa en el Esquema 4.1 el resultado de estas reacciones depende de las características electrónicas del grupo R. Así, el tratamiento de disoluciones amarillas de los derivados $(NBu_4)[Pt(bzq)(C{\equiv}CR)_2]$ (R = Ph y C_6H_4OMe-3) en acetona con $[Pb(HBpz_3)]Cl$ y $NaPF_6$ (Pt:Pb:Na 1:1:10), da como resultado la precipitación de sólidos amarillos de estequiometría $[Pt(bzq)(C{\equiv}CR)_2Pb(HBpz_3)]_2$ (R = Ph **28**, C_6H_4OMe-3 **29**) con rendimientos de aceptables a buenos (72% **28**, 56% **29**). Idénticos resultados se obtienen si se lleva a cabo la reacción con relación Pt:Pb:Na (2:1:10). La estequiometría de los compuestos **28** y **29** indica que los fragmentos aniónicos $[Pt(bzq)(C{\equiv}CR)]^-$ se neutralizan con una unidad catiónica, y su estudio cristalográfico permite formularlos como derivados dímeros $[\{Pt(bzq)(C{\equiv}CR)_2\}\{Pb(HBpz_3)\}]_2$. El plomo muestra una preferencia por el centro básico de platino, originando un fragmento bimetálico $[\{Pt(bzq)(C{\equiv}CR)_2\}\{Pb(HBpz_3)\}]$, que dimeriza mediante interacciones débiles $Pb^{II}\cdots\eta^2(C{\equiv}C)$, con lo que aumenta el entorno de coordinación del plomo.

Sin embargo, la reacción del derivado $(NBu_4)[Pt(bzq)(C{\equiv}CC_6H_4CF_3\text{-}4)_2]$, que contiene un sustituyente menos dador de electrones, en las mismas condiciones que los derivados anteriores, genera la formación de una disolución amarilla de la que se obtiene por evaporación de la acetona a sequedad y tratamiento con H_2O, un sólido

amarillo identificado como $(NBu_4)[\{Pt(bzq)(C{\equiv}CC_6H_4CF_3\text{-}4)_2\}_2\{Pb(HBpz_3)\}]$ **30** con buen rendimiento (90% **30**) (Esquema 4.1). En este caso se genera una entidad aniónica en la que dos fragmentos aniónicos $[Pt(bzq)(C{\equiv}CC_6H_4CF_3\text{-}4)_2]^-$ se conectan por una entidad catiónica $[Pb(HBpz_3)]^+$.

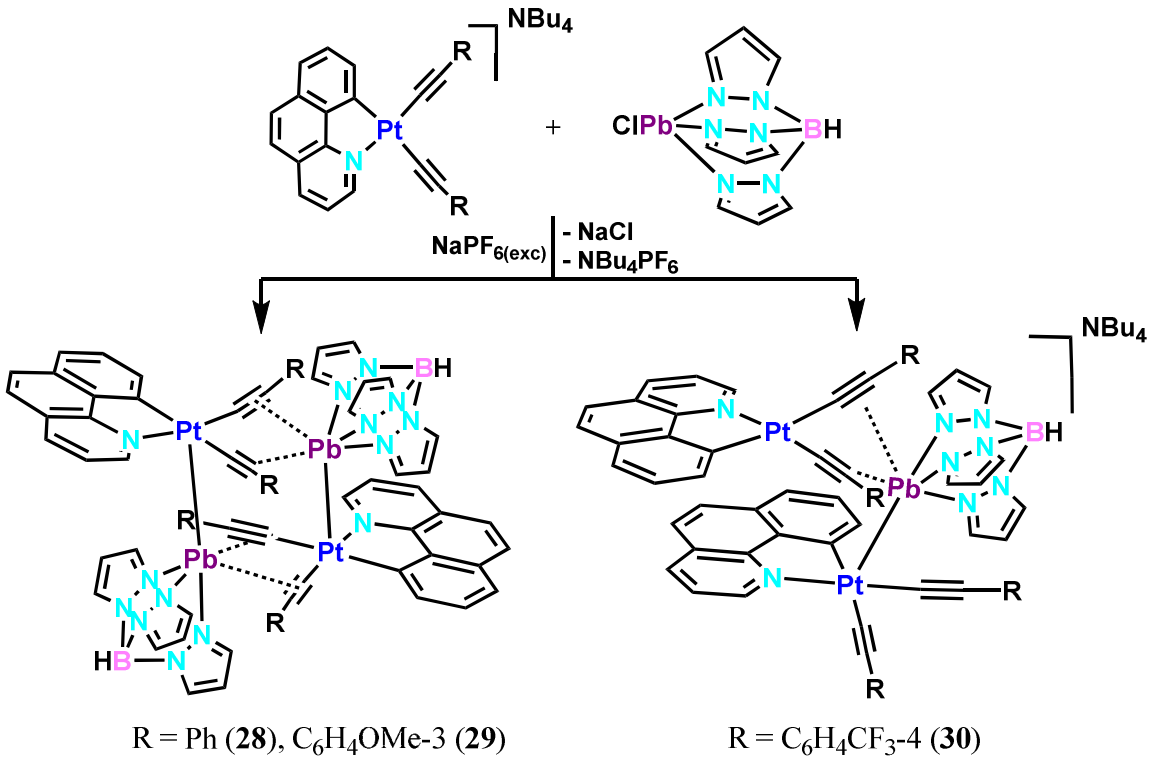

R = Ph (**28**), C_6H_4OMe-3 (**29**) R = $C_6H_4CF_3$-4 (**30**)

Esquema. 4.1

Estos derivados fueron caracterizados por difracción de Rayos X y por las técnicas espectroscópicas habituales [análisis elemental, espectroscopía de masas, IR, RMN (^1H, $^{13}C\{^1H\}$ y ^{19}F)]. Específicamente, para los derivados **28** y **29** se realizaron espectros unidimensionales PGSE y bidimensionales DOSY RMN de ^1H con el fin de intentar comprender su naturaleza en disolución.

4.1.1 Caracterización estructural por difracción de Rayos X

Se obtuvieron cristales amarillos adecuados para su estudio por difracción de Rayos X mediante lenta difusión de *n*-hexano sobre una disolución saturada de los clusters **28**–**30** en CH_2Cl_2. Las estructuras cristalinas de estos compuestos son de especial interés, ya que como se ha comentado anteriormente, el número de sistemas

descritos con enlaces Pt-Pb es extremadamente escaso y además representan uno de los pocos ejemplos descritos de sistemas con interacciones η^2–alquinilo$\cdots Pb^{II}$, junto con los derivados trinucleares de tipo sándwich Pt_2Pb[4] y tetranucleares Pt_2Pb_2[1] publicados por nuestro grupo de investigación.

Las estructuras cristalinas de los derivados **28** y **29** (Figuras 4.1 y 4.2 y Tablas 4.1 y 4.2) revelan la dimerización de la entidad básica PtPb originando una especie tetranuclear neutra de estequiometría Pt_2Pb_2. Así, dos fragmentos neutros dialquinilplatinato(II) tris(pirazolil)boratoplomo(II) $[\{Pt(bzq)(C{\equiv}CR)_2\}\{Pb(HBpz_3)\}]$ se conectan entre sí a través de interacciones muy débiles $Pb^{II}\cdots\eta^2(C{\equiv}C)$ entre los acetiluros del sustrato de platino $[Pt(bzq)(C{\equiv}CR)_2]^-$ y el plomo del grupo $[Pb(HBpz_3)]^+$ de otra unidad para generar las especies tetranucleares $[\{Pt(bzq)(C{\equiv}CR)_2\}\{Pb(HBpz_3)\}]_2$.

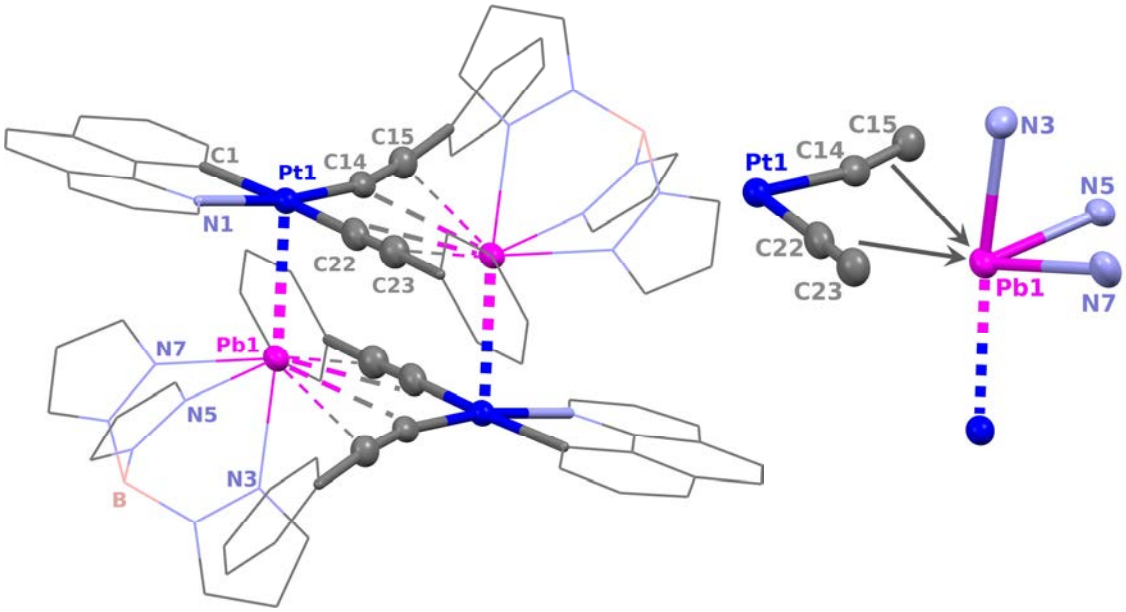

Figura 4.1: Estructura molecular del compuesto $[\{Pt(bzq)(C{\equiv}CPh)_2\}\{Pb(HBpz_3)\}]_2$ (**28**) y entorno de coordinación del Pb^{2+}

Tabla 4.1: Distancias [Å] y ángulos [º] más representativos de **28**

28			
Pt(1)-N(1)	2.066(7)	Pt(1)-C(1)	2.063(7)
Pt(1)-C(14)	2.019(9)	Pt(1) -C(22)	2.011(8)
C(14)-C(15)	1.203(12)	C(22)-C(23)	1.226(11)
Pb(1)-C(14)	3.027(8)	Pb(1)-C(22)	2.951(9)
Pb(1)-C(15)	3.132(8)	Pb(1)-C(23)	3.142(9)
Pb(1)-N(3)	2.499(6)	Pb(1)-N(5)	2.556(7)
Pb(1)-N(7)	2.432(6)	Pt(1)-Pb(1)	3.2313(4)
Pb(1)-Pt(1)-N(1)	87.25(18)	Pb(1)-Pt(1)-C(1)	104.20(19)
Pb(1)-Pt(1)-C(14)	95.1(2)	Pb(1)-Pt-(1)C(22)	81.6(2)
Pt(1)-C(14)-C(15)	176.6(7)	C(14)-C(15)-C(16)	178.4(9)
Pt(1)-C(22)-C(23)	168.1(7)	C(22)-C(23)-C(24)	174.4(9)
N(3)-Pb(1)-Pt(1)	168.51(16)	N(5)-Pb(1)-Pt(1)	108.13(16)
N(7)-Pb(1)-Pt(1)	91.37(14)	C(1)-Pt(1)-N(1)	80.9(3)

Tabla 4.2: Distancias [Å] y ángulos [º] más representativos de **29**·CH_2Cl_2

29· CH_2Cl_2			
Pt(1)-N(1)	2.058(5)	Pt(2)-N(2)	2.082(5)
Pt(1)-C(1)	2.044(6)	Pt(2)-C(41)	2.055(6)
Pt(1)-C(14)	1.957(6)	Pt(2)-C(54)	1.977(7)
Pt(1)-C(23)	2.014(6)	Pt(2)-C(63)	1.996(7)
C(14)-C(15)	1.223(8)	C(54)-C(55)	1.238(9)
C(23)-C(24)	1.214(9)	C(63)-C(64)	1.224(9)
Pb(1)-N(3)	2.500(5)	Pb(2)-N(9)	2.513(5)
Pb(1)-N(5)	2.492(5)	Pb(2)-N(11)	2.500(5)
Pb(1)-N(7)	2.521(6)	Pb(2)-N(13)	2.465(5)
Pb(1)-C(54)	3.124(8)	Pb(2)-C(14)	2.951(6)
Pb(1)-C(55)	3.186(8)	Pb(2)-C(15)	3.063(7)
Pb(1)-C(63)	2.966(6)	Pb(2)-C(23)	3.121(6)
Pb(1)-C(64)	3.013(5)	Pb(2)-C(24)	3.426(6)
Pt(1)-Pb(1)	3.3059(3)	Pt(2)-Pb(2)	3.0935(3)
Pb(1)-Pt(1)-N(1)	93.73(14)	Pb(2)-Pt(2)-N(2)	99.92(13)
Pb(1)-Pt(1)-C(1)	113.77(16)	Pb(2)-Pt(2)-C(41)	99.62(15)
Pb(1)-Pt(1)-C(14)	94.98(17)	Pb(2)-Pt(2)-C(54)	79.85(17)
Pb(1)-Pt(1)-C(23)	71.32(17)	Pb(2)-Pt(2)-C(63)	88.32(17)
Pt(1)-C(14)-C(15)	170.7(5)	Pt(2)-C(54)-C(55)	177.6(6)
C(14)-C(15)-C(16)	175.1(7)	C(54)-C(55)-C(56)	178.1(7)
Pt(1)-C(23)-C(24)	167.8(5)	Pt(2)-C(63)-C(64)	173.5(5)
C(23)-C(24)-C(25)	172.2(6)	C(63)-C(64)-C(65)	178.0(6)
C(1)-Pt(1)-N(1)	81.2(2)	C(41)-Pt(2)-N(2)	81.2(2)
N(3)- Pb(1)-Pt(1)	163.08(12)	N(13)- Pb(2)-Pt(2)	166.62(11)
N(5)- Pb(1)-Pt(1)	89.87(12)	N(9)- Pb(2)-Pt(2)	93.37(11)
N(7)- Pb(1)-Pt(1)	110.20(12)	N(11)- Pb(2)-Pt(2)	96.73(12)

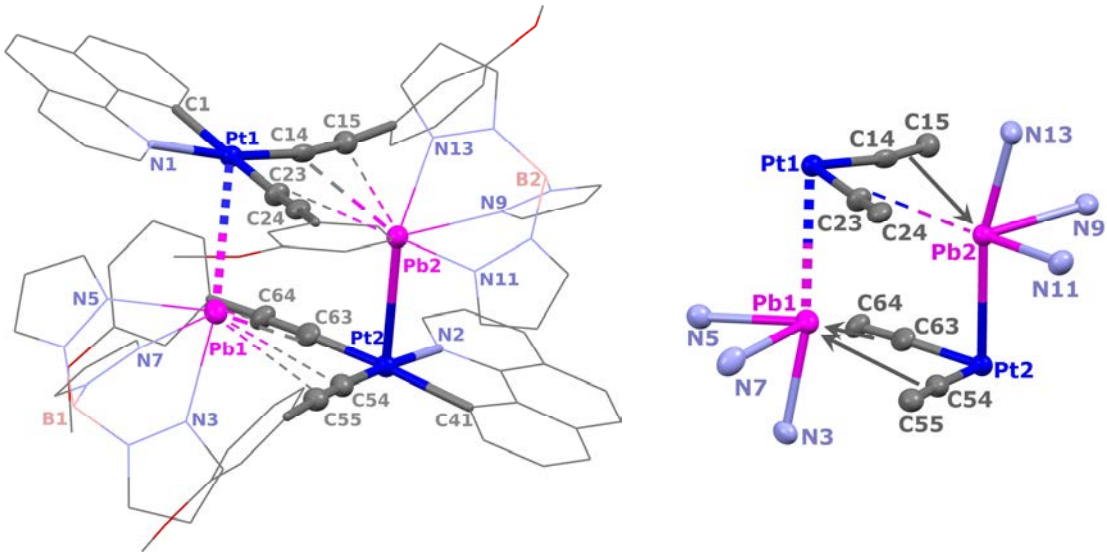

Figura 4.2: Estructura molecular del compuesto **29**·CH_2Cl_2 y entorno de coordinación del Pb^{2+}

El derivado **28** presenta un eje binario C_2 que hace que los dos fragmentos $[\{Pt(bzq)(C{\equiv}CPh)_2\}\{Pb(HBpz_3)\}]$ sean equivalentes, mientras que en el derivado **29** los fragmentos dimetálicos no son equivalentes. En consecuencia, en el derivado **28** hay una única distancia Pt-Pb [3.2313(4) Å], mientras que en **29** las distancias intermetálicas son asimétricas [Pt(1)-Pb(1) 3.3059(3), Pt(2)-Pb(2) 3.0935(3) Å]. Estas distancias son ligeramente más largas que la suma de los radios covalentes (2.82 Å),[8] pero notablemente más cortas que la suma de radios de van der Waals (3.77 Å),[9] encontrándose en el rango de las descritas en la bibliografía para otros compuestos Pt-Pb (2.642–3.313 Å).[1,4,10] Probablemente, las largas distancias intermetálicas Pt–Pb responden a la acción combinada de la presencia del ligando aniónico $[HBpz_3]^-$, que reduce la carga del ión Pb^{2+} y la escasa capacidad dadora del fragmento monoaniónico $[Pt(bzq)(C{\equiv}CR)_2]^-$. En ambos complejos el ángulo formado entre el vector Pt-Pb y la normal al plano de coordinación del Pt es de 12.34(12)º (**28**), 21.51(11)º y 11.67(9)º (**29**), lo que provoca que el ión plomo se encuentre prácticamente encima del Pt e interaccione con éste a través del orbital dz^2.

Adicionalmente, cada centro de plomo del grupo $[Pb(HBpz_3)]$ contacta débilmente con la densidad electrónica de ambos ligandos alquinilo de la otra unidad del dímero, con distancias Pb···C_α más cortas que las Pb···C_β [Pb···C_α/C_β 3.027(8), 2.951(9)/3.132(8), 3.142(9) Å **28**; 2.951(6)–3.124(8)/3.013(5)–3.426(6) Å **29**], siendo el más asimétrico el enlace Pb(2)···C(23)≡C(24) en el compuesto **29** [Pb···C_α/C_β

3.121(6)/3.426(6) Å]. Esta asimetría de los contactos Pb···C≡C se produce en el mismo sentido que en los derivados relacionados, previamente descritos[1,4,7] con una interacción fundamentalmente a través del C_α, pero las distancias Pb–C son significativamente más largas que en estos casos (ej. $[Pt_2Pb_2(C{\equiv}CTol)_8(acetone)_2]$ a 120 K Pb···C_α/C_β 2.693(6)–2.747(6)/2.822(7)–3.273(6) Å],[1] indicando que la interacción del Pb con los átomos de C de los alquinilos es relativamente débil. Estas distancias, sin embargo, se encuentran por debajo de la suma del radio de Van der Waals del C sp (1.78 Å)[11] y el radio covalente del plomo (1.47 Å) (suma 3.25 Å),[8] siendo las responsables de la estabilización de los dímeros en estado sólido. Los centros de Pb se disponen a 0.481 Å (**28**); 0.5381 Å Pb(1), 0.645 Å Pb(2) (**29**) del correspondiente plano de coordinación $[Pt(C{\equiv}CR)_2]$ con el que interaccionan (coordinación V-shape) y lejos del átomo de Pt. De hecho, las distancias Pt(1)–Pb(1') en **28** (3.900 Å) y en **29** [Pt(2)–Pb(1) 3.998 Å, Pt(1)–Pb(2) 3.920 Å] son claramente superiores al límite de van der Walls (3.77 Å), lo que refuerza la idea de que la estabilización del cúmulo tetranuclear, en sólido, se debe a las débiles interacciones Pb···η^2–C≡C. Por otra parte, la distancia transanular Pb···Pb [4.536 Å (**28**), 4.169 Å (**29**)] es más corta que la observada en los cúmulos $[Pt_2Pb_2(C{\equiv}CTol)_8S_X]$ (~5.131–5.436 Å) pero todavía superior a la suma de radios de van der Waals (4.04 Å), lo que descarta una interacción entre estos centros metálicos.

En el derivado **28** el núcleo metálico central $[Pt_2Pb_2]$ adopta una disposición plana (ángulo de torsión 0º) en forma de rombo ligeramente distorsionado con ángulos Pb–Pt–Pb (78.38º) y Pt–Pb–Pt (101.62º), que recuerda a algunos sistemas Pt-Tl relacionados preparados por el grupo.[12] Por su parte, el compuesto **29** presenta un núcleo romboidal no plano con un ángulo de torsión entre los enlaces Pt-Pb de 26.62º y ángulos Pb–Pt–Pb de 69.89º, 70.71º y Pt–Pb–Pt de 102.14º, 108.11º. Como puede observarse en las Figuras 4.1 y 4.2, el Pb presenta en ambos derivados un entorno octaédrico distorsionado, en el que se enlaza a los tres átomos de nitrógeno del ligando tris(pirazolil)borato, al centro de Pt de su unidad y a dos grupos alquinilo de la otra entidad. El análisis del entorno del Pb revela una ligera asimetría, con distancias Pb-N en los rangos [2.432(6)–2.556(7) (**28**); 2.492(5)–2.521(6) Pb(1); 2.465(5)–2.513(5) Å Pb(2) (**29**)], ángulo *transoidal* N3/13-Pb-Pt menor de 180º [168.51(16)º (**28**); 163.08(12)º (Pb1), 166.62(11)º (Pb2) (**29**)], y ángulos *cisoidales* N-Pb-N menores de 90º [73.35–77.98º (**28**); 72.42–76.27º (Pb1), 74.33–77.43º (Pb2) (**29**)]. Por su parte, el

ángulo formado por el centroide de los C acetilénicos, el Pb y el N en *trans* es muy inferior a 180º [146.05, 157.08º (**28**); 152.80, 153.25º (Pb1); 150.14, 156.89º Pb(2) (**29**)], lo que está de acuerdo con la coordinación V-shape para el Pb. Esta asimetría en el entorno de coordinación del Pb apuntaría a una cierta actividad del par solitario hacia el interior del dimetaciclo en la dirección transanular Pb···Pb. El resto de datos estructurales relativos al ligando $[HBpz_3]^-$ ajustan a los descritos en estructuras de polipirazolilboratos.[6,13]

La estructura del derivado trinuclear **30** (Figura 4.3, Tabla 4.3) es distinta a las anteriores y se puede describir como dos fragmentos aniónicos bis(alquinil)platinato(II) "$[Pt(bzq)(C{\equiv}CC_6H_4CF_3\text{-}4)_2]^-$" desplazados y orientados mutuamente *cis* (con disposición *anti* de los átomos de C y N en los ligandos bzq), conectados a través del catión $[Pb(HBpz_3)]^+$.

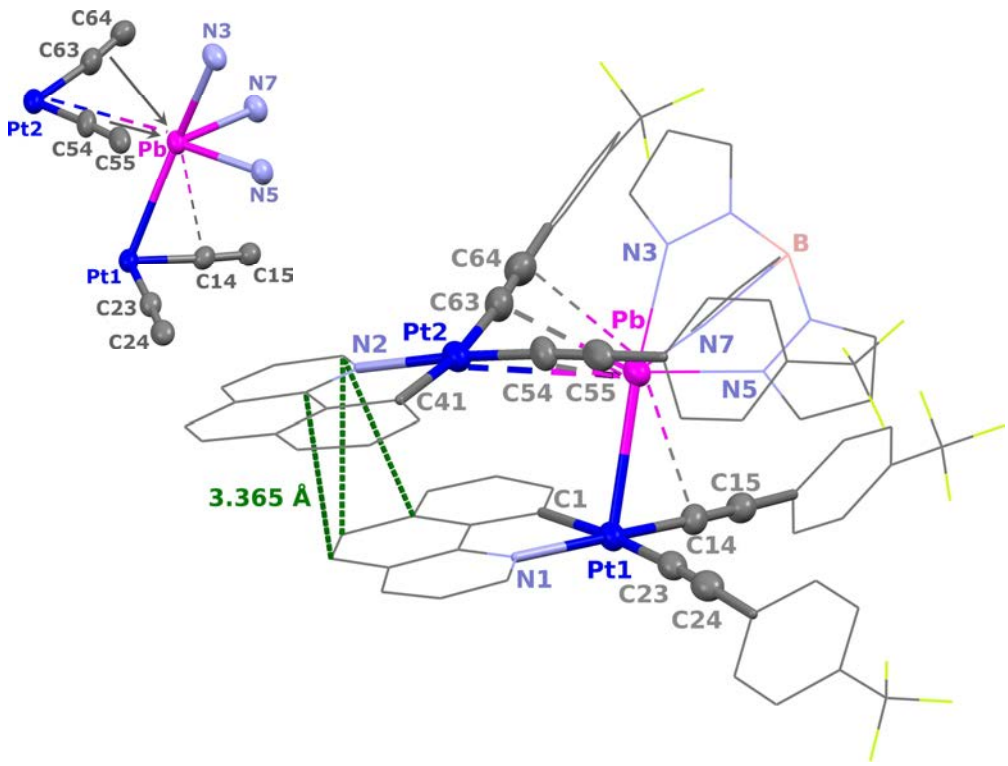

Figura 4.3: Estructura molecular del anión $[\{Pt(bzq)(C{\equiv}CC_6H_4CF_3\text{-}4)_2\}_2\{Pb(HBpz_3)\}]^-$ del compuesto **30**·$2CHCl_3$ y entorno de coordinación del Pb^{2+}

Tabla 4.3: Distancias [Å] y ángulos [º] más representativos de **30**·2$CHCl_3$

30·2$CHCl_3$			
Pt(1)-N(1)	2.083(5)	Pt(2)-N (2)	2.077(6)
Pt(1)-C(1)	2.049(6)	Pt(2)-C(41)	2.036(7)
Pt(1)-C(14)	1.952(6)	Pt(2)-C(54)	1.957(6)
Pt(1)-C(23)	2.028(6)	Pt(2)-C(63)	2.028(7)
C(14)-C(15)	1.218(8)	C(54)-C(55)	1.211(9)
C(23)-C(24)	1.198(9)	C(63)-C(64)	1.214(10)
Pb-C(54)	2.928(6)	Pb-C(63)	2.898(8)
Pb-C(55)	3.057(6)	Pb-C(64)	3.180(8)
Pb-C(14)	3.111(7)	Pb-N(5)	2.473(5)
Pb-N(3)	2.533(5)	Pb-N(7)	2.531(5)
Pt(1)-Pb	3.1125(3)	Pt(2)-Pb	3.6214(4)
C(1)-Pt(1)-N(1)	80.8(2)	C(41)-Pt(2)-N(2)	81.4(3)
Pt(1)-C(14)-C(15)	174.8(5)	Pt(2)-C(54)-C(55)	176.3(6)
C(14)-C(15)-C(16)	175.9(7)	C(54)-C(55)-C(56)	177.3(7)
Pt(1)-C(23)-C(24)	177.0(6)	Pt(2)-C(63)-C(64)	174.7(6)
C(23)-C(24)-C(25)	175.5(6)	C(63)-C(64)-C(65)	178.3(7)
N(3)-Pb-Pt(1)	162.41(12)	N(5)-Pb-Pt(1)	97.61(13)
N(7)-Pb-Pt(1)	117.76(13)	Pt(1)-Pb-Pt(2)	85.35(1)

Esta disposición estructural se parece a las encontradas en el derivado $(NBu_4)[\{Pt(bzq)(C{\equiv}CC_6H_4CF_3\text{-}4)_2\}_2\{Pb(O_2ClO_2)\}]$ previamente descrita por el grupo,[4] aunque muestra algunas diferencias. Así, en el anión $[\{Pt(bzq)(C{\equiv}CC_6H_4CF_3\text{-}4)_2\}_2Pb(O_2ClO_2)]^-$ el Pb^{2+} se coordina, aunque de forma asimétrica, a los dos platinos y a los cuatro ligandos alquinilo (dos de cada unidad) y completa su coordinación con dos enlaces asimétricos Pb–O (perclorato). Sin embargo, en el anión **30**$^-$, el Pb de la unidad $[Pb(HBpz_3)]^+$ se enlaza sólo al Pt de uno de los fragmentos [Pt–Pb(1) 3.1125(3) Å] y completa su entorno de coordinación interaccionando de forma más débil con el platino y los ligandos alquinilo de la segunda unidad [Pb–Pt(2) 3.6214(4) Å, Pb···C_α 2.898(8), 2.928(6) Å, Pb···C_β 3.057(6), 3.180(8) Å] y uno de los C_α, de la primera unidad [Pb···C_α 3.111 Å]. Tanto las distancias Pt–Pb como las interacciones Pb···η^2–C≡C son claramente más largas que las encontradas en el anión $[\{Pt(bzq)(C{\equiv}CC_6H_4CF_3\text{-}4)_2\}_2Pb(O_2ClO_2)]^-$ [Pt–Pb 2.875(5), 3.3136(5) Å; Pb···C_α 2.630(9)–2.772(10) Å].[4] Esto es de esperar ya que el ligando tridentado tris(pirazolil)borato $[HBpz_3]^-$ cede más densidad electrónica al átomo de plomo que el grupo bidentado $O_2ClO_2^-$ y presenta, además, un mayor impedimento estérico que este último. Este hecho provoca una menor interacción del ión Pb^{II} con los dos fragmentos de platino. El ángulo Pt–Pb–Pt en **30**$^-$ es menos agudo [85.35(1)º] que el observado en $[\{Pt(bzq)(C{\equiv}CC_6H_4CF_3\text{-}4)_2\}_2Pb(O_2ClO_2)]^-$ (~76º).

El entorno de coordinación del Pb se podría describir como bipirámide pentagonal distorsionada con el Pb coordinado en el eje axial al centro de Pt(1) y al N(3) [Pt(1)–Pb–N(3) 162.41(12)] del pirazolato y en el ecuatorial a los C≡C, a dos N de los grupos pirazolatos y al segundo centro de Pt(2). La notable asimetría de este entorno sugiere que el par solitario del Pb^{2+} es estereoquímicamente más activo que en los derivados **28** y **29**. Como consecuencia de esta asimetría, los ligandos benzoquinolato, aunque desplazados, se encuentran parcialmente eclipsados con una separación mínima entre ellos de 3.365 Å, que está en el rango descrito para las interacciones π···π, lo que podría contribuir a la estabilidad del anión (Figura 4.3).

Cada uno de los derivados estudiados presenta un empaquetamiento supramolecular diferente. Así, en el derivado **28** los dímeros $[\{Pt(bzq)(C{\equiv}CPh)_2\}\{Pb(HBpz_3)\}]_2$ empaquetan a través de interacciones secundarias débiles con distancias mínimas relativamente largas [2.615–2.862 Å ($H_{pz}\cdots\pi_{bzq}$), 2.800, 2.828 Å ($C_{pz}\cdots H_{bzq}$), 2.894 Å ($C_{Ph}\cdots H_{bzq}$), 3.285 Å ($C_{ph}\cdots C_{bzq}$), 2.792 Å ($C_{pz}\cdots H_{Ph}$)] (Figura 4.4). Por su parte, el derivado **29** empaqueta formando cadenas estabilizadas principalmente mediante interacciones π···π no paralelas entre los anillos ciclometalados (3.344 Å) (Figura 4.5 a en negro). Estas cadenas forman láminas a través de contactos bzq···bzq adicionales más desplazados (3.384 Å), como se refleja en la Figura 4.5 b (en naranja).

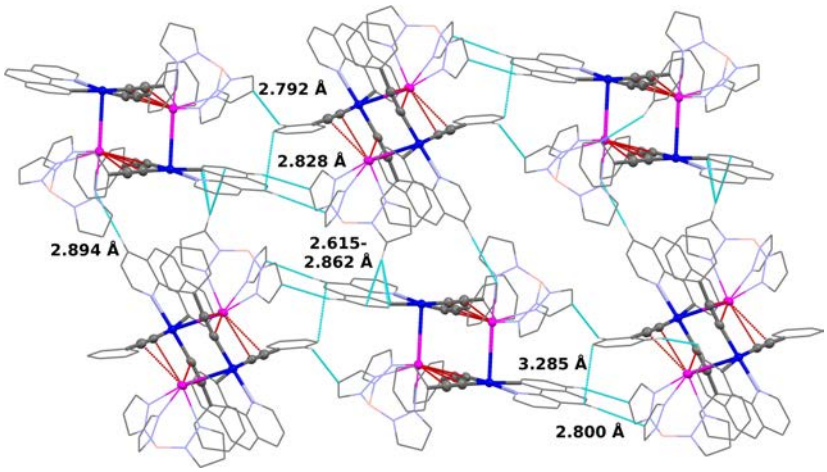

Figura 4.4: Estructura supramolecular de $[\{Pt(bzq)(C{\equiv}CPh)_2\}\{Pb(HBpz_3)\}]_2$ (**28**)

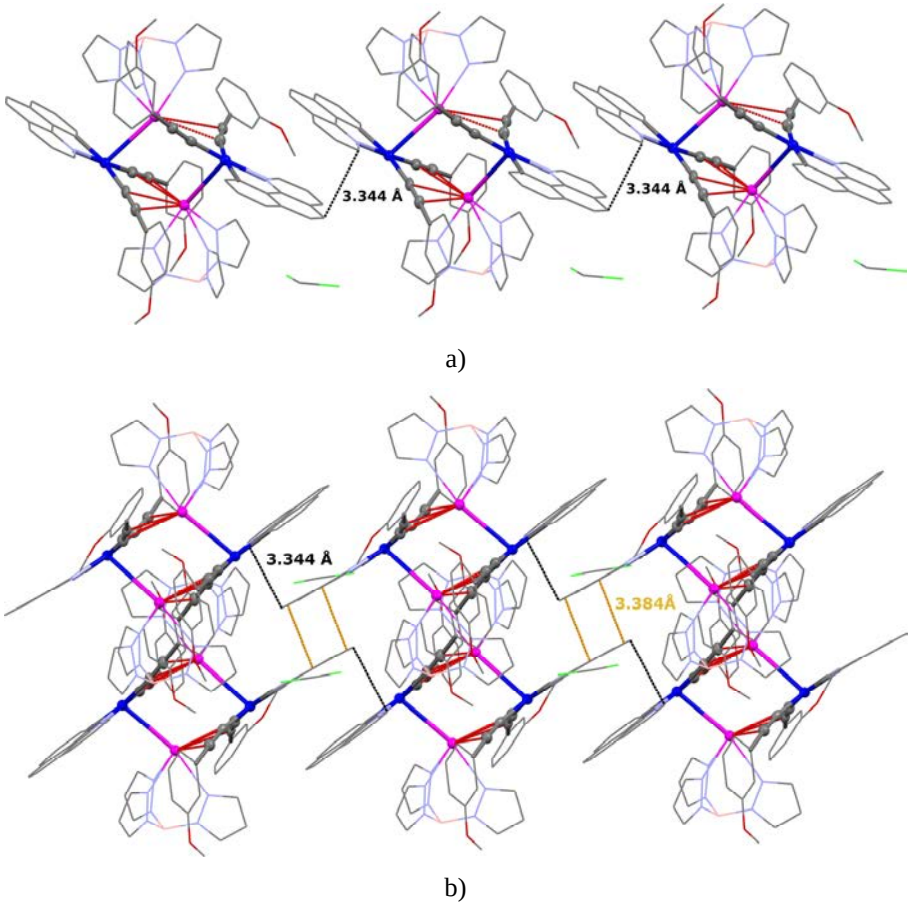

Figura 4.5: Estructura supramolecular de [{Pt(bzq)(C≡CC_6H_4OMe-3)$_2$}{Pb(HBpz_3)}]$_2$·CH_2Cl_2 (**29**·CH_2Cl_2) a) disposición en cadenas de las moléculas b) interacción entre las cadenas

En el derivado **30** los aniones $[Pt_2Pb]^-$ contactan formando dímeros mediante interacciones desplazadas bzq···bzq (3.233 Å) (Figura 4.6a en negro). Estos dímeros interaccionan entre sí a través de interacciones débiles entre los carbonos alquinílicos del fragmento PtPb [{Pt(bzq)(C≡C$C_6H_4CF_3$-4)$_2$}{Pb(HBpz_3)}] y el catión NBu_4^+ (2.735–2.896 Å) (Figura 4.6b en azul) e interacciones $H_{NBu_4}\cdots H_{bzq}$ (Figura 4.6b en naranja, 2.354 Å), $H_{pz}\cdots F_{CF3}$ (Figura 4.6b en violeta, 2.504 Å) y $H_{NBu_4}\cdots F_{CF_3}$ (Figura 4.6b en rosa, 2.636 Å) o entre H_{Ph}/C,H_{NBu_4}/F_{CF_3}/π_{bzq}/π_{Ph} y las moléculas de $CHCl_3$ de cristalización (Figura 4.6b en marrón).

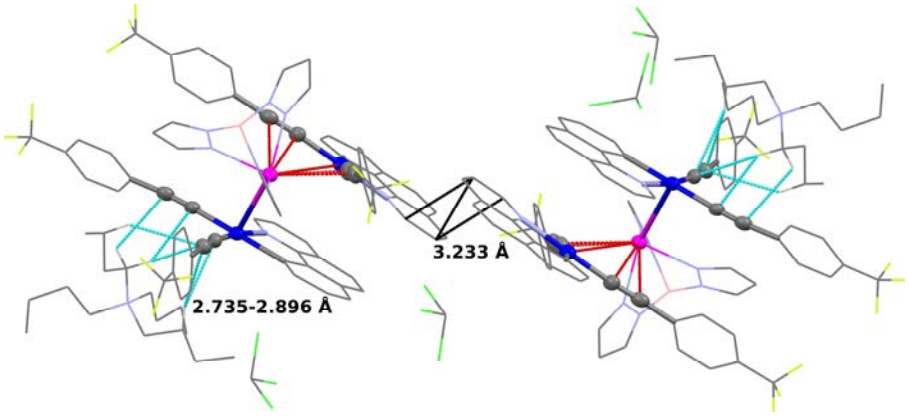

a)

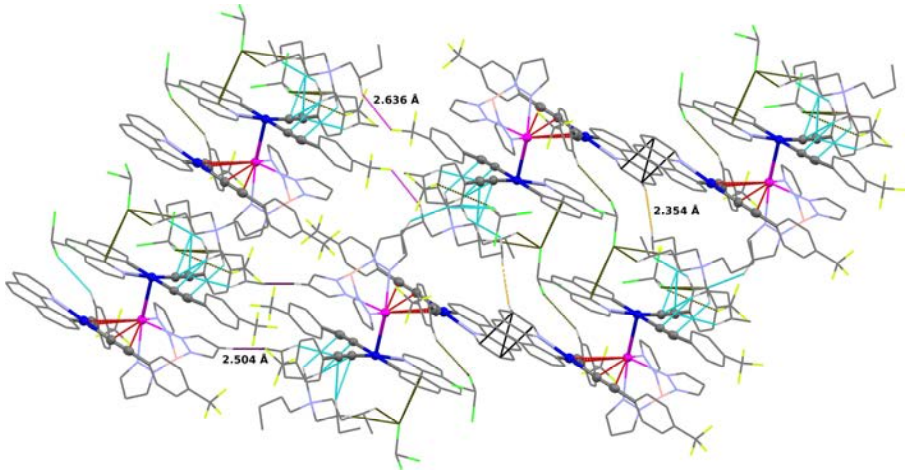

b)

Figura 4.6: Estructura supramolecular de $(NBu_4)[\{Pt(bzq)(C{\equiv}CC_6H_4CF_3\text{-}4)_2\}_2\{Pb(HBpz_3)\}]\cdot 2CHCl_3$ (**30**$\cdot 2CHCl_3$). La interacción bzq···bzq intramolecular dentro del cúmulo se ha omitido por claridad

4.1.2 Caracterización espectroscópica

Los clusters **28**–**30** se han caracterizado mediante las técnicas espectroscópicas habituales. Los espectros de masas (MALDI+) de los derivados **28** y **29** muestran picos que ajustan bien para el fragmento dinuclear $[\{Pt(bzq)(C{\equiv}CR)_2\}\{Pb(HBpz_3)\}]^+$ y los correspondientes a la pérdida de uno (**28**, **29**) o dos (**29**) ligandos alquinilo. Desafortunadamente, no se observa el pico correspondiente al fragmento tetranuclear $[\{Pt(bzq)(C{\equiv}CR)_2\}\{Pb(HBpz_3)\}]_2$, aunque en ambos se observa el pico con pérdida de un fragmento $[HBpz_3]^+$ ($[M–HBpz_3]^+$). Otro pico interesante es el correspondiente al fragmento ($[M/2+Pb(HBpz_3)]^+$) (**28**, **29**). Por su parte, en el espectro de masas (MALDI-) del derivado **30** se observan los picos moleculares con pérdida de NBu_4^+

correspondientes a [{Pt(bzq)(C≡CC$_6$H$_4$CF$_3$-4)$_2$}$_2${Pb(HBpz$_3$)}]$^-$ ([M-NBu$_4$]) y a [{Pt(bzq)(C≡CC$_6$H$_4$CF$_3$-4)$_2$}$_2${Pb}] ([M-NBu$_4$-HBpz$_3$]$^+$).

La conductividad molar del derivado aniónico **30** en CH$_3$CN 5 x 10^{-4} M (98 Ω^{-1}cm^{2}mol^{-1}) se acerca a los valores establecidos para un electrolito 1:1, aunque queda un poco por debajo, mientras que la conductividad de los derivados **28** y **29** en CH$_3$CN indican que las unidades neutras se mantienen en disolución.

Los espectros de IR de los derivados **28** y **29** muestran varias bandas de intensidad media–fuerte en el rango 2094-2060 cm^{-1} (**28**) y 2085, 2060 cm^{-1} (**29**) ligeramente desplazadas a menores frecuencias respecto a las observadas en los precursores (2103, 2090 R = Ph;[5] 2096, 2077 cm^{-1} R = C$_6$H$_4$OMe-3[7]), lo que sugiere una debilitación del triple enlace C≡C por la interacción π del centro de plomo con los fragmentos alquinílicos. El derivado **30** presenta tres bandas $\nu_{C\equiv C}$ en el rango 2111 a 2070 cm^{-1} con un hombro a 2040 cm^{-1} (precursor 2105, 2082 cm^{-1} R = C$_6$H$_4$CF$_3$-4[5]) en coherencia con la presencia de dos grupos alquinilo terminales y dos grupos que interaccionan con los iones Pb^{II}.

Tabla 4.4: Señales más características del grupo bzq en el RMN de ^{1}H (CDCl$_3$, δ en ppm, *J* en Hz) de los compuestos **28**–**30** y sus precursores

R =	Ph			C$_6$H$_4$OMe-3			C$_6$H$_4$CF$_3$-4		
	28	**Precursor[a]**	**Δ**	**29**	**Precursor[b]**	**Δ**	**30**	**Precursor[a]**	**Δ**
H^2	9.82	10.17	0.35	9.80	10.03	0.23	9.67	10.10	0.43
J^{195}Pt-H	29.6	25.0		31.2	28.7		28.7	27.3	
H^4	8.15	8.49	0.34	8.14	8.19	0.05	7.91	8.53	0.62
H^9	8.60	8.63	0.03	8.58	8.56	-	8.40	8.54	0.14
J^{195}Pt-H	38.9	43.0		38.6	38.8	0.02	37.7	41.0	

[a] RMN registrado en CD$_3$COCD$_3$[5], [b] CDCl$_3$[7]

Los espectros de RMN de ^{1}H a temperatura ambiente, asignados en base a espectros de correlación 2D COSY ^{1}H-^{1}H, confirman la interacción del centro de plomo con los fragmentos de platino (Ver Figura 4.7). En todos los derivados sólo se observa un grupo de señales para la bzq, por lo que, en el compuesto **30** los dos fragmentos de Pt(bzq)(C≡CC$_6$H$_4$CF$_3$-4)$_2$ se promedian en disolución durante el tiempo de respuesta de la técnica a temperatura ambiente. Las resonancias correspondientes al H^2, H^4 y H^9,

especialmente H^2, aparecen desplazadas a menores frecuencias en relación a las observadas en los precursores $(NBu_4)[Pt(bzq)(C{\equiv}CR)_2]$[5,7] (Tabla 4.4). Las constantes de acoplamiento a ^{195}Pt, características para H^2, H^9 y visibles en los compuestos **28**–**30**, son similares a las observadas en los precursores. Como se observa en la Tabla 4.4, el desplazamiento de las señales de los protones H^2 y H^4 es claramente menor en los derivados tetranucleares **28** y **29** que en el derivado trinuclear **30**, lo que está de acuerdo con una diferente interacción entre el centro de plomo y el sustrato de platino. Además, los espectros también confirman la presencia del grupo tris(pirazolil)borato, observándose como señal más característica un singlete en el rango 5.80-5.92 ppm asignada al protón H^4 de los grupos pirazolato, mientras que en el derivado **30** también se observan las señales características del grupo NBu_4^+.

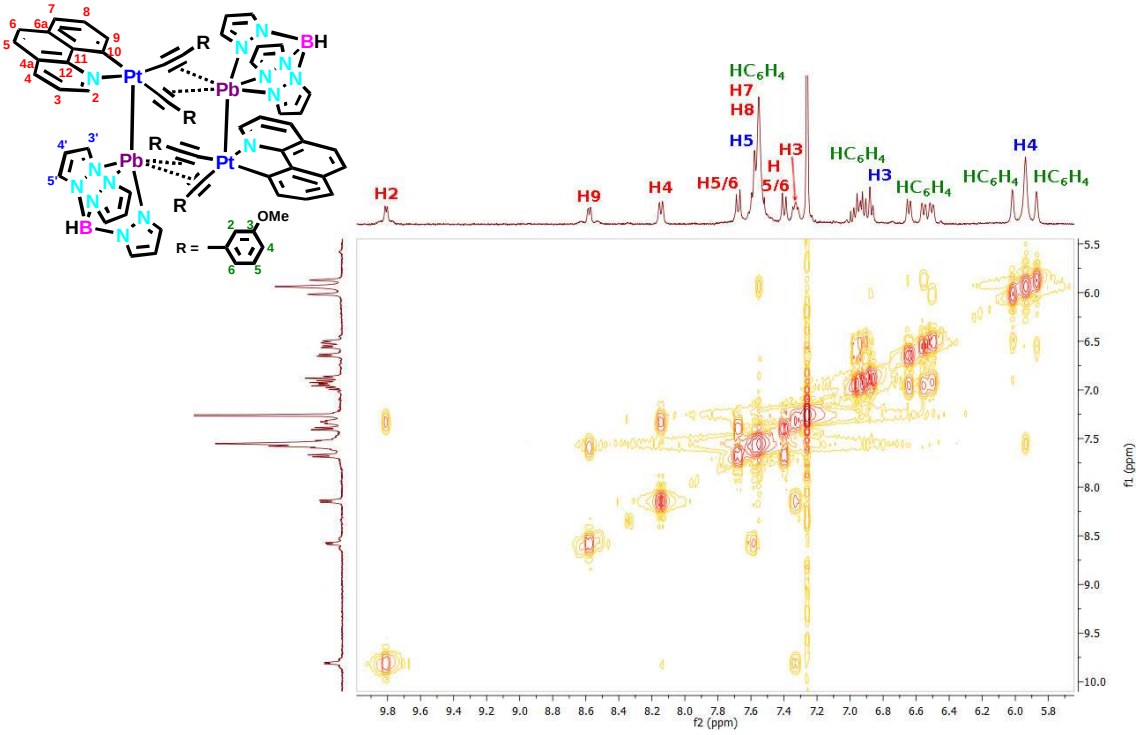

Figura 4.7: Sección del espectro de correlación ^1H-^1H del derivado **29** en $CDCl_3$

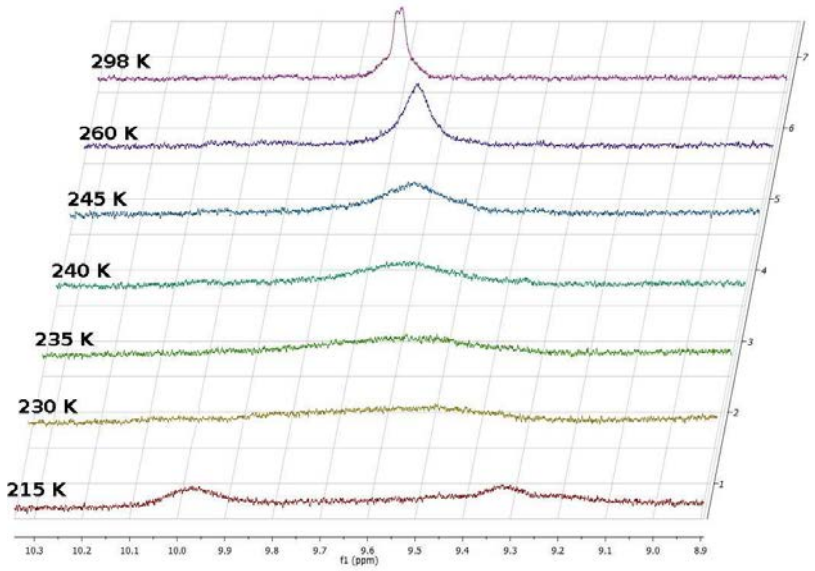

Figura 4.8: Sección de los espectros de RMN de ^{1}H en $CDCl_3$ a temperatura variable del complejo **30**

Se ha llevado a cabo un estudio de los espectros de RMN de ^{1}H del derivado **30** a temperatura variable (Figura 4.8). Se observa que al disminuir la temperatura las señales correspondientes al ligando bzq se ensanchan, llegando a la coalescencia a 230 K. A temperaturas inferiores a la de coalescencia se observa la aparición de 2 grupos de señales asignables al ligando bzq, lo que nos permite afirmar que el proceso que promediaba los grupos "Pt(bzq)(C≡C$C_6H_4CF_3$-4)$_2$" en disolución se frena al disminuir la temperatura. Desafortunadamente, la presencia de este equilibrio nos impide estudiar los posibles equilibrios de ruptura del cluster trinuclear **30**.

Debido a la baja solubilidad del compuesto **28** solamente se han podido registrar los espectros de RMN de ^{13}C de los derivados **29** y **30** aunque con baja resolución, incluso después de largos periodos de acumulación, en los que no se llegan a observar señales debidas a los carbonos cuaternarios. A pesar de esto, en ambos espectros se observa la presencia tanto del ligando ciclometalado bzq como del grupo tris(pirazolil)borato, siendo las señales más características de ambos grupos las asignadas al C^2 del grupo bzq (δ 150.5 **29**, 150.2 **30**) y al C^4 del tris(pirazolil)borato (δ 104.4).

El espectro de $^{195}Pt\{^{1}H\}$ del compuesto más soluble **29** muestra la presencia de un singlete a δ −3208, notablemente desapantallado respecto al correspondiente precursor (δ −3845), en coherencia con el decrecimiento en la densidad electrónica del

átomo de Pt debido a la formación del enlace Pt–Pb. Desafotunadamente, incluso con prolongada acumulación no se detectan los satélites por acoplamiento a Pb.

Como se ha observado en el estudio estructural, la entidad tetranuclear de los derivados **28** y **29** está formada por dos entidades dinucleares PtPb que interaccionan entre sí a través de contactos débiles $Pb^{II}\cdots\eta^2$–C≡C, que pueden romperse en disolución (Esquema 4.2). Con el fin de conocer la naturaleza de estas entidades en disolución se ha llevado a cabo un análisis de la estructura en disolución de estos derivados, mediante experimentos de difusión unidimensional PGSE ("Pulse Field Gradient Spin Echo")[14] y bidimensional DOSY ("Diffussion Ordered Spectroscopy")[15] y un estudio de RMN de ^{1}H a temperatura variable (en **28**).

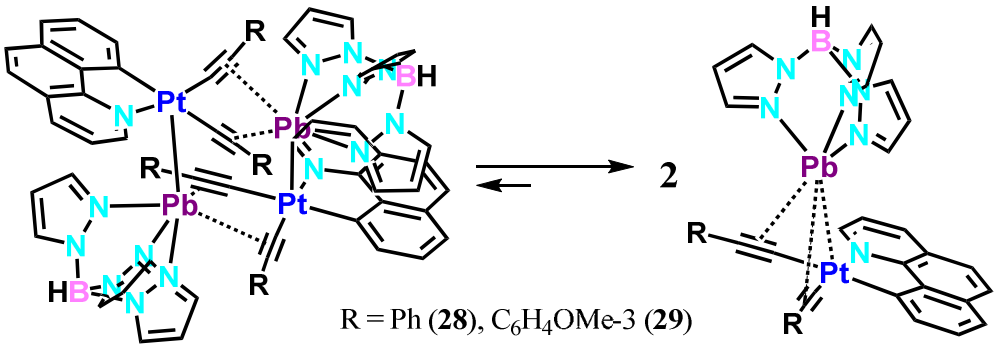

Esquema 4.2: Equilibrio propuesto entre las entidades tetra y binucleares para los derivados **28** y **29**

$$D = \frac{K_B T}{6\pi\eta r_H}$$

a)

$$I = I_o \exp(-D(2\pi\gamma \cdot \delta \cdot g)^2(\Delta - \delta/3) \cdot 10^4$$

b)

D = Coeficiente de Difusión,

η = Viscosidad del Disolvente

K_B = Constante de Boltzman

r_H = Radio hidrodinámico

I = Intensidad de la señal

I_o = Intensidad de la señal sin usar gradientes

Δ = Tiempo de Difusión

δ = Duración del gradiente

g = Fuerza del gradiente

γ = constante giromagnética

Ecuación 4.1: a) Ecuación de Stokes-Einstein, b) Ecuación de Stejskal-Tanner

La técnica PGSE permite medir el coeficiente de Difusión (D) de una molécula en una muestra de RMN y relacionarlo con el radio hidrodinámico (r_H) de dicha molécula en disolución mediante la ecuación de Stokes-Einstein (Ecuación 4.1a). Este método es útil para obtener una estimación rápida del tamaño molecular, ya que el radio hidrodinámico así calculado está correlacionado con el radio obtenido para la molécula en estado sólido mediante difracción de Rayos X de monocristal.[14]

El estudio de PGSE ^{1}H se ha llevado a cabo usando una secuencia de pulsos "Double Stimulated Echo Pulse Sequence" (Double STE)[16] en el que la intensidad de la señal (I) a un tiempo de relajación constante depende de la fuerza del gradiente (g) mediante la Ecuación 4.1b.

Los espectros se realizaron usando una disolución 0.2mM del compuesto **28** en $CDCl_3$ a 298 K actuando el disolvente como estandard interno, con una secuencia de pulsos de 90º. La duración del gradiente (δ) fue de 2 ms, el tiempo de difusión de 200 ms y la fuerza del gradiente g fue variando durante el experimento. Los espectros se adquirieron usando 32 K puntos. En la Figura 4.9a se muestra una sección de los espectros de RMN del experimento PGSE. Como se observa, la intensidad de las señales elegidas correspondientes al $H^{5'}$ del grupo pirazolato y del disolvente $CDCl_3$ disminuyen a medida que aumenta el gradiente. En la gráfica mostrada en la Figura 4.9b, generada usando el algoritmo exponencial estándar implementado en el software TOPSPIN, se representa la intensidad de la señal $H^{5'}{}_{pz}$ (I) frente a g, observándose una curva exponencial que permite obtener el coeficiente de Difusión D (7.781×10^{-10} m^2/s).

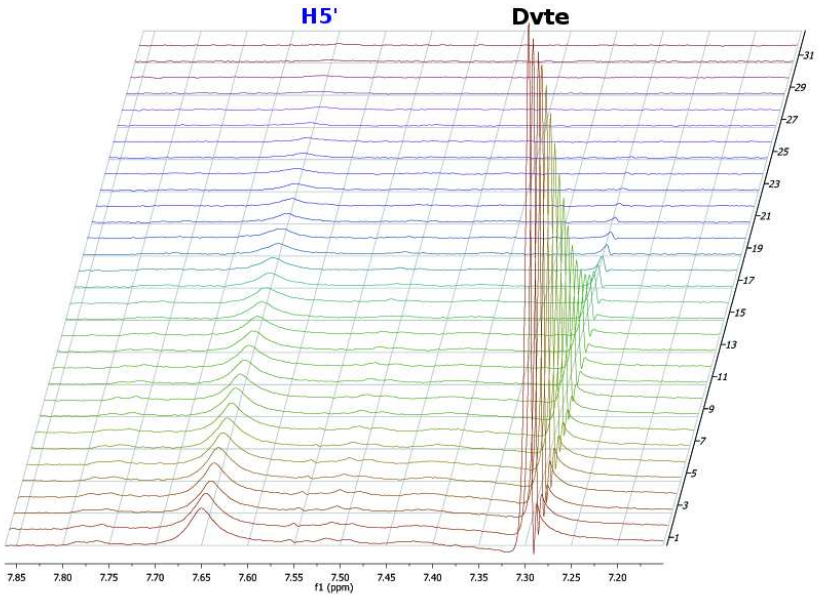

a)

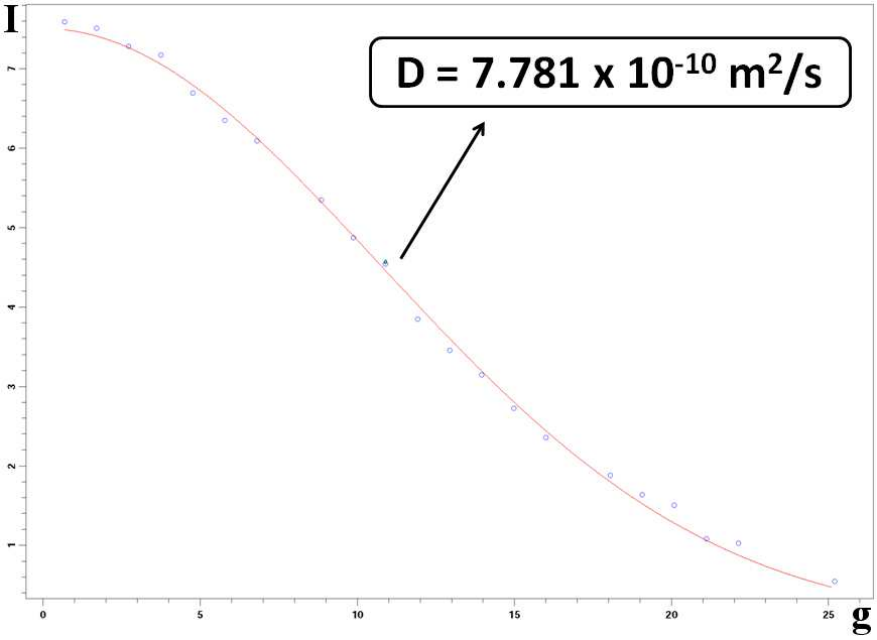

b)

Figura 4.9: a) Sección de los espectros de PGSE RMN de ^{1}H en $CDCl_3$ del complejo **28**, b) Representación gráfica de la I de la señal asignada al $H^{5'}_{pz}$ frente a g de donde se obtiene el Coeficiente de Difusión D del derivado **28**

La versión bidimensional de los espectros PGSE se conoce como DOSY y se ha aplicado con éxito en la caracterización de compuestos organometálicos en disolución,[17] análisis de mezclas,[18] identificación de enlaces de hidrógeno,[19] intercambios químicos[20] o caracterización de agregados moleculares o especies poliméricas.[17b,21]

Con el fin de comprobar la validez del valor de D obtenido mediante los espectros unidimensionales PGSE se ha correlacionado este valor con el obtenido a partir de los espectros bidimensionales DOSY.

Como se observa en la Figura 4.10 en el eje horizontal (ppm) aparecen las señales típicas del espectro de RMN de ^{1}H del derivado **28**, mientras que en el eje vertical (log D) éstas se resuelven en tantos grupos como derivados hay en la mezcla. En nuestro caso se observa un grupo de varias señales asignadas al derivado **28** y otro grupo de una señal asignado al disolvente. Además, vemos que el disolvente (log D = -8.569; D = 2.698 x 10^{-9} m^2/s) difunde más rápido que el compuesto **28** (log D = -9.108; D = 7.798 x 10^{-10} m^2/s) y que por tanto presenta un coeficiente de difusión mayor.

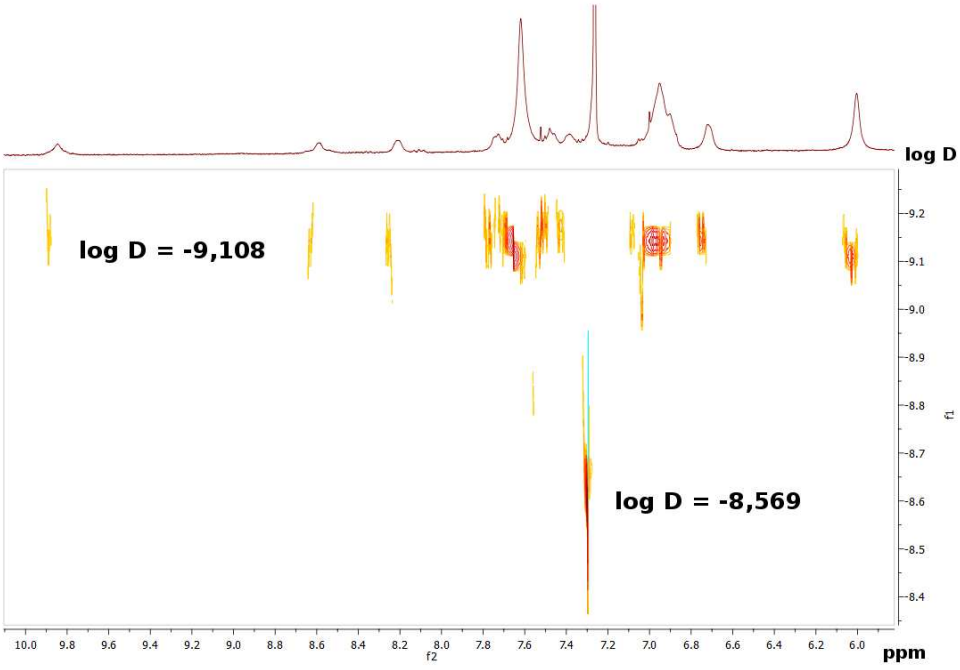

Figura 4.10: Espectro DOSY de ^{1}H del derivado **28**

Si se compara el valor de D para el derivado **28** obtenido mediante el espectro de bidimensional DOSY (D = 7.798 x 10^{-10} m^2/s) con el obtenido de los espectros unidimensionales PGSE (D = 7.781 x 10^{-10} m^2/s) se observa que estos valores son prácticamente iguales, lo que apoya tanto el resultado obtenido mediante los espectros unidimensionales como el valor de D. Una vez hallado el coeficiente de Difusión, y tomando como valor más exacto el obtenido mediante el estudio unidimensional podemos calcular con ayuda de la ecuación de Stokes-Einstein (Ecuación 4.1a) el r_H,

obteniendo un valor de 5.48 Å. Un estudio similar de PGSE en el derivado **29** aporta un valor de D de 6.753 x 10^{-10} m^2/s y un valor de r_H de 6.34 Å.

Para calcular el radio molecular teórico del derivado **28** y poder compararlo con el r_H obtenido experimentalmente se ha estimado el diámetro de una hipotética esfera formada por la molécula de la unidad tetranuclear a partir de los valores obtenidos por difracción de Rayos X, considerando la media entre la distancia máxima entre los dos grupos benzoquinolato (15.26 Å) y la distancia entre los dos átomos de B (11.56 Å). El diámetro así obtenido es ligeramente superior a 13 Å (13.41 Å), por lo que podemos asumir que el derivado tetranuclear **28** presenta un radio molecular de aproximadamente 6.5 Å, valor muy superior al r_H experimental en disolución, lo que pone en duda la presencia de la unidad tetranuclear en disolución. Otro método para calcular el volumen teórico tanto de la entidad binuclear como de la tetranuclear se basa en dividir el volumen de la celdilla unidad entre el número de entidades binucleares (4) o tetranucleares (2). En este método asumimos que se comete un gran porcentaje de error debido a que la estructura de la entidad binuclear se asemeja más a una pirámide que a una esfera. Aún así, el radio molecular obtenido para la entidad binuclear (5.78 Å) es claramente más cercano al obtenido experimentalmente (5.93 Å) que el obtenido para la tetranuclear tanto por este método (8.82 Å) como por el explicado anteriormente (6.5 Å). Para el derivado **29** el r_H teórico aplicando el volumen de la celdilla unidad es 7.36 Å para la entidad dinuclear y 9.27 Å para la tetranuclear, con lo que el r_H experimental 6.34 Å se acerca más a la binuclear. Estos cálculos apuntan a la ocurrencia de un proceso de disociación rápido de la entidad tetranuclear en disolución, manteniéndose las especias binucleares como especies mayoritarias (Esquema 4.2).

Por otro lado, por consideraciones entrópicas, podemos asumir que al disminuir la temperatura de la disolución este equilibrio se desplazaría en cierto grado hacia la izquierda, incrementándose la proporción de la entidad tetranuclear. Además, como se representa en el Esquema 4.2, podemos suponer que en la entidad binuclear el grupo $[Pb(HBpz_3)]$ podría cambiar su disposición desplazándose el Pb hacia los ligandos acetiluro de su fragmento de Pt y colocando el ligando tris(pirazolil)borato en una posición más perpendicular respecto al plano del platino que la observada en la entidad tetranuclear. Todo esto provocaría un desplazamiento de las señales de los espectros de RMN de ^1H al variar su temperatura.

Como se observa en la Figura 4.11 para el derivado **28** las señales representativas debidas a los hidrógenos H^2 y H^4 del grupo bzq, la asignada al $H^{4'}$ del grupo tris(pirazolil)borato y la asociada al H^2 del fenilo del ligando acetiluro se desplazan a frecuencias menores al disminuir la temperatura (δ 9.82, 298 K *vs* 9.69, 233 K H^2_{bzq}; 8.15, 298 K *vs* 8.06, 233 K H^4_{bzq}; 6.00, 298 K *vs* 5.84, 233 K $H^{4'}_{pz}$; 6.68, 298 K *vs* 6.46, 233 K H^2_{Ph}), mientras que la señal debida al H^9 se desplaza ligeramente hacia frecuencias mayores (δ 8.60, 298 K *vs* 8.66, 233 K H^9). Este resultado apoyaría un posible desplazamiento del equilibrio hacia la formación de las especies tetranucleares mediante asociación de las binucleares al disminuir la temperatura.

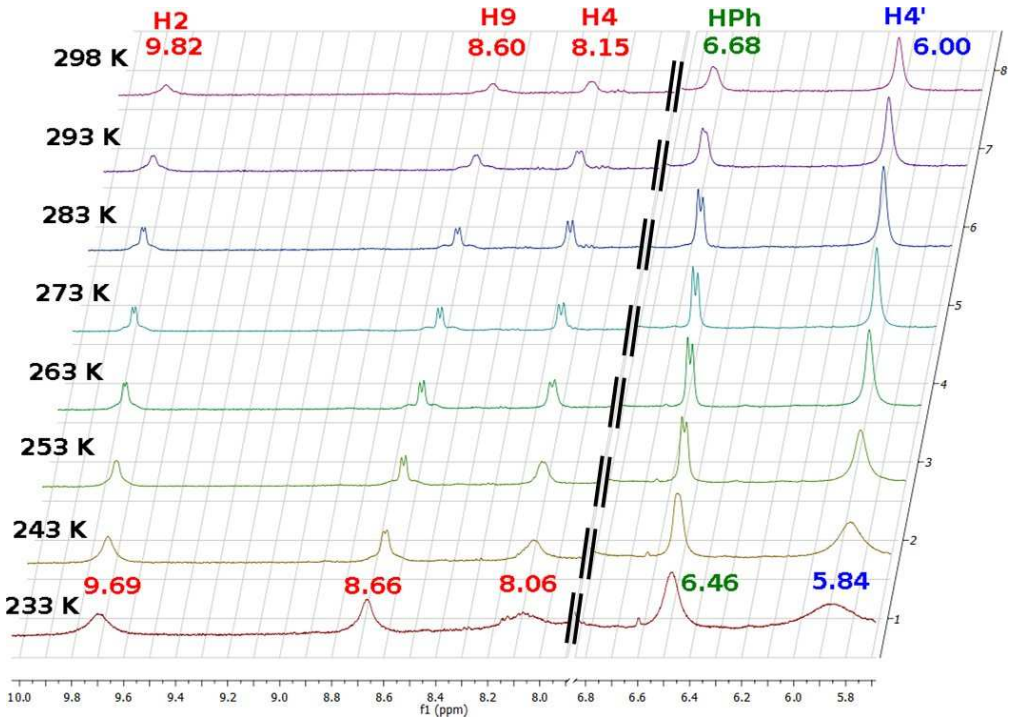

Figura 4.11: Secciones de los espectros de RMN de ^1H (en $CDCl_3$) del derivado **28** a varias temperaturas, donde se observan las variaciones en el desplazamiento de las señales asignadas a los hidrógenos H^2, H^9 y H^4 del ligando bzq (en rojo), H^2 del grupo fenilo (en verde) y $H^{4'}$ del ligando tris(pirazolil)borato (en azul) al variar la temperatura

Por tanto, y basándonos en los desplazamientos observados en las señales de RMN ^1H al variar la temperatura y en la similitud entre el radio hidrodinámico obtenido experimentalmente mediante espectros PGSE y el obtenido de la estructura de rayos X para la entidad binuclear, se puede concluir que la disolución a temperatura ambiente de los derivados **28** y **29** está formada por la entidad binuclear [{Pt(bzq)(C≡CR)$_2$}{Pb(HBpz$_3$)}] debido a la ruptura de las interacciones $Pb^{II}\cdots\eta^2$–C≡C en la entidad tetranuclear.

4.2 Propiedades ópticas

Como se ha comentado anteriormente, apenas se han estudiado las propiedades espectroscópicas de sistemas que contienen enlaces M···Pb. Con objeto de conocer más acerca de las propiedades del estado excitado de los complejos con enlaces Pt^{II}-Pb^{II}, hemos examinado las propiedades ópticas de los derivados **28**–**30**. En las Tablas 4.5 y 4.6 se recogen los datos de absorción y emisión de los tres derivados.

4.2.1 Espectros de absorción UV-Vis

Los derivados **28**–**30** muestran en disolución de CH_2Cl_2 absorciones intensas de alta energía (220–376 nm), asignadas a transiciones de tipo intraligando (^{1}IL $\pi\rightarrow\pi^*$, bzq, C≡CR) perturbadas por el platino. Los derivados **28** y **29**, probablemente monómeros [{Pt(bzq)(C≡CR)$_2$}{Pb(HBpz$_3$)}] en disolución, exhiben una absorción a baja energía, ausente en los precursores, responsable del color amarillo de las disoluciones de CH_2Cl_2 (Figura 4.12 para **29**). Esta absorción muestra una ligera dependencia con el sustituyente del ligando alquinilo (421 **28**, 424 nm **29**), observándose un desplazamiento al rojo en el complejo **29** con el sustituyente dador OMe en posición meta. Teniendo en cuenta estas características y asignaciones previas en sistemas heterometálicos relacionados con enlaces Pt–M, atribuimos de forma tentativa esta absorción de baja energía a una transición con un marcado carácter de transferencia de carga desde el fragmento "Pt(C≡CR)$_2$" a un estado que probablemente sea mezcla del ligando bzq y del fragmento {Pb(HBpz$_3$)} ^{1}L'LCT/^{1}ML'M'CT (L= bzq, L'= C≡CR, M = Pt, M' = Pb).

Tabla 4.5: Datos de absorción UV-visible de los derivados [{Pt(bzq)(C≡CR)$_2$}{Pb(HBpz$_3$)}]$_2$ (**28**, **29**) y (NBu$_4$)[{Pt(bzq)(C≡CC$_6$H$_4$CF$_3$-4)$_2$}$_2${Pb(HBpz$_3$)}] (**30**) y de los precursores (NBu$_4$)[Pt(bzq)(C≡CR)$_2$] en disolución 5 x 10^{-5} M de CH_2Cl_2 y en estado sólido (Reflectancia Difusa)

Compuesto	λ_{abs}/nm (10^3 ε $M^{-1}cm^{-1}$)
(NBu$_4$)[Pt(bzq)(C≡CPh)$_2$][5]	275 (231), 351 (18.1), 397 (10.3) **CH_2Cl_2** 280, 301, 351, 401, 443, 476 **sólido**
[{Pt(bzq)(C≡CPh)$_2$}{Pb(HBpz$_3$)}]$_2$ **28**	220 (151.1), 252 (97.3), 284 (74.6), 310$_{sh}$ (46.8), 338 (34.4), 376 (19.3), 421 (8.4) **CH_2Cl_2** 285, 305, 348, 389, 439, 475 **sólido**
(NBu$_4$)[Pt(bzq)(C≡CC$_6$H$_4$OMe-3]	220 (121.3), 268 (66.0), 283 (64.8), 307 (59.3), 350 (27.1), 400 (16.0) **CH_2Cl_2** 280, 302, 353, 391, 440, 474 **sólido**
[{Pt(bzq)(C≡CC$_6$H$_4$OMe-3)$_2$}{Pb(HBpz$_3$)}]$_2$ **29**	220 (186.3), 255 (94.2), 280 (72.5), 304 (63.3), 338 (38.5), 376 (21.2), 424 (7.7) **CH_2Cl_2** 284, 306, 351, 379, 436, 473 **sólido**
(NBu$_4$)[Pt(bzq)(C≡CC$_6$H$_4$CF$_3$-4][5]	265 (40.6), 306 (49.6), 346 (30.0), 392 (13.0) **CH_2Cl_2**[5] 278, 310, 335, 396, 416, 446, 480 **sólido**
(NBu$_4$)[{Pt(bzq)(C≡CC$_6$H$_4$CF$_3$-4)$_2$}$_2${Pb(HBpz$_3$)}] **30**	218 (113.9), 254 (119.2), 290$_h$ (68.0), 316 (39.5), 330 (34.6), 382 (33.5) **CH_2Cl_2** 282, 304, 335, 394, 425, 453, 483 **sólido**

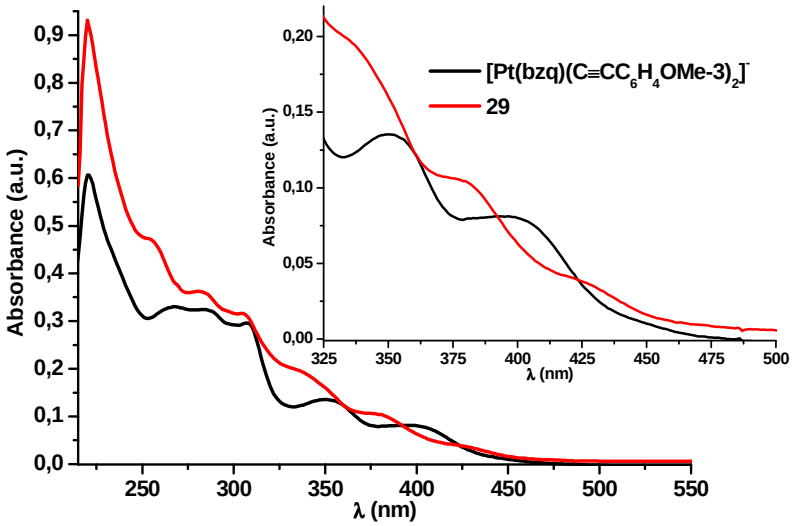

Figura 4.12: Espectros de absorción UV-vis en CH_2Cl_2 (5 x 10^{-5} M) de **29** y de su precursor y ampliación de la zona de baja energía

Sin embargo, el derivado trinuclear **30** muestra una absorción de baja energía a 382 nm, desplazada hacia el azul en relación a su precursor (392 nm), aunque con una cola que llega a ~ 460 nm (Figura 4.13). Este hecho apunta, al igual que los espectros de emisión en disolución (Ver siguiente apartado), a la diferente interacción de la unidad [Pb(HBpz$_3$)]$^+$ con los fragmentos [Pt(bzq)(C≡CR)$_2$]$^-$ y al carácter menos dador del ligando C≡CC$_6$H$_4$CF$_3$-4 en relación a los ligandos C≡CPh (**28**) y C≡CC$_6$H$_4$OMe-3 (**29**). En el derivado trinuclear **30** la contribución mayoritaria debe provenir de transiciones de transferencia de carga ligando (alquinilo o platino-alquinilo)–ligando

(benzoquinolato) ^{1}L'LCT o ^{1}ML'LCT, en las que la formación de las interacciones Pt···Pb aumenta la electrofilia del Pt provocando, en este caso, un incremento de la energía de la transición. Debido a la presencia de dos grupos bzq aceptores, probablemente la contribución de transferencia de carga de los fragmentos "$Pt(C{\equiv}CC_6H_4CF_3\text{-}4)_2$" al {$Pb(HBpz_3)$} sea menos determinante en este compuesto. No obstante, la zona de baja energía del derivado **30** no coincide con la del sustrato precursor, por lo que no podemos inferir que el complejo se disocie en disolución, como se observa también en los espectros de RMN de ^{1}H.

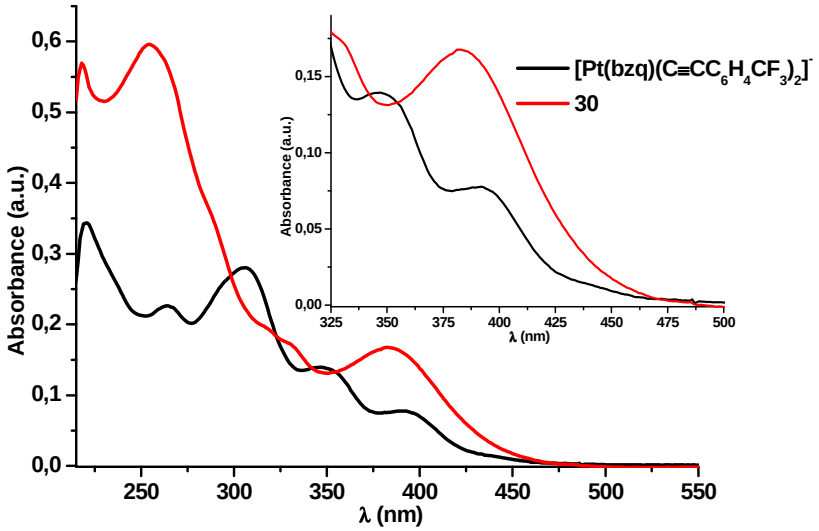

Figura 4.13: Espectros de absorción UV-vis en CH_2Cl_2 (5×10^{-5} M) de **30** y de su precursor y ampliación de la zona de baja energía

Los sólidos amarillos tetranucleares **28** y **29** se caracterizan en los espectros de Reflectancia Difusa por bandas de baja energía con máximos a 475 (**28**) y 473 nm (**29**), con cola hasta ~ 520 nm, mientras que el derivado amarillo trinuclear **30** presenta una banda de baja energía ligeramente desplazada hacia el rojo (483 nm) con una cola hasta ~ 550 nm (Figura 4.14).

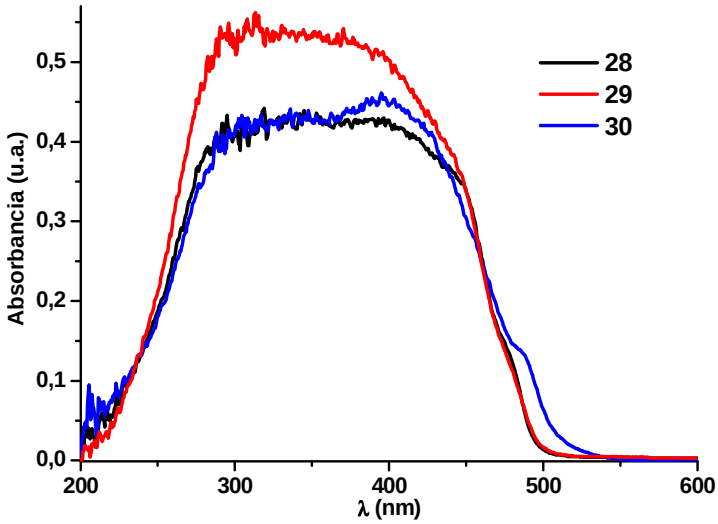

Figura 4.14: Espectros de absorción calculados a partir de los espectros de Reflectancia Difusa de los derivados **28**–**30** en estado sólido (diluido con SiO_2)

4.2.2 Espectros de emisión

Se han estudiado las propiedades emisivas de estos compuestos en estado sólido y en disolución de CH_2Cl_2 (5×10^{-5}–10^{-3} M) a 298 y 77 K . En la Tabla 4.6 únicamente se recogen los resultados de disoluciones diluídas, ya que no se aprecian diferencias significativas con el cambio de concentración. Así mismo, y con fines comparativos, en la Tabla 4.6 se recogen los datos de luminiscencia de los correspondientes productos de partida.

Todos los complejos obtenidos (**28**–**30**) son luminiscentes en estado sólido tanto a 298 como a 77 K (Figura 4.15). En sólido a 298 K muestran emisiones anchas asimétricas centradas a 505 nm en los derivados tetranucleares **28** y **29** y a 520 nm en el trinuclear **30**, con largos tiempos de vida media (7.4 **28**, 11.1 **29**, 7.1 μs **30**) y bajos rendimientos cuánticos (5.2 **28**, 1.2 **29**, 4.6 % **30**). Al bajar la temperatura hasta 77 K el color amarillo-naranja de la emisión se mantiene y los máximos apenas cambian, pero las bandas se estructuran (λ_{max} 505 **28**, **29**, 515 nm **30**) y los tiempos de vida media, como es de esperar, aumentan (19.7 **28**, 46.2 **29**, 30.4 μs **30**). Debemos indicar que las emisiones muestran el mismo patrón independientemente de la $\lambda_{excitación}$ elegida y que el

espaciado vibrónico es típico del grupo benzoquinolato, lo que sugiere su implicación en el estado emisivo.

Tabla 4.6: Datos extraídos de los espectros de emisión de los derivados $[\{Pt(bzq)(C{\equiv}CR)_2\}\{Pb(HBpz_3)\}]_2$ (**28**, **29**) y $(NBu_4)[\{Pt(bzq)(C{\equiv}CC_6H_4CF_3\text{-}4)_2\}_2\{Pb(HBpz_3)\}]$ (**30**) y de sus precursores $(NBu_4)[Pt(bzq)(C{\equiv}CR)_2]$ en estado sólido y disolución de CH_2Cl_2 a 298 y 77 K

Compuesto	Medio (T^a/K)	λ_{em}/nm (λ_{exc}/nm)	τ/μs	ϕ (%)
R = Ph	Sólido (298)	525 (365-450)		
	Sólido (77)	512_{max}, 454, 595 (365-475)		
	10^{-3} M (298)[a]	526 (462)		
	10^{-3} M (77)[a]	505_{max}, 538, 581 (350-470)		
28	Sólido (298)	505_{max}, 545_h (330-475)	7.4	5.2
	Sólido (77)	505_{max}, 543, 580 (365-450)	19.7	
	5×10^{-5} M (77)[b]	485_{max}, 523, 560, 620_h (365-450)		
R = C_6H_4OMe-3	Sólido (298)	520 (360-480)		
	Sólido (77)	515_{max}, 552, 596 (370-480)		
	10^{-3} M (298)	522_{max}, 580_h (370-480)		
	10^{-3} M (77)	498_{max}, 534, 573 (360-450)		
29	Sólido (298)	505_{max}, 560_h[c] (365-480)	11.1	1.2
	Sólido (77)	505_{max}, 541, 585 (365-450)	46.2	
	5×10^{-5} M (77)[b]	485_{max}, 523, 560, 625_h (365-430)		
R = $C_6H_4CF_3$-4	Sólido (298)	520 (340-390)		
	Sólido (77)	515_{max}, 550, 590 (365-490)		
	10^{-3} M (298)[a]	511 (461)		
	10^{-3} M (77)[a]	492_{max}, 526, 568 (350-440)		
30	Sólido (298)	520_{max}, 575_h[c] (330-480)	7.1	4.6
	Sólido (77)	515_{max}, 550, 595 (365-480)	30.4	
	5×10^{-5} M (298)	510_{max}, 540_h[c] (320-400)		
	5×10^{-5} M (77)	491_{max}, 527, 570, 605 (365-460)		

a) Datos tomados de la referencia; [5] b) No emisivo en disolución de CH_2Cl_2 a 298 K (5×10^{-5} – 10^{-3} M); c) Cola hasta ~ 650 (**28**, **29**), ~ 700 nm (**30**)

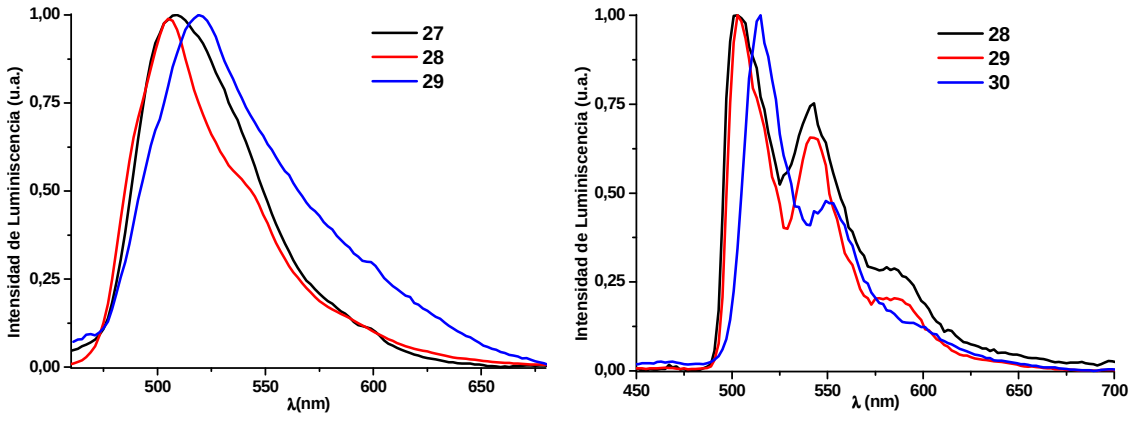

a) b)

Figura 4.15: Espectros de emisión normalizados (λ_{ex} 365 nm) de los derivados **28**–**30** en estado sólido a a) 298 K y b) 77 K

Con el fin de comparar las emisiones de los derivados **28**–**30** con las de los precursores aniónicos $(NBu_4)[Pt(bzq)(C{\equiv}CR)_2]$ (R= Ph, C_6H_4OMe-3, $C_6H_4CF_3$-4) se han registrado las emisiones de éstos en estado sólido a 298 y a 77 K (Tabla 4.6, Figura 4.16), ya que las emisiones publicadas[5] del derivado de Ph se habían realizado únicamente a temperatura ambiente en pastilla de KBr.

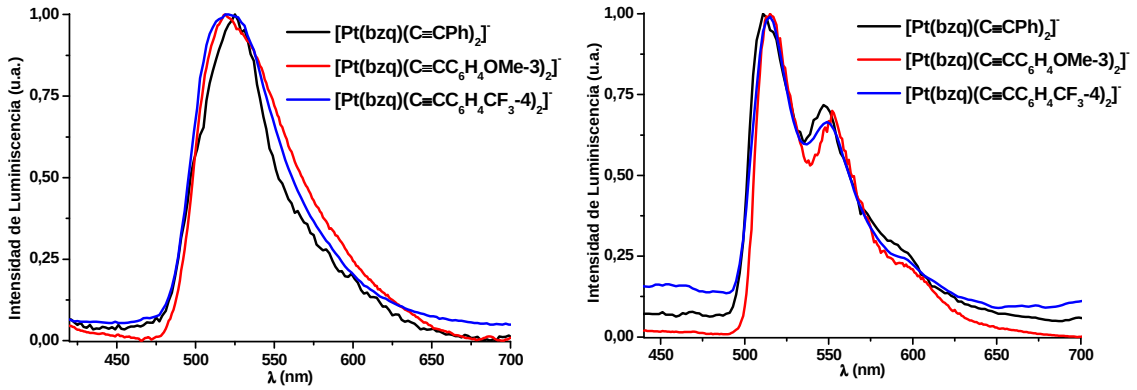

Figura 4.16: Espectros de emisión normalizados (λ_{ex} 365 nm) de los precursores en estado sólido a a) 298K y b) 77K

Éstas muestran a 298 K emisiones intensas asimétricas con λ_{max} a ~ 520 nm que se estructuran y se desplazan hacia el azul al bajar la temperatura hasta 77 K (512–515 nm). Estas emisiones se han atribuido mediante cálculos TD–DFT a estados excitados ^{3}L'LCT perturbados por el metal ^{3}[Pt(d)/π(C≡CR)→π*(bzq)].

Los derivados tetranucleares de Pb **28** y **29** muestran una escasa dependencia con los ligandos alquinilo, al igual que sucede con los precursores de Ph y C_6H_4OMe-3, pero se observa un ligero desplazamiento hacia el azul de su emisión con respecto a la de los sustratos precursores (Δ~20 nm). Sin embargo, el derivado trinuclear **30** apenas muestra diferencias con su precursor. Con estas consideraciones, la emisión de estos derivados podría ser asignada a una transferencia de carga fundamentalmente ligando (alquinilo o metal–alquinilo) – ligando (bzq) ^{3}L'LCT o ^{3}ML'LCT perturbada escasamente por la interacción Pt···Pb ^{3}[Pt/π(C≡CR)→ Pt(d)/Pb(sp)/π*(bzq)]. El desplazamiento al azul observado (en los tetranucleares) podría estar relacionado con la electrofilia del fragmento $Pb(HBpz_3)^+$ y la consiguiente estabilización del HOMO,

centrado en el fragmento "$Pt(C{\equiv}CR)_2$", al formarse los correspondientes enlaces $Pt^{II}\cdots Pb(HBpz_3)$. Este comportamiento es extraño, porque en general la implicación de un enlace Pt–Pb causa un claro desplazamiento hacia el rojo de la emisión.[1,4]

Desafortunadamente, los derivados tetranucleares **28** y **29** no presentan emisión a 298 K en disolución de CH_2Cl_2 (5 x 10^{-5}–10^{-3} M). Sin embargo, a baja temperatura (77 K) muestran una banda intensa y estructurada (λ_{max} 485 nm), ligeramente desplazada hacia el azul con respecto al sólido ($\Delta\sim$ 20 nm) y al correspondiente precursor ($\Delta\sim$20 nm **28**, 12 nm **29**) en estas condiciones (Figura 4.17 para **29**).

El pequeño rigidocromismo observado con respecto al precursor da idea de una cierta implicación del enlace $Pt\cdots Pb$ en disolución, es decir, que al menos la unidad binuclear PtPb se mantiene en los vidrios a 77 K. Esta emisión se asigna, como en estado sólido, a transferencia de carga ligando–ligando (alquinilo–bzq) perturbada escasamente por la interacción $Pt\cdots Pb$[3][$Pt/\pi(C{\equiv}CR)\rightarrow Pt(d)/Pb(sp)/\pi^*(bzq)$].

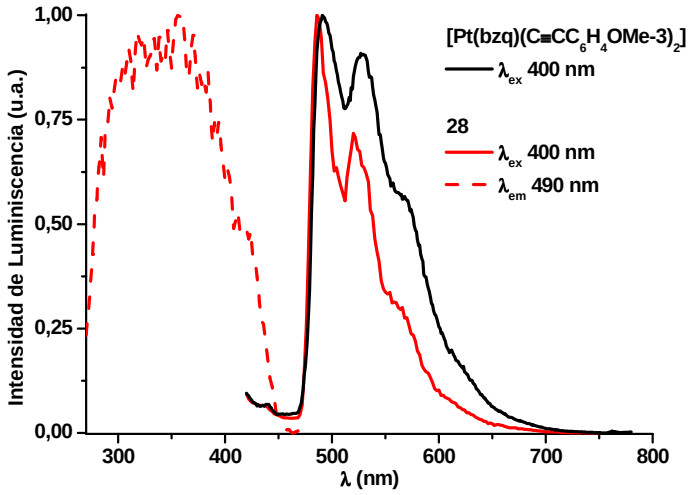

Figura 4.17: Espectros normalizados de excitación (línea discontinua) y de emisión (línea contínua) en disolución de CH_2Cl_2 (5 x 10^{-5}M) del derivado **29** y de emisión de su precursor a 77 K

Por otra parte, el derivado trinuclear **30** es emisivo en disolución de CH_2Cl_2 tanto a 298 como a 77 K. A temperatura ambiente muestra una banda ancha asimétrica, que se estructura y se desplaza hacia el azul al bajar la temperatura (510, 298 K *vs* 491 nm 77 K) (Figura 4.18). Esta emisión prácticamente coincide con la observada en el

precursor en el mismo medio tanto a temperatura ambiente como a 77 K (Tabla 4.6), por lo que esta emisión en disolución se podría atribuir a fosforescencia ^{3}L'LCT ^{3}[Pt(d)/π(C≡CR)→π*(bzq)] con escasa o nula participación de la interacción Pt···Pb. Adicionalmente, a 77 K aparece una pequeña banda adicional de baja energía a 605 nm, relacionada con un espectro de excitación distinto del de la banda estructurada, que se podría asignar tentativamente a la formación de excímeros favorecidos por la presencia de cortas interacciones π··π intramoleculares que se producen entre los grupos bzq (Figura 4.18), como se observa en la estructura cristalina.

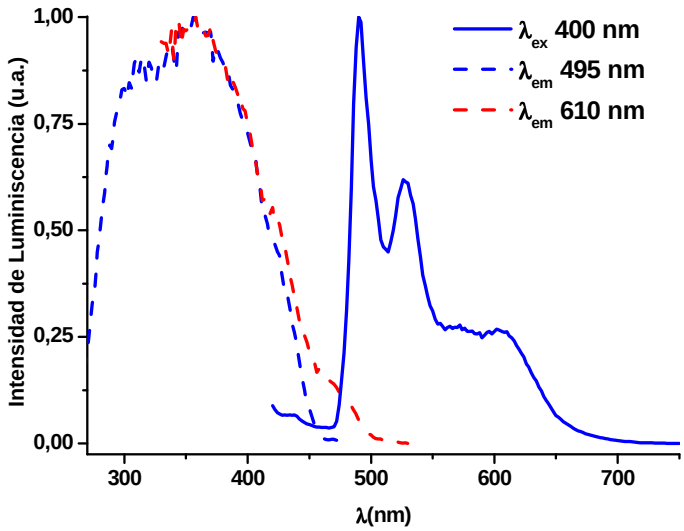

Figura 4.18: Espectros normalizados de excitación (línea discontinua) y de emisión (línea continua) del derivado **30** en disolución de CH_2Cl_2 5 x 10^{-5} M a 77 K

4.3 Resumen

Con el fin de seguir estudiando la influencia que tiene el cambio en la naturaleza electrónica de los centros de Pb^{II} sobre las estructuras y propiedades ópticas de sistemas platino–plomo–alquinilo, se ensayaron las reacciones de los compuestos cicloplatinados de Pt^{II} $(NBu_4)[Pt(bzq)(C{\equiv}CR)_2]$ (R = Ph, C_6H_4OMe-3 y $C_6H_4CF_3$-4) frente al derivado $[Pb(HBpz_3)]Cl$ en presencia de exceso de $NaPF_6$.

En el caso de los sustratos con R = Ph y C_6H_4OMe-3 las reacciones evolucionaron con la neutralización de los precursores monoaniónicos correspondientes, dando lugar a los derivados tetranucleares $[\{Pt(bzq)(C{\equiv}CR)_2\}\{Pb(HBpz_3)\}]_2$ (**28**, **29**), en los que el fragmento bimetálico $[\{Pt(bzq)(C{\equiv}CR)_2\}\{Pb(HBpz_3)\}]$ dimeriza mediante interacciones débiles $Pb^{II}\cdots\eta^2$ alquinilo, aumentando el entorno de coordinación del Pb. En la especie binuclear, el Pb^{II} de una unidad $\{Pb(HBpz_3)\}^+$ se conecta a un fragmento $\{Pt(bzq)(C{\equiv}CR)_2\}^-$ mediante un enlace Pt–Pb y completa una coordinación octaédrica distorsionada con una unidad *cis*–bis–η^2alquinilo del segundo $\{Pt(bzq)(C{\equiv}CR)_2\}^-$, originando un metalaciclo central de la forma $\{Pt(C{\equiv}C)_2\}_2Pb_2$ en la especie tetranuclear.

Sin embargo, con el sustrato que contiene el sustituyente menos dador de e^- ($C_6H_4CF_3$-4) se obtiene el derivado trinuclear aniónico $(NBu_4)[\{Pt(bzq)(C{\equiv}CC_6H_4CF_3\text{-}4)_2\}_2\{Pb(HBpz_3)\}]$ (**30**), en el que dos fragmentos aniónicos $\{Pt(bzq)(C{\equiv}CC_6H_4CF_3\text{-}4)_2\}^-$ desplazados y orientados mutuamente *cis*, se conectan a través del catión $\{Pb(HBpz_3)\}^+$.

Con el fin de conocer la naturaleza de las entidades **28** y **29** en disolución se llevó a cabo un análisis de la estructura en disolución de estos derivados mediante experimentos de difusión unidimensional PGSE, bidimensional DOSY y un estudio de RMN de ^1H a temperatura variable (**28**). Este estudio parece concluir que los derivados **28** y **29** están formados por la entidad binuclear $[\{Pt(bzq)(C{\equiv}CR)_2\}\{Pb(HBpz_3)\}]$ debido a la ruptura de las interacciones $Pb^{II}\cdots\eta^2$alquinilo en la entidad tetranuclear.

La absorción de más baja energía en los derivados tetranucleares **28** y **29** se atribuye de forma tentativa a una transición con un marcado carácter de transferencia de carga desde el fragmento "$Pt(C{\equiv}CR)_2$" a un estado con mezcla del ligando bzq y del fragmento {$Pb(HBpz_3)$} ^{1}L'LCT/^{1}ML'M'CT (L = bzq, L' = C≡CR, M = Pt, M' = Pb), mientras que en el derivado trinuclear **30**, la contribución mayoritaria se atribuye a transiciones de transferencia de carga ^{1}L'LCT o ^{1}ML'LCT, con menor contribución de transferencia de los fragmentos "$Pt(C{\equiv}CC_6H_4CF_3\text{-}4)_2$" al {$Pb(HBpz_3)$}.

La luminiscencia amarillo–naranja que se observa en los compuestos tetranucleares en estado sólido y en vidrios congelados a 77 K se desplaza hacia el azul respecto a los correspondientes sustratos de partida y se asigna a una transferencia de carga fundamentalmente ligando (alquinilo o metal–alquinilo)–ligando (bzq) ^{3}L'LCT o ^{3}ML'LCT, perturbada escasamente por la interacción Pt···Pb ^{3}[Pt/π(C≡CR)→Pt(d)/Pb(sp)/π*(bzq)]. Sin embargo la luminiscencia del trinuclear **30** tanto en sólido como en disolución (298 K, 77 K) apenas muestra diferencias con su precursor, por lo que la emisión se podría atribuir, al menos en fluido, a fosforescencia ^{3}L'LCT ^{3}[Pt(d)/π(C≡CR)→π*(bzq)] con escasa o nula participación de la interacción Pt···Pb. Las cortas interacciones π(bzq)··π(bzq) dan lugar a la presencia de una pequeña contribución excimérica en vidrio congelado.

4.4 Bibliografía

1. Berenguer, J. R.; Fernández, J.; Gil, B.; Lalinde, E.; Sánchez, S. *Chem. Eur. J.* **2014**, *20*, 2574.
2. Fernández, J., Tesis Doctoral, Universidad de La Rioja, 2011.
3. (a) Berenguer, J. R.; Gil, B.; Fernández, J.; Forniés, J.; Lalinde, E. *Inorg. Chem.* **2009**, *48*, 5250; (b) Berenguer, J. R.; Fernández, J.; Gil, B.; Lalinde, E.; Sánchez, S. *Inorg. Chem.* **2010**, *49*, 4232.
4. Berenguer, J. R.; Díez, A.; Fernández, J.; Forniés, J.; García, A.; Gil, B.; Lalinde, E.; Moreno, M. T. *Inorg. Chem.* **2008**, *47*, 7703.
5. Fernández, S.; Forniés, J.; Gil, B.; Gómez, J.; Lalinde, E. *Dalton Trans.* **2003**, 822.
6. Reger, D. L.; Huff, M. F.; Rheingold, A. L.; Haggerty, B. S. *J. Am. Chem. Soc.* **1992**, *114*, 579.
7. Díez, Á., Tesis Doctoral, Universidad de La Rioja, 2010.
8. Cordero, B.; Gómez, V.; Platero-Prats, A. E.; Reves, M.; Echeverría, J.; Cremades, E.; Barragán, F.; Álvarez, S. *Dalton Trans.* **2008**, 2832.
9. Bondi, A. *J. Phys. Chem.* **1964**, *68*, 441.
10. (a) Balch, A. L.; Fung, E. Y.; Nagle, J. K.; Olmstead, M. M.; Rowley, S. P. *Inorg. Chem.* **1993**, *32*, 3295; (b) Usón, R.; Forniés, J.; Falvello, L. R.; Usón, M. A.; Usón, I. *Inorg. Chem.* **1992**, *31*, 3697; (c) Ara, I.; Falvello, L. R.; Forniés, J.; Gómez-Cordón, J.; Lalinde, E.; Merino, R. I.; Usón, I. *J. Organomet. Chem.* **2002**, *663*, 284; (d) Casas, J. M.; Forniés, J.; Martín, A.; Orera, V. M.; Orpen, A. G.; Rueda, A. *Inorg. Chem.* **1995**, *34*, 6514; (e) Albano, V. G.; Castellari, C.; Monari, M.; De Felice, V.; Ferrara, M. L.; Ruffo, F. *Organometallics* **1995**, *14*, 4213.
11. Szafert, S.; Gladysz, J. A. *Chem. Rev.* **2003**, *103*, 4175.
12. (a) Forniés, J.; Fuertes, S.; Martín, A.; Sicilia, V.; Gil, B.; Lalinde, E. *Dalton Trans.* **2009**, 2224; (b) Díez, Á.; Fernández, J.; Lalinde, E.; Moreno, M. T.; Sánchez, S. *Inorg. Chem.* **2010**, *49*, 11606.
13. (a) Reger, D. L.; Ding, Y.; Rheingold, A. L.; Ostrander, R. L. *Inorg. Chem.* **1994**, *33*, 4226; (b) Janiak, C.; Temizdemir, S.; Scharmann, T. G.; Schmalstieg, A.; Demtschuk, J. *Z. Anorg. Allg. Chem.* **2000**, *626*, 2053.

14. (a) Valentini, M.; Pregosin, P. S.; Rüegger, H. *Organometallics* **2000**, *19*, 2551; (b) Johnson Jr, C. S. *Prog. Nucl. Magn. Reson. Spectrosc.* **1999**, *34*, 203.
15. Morris, K. F.; Johnson, C. S. *J. Am. Chem. Soc.* **1992**, *114*, 3139.
16. Khrapitchev, A. A.; Callaghan, P. T. *J. Magn. Res.* **2001**, *152*, 259.
17. (a) Schlörer, N. E.; Cabrita, E. J.; Berger, S. *Angew. Chem. Int. Ed.* **2002**, *41*, 107; (b) Keresztes, I.; Williard, P. G. *J. Am. Chem. Soc.* **2000**, *122*, 10228.
18. (a) Barjat, H.; Morris, G. A.; Smart, S.; Swanson, A. G.; Williams, S. C. R. *J. Magn. Reson. Ser. B* **1995**, *108*, 170; (b) Kapur, G. S.; Findeisen, M.; Berger, S. *Fuel* **2000**, *79*, 1347; (c) Politi, M.; Groves, P.; Chávez, M. I.; Cañada, F. J.; Jiménez-Barbero, J. *Carbohydr. Res.* **2006**, *341*, 84; (d) Allouche, L.; Marquis, A.; Lehn, J.-M. *Chem. Eur. J.* **2006**, *12*, 7520.
19. (a) Kapur, G. S.; Cabrita, E. J.; Berger, S. *Tetrahedron Lett.* **2000**, *41*, 7181; (b) Cabrita, E. J.; Berger, S. *Magn. Reson. Chem.* **2001**, *39*, S142.
20. (a) Cabrita, E. J.; Berger, S.; Bräuer, P.; Kärger, J. *J. Magn. Reson.* **2002**, *157*, 124; (b) Cabrita, E. J.; Berger, S. *Magn. Reson. Chem.* **2002**, *40*, S122.
21. (a) Viel, S.; Mannina, L.; Segre, A. *Tetrahedron Lett.* **2002**, *43*, 2515; (b) Díaz, M. D.; Berger, S. *Carbohydr. Res.* **2000**, *329*, 1; (c) Simova, S.; Berger, S. *J. Inclusion Phenom.* **2005**, *53*, 163.

CHAPTER 5

Pt_2Pb clusters $[\{Pt(C_6F_5)(C\hat{}N)\}_2Pb(SpyR\text{-}5)_2]$. Structures and photophysical responses driven by solvent interactions

Pt_2Pb clusters $[\{Pt(C_6F_5)(C\hat{}N)\}_2Pb(SpyR\text{-}5)_2]$. Structures and photophysical responses driven by solvent interactions

As commented in the Introduction, considerable efforts has been made in the preparation and study of the photophysical behavior of heterometallic Pt^{II}-d^{10} or Pt^{II}-d^8 systems. Notably, some of these systems have been found to be sensitive to external stimuli such as VOCs (vapoluminescence),[1] mechanical grinding (mechanochromism)[2] or temperature (thermochromism).[3] These phenomena have been usually correlated with subtle structural transformations, which are often associated with the formation/disruption or modification of metal-metal interactions or interligand $\pi\cdots\pi$ stacking, although for polymetallic systems exhibiting response to vapors, metal-ligand coordination/decoordination has been also demonstrated.[4]

In contrast, heteropolynuclear systems incorporating heavy metals with a valence shell $d^{10}s^2$ (Tl^I, Pb^{II}) have been comparatively much less explored. In the case of thallium, interesting families of heteronuclear Pt^{II}-Tl^I,[3b,c,5] having diverse structural configurations and exhibiting intriguing photophysical properties, have been also reported. In contrast, the number of polymetallic systems involving the harder Pb^{2+} ion in metallophilic interactions is quite limited[5n,6] and still little is known about their photoluminescence properties.[6d,e] In these heterometallic systems, the $6s^2$ electron lone pair of the heavy ion (Tl^I, Pb^{II}) usually exerts a remarkable structural influence depending on its stereoactivity.[7] This electronic and structural effect, attributed to ligand-to-metal charge transfer, is particularly relevant in lead(II) containing systems due to its higher charge, thus favoring the formation of more or less *hemi-directional* environments having a void in the coordination sphere of the Pb^{II}, which is occupied by the stereochemically active lone pair.

Our research group is interested in preparing platinum-lead(II) systems due to the well-known capacity of Pb^{II} to adopt a wide range of coordination numbers (from 2 to 12) and geometries arising from subtle changes in the stereochemical activity of the lone pair.[7] In particular, as it has been commented in the Introduction, when the lone

pair is active, it is expected that its degree of activity will be susceptible to the influence of external factors (binding of vapors, mechanical forces…) with concomitant changes in electronic structure and properties. This structural property might endow these Pt^{II}-Pb^{II} complexes with some unique properties, such as the response to external stimuli, thereby providing the opportunity of forming dynamic stimuli responsive materials.

As it has been described in the Introduction by using alkynyl platinates as basic building bloks and the $Pb(ClO_4)_2 \cdot 3H_2O$ salt, we have successfully prepared several sandwich type trinuclear Pt_2Pb[8] and tetranuclear Pt_2Pb_2[9]clusters, stabilized by a synergistic combination of η^1 and/or η^2 $Pb^{II}\cdots(C{\equiv}CR)$ and Pt^{II}-Pb^{II} bonding interactions, which have been demonstrated to display interesting photophysical properties depending on the topology and the alkynyl substituents. Notably, the emissive tetranuclear clusters [$Pt_2Pb_2(C{\equiv}CR)_8$] (R = Tol, C_6H_4OMe-3)[9] have a rather dynamic core sensitive to mechanical grinding and donor solvents. In particular, the remarkable and distinct vapochromic response observed has been ascribed to a fast creation/disruption of Pb-solvate clusters [$Pt_2Pb_2(C{\equiv}CR)_8S_x$] (S = donor volatile, $x \geq 2$) with concomitant geometrical and electronic changes.

In the search for new and more robust platinum-lead systems, we considered it of interest to explore its formation by self-assembly of neutral building precursors. Herein, we report the synthesis, spectroscopic, structural characterization and photophysical studies of a series of new luminescent Pt_2Pb clusters [{$Pt(C_6F_5)(C^N)$}$_2$Pb(SpyR-5)$_2$] (C^N = bzq, ppy; R = H, CF_3 **33**-**36**) studying the role of the cycloplatinated "Pt(C^N)" fragment and the basicity of the ancillary pyridine thiolate ligand in the structures and photophysical responses. The bzq derivatives (**33**, **34**) exhibited *vapoluminescence* behaviour (**34** also *vapochromic* behaviour) while the ppy/SpyR-5 derivative **35** (R = H) and **36** (R = CF_3) did not show *vapochromic* behaviour. In the case of **36** its structure and properties were found to depend on the crystallization conditions and displays also *mechanochromic* properties. To get insight into the nature of their photophysical properties, TD-DFT calculations were carried out in gas phase on some selected unsolvated and solvated clusters.

5.1 Synthesis and characterization

5.1.1 Synthesis

The trinuclear complexes [{Pt(C_6F_5)(bzq)}$_2$Pb(μ-SpyR-5)$_2$] (bzq = benzoquinolinyl, R = H **33**, CF_3 **34**) were obtained, in high yields, as orange solids by treatment of the acetone solvate [Pt(C_6F_5)(bzq)($OCMe_2$)][10] (**31**) with 0.5 equiv. of the appropriate *bis*(pyridinethiolate)lead(II). It is worth noting that both reactions evolve with formal thiolate transfer from Pb^{II} to Pt^{II}, keeping the two N atoms in the primary environment of the lead, plausibly favored by the soft nature of Pt^{II} (Scheme 5.1a).

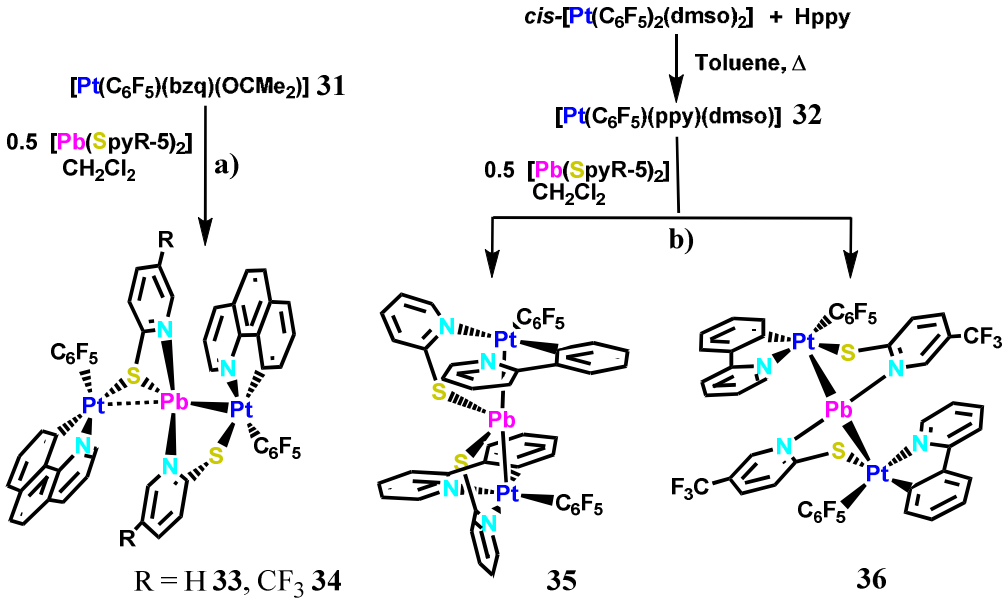

Scheme 5.1

The attempts to synthesize the acetone solvate [Pt(C_6F_5)(ppy)($OCMe_2$)] with the 2-phenylpyridine ligand (Hppy) under conditions similar to those described for **31** resulted unsuccessful. Fortunately, the synthesis of the targeted clusters [{Pt(C_6F_5)(ppy)}$_2$Pb(μ-SpyR-5)$_2$] (R = H **35**, CF_3 **36**), as orange (**35**) or yellow (**36**) solids, was achieved by using the dimethylsulphoxide solvate, [Pt(C_6F_5)(ppy)(dmso)] (**32**), as the precursor (Scheme 5.1b). Surprisingly, whereas the formation of **36** takes also place with thiolate transfer from Pb^{II} to Pt^{II}, in the case of cluster **35**, however, this transfer does not occur, keeping the sulphur coordinated to the Pb atom, as evidenced by X-ray. As shown in Scheme 5.1b, the precursor **32** was prepared following similar approaches to related aryl-cycloplatinate complexes, by refluxing a mixture of *cis*-[Pt(C_6F_5)$_2$(dmso)$_2$][11] and Hppy (1 equiv.) in toluene (32 h), and its structure was

identified by spectroscopic means (See Experimental) and X-ray crystallography (See Section 5.1.3).

5.1.2 NMR characterization

In solution, the most remarkable spectroscopic features of the precursor **32** are the high value of the ^{195}Pt-F_{ortho} coupling constant (494 Hz), consistent with the low *trans influence* of the N atom *trans* to the C_{ipso} atom of the C_6F_5 group, and the notable upfield shift of the *ortho*-H^9 proton of the ppy ligand (δ 6.41, $^3J_{Pt\text{-}H}$ 62.4 Hz) due to the anisotropic effect of the C_6F_5 ring.

Complexes **33–36** were characterized by standard analytical and spectroscopic techniques and its integrity in solution confirmed by multinuclear [^{1}H, ^{19}F (CD_2Cl_2, CD_3COCD_3) and ^{13}C{^{1}H}] NMR spectroscopy. For all complexes **33–36** only one set of cyclometalated, C_6F_5 and bridging SpyR groups was observed, even at low temperature, indicating that the structural differences between the two "Pt(C_6F_5)(C^N)(μ-SpyR)" fragments observed in the solid state for **33**, **34** and **36** around Pb^{II} are averaged in solution.

The most relevant features are provided by ^{19}F NMR spectroscopy. In a donor solvent such as CD_3COCD_3, the complexes exhibit the typical AA'MXX' pattern (2F_o, F_p, 2F_m), revealing that the pentafluorophenyl groups have free rotation about the Pt-C_{ipso}(C_6F_5) bonds. The *ortho*-fluorine signal is only flanked by platinum satellites pointing to the absence of F···Pb contacts in this donor solvent. However, it is worth noting that the ^{195}Pt-F_o coupling constants (382-408 Hz) are clearly smaller than those in the starting precursors (501 Hz **31**, 494 Hz **32**), thus supporting the integrity of Pt^{II}-Pb^{II}-Pt^{II} bonds. The remarkable reduction in the J ^{195}Pt-F_o value is consistent with the increase in the coordination number of the Pt center (from 4 to 5) upon formation of the Pt-Pb bonds. The ^{19}F NMR spectra were also recorded in CD_2Cl_2 revealing not only a more rigid behaviour but also the persistence of close contacts Pb···F_o in solution. In this solvent, at ambient temperature, the *ortho*-fluorine resonances are very broad indicative of dynamic behaviour. While in complexes with the substituted SpyCF_3 bridging ligand (**34** and **36**) two distinct very broad signals (*exo*- and *endo*-F_o) are seen, in complexes **33** and **35** both resonances are close to $T_{coalescence}$ (**33**) or slightly up (**35**

broad hump). Upon cooling to 186 K, two distinct F_o (*endo* and *exo*, and also two F_m) resonances appear in all complexes **33–36** (see Figure 5.1 for **34**). The *exo*-F_o atoms appear at low field (δ -115.7 for **36** to -116.3 **33**) with well-resolved platinum satellites, whereas the *endo*-F_o atoms are seen in the range (δ -123.1 for **36** to -124.6 for **34**), clearly flanked in **33–35** by two sets of satellites due to coupling to ^{207}Pb and ^{195}Pt, respectively (see Figure 5.2 for **34**). The *endo*-fluorine–lead coupling constants ($J^{207}_{Pb\text{-}^{19}F}$ 1564 **33**, 1594 **34** and 1557 Hz **35**) are larger than that previously reported for the tetranuclear anion $[Pb\{Pt(\mu\text{-}Cl)(C_6F_5)_2\}_3]^-$ (1140 Hz),[6d] which also displays close $F_o\cdots Pb$ contacts. Interestingly, the presence of these *endo*-$F_o\cdots Pb$ contacts is also reflected in the corresponding values of coupling constants $^3J_{Pt\text{-}Fo(endo)}$ (289-317 Hz), which decrease in relation to those observed for the *exo*-F_o (384-404 Hz).

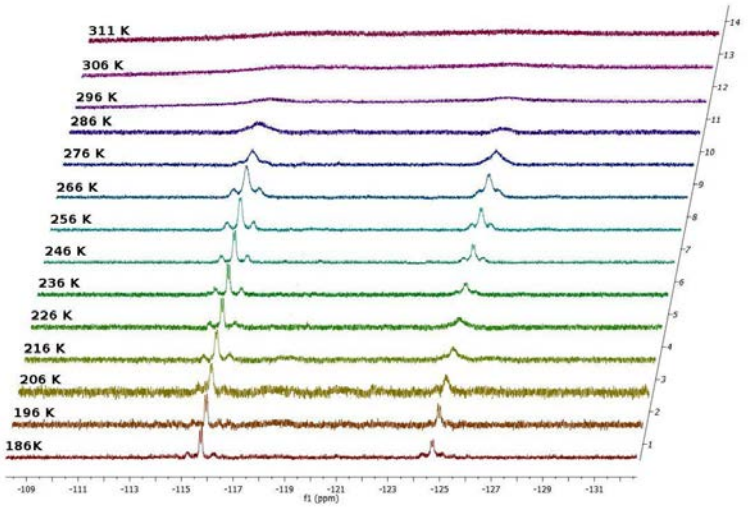

a)

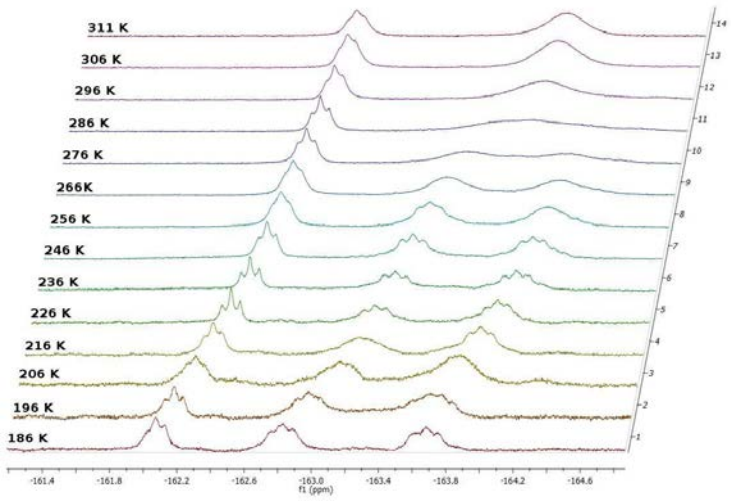

b)

Figure 5.1: Variable-temperature ^{19}F NMR spectra of **34** in CD_2Cl_2 (a) *ortho*-F region, b) *para* and *meta* region

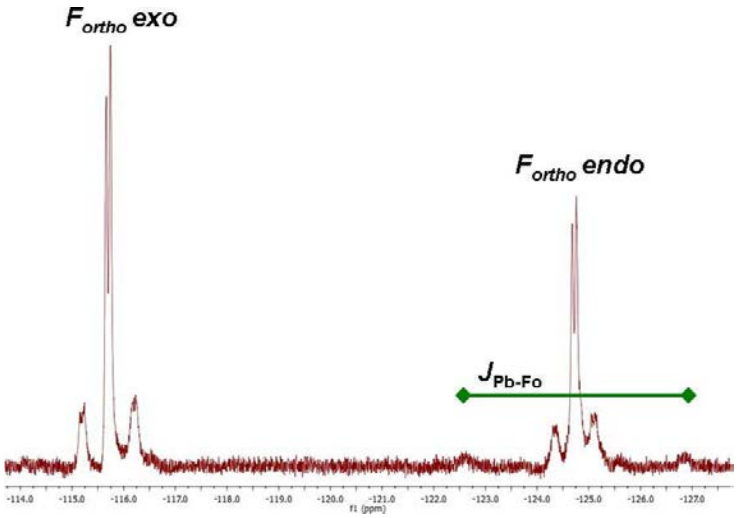

Figure 5.2: *ortho*-F region in the ^{19}F NMR spectrum of **34** in CD_2Cl_2 at 186 K

5.1.3 X-Ray diffraction

The X-ray structure of complex **32** (Figure 5.3, Table 5.1) exhibits the expected square-planar environment around platinum, having the C_6F_5 group coordinated in *cis* position to the metalated C(10) atom of the ppy ligand. The bond lengths and angles are not unusual,[10-12] and not unexpectedly, the complex crystallizes as head-to-tail dimers through moderate intermolecular interactions (3.270 Å) between the ppy ligands (Figure 5.3b).

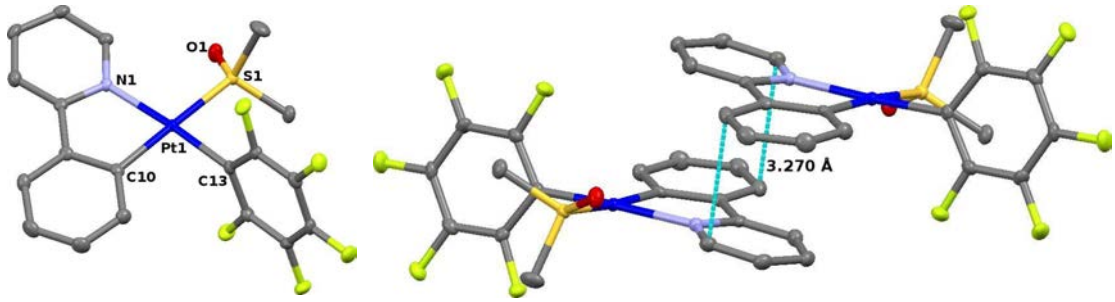

a) b)

Figure 5.3: a) Molecular view and b) Crystal packing of [Pt(C_6F_5)(ppy)(dmso)] (**32**) showing the intermolecular contacts

Table 5.1: Selected Distances [Å] and Angles [º] for complex **32**

32			
Pt1-S1	2.3116(7)	C10-Pt1-N1	80.37(10)
Pt1-N1	2.085(2)	S1-Pt1-C13	89.59(8)
Pt1-C10	2.017(7)	C10-Pt1-C13	92.34(11)
Pt1-C13	2.022(3)	S1-Pt1-N1	98.11(6)
S1-O1	1.486(2)	Pt1-S1-O1	117.76(9)

Table 5.2: Selected Distances [Å] and angles (º) of complexes **33**·1.5CH_2Cl_2, [**33·acetone**]·0.5 acetone, **34**·0.9CH_2Cl_2, [**34·(acetone)$_{1.5}$**], **35**·2$CHCl_3$, **36**·4C_6H_6, **36**·4$CHCl_3$, **36**·2CH_2Cl_2 and [**36·acetone**]

		Pt1-Pb1	Pt2-Pb1	Pb1-N2	Pb1-N4	Pb1-S1	Pb1-S2	Pb1-O	Pb1-F	Pt1-Pb1-Pt2	N2-Pb1-N4
33·1.5CH_2Cl_2		2.7832(3)	3.1642(3)	2.565(5)	2.683(5)		2.797(1)		Pb-F20 2.959(3)	140.75(1)	151.72(15)
[**33·acetone**]		2.9790(3)	2.8401(3)	2.497(4)	2.568(3)	3.186(1)		2.775(5)	Pb-F20 3.037(3)	133.29(1)	84.20(13)
34·0.9CH_2Cl_2		2.7774(4)	3.0877(4)	2.495(5)	2.775(5)		2.821(2)		Pb-F20 2.876(6) Pb-F45 3.058(4)	141.54(1)	153.15(16)
[**34·(acetone)$_{1.5}$**]	A	2.8654(6)	3.0902(6)	2.676(9)	2.608(9)		2.968(3)	Pb-O1 2.791(11) Pb-O2 2.937(9)	Pb-F20 2.895(8)	146.88(2)	144.7(3)
	B	2.8038(6)	3.1408(6)	2.634(9)	2.593(9)		2.872(3)	2.967	Pb'-F16' 2.829(8) Pb'-F45' 3.031(6)	149.64(2)	140.4(3)
35·2$CHCl_3$		2.8326(4)	2.8998(4)			2.767(2)	2.691(2)		Pb-F18 2.914(4) Pb-F40 2.874(6)	169.88(1)	
36·4C_6H_6		2.9469(1)		2.669(3)		2.957(1)			Pb-F18 2.997(2)	156.22(1)	155.47(14)
36·4$CHCl_3$		2.9222(4)		2.674(5)		3.024(2)			Pb-F18 3.075(3)	155.02(1)	154.2(2)
36·2CH_2Cl_2[a]		2.7840(5)	3.0596(5)	2.564(8)	2.679(7)		2.858(3)		Pb-F14 2.874(6) Pb-F37 3.191(5)	137.58(2)	159.9(3)
[**36·acetone**]		2.7863(2)	3.534	2.603(3)	2.566(3)		2.7728(8)	2.897	Pb-F14 2.912(2)	132.25	142.11(8)

[a] data of one (Pb1) of the three molecules (see SI for molecules associated to Pb2 and Pb3)

Interestingly, a visual and reversible change in the luminescence of **33** from *orange-red* to *yellow-orange* was observed in contact with a drop of acetone. We found the formation of two pseudopolymorphs depending on the solvent. Crystallization at low temperature from CH_2Cl_2/*n*-hexane or acetone/*n*-hexane produces orange crystals of stoichiometry [{$Pt(C_6F_5)(bzq)$}$_2$$Pb(Spy)_2$]·$1.5CH_2Cl_2$ (**33**·$1.5CH_2Cl_2$) and [{$Pt(C_6F_5)(bzq)$}$_2$$Pb(Spy)_2$(acetone)]·1.5acetone (**33·acetone**·1.5acetone), respectively. In the case of **34**, upon addition of a drop of acetone, not only a reversible change of the luminescence from *orange-yellow* to *yellow-green*, but also a visual color change of the solid from *orange* to *yellow* was observed. Thus, crystallization of **34** from CH_2Cl_2/*n*-hexane at -30ºC produced orange crystals of [{$Pt(C_6F_5)(bzq)$}$_2$$Pb(\mu\text{-}SpyCF_3)_2$]·$0.9CH_2Cl_2$ (**34**), whereas from acetone/*n*-hexane afforded yellow crystals of [{$Pt(C_6F_5)(bzq)$}$_2$$Pb(\mu\text{-}SpyCF_3)_2(acetone)_{1.5}$] [**34·(acetone)$_{1.5}$**].

The X-ray structures of **33**·$1.5CH_2Cl_2$ (**33**) (Figure 5.4, Tables 5.2 and A5.1) and **34**·$0.9CH_2Cl_2$ (**34**) (Figure 5.4, Tables 5.2 and A5.3) revealed the formation of a bent Pt-Pb-Pt core [140.753(9) (**33**), 141.54(1)º (**34**)] with a very short Pt-Pb bond [Pt(1)-Pb 2.7832(3) (**33**), 2.7774(4) Å (**34**)], supported by a bridging (μ-κ*N*,*S*) pyridine-2-thiolate ligand ($SpyR^-$), and a longer Pt-Pb [Pt(2)-Pb 3.1642(3) (**33**), 3.0877(4) Å (**34**)] bond, which is associated with the more unusual 6 e^- (μ-1κ*N*,*S*:2κ*S*) $SpyR^-$ bridging ligand. The short Pt-Pb distance is only slightly longer than the sum of the covalent radii (2.75 Å), and both distances are in the range reported for the relatively scarce number of species containing Pt-Pb bonds.[6a,b,6e-h,8] The Pb-N [2.565(5), 2.683(5) (**33**); 2.495(5), 2.775(5) Å (**34**)] and Pb-S(2) [2.797(1) (**33**), 2.821(2) Å (**34**)] distances are comparable to those reported for [$Pb(SpyCF_3\text{-}3)_2$].[14] The Pb-S(1) distances are too long [3.545(2) (**33**); 3.633(2) Å (**34**)] and clearly out of the reported range (2.45-3.03 Å) for primary coordination spheres in aggregated and base stabilized lead (II) thiolates.[15]

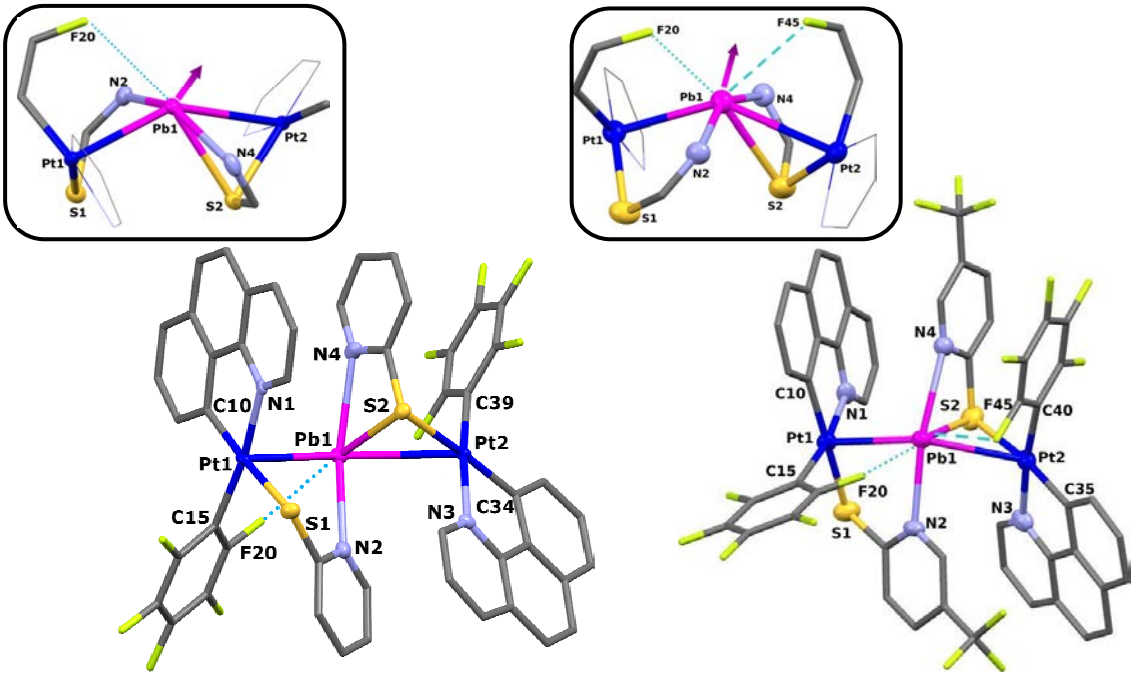

a) b)

Figure 5.4: a) Drawing of the structure of a) **33**·1.5 CH_2Cl_2 and b) **34**·0.9 CH_2Cl_2 (orange crystals) with a detail of the environment of Pb^{II} (The arrow suggests the direction where the lone pair is located)

As has been previously noted,[7a] the exact geometry around Pb^{II} is not easy to define. In these systems, the lead centre exhibits a *primary* "Pt_2N_2S" strongly distorted square pyramidal five-coordination, with the N atoms [N(2)-Pb-N(4) 151.72(15) (**33**); 153.15(16)º (**34**)] and the Pt atoms [Pt-Pb-Pt 140.753(9) (**33**), 141.54(1)º (**34**)] defining the basal positions and the bridging S(2) centre the apex (Figure 5.4) due to the acute angles S(2)-Pb-Pt(2) [47.24(3) **33**, 48.01 (4)º **34**] and S(2)-Pb-N(4) [57.61(11) **33**, 56.31 (4)º **34**]. The remarkable gap opposite to the sulphur centre is possibly occupied by the stereochemically active $6s^2$ lone pair (coordination as ψ–octahedron) (Figure 5.4). However, as shown in Figure 5.4a the environment of the lead in **33** is also supplemented by one secondary *intramolecular* interactions with the *ortho*-fluorine atoms, of one C_6F_5 ligand [Pb-F(20) 2.959 (3)],[16] whereas in **34** (Figure 5.4b) there are two intramolecular interactions of this type, one from each C_6F_5 ligand [Pb-F(20) 2.876(6) Å, Pb-F(45) 3.058(4) Å].[16] These interactions are weak, but as noted before, they are reflected in CD_2Cl_2 solution at low temperature in the fluorine-lead coupling constants (through space). The presence of two secondary Pb··F_o interactions in **34** is in contrast with the observation of only one in **33**. This feature could be associated with the lower basicity of the SpyCF_3-5 ligand in relation to the Spy in **33**, which is also

reflected in the $J_{Pb\text{-}Fo}$ value observed in CD_2Cl_2 solution (1594 in **34** *vs* 1552 Hz in **33**). An inspection of related bond lengths and contacts around Pb^{II} suggests that lone pair activity is somewhat more pronounced in the direction where the contacting atoms are located furthest [N(4) and F(40) in **33**, N(4) and F(45) in **34**].

Supramolecular packing of the crystal structure of **33** reveals the formation of dimers formed by short *intra*- (Spy···bzq) (3.158 Å) (yellow) and *intermolecular* (bzq···bzq) π···π (3.280 Å) (blue) contacts assisted by secondary H···F interactions (2.428 Å) (green). These dimers are further connected by π···π (bzq···bzq) contacts (3.326 Å) (blue) (Figure 5.5).

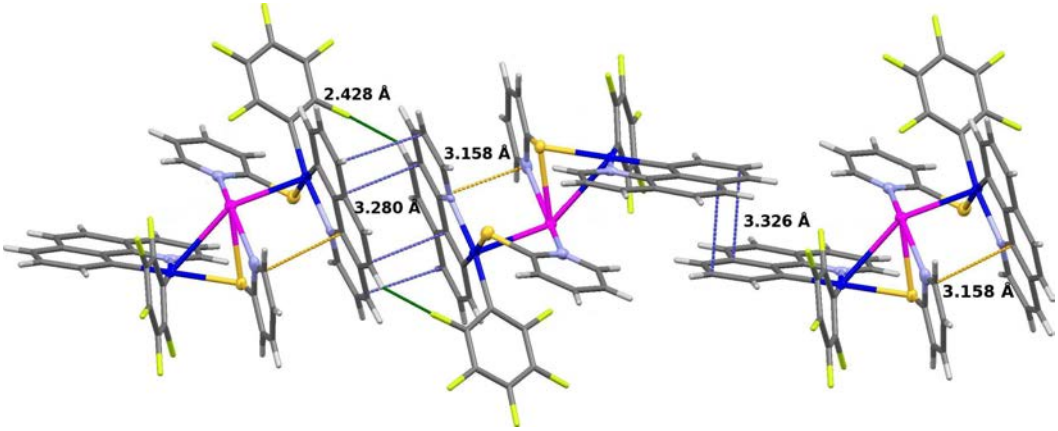

Figure 5.5: Crystal packing of **33**·1.5CH_2Cl_2 showing the intra and intermolecular π···π contacts (blue)

Interestingly, an analysis of the extended packing of **34** reveals that the void space around the lead(II) seems to be reduced by the occurrence of a short *intermolecular* fluorine···fluorine contact between F_o of two C_6F_5 [2.734(5) Å] rings of different Pt_2Pb clusters (Figure 5.6). This $F_o\cdot\cdot F_o$ interaction form dimers, which are further connected by *intermolecular* π··π [3.387(10) Å bzq···bzq] and reinforced by $F_o\cdot\cdot H$(bzq) interactions [2.426(5), 2.595(5) Å].

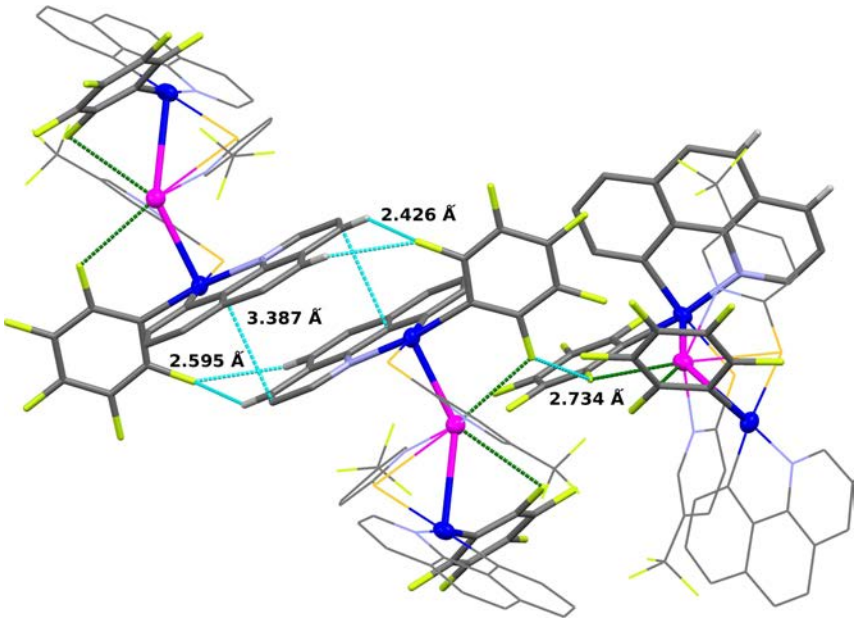

Figure 5.6: Crystal packing of **34**·0.9CH_2Cl_2 showing the intermolecular contacts

As has been previously noted, the treatment of **33** and **34** with a drop of acetone provokes a change in the luminescence (**33**) or in the luminescence and in the color (**34**). This fact encouraged us to crystallize these compounds from acetone/hexane.

The structure of [{Pt(C_6F_5)(bzq)}$_2$Pb(Spy)$_2$(acetone)]·1.5acetone (**33·acetone**·1.5acetone) (Figure 5.7, Table 5.2 and A5.2) shows that one of the two and a half molecules of acetone present in the lattice is directly ligated to the Pb^{II} centre, causing a remarkable change in its coordination sphere. The Pb-O distance [2.775(5) Å] falls within the reported range of Pb-O distances for the primary coordination sphere in lead(II) complexes.[7b] Further evidence for the coordination of acetone is the presence of a ν(C=O) band at 1696 cm^{-1}, lower than that of the free acetone (~ 1720 cm^{-1}). Curiously, the coordination of the acetone causes the rupture of the Pb···S bond (Figure 5.7) and enforces a small conformational change in the five membered ring (PbNCSPt), resulting in a final *cis* geometry of N atoms around Pb^{II} [N(2)-Pb-N(4) 84.20(13)º] and also in a more acute Pt-Pb-Pt angle [133.291(8)º] compared to that in **33**·1.5CH_2Cl_2. This rearrangement seems to be accompanied by a decrease in the lone pair activity in relation to **33**·1.5CH_2Cl_2 (also supported by TD-DFT). Thus, in **33·acetone** the local Pt_2N_2O environment around the Pb^{II} ion is more *holodirected*, and displays less asymmetric and slightly shorter (within average) Pb-N [2.497(4), 2.568(4) Å] and Pb^{II}-Pt [2.8401(3), 2.9790(3) Å] distances in relation to those found in **33**·1.5CH_2Cl_2. These

changes seem to be responsible for the observed vapoluminescent behaviour. In fact, despite the incorporation of a greater amount of acetone solvent (density: 2.046 **33·acetone** *vs* 2.221 g/cm^3 **33**·1.5CH_2Cl_2) both, the *intra* (Spy···bzq) (3.196 Å) (orange) and *inter* (bzq···bzq) π···π (3.222, 3.304 Å) (violet) and H···F (2.654 Å) (green) contacts are similar in both pseudopolymorphs (Figure 5.5 and 5.8).

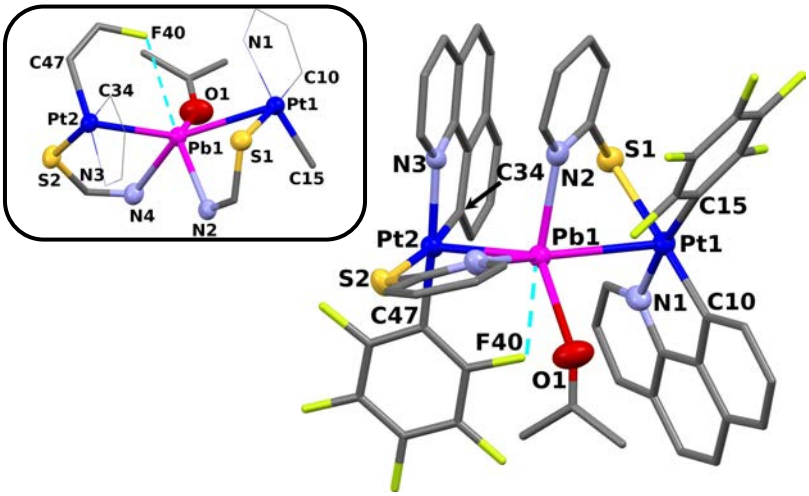

Figure 5.7: X-ray molecular structure of **33·acetone**·1.5acetone (yellow) showing its core (up left)

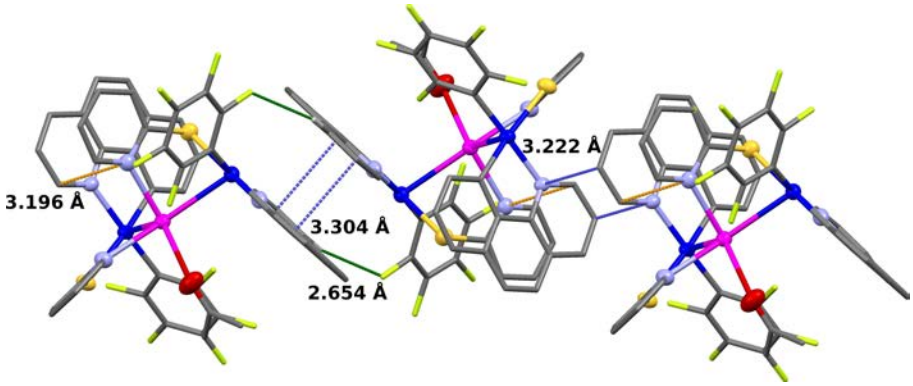

Figure 5.8: Crystal packing of **33·acetone**·1.5acetone showing the π···π intra and intermolecular contacts

Unlike the local Pt_2N_2S (*trans*-N,N) to Pt_2N_2O (*cis*-N,N) lead environment that was found for the bzq/Spy complex **33** upon incorporation of one molecule of acetone (**33** to **33·acetone**), the structure of the yellow form **34·(acetone)$_{1.5}$** (Figure 5.9, Tables 5.2 and A5.4) revealed that the incorporation of molecules of acetone takes place with minor changes in the *primary sphere* of coordination of Pb^{II}.

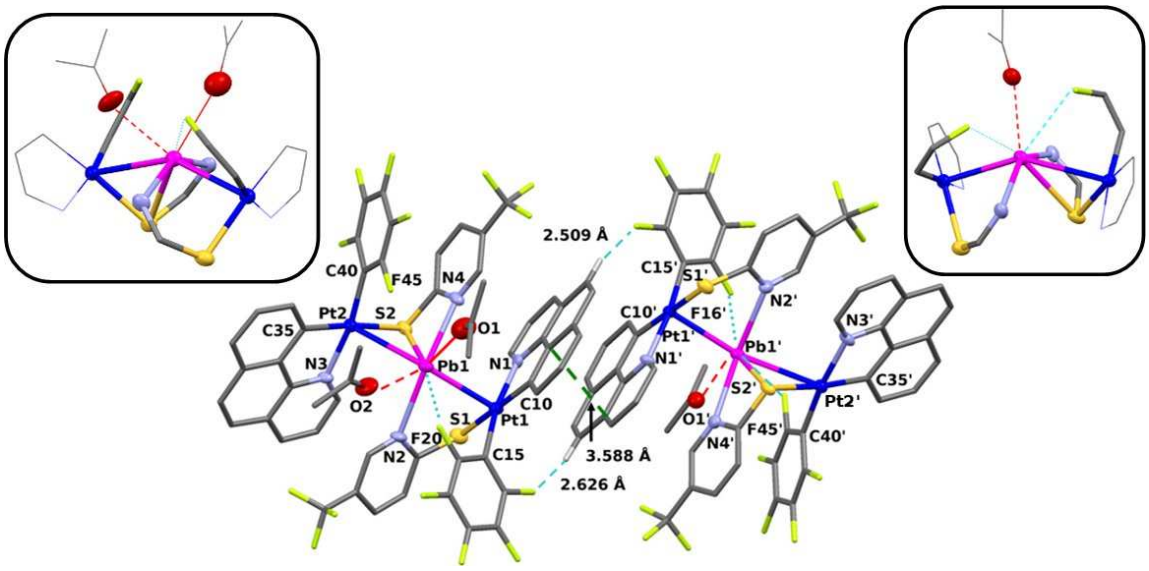

Figure 5.9: X-ray molecular structure of **34·(acetone)$_{1.5}$** (yellow) showing the two types of molecules: (left) molecule **A 34·(acetone)$_2$** with its core (top left) and (right) molecule **B** of **34·(acetone)** with its core (top right). Intermolecular π···π (bzq···bzq) and H_{bzq}···F_o interactions between molecules **A** and **B** are also included

Interestingly, the crystals of **34·(acetone)$_{1.5}$** ($P2_1$ space group) were found to contain two different molecules (labeled **A** and **B**) in the asymmetric unit having different and very weak Pb···O(acetone) secondary contacts within the van der Waals limit. Thus, while in the molecule **A** the lead is involved in two long Pb···acetone interactions [Pb···O 2.791(11) and 2.937(9) Å], retaining only one F_o contact [F(20)···Pb 2.895(8) Å], in the molecule**B** the Pb atom interacts more weakly with only one acetone molecule [Pb'-O' 2.967(8) Å] retaining the two F_o···Pb secondary contacts [2.829(8), 3.031(6) Å] observed in **34**. Although the Pb···O distances are slightly longer than those reported for the upper range in the primary coordination sphere of Pb^{II} (2.70 Å),[7b] the presence of these contacts in **34·(acetone)$_{1.5}$** provokes an increase in the Pb^{II} coordination number in relation to the unsolvated orange **34** (from 7 to 8), which is reflected in a less asymmetrical Pt_2N_2S local environment with bond lengths, on average, longer than those found in **34** (see Table 5.2). The more *holodirected* environment around the Pb in the acetone solvate **34·(acetone)$_{1.5}$** is evidenced by the wider Pt-Pb-Pt angle [146.88(2)º **A**, 149.64(2)º **B** in **34·(acetone)$_{1.5}$** *vs* 141.54(1)º in **34**] and more symmetrical Pb-N distances, though the N-Pb-N angle observed in both molecules **A** and **B** is more acute [144.7(3) **A**, 140.4(3)º **B** in **34·(acetone)$_{1.5}$** *vs* 153.15(16)º in **34**]. All of these structural details point to lower stereochemical activity of the lone pair in the yellow form **34·(acetone)$_{1.5}$** in relation to the orange **34**. As it is

illustrated in Figure 5.9, both molecules (**A** and **B**) are contacting through π···π (bzq) and F_o···H interactions involving one of the platinum fragments (Pt1, Pt1'). These intermolecular contacts are clearly weaker than those observed in **34** [π···π/F_o···H 3.588(20)/2.509(7), 2.626(7) Å **34·(acetone)$_{1.5}$** *vs* 3.387(10)/2.426(5), 2.595(5) Å **34**]. We hypothesize that not only the different coordination environment of the Pb center in both forms but also the packing changes play a role for the observed vapochromism and vapoluminescent behaviour of this cluster.

In contrast to benzoquinolinyl clusters (**33** and **34**), the molecular structure of the orange ppy/Spy derivative **35** (crystallized as **35**·2$CHCl_3$, Figure 5.10, Table 5.2 and A5.5) reveals the formation of a rather symmetrical and linear Pt_2Pb cluster [Pt-Pb-Pt 169.88(1)º], in which the N of the μ-κ*N*,*S*-Spy ligands are surprisingly ligated to the platinum centers [Pt-N 2.148(5), 2.120(6) Å]. The Pb center exhibits a *primary* "Pt_2S_2" four-coordination, with Pt-Pb [2.8326(4), 2.8998(4) Å] and Pb-S bonds shorter [2.691(2), 2.767(2) Å], on average, than those found in **33** and **34**, supplemented by two secondary Pb···F_o *intramolecular* interactions [2.874(6), 2.914(4) Å]. The *formally neutral* Pb center acquires a final slightly distorted octahedral coordination, as evidenced by the angles (S-Pb-S and F-Pb-F *ca* 96º) close to 90º, thus indicating that the stereochemical activity of the lone pair is negligible. This structural feature, together with the rather tight packing generated (Figure 5.10b), could explain the experimental observation that this cluster does not exhibit visual response (colour or luminescence) to vapour of donor solvents such as acetone, THF and NCMe. In this complex the Pb is well embedded and, presumably, the activation energy to cause structural changes is higher than those required for **33** and **34**.

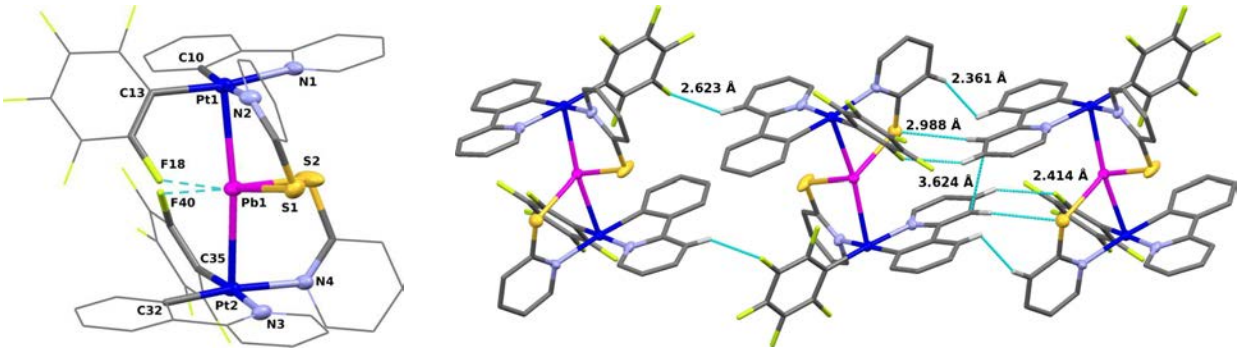

a) b)

Figure 5.10: a) Molecular structure and b) crystal packing of **35**·2$CHCl_3$ showing the closest intermolecular [$H_{ppy}\cdots$S 2.988(2) Å, $H_{ppy}\cdots F_{ortho}$ 2.414(4) Å, $H_{ppy}\cdots H_{spy}$ 2.361(1) Å and $H_{ppy}\cdots F_{metha}$ 2.623(4) Å] contacts. The ppy ligands are slipped and the shortest separation is long [3.624(13) Å]

As **35**, the ppy/SpyCF_3-5 complex **36**, isolated as a yellow solid by precipitation from a CH_2Cl_2 solution with *n*-hexane, did not showed visual changes to vapours. However, while exploring different crystallization conditions, we found that its colour (yellow or orange) and luminescence (yellow or orange-red) depend on the solvent, concentration and also the velocity of crystallization. Thus, slow crystallization from CH_2Cl_2, $CHCl_3$ or benzene always yielded yellow crystals. However, from very concentrated CH_2Cl_2 solution both yellow and dark-orange crystals separated, whereas pale-orange crystals were obtained from acetone (or acetone/hexane). In addition, we noted that fast evaporation of **36** to dryness in any of these solvents always generated an orange film with a very strong red luminescence. For cluster **36** we could crystallize four solvates that were subjected to X-ray crystallography (Figure 5.11, Tables 5.2 and A5.6–5.9): yellow crystals of stoichiometry **36**·4C_6H_6 and **36**·4$CHCl_3$ (hereafter **36-y**), pale-orange crystals of the solvate [{Pt(C_6F_5)(ppy)}$_2$Pb(SpyCF_3)$_2$(acetone)] [**36·acetone**] and orange crystals by cooling a concentrated solution of CH_2Cl_2 (**36**·2CH_2Cl_2, denoted as **36-o**).

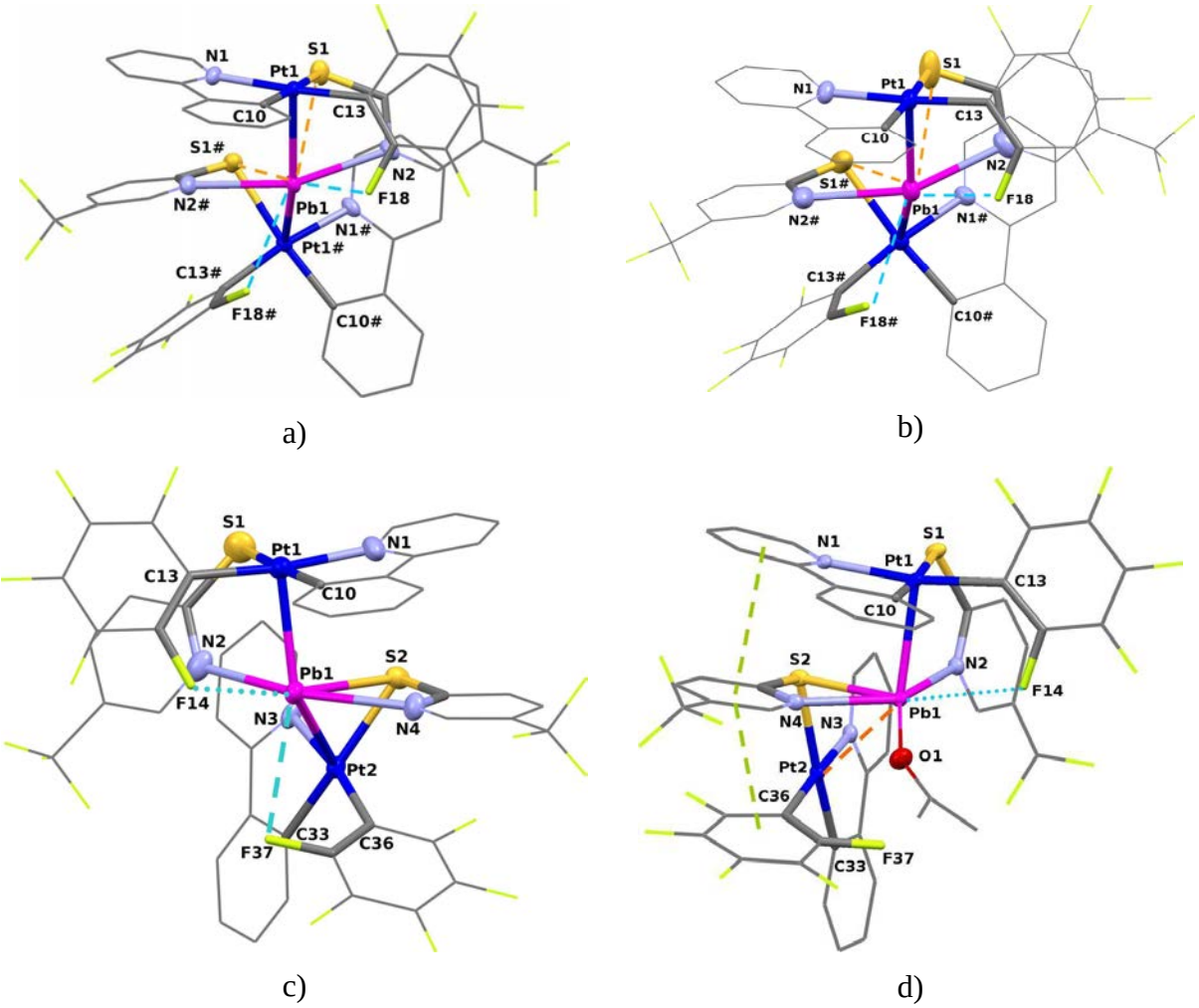

Figure 5.11: Molecular structure of a) **36**·4C_6H_6, b) **36**·4$CHCl_3$, (**36-y**), c) **36**·2CH_2Cl_2 (**36-o**) and d) **36·acetone**

The structures of the two yellow solvates are very similar (see Table 5.2) with only small differences in bond lengths and angles and clearly different from those of orange crystals **36-o** and **36·acetone**. The asymmetric unit of the orange crystals **36-o** is built by three rather similar molecules (Figure 5.12a, Table A5.6), and, therefore, only the data of one of them are included in Table 5.2. The structural details are comparable to those of orange crystals of **33** and **34** obtained from CH_2Cl_2. The Pb^{II} center (Figure 5.11c) also features a primary "Pt_2N_2S" coordination with *asymmetric* Pt-Pb [2.7840(5), 3.0596(5) Å)] and Pb-N [2.564(8), 2.679(7) Å] bond distances. Pb-S distances of 2.858(3) and 3.596(5) Å indicate that only one of the sulphur atoms takes part in the bonding, which is supplemented (up to 7), in the direction of the open void, by two long Pb-F_o contacts. The orientation of the Pt fragments (dihedral angle ~64º) leads to a Pt-Pb-Pt angle [137.58(2)º] more acute than those seen in **33** and **34**, whereas the N-Pb-N is more linear (~160º). In the crystal, the molecules are arranged in a head to head

manner through π···π interactions [ppy···ppy (3.235-3.355, 3.855 Å) and C_6F_5····C_6F_5 (3.232-3.325, 3.320 Å)] of different degrees to form extended chains, which are additionally connected by extensive H···F contacts (2.609-2.668 Å) (Figure 5.12).

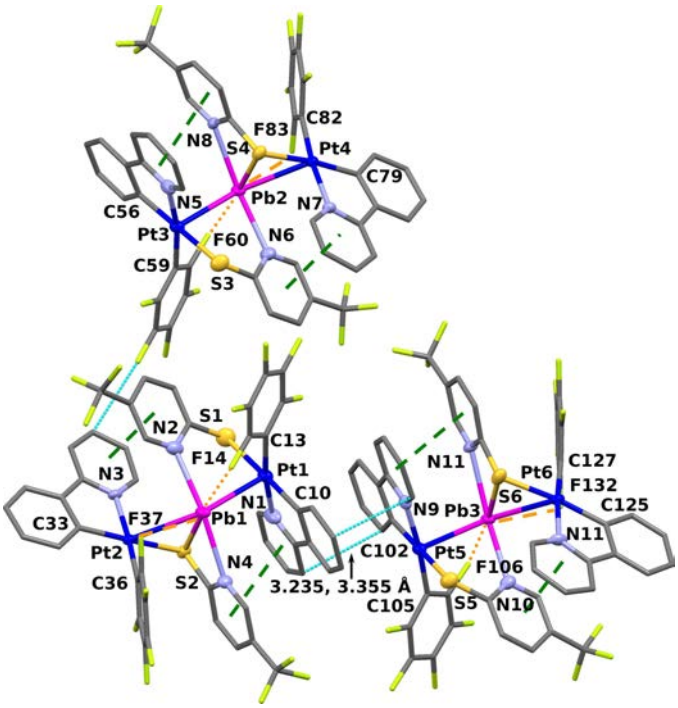

a)

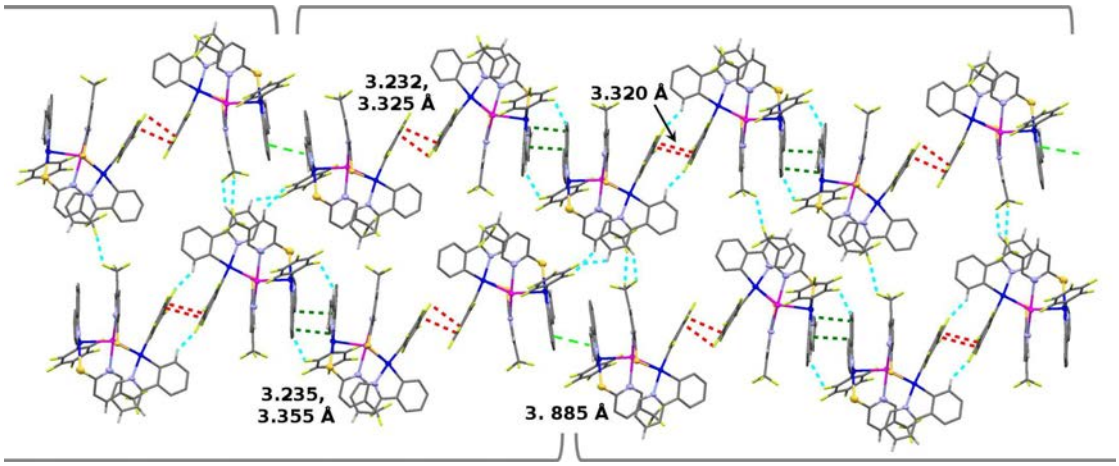

b)

Figure 5.12: Crystal packing of **36**·2CH_2Cl_2 (**36-o**) showing a) the three molecules of the asymmetric unit, the intermolecular π··π (ppy···ppy) [3.235(14), 3.355(16) Å] and C_{ppy}···F_m [3.081(12) Å] (blue) between the three molecules and the intramolecular π··π (ppy···Spy) (3.598, 3.844 Å) (green lines) and F_o···Pb (2.835-2.892; 3.128-3.232 Å) (orange), b) the intermolecular contacts. The supramolecular packing is formed by chains supported by intermolecular π··π interactions involving two ppy ligands [3.235, 3.355, 3.855 Å] (green) and two C_6F_5 (3.232-3.325 Å) (red). This chains interacts via $F_{C_6F_5}/_{CF_3}$···Hppy/Spy (2.609-2.668 Å) (blue)

In contrast, slow crystallization from benzene and $CHCl_3$ (and also from CH_2Cl_2) seems to allow a symmetrical coordination of both Pt units (dihedral angle *ca* 67º) around Pb^{II} in the yellow forms (**36-y**, see Figure 5.11a for **36**·$4C_6H_6$ and Figure 5.11b for **36**·$4CHCl_3$), pointing to a lower stereochemical activity of the lone pair. In both yellow crystals, the Pb is coordinated to the two Pt and N atoms of both platinum units with identical Pt-Pb (~ 2.95 in **36**·$4C_6H_6$, 2.92 Å in **36**·$4CHCl_3$) and Pb-N (~2.67 Å) bonds lengths, its formal coordination being increased (up to 8) with two clearly weaker Pb···S and Pb···F bonding interactions (Table 5.2). The Pb-S distances [2.957(1)-3.024(2) Å] are slightly larger than the shorter distances seen in **36-o** and bzq clusters (**33** and **34**), suggesting that the coordination of the thiolate is somewhat midway between μ-κ^2*N,S* and μ-κ^3*N,S,S*. Interestingly, the Pt-Pb-Pt angle also increases in relation to that observed in **36-o** being comparable to the angle N-Pb-N (~155, 154º). In the crystal the molecules also forms chains, but the main difference with the packing observed in **36-o** is that the neighbouring molecules are associated in a face to face manner through the ppy ligands (3.346 Å **36**·$4CHCl_3$; 3.689 **36**·$4C_6H_6$) (Figures 5.13 for **36**·$4CHCl_3$ and 5.14 for **36**·$4C_6H_6$).

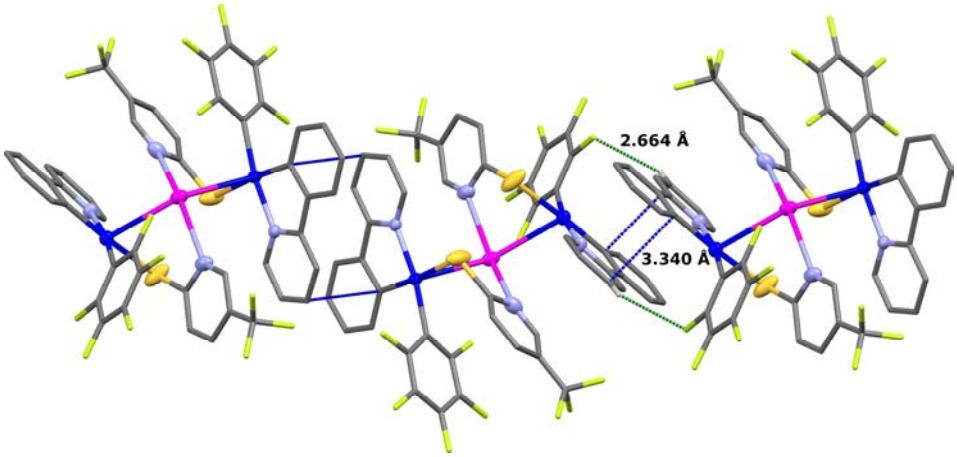

Figure 5.13: Crystal packing of **36**·$4CHCl_3$ showing the intermolecular contacts. The supramolecular packing is formed by chains supported by intermolecular π···π interactions involving two ppy ligands with an interplanar distance of 3 3.340(8) Å

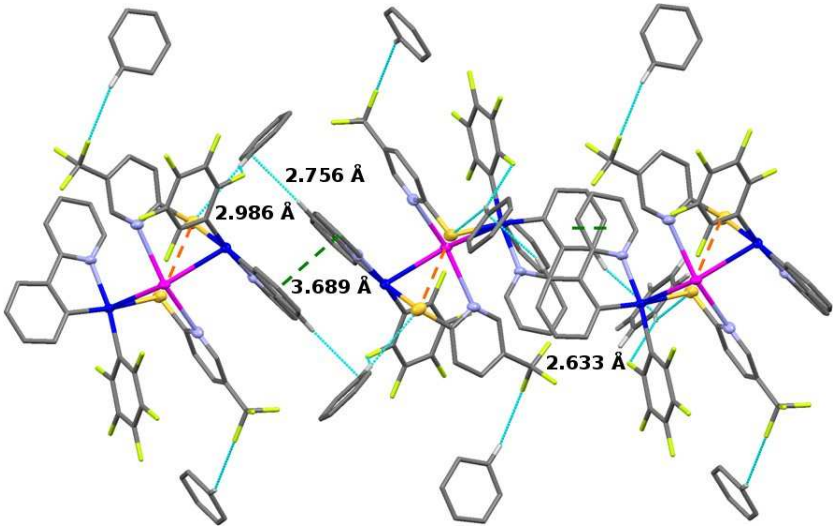

Figure 5.14: Crystal packing of **36**·4C_6H_6 showing the intermolecular contacts. The supramolecular packing is formed by chains supported by intermolecular π···π interactions involving two ppy ligands with interplanar distances of 3.689 Å. This π···π interaction is supported by $H_{ppy}\cdots C_{C_6H_6}$ [2.756(4) Å], $F_{C_6F_5}\cdots H_{C_6H_6}$ [2.633(2) Å] and $S\cdots C_{C_6H_6}$ [2.986(1) Å] secondary interactions

Interestingly, crystallization from acetone enforces an essentially perpendicular disposition of both Pt units (dihedral angle 80.23º), provoking an asymmetry greater than that observed in **36-o** and the presence of two very distinct Pt centers. In **36·acetone**, one of the Pt units is involved in a short Pt(1)-Pb bond [2.7863(2) Å] and the other in a weak contact [Pb-Pt(2) 3.534(1) Å] (Figure 5.11d). Similarly, one of the SpyCF$_3$-5 ligands chelates the Pb [Pb-S(2)/N(4) 2.7728(8)/2.566(3) Å] and is bonded to Pt(2) (μ-κ^3*N,S,S*), whereas the other behaves as typical μ-κ^2*N,S*. The remaining closest donor atoms around the Pb are one F_o [2.912(2) Å] and the oxygen of the acetone [2.897(3) Å]. The interaction with the solvent is very weak, consistent with this, the acetone molecules escape from the crystal in air, as confirmed by NMR spectroscopy. Interestingly, the conformation of the Pt coordination planes and the chelating thiolate bridge favours the presence of very close π···π *intramolecular* contacts (ppy···SpyCF$_3$···C_6F_5 3.443-3.437 Å), which likely also play an important role in the stabilization of this structure (Figure 5.11d). In addition, the trinuclear Pt_2Pb molecules are arranged so that the same ppy and C_6F_5 ligands are closely located in a head [ppy···ppy 3.345(5) Å] and tail [$C_6F_5\cdots C_6F_5$ 3.230(5) Å] fashion giving rise to a columnar network (Figure 5.15). This packing is somewhat comparable to that seen in **36-o** (Figure 5.12), but is in contrast with those observed for the yellow forms

(**36**·4C_6H_6 and **36**·4$CHCl_3$) mainly based in more tightly intermolecular π···π of ppy groups (Figures 5.13 and 5.14).

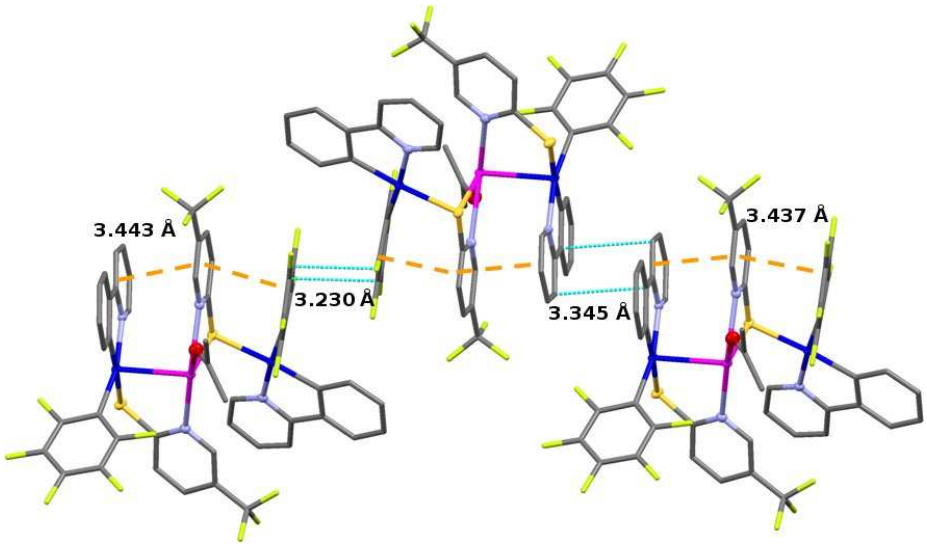

Figure 5.15: Crystal packing of **36·acetone** showing the intermolecular contacts. The supramolecular packing is formed by chains along the *c* crystallographic direction, supported by alternative intermolecular π···π (ppy-ppy) [3.345(5) Å] and (C_6F_5…C_6F_5) [3.230(5) Å] interactions

To help to clarify the photophysical behaviour we conclude this X-Ray diffraction section with a small summary about structural characteristics of these complexes.

Complex **35** (ppy/Spy) is generated through coordination of the pyridine-N atom to the Pt centers, whereas the formation of **33**, **34** (bzq) and **36** (ppy ($SpyCF_3$) is accompanied by a formal thiolate transfer from Pb^{II} to Pt^{II}, keeping the two N in the primary environment of the lead. In **35**, the neutral Pb center adopts a rather stable and symmetrical "Pt_2S_2" coordination sphere, supplemented by two Pb-F_o contacts.

For **33** and **34** two pseudopolymorphs were found depending on the solvent (CH_2Cl_2 or acetone) with changes in the coordination mode of the SpyR ligands, intermetallic Pt-Pb bonds and secondary intra and intermolecular contacts induced by Pb-solvent binding. In the unsolvated systems the Pb^{II} exhibits an asymmetric "Pt_2N_2S" (*trans*-N,N) environment with changes to a more symmetric in their acetone adducts ["PtN_2O" (*cis*-N,N) **33·acetone** or "PtN_2SO_2/ PtN_2SO" in **34·(acetone)$_{1.5}$**].

Complex **36** crystallizes in different forms depending on the solvent and crystallization conditions, a symmetrical (yellow **36-y**), and two asymmetrical with short Pt-Pb bonds [pale-orange (**36·acetone**) and orange **36**·$2CH_2Cl_2$ (**36-o**)]. Notably, slow crystallization and low concentration favour the formation of the thermodynamically more stable yellow form, whereas fast crystallization gives rise orange solids. We note that an asymmetrical environment around the Pb^{II} (*hemidirected*) point to a greater stereochemical activity of the lone pair on the Pb^{II}.

5.2 Photophysical properties

The detailed data of the photophysical properties of all derivatives **32-36** are compiled in Tables 5.3 (UV-vis solution and solid), 5.4 (emission in solid state) and A5.10 (emission in solution)

Table A5.3: Absorption data for compounds [Pt(C_6F_5)(ppy)(dmso)] (**32**), [{Pt(C_6F_5)(C^N)}$_2$Pb(SpyR)$_2$] (**33**–**36**) at room temperature (5 x 10^{-5} M solutions and solid state[a])

Compound	λ_{abs}/nm (10^3 ε $M^{-1}cm^{-1}$)
[Pt(C_6F_5)(ppy)(dmso)] **(32)**	246 (28.8), 253 (29.5), 297 (7.4), 313 (8.5), 323 (10.2), 350 (3.9), 365 (2.7) **CH_2Cl_2** 315 (6.2), 347 (4.3), 365 (3.0), 395 (1.7) **Acetone** 243 (17.8), 253 (18.8), 280 (8.9), 288 (7.8), 313 (5.2), 323 (5.1), 352 (2.9), 400 (1.1) **2-MeTHF** 234, 256, 280, 321, 363, tail to 400 **Solid**
[{Pt(C_6F_5)(bzq)}$_2$Pb(Spy)$_2$] **(33)**	215 (46.4), 240 (75.2), 310 (30.1), 357 (17.3), 405 (11.4), 455 (5.6), 485_{sh} (2.6) **CH_2Cl_2** 354 (20.1), 401 (11.7), 454 (4.9), 485_{sh} (2.5) **Acetone** 249, 307, 350, 415, 480, tail to 550 **Solid**
33-acetone	260 , 315, 365, 440, 495, tail to 560 **Solid**
[{Pt(C_6F_5)(bzq)}$_2$Pb(SpyCF$_3$)$_2$] **(34)**	245 (79.5), 308 (38.3), 365 (20.1), 400 (13.3), 450 (6.6), 485_{sh} (2.5) **CH_2Cl_2** 343 (10.2), 360 (8.5), 400 (5.4), 450 (2.3), 480_{sh} (1.1) **Acetone** 254, 290, 319, 352, 370, 397, 446, 500, tail to 560 **Solid**
34-acetone	255, 290, 316, 400, 448, 490, tail to 550 **Solid**
[{Pt(C_6F_5)(ppy)}$_2$Pb(Spy)$_2$] **(35)**	255 (55.0), 295 (33.1), 332 (21.5), 360 (15.9), 410 (11.0), 455 (4.8), 485_{sh} (2.5) **CH_2Cl_2** 342 (10.1), 365 (7.6), 410 (5.3), 460 (2.3)*** Acetone** 227, 260, 300, 339, 362, 414, 485, tail to 560 **Solid**
[{Pt(C_6F_5)(ppy)}$_2$Pb(SpyCF$_3$)$_2$] **(36)**	255 (48.3), 290 (34.6), 323 (23.2), 355 (17.8), 395 (13.6), 445 (5.7), 485_{sh} (2.8) **CH_2Cl_2** 330 (10.5), 355 (7.7), 390 (6.2), 440 (1.9)*** Acetone** 230, 260, 285, 325, 360, 395, 430, 442, 470 tail to 540 **Solid**
36-acetone	230, 260, 285, 330, 360, 385, 425, 450, 482, 500 tail to 570 **Solid**
36 grinding	230, 260, 295, 405, 480 tail to 540 **Solid**

a) Diffuse Reflectance, * Tail to 530 nm

Table 5.4: Photophysical data for complexes [$Pt(C_6F_5)$(ppy)(dmso)] (**32**), [{$Pt(C_6F_5)(C^N)$}$_2$Pb(SpyR)$_2$] (**33** – **36**) in the solid state at 298 and 77 K

Compound	T[a]/K	λ_{em}/nm[d]	τ (μs)	ϕ [a]	k_r [b]	k_{nr} [c]
[$Pt(C_6F_5)$(ppy)(dmso)] (**32**)	298 77	490, 518$_{max}$ 500$_{max}$, 537	20.1 70.0	13	6.5 x 10^3	5.7 x 10^4
[{$Pt(C_6F_5)$(bzq)}$_2$Pb(Spy)$_2$] (**33**)	298 77	620 620	1.6 5.2	34	2.1 x 10^5	9.5 x 10^5
33-Acetone	298 77	580 577	0.5 9.3	14	2.8 × 10^5	1.7 × 10^6
33- CH_3CN	298 77	585 570	0.5 11	15	3.0 × 10^5	1.7 × 10^6
33-MeOH	298 77	576 575	0.3 12.9	17	5.6 × 10^5	2.8 × 10^6
33-THF	298 77	570 563	0.6 7.7	21	3.5 × 10^5	1.3 × 10^6
[{$Pt(C_6F_5)$(bzq)}$_2$Pb($SpyCF_3$)$_2$] (**34**)	298 77	580 570	3.6(18%); 5(82%) 9.8	32.2	3.0 x 10^5	1.4 x 10^6
34-Grinding	298 77	610 600	0.1(47%); 0.5(53%) 7.1	10.6	3.4 x 10^5	3.6 x 10^6
34-Acetone	298 77	545 535	0.2(24%); 0.4 (76%) 11.5	22.8	6.5 x 10^5	3.7 x 10^6
34-THF	298 77	575 570	0.2(37%); 0.4(63%) 11.0	12.4	3.8 x 10^5	3.5 x 10^6
34-MeOH	298 77	558 545	0.08(47%); .2(53%) 15.7	8.6	6.0 x 10^5	7.6 x 10^6
34-CH_3CN	298 77	550 550	0.3 (27%); 0.8(73%) 12.5	29	4.4 x 10^5	2.1 x 10^6
34-C_6H_6	298 77	570 570	0.3 (57%); 0.7 (43%) 10.4	19.5	4.1 x 10^5	2.6 x 10^6
[{$Pt(C_6F_5)$(ppy)}$_2$Pb(Spy)$_2$] (**35**)	298 77	620 616	3.2(13%); 0.6(87%) 7.2	13.8	1.5 x 10^5	1.2 x 10^6
[{$Pt(C_6F_5)$(ppy)}$_2$Pb($SpyCF_3$)$_2$] (**36**) yellow solid[e]	298 77	550 550	0.3 (24%); 0.9 (76%) 11.7	34.6	4.6 x 10^5	2.0 x 10^6
36-o (crystals)	298 77	610 630	1.24 6.5	14.0	1.1 x 10^5	9.4 x 10^5
36·acetone (crystals)	298 77	570 550	0.05(34%); 0.58(66%) 12.9	3.4	8.5 x 10^4	2.6 x 10^6
36 (red solid, from CH_2Cl_2)	298 77	660 650	0.4 (69%); 0.8 (31%) 4.4	39.6	7.6 x 10^5	3.2 x 10^6
36 (pale-orange, from acetone)	298 77	630 645	0.08(79%); 0.2(21%) 8.8	24.5	2.3 x 10^6	1.3 x 10^7
36-Grinding	298 77	600 600	0.1(23%); 0.7(77%) 7.7	5.2	9.3 x 10^4	1.9 x 10^6

a) (%) Determined by the absolute method using an integrated sphere. b) $k_r = \phi/\tau_{average}$. c) $k_{nr} = 1/\tau_{average}(1-\phi)$. d) λ_{exc} for **32** 365 nm; λ_{exc} for **33–36** 395-500 nm. e) from THF and CH_3CN weak emission centred at 580 and 600 nm, respectively

[Pt(ppy)(C_6F_5)(dmso)] (**32**). The precursor **32** shows intense absorptions (CH_2Cl_2) in the range 246-323 nm, attributable to metal perturbed ππ* intraligand (^{1}IL, bzq, C_6F_5) transitions, and two additional less intense bands at 350, 365 nm, which, with reference to previous assignments,[12e,f] are attributed to an admixture of ^{1}IL and ^{1}MLCT

(Table A5.3). The low-energy absorption showed a remarkable solvent dependence, shifting to lower energies in acetone or 2-MeTHF, indicating that it possesses a significant charge transfer character. Upon photoexcitation, it displays a structured emission (CH_2Cl_2 484, 518, 555 nm), which has negligible solvent and concentration dependence and exhibits a slight rigidochromism at 77 K (Table A5.10). In the solid state, the emission is somewhat broader, showing a slight red shift (Table 5.4), 490 nm 298 K, 500 nm 7 7K), probably because of the short $\pi\cdot\cdot\pi$ intermolecular interactions, as observed by X-ray. The structuration and long lifetime (20.1 μs, 298 K) suggest a predominant ^{3}LC transition with some ^{3}MLCT.

[{Pt(C_6F_5)(C^N)}$_2$Pb(μ-SpyR)$_2$]. The detailed data of the photophysical properties of the clusters **33**–**36** in solution and in solid state are compiled in Tables 5.3, 5.4 and A5.10.

5.2.1 Solution

Complexes **33**–**36** all exhibit rather similar UV-vis profiles in CH_2Cl_2 or acetone solutions. In particular, the formation of the clusters is characterized by the presence of two visible low energy absorptions (with a shoulder at *ca* 485 nm) in the range 390-485 nm tailing to 520-530 nm. According to TD-DFT calculations in the gas phase for **33**, **34** and **36** (See Section 5.3), these transitions mainly could be ascribed to admixtures of thiolate to cluster [(SpyR)→Pb,Pt] ^{1}L'CCT and ^{1}L'LCT [SpyR→C^N] charge transfer with some ^{1}MM'CT contribution. In agreement with this assignment, no noticeable changes were observed from the bzq (**33**/**34**) to the ppy (**35**/**36**) complexes and only minor blue shifts were detected from the Spy to the SpyCF_3 (see Table 5.3 and Figure A5.1 for **35** and **36**).

Upon photoexcitation into the low-energy bands (395-500 nm), the complexes display a broad featureless weak emission centered at 620 nm for the Spy derivatives (**33**, **35**) and slightly blue-shifted for SpyCF_3 complexes (600 **34**, 610 nm **36**) in fluid CH_2Cl_2 solution. In acetone solution, the emission is weaker but the maxima, clearly measured at higher concentration (10^{-3} M), remain essentially unchanged (see Table A5.10). This emission can be attributed to phosphorescence ligand-to-cluster ^{3}L'CCT

[(SpyR)→Pb,Pt] with some ^{3}MM'CT (M = Pt, M' = Pb) and ^{3}L'LCT [(SpyR)→C^N] character, as supported by TD-DFT studies. Upon cooling at 77 K, the intensity of the emissions increases remarkably. Curiously, whereas the Spy bridged complexes displayed only one band with a remarkable (570 nm **33**) or slight (600 nm **35**) rigidochromism in CH_2Cl_2 glasses, several bands were observed for the $SpyCF_3$ derivatives (555, 645_{max}, 730 nm **34**; 540, 640_{max}, 720 nm **36**, Figure 5.16). These bands are related to different excitation profiles, suggesting the presence of different emissive manifolds. It is likely that the main band and the small high-energy component originate from two different conformations of the pyridinethiolate-Pt fragments around the Pb^{II} formed in the freezing process, while the low energy manifold (720-730 nm) could be ascribed to excimers or aggregates ($\pi\cdots\pi$ or Pt$\cdots$Pt), which are well known in Pt^{II} cycloplatinate complexes. In acetone glasses, the emission maximum of **33** is also blue-shifted (570 nm), whereas those of **34** and **36** are similar to those observed in fluid solution (600 **34**, 595 nm **36**). In complex **35** two emission bands (575, 620 nm), probably related to two different conformers, were observed.

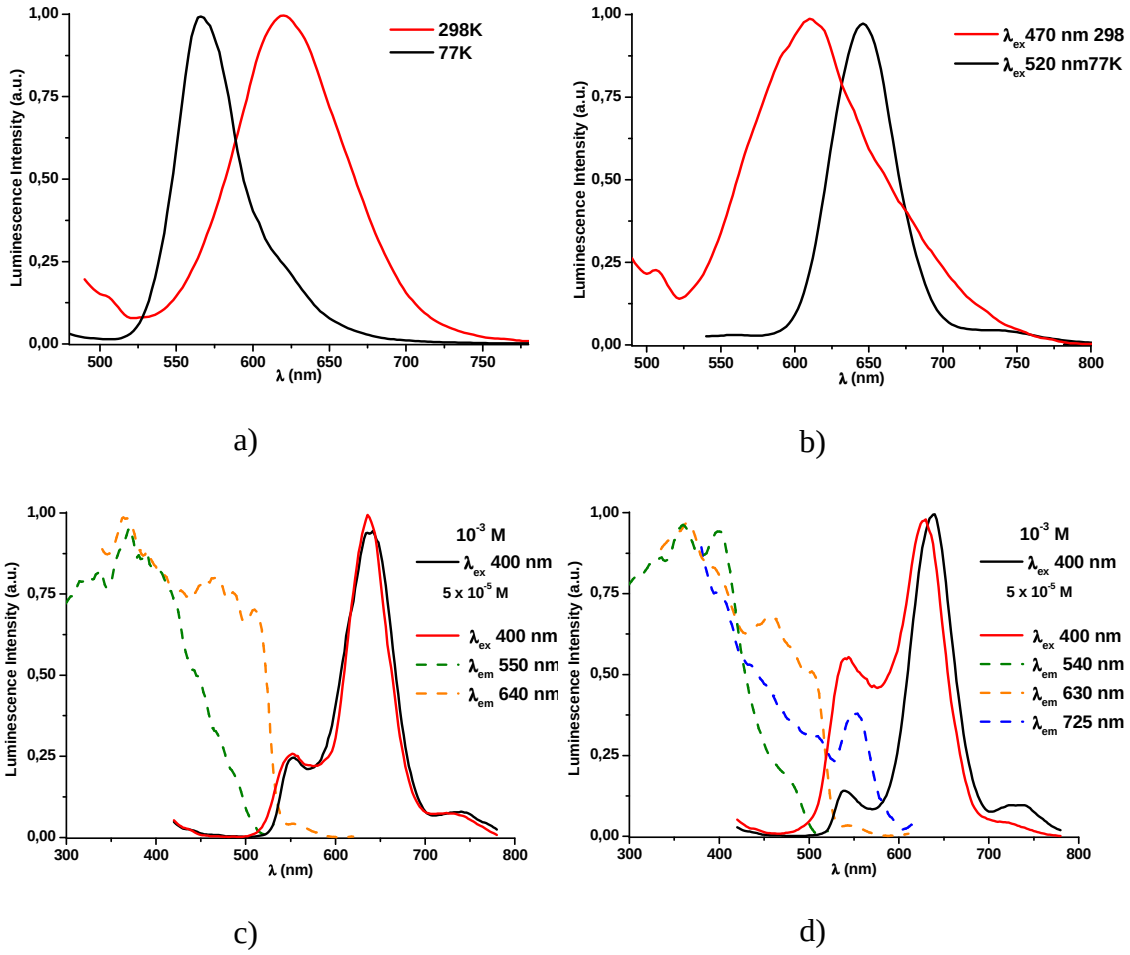

Figure 5.16: Experimental emission spectra of 10^{-3} M CH_2Cl_2 solution of a) **33** (λ_{ex} 460 nm) and b) **35**. Emission (solid line) and excitation (dotted line) spectra of CH_2Cl_2 solutions at 77 K of c) **34** and d) **36**

5.2.2 Solid state

The photophysical characteristics in solid state are compiled in Table 5.4 (Table 5.3 for reflectance) and illustrative examples are given in Figures 5.17-5.19 and 5.21-5.25. We note that the as-obtained solids (orange **33**–**35** and yellow **36**) are free of solvent, as confirmed by NMR spectroscopy. They are characterized by broad low energy absorptions (400-490 nm) tailing to *ca* 530 nm (**36**) or 560 nm (**33**–**35**), which are ascribed to mixed ^{1}L'CCT [(SpyR)→Pb,Pt]/^{1}L'LCT (thiolate→C^N) transitions, to which additional contribution from extensive π···π contacts (as supported by X-ray) cannot be discarded.

Under irradiation (λ_{ex} 395–500 nm) the as-synthesized solids display a bright orange (620 nm **33**, **35**; 580 nm **34**) or yellow (550 nm **36**) emission, whose maxima remain essentially unchanged at 77 K (Table 5.3 and Figure 5.17). The lifetimes are in the microsecond domain, implying a triplet excited state with phosphorescence character, and increase remarkably at 77 K, likely due to suppression of thermally activated nonradiative processes. We noted that for **34**–**36**, at room temperature, the emission decays were best fitted with two components, which might be attributed to small different structural environments, as was recently shown by Coppens in copper complexes.[17] The observed blue shift in complexes **34** and **36** can be attributed to the lower donor character of the $SpyCF_3$ ligand, supporting a significant ^{3}L'CCT character for the emission.

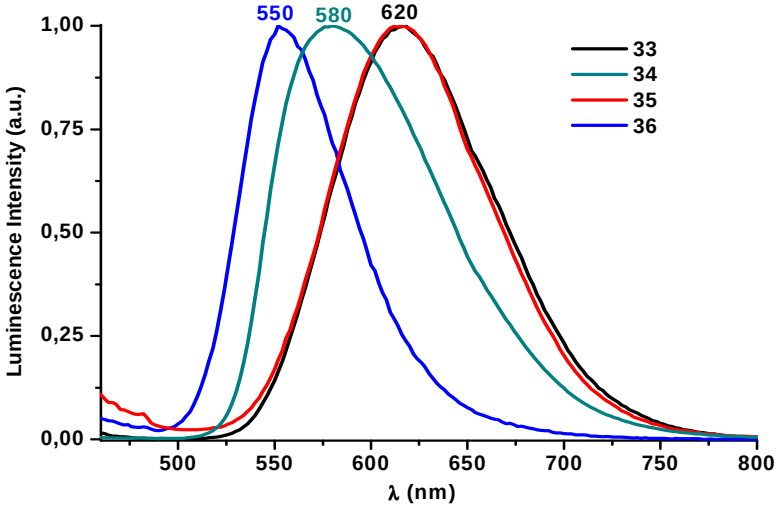

Figure 5.17: Comparative normalized solid state emission spectra (298 K, λ_{exc} 440 nm) of **33**–**36**

5.2.3 Vapochromism and mechanochromism properties

As mentioned in the Introduction, the flexibility of coordination of Pb allows it to modify its coordination through tuning the degree of stereochemical activity of the lone pair, which seems to be decisive in the observed vapochromic behavior of the bzq complexes **33** and **34** and in the mechanochromism of **34** and **36**. As noted before, in the case of complex solid **35**, its exposure to vapors or a drop of solvents of different VOCs has no visual effect in the color or emission. This behavior could be related to the rather stable octahedral geometry around the formally neutral Pb^{II} center with the Spy acting as a symmetrical μ-κ^2 *N*(Pt),*S*(Pb) ligands.

As was previously mentioned the as-obtained powder bzq/Spy complex **33** shows the same color (orange) in the crystalline form (**33**·1.5CH_2Cl_2) and the acetone adduct **33-acetone**, but when powder **33** is exposed to Me_2CO vapour, the solid-state luminescence colour changes from orange-red (620 nm, ϕ 34%) to yellow-orange (580 nm, ϕ 14%) in a few minutes (~ 10 min), indicating that the transformation has occurred. As is seen in Figure 5.18, both **33** and **33-acetone** display similar excitation spectra, which suggests that the blue-shift in the emission of **33-acetone** in relation to that of **33** could be related to a smaller Stockes shift in the aceton solvate (4593 cm^{-1} **33** *vs* 3231 cm^{-1} **33-acetone**)

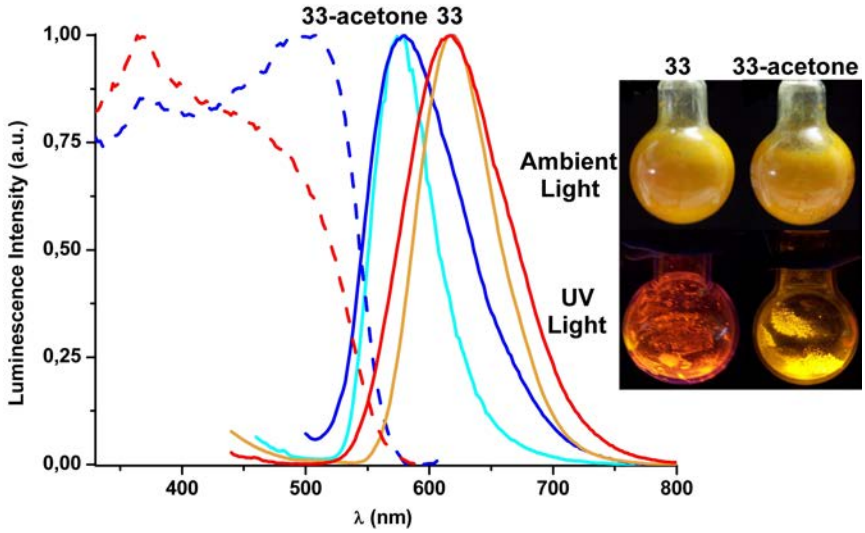

Figure 5.18: Normalized excitation (dotted lines) and emission (solid lines) of a) **33** and **33-acetone** in the solid state at 298 K (red and deep blue) and at 77 K (orange and light blue). Photographs show the colour and luminescence changes of **33** after addition of a drop of acetone

On standing, the acetone was completely lost in ~12h, recovering **33**. The desolvation, when passing a stream of air onto the sample **33-acetone**, was monitored by emission spectroscopy (Figure 5.19a) and the results showed a gradual change from **33-x(acetone)** to **33**, so we can not discard the formation of intermediate species. We note that the **33-acetone** to **33** process takes place also by grinding **33-acetone** in a ceramic mortar (Figure A5.2). Subsequent treatment of the crushed powder **33** with a drop of acetone leads again to the initial yellow-orange emissive phase [**33-x(acetone)**]. The characteristic emission of **33** and **33-acetone** can be recovered several times by sequential and repetitive paths (grinding and treatment with acetone).

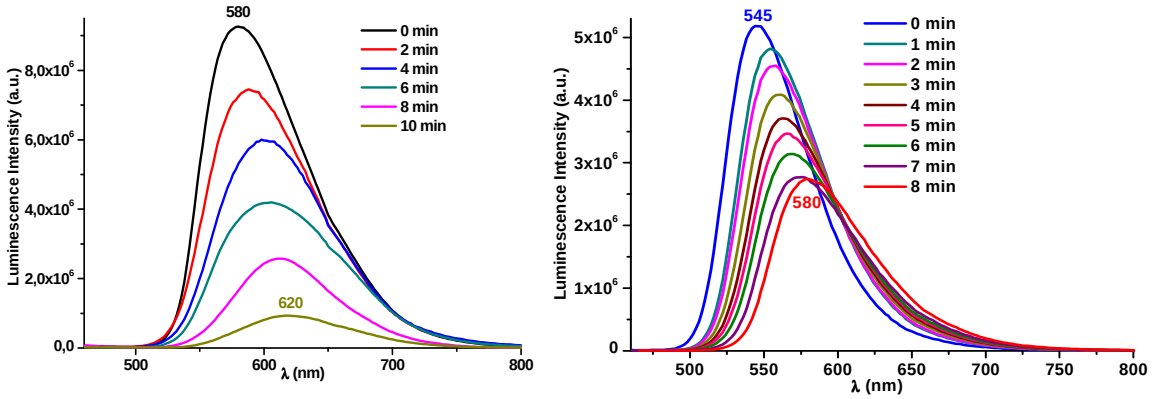

a) b)

Figure. 5.19: Monitoring of the desolvatation by emission spectroscopy with the time, passing a stream of air, of a) **33**·x(acetone) b) **34**·x(acetone)

The loss of acetone molecules, determined by TGA (Figure A5.3), fits to a molar ratio acetone/**33** of *ca.* 2:1 [**33-x(acetone), x** ~ 2]. Conclusively, powder X-ray diffraction (PXRD) diagrams were recorded for solid samples of **33** and **33** exposed to saturated acetone vapour [**33-x(acetone)**] at 298 K. The diffraction peaks correspond approximately to those calculated from the diffraction data of the single crystal X-ray analysis of **33**· 1.5CH_2Cl_2 and **33**·**acetone**· 1.5acetone, respectively (Figure 5.20).

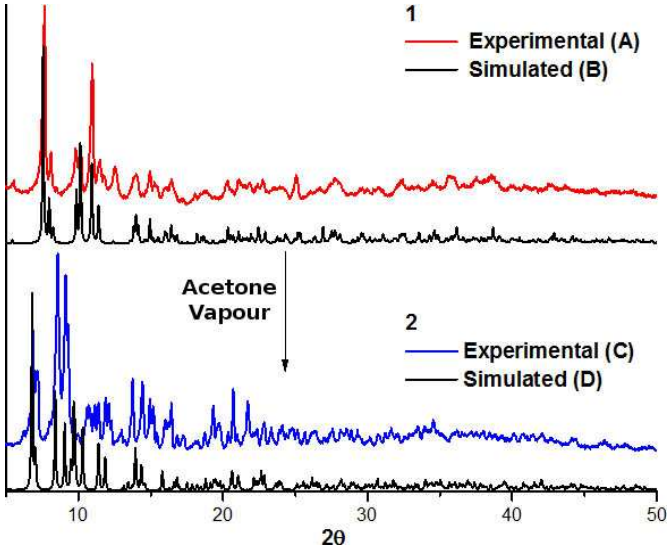

Figure 5.20: Powder diffraction patterns for: (A) experimental data from the ground state **33**, (B) computed pattern from the single crystal data for **33**· 1.5CH_2Cl_2. (C) experimental data from the sample **33** after exposure to acetone vapour [**33**·**x(acetone)**]. (D) computed pattern from the single crystal data for **33**·**acetone**· 1.5acetone

Vapour response of **33** to other donor solvents such as MeCN, MeOH and THF is also relatively fast [MeCN (~10 min) > MeOH (20 min) > THF (30 min)], provoking a distinct shift to the yellow region in the photoemission (Figure 5.21a Table 5.4). However, no-donor solvents such as toluene, hexane or even diethyl-ether do not trigger a response. The solvated products, **33**-x(solvent), possibly similar to **33·acetone**-x(acetone), were obtained as pure phases by addition of a drop of the respective solvent to **33**. The desolvation process for **33**-THF, examined by emission spectroscopy, followed a similar pattern to **33·acetone**-x(acetone). It is assumed that these donor solvents L are able to approach to the Pb^{II}, causing a change in the local environment from a distorted *hemidirected* "Pt_2N_2S" to a more symmetrical "Pt_2N_2L" as seen in the X-Ray studies of **33·acetone**. As listed in Table 5.4, in the solvates the phosphorescence yields are smaller and the calculated non-radiative constants, k_{nr}, are larger than those of **33** which is absent in the solvate. The presence of a more rigid $6e^-$ Spy^- bridging ligand in **33** could explain the lower observed k_{nr} values.

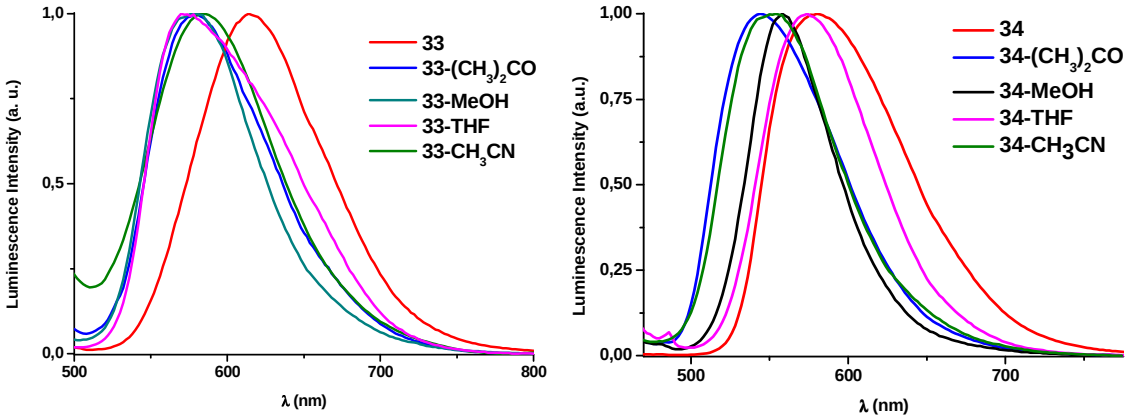

a) b)

Figure. 5.21: Normalized emission spectra after treating a) **33** and b) 34 with a drop of the respective solvent at 298 K

In contrast, as commented before, color and luminescence changes were observed for **34** (powder and crystalline) and the acetone solvate **34·(acetone)**$_{1.5}$. Thus, when **34** was treated with a drop of acetone, a color change occurred from orange to yellow under ambient light and the bright yellow-orange luminescence turned to yellow-green under UV-light (Figure 5.22). This behavior, visible to the naked eye, is reflected in a slight blue-shift in the diffuse reflectance spectra (Figure 5.23a) and in the corresponding emission spectra. As is illustrated in Figure 5.22, a significant blue shift from 580 to 545 nm is observed in the emission at 298 K, which is slightly blue-shifted

at 77 K (535 nm). In contrast to the bzq/Spy complex (**33**), in this case **34** and **34·(acetone)$_{1.5}$** display different excitation spectra, giving rise to similar Stokes shifts. Considering the increase in the Pb coordination due to weak contacts to the acetone molecules and the larger π···π stacking observed in the XRD of **34·(acetone)$_{1.5}$**, these changes are attributed to the concomitant result of both effects. Interaction with the solvent molecules likely somewhat decreases the electrophilicity of the lead center, increasing the energy of the LUMO and the gap of the transition.

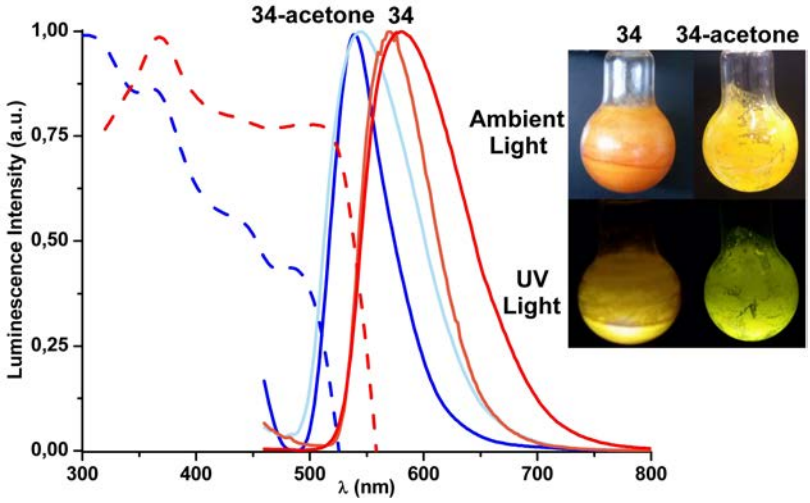

Figure 5.22: Normalized excitation (dotted lines) and emission (solid lines) of **34** and **34-acetone** (powders) at 298 K (red and deep blue) and at 77 K (orange and light blue). Photographs show the colour and luminescence changes of **34** after addition of a drop of acetone

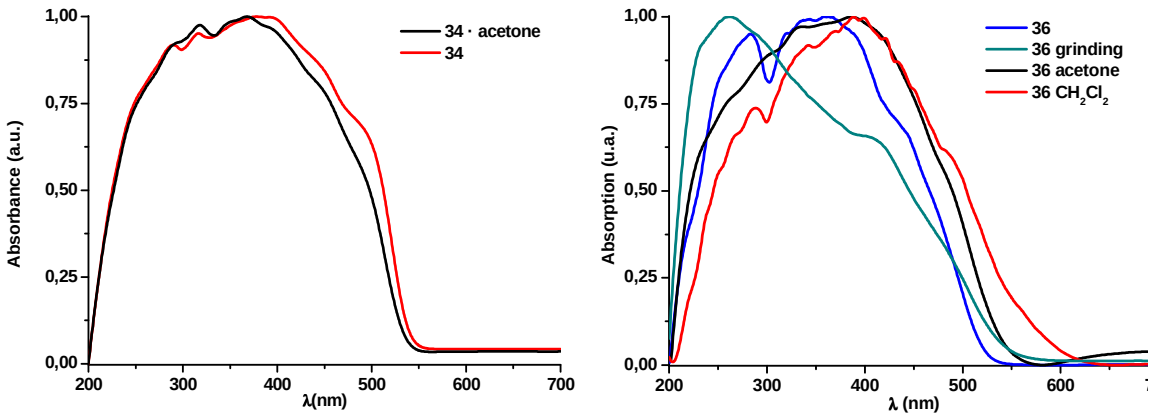

a) b)

Figure 5.23: a) Experimental of absorption spectra in solid state of a) **34** and **34-acetone** and b) **36**, **36 grinding**, **36-acetone, 36·CH_2Cl_2**

Similar response in color and luminescence was observed when solid **34** was exposed to acetone vapors at 298 K for a few minutes (~ 15 min), indicating that the transformation of **34** to **34-acetone** [likely similar to **34·(acetone)$_{1.5}$**] has occurred. On standing, the acetone was completely lost in ~ 12 h, with recovering of **34**. Desolvation by passing of a stream of air onto the sample of **34-acetone**, monitored using emission spectroscopy (Figure 5.19b), showed also a gradual change from **34-acetone** to **34**, therefore we cannot discard the formation of intermediate species.

The response to other vapors was also examined (Figure 5.21b at 298 K and Table 5.4). Moderate and relatively fast color and emission changes were also observed with MeCN and MeOH [MeCN (~15 min) > MeOH (20 min)]. Only minor changes were detected in the emission maxima upon sorption of THF and benzene after prolonged exposure (45 min for THF, C_6H_6), but the quantum efficiencies and the measured lifetimes decrease significantly, pointing to the occurrence of structural modifications (probably through the packing), which have a negative impact on the emission. Poor solvents such as *n*-hexane and diethyl-ether, however, did not trigger a response. It is reasonable to conclude that the donor solvents (acetone, NCMe, MeOH) and probably also THF are able to contact to the Pb^{II} center in a way similar to that described for **34·(acetone)$_{1.5}$**, provoking an increase in the Pb^{II} coordination number (more *holodirected* Pb^{II} environment) and changes in the packing, explaining the different emission observed. In any case, the vapor induced responses are slightly smaller than those reported for the system **33**/**33-solvent**, for which a change from a local Pt_2N_2S environment (*trans*-N,N) to Pt_2N_2O (*cis*-N,N) around the Pb^{II} was confirmed by XRD. We also observed that the color and the emission of **34** are slightly red-shifted by crushing the solid in a ceramic mortar (see Table 5.4).

As noted before, the color and emission characteristics of the ppy/SpyCF_3 complex **36** are significantly altered depending on the crystallization conditions (see Figure 5.23b for reflectance). The yellow microcrystalline solid **36-y** displays an intense yellow emission (550 nm, ϕ 34.6 %), while dried pale-orange crystals prepared from acetone (**36·acetone** form) exhibit a weaker yellow-orange emission (570 nm, ϕ 3.4%) and the orange crystals **36-o** (from concentrated CH_2Cl_2 solution) emit at 610 nm (ϕ 14 %) (Table 5.4, Figure 5.24). The notable red-shift of the orange forms could be mainly

ascribed to the presence of one very short Pt-Pb bond (~ 2.78 Å in the orange forms **36-o** and **36·acetone** *vs* ~ 2.95 Å in the yellow **36**·$4C_6H_6$ and 2.92 Å in **36**·$4CHCl_3$). The relatively strong *intramolecular* (in **36·acetone**) and *intermolecular* π···π interactions (in both orange forms) presumably also reduce the gap of the transition and favour exciton coupling.

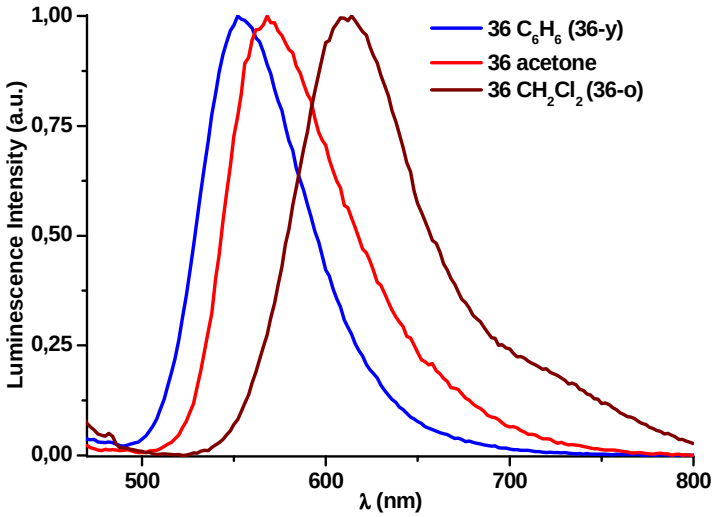

Figure 5.24: Normalized emission spectra of crystals **36**·C_6H_6 (**36-y**), **36**·acetone and **36**·CH_2Cl_2 (**36-o**) (298 K, λ_{exc} 420 nm)

As seen in Figure 5.11, these forms (**36-o** and **36·acetone)** are generated by the twisting of the second platinum fragment associated with the μ-κ^3*N,S,S* bridging ligand around the lead center, which closes the Pt-Pb-Pt angle by *ca.* 20º in relation to that of **36-y**, and seems to be favoured in acetone solution or under kinetic conditions by quick precipitation from different solvents. The remarkable structural difference between the yellow **36-y** and the orange form **36-o** could explain the inability of acetone and other solvent vapors to promote the change, which is, however, observed by dissolving the yellow solid in the corresponding solvent. Thus, although the examined solvent vapors (NCMe, THF, acetone, benzene,...) have no visual change on the yellow solid **36**, the emissions of the solids (from pale-orange to orange-red) obtained by fast precipitation after dissolution of **36** in different solvents range from 580 nm in THF to 660 nm in CH_2Cl_2 (Figure 5.25). Interestingly, we also found that the initial yellow form was easily recovered by stirring the orange or orange-red solids in *n*-hexane for *ca.* 2 h. By heating the red solid obtained from CH_2Cl_2 at *ca* 80º C, its colour slowly blue shifts yielding a final pale-orange after 24 h. These facts suggest that fast crystallizations

probably give rise to structures with low symmetry environments at Pb and short Pt-Pb distances, which slowly undergo conformational switching to more symmetrical and stable structures by stirring in hexane or prolonged heating.

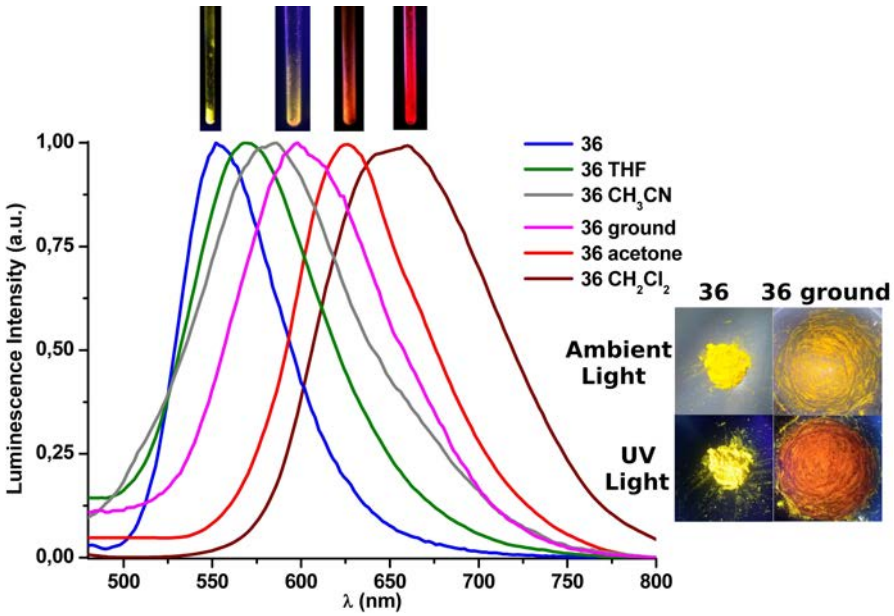

Figure 5.25: Normalized emission spectra of the unground yellow solid **36**, **36-ground**, and those solids obtained (orange-red) by evaporation of the appropriate solution of complex **36** in different solvents. Photographs show the colour and the luminescence change of **36** after grinding

We also found that this cluster exhibited notable *mechanochromic* behaviour, which is illustrated in Figure 5.25. Thus, after the yellow solid was ground, the resulting orange powder showed a red shift in its absorption (Figure 5.23b) and emission spectra (λ_{max} 600 nm) with a remarkable decrease in its quantum yield (ϕ 5.2). The remarkable red shift in the crushed powder suggests that, after grinding, some clusters could present an asymmetric structure (similar to **36-o** or **36·acetone**) with one very short Pt-Pb bond and close $\pi\cdots\pi$ stacking interactions. This behaviour is not surprising as most of the *mechanochromic* luminescent transition metal complexes are related to modulation of metallophilic interactions, and is further support of the influence of the Pt-Pb bond in the excited state.

5.3 Theoretical calculations

To gain some insight into the photophysics of these complexes, we performed theoretical calculations in the gas phase for the solvent-free clusters **33**, **34** and **36** and for the three solvate molecules **33·acetone**, **34·(acetone)$_2$** (molecule **A** of the lattice) and **36·acetone**. The S_0 and T_1 state geometries were optimized at the B3LYP/LanL2DZ(Pt and Pb)/6-31G**(ligand atoms) level. The most important geometrical parameters (bond lengths and angles) are given in Table A5.11. Detailed orbital compositions and electron-density contours are detailed in Figures 5.26, 5.28, A5.4–A5.6 and Tables A5.12 and A5.13.

The calculations (state S_0) agree reasonably well with the geometrical parameters obtained in the X-ray structures for all complexes except for **34·(acetone)$_2$**. Thus, for complexes **33**, **33·acetone**, **34**, and **36·acetone**, calculations reproduce the asymmetric Pt-Pb distances, although in both complexes the short distance fits better that the long distance [Pt-Pb experimental. 2.7774(4), 3.0877(4) Å *vs* calculated 2.832, 3.507 Å for **34**]. It should be noted that the B3LYP functional trends to overestimate bond lengths. Interestingly, the free solvent optimized structure for complex **36** is essentially symmetrical and reproduces the structural data found for the symmetrical yellow forms **36-y** obtained in benzene (**36**$\cdot 4C_6H_6$) and chloroform (**36**$\cdot 4CHCl_3$) or by slow crystallization [experimental 2.9222(4) Å *vs* calculated 2.920, 2.922 Å, see Table A5.11], thus supporting the thermodynamic stability of this conformation. In the case of model complex **34·(acetone)$_{1.5}$**, the obtained S_0 geometry does not reproduce the X-ray geometry, showing remarkably larger Pt-Pb distances [2.8654(6), 3.092(6) Å *vs* calculated. 3.709, 3.710 Å] and a wider Pt-Pb-Pt angle [146.88(2)º vs 179.71º] and, in contrast, relatively shorter Pb-N and Pb-S bond lengths (See Table A5.11). Therefore, TD-DFT and energy emission calculations were carried out only for **33**, **33·acetone**, **34**, **36**, and **36·acetone**.

The study of the composition of frontier molecular orbitals in terms of ligands and metals (Figure 5.26, Table A5.12) of complex **33** and **33·acetone** shows that the HOMO are mainly located on the Pt(1)/bzq(1)/Spy(1), while the LUMO has contribution from the metals associated to the short Pb-Pt bond and the corresponding bzq ligand [Pb 14%, Pt(1) 10%, bzq(1) 54% in **33** and bzq(2) (69%) in **33·acetone**]. In

contrast, for **34** the HOMO and the HOMO-1 are mainly located on the Pt(2)/bzq(2) and Pt(1)/bzq(1)/Spy(1), respectively, and the LUMO has similar contribution than in **33** [Pb 18%, Pt(1) 12%, bzq(1) 54%]. For the symmetrical **36** and asymmetrical **36·acetone**, the composition of the frontier molecular orbitals is very different despite the almost negligible contribution of the acetone molecule in **36·acetone**. Thus, for complex **36** having a symmetrical conformation, the HOMO and HOMO-1 are well distributed along both Pt units and the two bridging pyridinethiolate groups, with a large contribution of the latter (i.ex. HOMO: Spy 51%, Pt 22%, ppy 25%), and the LUMO is mainly contributed from the Pb and the two Pt fragments [Pb 15%, Pt(1,2) 18 %, ppy 53%] having Pt-Pb-Pt bonding character. In contrast, in **36·acetone** while the HOMO is located on the pending Pt unit [Pt(2) 38%, ppy(2) 50%], the HOMO-1 is mainly derived from the Spy bridging group associated with the short Pt(1)-Pb bond [Pt(1) 9% Spy(1) 83%]. In this solvate the LUMO has the highest heterometallic contribution being located on the short Pb-Pt(1) bond (Pb 24 %, Pt 15 %), also having bonding character, and the associated ppy(1) ligand.

Time-dependent (TD-DFT) calculations (Table A5.14) in the gas phase show that the lowest calculated energy absorptions (445 nm **33**; 453 nm **33·acetone**; 446 nm **34**; 424 nm **36**, 460, 463 nm **36·acetone**) are in agreement with the trend observed experimentally (480 nm **33**, 495 nm **33·acetone**, 484 nm **34**, 442 nm **36-y**, 500 nm **36·acetone**) in the solid state. For complex **33** and **33· acetone**, the lowest energy transition (Table A5.14) it is computed as HOMO to LUMO transition. Therefore the electron density moves from thiolate-κ*S*,*N* ligand to Pb-Pt bond/bzq, being mainly ascribed to ^{1}L'CCT/^{1}L'LCT admixture ^{1}[Spy→Pb,Pt(bzq)].

For complex **34**, the lowest energy transition is rather similar to the observed in **33**. The lowest energy transition (Table A5.14) it is assigned to a HOMO-1(85%)+HOMO(11%) to LUMO transition having, therefore, strong contribution from the Spy-κ*S*,*N* short bonded [bzqPt](1)-Pb fragment and a minor contribution of the second [bzqPt](2). In this case this transition mainly moves electron density from the thiolate-κ*S*,*N* ligand to the Pb-Pt bond/bzq, being ascribed to ^{1}L'CCT/^{1}L'LCT admixture ^{1}[Spy→Pb,Pt(bzq)], somewhat perturbed by CT from the second Pt(bzq) (^{1}MM'CT).

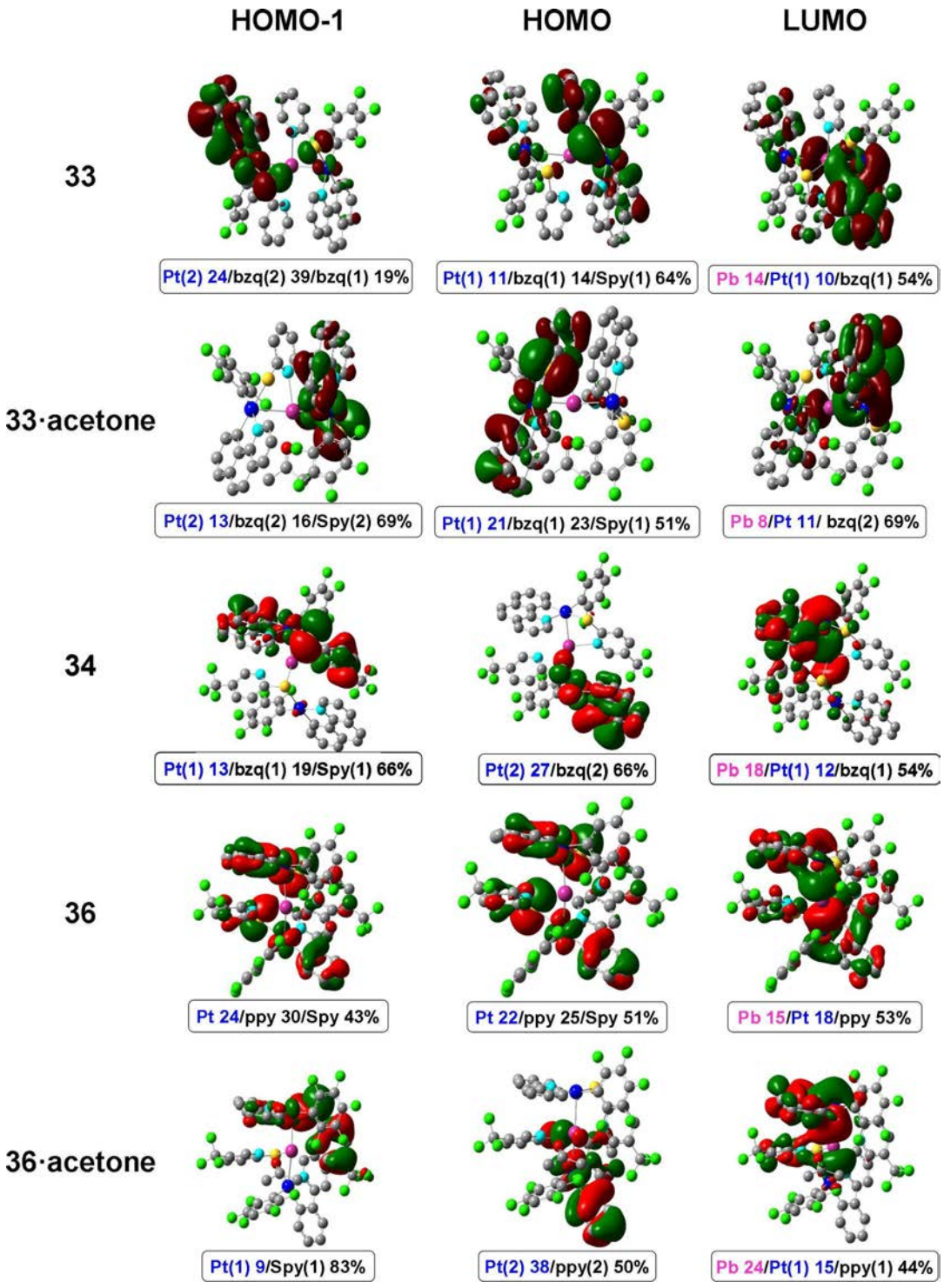

Figure 5.26: HOMO-1, HOMO and LUMO of complexes **33**, **33·acetone**, **34**, **36** and **36·acetone**

In the symmetrical complex **36** (yellow form), the lowest electronic transition computed (HOMO-1 to LUMO) mainly transfers charge from both Spy ligands and the Pt atoms to the two Pt-Pb bonds in the Pt_2Pb unit and ppy coligands, also being identified as ^{1}L'CCT/^{1}L'LCT ^{1}[Spy→Pb,Pt(ppy)]. As far as the solvate **36·acetone** is

concerned, the lowest transition calculated at 463 (HOMO to LUMO) has a remarkable charge transfer from the pendant [Pt(ppy)](2) unit to the short Pb-Pt(1) bond and the ppy(1) coligand, mainly being ascribed to metal-metal charge transfer (^{1}MM'CT) mixed with ^{1}L'L'CT (ppy to ppy). This transition lies very close to the next one (460 nm) which has, however, strong thiolate to cluster ^{1}[Spy→Pb,Pt(1)] charge transfer.

Details of the optimized triplet state geometries for all complexes are collected in Table A5.11. A comparison of the bond lengths in the optimized S_0 state and the T_1 state for **33** and **33·acetone** reveals that upon photoexcitation complex **33** rearranges to a more symmetrical Pt_2N_2S core (Pt-Pb bond 2.988, 3.132 Å T_1 *vs* 2.817, 3.222 Å S_0) (Figure 5.27), whereas in the solvate complex **33·acetone**, the changes in the Pt_2N_2O core are negligible (Pt-Pb bond 3.013, 2.923 Å T_1 *vs* 3.020, 2.867 Å S_0). The different Stokes shift (4593 cm^{-1} **33** *vs* 3231 cm^{-1} **33·acetone**) reflects the smaller geometrical change in the excited state of the more symmetrical solvate **33·acetone** and it is consistent with the observed blue shift in the emission. This result is in line with previous studies of s^2 complexes, which suggested that distortion in *hemidirected* structures is reduced (or even eliminated) in the excited state.[18] To investigate this, additional natural bond orbital (NBO) analysis (Table 5.6) were performed to estimate the hybridization of the lone pair on Pb^{II} ion, both in the S_0 and T_1 states. This study confirms, in the ground S_0 state, that there is greater p-character in the asymmetrical complex **33** (2.42% p **33** *vs* 0.34% p **33·acetone**) and decreases in the corresponding T_1 state (2.03% p **33**).

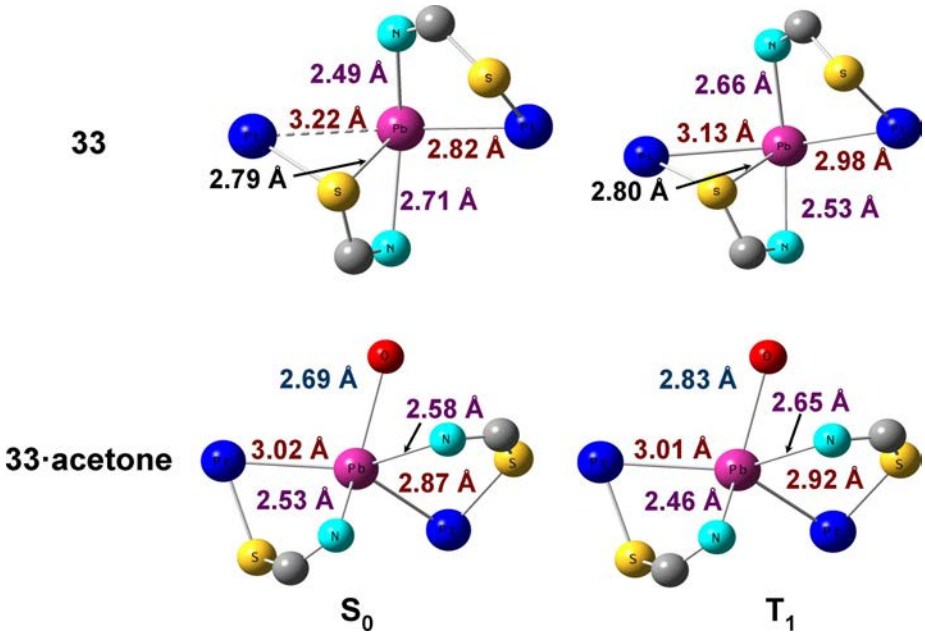

Figure 5.27: Optimized structures (S_0 and T_1 state) in **33**

Table 5.6: NBO analysis of Pb(II) for **33** and **33·acetone**

	Natural electron configuration	Lone pair NBO on Pb	Lone pair occupancy
33 (S_0)	6s(1.83) 6p(0.78) 7p(0.03)	s(97.58%) p 0.02(2.42%)	1.86803
33 (T_1)	6s(1.84) 6p(0.96) 7p(0.02)	s(97.97%) p 0.02(2.03%) s(97.90%) p 0.02(2.10%)	0.93504 0.93663
33·acetone (S_0)	6s(1.81) 6p(0.68) 7p(0.02)	s(99.66%) p 0.00(0.34%)	1.81125
33·acetone (T_1)	6s(1.81) 6p(0.77) 7p(0.03)	s(99.17%) p 0.01(0.83%) s(99.39%) p 0.01(0.61%)	0.91419 0.91223

The behavior of **34** resembles that found for **33** and upon photoexcitation also rearranges to a geometry more symmetric than that calculated for the ground state with similar Pt-Pb lengths (3.101, 3.166 Å T_1 *vs* 2.832, 3.507 Å S_0). The triplet state geometry of **36** displays a symmetrical environment around Pb, with small changes in the Pt-Pb distances (2.793, 2.906 Å T_1 *vs* 2.920, 2.922 Å S_0) relative to S_0. Notably, the Pt-Pb-Pb angle opens from 146.30º in S_0 to 166.91º in T_1, reflecting the role of the trimetallic unit in the excited state. In the corresponding optimized T_1 state of **36·acetone**, the most relevant feature is the significant withdrawal of the pendant Pt(2) fragment (Pt-Pb distances 2.883, 4.393 T_1 *vs* 2.842, 3.858 Å S_0), which is compensated by the approach of the acetone molecule (2.683 T_1 *vs* 2.961 Å S_0).

As seen in Figure 5.28 for **33**, **33·acetone**, **34**, **36**, and **36·acetone**, the HSOMO, from which the emission is produced, have, in all complexes, bonding character within the Pt-Pb-Pt entity and also a remarkable contribution from one of the π*C^N ligands,

specially in bzq complexes **33**, **33·acetone** and **34** (Pt_2Pb 46% bzq 41% **33**; Pt_2Pb 25% bzq 66% **33·acetone**; Pt_2Pb 43% bzq 40% **34**; Pt_2Pb 55% ppy 24% **36**; Pt_2Pb 59% ppy 22% **36·acetone**). It is worthnoting that the contribution of the Spy ligands and the associated Pt(bzq) fragment in all the computed LSOMOs [μ-Spy 48% Ptbzq 50% **33**; μ-Spy 35% Ptbzq 64% **33·acetone**; μ-Spy 37% Ptbzq 62% **34**; μ-Spy 11% Ptbzq 28% **36**; μ-Spy 30% Ptbzq 15% **36·acetone**] (Figure 5.28) is in agreement with the different emission energies observed in complexes **33**, **33·acetone**, **34**, **36** and **36·acetone**. The very asymmetric geometry calculated for **36·acetone**, in both S_0 and T_1, is reflected in the asymmetrical contribution of both Pt fragments with a negligible contribution of the pendant [Pt(ppy)](2) in the excited state. The shorter Pt-Pb distance in **36·acetone** relative to that in **36** and greater metallic contribution (55% **36** *vs* 59% **36·acetone**) is in line with the red-shift observed in the emission of the solvate complex. The calculated emission energy, as the difference between the energy of T_1 and the energy of the singlet state with the optimized triplet state phosphorescence (560 nm for **33**, 531 nm for **33·acetone**, 568 nm for **34**, 537 nm for **36** and 547 nm for **36·acetone**) agree qualitatively with the experimental data (620 nm for **33**; 580 nm for **33·acetone**; 580 nm for **34**, 550 nm for **36** and 570 nm for **36·acetone**), supporting a ligand-to-cluster ^{3}L'CCT [Spy→Pt,Pb] excited state with some ^{3}MM'CT and ^{3}L'LCT (Spy to C^N) character.

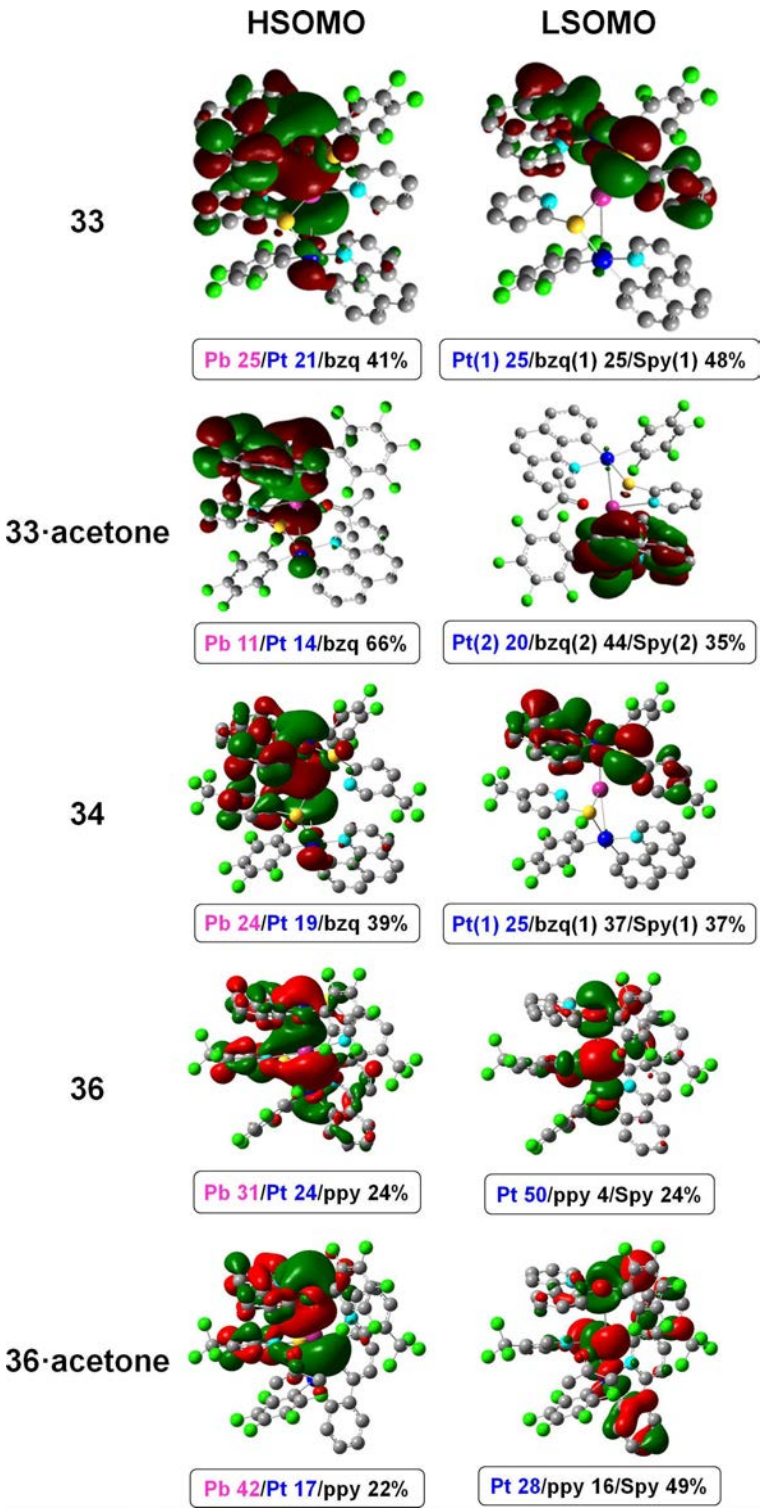

Figure 5.28: HSOMO and LSOMO of complexes **33**, **33·acetone**, **34**, **36** and **36·acetone**

5.4 Summary

In summary, in this Chapter two distinct types of Pt_2Pb clusters [{$Pt(C_6F_5)(C^N)$}$_2$Pb(μ-SpyR)$_2$] were prepared by reaction of the corresponding solvate complexes [$Pt(C_6F_5)$(bzq)($OCMe_2$)] (**31**) and [$Pt(C_6F_5)$(ppy)(dmso)] (**32**) with Pb(SpyR-5)$_2$ (R = H, CF_3), and a detailed study of their structures and photophysical properties is reported.

In spite of the fact that all clusters feature two Pt-Pb bonds supported by two bridging pyridine-2-thiolate ligands, the notable differences in the Pb environment and, consequently, in the stereochemical activity of the $6s^2$ lone pair strongly affect their photophysical response. It was found that only the presence of *asymmetric* (*hemidirected*) environments around the Pb^{II} seems to provoke stimulus-responsive luminescent behaviour.

Thus, the ppy/Spy cluster (**35**), formed by coordination of the pyridine-N atoms to the Pt center, displays a *symmetrical* "PbS_2Pt_2" core and exhibits a strong emission (mainly ^{3}LCCT in nature), which is not sensitive to external stimuli.

Unlike of **35**, clusters **33**, **34** (bzq) and **36** (ppy, SpyCF_3), formed by a formal thiolate S-transfer from Pb^{II} to Pt^{II}, show an *asymmetrical* coordination around the formally changed Pb^{II} ion in which the $6s^2$ lone pair is stereochemically active and are sensitive to external stimuli (vapours and/or mechanical grinding). For these clusters, several pseudopolymorphs (solvates) were crystallized depending on the solvent (**33**, **34**) and crystallization conditions (**36**), which allow us to rationalize their properties. Thus, in **33** and **34** (bzq) the Pb^{II} exhibits an *asymmetric* "Pt_2N_2S" (*trans*-N,N) environment, which change to a more *symmetric* environment in their acetone adducts ["Pt_2N_2O" (*cis*-N,N) (**33·acetone**) or "$Pt_2N_2SO_2$"/"Pt_2N_2SO" [**34·(acetone)$_{1.5}$**]], pointing a lower stereochemical activity of the lone pair in the acetone forms. In both clusters, the bright orange emission of the as-obtained solids, ascribed to ^{3}L'CCT [SpyR→Pb,Pt] states with some ^{3}MM'CT (M = Pt, M' = Pb) and ^{3}L'LCT (Spy→C^N) character, exhibit a significant and reversible blue-shift vapoluminescence response (by *ca.* 50 nm, **34** shows also colour changes) upon exposure to donor solvents. This

response results from changes in the environment of the Pb^{II} ion from an asymmetric (*hemidirected*) to a more symmetric (*holodirected*) upon solvent binding. In the case of **33**, TD-DFT calculations suggest that the change in emission colour is related to a smaller Stokes shift (in **33·acetone**), attributed to a different distortion of the geometry (in **33** and in **33·acetone**) around the Pb^{II} center upon photoexcitation. However, in the system **34**, in which both forms show similar Stokes shifts, these changes are attributed to the concomitant effect of a more *holodirected* Pb environment and larger $\pi\cdots\pi$ stacking in the acetone form.

For **36** (ppy/SpyCF_3), three forms having different environments around the Pb^{II} ion and, hence, different emissions were found, depending on the solvent and crystallization conditions. In most of the solvents (CH_2Cl_2, $CHCl_3$, C_6H_6) slow crystallization generates a yellow form (**36-y**) with a primary *symmetrical* "Pt_2N_2" environment, supplemented up to 8 with weak contacts to the S and F_o, which displays an intense yellow emission. Fast crystallization from CH_2Cl_2 (or concentrated solution) gives rise to orange (**36-o**) or pale-orange (**36·acetone**) crystals with a very *asymmetric* primary ("Pt_2N_2S" **36-o**, "PtN_2S" **36·acetone**) coordination, supplemented by weak contacts (two F_o **36-o**; one F_o and O for **36·acetone**). In these coloured forms, the most distinct feature is the twisting of one of the Pt units, shortening one of the Pt-Pb bonds to ~ 2.78 Å. Curiously, in contrast with the behaviour of the bzq clusters (**33** and **34**), in the solvate **36·acetone** the binding of acetone entails the *greatest asymmetry* (with a perpedicular orientation of the Pt fragments), which provokes the rupture of one of the Pt-Pb bonds that, in turn, is compensated by the presence of strong $\pi\cdots\pi$ intramolecular interactions. The lack of vapoluminescent response to vapour donor solvents (and even a drop of solvent) of the yellow solid **36** may be attributed to the marked structural differences between the yellow and solvate **36·acetone** forms, which makes its transformation difficult in rigid media. In fact, the more symmetrical and *holodirected* coordination at Pb^{II} (yellow form) seems to be the most thermodynamically stable form, as it is generated from the orange forms by stirring in hexane (sonication or prolonged heating). Theoretical calculations of **36** and **36·acetone** reproduce the observed *symmetrical* (**36**) and *asymmetrical* (**36·acetone**) environments around Pb and the energy of the emissions, supporting ligand-cluster ^{3}LCCT [SpyR→Pb,Pt] state with some ^{3}MM'CT and ^{3}LLCT character. Notably, the amorphous solids generated upon

dissolution/evaporation of **36** in different solvents exhibit intense emission in a wide range from 580 nm (THF) to 660 nm (CH_2Cl_2) (depending on the solvent), a feature which is ascribed to the formation of metastable kinetic forms, presumably having an asymmetric environment at Pb and a short Pt-Pb bond. The yellow solid also shows *mechanochromic* behaviour, with a remarkable red-shift in colour and luminescence upon grinding, which is ascribed to the transformation of the symmetrical form to more asymmetrical structures (similar to **36-o** or **36·acetone**) by mechanical stimuli.

5.6 References

1. (a) Zhao, Q.; Li, F.; Huang, C. *Chem. Soc. Rev.* **2010**, *39*, 3007; (b) Zhang, X.; Li, B.; Chen, Z. H.; Chen, Z. N. *J. Mater. Chem.* **2012**, *22*, 11427; (c) Wenger, O. S. *Chem. Rev.* **2013**, *113*, 3686; (d) Shan, G.-G.; Li, H.-B.; Cao, H.-T.; Zhu, D.-X.; Li, P.; Su, Z.-M.; Liao, Y. *Chem. Commun.* **2012**, *48*, 2000; (e) Lefebvre, J.; Korcok, J. L.; Katz, M. J.; Leznoff, D. B. *Sensors* **2012**, *12*, 3669.
2. (a) Balch, A. L. *Angew. Chem. Int. Ed.* **2009**, *48*, 2641; (b) Zhang, X.; Chi, Z.; Zhang, Y.; Liu, S.; Xu, J. *J. Mater. Chem. C* **2013**, *1*, 3376; (c) Ni, J.; Zhang, X.; Wu, Y. H.; Zhang, L. Y.; Chen, Z. N. *Chem. Eur. J.* **2011**, *17*, 1171; (d) Lasanta, T.; Olmos, M. E.; Laguna, A.; López-de-Luzuriaga, J. M.; Naumov, P. *J. Am. Chem. Soc.* **2011**, *133*, 16358; (e) Osawa, M.; Kawata, I.; Igawa, S.; Hoshino, M.; Fukunaga, T.; Hashizume, D. *Chem. Eur. J.* **2010**, *16*, 12114.
3. (a) Rachford, A. A.; Castellano, F. N. *Inorg. Chem.* **2009**, *48*, 10865; (b) Forniés, J.; Fuertes, S.; Martín, A.; Sicilia, V.; Gil, B.; Lalinde, E. *Dalton Trans.* **2009**, 2224; (c) Falvello, L. R.; Forniés, J.; Garde, R.; García, A.; Lalinde, E.; Moreno, M. T.; Steiner, A.; Tomás, M.; Usón, I. *Inorg. Chem.* **2006**, *45*, 2543; (d) Omary, M. A.; Mohamed, A. A.; Rawashdeh-Omary, M. A.; Fackler Jr, J. P. *Coord. Chem. Rev.* **2005**, *249*, 1372.
4. (a) Lefebvre, J.; Batchelor, R. J.; Leznoff, D. B. *J. Am. Chem. Soc.* **2004**, *126*, 16117; (b) Strasser, C. E.; Catalano, V. J. *J. Am. Chem. Soc.* **2010**, *132*, 10009; (c) Laguna, A.; Lasanta, T.; López-de-Luzuriaga, J. M.; Monge, M.; Naumov, P.; Olmos, M. E. *J. Am. Chem. Soc.* **2010**, *132*, 456; (d) Fernández, E. J.; López-de-Luzuriaga, J. M.; Monge, M.; Olmos, M. E.; Puelles, R. C.; Laguna, A.; Mohamed, A. A.; Fackler Jr, J. P. *Inorg. Chem.* **2008**, *47*, 8069.
5. (a) Ara, I.; Berenguer, J. R.; Forniés, J.; Gómez, J.; Lalinde, E.; Martín, A.; Merino, R. *Inorg. Chem.* **1997**, *36*, 6461; (b) Berenguer, J. R.; Forniés, J.; Gómez, J.; Lalinde, E.; Moreno, M. T. *Organometallics* **2001**, *20*, 4847; (c) Charmant, J. P. H.; Forniés, J.; Gómez, J.; Lalinde, E.; Merino, R. I.; Moreno, M. T.; Orpen, A. G. *Organometallics* **2003**, *22*, 652; (d) Berenguer, J. R.; Forniés, J.; Gil, B.; Lalinde, E. *Chem. Eur. J.* **2006**, *12*, 785; (e) Díez, Á.; Fernández, J.; Lalinde, E.; Moreno, M. T.; Sánchez, S. *Inorg. Chem.* **2010**, *49*, 11606; (f) Díez, A.; Forniés, J.; Gómez, J.; Lalinde, E.; Martín, A.; Moreno, M. T.; Sánchez, S. *Dalton Trans.* **2007**, 3653; (g) Forniés, J.; García, A.; Lalinde, E.; Moreno, M. T. *Inorg. Chem.* **2008**, *47*,

3651; (h) Belío, Ú.; Fuertes, S.; Martín, A. *Inorg. Chem.* **2013**, *52*, 5627; (i) Usón, R.; Forniés, J.; Tomás, M.; Garde, R. *Inorg. Chem.* **1997**, *36*, 1383; (j) Wu, G.; Wang, D. *J. Cluster Sci.* **2007**, *18*, 406; (k) Nagle, J. K.; Balch, A. L.; Olmstead, M. M. *J. Am. Chem. Soc.* **1988**, *110*, 319; (l) Stork, J. R.; Olmstead, M. M.; Balch, A. L. *J. Am. Chem. Soc.* **2005**, *127*, 6512; (m) Stork, J. R.; Olmstead, M. M.; Fettinger, J. C.; Balch, A. L. *Inorg. Chem.* **2006**, *45*, 849; (n) Balch, A. L.; Rowley, S. P. *J. Am. Chem. Soc.* **1990**, *112*, 6139; (o) Renn, O.; Lippert, B.; Mutikainen, I. *Inorg. Chim. Acta* **1993**, *208*, 219; (p) Oberbeckmann-Winter, N.; Braunstein, P.; Welter, R. *Organometallics* **2004**, *23*, 6311; (q) Song, H. B.; Zhang, Z. Z.; Hui, H.; Che, C. M.; Mak, T. C. W. *Inorg. Chem.* **2002**, *41*, 3146; (r) Quadrelli, E. A.; Davies, J. E.; Johnson, B. F. G.; Feeder, N. *Chem. Commun.* **2000**, 1031; (s) Chen, W.; Liu, F.; Xu, D.; Matsumoto, K.; Kishi, S.; Kato, M. *Inorg. Chem.* **2006**, *45*, 5552.

6. (a) Balch, A. L.; Fung, E. Y.; Nagle, J. K.; Olmstead, M. M.; Rowley, S. P. *Inorg. Chem.* **1993**, *32*, 3295; (b) Usón, R.; Forniés, J.; Falvello, L. R.; Usón, M. A.; Usón, I. *Inorg. Chem.* **1992**, *31*, 3697; (c) Albano, V. G.; Castellari, C.; Monari, M.; De Felice, V.; Ferrara, M. L.; Ruffo, F. *Organometallics* **1995**, *14*, 4213; (d) Ara, I.; Falvello, L. R.; Forniés, J.; Gómez-Cordón, J.; Lalinde, E.; Merino, R. I.; Usón, I. *J. Organomet. Chem.* **2002**, *663*, 284; (e) Casas, J. M.; Forniés, J.; Martín, A.; Orera, V. M.; Orpen, A. G.; Rueda, A. *Inorg. Chem.* **1995**, *34*, 6514; (f) Catalano, V. J.; Bennett, B. L.; Noll, B. C. *Chem. Commun.* **2000**, 1413; (g) Heitmann, D.; Pape, T.; Hepp, A.; Mück-Lichtenfeld; S. Grimme; Ekkehardt-Hahn, F. *J. Am. Chem. Soc.* **2011**, *133*, 11118; (h) Braunschweig, H.; Damme, A.; Dewhurst, R. D.; Hupp, F.; Jiménez-Halla, J. O. C.; Radacki, K. *Chem. Commun.* **2012**, *48*, 10410.
7. (a) Shimoni-Liuny, L.; Glusker, J. P.; Bock, C. W. *Inorg. Chem.* **1998**, *37*, 1853; (b) Davidovich, R. L.; Stavila, V.; Marinin, D. V.; Voit, E. I.; Whitmire, K. H. *Coord. Chem. Rev.* **2009**, *253*, 1316; (c) Davidovich, R. L.; Stavila, V.; Whitmire, K. H. *Coord. Chem. Rev.* **2010**, *254*, 2193; (d) Gourlaouen, C.; Gérard, H.; Piquemal, J.-P.; Parisel, O. *Chem. Eur. J.* **2008**, *14*, 2730; (e) Greer, B. J.; Michaelis, V. K.; Katz, M. J.; Leznoff, D. B.; Schreckenbach, G.; Kroeker, S. *Chem. Eur. J.* **2011**, *17*, 3609.
8. Berenguer, J. R.; Díez, A.; Fernández, J.; Forniés, J.; García, A.; Gil, B.; Lalinde, E.; Moreno, M. T. *Inorg. Chem.* **2008**, *47*, 7703.

9. Berenguer, J. R.; Fernández, J.; Gil, B.; Lalinde, E.; Sánchez, S. *Chem. Eur. J.* **2014**, *20*, 2574.
10. Berenguer, J. R.; Lalinde, E.; Moreno, M. T.; Sánchez, S.; Torroba, J. *Inorg. Chem.* **2012**, *51*, 11665.
11. Yagyu, T.; Ohashi, J.-I.; Maeda, M. *Organometallics* **2007**, *26*, 2383.
12. (a) Martín, A.; Belío, Ú.; Fuertes, S.; Sicilia, V. *Eur. J. Inorg. Chem.* **2013**, 2231; (b) Sasaki, I.; Bijani, C.; Ladeira, S.; Bourdon, V.; Faller, P.; Hureau, C. *Dalton Trans.* **2012**, *41*, 6404; (c) Owen, J. S.; Labinger, J. A.; Bercaw, J. E. *J. Am. Chem. Soc.* **2004**, *126*, 8247; (d) Newman, C. P.; Casey-Green, K.; Clarkson, G. J.; Cave, G. W. V.; Errington, W.; Rourke, J. P. *Dalton Trans.* **2007**, 3170; (e) Ghavale, N.; Wadawale, A.; Dey, S.; Jain, V. K. *J. Organomet. Chem.* **2010**, *695*, 1237; (f) Rao, Y.-L.; Wang, S. *Inorg. Chem.* **2009**, *48*, 7698.
13. Berenguer, J. R.; Lalinde, E.; Martin, A.; Moreno, M. T.; Ruiz, S.; Sánchez, S.; Shahsavari, H. R. *Chem. Commun.* **2013**, *49*, 5067.
14. Sousa-Pedrares, A.; Casanova, M. I.; García-Vázquez, J. A.; Durán, M. L.; Romero, J.; Sousa, A.; Silver, J.; Titler, P. J. *Eur. J. Inorg. Chem.* **2003**, 678.
15. (a) Rekken, B. D.; Brown, T. M.; Olmstead, M. M.; Fettinger, J. C.; Power, P. P. *Inorg. Chem.* **2013**, *52*, 3054; (b) Rossini, A. J.; Macgregor, A. W.; Smith, A. S.; Schatte, G.; Schurko, R. W.; Briand, G. G. *Dalton Trans.* **2013**, *42*, 9533.
16. We note that in this work we accept 3.20 Å as the upper limit of the Pb-F distance. At values above this we consider the Pb-F distances negligible. The limit is below than the van der Waals limit (PbII…F 3.46 Å) but it is longer than the sun of covalent radii of Pb (1.46 Å) and van der Waals radii of F (1.47 Å) (2.93 Å) and of course than the primary coordination sphere of the PbII atom, which can be considered as sum of ionic radii of PbII [CN 6, 1.19 Å and F- 1.285 Å (2.475 Å)]. .
17. Makal, A.; Benedict, J.; Trzop, E.; Sokolow, J.; Fournier, B.; Chen, Y.; Kalinowski, J. A.; Graber, T.; Henning, R.; Coppens, P. *J. Phys. Chem. A* **2012**, *116*, 3359.
18. Vogler, A.; Nikol, H. *Pure Appl. Chem.* **1992**, *64*, 1311.

5.5 Appendix

Table A5.1: Selected distances [Å] and angles [º] for **33**·1.5CH_2Cl_2

33·1.5CH_2Cl_2			
Pt1-S1	2.383(1)	Pt2-S2	2.412(1)
Pt1-N1	2.086(4)	Pt2-N3	2.099(4)
Pt1-C10	2.021(5)	Pt2-C34	2.011(5)
Pt1-C15	2.023(5)	Pt2-C39	2.007(5)
Pt1-Pb1	2.7832(3)	Pt2-Pb1	3.1642(3)
Pb1-N2	2.565(5)	Pb1-N4	2.683(5)
Pb1-S1	3.545(2)	Pb1-S2	2.797(1)
S1-C25	1.761(6)	S2-C49	1.773(6)
Pb1⋯Cl1	3.640(6)		
Pt1-Pb1-Pt2	140.753(9)	N2-Pb1-N4	151.72(15)
Pt1-Pb1-S2	98.06(3)	Pt2-Pb1-S2	47.24(3)
Pt1-Pb1-N2	79.95(10)	Pt1-Pb1-N4	95.68(10)
S2-Pb1-N4	57.61(11)	S2-Pb1-N2	95.07(10)
N4-Pb1-Pt2	80.83(10)	N2-Pb1-Pt2	85.14(10)
C10-Pt1-N1	81.72(19)	N3-Pt2-C34	81.93(19)
S1-Pt1-C15	89.46(16)	S2-Pt2-C39	95.35(15)
Pt1-S1-C25	104.59(18)	Pt2-S2-C49	106.11(18)
S1-C25-N2	118.4(4)	S2-C49-N4	115.6(4)
S1-Pt1-Pb1	86.29(3)	S2-Pt2-Pb1	58.35(3)
Pb1-N2-C25	120.5(4)	Pb1-N4-C49	100.6(3)
Pb1-S2-Pt2	74.41(4)		

Table A5.2:. Selected bond lengths [Å] and angles [º] for **33**·1.5acetone

33·1.5acetone			
Pt1-S1	2.4138(13)	Pt2-S2	2.3679(12)
Pt1-N1	2.102(4)	Pt2-N3	2.091(4)
Pt1-C10	2.022(5)	Pt2-C34	2.020(4)
Pt1-C15	2.011(4)	Pt2-C39	2.024(5)
Pb1-Pt1	2.9790(3)	Pb1-Pt2	2.8401(3)
Pb1-N2	2.497(4)	Pb1-N4	2.568(4)
S1-C25	1.761(5)	S2-C49	1.745(5)
Pb1-S1	3.186(1)	Pb1-S2	3.678(3)
Pb1-O1	2.775(5)	C50-O1	1.189(9)
Pt1-Pb1-Pt2	133.291(8)	N2-Pb1-N4	84.20(13)
O1-Pb1-Pt1	87.5(1)	O1-Pb1-Pt2	123.8(1)
N2-Pb1-Pt1	80.47(9)	N4-Pb1-Pt2	85.51(9)
N1-Pt1-C10	81.5(2)	N3-Pt2-C34	81.45(17)
Pt2-Pb1-N2	102.52(9)	Pt1-Pb1-N4	140.51(9)
S1-Pt1-C15	89.78(13)	S2-Pt2-C39	87.92(14)
Pt1-S1-C25	103.34(16)	Pt2-S2-C49	116.81(16)
S1-C25-N2	117.5(4)	S2-C49-N4	122.3(4)
S1-Pt1-Pb1	71.56(3)	S2-Pt2-Pb1	89.39(3)
Pb1-N4-C49	120.7(3)	Pb1-N2-C20 (Spy)	121.3(12)
Pb1-O1-C50	136.2(5)		

Table A5.3: Selected Distances [Å] and Angles [°] for **34**·0.9CH_2Cl_2

34·0.9CH_2Cl_2			
Pt1-S1	2.381(2)	Pt2-S2	2.416(2)
Pt1-N1	2.094(5)	Pt2-N3	2.103(6)
Pt1-C10	2.038(6)	Pt2-C35	2.003(7)
Pt1-C15	2.036(6)	Pt2-C40	2.030(7)
Pt1-Pb1	2.7774(4)	Pt2-Pb1	3.0877(4)
S1-C25	1.7410(7)	S2-C50	1.766(7)
Pb1-N2	2.495(5)	Pb1-N4	2.775(5)
Pb1-S1	3.633(2)	Pb1-S2	2.8214(19)
Pt1-Pb1-Pt2	141.54(1)	N2-Pb1-N4	153.15(16)
S2-Pb1-N2	97. 29(13)	S2-Pb1-N4	56.31(12)
Pt1-Pb1-N2	81.43(13)	Pt2-Pb1-N2	81.27(12)
Pt1-Pb1-N4	97.82(11)	Pt2-Pb1-N4	83.12(11)
Pt1-Pb1-S2	101.02(4)	Pt2-Pb1-S2	48.01(4)
N1-Pt1-C10	81.7(2)	N3-Pt2-C35	81.8(3)
S1-Pt1-C15	92.46(18)	S2-Pt2-C40	96.46(19)
S1-Pt1-Pb1	89.20(5)	S2-Pt2-Pb1	60.22(5)
Pb1-N2-C25	122.6(4)	Pb1-N4-C50	99.3(4)
Pt1-S1-C25	108.1(2)	Pt2-S2-C50	109.9(2)
S1-C25-N2	120.9(5)	S2-C50-N4	116.6(5)
S1-Pb1-S2	83.08	Pb1-S2-Pt2	71.78(5)

Table A5.4: Selected Distances [Å] and Angles [°] for [**34·(acetone)$_{1.5}$**]

[**34·(acetone)$_{1.5}$**]			
(Molecule A)		**(Molecule B)**	
Pt1-S1	2.395(3)	Pt1'-S1'	2.390(3)
Pt1-N1	2.116(9)	Pt1'-N1'	2.105(9)
Pt1-C10	2.042(11)	Pt1'-C10'	2.009(11)
Pt1-C15	2.066(10)	Pt1'-C15'	2.045(11)
Pt2-S2	2.414(3)	Pt2'-S2'	2.431(3)
Pt2-N3	2.101(9)	Pt2'-N3'	2.090(9)
Pt2-C35	2.023(11)	Pt2'-C35'	2.017(11)
Pt2-C40	2.029(12)	Pt2'-C40'	2.000(12)
Pt1-Pb1	2.8654(6)	Pt1'-Pb1'	2.8038(6)
Pt2-Pb1	3.0902(6)	Pt2'-Pb1'	3.1408(6)
Pb1-N2	2.676(9)	Pb1'-N2'	2.634(9)
Pb1-N4	2.680(9)	Pb1'-N4'	2.593(9)
S2-C50	1.777(12)	S2'-C50'	1.779(12)
S1-C25	1.758(13)	S1'-C25'	1.729(11)
Pb1-S2	2.968(3)	Pb1'-S2'	2.872(3)
Pb1-S1	3.626(3)	Pb1'-S1'	3.600(3)
Pb1-O1	2.791(1)	Pb1'-O1'	2.967(8)
Pb1-O2	2.937(9)		
Pt1-Pb1-Pt2	146.88(2)	Pt1'-Pb1'-Pt2'	149.64(2)
N2-Pb1-N4	144.7(3)	N2'-Pb1'-N4'	140.4(3)
O1-Pb1-Pt1	91.91	O1'-Pb1'-Pt1'	92.86
O1-Pb1-Pt2	114.73	O1'-Pb1'-Pt2'	115.00
O2-Pb1-Pt1	128.22		
O2-Pb1-Pt2	76.17		
Pt1-Pb1-S2	102.32(6)	Pt1'-Pb1'-S2'	107.69(6)
Pt1-Pb1-N2	76.8(2)	Pt1'-Pb1'-N2'	77.2(2)
Pt1-Pb1-N4	91.4(2)	Pt1'-Pb1'-N4'	97.5(2)
N2-Pb1-Pt2	91.6(2)	N2'-Pb1'-Pt2'	83.4(2)
S2-Pb1-N4	55.6(2)	S2'-Pb1'-N4'	57.3(2)
N4-Pb1-Pt2	80.2(2)	N4'-Pb1'-Pt2'	82.9(2)

S2-Pb1-N2	94.0(2)	S2'-Pb1'-N2'	86.6(2)
Pt2-Pb1-S2	46.90(6)	Pt2'-Pb1'-S2'	47.43(6)
S1-Pb1-S2	76.58	S1'-Pb1'-S2'	76.96
C10-Pt1-N1	82.2(4)	C10'-Pt1'-N1'	81.5(4)
S1-Pt1-C15	90.7(3)	S1'-Pt1'-C15'	90.0(3)
N3-Pt2-C35	81.6(4)	N3'-Pt2'-C35'	81.5(4)
S2-Pt2-C40	93.6(4)	S2'-Pt2'-C40'	95.9(3)
Pt1-S1-C25	104.5(4)	Pt1'-S1'-C25'	105.0(4)
Pt2-S2-C50	102.8(4)	Pt2'-S2'-C50'	105.4(4)
S1-C25-N2	119.5(9)	S1'-C25'-N2'	119.3(9)
S2-C50-N4	116.6(9)	S2'-C50'-N4'	114.5(9)
S1-Pt1-Pb1	86.65(8)	S1'-Pt1'-Pb1'	87.37(8)
S2-Pt2-Pb1	63.90(7)	S2'-Pt2'-Pb1'	60.46(7)
Pb1-S2-Pt2	69.20(8)	Pb1'-S2'-Pt2'	72.10(8)
Pb1-N2-C25	119.5(8)	Pb1'-N2'-C25'	120.3(8)
Pb1-N4-C50	104.1(7)	Pb1'-N4'-C50'	104.1(7)

Table A5.5: Selected Distances [Å] and Angles [º] for **35**·2$CHCl_3$

35·2$CHCl_3$			
Pt1-S1	3.606	Pt2-S2	3.589
Pt1-N1	2.067(6)	Pt2-N3	2.084(5)
Pt1-C10	2.016(6)	Pt2-C32	2.013(7)
Pt1-C13	2.027(7)	Pt2-C35	2.045(7)
Pt1-N2	2.148(5)	Pt2-N4	2.120(6)
Pt1-Pb1	2.8326(4)	Pt2-Pb1	2.8998(4)
S1-C19	1.750(7)	S2-C41	1.747(8)
Pb1-S1	2.7670(19)	Pb1-S2	2.691(2)
Pt1-Pb1-Pt2	169.88(1)	S1-Pb1-S2	96.16(8)
Pt1-Pb1-S1	80.16(4)	Pt2-Pb1-S1	109.96(4)
Pt1-Pb1-S2	99.70(4)	Pt2-Pb1-S2	79.78(5)
N1-Pt1-C10	80.9(3)	N3-Pt2-C32	80.9(3)
N2-Pt1-C13	87.6(2)	N4-Pt2-C35	90.1(3)
N2-Pt1-Pb1	95.20(15)	N4-Pt2-Pb1	94.81(15)
Pt1-N2-C19	127.0(4)	Pt2-N4-C41	126.8(5)
Pb1-S1-C19	107.3(2)	Pb1-S2-C41	109.8(3)
S1-C19-N2	123.3(5)	S2-C41-N4	122.8(6)

Table A5.6: Selected Distances [Å] and Angles [º] for **36**·2CH_2Cl_2

36·2CH_2Cl_2					
Pt1-S1	2.390(3)	Pt3-S3	2.393(3)	Pt5-S5	2.396(3)
Pt1-N1	2.094(8)	Pt3-N5	2.107(8)	Pt5-N9	2.072(8)
Pt1-C10	2.052(10)	Pt3-C56	2.043(10)	Pt5-C102	2.026(9)
Pt1-C13	2.030(9)	Pt3-C59	2.049(9)	Pt5-C105	2.023(9)
Pt1-Pb1	2.7840(5)	Pt3-Pb2	2.7765(5)	Pt5-Pb3	2.7574(5)
Pb1-N2	2.564(8)	Pb2-N6	2.548(8)	Pb3-N10	2.512(7)
Pb1-S1	3.638	Pb2-S3	3.565	Pb3-S5	3.515
S1-C23	1.756(12)	S3-C69	1.733(11)	S5-C115	1.727(11)
Pt2-S2	2.413 (2)	Pt4-S4	2.412(2)	Pt6-S6	2.416(3)
Pt2-N3	2.094(7)	Pt4-N7	2.098(7)	Pt6-N11	2.101(7)
Pt2-C33	2.021(9)	Pt4-C79	2.012(9)	Pt6-C125	2.018(9)
Pt2-C36	2.021(9)	Pt4-C82	2.012(9)	Pt6-C127	2.039(9)
Pt2-Pb1	3.0596(5)	Pt4-Pb2	3.0258(5)	Pt6-Pb3	3.0554(5)
Pb1-N4	2.679(7)	Pb2-N8	2.678(7)	Pb3-N12	2.708(7)

Pb1-S2	2.858(3)	Pb2-S4	2.888(3)	Pb3-S6	2.896(3)
S2-C46	1.773(9)	S4-C92	1.756 (9)	S6-C137	1.764(9)
C10-Pt1-N1	81.6 (4)	C56-Pt3-N5	80.9(4)	C102-Pt5-N9	80.3(4)
S1-Pt1-C13	88.0(3)	S3-Pt3-C59	89.1(4)	S5-Pt5-C105	89.8(3)
Pt1-S1-C23	106.7(4)	Pt3-S3-C69	107.7(3)	Pt5-S5-C115	106.7(3)
S1-C23-N2	119.6(8)	S3-C69-N6	120.1(7)	S5-C115-N10	119.6(7)
S1-Pt1-Pb1	89.01(7)	S3-Pt3-Pb2	86.86(7)	S5-Pt5-Pb3	85.72(7)
Pb1-N2-C23	122.0(7)	Pb2-N6-C69	119.6(6)	Pb3-N10-C115	119.9(6)
Pt2-Pb1-S2	47.97(5)	Pt4-Pb2-S4	48.07(5)	Pt6-Pb3-S6	47.80(5)
Pt2-Pb1-S1	102.42	Pt4-Pb2-S3	102.08	Pt6-Pb3-S5	97.34
Pt1-Pb1-N2	81.1(2)	Pt3-Pb2-N6	82.37(18)	Pt5-Pb3-N10	81.15(18)
N2-Pb1-Pt2	83.65(18)	N6-Pb2-Pt4	84.47(18)	N10-Pb3-Pt6	79.88(17)
S1-Pb1-N2	47.61	S3-Pb2-N6	48.78	S5-Pb3-N10	48.94
S1-Pb1-N4	120.98	S3-Pb2-N8	116.42	S5-Pb3-N12	117.62
Pb1-S1-Pt1	49.92	Pb2-S3-Pt3	51.05	Pb3-S5-Pt5	51.46
Pt1-Pb1-Pt2	137.58(2)	Pt3-Pb2-Pt4	137.93(2)	Pt5-Pb3-Pt6	136.84(2)
C33-Pt2-N3	81.1(3)	C79-Pt4-N7	81.0(3)	C125-Pt6-N11	80.0(4)
S2-Pt2-C36	95.5(2)	S4-Pt4-C82	95.4(2)	S6-Pt6-C127	94.6(2)
Pt2-S2-C46	111.0(3)	Pt4-S4-C92	111.9(3)	Pt6-S6-C137	113.6(3)
S2-C46-N4	116.1(6)	S4-C92-N8	118.2(7)	S6-C137-N12	117.4(7)
S2-Pt2-Pb1	61.64(6)	S4-Pt4-Pb2	62.98(6)	S6-Pt6-Pb3	62.65(7)
Pb1-N4-C46	102.1(5)	Pb2-N8-C92	101.0(5)	Pb3-N12-C137	101.3(5)
Pt1-Pb1-S1	41.07	Pt3-Pb2-S3	42.09	Pt5-Pb3-S5	42.82
Pt1-Pb1-S2	97.97(5)	Pt3-Pb2-S4	96.48(5)	Pt5-Pb3-S6	99.62(5)
N4-Pb1-Pt2	83.63(16)	N8-Pb2-Pt4	84.41(15)	N12-Pb3-Pt6	85.49(16)
Pt1-Pb1-N4	98.05(16)	Pt3-Pb2-N8	93.84(15)	Pt5-Pb3-N12	98.77(16)
S2-Pb1-N4	56.85(17)	S4-Pb2-N8	56.94 (17)	S6-Pb3-N12	56.57(17)
S2-Pb1-N2	103.21(19)	S4-Pb2-N6	102.26(19)	S6-Pb3-N10	101.41(18)
Pb1-S2-Pt2	70.39(6)	Pb2-S4-Pt4	68.95(6	Pb3-S6-Pt6	69.55(7)
N2-Pb1-N4	159.9(3)	N6-Pb2-N8	158.5(3)	N10-Pb3-N12	157.8(2)

Table A5.7: Selected Distances [Å] and Angles [°] for **36**·4C_6H_6

36·4C_6H_6			
Pt1-S1	2.4288(9)	Pt1-Pb1	2.9469(1)
Pt1-N1	2.083(3)	Pb1-N2	2.669(3)
Pt1-C10	2.005(3)	Pb1-S1	2.9566(11)
Pt1-C13	2.024(3)	S1-C19	1.758(4)
C10-Pt1-N1	80.66(13)	Pt1-Pb1-N2	82.44(6)
S1-Pt1-C13	93.08(9)	N2#-Pb1-Pt1	92.53(6)
S1-Pt1-Pb1	65.91(3)	S1-Pb1-N2	55.73(7)
Pt1-S1-C19	104.47(12)	S1-Pb1-N2#	103.40(7)
Pb1-S1-Pt1	65.50(2)	S1-C19-N2	116.1(3)
Pb1-N2-C19	104.0(2)	S1-Pb1-S1#	77.59(4)
Pt1-Pb1-S1#	109.90(2)	Pt1-Pb1-S1	48.59(2)
Pt1-Pb1-Pt1#	156.22(1)	N2-Pb1-N2#	155.47(14)

Table A5.8: Selected Distances [Å] and Angles [°] for **36**·4$CHCl_3$

36·4$CHCl_3$			
Pt1-S1	2.4199(16)	Pt1-Pb1	2.9222(4)
Pt1-N1	2.085(4)	Pb1-N2	2.674(5)
Pt1-C10	2.005(5)	Pb1-S1	3.024(2)
Pt1-C13	2.028(6)	S1-C23	1.753(7)
C10-Pt1-N1	80.9(2)	Pt1-Pb1-N2	81.27(11)
S1-Pt1-C13	92.09(16)	N2#-Pb1-Pt1	93.16(10)
S1-Pt1-Pb1	68.19(6)	S1-Pb1-N2	55.15(12)
Pt1-S1-C23	104.7(2)	S1-Pb1-N2#	102.79(11)
Pb1-S1-Pt1	63.81(5)	S1-C23-N2	116.6(5)
Pb1-N2-C23	105.2(4)	S1-Pb1-S1#	76.92(7)
Pt1-Pb1-S1#	109.30(4)	Pt1-Pb1-S1	48.00(3)
Pt1-Pb1-Pt1#	155.019(14)	N2-Pb1-N2#	154.2(2)

Table A5.9: Selected Distances [Å] and Angles [°] for [**36·acetone**]

[**36·acetone**]			
Pt1-S1	2.3939(7)	Pt2-S2	2.3884(7)
Pt1-N1	2.087(2)	Pt2-N3	2.089(3)
Pt1-C10	2.017(3)	Pt2-C33	2.001(3)
Pt1-C13	2.018(3)	Pt2-C36	2.011(3)
Pt1-Pb1	2.7863(2)	Pt2-Pb1	3.5344(2)
Pb1-N2	2.603(3)	Pb1-N4	2.566(3)
Pb1-S1	3.833	Pb1-S2	2.7728(8)
S1-C23	1.741(3)	S2-C46	1.7663(3)
Pb1-O1	2.897		
C10-Pt1-N1	80.66(11)	C33-Pt2-N3	81.09(11)
S1-Pt1-C13	88.64(8)	S2-Pt2-C36	92.63(8)
Pt1-S1-C23	109.08(10)	Pt2-S2-C46	109.22(10)
S1-C23-N2	120.5(2)	S2-C46-N4	114.9(2)
S1-Pt1-Pb1	95.15(2)	S2-Pt2-Pb1	51.51
Pb1-N2-C23	126.43(19)	Pb1-N4-C46	101.94(18)
Pt2-Pb1-S2	42.39	Pt1-Pb1-S1	38.47
Pt2-Pb1-S1	102.30	Pt1-Pb1-S2	93.04(2)
Pt1-Pb1-N2	80.33(5)	N4-Pb1-Pt2	78.07
N2-Pb1-Pt2	78.95	Pt1-Pb1-N4	93.48(5)
S1-Pb1-N2	44.43	S2-Pb1-N4	55.88(6)
S1-Pb1-N4	113.32	S2-Pb1-N2	83.98(6)
Pb1-S1-Pt1	46.39	Pb1-S2-Pt2	86.10(2)
Pt1-Pb1-Pt2	132.25	N2-Pb1-N4	142.11(8)
O1-Pb1-Pt1	105.34	O1-Pb1-Pt2	114.50

Table A5.10: Photophysical data for complexes $[Pt(C_6F_5)(ppy)(dmso)]$ (**32**), $[\{Pt(C_6F_5)(C\hat{}N)\}_2Pb(SpyR)_2]$ (**33**–**36**) in solution (CH_2Cl_2 and acetone) at 298 and 77 K

Compound	Media/M (T^a/K)	λ_{em}/nm (λ_{exc}/nm)
$[Pt(C_6F_5)(ppy)(dmso)]$ **(32)**	CH_2Cl_2 5×10^{-5} M (298)[a]	484_{max}, 518, 555_{sh} (365-400)
	CH_2Cl_2 5×10^{-5} M (77)[a]	476_{max}, 515, 547 (365)
	Acetone 5×10^{-5} M (298)[a]	485_{max}, 518, 550_{sh} (380)
	Acetone 5×10^{-5} M (77)[a]	482_{max}, 518, 550 (355 or 400)
$[\{Pt(C_6F_5)(bzq)\}_2Pb(Spy)_2]$ **(33)**	CH_2Cl_2 10^{-3} M (298)	620 (470)
	CH_2Cl_2 10^{-3} M (77)	570 (460)
	CH_2Cl_2 5×10^{-5} M (298)	620 (460)
	CH_2Cl_2 5×10^{-5} M (77)	560 (460)
	Acetone 10^{-3} M (298)	620 (480)
	Acetone 10^{-3} M (77)	570 (365-520)
	Acetone 5×10^{-5} M (77)[b]	570 (480-515)
$[\{Pt(C_6F_5)(bzq)\}_2Pb(SpyCF_3)_2]$ **(34)**	CH_2Cl_2 10^{-3} M (298)	600 (450-470)
	CH_2Cl_2 5×10^{-5} M (298)	605_{weak} (460)
	CH_2Cl_2 5×10^{-5} M (77)[a]	555, 645_{max}, 730 (480)
		645_{max}, 730 (520)
	Acetone 10^{-3} M (298)	600 (440-470)
	Acetone 10^{-3} M (77)	600_{max}, 700_{sh} (460-500)
	Acetone 5×10^{-5} M (77)[b]	600_{max}, 715 (450)
$[\{Pt(C_6F_5)(ppy)\}_2Pb(Spy)_2]$ **(35)**	CH_2Cl_2 10^{-3} M (298)	620 (450)
	CH_2Cl_2 10^{-3} M (77)	600 (520)
	CH_2Cl_2 5×10^{-5} M (298)	620 (480)
	CH_2Cl_2 5×10^{-5} M (77)	600 (480)
	Acetone 10^{-3} M (298)	620 (440)
	Acetone 10^{-3} M (77)	575_{max}, 620 (440)
		575, 620 (480-520)
		620 (540)
	Acetone 5×10^{-5} M (77)[b]	575 (440)
		$575,620_{max}$ (480)
$[\{Pt(C_6F_5)(ppy)\}_2Pb(SpyCF_3)_2]$ **(36)**	CH_2Cl_2 10^{-3} M (298)	610 (440)
	CH_2Cl_2 10^{-3} M (77)	640_{max}, 730 (365-540)
	CH_2Cl_2 5×10^{-5} M (298)	610 (365-480)
	CH_2Cl_2 5×10^{-5} M (77)	540, 640_{max}, 720 (480)
		640_{max}, 720 (520-560)
	Acetone 10^{-3} M (298)	610 (440)
	Acetone 10^{-3} M (77)	600_{max}, 710 (365-480)
	Acetone 5×10^{-5} M (77)[b]	595_{max}, 700 (440)

a) Similar pattern at 10^{-3} M. b) Non emissive at 298 K

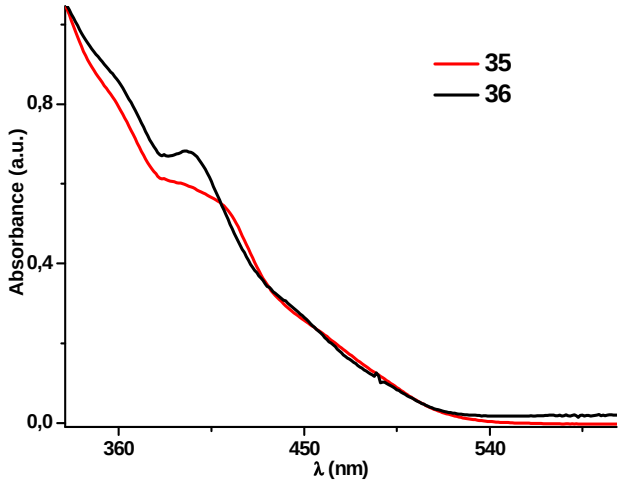

Figure A5.1: Low-energy region of normalized absorption spectra of **35** and **36** in CH_2Cl_2 at 298 K

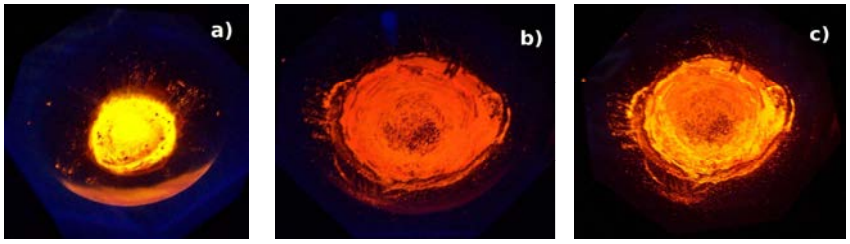

Figure A5.2: Photographs show luminescence change of **33·acetone** under UV light irradiation (365 nm): a) solvated form of **33·acetone**, b) after grinding (to give **33**) c) after addition to b of a drop of acetone (showing the partial recovering of **33·acetone**)

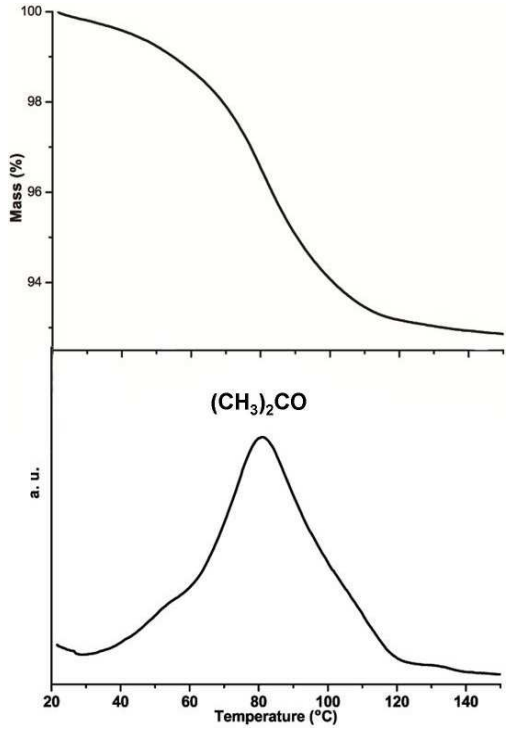

Figure A5.3: Thermogravimetric analyses showing the weight lost in the sample **33·x(acetone)**

Table A5.11: Selected distances (A) and angles (deg) for the computed structures of **33**, **33·acetone**, **34**, **34·(acetone)$_2$**, **36** and **36·acetone**

	33		
	X-Ray (33·1.5CH_2Cl_2)	**S_0**	**T_1**
Pt(1)-Pb	2.7832(3)	2.817	2.988
Pt(1)-S(1)	2.383(1)	2.426	2.361
Pt(1)-N(1)	2.086(4)	2.123	2.109
Pt(2)-Pb	3.1642(3)	3.222	3.132
Pt(2)-S(2)	2.412(1)	2.485	2.483
Pt(2)-N(3)	2.099(4)	2.128	2.127
Pb-N(2)	2.565(5)	2.490	2.662
Pb-N(4)	2.683(5)	2.709	2.528
Pb-S(1)	3.545(2)	3.596	3.707
Pb-S(2)	2.797(1)	2.794	2.801
Pt(1)-Pb-Pt(2)	140.753(9)	146.89	143.26
N(2)-Pb-N(4)	151.72(15)	148.69	149.30
	33·acetone		
	X-Ray (33·acetone)	**S_0**	**T_1**
Pt(1)-Pb	2.9790(3)	3.020	3.013
Pt(1)-S(1)	2.4138(13)	2.445	2.459
Pt(1)-N(1)	2.102(4)	2.128	2.128
Pt(2)-Pb	2.8401(3)	2.867	2.923
Pt(2)-S(2)	2.3679(12)	2.435	2.375
Pt(2)-N(3)	2.091(4)	2.125	2.105
Pb-N(2)	2.497(4)	2.531	2.466
Pb-N(4)	2.568(4)	2.581	2.653
Pb-S(1)	3.186(1)	3.304	3.109
Pb-S(2)	3.678(3)	3.568	3.641
Pb-O(1)	2.775(5)	2.693	2.832
Pt(1)-Pb-Pt(2)	133.291(8)	134.52	136.19
N(2)-Pb-N(4)	84.20(13)	86.29	84.58
	34		
	X-Ray (34.0.9CH_2Cl_2)	**S_0**	**T_1**
Pt(1)-Pb	2.7774(4)	2.832	3.101
Pt(1)-S(1)	2.381(2)	2.476	2.412
Pt(1)-N(1)	2.094(5)	2.160	2.147
Pt(2)-Pb	3.0877(4)	3.507	3.166
Pt(2)-S(2)	2.416(2)	2.558	2.554
Pt(2)-N(3)	2.103(6)	2.160	2.161
Pb-N(2)	2.495(5)	2.505	2.775
Pb-N(4)	2.775(5)	2.763	2.528
Pb-S(1)	3.633	3.670	3.757
Pb-S(2)	2.8214(19)	2.802	2.841
Pt(1)-Pb-Pt(2)	141.54(1)	148.09	148.10
N(2)-Pb-N(4)	153.15(16)	145.80	150.15
	34·(acetone)$_2$		
	X-Ray 34·(acetone)$_2$ Molecule A	**S_0**	**T_1**
Pt(1)-Pb	2.8654(6)	3.709	3.219
Pt(1)-S(1)	2.395(3)	2.527	3.388
Pt(1)-N(1)	2.116(9)	2.157	2.151
Pt(2)-Pb	3.092(6)	3.710	3.388
Pt(2)-S(2)	2.414(3)	2.526	2.533
Pt(2)-N(3)	2.101(9)	2.157	2.159
Pb-N(2)	2.676(9)	2.595	3.075
Pb-N(4)	2.680(9)	2.596	2.447
Pb-S(1)	3.626	2.884	3.902
Pb-S(2)	2.968(3)	2.884	2.945
Pb-O(1)	2.791	2.951	2.649

Pb-O(2)	2.937	2.952	3.927
Pt(1)-Pb-Pt(2)	146.88(2)	179.71	143.19
36			
	X-Ray (36·4CHCl$_3$)	**S_0**	**T_1**
Pt-Pb	2.9222(4)	2.920, 2.922	2.793, 2.906
Pt-S	2.4199(16)	2.505, 2.506	2.501, 2.578
Pt-N	2.085(4)	2.150, 2.150	2.156, 2.153
Pb-N(2)	2.674(5)	2.652, 2.653	2.595, 2.530
Pb-S(1)	3.024(2)	3.337, 3.326	3.641, 2.874
Pt(1)-Pb-Pt(1#)	155.019(14)	146.30	166.91
N(2)-Pb-N(2#)	154.2(24)	162.58	166.27
36·acetone			
	X-Ray (36·acetone)	**S_0**	**T_1**
Pt(1)-Pb	2.7863(2)	2.842	2.883
Pt(1)-S(1)	2.3939(7)	2.482	2.459
Pt(1)-N(1)	2.087(2)	2.149	2.145
Pt(2)-Pb	3.534	3.858	4.393
Pt(2)-S(2)	2.3884(7)	2.539	2.450
Pt(2)-N(3)	2.089(3)	2.140	2.150
Pb-N(2)	2.603(3)	2.577	2.724
Pb-N(4)	2.566(3)	2.627	2.515
Pb-S(1)	3.833	3.772	3.908
Pb-S(2)	2.7728(8)	2.863	3.047
Pb-(O)	2.897	2.961	2.683
Pt(1)-Pb-Pt(2)	132.25	140.92	143.02
N(2)-Pb-N(4)	142.11(8)	141.68	132.89

Table A5.12: Composition (%) of frontier MOs in the ground state for **33**, **33·acetone**, **34**, **36** and **36·acetone** in gas phase

33									
MO	**Energy**	**Pt(1)**	**bzq(1)**	**Spy(1)**	**Pb**	**Pt(2)**	**bzq(2)**	**Spy(2)**	**C_6F_5**
L+4	-1.20	1	22	19	6	2	15	34	2
L+3	-1.25	1	43	15	1	3	30	7	0
L+2	-1.57	6	55	2	14	2	15	4	1
L+1	-1.86	0	29	1	1	3	65	0	1
LUMO	-2.14	10	54	2	14	4	9	5	2
HOMO	-5.75	11	14	64	0	3	5	1	1
H-1	-5.90	2	19	5	1	24	39	9	0
H-2	-6.21	10	21	5	10	25	3	8	19
H-3	-6.28	4	4	3	1	20	3	2	63
H-4	-6.31	9	18	5	0	4	1	0	62
33·acetone										
MO	**Energy**	**Pt(1)**	**bzq(1)**	**Spy(1)**	**Pb**	**Pt(2)**	**bzq(2)**	**Spy(2)**	**C_6F_5**	**$(CH_3)_2CO$**
L+4	-1.11	2	3	40	2	1	50	1	1	0
L+3	-1.14	4	66	10	4	0	1	13	1	0
L+2	-1.48	2	14	14	10	7	48	2	1	1
L+1	-1.69	3	77	0	2	1	16	0	1	0
LUMO	-2.03	3	7	3	8	8	69	1	1	0
HOMO	-5.50	21	23	51	1	1	1	1	1	0
H-1	-5.67	0	0	0	0	13	16	69	0	0
H-2	-5.84	33	16	5	13	18	3	7	4	2
H-3	-6.14	17	16	6	0	1	6	2	53	0
H-4	-6.17	4	22	26	0	4	21	8	14	0
34										
MO	**Pt(1)**	**bzq(1)**	**Spy-CF_3(1)**	**C_6F_5(1)**	**Pt(2)**	**bzq(2)**	**Spy-CF_3(2)**	**C_6F_5(2)**	**Pb**	
L+4	2	37	12	0	2	2	42	1	2	
L+3	3	5	70	1	1	3	13	0	3	
L+2	4	24	5	1	1	49	8	0	8	

L+1	2	37	1	0	4	44	5	1	8
LUMO	12	54	2	2	2	3	6	1	18
HOMO	0	0	1	0	27	66	5	0	1
H-1	13	19	66	1	1	0	0	0	0
H-2	0	1	0	0	23	5	4	67	0
H-3	6	9	2	1	65	6	2	5	4
H-4	10	40	7	38	2	1	1	1	0

36

MO	**Pt(1)**	**ppy (1)**	**Spy-CF_3(1)**	**C_6F_5(1)**	**Pt(2)**	**ppy(2)**	**Spy-CF_3(2)**	**C_6F_5(2)**	**Pb**
L+4	2	19	21	0	2	21	20	0	15
L+3	2	11	36	1	2	12	36	1	1
L+2	2	31	9	1	2	29	10	1	15
L+1	3	19	15	1	3	20	15	1	21
LUMO	9	27	6	1	9	26	6	1	15
HOMO	12	14	28	1	10	11	23	1	0
H-1	11	14	20	1	13	16	23	1	1
H-2	26	8	4	6	26	8	4	6	12
H-3	6	4	5	35	6	4	5	35	0
H-4	5	4	7	34	5	4	7	34	0

36·acetone

MO	**Pt(1)**	**ppy(1)**	**Spy-CF_3(1)**	**C_6F_5(1)**	**Pt(2)**	**ppy(2)**	**Spy-CF_3(2)**	**C_6F_5(2)**	**Pb**	**Acet.**
L+4	2	71	2	0	1	2	16	0	4	1
L+3	5	6	75	2	1	1	4	0	6	0
L+2	0	4	1	0	5	74	16	1	0	0
L+1	1	38	1	0	3	15	37	1	5	0
LUMO	15	44	2	2	1	1	9	0	24	1
HOMO	0	0	0	0	38	50	9	0	2	0
H-1	9	7	83	0	0	0	1	0	0	0
H-2	1	0	1	0	77	8	3	10	1	0
H-3	1	0	0	0	35	3	3	58	0	0
H-4	9	11	16	50	1	10	2	0	1	0

Table A5.13: Composition (%) of frontier MOs for the computed T_1 for **33**, **33·acetone**, **34**, **36** and **36·acetone** in gas phase

	33							
	Pt(1)	bzq(1)	Spy (1)	Pt(2)	bzq(2)	Spy (2)	C_6F_5	Pb
HSOMO	15	37	3	6	4	8	2	25
LSOMO	25	25	48	0	1	0	1	0
	33·acetone							
	Pt(1)	bzq(1)	Spy (1)	Pt(2)	bzq(2)	Spy (2)	C_6F_5	Pb
HSOMO	3	2	6	11	64	1	2	11
LSOMO	0	0	1	20	44	35	0	0

	34								
	Pt(1)	bzq(1)	Spy-CF_3(1)	C_6F_5(1)	Pt(2)	bzq(2)	Spy-CF_3(2)	C_6F_5(2)	Pb
HSOMO	13	37	2	1	6	3	13	1	24
LSOMO	25	37	37	1	0	0	0	0	0
	36								
	Pt(1)	ppy(1)	Spy-CF_3(1)	C_6F_5(1)	Pt(2)	ppy(2)	Spy-CF_3(2)	C_6F_5(2)	Pb
HSOMO	13	14	3	2	11	10	15	1	31
LSOMO	26	2	11	3	24	2	13	2	17
	36·acetone								
	Pt(1)	ppy(1)	Spy-CF_3(1)	C_6F_5(1)	Pt(2)	ppy(2)	Spy-CF_3(2)	C_6F_5(2)	Pb
HSOMO	16	22	3	3	1	0	13	0	42
LSOMO	11	4	30	1	17	12	19	0	4

Table A5.14: Selected vertical excitation energies computed by TD-DFT with the orbitals involved for **33**, **33·acetone**, **34**, **36** and **36·acetone**

	λ (nm)	*f* [a]	Transition
			33
S_1	445.44	0.019	HOMO→LUMO (93%)
S_2	411.18	0.0231	HOMO-1→LUMO (66%), HOMO-1→LUMO+1 (19%)
S_3	385.59	0.0117	HOMO→LUMO+1 (64%), HOMO-2→LUMO (15%)
S_4	377.16	0.0529	HOMO-2→LUMO (69%), HOMO→LUMO+1 (14%)
S_5	376.41	0.0187	HOMO-1→LUMO+1 (65%), HOMO→LUMO+1 (9%)
S_6	366.04	0.0168	HOMO-4→LUMO (62%), HOMO-3→LUMO (25%)
S_7	360.26	0.0223	HOMO→LUMO+2 (80%)
S_8	359.34	0.0107	HOMO-3→LUMO (46%), HOMO-4→LUMO (18%), HOMO-5→LUMO (17%)
S_9	355.18	0.0882	HOMO-5→LUMO (55%), HOMO-3→LUMO (15%)
S_{10}	337.90	0.0584	HOMO→LUMO+3 (28%), HOMO→LUMO+5 (27%), HOMO→LUMO+4 (24%)
			33·acetone
S_1	453.24	0.0044	HOMO→LUMO (89%)
S_2	439.94	0.0149	HOMO-1→LUMO (95%)
S_3	410.27	0.0234	HOMO→LUMO+1 (76%), HOMO-2→LUMO (16%)
S_4	397.45	0.0868	HOMO-2→LUMO (76%), HOMO→LUMO+1 (12%)
S_5	381.17	0.0128	HOMO→LUMO+2 (81%)
S_6	367.59	0.0213	HOMO-2→LUMO+1 (58%), HOMO-5→LUMO+2 (12%), HOMO-1→LUMO+1 (12%)
S_7	352.56	0.0109	HOMO-1→LUMO+2 (46%), HOMO-1→LUMO+1 (20%), HOMO-5→LUMO (11%)
S_8	350.12	0.0524	HOMO→LUMO+3 (53%), HOMO→LUMO+4 (26%)
S_9	344.12	0.0156	HOMO-6→LUMO (80%)
S_{10}	341.01	0.0432	HOMO→LUMO+4 (35%), HOMO→LUMO+3 (24%), HOMO-2→LUMO+2 (22%),
			34
S_1	446.3	0.0366	H-1->LUMO (85%), HOMO->LUMO (11%)
S_2	404.8	0.0202	HOMO->L+1 (62%), HOMO->L+2 (25%)
S_3	391.8	0.0548	H-3->LUMO (53%), H-2->LUMO (15%), H-4->LUMO (12%)
S_4	384.5	0.0205	H-4->LUMO (74%), H-5->LUMO (12%)
S_5	379.9	0.0232	H-5->LUMO (61%), H-3->LUMO (14%)
S_6	375.5	0.0104	H-1->L+1 (49%), H-1->L+2 (10%), HOMO->L+2 (18%)
S_7	373.1	0.0356	HOMO->L+2 (38%), H-1->L+1 (28%), HOMO->L+1 (13%)
			36
S_1	424.5	0.0284	H-1->LUMO (95%)
S_2	405.6	0.0598	HOMO->L+1 (92%)
S_3	377.3	0.1142	H-2->LUMO (83%), H-3->LUMO (7%)
S_4	370.1	0.0328	H-3->LUMO (82%), HOMO->L+2 (5%)
S_5	360.0	0.0138	H-1->L+2 (49%), H-5->LUMO (18%), HOMO->L+2 (11%)
			36·acetone
S_1	462.8	0.0101	HOMO->LUMO (94%)
S_2	460.2	0.0181	H-1->LUMO (96%)
S_3	408.6	0.0374	H-2->LUMO (95%)
S_4	392.9	0.0232	HOMO->L+2 (35%), HOMO->L+1 (28%), H-3->LUMO (27%)
S_5	377.8	0.0166	H-6->LUMO (69%), HOMO->L+2 (10%), HOMO->L+1 (9%)
S_6	349.7	0.0195	H-8->LUMO (50%), H-9->LUMO (18%), H-7->LUMO (6%)

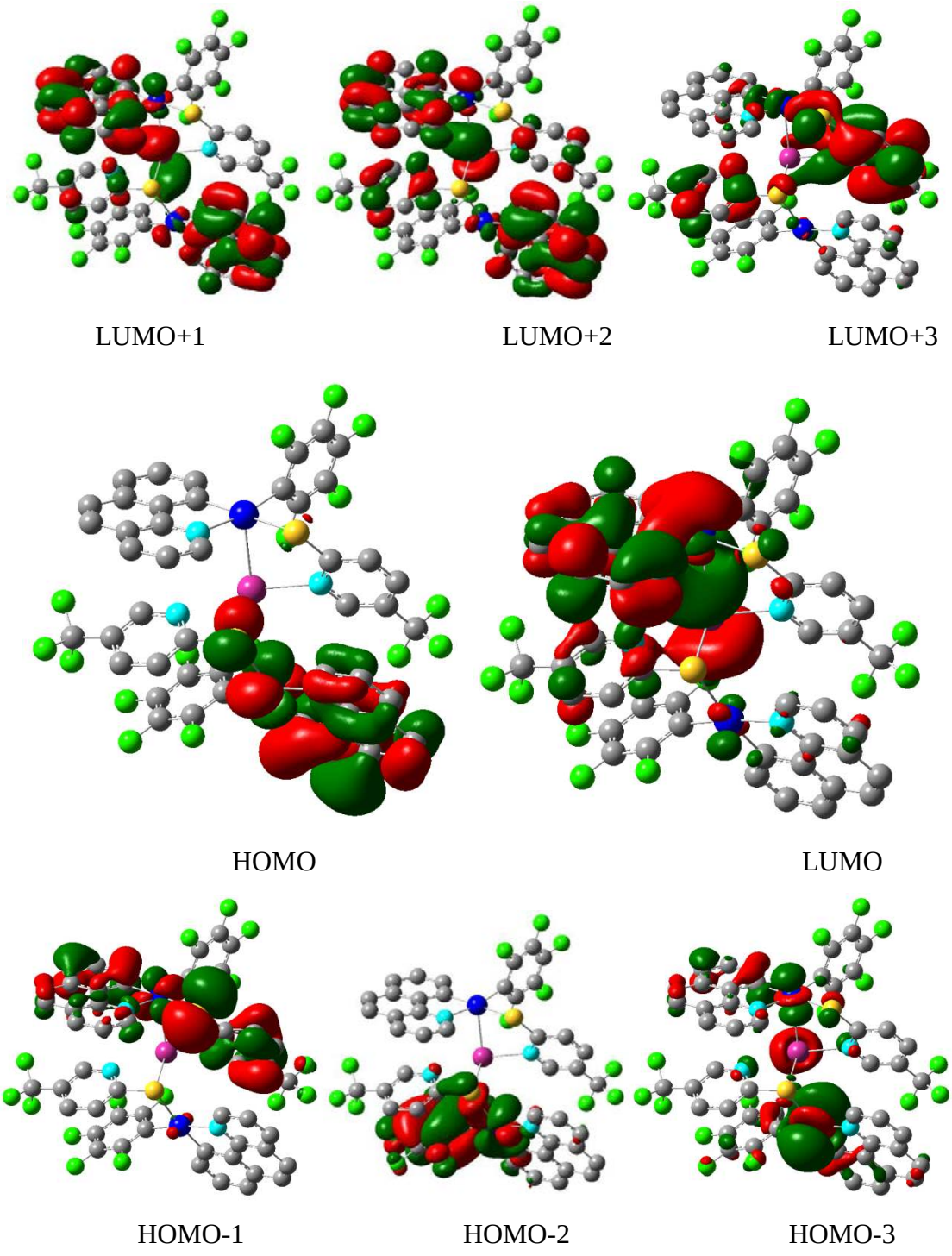

Figure A5.4: Frontier MOs of **34** optimized in the ground state

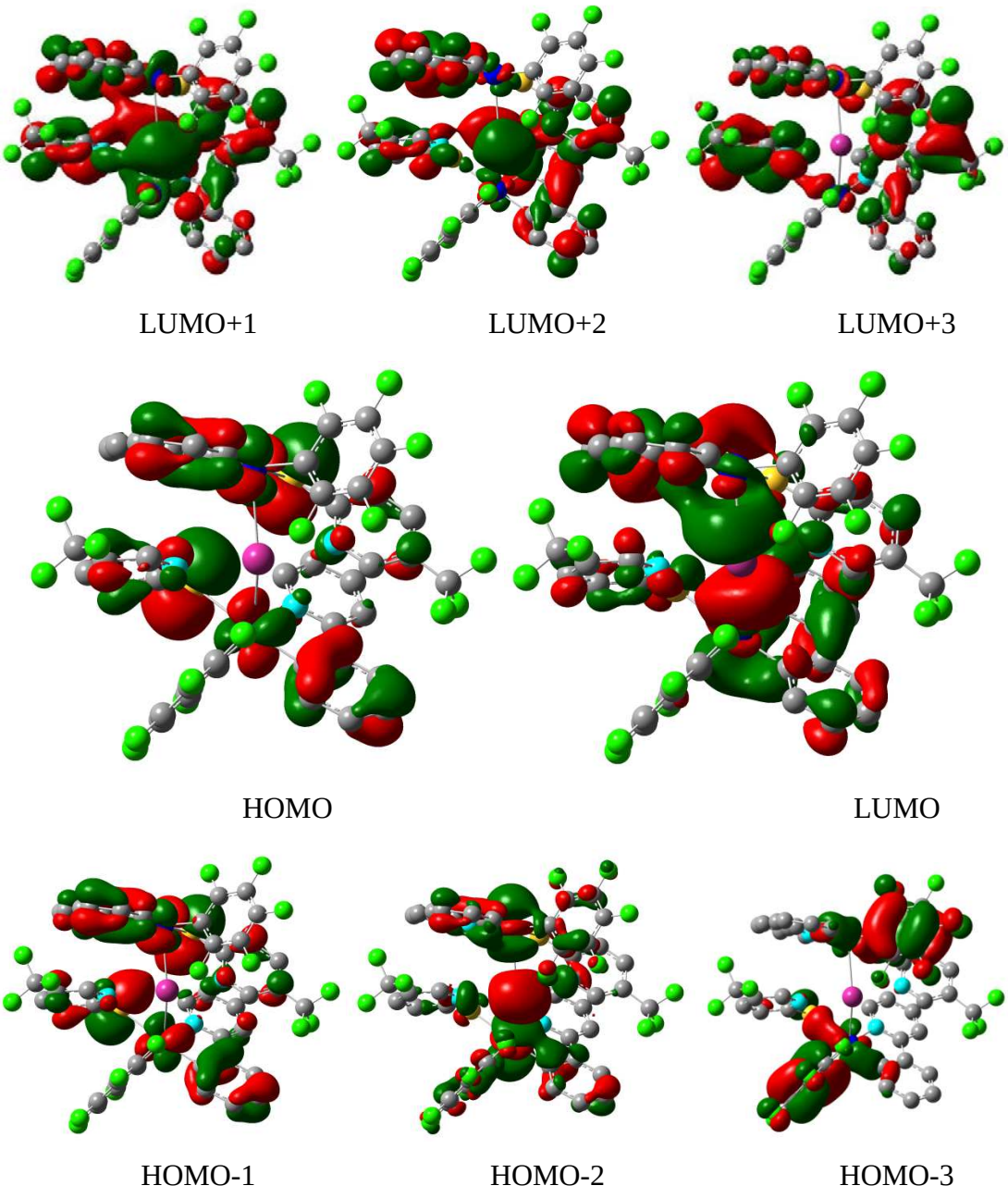

Figure A5.5: Frontier MOs of **36** optimized in the ground state

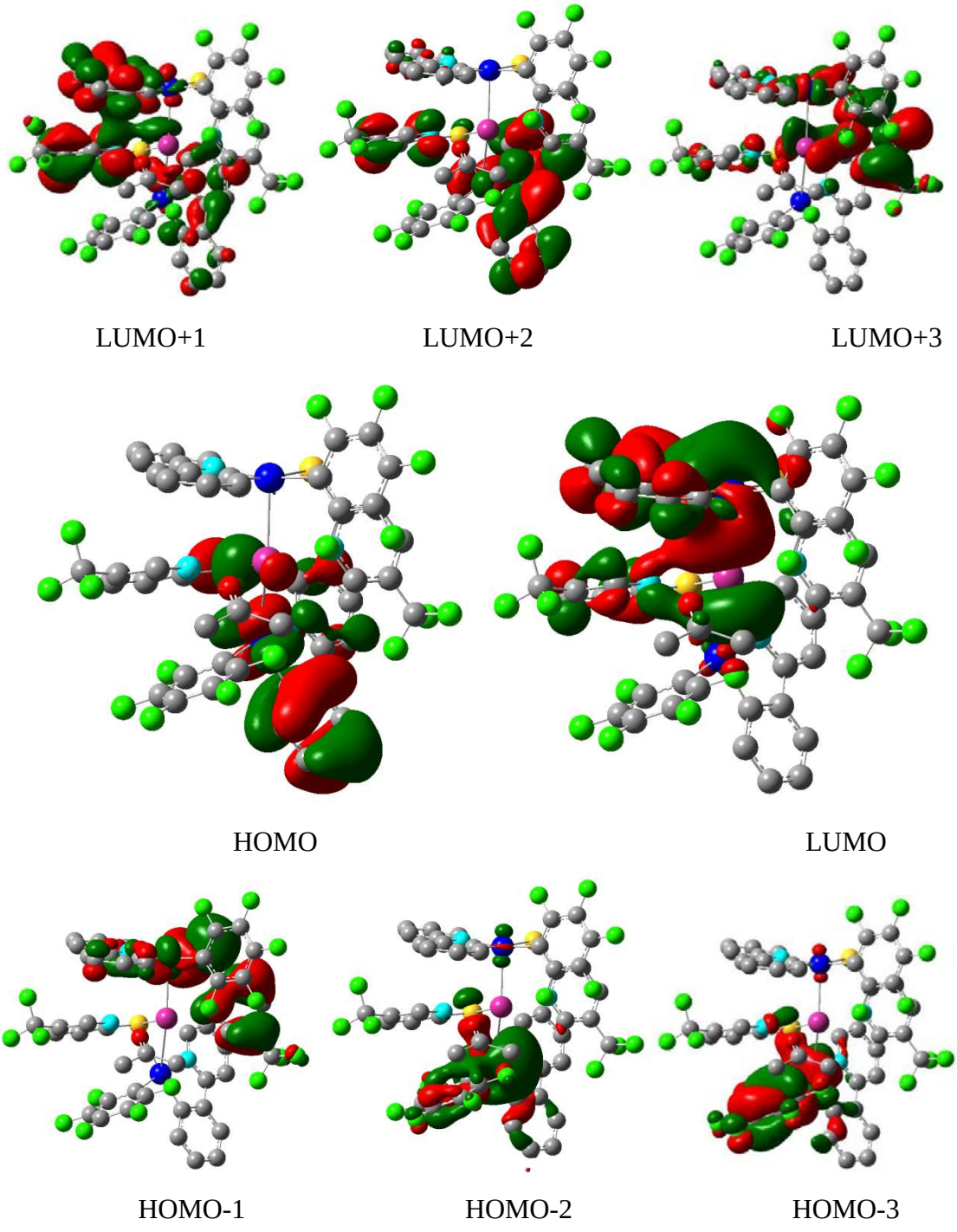

Figure A5.6: Frontier MOs of **36·acetone** optimized in the ground state

SUMMARY AND CONCLUSIONS

Summary and Conclusions

Summary

Chapter 1. Cycloplatinated complexes with escorpionate ligands

In this Chapter, three series of neutral [Pt(C^N){$H_2B(pz)_2$}] (**1**-**3**) and cationic [Pt(C^N){$H_2C(pz)_2$}]$^+$ (**4**-**6**), [Pt(C^N){$HC(pz)_3$}]$^+$ (**7**-**9**) (C^N = bzq, ppy, pq) cyclometalated complexes containing poly(pyrazolyl)borate and methane as ancillary ligands have been prepared by bridge splitting and chloride substitution reactions from the precursors [Pt(C^N)(μ-Cl)]$_2$ and the corresponding ligand. The neutral tris(pyrazolyl)borate [Pt(pq){$HB(pz)_3$}] **10** complex was also prepared following a similar methodology, but the related benzoquinolate and phenylpyridinate derivatives were inaccessible by this route due to the ease of formation of binuclear systems [Pt(C^N)(μ-pz)]$_2$ (mixture of *cis* and *trans* isomers) involving B-N bonds rupture.

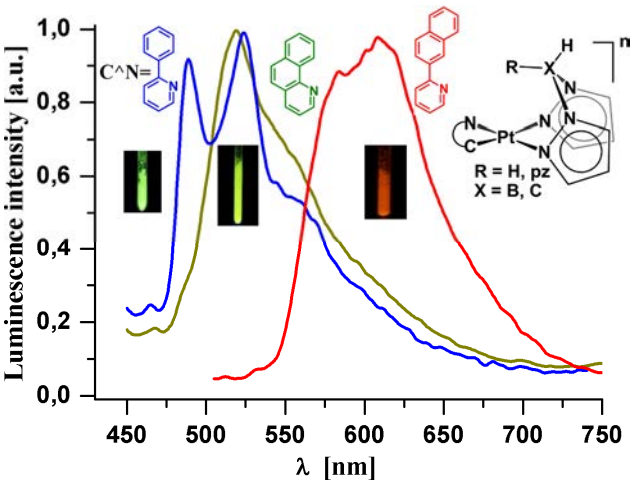

The photophysical properties have been modulated by the cyclometalating (L) and chelating (L') ligands. Both, absorption and emission features are distinctly red-shifted following the energy order (*pq* < *bzq* < *ppy*) and hence are mainly associated with mixed IL/MLCT transitions. Compared with the neutral complexes (**1**-**3**, **10**), energy absorption and emission in most of the related cationic derivatives are blue-shifted, in agreement with an increased contribution from the IL state and a decrease in the MLCT character. These trends are correlated with electrochemical measurements.

This study reveals that in diluted fluid solution, the complexes containing the planar *bzq* ligand (**1**, **4**, **7**) and some of the derivatives with the tris(pyrazolyl)methane group [$HC(pz)_3$] also exhibit fluorescence and/or excimer fluorescence. Time-resolved

emission studies suggest that the fluorescence is *delayed fluorescence*. This is also coherent with an additional solvent-dependence study on complex **1**, which indicates that in the less polar solvent used (toluene), the fluorescence disappears and the ^{3}ILCT/^{3}MLCT is stabilized. In glass state, the triplet manifold is also stabilized and only phosphorescence emission is observed. Probably due to steric hindrance of the bulky ligands, no low-energy emissions due to excimer and/or aggregates are found (298 K, 77 K) even in concentrated solutions. Only in the cationic [HC(pz)$_3$] complex **7**, excimeric emission is observed even in diluted glasses (77 K) and emission from aggregates also appears at a longer wavelength in concentrated glasses.

TD-DFT calculations have been carried out on the neutral **1** and the cationic **7-9** complexes. On the basis of these calculations, the lowest energy absorption is suggested to be ^{1}ILCT/^{1}MLCT in nature in **1** and in the [HC(pz)$_3$] series (**7-9**), this transition is mainly ^{1}ILCT combined with ^{1}MLCT/^{1}ML'CT for **9** or ML'CT for **7** and **8**. The TD-DFT calculations of the optimization of the lowest-lying triplet excited states responsible for the phosphorescence of these complexes indicates that whereas in the neutral derivative **1** this emission has mainly a ^{3}ILCT origin with mixing ^{3}MLCT character, in the cationic derivatives **7-9**, it would arise from a ^{3}ILCT transition mixed with ^{3}ML'CT (specially in **8**) and with some of ^{3}MLCT in **9**.

Chapter 2. Phenylquinoline and Phenylquinolinyl Alkynyl Based Pt^{II} Complexes

Chapter 2 details the reactions of the phenylquinolinyl derivative [Pt(pq)(μ-Cl)]$_2$ with LiC≡CR. Depending on the substituents in the alkynyl group and the reaction conditions two different series of alkynyl Pt(II) complexes have been obtained. We have investigated the phosphorescent characteristics of two very different series of alkynyl Pt(II) complexes.

On one hand, unusual tris(alkynyl) monoanionic (NBu$_4$)[Pt(C≡CR)$_3$(Hpq)] (**13-15**) complexes containing the *N*-coordinated phenylquinoline (Hpq) ligand were generated by

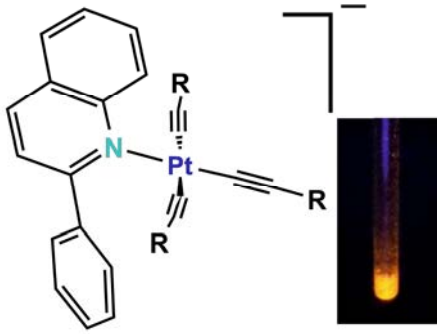

R = Tol, C_6H_4OMe-3, $C_6H_4CF_3$-4

using excess of *arylethynyl* lithium. Their formation involves a rare de-orthometalation process which, to our knowledge, has no precedent in the chemistry of σ-alkynyl/cyclometalated complexes. These complexes display yellow-orange emissions in rigid media which are ascribed, on the basis of DFT calculations, to a mixed alkynyl-metal to phenylquinoline ^{3}[(L'+M)LCT] excited estate. The energy of this emission is perturbed in the solid state for **14** by the presence of *intermolecular* $O_{methoxy}\cdots H_{Hpq}$ contacts, as supported by X-ray.

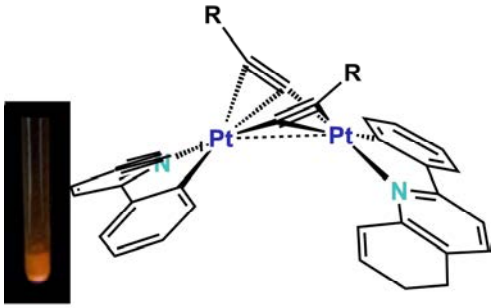

R = ^{t}Bu, Tol, C_6H_4OMe-3, $C_6H_4CF_3$-4

By the other hand, cyclometalated binuclear [Pt(pq)(μ−κC^{α}:η^{2}C≡CR)]$_2$ (**16**-**19**) complexes, featuring a double σ/π alkynyl bridging ligand system, have been successfully prepared employing a more adequate stoichiometry of the alkynylating agent. The X-ray diffraction studies of **16** (R = ^{t}Bu) and **17** (R = Tol) reveal the formation of butterfly structures with short Pt···Pt separations (shorter in **16**) stabilized by η^2-C≡CR asymmetrical (**16**) or symmetrical (**17**) linkages, which seem to play a major role in their photophysical behavior.

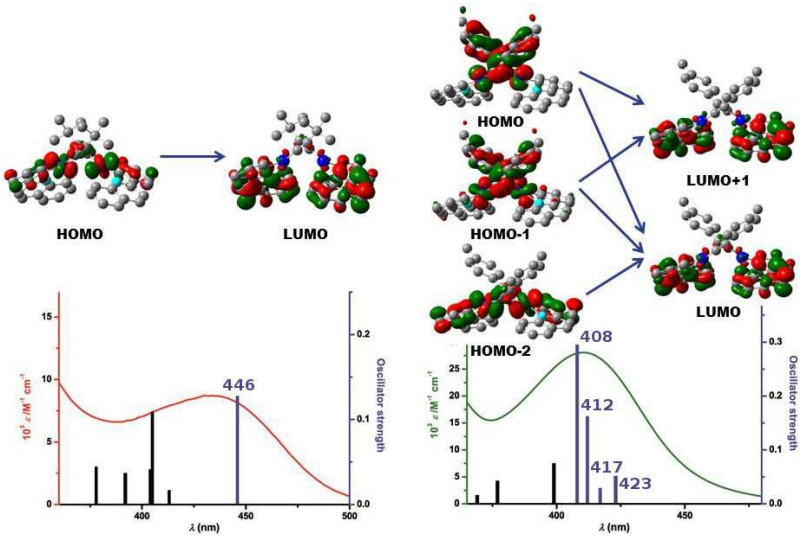

Their emissions are clearly influenced by the nature of substituents on the alkynyl ligands and correlate with the observed intramolecular Pt···Pt distances. For complex **16** with an alkyl substituent (^{t}Bu) and featuring a short Pt····Pt distance, the emission is located within the dimetallacycle core $Pt_2(C{\equiv}C)_2$ with some alkynyl to pq charge transfer ^{3}[(MM+L')LCT] excited state. However in **17**, with the tolyl substituent and a longer Pt····Pt distance, the emission mainly arises from a ^{3}L'LCT excited state with minor contribution of ^{3}MMLCT

character. Intriguingly, the emissions profiles of **18** and **19** in solid state (77 K) and those of all complexes in glasses are characteristic of a *monomer-like* ^{3}[(L'+M)LCT] excited state with a negligible contribution of the Pt···Pt interaction. We attributed this behavior to the formation of bent $Pt_2(C{\equiv}C)_2$ cores with longer Pt···Pt distances to those found for **16** and **17** in solid state (> 3.2 Å) and in the fast frozen process. Although the generation of planar $Pt_2(C{\equiv}C)_2$ cores with long metal-metal separation could not be completely excluded, it is seems less likely due to geometrical constraints of the pq ligands.

In contrast to the behavior described in the Introduction for di and oligonuclear cycloplatinate derivatives stabilized by other types of bridging ligands and weak Pt···Pt interactions, the theoretical studies on diplatinum complexes **16** and **17** indicate that the utilization of two alkynyls as unique bridging groups introduces a remarkable change in the nature of the HOMO, not only because the favorable Pt(dπ)/π(C≡C) electronic interaction within the $Pt_2(C{\equiv}C)_2$ core as found in **16**, but also due to the possible delocalization through the substituents as is seen in **17**. Optimization of the T_1 excited state of **17** suggests that upon excitation not only a shortening of the Pt···Pt distance takes place but also a change in the alkynyl bonding fashion from asymmetric (μ-σ/πC≡C^{t}Bu) to a symmetrical (μ-η^{1}C≡C^{t}Bu).

Chapter 3. Reactivity of [Pt(pq)(μ–κC$^\alpha$:η^2-C≡C^{t}Bu)]$_2$ toward donor ligands. Solution behavior and photophysical properties

This Chapter summarizes the result of the reactions of [Pt(pq)(μ–κC$^\alpha$:η^2-C≡C^{t}Bu)]$_2$ (**16**) toward different donor ligands.

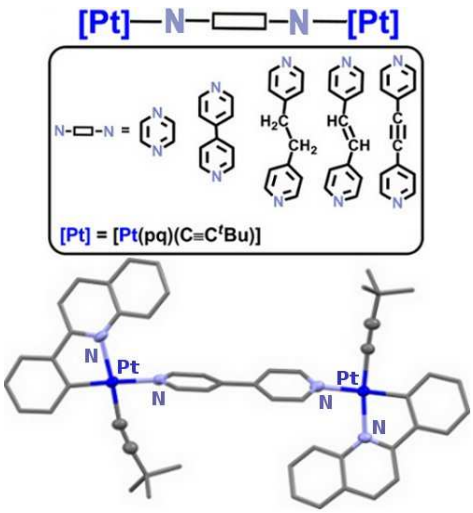

The first part of the Chapter focuses on the bridge-splitting reactions of **16** with bidentate N-donor ligands of different lengths and flexibility and one *N*-tridentate ligand to form binuclear [{Pt(pq)(C≡C^{t}Bu)}$_2$(μ-L)] (**20a-24a)** and trinuclear [{Pt(pq)(C≡C^{t}Bu)}$_3$(μ-L)] (**25a**) derivatives. The structures of **21a** and **23a** have

been confirmed by X-ray crystallography. Probably due to the *trans* labilizing effect of the *C*-cyclometalating atom and the high stability of **16**, these complexes rearrange in solution giving rise to a dynamic equilibrium between the diplatinum complexes (**20a**-**24a**), the mononuclear species [Pt(pq)(C≡C^{t}Bu)(L-κ*N*)] (**20b**-**24b**), the precursor (**16**) and the free ligand (L), as confirmed by ^{1}H NMR experiments. The equilibrium is affected by the concentration, temperature and solvent polarity. The higher proportion of the bimetallic species (**a**) in solution was found with the more flexible and donor ligands (bpa, bpe), in concentrated solutions, at low temperatures and with less polar solvents.

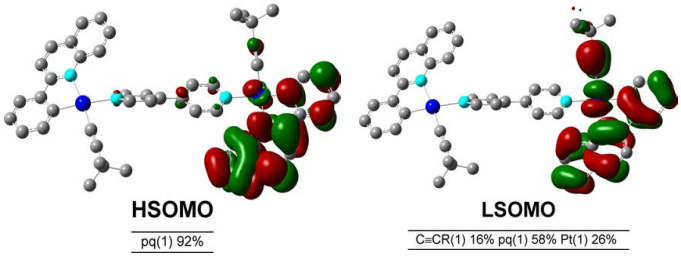

TD-DFT calculations on **21a** allow to assign the low-energy absorption band in solid state to Pt(pq)(C≡C^{t}Bu) to ***N-N*** linker charge transfer (500-540 nm) ^{1}[(M+L+L')L''CT], whereas in CH_2Cl_2 solution the low energy band (408-413 nm) is ascribed mainly to admixture of platina/alkynyl to cyclometalate (pq) charge transfer ^{1}[d(Pt)/C≡C→π*(pq)] ^{1}[(M+L')LCT], although some contribution to the *N*-donor ligand ^{1}[d(Pt)/C≡C→π*(*N*-donor)] cannot be discarded. These assemblies show a stronger luminescence than the starting material (**16**). The emission properties of the bpe-dimer **23a** in solid state are consistent with a predominantly bpe-centered ^{3}IL ^{3}(ππ*) excited state, whereas **20a** and **21a** exhibit emission from an admixture platina/alkynyl to cyclometalated (pq) charge transfer ^{3}[(M+L')LCT], supported by DFT calculations on **21a** and in the remaining complexes some additional contribution of the central *N*-linker can be invoked. The emission in solution of the binuclear species (**a**) (predominant in mixtures **16**:L 1:1) and the mononuclear species (**b**) (predominant in mixtures **16**:L 1:4) is rather similar, suggesting a similar excited state for both types of species, attributed in all complexes to ^{3}[(M+L')LCT]. Experimental data and theoretical calculations suggest that the excitation of the molecule seems to introduce a remarkable change in the nature of the HOMO-LUMO/SOMO-1-SOMO, rising the energy of the π* diimine-based orbitals above the cyclometalated-based orbitals.

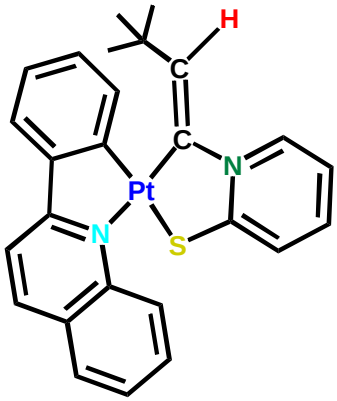

On the other hand, the second part of this Chapter is centered in the reactivity of **16** with 2- and 4- thiolpyridine. The position of the sulfur atom in the pyridine ring determines the geometry of the obtained complexes. The reaction with 2-thiolpyridine gives rise the mononuclear complex [Pt(pq){(κ*C*:κ*S*-2-SC_5H_4N-C=CH^{t}Bu}] (**26**) with a vinylthione molecule as ligand. Its structure has been confirmed by X-Ray diffraction observing the presence of a solid solution from both geometries (*Z* and *E*) in the ^{t}Bu residue of the alkynyl fragment. The formation of this complex implies the *intramolecular* addition of the N-H bond of the mercaptopyridine ligand through the $C^{\alpha}\equiv C^{\beta}$ triple bond of the alkynyl fragment, giving rise a new vinylthione C(NC_5H_4S-2)=CH^{t}Bu molecule acting as a chelatig κ*C*,*S* ligand, forming an unusual platinaheterocyle of five members. The mechanism of its formation has been proposed by a variable temperature ^{1}H NMR study.

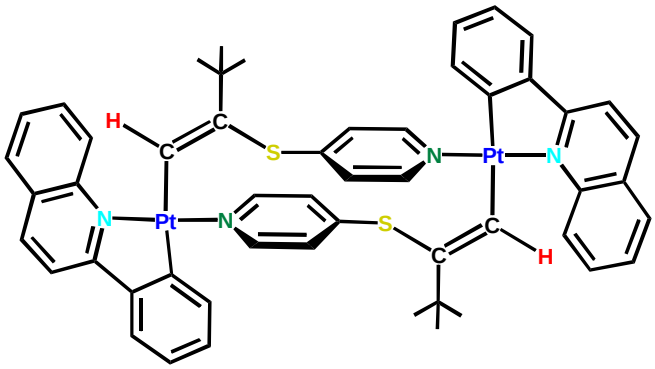

The thermal and photochemical *Z*/*E* isomerization of this compound have been studied. This study permits to discard the thermal isomerization, and to reach the photostationary state in the photoisomerization process after ~ 30 minutes of irradiation at λ > 360 nm with a 55/45 (*Z*/*E*) ratio.

The reaction with 4-thiolpyridine proceeds with formation of the cyclic bimetallic complex [Pt(pq){μ-*Z*-κ*C*:κ*N*-C=CH(^{t}Bu)-4-SC_5H_4N}]$_2$ (**27**), which contains a pyridyl-vinyl-thioether bridging system between the two platinum centers, formed by a formal hydrothiolation process of the alkynyl fragment.

In **26**, the lowest energy absorption band is substantially red shifted compared to that of the starting material and is associated with an heterocyclic ring-to-cyclometalated pq ligand ^{1}L'LCT or heterocycle/metal-to-pq ^{1}ML'LCT transition.

However in **27** the lowest-energy band is slightly blue-shifted, being tentatively ascribed to typical ^{1}LC/^{1}MLCT located on the Pt units.

Both complexes show a more intense emission than the precursor **16**. Complex **26** shows different emission in solid state or in solution. Thus, in the solid state it displays a broad asymmetric band, considerably red-shifted in relation to **16**, whereas in CH_2Cl_2 solution the emission is blue-shifted respect to the solid. This suggests that the emission in the solid can be influenced by the close π···π ligand-type (pq-pq) interactions and ascribed to platinum heterocycle-to-ligand (pq)/ligand (pq) charge transfer ^{3}[(M+L')LLCT], whereas in solution these π···π (pq-pq) interactions are loosed. Thus, the emission in solution is adscribed to an admixture ^{3}[(M+L')LCT] ^{3}[Pt(d)/heterocycle→ π*(bzq)] excited state.

Complex **27** exhibits in the solid state a broad asymmetric band that suffers a slightly blue-shift in CH_2Cl_2 solution, pointing to an admixture ^{3}MLCT/^{3}LC contribution.

Chapter 4. Reactivity of $(NBu_4)[Pt(bzq)(C{\equiv}CR)_2]$ toward $[Pb(HBpz_3)]^+$

In order to study the influence of the change in the electronic nature of Pb^{II} centers on the structures and optical properties of lead-platinum-alkynyl systems, the reactions of cyclometalated Pt^{II} compounds $(NBu_4)[Pt(bzq)(C{\equiv}CR)_2]$ (R = Ph, C_6H_4OMe-3 y $C_6H_4CF_3$-4) with $[Pb(HBpz_3)]Cl$ and excess of $NaPF_6$ were tested.

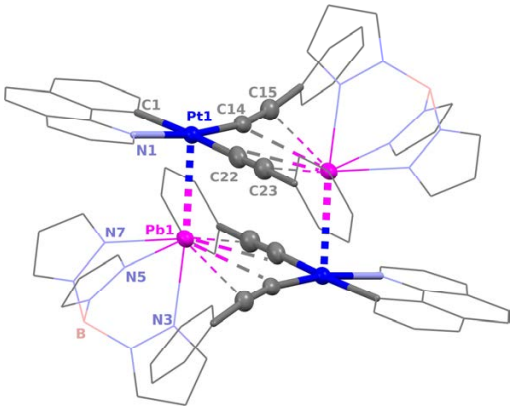

In the case of the compounds with R = Ph and C_6H_4OMe-3, the reactions evolve with the neutralization of the corresponding monoanionic precursors, giving rise to the tetranuclear derivatives $[Pt(bzq)(C{\equiv}CR)_2\{Pb(HBpz_3)\}]_2$ (**28**, **29**), where the bimetallic fragment $[\{Pt(bzq)(C{\equiv}CR)_2\}\{Pb(HBpz_3)\}]$ dimerizes through weak or short $Pb^{II}\cdots\eta^2$alkynyl interactions, increasing the coordination

environment of Pb. In the binuclear derivatives, the lead center of the $\{Pb(HBpz_3)\}^+$ unit interacts with the $\{Pt(bzq)(C\equiv CR)_2\}^-$ fragment through a Pt-Pb bond and completes its coordination sphere through $Pb^{II}\cdots\eta^2$alkynyl interactions with the *cis*–bis–η^2alkynyl of the second $\{Pt(bzq)(C\equiv CR)_2\}^-$.

However, with the substrate containing the less electron donor substituent ($C_6H_4CF_3$-4), the trinuclear anionic derivative $(NBu_4)[\{Pt(bzq)(C\equiv CC_6H_4CF_3\text{-}4)_2\}_2\{Pb(HBpz_3)\}]_2$ (**30**) was obtained, in wich two anionic $\{Pt(bzq)(C\equiv CR)_2\}^-$ fragments displaced and mutually oriented in a *cis* position are connected through the $\{Pb(HBpz_3)\}^+$ cation.

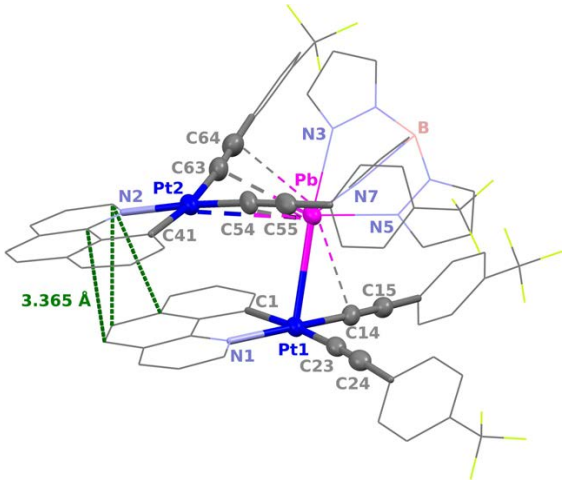

In order to understand the behaviour of **28** and **29** in solution unidimensional (PGSE) and bidimesional (DOSY) diffusion experiments and a variable temperature ^1H RMN study (**28**) were carried out. According to these measurements, we conclude that the solutions of **28** and **29** are mainly formed by the binuclear entity $[\{Pt(bzq)(C\equiv CR)_2\}\{Pb(HBpz_3)\}]$, due to the rupture of the $Pb^{II}\cdots\eta^2$alkynyl interactions of the tetranuclear entity.

The lowest energy absorption bands in **28** and **29** are tentatively attributed to a transition with a marked charge transfer character from the "$Pt(C\equiv CR)_2$" fragment to a bzq/$\{Pb(HBpz_3)\}$ mixed state ^{1}L'LCT/^{1}ML'M'CT (L = bzq, L' = C≡CR, M = Pt, M' = Pb), while in the trinuclear derivative **30**, the more important contribution must come from a charge transfer transition ^{1}L'LCT o ^{1}ML'LCT, with less contribution of the "$Pt(C\equiv CR)_2$" to $\{Pb(HBpz_3)\}$ transition.

The yellow-orange luminescence observed in the tetranuclear compounds in solid state and glassy solution are blue shifted respect to the starting materials and are assigned to an alkynyl or metal-alkynyl to ligand (bzq) charge transfer transition

^{3}L'LCT o ^{3}ML'LCT, scarcely perturbed for the Pt···Pb interaction ^{3}[Pt/π(C≡CR)→Pt(d)/Pb(sp)/π*(bzq)].

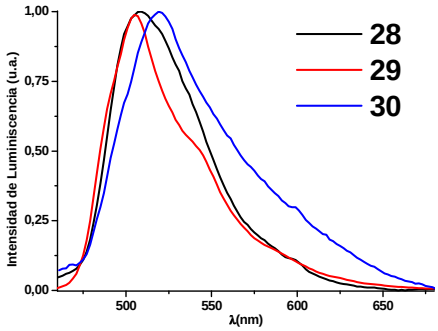

Nevertheless, the luminescence of the trinuclear compound **30**, both in solid and in solution (298 and 77 K), do not show differences with the starting material, so the emission could be attributed, at least in fluid to a ^{3}L'LCT ^{3}[Pt(d)/π(C≡CR)→π*(bzq)] transition, with few or no participation of the Pt···Pb interaction. The short intermolecular π(bzq)··π(bzq) interactions observed in X- Ray crystallography could be responsible of the presence of a small additional excimeric contribution in glassy state (77 K).

Chapter 5. Pt_2Pb Clusters [{Pt(C_6F_5)(C^N)}$_2$Pb(SpyR-5)$_2$]. Structures and Photophysical Responses Driven by Solvent Interactions

In this Chapter, two distinct types of Pt_2Pb clusters [{Pt(C_6F_5)(C^N)}$_2$Pb(μ-SpyR)$_2$] (**33**–**36**) were prepared by reaction of the corresponding solvate complexes [Pt(C_6F_5)(bzq)($OCMe_2$)] and [Pt(C_6F_5)(ppy)(dmso)] with Pb(SpyR-5)$_2$ (R = H, CF_3), and a detailed study of their structures and photophysical properties is reported.

In spite of the fact that all clusters feature two Pt-Pb bonds supported by two bridging pyridine-2-thiolate ligands, the notable differences in the Pb environment and, consequently, in the stereochemical activity of the $6s^2$ lone pair strongly affect their photophysical response. It was found that only the presence of *asymmetric* (*hemidirected*) environments around the Pb^{II} seems to provoke stimulus-responsive luminescent behaviour.

Thus, the ppy/Spy cluster (**35**), formed by coordination of the pyridine-N atoms to the Pt center, displays a *symmetrical* "PbS_2Pt_2" core and exhibits a strong emission (mainly ^{3}LCCT in nature), which is not sensitive to external stimuli.

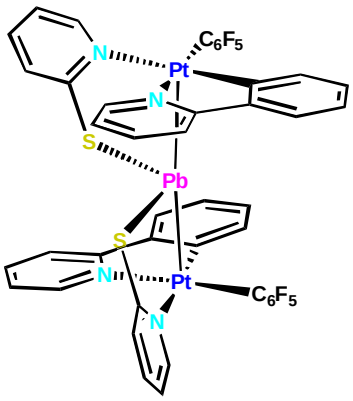

35

Unlike of **35**, clusters **33**, **34** (bzq) and **36** (ppy, $SpyCF_3$), formed by a formal thiolate S-transfer from Pb^{II} to Pt^{II}, show an *asymmetrical* coordination around the formally changed Pb^{II} ion in which the $6s^2$ lone pair is stereochemically active and are sensitive to external stimuli (vapours and/or mechanical grinding). For these clusters, several pseudopolymorphs (solvates) were crystallized depending on the solvent (**33**, **34**) and crystallization conditions (**36**), which allow us to rationalize their properties. Thus, in **33** and **34** (bzq) the Pb^{II} exhibits an *asymmetric* "Pt_2N_2S" (*trans*-N,N) environment, which change to a more *symmetric* environment in their acetone adducts ["Pt_2N_2O" (*cis*-N,N) (**33·acetone**) or "$Pt_2N_2SO_2$"/"Pt_2N_2SO" [**34·(acetone)$_{1.5}$**]], pointing a lower stereochemical activity of the lone pair in the acetone forms. In both clusters, the bright orange emission of the as-obtained solids, ascribed to ^{3}L'CCT [SpyR→Pb,Pt] states with some ^{3}MM'CT (M = Pt, M' = Pb) and ^{3}L'LCT (Spy→C^N) character, exhibit a significant and reversible blue-shift vapoluminescence response (by *ca.* 50 nm, **34** shows also colour changes) upon exposure to donor solvents. This response results from changes in the environment of the Pb^{II} ion from an asymmetric (*hemidirected*) to a more symmetric (*holodirected*) upon solvent binding. In the case of **33**, TD-DFT calculations suggest that the change in

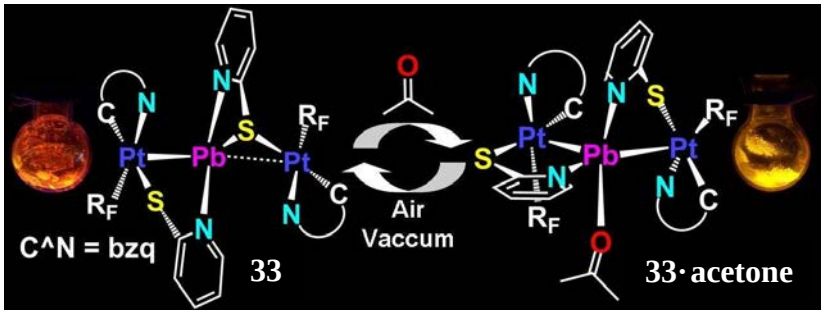

emission colour is related to a smaller Stokes shift (in **33·acetone**), attributed to a different distortion of the geometry (in **33** and in **33·acetone**) around the Pb^{II} center upon photoexcitation. However, in the system **34**, in which both forms show similar Stokes shifts, these changes are attributed to the concomitant effect of a more *holodirected* Pb environment and larger π···π stacking in the acetone form.

For **36** (ppy/$SpyCF_3$), three forms having different environments around the Pb^{II} ion and, hence, different emissions were found, depending on the solvent and

crystallization conditions. In most of the solvents (CH_2Cl_2, $CHCl_3$, C_6H_6) slow crystallization generates a yellow form (**36-y**) with a primary *symmetrical* "Pt_2N_2" environment, supplemented up to 8 with weak contacts to the S and F_o, which displays an intense yellow emission. Fast crystallization from CH_2Cl_2 (or concentrated solution) gives rise to orange (**36-o**) or pale-orange (**36·acetone**) crystals with a very *asymmetric* primary ("Pt_2N_2S" **36-o**, "PtN_2S" **36·acetone**) coordination, supplemented by weak contacts (two F_o **36-o**; one F_o and O for **36·acetone**). In these coloured forms, the most distinct feature is the twisting of one of the Pt units, shortening one of the Pt-Pb bonds to ~ 2.78 Å. Curiously, in contrast with the behaviour of the bzq clusters (**33** and **34**), in the solvate **36·acetone** the binding of acetone entails the *greatest asymmetry* (with a perpedicular orientation of the Pt fragments), which provokes the rupture of one of the

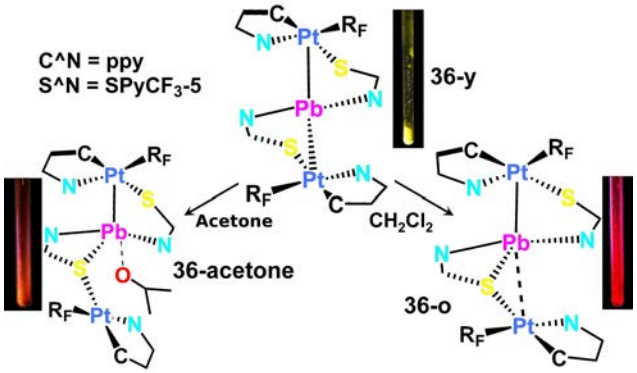

Pt-Pb bonds that, in turn, is compensated by the presence of strong π··π *intramolecular* interactions. The lack of vapoluminescent response to vapour donor solvents (and even a drop of solvent) of the yellow solid **36** may be attributed to the marked structural differences between the yellow and solvate **36·acetone** forms, which makes its transformation difficult in rigid media. In fact, the more symmetrical and *holodirected* coordination at Pb^{II} (yellow form) seems to be the most thermodynamically stable form, as it is generated from the orange forms by stirring in hexane (sonication or prolonged heating). Theoretical calculations of **36** and **36·acetone** reproduce the observed *symmetrical* (**36**) and *asymmetrical* (**36·acetone**) environments around Pb and the energy of the emissions, supporting ligand-cluster ^{3}LCCT [SpyR→Pb,Pt] state with some ^{3}MM'CT and ^{3}LLCT character. Notably, the amorphous solids generated upon dissolution/evaporation of **36** in different solvents exhibit intense emission in a wide range from 580 nm (THF) to 660 nm (CH_2Cl_2) (depending on the solvent), a feature which is ascribed to the formation of metastable kinetic forms, presumably having an asymmetric environment at Pb and a short Pt-Pb bond. The yellow solid also shows *mechanochromic* behaviour, with a remarkable red-shift in colour and luminescence upon grinding, which is ascribed to the transformation of the symmetrical form to more asymmetrical structures (similar to **36-o** or **36·acetone**) by mechanical stimuli.

Conclusions

This Memory has focused on the preparation of cyclometalated mononuclear and homodinuclear Pt^{II} and heteropolynuclear Pt^{II}-Pb^{II} species, with special emphasis in the study of their crystalline structures and their photophysical properties.

To this aim several families of neutral and cationic species with scorpionate-type ligands bis and tris(pyrazolyl)borate or methane and different cyclometalated groups have been prepared. Their photophysical and electrochemical properties are tuned by both, the cyclometalated ligands and the chelating ligands, as it has been established experimentally and supported by theoretical calculations on chosen models.

We have successfully obtained two families of alkynyl Pt^{II} derivatives: i) unusual anionic mononuclear tris(alkynyl) complexes $(NBu_4)[Pt(Hpq\text{-}\kappa\text{-}N)(C{\equiv}CR)_3]$, with the *N*-coordinated Hpq ligand and, ii) binuclear cyclometalated derivatives $[Pt(pq)(\mu{-}\kappa C^{\alpha}{:}\eta^2\text{-}C{\equiv}CR)]_2$, stabilized by a double σ/π alkynyl bridging system, depending on the substituents of the alkynyl ligands and the reaction conditions. We have investigated how the variation of the alkynyl ligands affect to their photophysical properties, which have been rationalized on the basis of their crystalline and electronic structures using theoretical calculations.

The reactivity of the *tert*-butyl binuclear derivative $[Pt(pq)(\mu{-}\kappa C^{\alpha}{:}\eta^2\text{-}C{\equiv}C^{t}Bu)]_2$ toward several bi- and tridentate nitrogen donor ligands has been studied allowing us to prepare binuclear derivatives, $[\{Pt(pq)(C{\equiv}C^{t}Bu)\}_2(\mu\text{-}L)]$, with the *N*,*N*-donor bridging both metallic centers, and a trinuclear branched complex $[\{Pt(pq)(C{\equiv}C^{t}Bu)\}_3(\mu\text{-}L)]$. In these systems, the equilibria stablished in solution and the photophysical properties in the solid state and in solution have been analyzed in detail, using also theoretical calculations.

In complex $[Pt(pq)(\mu{-}\kappa C^{\alpha}{:}\eta^2\text{-}C{\equiv}C^{t}Bu)]_2$, the activation reactions of the alkynyl group with 2- and 4-thiolpyridine take place with formal *intra*- and *intermolecular* hydroamination and hydrothiolation processes, respectively, affording the complexes $[\overline{Pt(pq)\{(\kappa C{:}\kappa S\text{-}2\text{-}SC_5H_4N\text{-}C{=}CH^{t}Bu\}}]$ and $[Pt(pq)\{\mu\text{-}Z\text{-}\kappa C{:}\kappa N\text{-}C{=}CH(^{t}Bu)\text{-}4\text{-}$

$SC_5H_4N\}]_2$. The position of the sulphur atom in the pyridine ring determines not only the geometry of the obtained complexes but also the observed optical properties.

Novel families of luminescent heteronuclear systems with cycloplatinated fragments and Pt-Pb bonds have been synthesized.

Thus, by using $[Pt(bzq)(C{\equiv}CR)_2]^-$ and $\{Pb(HBpz_3)\}^+$ as building blocks, novel tetranuclear clusters $[\{Pt(bzq)(C{\equiv}CR)_2\}\{Pb(HBpz_3)\}]_2$ and the trinuclear complex $(NBu_4)[\{Pt(bzq)(C{\equiv}CC_6H_4CF_3\text{-}4)_2\}_2\{Pb(HBpz_3)\}]$, stabilized by Pt···Pb bonds and/or $Pb^{II}\cdots\eta^2(C{\equiv}CR)$ interactions have been obtained. The nature of the tetranuclear derivatives in solution has been assessed by PGSE, DOSY and variable-temperature ^1H NMR studies. We have also carried out a comparative study of their optical properties in relation to those of the corresponding precursors.

Finally, two distinct types of Pt_2Pb luminescent clusters of stoichiometry $[\{Pt(C_6F_5)(C\text{^}N)\}_2Pb(SpyR\text{-}5)_2]$ (C^N = bzq, ppy; R = H, CF_3), stabilized by μ-SpyR groups and Pt-Pb bonds, were also prepared. In the ppy/Spy derivative the pyridine-*N* donor atoms coordinate to the Pt^{II} centers while the Pb^{II} retains the coordination of the two sulphur thiolate atoms. However, the formation of the rest of compounds occurs with a formal thiolate transfer form Pb^{II} to Pt^{II}, keeping the two N atoms in the primary environment of the lead. These clusters crystallize as several pseudopolymorphs depending on the solvent (bzq, SpyR) and crystallization conditions (ppy, $SpyCF_3$). The observed structural diversity relies on changes in the coordination mode of the SpyR ligands, the intermetallic Pt-Pb bonds and the presence of secondary *intra-* and/or *intermolecular* contacts induced by Pb-solvent binding. These changes, which are related with subtle changes in the stereochemical activity of the lone pair, have also a remarkable impact in the emissive state [^{3}L'CCT/^{3}L'LCT, SpyR→Pb,Pt/(C^N) in nature] and in the colour of the emission.

From this study, it is clear that only the presence of asymmetric *hemidirected* environments around the lead center seems to produce a luminescent response to external stimuli. Thus, the bzq clusters display a distinct and fast reversible blue-shift vapoluminescent response to donor solvents, which has been correlated with changes in

the environment of the Pb^{II} ion from an asymmetric *hemidirected* to a more symmetric *holodirected* environment upon solvent binding.

Although the ppy derivatives do not show a vapoluminescent response, the cluster with ppy and $SpyCF_3$ displays a rich polymorphism. Depending on the solvent and the velocity of crystallization several forms with different Pt···Pb separations and different Pb^{II} environments and, consequently, different emissions were isolated. Slow crystallization and low concentration favour the formation of thermodynamically more stable symmetric yellow form, whereas fast crystallization gives rise to the most asymmetric orange form, with a remarkable red-shift of the emission. Transformation of the symmetric form to more asymmetric forms is also possible by mechanical stimuli. The mechanochromic behaviour produces changes in the color and in the emission and it is reversible. To gain insight into the vapochromic and mecanochromic behaviours of these compounds, theoretical calculations on selected clusters and solvates have been performed.

CONCLUSIONES

Conclusiones

En esta Memoria se ha abordado la preparación de especies ciclometaladas mononucleares y homodinucleares de Pt^{II} y heteropolinucleares Pt^{II}-Pb^{II}, con especial énfasis en el estudio de sus estructuras cristalinas y de sus propiedades fotofísicas.

Se han preparado especies neutras y catiónicas con ligandos escorpionato bis y tris(pirazolil)borato o metano y distintos ligandos ciclometalados. Sus propiedades fotofísicas y electroquímicas se pueden modular tanto por los ligandos ciclometalados como por los ligandos quelato de tipo escorpionato, justificándose estas variaciones mediante cálculos teóricos en modelos escogidos.

Se han obtenido dos familias de alquinil derivados de Pt^{II}: i) los inusuales complejos aniónicos mononucleares tris(alquinilo) $(NBu_4)[Pt(Hpq\text{-}\kappa\text{-}N)(C{\equiv}CR)_3]$, con el ligando Hpq coordinado a través del nitrógeno y ii) los derivados ciclometalados binucleares $[Pt(pq)(\mu\text{–}\kappa C^{\alpha}\text{:}\eta^2\text{-}C{\equiv}CR)]_2$, estabilizados mediante un sistema de doble puente σ/π alquinilo, dependiendo de los sustituyentes de los ligandos alquinilo y de las condiciones de reacción. Hemos investigado cómo la variación del ligando alquinilo afecta a sus propiedades fotofísicas, que se han racionalizado analizando sus estructuras cristalinas y electrónicas mediante cálculos teóricos.

Se han estudiado las reacciones del *tert*-butil derivado binuclear $[Pt(pq)(\mu\text{–}\kappa C^{\alpha}\text{:}\eta^2\text{-}C{\equiv}C^{t}Bu)]_2$ frente a varios ligandos dadores. Las reacciones con ligandos nitrógeno dadores bi o tri dentados han dado lugar a derivados binucleares con los ligandos *N*,*N*-dadores puente entre ambos centros metálicos $[\{Pt(pq)(C{\equiv}C^{t}Bu)\}_2(\mu\text{-}L)]$ y el derivado trinuclear $[\{Pt(pq)(C{\equiv}C^{t}Bu)\}_3(\mu\text{-}L)]$ de tipo ramificado. En estos sistemas se ha analizado la presencia de equilibrios en disolución y sus propiedades fotofísicas tanto en estado sólido como en disolución, apoyado con cálculos teóricos.

Las reacciones de activación de los ligandos alquinilo en el sustrato binuclear de ^{t}Bu con 2- y 4-tiolpiridina evolucionan con procesos *intra-* e *intermoleculares* de hidroaminación y de hidrotiolación lo que nos permite obtener los sustratos $[Pt(pq)\{(\kappa C\text{:}\kappa S\text{-}2\text{-}SC_5H_4N\text{-}C{=}CH^{t}Bu\}]$ y $[Pt(pq)\{\mu\text{-}Z\text{-}\kappa C\text{:}\kappa N\text{-}C{=}CH(^{t}Bu)\text{-}4\text{-}$

$SC_5H_4N\}]_2$, respectivamente. La posición del átomo de azufre en el anillo piridínico determina no sólo la geometría de los complejos obtenidos sino también las propiedades ópticas observadas.

Se han sintetizado varias familias de sistemas luminiscentes heteronucleares con fragmentos cicloplatinados y enlaces Pt-Pb.

Así, utilizando como precursores las especies $[\{Pt(bzq)(C{\equiv}CR)_2\}^-$ y $Pb(HBpz_3)\}^+$, se han obtenido los clusters tetranucleares $[\{Pt(bzq)(C{\equiv}CR)_2\}\{Pb(HBpz_3)\}]_2$ y el compuesto trinuclear $(NBu_4)[\{Pt(bzq)(C{\equiv}CC_6H_4CF_3\text{-}4)_2\}_2\{Pb(HBpz_3)\}]$, estabilizados mediante enlaces $Pt\cdot\cdot Pb$ y/o interacciones $Pb^{II}\cdot\cdot\eta^2(C{\equiv}CR)$. En los derivados tetranucleares se han realizado estudios PGSE, DOSY y RMN de ^1H de temperatura variable para estudiar su naturaleza en disolución, y en todos ellos se ha realizado un estudio comparativo de sus propiedades ópticas en relación a las de los sustratos de partida.

Se han estudiado en detalles dos tipos de clusters Pt_2Pb luminiscentes, con estequiometría $[\{Pt(C_6F_5)(C\text{^}N)\}_2Pb(SpyR\text{-}5)_2]$ (C^N = bzq, ppy; R = H, CF_3), estabilizados por puentes μ-SpyR y enlaces Pt-Pb. Mientras el derivado con C^N = ppy y R = H coordina los átomos de nitrógeno de la piridina a los centros de Pt^{II}, en el resto de compuestos se produce una transferencia formal del tiolato desde el Pb^{II} al Pt^{II}, manteniendo los dos átomos de Nitrógeno coordinados al Pb^{II}. En estos derivados se pueden cristalizar varios pseudopolimorfos dependiendo del disolvente (bzq, SpyR) y de las condiciones de cristalización (ppy, $SpyCF_3$). Esta diversidad estructural proviene de distintos modos de coordinación de los ligandos SpyR, de las distancias intermetálicas $Pt\cdot\cdot Pb$ y de contactos secundarios intra- e intermoleculares inducidos por la coordinación del disolvente al centro de Pb. Estos cambios, que están estrechamente relacionados con la actividad estereoquímica del par solitario del Pb^{II} tiene también un notable impacto en el estado emisivo y en el color de la emisión [de naturaleza ^{3}L'CCT/^{3}L'LCT: SpyR→Pb,Pt/(C^N)]. Parece claro que sólo la presencia de entornos *hemidirigidos* asimétricos provocan una respuesta luminiscente hacia estímulos externos. Los clusters de bzq muestran una respuesta vapoluminiscente hacia el azul rápida y reversible cuando están en presencia de disolventes dadores, asociada con

cambios en el entorno del ión Pb^{II} desde un entorno asimétrico *hemidirigido* a un entorno más simétrico y *holodirigido* tras la coordinación de la molécula dadora.

Aunque los derivados de ppy no muestran respuesta vapoluminiscente, el cluster de ppy y $SpyCF_3$ presenta un rico polimorfismo con tres formas diferentes e interconvertibles en función del disolvente y la velocidad de cristalización, en las que aparecen distintos entornos en el Pb^{II}, distintas separaciones Pt··Pb y diferentes emisiones. La lenta cristalización y baja concentración favorece la formación de la forma más simétrica, termodinámicamente más estable, mientras que la rápida cristalización favorece la formación de la forma más asimétrica con un notable desplazamiento hacia el rojo de la emisión. La transformación de la forma más simétrica a la más asimétrica es posible también por estímulo mecánico. Este comportamiento mecanocrómico produce cambios tanto en el color como en la luminiscencia y es reversible. Para comprender el comportamiento vapoluminiscente, vapocrómico y mecanocrómico de estos compuestos se han realizado cálculos TD-DFT sobre algunos de estos clusters y sus solvatos.

EXPERIMENTAL

Experimental

A) Instrumental and spectroscopic techniques

Elemental analyses.

C, H and N elemental analyses have been carried out with a Carlo Erba EA1110 CHNS/O microanalyzer.

Mass spectra.

The Electrospray Mass spectra were performed using a VG Autospec double-focusing mass spectrometer operating in the negative FAB mode or a HP5989B mass spectrometer with interphase API-ES HP 59987A. MALDI-TOF spectra have been recorded in a Microflex MALDI-TOF Bruker spectrometer operating in the linear and reflector modes using dithranol as matrix in those cases that it was needed.

IR spectra

The IR spectra have been recorded in a Nicolet Nexus FT-IR spectrometer between 4000 and 200 cm^{-1}. These spectra have been done in most cases using Nujol mulls between polyethylene sheets (Nujol absorptions: 2900, 1452, 1377, 1362 cm^{-1}) and, for some compounds, from KBr pellets.

Cyclic Voltametry

Cyclic voltametry measurements were carried out in CH_3CN solution (5×10^{-4} M of the complex and 0.1 M of NBu_4PF_6.as the supporting electrolyte), using a three-electrode configuration (Pt disk as working electrode, Pt-wire counter electrode, Ag/AgCl referente electrode) on a Voltalab PST 050.

NMR characterization

The ^{1}H, ^{19}F, $^{13}C\{^{1}H\}$, and $^{195}Pt\{^{1}H\}$ NMR experiments described in this memory and in the rest of the experimental section were recorded on a Bruker ARX 300 and/or a Bruker AVANCE 400 spectrometer. Chemical shifts are reported in parts per million (ppm) relative to the appropriate external standard for each of the nuclei, and coupling constants are given in Hz.

^{1}H-PGSE measurements

^{1}H–PGSE measurements were carried out using the double stimulated echo pulse sequence (Double STE) on a bruker AVANCE 400 equiped with a BBI H-BB Z-GRD probe at 298 K without spinning using $CHCl_3$ as internal standard, the dependence of the resonance intensity I on a constant waiting time and on a variety gradient strength g in described bt the equation. 1:

$$I = I_o \exp(-D(2\pi\gamma \cdot \delta \cdot g)^2(\Delta-\delta/3) \cdot 10^4$$

I = Intensity of the observed spin-echo

I_o = Intensity of the observed spin-echo without gradients

Δ = Delay between the midpoints of the gradients

δ = Length of the gradient pulse

g = Strenght of the gradient

γ = Magnetogyric ratio

Equation 1

The pulse sequence was composed of 90º pulses. The duration of the gradients (δ) was 2 ms, the delay Δ was 200 ms and the strength g was varied during the experiment. The spectra were acquired using 32*K* (K = 1000) points. The exponential plots of I *versus* g were fitted using a standard exponential algorithm implemented in TOPSPIN software

Using the obtained diffusion coefficient D of the sample and the internal standard, and through the Stokes-einstein equation (equation. 2), an accurate value of the hydrodynamic radius r_H can be obtained in each case

$$D = \frac{K_B T}{6\pi\eta r_H}$$

D = Diffusion coefficient,

η = Solvent viscosity

K_B = Boltzman constant

r_H = Hydrodynamic radius

Equation 2

Molar conductivities

The Molar Conductivities described for some of the complexes were measured in solution (ca. 5×10^{-4} M) using a Crison GLP31 conductimeter. The type of electrolyte is established taking into account ranges previously reported.[1] Additional values in CH_2Cl_2 are included in the Table:

	Electrolyte 1:1	Electrolyte 2:1	Electrolyte 3:1	Electrolyte 4:1
Acetone	100-140	160-200	440	
Acetonitrile	120-160	220-300	340-420	>500
DCM	~ 33*			

* Molar conductivities of $(NBu_4)(ClO_4)$ (33.3 $\Omega^{-1}.cm^2.mol^{-1}$) and $(NBu_4)(PF_6)$ (33.8 $\Omega^{-1}.cm^2.mol^{-1}$).

UV-vis spectroscopy

UV-Vis spectra were recorded on a Hewlet Packard 8453 spectrometer. The DRUV (diffuse reflectance ultraviolet) in the solid state have been using a Shimadzu UV-3600 spectrometer with a Harrick Praying Mantis accessory coupled to it. Samples were prepared mixing the complex with KBr or SiO_2, and the reflectance information transformed following the Kubelka-Munk function.

Emission spectroscopy and lifetime measurements

Excitation and emission spectra were obtained on a Jobin-Yvon Horiba Fluorolog 3-11 Tau-3 spectrofluorimeter. The lifetime measurements were performed operating in the phosphorimeter mode (with a F1-1029 lifetime emission PMT assembly, using a 450 W Xe lamp) or using a Data station HUB-B with a nanoLED controller DAS6. Quantum yields in the solid state were measured using a F-3018 Integrating Sphere mounted on a Fluorolog 3-11 Tau-3 spectrofluorimeter. Data have been fittered using the JobinYvon software package and Origin 7.5.

X-Ray powder diffraction

X-ray powder diffraction patterns were obtained at room temperature using a Rigaku D/max 2500 rotating anode generator by using graphite-monochromated CuK operating at 40 kV and 80 mA. Powder diffraction patterns were collected between 2θ of 3° and 50° with a 2θ stepping angle of 0.03° and an angle dwell of 1 s

Thermogravimetric analyses

TGA (*Themal Gravimetric Analysis*) were recorded on a TA Instrument SDT 2960 using 2-10 mg samples at 10ºC/min rate in 30-600ºC range under nitrogen, and in the 600-750ºC range in air.

Theorethical calculations

All calculations included in the memory have been carried out by Sergio Sanchez using the corresponding molecular geometry obtained through X-ray diffraction analysis. Keeping all distances, angles and dihedral angles frozen, single point calculations with the Gaussian 03[2] program by density functional theory were performed, using Becke's three-parameter functional combined with Lee–Yang–Parr's correlation functional[3] (B3LYP) for the ligand atoms, along with the LanL2DZ basis set for the metal centers. The time-dependent density-functional theory (TD-DFT) calculation was carried out using the polarized continuum model approach implemented in the Gaussian 03 software. Percentage compositions of molecular orbitals were calculated using the AOMix program[4]

X-Ray crystallography

X-ray intensity data has been collected with a NONIUS-κCCD area-detector diffractometer, using graphite-monochromated Mo K_α radiation. Images were processed using the suite of programs DENZO and SCALEPACK, in those cases that the absorption correction was carried out at this point.[5] Details concerning structural resolution, including special methodology, are included in section D.

B) Synthesis of the starting materials

The starting materials are prepared following reported procedures

$[Pt(\eta^3\text{-}C_4H_7)(\mu\text{-}Cl)]_2$[6]

$[Pt(bzq)(\mu\text{-}Cl)]_2$ [7]

$[Pt(ppy)(\mu\text{-}Cl)]_2$ [8]

$K[HB(pz)_2]$ [9]

$K[HB(pz)_3]$ [9]

$HC(pz)_3$ [10]

$[H_2C(pz)_2]$[11]

di(4-pyridyl)acetylene [12]

1,3,5-tris(pyridine-4-ylethynyl)benzene [13]

$NBu_4[Pt(bzq)(C{\equiv}CR)_2]$ (R = Ph,[14] C_6H_4OMe-3,[15] $C_6H_4CF_3$-4[14])

$[Pb\{HB(pz)_3\}Cl]$[16]

cis-$[Pt(C_6F_5)_2(dmso)_2]$[17]

$[Pt(C_6F_5)(bzq)(acetone)]$ (**31**)[18]

$[Pb(Spy)_2]$[19]

$[Pb(SpyCF_3\text{-}5)_2]$[19]

Preparation of **$[Pt(pq)(\mu\text{-}Cl)]_2$.**

A suspension of $[Pt(\eta^3\text{-}2Me\text{-}C_3H_4)(\mu\text{-}Cl)]_2$ (1g, 1.75 mmoles) in xylene (10 mL) was treated with 2-Phenylquinoline (0.718 g, 3.50 mmoles) and the mixture refluxed for 2 h. The resulting orange solid was filtered and washed with xylene (5 mL) and diethyl ether (2 mL) (1.3 g, 86%).

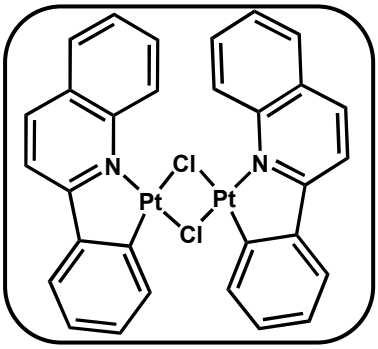

Anal. Calcd for $C_{30}H_{20}N_2Pt_2Cl_2$ (868.03): C, 41.47; H, 2.32; N, 3.23. Found: C, 41.41; H, 2.13; N, 3.25.

MALDI-TOF (+): *m/z* (%) 869.7 (100) $[M]^+$, 833.68 (86) $[M\text{-}Cl]^+$.

The low solubility of this complex precludes its characterization by NMR spectroscopy.

C) Synthesis of new complexes

Preparation of **[Pt(bzq){$H_2B(pz)_2$}] (1)**

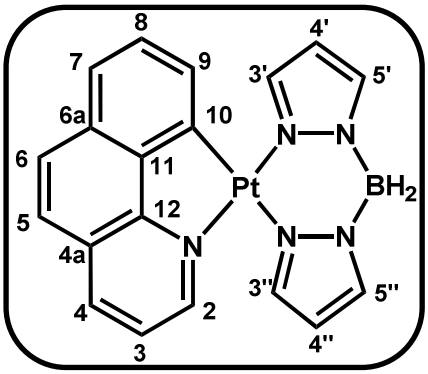

To a yellow suspension of [Pt(bzq)(μ-Cl)]$_2$ (0.500 g, 0.612 mmoles) in acetone (30 mL) was added 0.455 g (2.446 mmoles) of K[$H_2B(pz)_2$]. After 30 minutes of reaction, the white solid precipitated (KCl) was filtered through Celite and the yellow solution was evaporated to dryness. The residue was treated with CH_2Cl_2 (30 mL) and filtered again through Celite. Evaporation of the resulting filtrate and addition of EtOH (10 mL) yielded **1** as a yellow solid (0.273 g, 43%).

Anal. Calcd for $C_{19}H_{16}N_5BPt$ (520.25) C, 43.86; H, 3.10; N, 13.46. Found: C, 43.67; H, 3.21; N, 13.17 %.

MALDI-TOF (+): *m/z* (%) 519.1 (100) $[M-H]^+$.

IR (Nujol) (cm^{-1}): $\nu(B-H)_{st}$ 2407 (s).

^{1}H NMR (δ, 300.13 MHz, CD_3COCD_3): 9.01 (d, J_{H-H} = 5.4, $^3J_{Pt-H}$ = 32.9, 1H, H^2_{bzq}), 8.70 (d, J_{H-H} = 7.8, 1H, H^4_{bzq}), 7.98 (s, 2 H, $H^{5'}_{pz}$, $H^{5''}_{pz}$), 7.89 (AB, J_{H-H} = 10.2, δ_A = 7.95, δ_B = 7.83, 2H, H^5_{bzq}, H^6_{bzq}), 7.80 (s, 2H, $H^{3'}_{pz}$, $H^{3''}_{pz}$), 7.78 (d, J_{H-H} = 7.1, 1H, H^3_{bzq}), 7.73 (d, J_{H-H} = 7.9, 1H, H^7_{bzq}), 7.56 (t, J_{H-H} = 7.5, 1H, H^8_{bzq}), 7.48 (d, $^3J_{Pt-H}$ = 37.8, J_{H-H} = 7.2, 1H, H^9_{bzq}), 6.45 (t, J_{H-H} = 1.8, 1H, $H^{4'/4''}_{pz}$), 6.41 (t, J_{H-H} = 2.0, 1H, $H^{4'/4''}_{pz}$), 3.89 (t_{br}, J_{B-H} = 161.2, 2H, HBH_2).

^{13}C{^{1}H} NMR (δ, 75.5 MHz, $CDCl_3$): 157.5 (s, C^{10}_{bzq}), 148.3 (s, $^2J_{Pt-C}$ = 26.7, C^2_{bzq}), 142.0 (s, $^2J_{Pt-C}$ = 79.1, $C^{3'}_{pz}$), 140.3 (s, C^{12}_{bzq}), 140.0 (s, $^2J_{Pt-C}$ = 24.3, $C^{3''}_{pz}$), 137.7 (s, C^4_{bzq}), 136.5 (s, $C^{5''}_{pz}$), 136.3 (s, $^3J_{Pt-C}$ = 35.0, $C^{5'}_{pz}$), 133.8 (s, C^{11}_{bzq}), 131.7 (s, $^2J_{Pt-C}$ = 64.6, C^9_{bzq}), 130.0 (s, C^6_{bzq} + C^{6a}_{bzq}), 129.3 (s, $^4J_{Pt-C}$ = 54.0, C^7_{bzq}), 127.1 (s, C^{4a}_{bzq}), 123.1 (s, C^5_{bzq}), 122.2 (s, C^8_{bzq}), 120.9 (s, $^3J_{Pt-C}$ = 38.0, C^3_{bzq}), 105.7 (s, $^3J_{Pt-C}$ = 18.2, $C^{4''}_{pz}$, $^3J_{Pt-C}$ = 50.15, $C^{4'}_{pz}$).

Preparation of **[Pt(ppy){$H_2B(pz)_2$}] (2)**

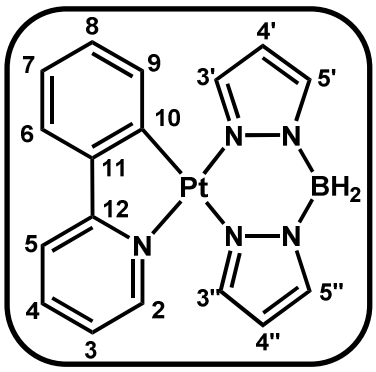

The synthesis of this complex has been previously described. [20] In this work, **2** was obtained as a yellow solid, following the same procedure than that described for **1** starting from [Pt(ppy)(μ-Cl)]$_2$ (0.200 g, 0.252 mmoles) and K[$H_2B(pz)_2$] (0.189 g, 1.008 mmoles) (0.096 g, 79%).

Anal. Calcd for $C_{17}H_{16}N_5BPt$ (496.24): C, 41.15; H, 3.25; N, 14.11. Found: C, 40.78; H, 2.99; N, 13.82 %.

MALDI-TOF (+): *m/z* (%) 495.1 (52) $[M-H]^+$.

IR (Nujol) (cm^{-1}): $\nu(B\text{-}H)_{st}$ 2413 (s).

^{1}H NMR (δ, 300.13 MHz, CD_3COCD_3): 8.68 (d, $J_{H\text{-}H}$ = 5.7, $^3J_{Pt\text{-}H}$ = 37, 1H, H^2_{ppy}), 8.15 (t, $J_{H\text{-}H}$ = 8, 1H, H^4_{ppy}), 8.08 (d, $J_{H\text{-}H}$ = 7.3, 1H, H^5_{ppy}), 7.80 (s, 1H, $H^{3''}_{pz}$), 7.75 (m, 4H, $H^{3'}_{pz}$, $H^{5'}_{pz}$, $H^{5''}_{pz}$, H^6_{ppy}), 7.39 (t, $J_{H\text{-}H}$ = 5.7, H^3_{ppy}), 7.20 (d, $J_{H\text{-}H}$ = 3.6, $^3J_{Pt\text{-}H}$ = 35.6, 1H, H^9_{ppy}), 7.16 (d, $J_{H\text{-}H}$ = 4.3, 1H, $H^{7/8}_{ppy}$), 7.14 (d, $J_{H\text{-}H}$ = 4.7, 1H, $H^{7/8}_{ppy}$), 6.39 (t, $J_{H\text{-}H}$ = 2.0, 1H, $H^{4''}_{pz}$), 6.36 (t, $J_{H\text{-}H}$ = 1.8, 1H, $H^{4'}_{pz}$), 3.88 (t_{br}, $J_{B\text{-}H}$ = 143.3, 2H, HBH_2).

$^{13}C\{^1H\}$ NMR (δ, 75.5 MHz, CD_3COCD_3): 168.6 (s, C^{10}_{ppy}), 150.5 (s, $^2J_{Pt\text{-}C}$ = 19.7, C^2_{ppy}), 146.6 (s, C^{12}_{ppy}), 144.2 (s, C^{11}_{ppy}), 142.8 (s, $^2J_{Pt\text{-}C}$ = 80.4, $C^{3'}_{pz}$), 141.3 (s, $^2J_{Pt\text{-}C}$ = 24.5, $C^{3''}_{pz}$), 140.3 (s, $^4J_{Pt\text{-}C}$ = 7.8, C^4_{ppy}), 137.0 (s, $^3J_{Pt\text{-}C}$ = 10.5, $C^{5''}_{pz}$), 136.8 (s, $^3J_{Pt\text{-}C}$ = 30.1, $C^{5'}_{pz}$), 134.5 (s, $^2J_{Pt\text{-}C}$ = 58.4, C^9_{ppy}), 130.1 (s, $^3J_{Pt\text{-}C}$ = 51.9, C^8_{ppy}), 124.6 (s, $J_{Pt\text{-}C}$ = 38.6, C^6_{ppy}, C^7_{ppy}), 123.6 (s, $^3J_{Pt\text{-}C}$ = 33.4, C^3_{ppy}), 120.2 (s, $^3J_{Pt\text{-}C}$ = 42.1, C^5_{ppy}), 106.5 (s, $^3J_{Pt\text{-}C}$ = 51.4, $C^{4'}_{pz}$, $^3J_{Pt\text{-}C}$ = 18.1, $C^{4''}_{pz}$).

Preparation of **[Pt(pq){$H_2B(pz)_2$}] (3)**

The complex was prepared as an orange solid in a similar way to **1** starting from $[Pt(pq)(\mu\text{-}Cl)]_2$ (0.200 g, 0.229 mmoles) and $K[H_2B(pz)_2]$ (0.173 g, 0.920 mmoles) (0.192 g, 76%).

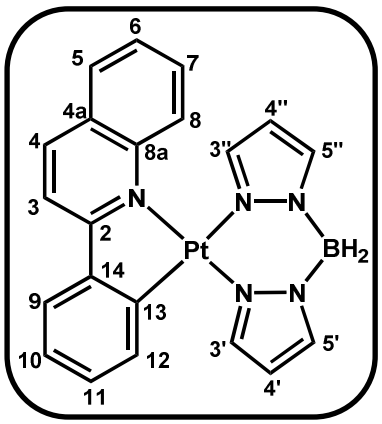

Anal. Calcd for $C_{21}H_{18}N_5BPt$ (546.31): C, 46.17; H, 3.32; N, 12.82. Found: C, 45.92; H, 3.15; N, 12.63 %.

MALDI-TOF (+): *m/z* (%) 545.1 (100) $[M\text{-}H]^+$.

IR (Nujol) (cm^{-1}): $\nu(B\text{-}H)_{st}$ 2431 (m, br).

^{1}H NMR (δ, 400.17 MHz, CD_3COCD_3): 8.53 (d, $J_{H\text{-}H}$ = 8.6, 2H, $H^{3/4}{}_{pq}$), 8.07 (d, $J_{H\text{-}H}$ = 8.6, 2H, $H^{3/4}{}_{pq}$), 7.88 (d, $J_{H\text{-}H}$ = 7.6, $H^{8}{}_{pq}$), 7.76 (d, $J_{H\text{-}H}$ = 5.4, $H^{9}{}_{pq}$), 7.63 (d, $J_{H\text{-}H}$ = 2.4, $H^{5'}{}_{pz}$), 7.61 (d, $J_{H\text{-}H}$ = 1.8, $H^{5''}{}_{pz}$), 7.54 (d, $J_{H\text{-}H}$ = 9.1, $H^{5}{}_{pq}$), 7.51 (d, $J_{H\text{-}H}$ = 1.5, $H^{3'}{}_{pz}$), 7.41 (t, $J_{H\text{-}H}$ = 7, $H^{7}{}_{pq}$), 7.22 (t, $J_{H\text{-}H}$ = 7.1, $H^{6}{}_{pq}$), 7.12 (t, $J_{H\text{-}H}$ = 4.0, $H^{10}{}_{pq}$), 7.10 (t, $J_{H\text{-}H}$ = 4, $H^{12}{}_{pq}$), 7.09 (d, $J_{H\text{-}H}$ = 3.4, $H^{11}{}_{pq}$), 6.70 (d, $J_{H\text{-}H}$ = 1.7, $H^{3''}{}_{pz}$), 6.20 (t, $J_{H\text{-}H}$ = 2.3, $H^{4'}{}_{pz}$), 5.96 (t, $J_{H\text{-}H}$ = 2.1, $H^{4''}{}_{pz}$), 3.97 (br, 2H, HBH_2).

^{13}C{^{1}H} NMR (δ, 75.5 MHz, CD_3COCD_3): 170.0 (s, $C^{2}{}_{pq}$), 149.2 (s, $C^{8a}{}_{pq}$), 148.4 (s, $C^{13}{}_{pq}$), 147.9 (s, $C^{14}{}_{pq}$), 142.8 (s, $^2J_{Pt\text{-}C}$ = 83.0, $C^{3'}{}_{pz}$), 142.3 (s, $^2J_{Pt\text{-}C}$ = 29.6, $C^{3''}{}_{pz}$), 140.9 (s, $^4J_{Pt\text{-}C}$ = 4.1, $C^{4}{}_{pq}$), 137.2 (s, $^3J_{Pt\text{-}C}$ = 16.7, $C^{5'}{}_{pz}$), 136.3 (s, $^3J_{Pt\text{-}C}$ = 8.1 $C^{5''}{}_{pz}$), 134.8 (s, $^2J_{Pt\text{-}C}$ = 58.5, $C^{12}{}_{pq}$), 130.2 (s, $C^{6}{}_{pq}$), 130.1 (s, $^3J_{Pt\text{-}C}$ = 50.7, $C^{11}{}_{pq}$), 129.0 (s, $C^{8}{}_{pq}$), 129.0 (s, $C^{4a}{}_{pq}$), 127.6 (s, $^4J_{Pt\text{-}C}$ = 30.3, $C^{5}{}_{pq}$, $C^{7}{}_{pq}$), 126.5 (s, $^3J_{Pt\text{-}C}$ = 35.7, $C^{9}{}_{pq}$), 124.0 (s, $C^{10}{}_{pq}$), 117.9 (s, $^4J_{Pt\text{-}C}$ = 44.4 , $C^{3}{}_{pq}$), 106.2 (s, $^3J_{Pt\text{-}C}$ = 52.5, $C^{4'}{}_{pz}$), 105.9 (s, $^3J_{Pt\text{-}C}$ = 20.2, $C^{4''}{}_{pz}$).

Preparation of **[Pt(bzq){$H_2C(pz)_2$}]PF_6 (4)**

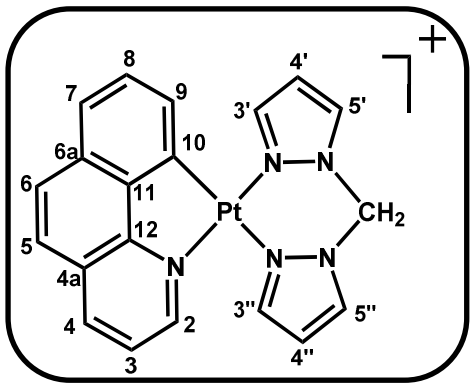

This complex was prepared as a yellow solid following the procedure described for **1** but using $[Pt(bzq)(\mu\text{-}Cl)]_2$ (0.200 g, 0.245 mmoles), $[H_2C(pz)_2]$ (0.109 g, 0.735 mmoles) and $NaPF_6$ (0.123 g, 0.735 mmoles) (0.245 g, 75%).

Anal. Calcd for $C_{20}H_{16}N_5PtPF_6$ (666.43): C, 36.05; H, 2.42; N, 10.51. Found: C, 36.18; H, 2.08; N, 10.80 %.

ESI-MS (+): *m/z* (%) 521.1 (100) $[M\text{-}PF_6]^+$, 589.4 (24) $[M\text{-}PF_6\text{+}pz]^+$.

Λ_M (CH_3CN): 149.3 $\Omega^{-1}cm^{-2}mol^{-1}$.

^{1}H NMR (δ, 400.17 MHz, CD_3COCD_3): 9.08 (d, $J_{H\text{-}H}$ = 5.3, $^3J_{Pt\text{-}H}$ = 41.0, 1H, $H^2{}_{bzq}$), 8.82 (d, $J_{H\text{-}H}$ = 8.1, 1H, $H^4{}_{bzq}$), 8.56 (d, $J_{H\text{-}H}$ = 2.3, 2H, $H^{5'}{}_{pz}$, $H^{5''}{}_{pz}$), 8.48 (d, $J_{H\text{-}H}$ = 2.1, 2H, $H^{3'}{}_{pz}$, $H^{3''}{}_{pz}$), 8.0 (AB $J_{H\text{-}H}$ = 8.8, δ_A = 8.04, δ_B = 7.93, 2H, $H^5{}_{bzq}$, $H^6{}_{bzq}$), 7.86 (m, 2H, $H^3{}_{bzq}$, $H^7{}_{bzq}$), 7.64 (t, $J_{H\text{-}H}$ = 7.6, 1H, $H^8{}_{bzq}$), 7.45 (d, $J_{H\text{-}H}$ = 7.3, $^3J_{Pt\text{-}H}$ = 34.7, 1H, $H^9{}_{bzq}$), 7.35 (AB, $J_{H\text{-}H}$ = 14.7, δ_A = 7.33, δ_B = 7.37, 2H, HCH_2), 6.88 (t, $J_{H\text{-}H}$ = 4.77, 1H, $H^{4'}{}_{pz}$), 6.87 (t, $J_{H\text{-}H}$ = 5.16, 1H, $H^{4''}{}_{pz}$).

^{13}C{^{1}H} NMR (δ, 75.5 MHz, CD_3COCD_3): 154.4 (s, $C^{10}{}_{bzq}$), 154.3 (s, $^2J_{Pt\text{-}C}$ = 23.8, $C^2{}_{bzq}$), 150.2 (s, $^2J_{Pt\text{-}C}$ = 68.3, $C^{3'}{}_{pz}$), 149.0 (s, $^2J_{Pt\text{-}C}$ = 19.0, $C^{3''}{}_{pz}$), 148.2 (s, $C^{10b}{}_{bzq}$), 144.4 (s, $C^4{}_{bzq}$), 139.9 (s, $^3J_{Pt\text{-}C}$ = 17.2, $C^{5'}{}_{pz}$), 139.7 (s, $C^{5''}{}_{pz}$), 138.7 (s, $C^{10a}{}_{bzq}$), 135.2 (s, $^2J_{Pt\text{-}C}$ = 65.1, $C^9{}_{bzq}$), 134.4 (s, $C^6{}_{bzq}$, $C^{6a}{}_{bzq}$), 134.0 (s, $C^7{}_{bzq}$), 132.1 (s, $C^{4a}{}_{bzq}$), 128.8 (s, $C^5{}_{bzq}$), 128.2 (s, $C^8{}_{bzq}$), 127.2 (s, $^3J_{Pt\text{-}C}$ = 27.0, $C^3{}_{bzq}$), 114.1 (s, $^3J_{Pt\text{-}C}$ = 49.7, $C^{4'}{}_{pz}$), 113.9 (s, $^3J_{Pt\text{-}C}$ = 16.0, $C^{4''}{}_{pz}$), 68.6 (s, $^3J_{Pt\text{-}C}$ = 28.0, C_{CH}).

Preparation of **[Pt(ppy){$H_2C(pz)_2$}]PF_6 (5)**

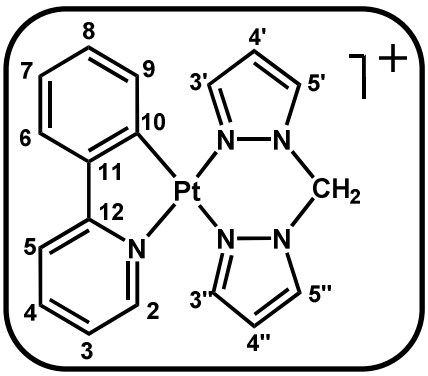

This complex was prepared as a yellow solid in a similar way to complex **4** starting from [Pt(ppy)(μ-Cl)]$_2$ (0.250 g, 0.325 mmoles), [$H_2C(pz)_2$] (0.145 g, 0.975 mmoles) and $NaPF_6$ (0.164 g, 0.975 mmoles), (0.294 g, 70%).

Anal. Calcd for $C_{18}H_{16}N_5PtPF_6$ (642.41): C, 33.65; H, 2.51; N, 10.90. Found: C, 33.27; H, 2.24; N, 10.66 %.

MALDI-TOF (+): *m/z* (%) 497.1 (100) $[M\text{-}PF_6]^+$.

Λ_M (CH_3CN): 137.2 $\Omega^{-1}cm^{-2}mol^{-1}$.

^{1}H NMR (δ, 400.17 MHz, CD_3COCD_3): 8.74 (d, $J_{H\text{-}H}$ = 5.7, $^3J_{Pt\text{-}H}$ = 37.7, 1H, H^2_{ppy}), 8.51 (m, 2H, $H^{5'}_{pz}$, $H^{5''}_{pz}$), 8.38 (d, $J_{H\text{-}H}$ = 2.0, 1H, $H^{3'/3''}_{pz}$), 8.28 (d, $J_{H\text{-}H}$ = 1.9, 1H, $H^{3'/3''}_{pz}$), 8.22 (m, 2H, H^4_{ppy}, H^5_{ppy}), 7.83 (d, $J_{H\text{-}H}$ = 7.4, 1H, H^9_{ppy}), 7.52 (t, $J_{H\text{-}H}$ = 7.4, 1H, H^3_{ppy}), 7.29 (AB, $J_{H\text{-}H}$ = 14.4, δ_A = 7.32 δ_B = 7.27, 2H, HCH_2), 7.25 (m, $J_{H\text{-}H}$ = 7.1, 2H, H^7_{ppy}, H^8_{ppy}), 7.16 (d, $J_{H\text{-}H}$ = 7.2, 1H, H^6_{ppy}), 6.83 (t, $J_{H\text{-}H}$ = 2.5, 1H, $H^{4''}_{pz}$), 6.81 (t, $J_{H\text{-}H}$ = 2.6, 1H, $H^{4'}_{pz}$).

^{13}C{^{1}H} NMR (δ, 75.5 MHz, CD_3COCD_3): 167.8 (s, C^{10}_{ppy}), 150.9 (s, $^2J_{Pt\text{-}C}$ = 20.2, C^2_{ppy}), 146.1 (s, $^2J_{Pt\text{-}C}$ = 68.7, $C^{3'}_{pz}$), 144.8 (s, $^2J_{Pt\text{-}C}$ = 15.1, $C^{3''}_{pz}$), 141.7 (s, C^4_{ppy}), 139.7 (s, C^{12}_{ppy}), 136.1 (s, $^4J_{Pt\text{-}C}$ = 42.1, $C^{5'}_{pz}$), 135.5 (s, $C^{5''}_{pz}$), 133.7 (s, $^2J_{Pt\text{-}C}$ = 56.3, C^9_{ppy}), 131.0 (s, C^{11}_{ppy}), 130.7 (s, $^3J_{Pt\text{-}C}$ = 50.5, C^8_{ppy}), 126.1 (s, C^7_{ppy}), 125.1 (s, $^3J_{Pt\text{-}C}$ = 35.7, C^6_{ppy}), 124.4 (s, $^3J_{Pt\text{-}C}$ = 26.5, C^3_{ppy}), 120.7 (s, $^3J_{Pt\text{-}C}$ = 44.8, C^5_{ppy}), 110.0 (s, $^3J_{Pt\text{-}C}$ = 48.6, $C^{4'}_{pz}$), 109.8 (s, $^3J_{Pt\text{-}C}$ = 16.2, $C^{4''}_{pz}$), 64.6 (s, $^3J_{Pt\text{-}C}$ = 26.7, C_{CH}).

Preparation of **[Pt(pq){$H_2C(pz)_2$}]PF_6 (6)**

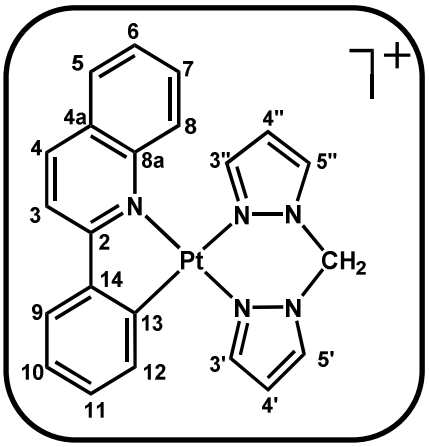

This complex was prepared as an orange solid in a similar way to complex **4** starting from [Pt(pq)(μ-Cl)]$_2$ (0.200 g, 0.230 mmoles), [$H_2C(pz)_2$] (0.102 g, 0.690 mmoles) and $NaPF_6$ (0.116 g, 0.690 mmoles), (0.226 g, 71%).

Anal. Calcd for $C_{22}H_{18}N_5PtPF_6$ (692.47): C, 38.16; H, 2.62; N, 10.11. Obtenidos: C, 38.44; H, 2.37; N, 10.50 %.

ESI-MS (+): *m/z* (%) 547.1 (100) $[M\text{-}PF_6]^+$.

Λ_M (CH_3CN): 136.8 $\Omega^{-1}cm^{-2}mol^{-1}$.

^{1}H NMR (δ, 400.17 MHz, CD_3COCD_3): 8.79 (d, $J_{H\text{-}H}$ = 8.6, 2H, $H^{3/4}{}_{pq}$), 8.53 (d, $J_{H\text{-}H}$ = 2.6, 1H, $H^{5'}{}_{pz}$), 8.48 (d, $J_{H\text{-}H}$ = 2.4, 1H, $H^{5''}{}_{pz}$), 8.32 (d, $J_{H\text{-}H}$ = 8.6, 2H, $H^{3/4}{}_{pq}$), 8.13 (d, $J_{H\text{-}H}$ = 8.3, 1H, $H^{8}{}_{pq}$), 8.09 (d, $J_{H\text{-}H}$ = 2.1, 1H, $H^{3'}{}_{pz}$), 8.00 (d, $J_{H\text{-}H}$ = 8.7, 1H, $H^{5}{}_{pq}$), 7.99 (d, $J_{H\text{-}H}$ = 6.4, 1H, $H^{9}{}_{pq}$), 7.66 (d, $J_{H\text{-}H}$ = 7.4, 1H, $H^{7}{}_{pq}$), 7.51 (t, $J_{H\text{-}H}$ = 8.4, 1H, $H^{6}{}_{pq}$), 7.49 (AB, $J_{H\text{-}H}$ = 15.7, δ_A = 7.59 δ_B = 7.38, 2H, HCH_2), 7.45 (d, $J_{H\text{-}H}$ = 1.9, 1H, $H^{3''}{}_{pz}$), 7.34 (t, $J_{H\text{-}H}$ = 7.4, 1H, $H^{10}{}_{pq}$), 7.31 (t, $J_{H\text{-}H}$ = 7.4, 1H, $H^{11}{}_{pq}$), 7.20 (d, $J_{H\text{-}H}$ = 7.4, $^3J_{Pt\text{-}C}$ = 32.0, 1H, $H^{12}{}_{pq}$), 6.79 (t, $J_{H\text{-}H}$ = 2.5, 1H, $H^{4'}{}_{pz}$), 6.57 (t, $J_{H\text{-}H}$ = 2.3, 1H, $H^{4''}{}_{pz}$).

^{13}C{^{1}H} NMR (δ, 100.67 MHz, CD_3COCD_3): 169.9 (s, $C^{2}{}_{pq}$), 147.9 (s, $C^{8a}{}_{pq}$), 147.4 (s, $C^{13}{}_{pq}$), 146.3 (s, $^2J_{Pt\text{-}C}$ = 73.9, $C^{3'}{}_{pz}$), 145.8 (s, $C^{3''}{}_{pz}$), 144.5 (s, $C^{14}{}_{pq}$), 142.3 (s, $C^{4}{}_{pq}$), 136.0 (s, $^3J_{Pt\text{-}C}$ = 16.5, $C^{5'}{}_{pz}$), 135.0 (s, $C^{5''}{}_{pz}$), 134.1 (s, $^2J_{Pt\text{-}C}$ = 57.6, $C^{12}{}_{pq}$), 131.2 (s, $C^{6}{}_{pq}$), 130.8 (s, $^3J_{Pt\text{-}C}$ = 52.4, $C^{11}{}_{pq}$), 129.6 (s, $C^{8}{}_{pq}$), 129.1 (s, $C^{4a}{}_{pq}$), 128.2 (s, $^4J_{Pt\text{-}C}$ = 36.9, $C^{5/7}{}_{pq}$), 127.4 (s, $^4J_{Pt\text{-}C}$ = 28.7, $C^{5/7}{}_{pq}$), 127.0 (s, $^3J_{Pt\text{-}C}$ = 27.6, $C^{9}{}_{pq}$), 126.2 (s, $C^{10}{}_{pq}$), 118.1 (s, $^3J_{Pt\text{-}C}$ = 47.7, $C^{3}{}_{pq}$), 109.7 (s, $^3J_{Pt\text{-}C}$ = 51.4, $C^{4'}{}_{pz}$), 109.3 (s, $C^{4''}{}_{pq}$), 64.7 (s, $^3J_{Pt\text{-}C}$ = 27.4, C^{8} CH).

Preparation of **[Pt(bzq){HC(pz)$_3$}]PF$_6$ (7)**

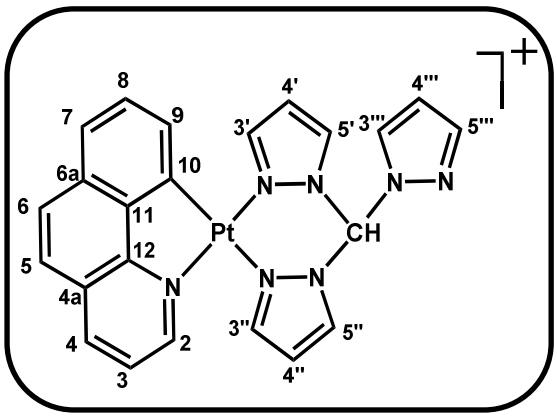

A mixture of [HC(pz)$_3$] (0.157 g, 0.734 mmoles), NaPF$_6$ (0.123 g, 0.734 mmoles) and [Pt(bzq)(μ-Cl)]$_2$ (0.300 g, 0.367 mmoles) was stirred in acetone (20 mL) for 1 h. The final mixture was evaporated to dryness and treated with CH_2Cl_2 (15 mL) yielding a yellow solid, which was washed with H_2O (3 x 5 mL) and EtOH (3 x 5mL). Recrystallization of the crude solid in a mixture of CH_3CN/^{i}PrOH at -30ºC yielded **7** as a yellow microcrystalline solid (0.366 g, 68%).

Anal. Calcd for $C_{23}H_{18}N_7PtPF_6$ (732.50): C, 37.71; H, 2.48; N, 13.39. Found: C, 37.34; H, 2.54; N, 13.14 %.

ESI-MS (+): *m/z* (%) 587.1 (100) $[M\text{-}PF_6]^+$.

Λ_M (CH_3CN): 126.0 $\Omega^{-1}cm^{-2}mol^{-1}$.

^{1}H NMR (δ, 300.13 MHz, CD_3COCD_3): 9.45 (s, 1H, HCH), 9.04 (d, $J_{H\text{-}H}$ = 5.3, $^3J_{Pt\text{-}H}$ = 39.9, 1H, H^2_{bzq}), 8.95 (d, $J_{H\text{-}H}$ = 2.7, 2H, $H^{5'}_{pz}$, $H^{5''}_{pz}$), 8.77 (d, $J_{H\text{-}H}$ = 8.1, 1H, H^4_{bzq}), 8.67 (s, 2H, $H^{3'}_{pz}$, $H^{3''}_{pz}$), 8.29 (s, br, 1H, $^{3'''}$ /$^{5'''}_{pz}$), 7.90 (AB, $J_{H\text{-}H}$ = 8.8, δ_A = 7.93 δ_B = 7.87, 2H, H^5_{bzq}, H^6_{bzq}), 7.84 (s, 1H, H^3_{bzq}), 7.82 (d, $J_{H\text{-}H}$ = 2.4, 1H, $H^{3'''/5'''}_{pz}$), 7.78 (d, $J_{H\text{-}H}$ = 7.6, 1H, H^7_{bzq}), 7.57 (t, $J_{H\text{-}H}$ = 7.6 Hz, 1H, H^8_{bzq}), 7.36 (d, $J_{H\text{-}H}$ = 7.3, $^3J_{Pt\text{-}H}$ = 33.8, 1H, H^9_{bzq}), 7.06 (t, $J_{H\text{-}H}$ = 2.5, 2H, $H^{4'}_{pz}$, $H^{4''}_{pz}$), 6.23 (s, br, 1H, $H^{4'''}_{pz}$).

The low solubility of this complex precludes its characterization by $^{13}C\{^1H\}$ NMR.

Preparation of [**Pt(ppy){HC(pz)$_3$}]PF$_6$ (8)**

Complex **8** was prepared as a yellow solid by a similar procedure to **7** from [Pt(ppy)(μ-Cl)]$_2$ (0.300 g, 0.390 mmoles), [HC(pz)$_3$] (0.167 g, 0.780 mmoles) and NaPF$_6$ (0.131 g, 0.780 mmoles). In this case the solid obtained after washing with H$_2$O and EtOH is analytically pure (0.383 g, 70%).

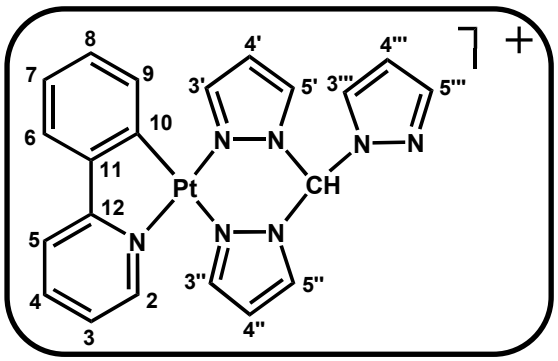

Anal. Calcd for C$_{21}$H$_{18}$N$_7$PtPF$_6$ (708.47): C, 35.60; H, 2.56; N, 13.84. Found: C, 35.63; H, 2.47; N, 13.75 %.

ESI-MS (+): *m/z* (%) 563.1 (100) [M-PF$_6$]$^+$.

Λ_M (CH$_3$CN): 137.0 Ω^{-1}cm^{-2}mol^{-1}.

^{1}H NMR (δ, 300.13 MHz, CD$_3$COCD$_3$): 9.40 (s, 1H, H$_{CH}$), 8.90 (d, $J_{H\text{-}H}$ = 2.5, 2H, H$^{5'}{}_{pz}$, H$^{5''}{}_{pz}$), 8.66 (d, $J_{H\text{-}H}$ = 5.4, $^3J_{Pt\text{-}H}$ = 35.1, 1H, H$^2{}_{bzq}$), 8.45 (s, $^3J_{Pt\text{-}H}$ = 31.0, 2H, H$^{3'}{}_{pz}$, H$^{3''}{}_{pz}$), 8.27 (s, 1H, H$^{5'''/3'''}{}_{pz}$), 8.20 (t, $J_{H\text{-}H}$ = 7.8, 1H, H$^4{}_{bzq}$), 8.10 (d, $J_{H\text{-}H}$ = 7.8, 1H, H$^5{}_{bzq}$) 7.87 (s, 1H, H$^{5'''/3'''}{}_{pz}$), 7.73 (d, $J_{H\text{-}H}$ = 6.3, 1H, H$^9{}_{bzq}$), 7.45 (t, $J_{H\text{-}H}$ = 5.9, 1H, H$^3{}_{bzq}$), 7.19 (d, $J_{H\text{-}H}$ = 5.8 Hz, 1H, H$^8{}_{bzq}$), 7.17 (t, $J_{H\text{-}H}$ = 6.0, 1H, H$^7{}_{bzq}$), 7.06 (d, $J_{H\text{-}H}$ = 7.1 Hz, 1H, H$^6{}_{bzq}$), 6.99 (s, 2H, H$^{4''}{}_{pz}$, H$^{4'}{}_{pz}$), 6.34 (s, 1H, H$^{4'''}{}_{pz}$).

Its low solubility precludes its characterization by ^{13}C{^{1}H} NMR.

Preparation of **[Pt(pq){HC(pz)$_3$}]PF$_6$ (9)**

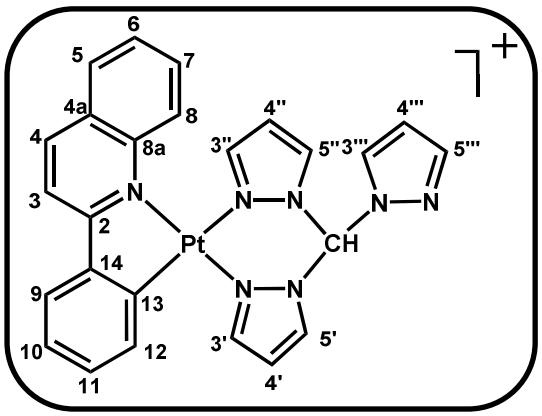

A mixture of [HC(pz)$_3$] (0.172 g, 0.804 mmoles), NaPF$_6$ (0.135 g, 0.804 mmoles) and [Pt(pq)(μ-Cl)]$_2$ (0.350 g, 0.402 mmoles) in acetone (20 mL) was stirred for 1.5 h. The solvent was removed and the complex extracted with CH_2Cl_2 (20 mL) and filtered through Celite to eliminate NaCl. The resulting orange filtrate was evaporated to dryness and treated with EtOH (10 mL) to give **9** as an orange solid, which was filtered and washed with diethyl ether (5 mL) (0.453 g, 74%).

Anal. Calcd for $C_{25}H_{20}N_7PtPF_6$ (758.53): C, 39.59; H, 2.66; N, 12.93. Found: C, 39.87; H, 2.48; N, 12.57 %.

ESI-MS(+): *m/z* (%) 614.2 (100) $[M\text{-}PF_6]^+$.

Λ_M (CH_3CN): 131.6 $\Omega^{-1}cm^{-2}mol^{-1}$.

^{1}H NMR (δ, 300.13 MHz, CD_3COCD_3): 9.53 (s, 1H, C-H$_{CH}$), 8.96 (s, 2H, H$^{5'}{}_{pz}$, H$^{5''}{}_{pz}$), 8.72 (d, $J_{H\text{-}H}$ = 8.6, 2H, H$^{3/4}{}_{pq}$), 8.36 (s, 2H, H$^{3'}{}_{pz}$, H$^{3''}{}_{pz}$), 8.23 (d, $J_{H\text{-}H}$ = 8.6, 2H, H$^{3/4}{}_{pq}$), 8.12 (s, br, 1H, H$^{3'''/5'''}{}_{pz}$), 8.07 (d, $J_{H\text{-}H}$ = 7.8, 1H, H$^{8}{}_{pq}$), 7.91 (d, $J_{H\text{-}H}$ = 7.1, 1H, H$^{9}{}_{pq}$), 7.71 (s, br, 1H, H$^{3'''/5'''}{}_{pz}$), 7.65 (d, $J_{H\text{-}H}$ = 7.2, 1H, H$^{5}{}_{pq}$), 7.61 (t, $J_{H\text{-}H}$ = 6.2, 1H, H$^{6}{}_{pq}$), 7.49 (t, $J_{H\text{-}H}$ = 7.7, 1H, H$^{7}{}_{pq}$), 7.26 (m, 3H, H$^{10}{}_{pq}$, H$^{11}{}_{pq}$, H$^{12}{}_{pq}$), 7.02 (s, 2H, H$^{4'}{}_{pz}$, H$^{4''}{}_{pz}$), 6.63 (s, 1H, H$^{4'''}{}_{pz}$).

^{13}C{^{1}H} NMR (δ, 100.67 MHz, CD_3COCD_3): 168.9 (s, $^2J_{Pt\text{-}C}$ = 84.5, C$^{2}{}_{pq}$), 147.8 (s, $^2J_{Pt\text{-}C}$ = 61.8 Hz, C$^{3'}{}_{pz}$), 147.0 (s, $J_{Pt\text{-}C}$ = 47.6, C$^{13}{}_{pq}$, C$^{14}{}_{pq}$), 146.3 (s, C$_{pz}$), 143.7 (s, C$_{pz}$), 141.4 (s, C$^{4}{}_{pq}$), 137.9 (s, C$_{pz}$), 133.0 (s, $^2J_{Pt\text{-}C}$ = 53.0, C$^{12}{}_{pq}$), 130.2 (s, C$^{6}{}_{pq}$), 129.7 (s, $^3J_{Pt\text{-}C}$ = 49.1, C$^{11}{}_{pq}$), 128.6 (s, C$^{8}{}_{pq}$), 128.1 (s, $^2J_{Pt\text{-}C}$ = 20.7, C$^{4a}{}_{pq}$), 127.3 (s, C$^{5/7}{}_{pq}$), 126.5 (s, $^4J_{Pt\text{-}C}$ = 24.5, C$^{5/7}{}_{pq}$), 126.1 (s, $^3J_{Pt\text{-}C}$ = 35.8, C$^{9}{}_{pq}$), 125.3 (s, C$^{10}{}_{pq}$), 117.2 (s, $^3J_{Pt\text{-}C}$ = 48.1, C$^{3}{}_{pq}$), 109.6 (s, $^3J_{Pt\text{-}C}$ = 44.7, C$^{4'}{}_{pz}$), 108.3 (s, C$^{4''}{}_{pz}$, C$^{4'''}{}_{pz}$), 80.7 (s, C$_{CH}$).

Preparation of [Pt(pq){HB(pz)$_3$}] (10)

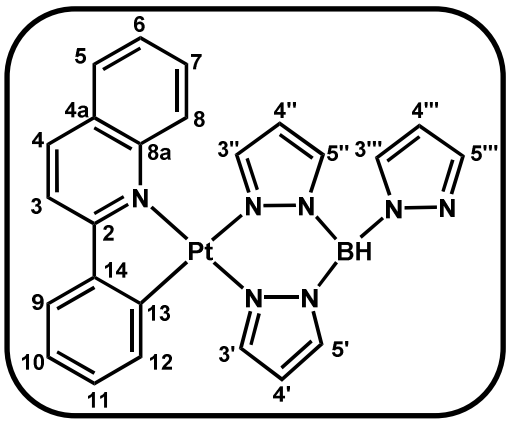

Complex **10** was prepared as an orange solid in a similar way to complex **9** starting from [Pt(pq)(μ-Cl)]$_2$ (0.250 g, 0.287 mmoles) and K[HB(pz)$_3$] (0.147 mg, 0.575 mmoles) by stirring of 30 minutes (0.270 g, 77%).

Anal. Calcd for $C_{24}H_{20}N_7PtB$ (612.15). C, 47.05; H, 3.29; N, 16.01. Found: C, 46.50; H, 3.46; N 15.41 %.

ESI-MS(+): *m/z* (%) 612.5 (100) $[M]^+$.

IR (cm^{-1}): ν(B-H)$_{st}$ 2419 (m, br).

^{1}H NMR (δ, 300.13 MHz, CD_3COCD_3): 8.50 (s, br, 2H, $H^{3'/3''}{}_{pz}$), 8.50 (d, J_{H-H} = 8.6, 2H, $H^{3/4}{}_{pq}$), 8.02 (d, J_{H-H} = 8.6, 2H, $H^{3/4}{}_{pq}$), 8.02 (s, br, 2H, $H^{5'/5''}{}_{pz}$), 7.84 (s, br, 2H, $H^{8}{}_{pq}$, $H^{3'''/5'''}{}_{pz}$), 7.73 (s, br, 1H, $H^{9}{}_{pq}$), 7.68 (s, br, 2H, $H^{3'''/5'''}{}_{pz}$), 7.47 (d, J_{H-H} = 8.8, 1H, $H^{5}{}_{pq}$), 7.39 (t, J_{H-H} = 7.3, 1H, $H^{7}{}_{pq}$), 7.19 (t, br, J_{H-H} = 7.2, 1H, $H^{6}{}_{pq,}$), 7.10 (m, 3H, $H^{10/11/12}{}_{pq}$), 6.76 (s, br, 1H, $H^{4'''}{}_{pz}$), 6.34 (s, br, 1H, $H^{4'/4''}{}_{pz}$), 6.02 (s, br, 1H, $H^{4'/4''}{}_{pz}$).

^{13}C{^{1}H} NMR (δ, 100.67 MHz, CD_3COCD_3): 152.6 (s), 151.9 (s), 148.6 (s, C_{pz}), 147.3 (s, C_{pz}), 145.2 (s, $C^{4}{}_{pq}$), 138.8 (s, $C^{10/11/12}{}_{pq}$), 134.5 (s, $C^{10/11/12}{}_{pq}$), 134.2 (s, $C^{6}{}_{pq}$), 133.1 (s, $C^{8}{}_{pq}$), 131.9 (s, $C^{5}{}_{pq}$, $C^{7}{}_{pq}$), 130.7 (s, $C^{9}{}_{pq}$), 129.1 (s, $C^{10/11/12}{}_{pq}$), 122.0 (s, $C^{3}{}_{pq}$), 110.2 (s, $C^{4'}{}_{pz}$, $C^{4''}{}_{pz}$).

Reaction of **[Pt(bzq)(μ-Cl)]$_2$ with K[HB(pz)$_3$] (11).**

A yellow suspension of [Pt(bzq)(μ-Cl)]$_2$ (0.250 g, 0.306 mmoles) in 20 mL of acetone was treated with 0.150 g (0.612 mmoles) of K[HB(pz)$_3$] and stirred for 30 min. The mixture was evaporated to dryness, treated with CH_2Cl_2 (15 mL) and filtered over Celite. The orange filtrate was evaporated to dryness and the residue treated with EtOH (10 mL). The resulting orange solid was recrystallized from a mixture of CH_2Cl_2/Hexane at -30ºC to precipitate yellow crystals identified as *trans*-[Pt(bzq)(μ-pz)]$_2$ **11** (0.040 g). From the ethanolic filtrate an additional pale orange solid was obtained (0.100 g) identified as a mixture of *cis* and *trans*-[Pt(bzq)(μ-pz)]$_2$.

Reaction of **[Pt(ppy)(μ-Cl)]$_2$ with K[HB(pz)$_3$] (12).**

0.199 g (0.780 mmoles) of K[HB(pz)$_3$] was added to a yellow suspension of [Pt(ppy)(μ-Cl)]$_2$ (0.300 g, 0.400 mmoles) in acetone. After 30 min the mixture was evaporated to dryness, treated with CH_2Cl_2 (20 mL) and filtered over Celite. The filtrate was evaporated to dryness and the residue was treated with EtOH (10 mL) causing the precipitation of a yellow solid identified as a mixture of *trans*-[Pt(ppy)(μ-pz)]$_2$, *cis*-[Pt(ppy)(μ-pz)]$_2$ and [Pt(ppy){HB(pz)$_3$}] (**12**). After successive crystallizations **12** was separated as a pure solid in low yield (0.027 g, 5%).

Preparation of (**NBu_4)[Pt(Hpq-κ^2N)(C≡CTol)$_3$] (13)**

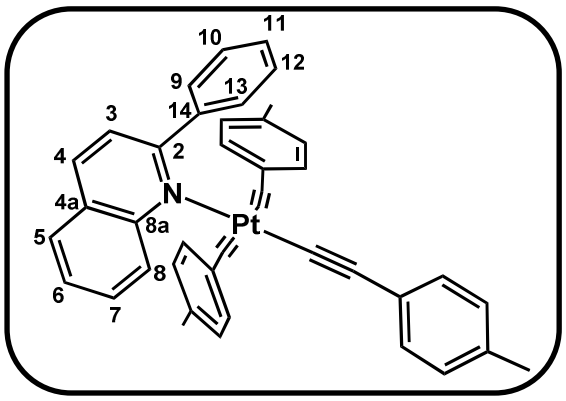

$[Pt(pq)(\mu\text{-}Cl)]_2$ (0.300 g, 0.345 mmol) was added to a solution of LiC≡CTol (2.76 mmol) (1:8 molar ratio), prepared from HC≡CTol (0.350 mL, 2.76 mmol) and $LiBu^n$ (1.73 mL, 1.6 N, 2.76 mmol) in diethyl ether/*n*-hexane (60 mL) at -20ºC, and the mixture was stirred at room temperature *ca*. 2 h. The solvent was evaporated to dryness and the orange solid residue extracted with a mixture of cold ^{i}PrOH/deoxygenated water (5/40 mL). The resulting orange solution was rapidly filtered under N_2 through celite and the filtrate treated with vigorous stirring with a solution of NBu_4Br (0.222 g, 0.689 mmol) in 5 mL of deoxygenated H_2O. The filtrate was evaporated to 5 mL and treated with 20 mL of dried CH_2Cl_2. The organic layer was dried with $MgSO_4$ and filtered over celite. The filtrate was evaporated to dryness and treated with 30 mL of ^{i}PrOH to afford **13** as an orange solid (0.171 g, 30%). Similar results were obtained using a 1:5 molar ratio.

Anal. Calcd for $C_{58}H_{68}N_2Pt$ (988.25): C, 70.49; H, 6.94; N, 2.83. Found: C, 69.67; H, 6.56; N, 3.07.

MALDI-TOF (-): *m/z* (%) 540 (46) $[Pt(C{\equiv}CTol)_3]^-$, 629 (100) $[Pt(pq)(C{\equiv}CTol)_2]^-$.

IR (Nujol) (cm^{-1}): ν(C≡C) 2111 (s), 2083 (s).

Λ_M(Acetone): 136.3 $\Omega^{-1}cm^2mol^{-1}$.

^{1}H NMR (δ, 400.17 MHz, $CDCl_3$): 10.66 (d, $J_{H\text{-}H}$ = 8.5, H^{13}_{Hpq}), 8.65 (d, $J_{H\text{-}H}$ = 7.3, $J_{Pt\text{-}H}$ = 40.9, H^8_{Hpq}), 8.05 (AB, $J_{H\text{-}H}$ = 8.7, δ_A = 8.16, δ_B = 7.87, H^3_{Hpq}, H^4_{Hpq}), 7.64 (d, $J_{H\text{-}H}$ = 9.2, H^5_{Hpq}), 7.40 (m, H^9_{Hpq}, H^{10}_{Hpq}, H^{11}_{Hpq}, H^{12}_{Hpq}), 7.32 (AB, $J_{H\text{-}H}$ = 7.7, δ_A = 7.66 , δ_B = 6.97, 12H, CH, Tol), 7.05 (d, $J_{H\text{-}H}$ = 7.5, H^7_{Hpq}), 6.95 (t, $J_{H\text{-}H}$ = 8.2, H^6_{Hpq}), 3.23 (m, 8H, NCH_2, NBu_4), 2.28 (s, 3H, CH_3, Tol), 2.27 (s, 6H, CH_3, Tol), 1.32 (m, 8H, -CH_2-, NBu_4), 1.08 (q, 8H, -CH_2-, NBu_4), 0.66 (t, 12H, -CH_3, NBu_4).

Its low solubility precludes its characterization by $^{13}C\{^1H\}$ and $^{195}Pt\{^1H\}$ NMR.

Preparation of (**NBu$_4$)[Pt(Hpq-κ*N*)(C≡CC$_6$H$_4$OMe-3)$_3$] (14)**

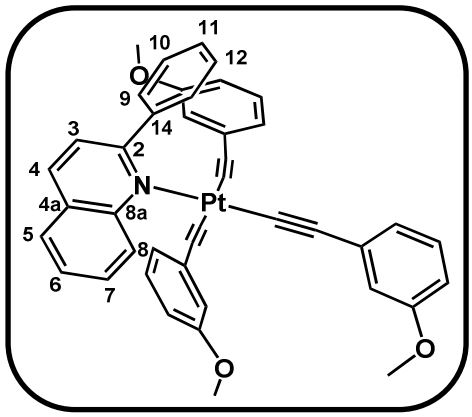

[Pt(pq)(μ-Cl)]$_2$ (0.300 g, 0.345 mmol) was added to a fresh (-20ºC) solution of LiC≡CC$_6$H$_4$OMe-3 (2.76 mmol) (1:8 molar ratio) in diehtyl ether/*n*-hexane (60 mL) at -20ºC and the mixture was allowed to warm to room temperature. After stirring *ca*. 2 h the solvent was evaporated to dryness and the resulting orange solid was extracted with cold ^{i}PrOH/CH$_2$Cl$_2$ (50/10 mL). The resulting orange suspension was rapidly filtered under N$_2$ over celite and the filtrate treated with a solution of NBu$_4$Br (0.222 g, 0.689 mmol) in deoxygenated H$_2$O (5 mL) to yield **14** as a dark orange solid (0.171 g, 48%). Similar results were obtained using a 1:5 molar ratio.

Anal. Calcd for C$_{58}$H$_{68}$N$_2$O$_3$Pt$_2$ (1036.25): C, 67.23; H, 6.61; N, 2.70. Found: C, 67.03; H, 6.41; N, 2.63.

MALDI-TOF (-): *m/z* (%) 588 (21) [Pt(C≡CC$_6$H$_4$OMe-3)$_3$]$^-$, 661 (100) [Pt(pq)(C≡CC$_6$H$_4$OMe-3)$_2$]$^-$.

IR (Nujol) (cm^{-1}): ν(C≡C) 2110 (s), 2073 (s).

Λ_M (Acetone): 130.6 Ω^{-1}cm^{2}mol^{-1}.

^{1}H NMR (δ, 400.17 MHz, CDCl$_3$): 10.60 (d, $J_{H\text{-}H}$ = 8.7, H^{13}$_{Hpq}$), 8.62 (d, $J_{H\text{-}H}$ = 7.3, $J_{Pt\text{-}H}$ = 44.6, H^8$_{Hpq}$), 8.16 (d, $J_{H\text{-}H}$ = 8.1, H^9$_{Hpq}$), 8.05 (AB, $J_{H\text{-}H}$ = 9.0, δ_A = 8.20, δ_B = 7.89, H^3$_{Hpq}$, H^4$_{Hpq}$), 7.60 (m, H^5$_{Hpq}$, H^{11}$_{Hpq}$, H^{12}$_{Hpq}$), 7.52 (t, $J_{H\text{-}H}$ = 7.5, H^{10}$_{Hpq}$), 7.42 (t, $J_{H\text{-}H}$ = 7.5, H^6$_{Hpq}$), 7.21 (t, $J_{H\text{-}H}$ = 8.6, H^7$_{Hpq}$), 7.07 (m, 6H, C$_6$H$_4$), 6.93 (s, 3H, C$_6$H$_4$), 6.63 (m, 3H, C$_6$H$_4$), 3.79 (s, 3H, OMe), 3.74 (s, 6H, OMe), 3.31 (m, 8H, NCH$_2$, NBu$_4$), 1.42 (m, 8H, -CH$_2$-, NBu$_4$), 0.85 (q, 8H, -CH$_2$-, NBu$_4$), 0.74 (t, 12H, -CH$_3$, NBu$_4$).

^{13}C{^{1}H} NMR (δ, 75.5 MHz, CDCl$_3$): 170.0 (s, C^2$_{Hpq}$), 167.9 (s, C^{8a}$_{Hpq}$), 158.9 (s, C$_{Ph}$), 158.6 (s, C^3$_{Ph}$), 148.9 (s, C^{4a}$_{Hpq}$), 138.0 (s, C^8$_{Hpq}$), 137.7 (s, C^4$_{Hpq}$), 132.6 (s, C^{13}$_{Hpq}$), 129.6 (s, C^7$_{Hpq}$), 129.2 (s, C^{12}$_{Hpq}$), 128.6 (s, C^{10}$_{Hpq}$), 128.1 (s, C$_{Ph}$), 127.7 (s, C$_{Ph}$), 127.6

(s, C^{14}_{Hpq}), 127.3 (s, C^{9}_{Hpq}), 126.5 (s, C^{11}_{Hpq}), 125.7 (s, C^{6}_{Hpq}), 124.4 (s, C^{5}_{Hpq}), 123.9 (s, C_{Ph}), 123.6 (s, C_{Ph}), 121.7 (s, C_{Ph}), 116.5 (s, C^{3}_{Hpq}), 116.3 (s, C_{Ph}), 116.0 (s, C_{Ph}), 110.1 (s, C_{Ph}), 58.5 (s, N-CH_2, NBu_4), 54.8 (s, CH_3, OMe), 54.7 (s, CH_3, OMe), 23.9 (s, -CH_2-, NBu_4), 19.2 (s, -CH_2-, NBu_4), 13.3 (s, -CH_3, NBu_4).

The low solubility of this complex precludes its characterization by $^{195}Pt\{^{1}H\}$ NMR.

Preparation of **$(NBu_4)[Pt(Hpq\text{-}\kappa N)(C{\equiv}CC_6H_4CF_3\text{-}4)_3]$ (15)**

Complex **15** was obtained as an orange solid in the similar way as **13**, starting from $[Pt(pq)(\mu\text{-}Cl)]_2$ (0.300 g, 0.345 mmol) and $LiC{\equiv}CC_6H_4CF_3$-4 (2.76 mmol), but the residue was extracted only with cold ^{i}PrOH (50 mL); (0.460 g, 58%). Similar results are obtained with a 1:5 molar ratio.

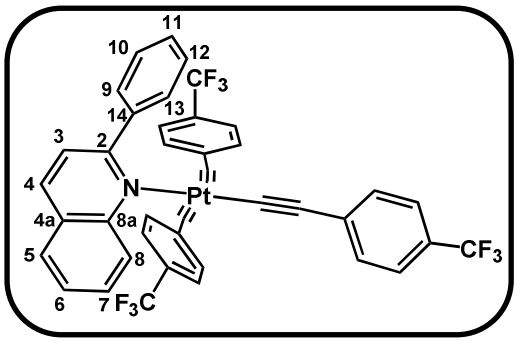

Anal. Calcd for $C_{58}H_{59}F_9N_2Pt$ (1149.42): C, 60.57; H, 5.17; N, 2.44. Found: C, 60.06; H, 5.42; N, 2.63.

MALDI-TOF (-): *m/z* (%) 702 (7) $[Pt(C{\equiv}CC_6H_4CF_3\text{-}4)_3]^-$, 737 (100) $[Pt(pq)(C{\equiv}CC_6H_4CF_3\text{-}4)_2]^-$.

IR (Nujol) (cm^{-1}): ν(C≡C) 2112 (s), 2085 (s).

Λ_M (Acetone): 113.1 $\Omega^{-1}cm^2mol^{-1}$.

^{1}H NMR (δ, 400.17 MHz, $CDCl_3$): 10.49 (d, $J_{H\text{-}H}$ = 8.9, H^{13}_{Hpq}), 8.53 (d, $J_{H\text{-}H}$ = 7.3, $J_{Pt\text{-}H}$ = 39.1, H^{8}_{Hpq}), 8.07 (AB, $J_{H\text{-}H}$ = 8.8, δ_A = 8.23, δ_B = 7.89, H^{3}_{Hpq}, H^{4}_{Hpq}), 7.70 (d, $J_{H\text{-}H}$ = 7.7, H^{9}_{Hpq}), 7.67 (d, $J_{H\text{-}H}$ = 8.2, H^{5}_{Hpq}), 7.61 (t, $J_{H\text{-}H}$ = 7.7, H^{12}_{Hpq}), 7.45 (t, $J_{H\text{-}H}$ = 8.2, $H^{10/11}_{Hpq}$), 7.42 (AB, $J_{H\text{-}H}$ = 8.2, δ_A = 7.47, δ_B = 7.37, 12H, C_6H_4), 7.40 (t, $J_{H\text{-}H}$ = 8.3, $H^{10/11}_{Hpq}$), 7.20 (t, $J_{H\text{-}H}$ = 7.2, H^{7}_{Hpq}), 7.07 (t, $J_{H\text{-}H}$ = 7.1, H^{6}_{Hpq}), 3.19 (m, 8H, NCH_2, NBu_4), 1.33 (m, 8H, -CH_2-, NBu_4), 1.09 (q, 8H, -CH_2-, NBu_4), 0.67 (t, 12H, -CH_3, NBu_4).

^{13}C{^{1}H} NMR (δ, 75.5 MHz, $CDCl_3$): 169.9 (s, C^{2}_{Hpq}), 167.1 (s, C^{8a}_{Hpq}), 148.6 (s, C^{4a}_{Hpq}), 138.4 (s, C^{4}_{Hpq}), 138.2 (s, C^{8}_{Hpq}), 132.5 (s, C^{13}_{Hpq}), 131.4 (s, C_{Ph}), 131.1 (s, C_{Ph}), 130.1 (s, C^{7}_{Hpq}), 129.6 (s, C^{12}_{Hpq}), 127.9 (s, C^{14}_{Hpq}), 127.0 (s, C^{9}_{Hpq}), 126.2 (s, C^{11}_{Hpq}), 124.8 (s, C^{5}_{Hpq}), 124.7 (s, C_{Ph}, C^{10}_{Hpq}), 122.4 (s, C^{6}_{Hpq}), 116.9 (s, C^{3}_{Hpq}), 111.3 (s, $C^{\beta}_{C\equiv C}$ *trans* to C≡C), 106.8 (s, $C^{\alpha}_{C\equiv C}$ *trans* to C≡C), 101.5 (s, $C^{\beta}_{C\equiv C}$ *trans* to N_{Hpq}), 100.7 (s, $C^{\alpha}_{C\equiv C}$ *trans* to N_{Hpq}), 58.9 (s, N-CH_2, NBu_4), 31.0 (s, CF_3), 24.2 (s, -CH_2-, NBu_4), 19.5 (s, -CH_2-, NBu_4), 13.5 (s, -CH_3, NBu_4).

^{19}F NMR (δ, 282.48 MHz, $CDCl_3$): -62.25 (s, br, CF_3).

^{195}Pt{^{1}H} NMR (δ, 86.0 MHz, $CDCl_3$, 252 K): -3845 (s, br).

Preparation of **[Pt(pq)(μ–κC^{α}:η^2-C≡C^{t}Bu)]$_2$ (16)**

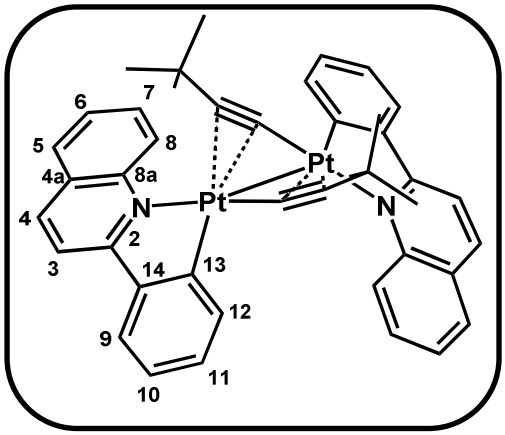

[Pt(pq)(μ-Cl)]$_2$ (0.600 g, 0.690 mmol) was added to a fresh (-20ºC) solution of LiC≡C^{t}Bu (2.070 mmol) (1:3 molar ratio) in 60 mL of diethyl ether/*n*-hexane and the mixture was stirred at room temperature for 2 h. The resulting orange suspension was evaporated to dryness and the final residue was treated with CH_2Cl_2 (25 mL). The orange solution was filtered through celite, the orange filtrate evaporated to dryness and the residue treated with cold ^{i}PrOH (15 mL), yielding **16** as an orange solid (0.562 g, 85%). Similar results were obtained with a 1:5 molar ratio.

Anal. Calcd for $C_{42}H_{38}N_2Pt_2$ (960.23): C, 52.50; H, 3.99; N, 2.92. Found: C, 52.21; H, 4.16; N, 2.95.

MALDI-TOF (+): *m/z* 879 (62) [M-C≡C^{t}Bu]$^+$, 944 (60) [M-CH_3]$^+$, 960 (100) [M]$^+$, 976 (30) [M+CH_3]$^+$.

IR (KBr) (cm^{-1}): ν(C≡C) 2030 (s), 2026 (sh).

^{1}H NMR (δ, 400.17 MHz, $CDCl_3$): 9.76 (d, $J_{H\text{-}H}$ = 8.8, 2H$^8_{pq}$), 8.30 (d, $J_{H\text{-}H}$ = 7.2, $J_{Pt\text{-}H}$ = 72.1, 2H$^{12}_{pq}$), 8.08 (AB, $J_{H\text{-}H}$ = 9.0, δ_A = 8.27, δ_B = 7.88, 2H$^3_{pq}$, 2H$^4_{pq}$), 7.79 (t, $J_{H\text{-}H}$ = 8.4, 2H$^7_{pq}$), 7.77 (d, $J_{H\text{-}H}$ = 9.0, 2H$^5_{pq}$), 7.73 (d, $J_{H\text{-}H}$ = 7.7, 2H$^9_{pq}$), 7.51 (t, $J_{H\text{-}H}$ = 7.4, 2H$^6_{pq}$), 7.32 (t, $J_{H\text{-}H}$ = 6.8, 2H$^{11}_{pq}$), 7.23 (t, $J_{H\text{-}H}$ = 7.4 2H$^{10}_{pq}$), 0.96 (s, 18H, CH_3).

^{13}C{^{1}H} NMR (δ, 75.5 MHz, $CDCl_3$): 166.7 (s, C$^2_{pq}$), 149.0 (s, C$^{8a}_{pq}$), 147.9 (s, C$^{13}_{pq}$), 145.6 (s, C$^{14}_{pq}$), 138.4 (s, C$^{12}_{pq}$, C$^4_{pq}$), 131.0 (s, C$^{11}_{pq}$), 130.5 (s, C$^8_{pq}$), 129.7 (s, C$^5_{pq}$), 128.1 (s, C$^{4a}_{pq}$), 127.3 (s, C$^7_{pq}$), 126.6 (s, C$^6_{pq}$), 125.3 (s, C$^9_{pq}$), 123.5 (s, C$^{10}_{pq}$), 116.8 (s, C$^3_{pq}$), 112.4 (s, C$^{\beta}_{C\equiv C}$), 82.1 (s, C$^{\alpha}_{C\equiv C}$) 32.1 (s, -CH_3), 31.2 (s, *C*(CH_3)).

^{195}Pt{^{1}H} NMR (δ, 86.0 MHz, $CDCl_3$): -3625.8 (s, br).

Preparation of **[Pt(pq)(μ–κC^{α}:η^2-C≡CTol)]$_2$ (17)**

Complex **17** was prepared as an orange solid in a similar way to **16** starting from [Pt(pq)(μ-Cl)]$_2$ (0.300 g, 0.345 mmol) and LiC≡CTol (1.035 mmol). The obtained brown solid was crystalized from CH_2Cl_2/^{i}PrOH to afford **17** as a light brown solid (0.309 g, 87%).

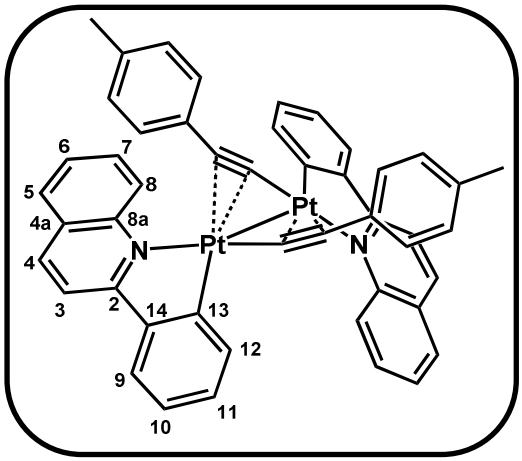

Anal. Calcd for $C_{48}H_{34}N_2Pt_2$ (1028.20): C, 56.02; H, 3.33; N, 2.72. Found: C, 56.34; H, 3.60; N, 2.59.

MALDI-TOF (+): *m/z* (%) 913 (30) $[M\text{-}C{\equiv}CTol]^+$, 1028 (100) $[M]^+$.

IR (KBr) (cm^{-1}): ν(C≡C) 2019 (sh), 2002 (s).

^{1}H NMR (δ, 400.17 MHz, $CDCl_3$): 9.48 (d, $J_{H\text{-}H}$ = 9.2, 2H$^8_{pq}$), 8.44 (d, $J_{H\text{-}H}$ = 6.7, $J_{Pt\text{-}H}$ = 69.5, 2H$^{12}_{pq}$), 8.03 (AB, $J_{H\text{-}H}$ = 8.6, δ_A = 8.16, δ_B = 7.89, 2H$^3_{pq}$, 2H$^4_{pq}$), 7.81 (d, $J_{H\text{-}H}$ = 7.2, 2H$^9_{pq}$), 7.59 (m, 2H$^7_{pq}$), 7.56 (d, $J_{H\text{-}H}$ = 8.2, 2H$^5_{pq}$), 7.41 (t, $J_{H\text{-}H}$ = 7.4, 2H$^6_{pq}$), 7.32 (t, $J_{H\text{-}H}$ = 7.1, 2H$^{11}_{pq}$), 7.23 (d, $J_{H\text{-}H}$ = 7.1, 2H$^{10}_{pq}$), 6.87 (AB, $J_{H\text{-}H}$ = 7.6, δ_A = 7.18, δ_B = 6.56, 8H, C_6H_4), 2.04 (s, 6H, CH_3, Tol).

^{13}C{^{1}H} NMR (δ, 75.5 MHz, $CDCl_3$): 166.7 (s, C$^2_{pq}$), 148.8 (s, C$^{8a}_{pq}$), 147.9 (s, C$^{13}_{pq}$), 145.7 (s, C$^{14}_{pq}$), 138.8 (s, C$^4_{pq}$), 138.0 (s, C$^{12}_{pq}$), 136.5 (s, C_6H_4), 132.1 (s, C_6H_4), 131.0 (s, C$^6_{pq}$), 130.1 (s, C$^5_{pq}$), 127.9 (s, C$^8_{pq}$, C_6H_4), 127.7 (s, C$^{4a}_{pq}$), 127.1 (s, C$^7_{pq}$), 126.3 (s, C$^{11}_{pq}$), 125.6 (s, C$^9_{pq}$), 123.9 (s, C$^{10}_{pq}$), 123.5 (s, C$^{ipso}C_6H_4$), 116.5 (s, $J_{Pt\text{-}C}$= 28.9, C$^3_{pq}$), 102.6 (s, C$^{\beta}_{C\equiv C}$), 91.8 (s, C$^{\alpha}_{C\equiv C}$), 31.1 (s, *C*(CH_3)), 21.3 (s, *C*H_3, Tol). ^{195}Pt{^{1}H} NMR (δ, 86.0 MHz, $CDCl_3$): -3596.2 (s, br).

The low solubility of this complex precludes its characterization by ^{195}Pt{^{1}H} NMR.

Preparation of **[Pt(pq)(μ–κC^{α}:η^2-C≡CC_6H_4OMe-3)]$_2$ (18)**

Complex **18** was prepared in a similar way to **16** starting from [Pt(pq)(μ-Cl)]$_2$ (0.300 g, 0.345 mmol) and LiC≡CC_6H_4OMe-3 (1.035 mmol). The obtained brown solid was crystalized from CH_2Cl_2/*i*-PrOH to afford **18** as a brown solid (0.308 g, 84%).

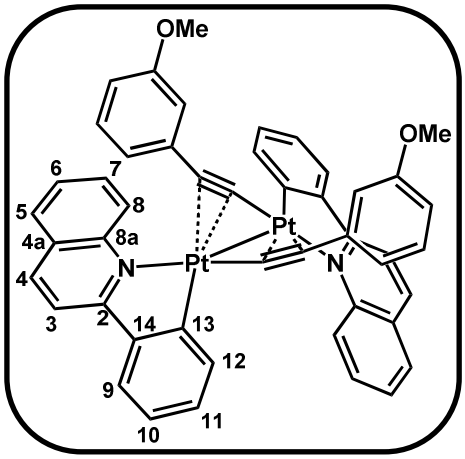

Anal. Calcd for $C_{48}H_{34}N_2O_2Pt_2$ (1060.19): C, 54.34; H, 3.23; N, 2.64. Found: C, 53.41; H, 3.87; N, 2.45.

MALDI-TOF (+): *m/z* (%) 929 (20) [M-C≡CC_6H_4OMe-3]$^+$, 1060 (100) [M]$^+$.

IR (KBr) (cm^{-1}): ν(C≡C) 2009 (s).

^{1}H NMR (δ, 300.13 MHz, $CDCl_3$): 9.41 (d, $J_{H\text{-}H}$ = 8.7, 2H^8$_{pq}$), 8.41 (d, $J_{H\text{-}H}$ = 7.1, $J_{Pt\text{-}H}$ = 75.7, 2H^{12}$_{pq}$), 8.05 (AB, $J_{H\text{-}H}$ = 8.5, δ_A = 8.19, δ_B = 7.90, 2H^3$_{pq}$, 2H^4$_{pq}$), 7.80 (d, $J_{H\text{-}H}$ = 7.3, 2H^9$_{pq}$), 7.58 (d, $J_{H\text{-}H}$ = 7.6, 2H^5$_{pq}$), 7.57 (t, $J_{H\text{-}H}$ = 7.6, 2H^7$_{pq}$), 7.40 (t, $J_{H\text{-}H}$ = 7.1, 2H^6$_{pq}$), 7.32 (m, 2H^{10}$_{pq}$, 2H^{11}$_{pq}$), 6.97 (d, $J_{H\text{-}H}$ = 7.3, 2H$^{4/6}$$C_6H_4$), 6.77 (s, 2H^2$C_6H_4$), 6.71 (t, $J_{H\text{-}H}$ = 7.9, 2H^5C_6H_4), 6.39 (d, $J_{H\text{-}H}$ = 8.1, 2H$^{4/6}$$C_6H_4$), 3.40 (s, 6H, OMe).

^{13}C{^{1}H} NMR (δ, 75.5 MHz, $CDCl_3$): 139.0 (s, C^4$_{pq}$), 137.9 (s, C^{12}$_{pq}$), 131.2 (s, C^6$_{pq}$), 130.3 (s, C^5$_{pq}$), 128.2 (s, C_6H_4), 127.7 (s, C^8$_{pq}$), 127.1 (s, C^7$_{pq}$), 126.5 (s, C^{11}$_{pq}$), 125.7 (s, C_6H_4), 125.5 (s, C^9$_{pq}$), 124.1 (s, C^{10}$_{pq}$), 116.4 (s, C^3$_{pq}$), 116.1 (s, C_6H_4), 114.0 (s, C_6H_4), 55.1 (s, OMe).

The low solubility of this complex precludes its characterization by ^{195}Pt{^{1}H} NMR.

Preparation of **[Pt(pq)(μ–κC^{α}:η^2-C≡C$C_6H_4CF_3$-4)]$_2$ (19)**

Complex **19** was prepared as a dark orange solid in a similar way to **16** starting from [Pt(pq)(μ-Cl)]$_2$ (0.300 g, 0.345 mmol) and LiC≡C$C_6H_4CF_3$-4 (1.035 mmol) (0.212 g, 54%).

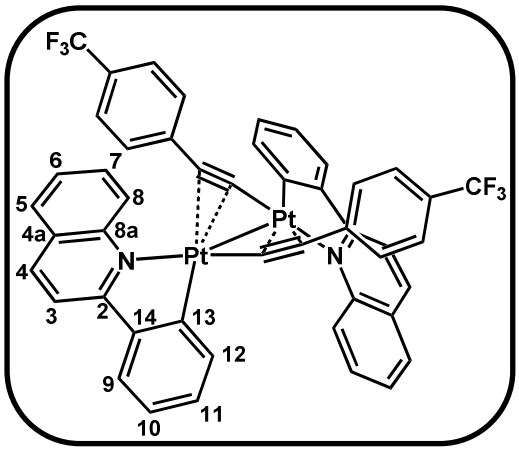

Anal. Calcd for $C_{48}H_{28}F_6N_2Pt_2$ (1136.89): C, 50.70; H, 2.48; N, 2.46. Found: C, 50.55; H, 2.53; N, 2.34.

MALDI-TOF (+): *m/z* (%) 967 (23) [M-C≡C$C_6H_4CF_3$-4]$^+$, 1136 (100) [M]$^+$.

IR (KBr) (cm^{-1}): ν(C≡C) 2040 (m), 1993 (s).

^{1}H NMR (δ, 400.17 MHz, $CDCl_3$): 9.31 (d, $J_{H\text{-}H}$ = 8.7, 2H$^8_{pq}$), 8.36 (d, $J_{H\text{-}H}$ = 7.2, $J_{Pt\text{-}H}$ = 71.5, 2H$^{12}_{pq}$), 8.07 (AB, $J_{H\text{-}H}$ = 8.7, δ_A = 8.21, δ_B = 7.93, 2H$^3_{pq}$, 2H$^4_{pq}$), 7.84 (d, $J_{H\text{-}H}$ = 7.5, 2H$^9_{pq}$), 7.59 (d, $J_{H\text{-}H}$ = 7.6, 2H$^5_{pq}$), 7.58 (t, $J_{H\text{-}H}$ = 8.2, 2H$^7_{pq}$), 7.44 (t, $J_{H\text{-}H}$ = 7.2, 2H$^6_{pq}$), 7.36 (t, $J_{H\text{-}H}$ = 7.2, 2H$^{10}_{pq}$, 2H$^{11}_{pq}$), 7.18 (AB, $J_{H\text{-}H}$ = 7.9, δ_A = 7.33, δ_B = 7.02, 8H, C_6H_4).

^{13}C{^{1}H} NMR (δ, 100.6 MHz, $CDCl_3$): 166.8 (s, C$^2_{pq}$), 147.9 (s, C$^{8a}_{pq}$), 147.7 (s, C$^{13}_{pq}$), 145.6 (s, C$^{14}_{pq}$), 139.4 (s, C$^4_{pq}$), 137.6 (s, C$^{12}_{pq}$), 132.1 (s, C^2 C_6H_4), 131.3 (s, C$^6_{pq}$), 130.3 (s, C$^7_{pq}$), 128.3 (q, $J_{C\text{-}F}$= 32, *C*-CF_3), 127.7 (s, C$^{4a}_{pq}$), 127.4 (s, C$^5_{pq}$), 127.2 (s, C$^8_{pq}$), 126.6 (s, C$^{11}_{pq}$), 125.9 (s, C$^9_{pq}$), 124.5 (s, C$^{10}_{pq}$), 124.0 (q, $J_{C\text{-}F}$= 272, CF_3), 124.1 (q, $J_{C\text{-}F}$= 4, C^3 C_6H_4), 116.1 (s, $J_{Pt\text{-}C}$ = 27, C$^3_{pq}$), 101.7 (s, $J_{Pt\text{-}C}$ ~ 410, C$^{\beta}_{C\equiv C}$), 97.1 (s, $J_{Pt\text{-}C}$ ~ 1460, C$^{\alpha}_{C\equiv C}$), 29.8 (s, *C*CF_3).

^{19}F NMR (δ, 282.48 MHz, $CDCl_3$): -63.0 (s, CF_3).

^{195}Pt{^{1}H} NMR (δ, 86.0 MHz, $CDCl_3$): -3598 (s, br).

Preparation of **[{Pt(pq)(C≡C^{t}Bu)}$_2$(μ-pyz)] (20a)**

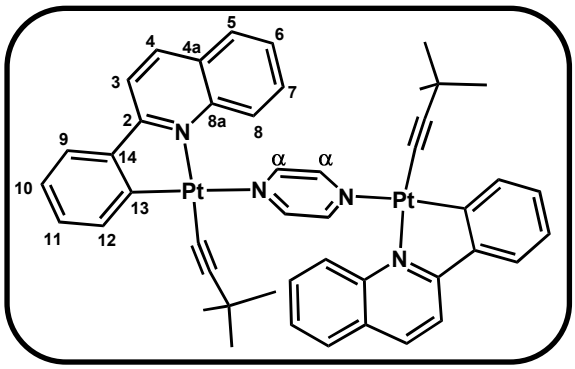

A solution of [Pt(pq)(μ–κC$^{\alpha}$:η^2-C≡C^{t}Bu)]$_2$ (**16**) (0.100 g, 0.104 mmol) in CH_2Cl_2 (20 mL) was treated with pyrazine (pyz) (0.017 g, 0.208 mmol) and the mixture was stirred for 3h. Evaporation to small volume (2 mL) afforded **20a** as an orange solid, which was filtered and washed with *n*-hexane (5 mL) (0.089 g, 82%).

Anal. Calcd for $C_{46}H_{42}N_4Pt_2$ (1041.01): C, 53.07; H, 4.07; N, 5.38. Found: C, 53.32; H, 4.11; N, 5.12.

ESI (+): *m/z* (%) 481 (77) [Pt(pq)(C≡C^{t}Bu)]$^+$, 879 (41) [Pt$_2$(pq)$_2$(C≡C^{t}Bu)]$^+$, 961 (100) [{Pt(pq)(C≡C^{t}Bu)}$_2$]$^+$, 1041 (7) [M]$^+$.

IR (KBr) (cm^{-1}): ν(C≡C) 2110 (m).

^{1}H NMR (δ, 300.13 MHz, $CDCl_3$) (**20a:16:20b:free ligand, ~1:13.1:6.2:8.9**): 9.75 (d, $J_{H\text{-}H}$ = 8.6, H$^8_{pq}$ **16**), 8.90-8.84 (m, H$^{\alpha}_{pyz}$ **20a**, H$^{\alpha}_{pyz}$ **20b**), 8.63 (s, H$^{\alpha}_{pyz}$ **20b**), 8.60 (s, H$^{\alpha}_{pyz}$ **free**), 8.42 (d, $J_{H\text{-}H}$ = 7.4, H$^{12}_{pq}$ **20a**, **20b**), 8.30 (d, $J_{H\text{-}H}$ = 7.5, H$^{12}_{pq}$ **16**, H$^{3/4}_{pq}$ **20a**, **20b**), 8.27 (d, $J_{H\text{-}H}$ = 8.9, H$^{3/4}_{pq}$ **16**); 7.96 (d, $J_{H\text{-}H}$ = 8.0, H$^{3/4}_{pq}$ **20a**, **20b**), 7.89 (d, $J_{H\text{-}H}$ = 8.7, H$^{3/4}_{pq}$ **16**), 7.80-7.72 (m, H$^{8/5}_{pq}$ **20a**, **20b**; H$^7_{pq}$, H$^5_{pq}$, H$^9_{pq}$ **16**), 7.65 (d, $J_{H\text{-}H}$ = 6.5, H$^9_{pq}$ **20a**, **20b**), 7.51 (t, $J_{H\text{-}H}$ = 7.1, H$^6_{pq}$ **16**), 7.49-7.29 (m, H$^{8/5}_{pq}$, H$^{7/6}_{pq}$ **20a**, **20b**; H$^{11}_{pq}$ **16**), 7.34 (t, $J_{H\text{-}H}$ = 8.1, H$^{11}_{pq}$ **16**), 7.23-7.12 (m, H$^{11}_{pq}$, H$^{10}_{pq}$, H$^{7/6}_{pq}$ **20a**, **20b**; H$^{10}_{pq}$ **16**); 1.28 (s, HCH_3 **20a**, **20b**), 0.96 (s, HCH_3 **16**).

Data of the **16**:**pyz**, 1:20: (**20a:16:20b:free ligand, ~1:0:7:82**). **^{1}H NMR (δ, 400.17 MHz, $CDCl_3$):** 8.83 (s, H$^{\alpha}_{pyz}$ **20a**); 8.81 (s, H$^{\alpha}_{pyz}$ **20b**), 8.59 (s, H$^{\alpha}_{pyz}$ **20b**, H$^{\alpha}_{pyz}$ **free**), 8.38 (d, $J_{H\text{-}H}$ = 7.9, H$^{12}_{pq}$ **20a**, **20b**), 8.29 (d, $J_{H\text{-}H}$ = 8.5, H$^{3/4}_{pq}$ **20a**, **20b**), 7.94 (d, $J_{H\text{-}H}$ = 8.7, H$^{3/4}_{pq}$ **20a**, **20b**), 7.80 (d, $J_{H\text{-}H}$ = 7.9, H$^{8/5}_{pq}$ **20a**, **20b**), 7.63 (d, $J_{H\text{-}H}$ = 7.8, H$^9_{pq}$ **20a**, **20b**), 7.39-7.35 (m, H$^{8/5}_{pq}$, H$^{7/6}_{pq}$ **20a**, **20b**), 7.20-7.09 (m, H$^{11}_{pq}$, H$^{7/6}_{pq}$, H$^{10}_{pq}$ **20a**, **20b**), 1.27 (s, HCH_3 **20a**, **20b**).

Preparation of **[{Pt(pq)(C≡C^{t}Bu)}$_2$(μ-bpy)] (21a)**

A solution of [Pt(pq)(μ−κC$^{\alpha}$:η^2-C≡C^{t}Bu)]$_2$ (**16**) (0.100 g, 0.104 mmol) in CH_2Cl_2 (20 mL) was treated with 4,4'-bipyridine (0.016 g, 0.104 mmol) and the obtained solution was stirred for 2h. Evaporation to small volume (2 mL) and treating with *n*-hexane (10 mL) afforded **21a** as an orange microcrystalline solid (0.073 g, 63%).

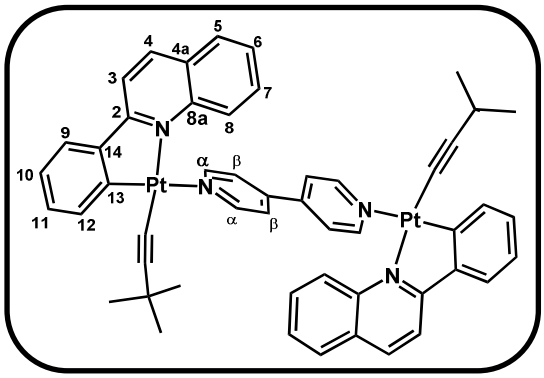

Anal. Calcd for $C_{52}H_{46}N_4Pt_2$ (1117.14): C, 55.91; H, 4.15; N, 5.02. Found: 55.74; H, 3.93; N, 4.86.

ESI (+): *m/z* (%) 481 (100) [Pt(pq)(C≡C^{t}Bu)]$^+$, 637 (6) [Pt(pq)(C≡C^{t}Bu)(bpy)]$^+$, 879 (10) [Pt$_2$(pq)$_2$(C≡C^{t}Bu)]$^+$, 961 (77) [{Pt(pq)(C≡C^{t}Bu)}$_2$]$^+$, 1117 (3) [M]$^+$.

IR (KBr) (cm^{-1}): ν(C≡C) 2117 (m).

^{1}H NMR (δ, 400.17 MHz, 293 K, $CDCl_3$) (**21a:16:21b:free ligand, ~1:0.8:1.3:0.2**): 9.75 (d, $J_{H\text{-}H}$ = 8.6, H$^8_{pq}$ **16**), 9.00 (d, $J_{H\text{-}H}$ = 5.9, H$^{\alpha}_{bpy}$ **21a**), 8.96 (d, $J_{H\text{-}H}$ = 5.8, H$^{\alpha}_{bpy}$ **21b**), 8.79 (d, $J_{H\text{-}H}$ = 5.3, H$^{\alpha}_{bpy}$ **21b**), 8.75 (d, $J_{H\text{-}H}$ = 5.1, H$^{\alpha}_{bpy}$ **free**), 8.44 (d, $J_{H\text{-}H}$ = 7.4, $J_{Pt\text{-}H}$ = 67.6, H$^{12}_{pq}$ **21a**, **21b**), 8.30 (d, $J_{H\text{-}H}$ = 8.4, H$^{12}_{pq}$ **16**, H$^{3/4}_{pq}$ **21a**, **21b**), 8.27 (d, $J_{H\text{-}H}$ = 9.8, H$^{3/4}_{pq}$ **16**), 7.96 (d, $J_{H\text{-}H}$ = 8.8, H$^{3/4}_{pq}$ **21a**, **21b**), 7.88 (d, $J_{H\text{-}H}$ = 8.6, H$^{3/4}_{pq}$ **16**), 7.79 (m, H$^{8/5}_{pq}$ **21a**, **21b**; H$^7_{pq}$, H$^5_{pq}$ **16**), 7.73 (d, $J_{H\text{-}H}$ = 7.9, H$^9_{pq}$ **16**), 7.65 (d, $J_{H\text{-}H}$ = 7.7, H$^9_{pq}$ **21a**, **21b**), 7.61-7.54 (m, H$^{\beta}_{bpy}$ **21a**, H$^{\beta}_{bpy}$ **21b**, H$^{\beta}_{bpy}$ **free**), 7.54 (m, H$^{8/5}_{pq}$ **21a**, **21b**, H$^6_{pq}$ **16**), 7.36 (t, $J_{H\text{-}H}$ = 7.8, H$^{7/6}_{pq}$ **21a**, **21b**), 7.34 (t, $J_{H\text{-}H}$ = 8.1, H$^{11}_{pq}$ **16**), 7.20 (m, H$^{11}_{pq}$ **21a**, **21b**, H$^{10}_{pq}$ **16**), 7.12 (m, H$^{7/6}_{pq}$, H$^{10}_{pq}$ **21a**, **21b**), 1.30 (s, HCH$_3$ **21a**, **21b**), 0.96 (s, HCH$_3$ **16**). **^{1}H NMR (δ, 400.17 MHz, 218 K, $CDCl_3$)** (**21a:16:21b:free ligand, ~1:0.4:0.8:0.1**). **^{1}H NMR (δ, 400.17 MHz, 293 K, CD_3COCD_3):** (**21a:16:21b:free ligand, ~1:2.2:2.4:1.2**)

Data of the **16**:**bpy**, 1:4: (**21a:16:21b:free ligand, ~1:0:8:14**). **^{1}H NMR (δ, 400.17 MHz, $CDCl_3$):** 9.00 (d, $J_{H\text{-}H}$ = 6.0, H$^{\alpha}_{bpy}$ **21a**), 8.94 (d, $J_{H\text{-}H}$ = 5.8, H$^{\alpha}_{bpy}$ **21b**), 8.78 (d, $J_{H\text{-}H}$ = 5.3, H$^{\alpha}_{bpy}$ **21b**), 8.74 (d, $J_{H\text{-}H}$ = 4.9, H$^{\alpha}_{bpy}$ **free**), 8.44 (d, $J_{H\text{-}H}$ = 7.5, $J_{Pt\text{-}H}$ = 67.6,

1H, H^{12}_{pq} **21a**, **21b**), 8.28 (d, $J_{H\text{-}H}$ = 8.6, $H^{3/4}_{pq}$ **21a**, **21b**), 7.94 (d, $J_{H\text{-}H}$ = 8.6, $H^{3/4}_{pq}$ **21a**, **21b**), 7.78 (d, $J_{H\text{-}H}$ = 7.8, $H^{8/5}_{pq}$ **21a**, **21b**), 7.64 (d, $J_{H\text{-}H}$ = 7.5, H^{9}_{pq} **21a**, **21b**), 7.58 (d, $J_{H\text{-}H}$ = 5.7, H^{β}_{bpy} **21b**), 7.55 (d, $J_{H\text{-}H}$ = 5.6, H^{β}_{bpy} **21b**), 7.53 (d, $J_{H\text{-}H}$ = 5.1, H^{β}_{bpy} **free**), 7.51 (d, $J_{H\text{-}H}$ = 7.7, $H^{8/5}_{pq}$ **21a**, **21b**), 7.32 (t, $J_{H\text{-}H}$ = 7.5, $H^{7/6}_{pq}$ **21a**, **21b**), 7.18 (t, $J_{H\text{-}H}$ = 7.1, H^{11}_{pq} **21a**, **21b**), 7.10 (t, $J_{H\text{-}H}$ = 7.1, $H^{7/6/10}_{pq}$ **21a**, **21b**), 7.08 (t, $J_{H\text{-}H}$ = 7.6, $H^{7/6/10}_{pq}$ **21a**, **21b**), 1.28 (s, HCH_3 **21a**, **21b**).

Preparation of **[{Pt(pq)(C≡C^{t}Bu)}$_2$(μ-bpa)] (22a)**

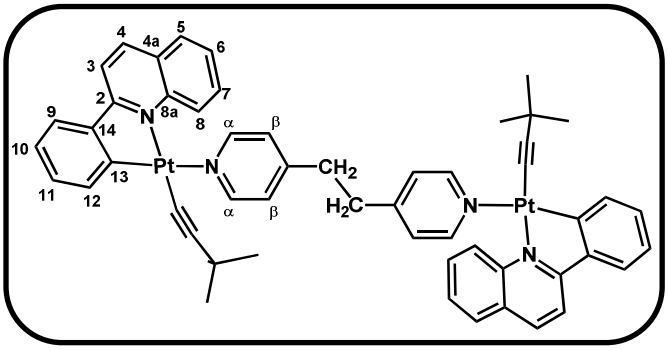

A solution of [Pt(pq)(μ−κC$^{\alpha}$:η^2-C≡C^{t}Bu)]$_2$ (**16**) (0.100 g, 0.104 mmol) in CH_2Cl_2 (20 mL) was treated with bis(4-pyridine)ethane (0.018 g, 0.104 mmol) and the obtained solution was stirred for 2h. Evaporation to small volume (2 mL) and treating with Et_2O (10 mL) afforded **22a** as an orange microcrystalline solid (0.100 g, 85%).

Anal. Calcd for $C_{54}H_{50}N_4Pt$ (1141.33): C, 56.64; H, 4.40; N, 4.89. Found: 56.43; H, 4.31; N, 5.10.

ESI (+): *m/z* (%) 481 (72) [Pt(pq)(C≡C^{t}Bu)]$^+$, 662 (4) [Pt(pq)(C≡C^{t}Bu)(bpa)]$^+$, 879 (50) [Pt$_2$(pq)$_2$(C≡C^{t}Bu)]$^+$, 961 (100) [{Pt(pq)(C≡C^{t}Bu)}$_2$]$^+$, 1145 (16) [M]$^+$.

IR (KBr) (cm^{-1}): ν(C≡C) 2119 (m).

^{1}H NMR (δ, 400.17 MHz, $CDCl_3$) (**22a:16:22b:free ligand, ~1:0.4:0.9:0.1**): 9.75 (d, $J_{H\text{-}H}$ = 8.6, H$^8_{pq}$ **16**), 8.74 (d, $J_{H\text{-}H}$ = 5.7, H$^{\alpha}_{py}$ **22a**), 8.69 (d, $J_{H\text{-}H}$ = 6.1, H$^{\alpha}_{py}$ **22b**), 8.52 (d, $J_{H\text{-}H}$ = 5.4, H$^{\alpha}_{py}$ **22b**), 8.50 (d, $J_{H\text{-}H}$ = 5.4, 1H, H$^{\alpha}_{py}$ **free**), 8.42 (d, $J_{H\text{-}H}$ = 7.5, $J_{Pt\text{-}H}$ = 61.6, H$^{12}_{pq}$ **22a**, **22b**), 8.30 (d, $J_{H\text{-}H}$ = 7.6, H$^{12}_{pq}$ **16**), 8.27 (d, $J_{H\text{-}H}$ = 8.7, H$^{3/4}_{pq}$ **22a**, **22b**, H$^{3/4}_{pq}$ **16**), 7.94 (d, $J_{H\text{-}H}$ = 8.7, H$^{3/4}_{pq}$ **22a**, **22b**), 7.88 (d, $J_{H\text{-}H}$ = 8.7, H$^{3/4}_{pq}$ **16**), 7.80-7.73 (m, H$^{8/5}_{pq}$ **22a**, **22b**; H$^5_{pq}$, H$^7_{pq}$, H$^9_{pq}$ **16**), 7.64 (d, $J_{H\text{-}H}$ = 7.4, H$^9_{pq}$ **22a**, **22b**), 7.53-7.45 (m, H$^{8/5}_{pq}$ **22a**, **22b**, H$^6_{pq}$ **16**), 7.35-7.29 (m, H$^{7/6}_{pq}$ **22a**, **22b**, H$^{11}_{pq}$ **16**), 7.22-7.16 (m, H$^{11}_{pq}$ **22a**, **22b**, H$^{10}_{pq}$ **16**), 7.11 (d, $J_{H\text{-}H}$ = 5.4, H$^{\beta}_{py}$ **22a**, H$^{\beta}_{py}$**22b**), 7.08-7.04 (m, H$^{\beta}_{py}$ **22b**, H$^{\beta}_{py}$ **free**), 7.00 (d, $J_{H\text{-}H}$ = 7.8, H$^{7/6}_{pq}$, H$^{10}_{pq}$ **22a**, **22b**), 3.03 (s, HCH_2 **22a**), 3.00 (s, HCH_2 **22b**), 2.98 (s, HCH_2 **free**), 1.28 (s, HCH_3 **22a**, **22b**), 0.96 (s, HCH_3 **16**).

Data of the **16**:**bpa**, 1:4: (**22a:16:22b:free ligand, ~1:0:6:9**). **^{1}H NMR (δ, 400.17 MHz, $CDCl_3$):** 8.74 (d, $J_{H\text{-}H}$ = 6.3, H$^{\alpha}_{py}$ **22a**), 8.69 (d, $J_{H\text{-}H}$ = 6.3, H$^{\alpha}_{py}$ **22b**), 8.52 (d, $J_{H\text{-}H}$ = 5.4, H$^{\alpha}_{py}$ **22b**), 8.50 (d, $J_{H\text{-}H}$ = 5.4, 1H, H$^{\alpha}_{py}$ **free**), 8.42 (d, $J_{H\text{-}H}$ = 7.4, $J_{Pt\text{-}H}$ = 63.5, H$^{12}_{pq}$ **22a**, **22b**), 8.26 (d, $J_{H\text{-}H}$ = 8.7, H$^{3/4}_{pq}$ **22a**, **22b**), 7.93 (d, $J_{H\text{-}H}$ = 8.8, H$^{3/4}_{pq}$ **22a**, **22b**), 7.77

(d, $J_{H\text{-}H}$ = 7.9, $H^{8/5}_{pq}$ **22a**, **22b**), 7.63 (d, $J_{H\text{-}H}$ = 7.3, H^{9}_{pq} **22a**, **22b**), 7.46 (d, $J_{H\text{-}H}$ = 8.9, $H^{8/5}_{pq}$ **22a**, **22b**), 7.33 (d, $J_{H\text{-}H}$ = 7.5, $H^{7/6}_{pq}$ **22a**, **22b**), 7.17 (d, $J_{H\text{-}H}$ = 7.1, H^{11}_{pq} **22a**, **22b**), 7.11 (d, $J_{H\text{-}H}$ = 7.0, H^{β}_{py} **22a**, $H^{\beta}_{py\ 22}$**3b**), 7.07 (d, $J_{H\text{-}H}$ = 4.1, H^{β}_{py} **22b**, H^{β}_{py} **free**); 7.00 (d, $J_{H\text{-}H}$ = 7.7, $H^{7/6}_{pq}$, H^{10}_{pq} **22a**, **22b**), 3.03 (s, HCH_2 **22a**), 3.00 (s, HCH_2 **22b**), 2.98 (s, HCH_2 **free**), 1.27 (s, HCH_3 **22a**, **22b**).

Preparation of **[{Pt(pq)(C≡C^{t}Bu)}$_2$(μ-bpe)] (23a)**

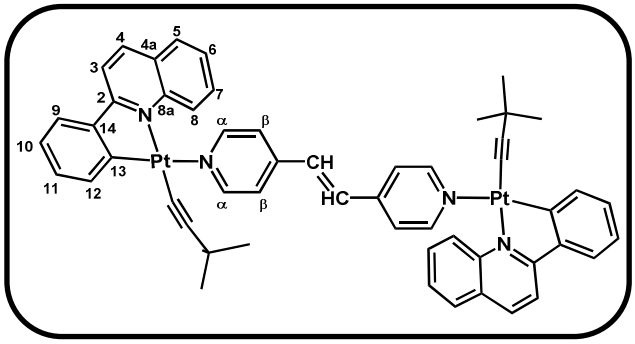

A solution of [Pt(pq)(μ–κC$^{\alpha}$:η^2-C≡C^{t}Bu)]$_2$ (**16**) (0.100 g, 0.104 mmol) in CH_2Cl_2 (20 mL) was treated with 1,2-di(4-pyridyl)ethylene (0.019 g, 0.104 mmol). Stirring at room temperature for 3h caused the precipitation of **23a** as an orange solid (0.070 g, 59%).

Anal. Calcd for $C_{54}H_{48}N_4Pt_2$ (1143.18): C, 56.74; H, 4.23; N, 4.90. Found: C, 56.59; H, 4.23; N, 4.87.

ESI (+): *m/z* (%) 481 (100) [Pt(pq)(C≡C^{t}Bu)]$^+$, 663 (6) [Pt(pq)(C≡C^{t}Bu)(bpe)]$^+$, 879 (8) [Pt$_2$(pq)$_2$(C≡C^{t}Bu)]$^+$, 961 (90) [{Pt(pq)(C≡C^{t}Bu)}$_2$]$^+$, 1143 (3) [M]$^+$.

IR (KBr) (cm^{-1}): ν(C≡C) 2115 (s).

^{1}H NMR (δ, 400.17 MHz, $CDCl_3$) (**23a:16:23b:free ligand, ~1:0.5:0.9:0.1**): 9.75 (d, $J_{H\text{-}H}$ = 8.5, H^8$_{pq}$ **16**), 8.85 (d, $J_{H\text{-}H}$ = 5.4, H$^{\alpha}$$_{py}$ **23a**), 8.82 (d, $J_{H\text{-}H}$ = 4.9, H$^{\alpha}$$_{py}$ **23b**), 8.66 (d, $J_{H\text{-}H}$ = 4.9, 1H, H$^{\alpha}$$_{py}$ **23b**), 8.64 (d, $J_{H\text{-}H}$ = 4.7, 1H, H$^{\alpha}$$_{py}$ **free**), 8.43 (d, $J_{H\text{-}H}$ = 7.8, $J_{Pt\text{-}H}$ = 61.4, 1H, H^{12}$_{pq}$ **23a**, **23b**), 8.31-8.26 (m, H$^{3/4}$$_{pq}$ **23a**, **23b**; H^{12}$_{pq}$, H$^{3/4}$$_{pq}$ **16**), 7.96 (d, $J_{H\text{-}H}$ = 8.6, H$^{3/4}$$_{pq}$ **23a**, **23b**), 7.89 (d, $J_{H\text{-}H}$ = 8.4, H$^{3/4}$$_{pq}$ **16**), 7.79 (d, $J_{H\text{-}H}$ = 7.9, H$^{8/5}$$_{pq}$ **23a**, **23b**; H^7$_{pq}$, H^5$_{pq}$ **16**), 7.73 (d, $J_{H\text{-}H}$ = 8.0, H^9$_{pq}$ **16**), 7.65 (d, $J_{H\text{-}H}$ = 7.4, H^9$_{pq}$ **23a**, **23b**), 7.55-7.49 (m, H$^{8/5}$$_{pq}$ **23a**, **23b**, H^6$_{pq}$ **16**), 7.42-7.37 (m, H$^{\beta}$$_{py}$ **23a**, H$^{\beta}$$_{py}$ **23b**, H$^{\beta}$$_{py}$ **free**), 7.35-7.30 (m, H$^{7/6}$$_{pq}$ **23a**, **23b**, H^{11}$_{pq}$ **16**), 7.26-7.19 (m, H$_{C=CH}$ **23a**, H$_{C=CH}$ **23b**, H$_{C=CH}$ **free**, H^{10}$_{pq}$ **16**), 7.11 (d, $J_{H\text{-}H}$ = 7.0, H$^{7/6}$$_{pq}$, H^{10}$_{pq}$ **23a**, **23b**), 1.29 (s, HCH$_3$ **23a**, **23b**), 0.96 (s, HCH$_3$ **16**).

Data of the **16**:**bpe**, 1:4: (**23a:16:23b:free ligand, ~1:0:5:8**). **^{1}H NMR (δ, 400.17 MHz, $CDCl_3$):** 8.83 (d, $J_{H\text{-}H}$ = 5.9, H$^{\alpha}$$_{py}$ **23a**), 8.81 (d, $J_{H\text{-}H}$ = 6.0, H$^{\alpha}$$_{py}$ **23b**), 8.65 (d, $J_{H\text{-}H}$ = 5.6, H$^{\alpha}$$_{py}$ **23b**), 8.63 (d, $J_{H\text{-}H}$ = 5.4, H$^{\alpha}$$_{py}$ **free**), 8.44 (d, $J_{H\text{-}H}$ = 7.3, $J_{Pt\text{-}H}$ = 62.0, H^{12}$_{pq}$ **23a**, **23b**), 8.28 (d, $J_{H\text{-}H}$ = 8.7, H$^{3/4}$$_{pq}$ **23a**, **23b**), 7.95 (d, $J_{H\text{-}H}$ = 8.7, H$^{3/4}$$_{pq}$ **23a**, **23b**), 7.78 (d, $J_{H\text{-}H}$ = 7.8, H$^{8/5}$$_{pq}$ **23a**, **23b**), 7.64 (d, $J_{H\text{-}H}$ = 7.6, H^9$_{pq}$ **23a**, **23b**), 7.53 (d, $J_{H\text{-}H}$ = 8.7, H$^{8/5}$$_{pq}$ **23a**, **23b**), 7.40 (d, $J_{H\text{-}H}$ = 5.5, H$^{\beta}$$_{py}$ **23b**), 7.39 (d, $J_{H\text{-}H}$ = 5.5, H$^{\beta}$$_{py}$ **free**), 7.34 (t, $J_{H\text{-}H}$ =

7.6, $H^{7/6}_{pq}$ **23a**, **23b**), 7.32 (s, $H_{C=C}$ **23a**), 7.29 (s, $H_{C=C}$ **23b**), 7.23 (s, $H_{C=C}$ **23b**), 7.21 (s, $H_{C=C}$ **free**), 7.18 (t, $J_{H\text{-}H}$ = 8.3, H^{11}_{pq} **23a**, **23b**), 7.11 (t, $J_{H\text{-}H}$ = 7.5, $H^{7/6}_{pq}$, H^{10}_{pq} **23a**, **23b**), 1.29 (s, HCH_3 **23a**, **23b**).

Preparation of **[{Pt(pq)(C≡C^{t}Bu)}$_2$(μ-bpac)] (24a)**

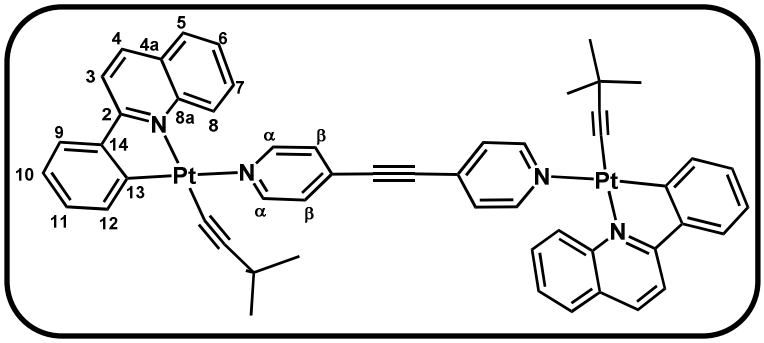

A solution of [Pt(pq)(μ–κC$^{\alpha}$:η^2-C≡C^{t}Bu)]$_2$ (**16**) (0.100 g, 0.104 mmol) in CH_2Cl_2 (20 mL) was treated with di(4-pyridyl)acetylene (0.038 g, 0.208 mmol) and the mixture was stirred for 12h. Evaporation to small volume (2 mL) and treating with *n*-hexane (5 mL) gave **24a** as an orange microcrystalline solid (0.085 g, 72%).

Anal. Calcd for $C_{54}H_{46}N_4Pt_2$ (1141.16): C, 56.84; H, 4.06; N, 4.91. Found: C, 56.47; H, 4.08; N, 4.78.

ESI (+): *m/z* (%) 481 (100) [Pt(pq)(C≡C^{t}Bu)]$^+$, 663 (6) [Pt(pq)(C≡C^{t}Bu)(bpac)]$^+$, 879 (55) [Pt$_2$(pq)$_2$(C≡C^{t}Bu)]$^+$, 961 (86) [{Pt(pq)(C≡C^{t}Bu)}$_2$]$^+$, 1141 (3) [M]$^+$.

IR (KBr) (cm^{-1}): ν(C≡C)$_{(\text{internal C≡C})}$ 2223 (w), ν(C≡C) 2118 (s).

^{1}H NMR (δ, 300.13 MHz, CDCl$_3$) (**24a:16:24b:free ligand, ~1:0.9:1.4:0.2**): 9.75 (d, $J_{H\text{-}H}$ = 8.6, H$^8_{pq}$ **16**), 8.89 (d, $J_{H\text{-}H}$ = 5.6, H$^{\alpha}_{py}$ **24a**), 8.86 (d, $J_{H\text{-}H}$ = 5.6, H$^{\alpha}_{py}$ **24b**), 8.68 (d, $J_{H\text{-}H}$ = 4.5, H$^{\alpha}_{py}$ **24b**), 8.66 (d, $J_{H\text{-}H}$ = 6.0, H$^{\alpha}_{py}$ **free**), 8.41 (d, $J_{H\text{-}H}$ = 7.0, $J_{Pt\text{-}H}$ = 62.3, H$^{12}_{pq}$ **24a**, **24b**), 8.31-8.26 (m, H$^{12}_{pq}$, H$^{3/4}_{pq}$ **16**, H$^{3/4}_{pq}$ **24a**, **24b**), 7.96 (d, $J_{H\text{-}H}$ = 8.6, H$^{3/4}_{pq}$ **24a**, **24b**), 7.89 (d, $J_{H\text{-}H}$ = 8.6, H$^{3/4}_{pq}$ **16**), 7.80-7.77 (m, H$^{8/5}_{pq}$ **24a**, **24b**; H$^7_{pq}$, H$^5_{pq}$ **16**), 7.73 (d, $J_{H\text{-}H}$ = 7.9, H$^9_{pq}$ **16**), 7.65 (d, $J_{H\text{-}H}$ = 7.2, H$^9_{pq}$ **24a**, **24b**), 7.53-7.48 (m, H$^{8/5}_{pq}$ **24a**, **24b**, H$^6_{pq}$ **16**), 7.41 (m, H$^{\beta}_{py}$ **24a**, H$^{\beta}_{py}$ **24b**, H$^{\beta}_{py}$ **free**), 7.39-7.32 (m, H$^{7/6}_{pq}$ **24a**, **24b**, H$^{11}_{pq}$ **16**), 7.19-7.09 (m, H$^{7/6}_{pq}$, H$^{11}_{pq}$, H$^{10}_{pq}$ **24a**, **24b**; H$^{10}_{pq}$ **16**), 1.29 (s, HCH$_3$ **24a**, **24b**), 0.96 (s, HCH$_3$ **16**).

Data of the **16**:**bpac**, 1:4: (**24a:16:24b:free ligand, ~1:0:4:7**). **^{1}H NMR (δ, 400.17 MHz, CDCl$_3$):** 8.90 (d, $J_{H\text{-}H}$ = 5.9, H$^{\alpha}_{py}$ **24a**), 8.87 (d, $J_{H\text{-}H}$ = 6.4, H$^{\alpha}_{py}$ **24b**), 8.68 (d, $J_{H\text{-}H}$ = 5.8, H$^{\alpha}_{py}$ **24b**), 8.66 (d, $J_{H\text{-}H}$ = 5.8, H$^{\alpha}_{py}$ **free**), 8.44 (d, $J_{H\text{-}H}$ = 6.1, H$^{12}_{pq}$ **24a**, **24b**), 8.29 (d, $J_{H\text{-}H}$ = 8.2, H$^{3/4}_{pq}$ **24a**, **24b**), 7.95 (d, $J_{H\text{-}H}$ = 8.8, H$^{3/4}_{pq}$ **24a**, **24b**), 7.80 (d, $J_{H\text{-}H}$ = 8.0, H$^{8/5}_{pq}$ **24a**, **24b**), 7.65 (d, $J_{H\text{-}H}$ = 7.7, H$^9_{pq}$ **24a**, **24b**), 7.50 (d, $J_{H\text{-}H}$ = 9.7, H$^{8/5}_{pq}$ **24a**,

24b), 7.42 (d, $J_{H\text{-}H}$ = 7.2, $H^{\beta}{}_{py}$ **24a**, **24b**), 7.41 (d, $J_{H\text{-}H}$ = 5.9, $H^{\beta}{}_{py}$ **24b**, **free**), 7.36 (t, $J_{H\text{-}H}$ = 7.0, $H^{7/6}{}_{pq}$ **24a**, **24b**), 7.21-7.07 (m, $H^{7/6}{}_{pq}$, $H^{10}{}_{pq}$, $H^{11}{}_{pq}$ **24a**, **24b**), 1.30 (s, HCH_3 **24a**, **24b**).

Preparation of **[{Pt(pq)(C≡C^{t}Bu)}$_3$(μ-tpab)] (25a)**

A solution of [Pt(pq)(μ–κC$^\alpha$:η^2-C≡C^{t}Bu)]$_2$ (**16**) (0.150 g, 0.156 mmol) in CH_2Cl_2 (20 mL) was treated with 1,3,5,-tris(pyridine-4-ylethynyl)benzene (0.040 g, 0.104 mmol) (molar ratio 3:2) and the orange solution was stirred for 4 h. Evaporation to small volume (2 mL) and treating with *n*-hexane (5 mL) gave **25a** as an orange microcrystalline solid (0.152 g, 80%).

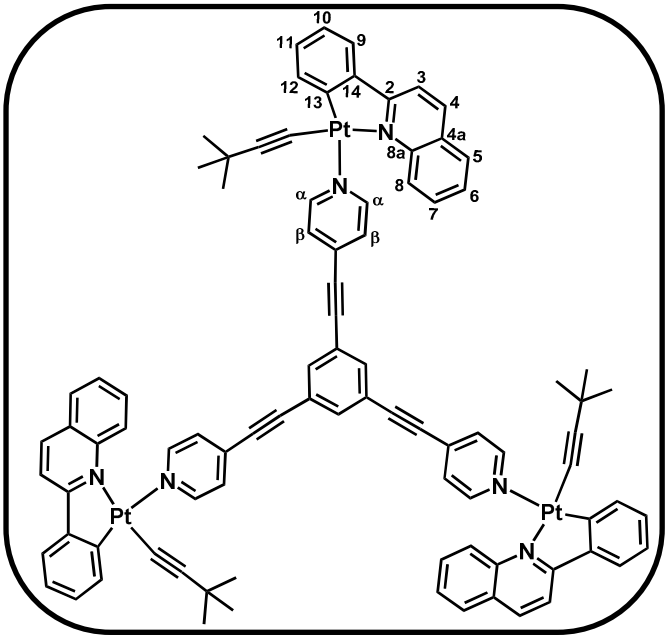

Anal. Calcd for $C_{90}H_{72}N_6Pt_3$ (1822.87): C, 59.30; H, 3.98; N, 4.61. Found: C, 59.19; H, 3.92; N, 4.40.

ESI (+): *m/z* (%) 879 (51) $[Pt_2(pq)_2(C{\equiv}C^tBu)]^+$, 961 (100) $[\{Pt(pq)(C{\equiv}C^tBu)\}_2]^+$, 1342 (21) $[Pt_2(pq)_2(C{\equiv}C^tBu)_2L]^+$, 1660 (3) $[M\text{-}2C{\equiv}C^tBu]^+$, 1823 (2) $[M]^+$.

IR (KBr) (cm^{-1}): ν(C≡C)$_{(internal\ C\equiv C)}$ 2212 (m), ν(C≡C) 2115 (m).

^{1}H NMR (δ, 300.13 MHz, CDCl$_3$): 9.75 (d, $J_{H\text{-}H}$ = 8.6, H$^8_{pq}$ **16**), 8.85 (m, H$^\alpha_{py}$ **25a**, H$^\alpha_{py}$ **25b**), 8.65 (m, H$^\alpha_{py}$ **25b**, H$^\alpha_{py}$ **free**), 8.42 (d, $J_{H\text{-}H}$ = 8.3, H$^{12}_{pq}$ **25a**, **25b**), 8.30 (d, $J_{H\text{-}H}$ = 7.3, H$^{12}_{pq}$ **16**, H$^{3/4}_{pq}$ **25a**, **25b**), 8.27 (d, $J_{H\text{-}H}$ = 7.9, H$^{3/4}_{pq}$ **16**), 7.96 (d, $J_{H\text{-}H}$ = 8.3, H$^{3/4}_{pq}$ **25a**, **25b**), 7.89 (d, $J_{H\text{-}H}$ = 8.8, H$^{3/4}_{pq}$ **16**), 7.80-7.72 (m, H$^{8/5}_{pq}$ **25a**, **25b**; H$^7_{pq}$, H$^5_{pq}$, H$^9_{pq}$ **161**, H$^\beta_{py}$ **25a**, C-*H*C$_6$H$_3$ **25a**, C-*H*C$_6$H$_3$ **25b**, C-*H*C$_6$H$_3$ **free**), 7.66-7.62 (m, H$^9_{pq}$ **25a**, **25b**, H$^\beta_{py}$ **25b**), 7.53-7.49 (m, H$^{8/5}_{pq}$ **25a**, **25b**, H$^6_{pq}$ **16**), 7.39-7.42 (m, H$^\beta_{py}$ **free**, H$^{7/6}_{pq}$ **25a**, **25b**, H$^{11}_{pq}$ **16**), 7.19-7.10 (m, H$^{7/6}_{pq}$, H$^{11}_{pq}$, H$^{10}_{pq}$ **25a**, **25b**; H$^{10}_{pq}$ **16**), 1.30 (s, HCH$_3$ **25a**, **25b**), 0.96 (s, HCH$_3$ **16**).

Data of the **16**:**tpab**, 1:4. **^{1}H NMR (δ, 400.17 MHz, CDCl$_3$):** 8.85 (d, $J_{H\text{-}H}$ = 4.6, H$^\alpha_{py}$ **25a**), 8.81 (d, $J_{H\text{-}H}$ = 4.8, H$^\alpha_{py}$ **25b**), 8.64 (d, $J_{H\text{-}H}$ = 4.2, H$^{\alpha 2}_{py}$ **25b**, H$^\alpha_{py}$ **free**), 8.42 (d, $J_{H\text{-}H}$ = 7.4, H$^{12}_{pq}$ **25a**, **25b**), 8.29 (d, $J_{H\text{-}H}$ = 8.6, H$^{3/4}_{pq}$ **25a**, **25b**), 7.95 (d, $J_{H\text{-}H}$ = 8.6,

$H^{3/4}{}_{pq}$ **25a**, **25b**), 7.82-7-79 (m, $J_{H\text{-}H}$ = 8.0, $H^{8/5}{}_{pq}$ **25a**, **25b**, $H^{\beta}{}_{py}$ **25a**), 7.78 (s, C-*H*C_6H_3 **25a**), 7.76 (s, C-*H*C_6H_3 **25b**), 7.75 (s, C-*H*C_6H_3 **free**), 7.64 (d, $J_{H\text{-}H}$ = 7.9, $H^{9}{}_{pq}$ **25a**, **25b**), 7.60 (d, $J_{H\text{-}H}$ = 5.4, $H^{\beta}{}_{py}$ **25b**), 7.51 (d, $J_{H\text{-}H}$ = 8.9, $H^{8/5}{}_{pq}$ **25a**, **25b**), 7.40-7.37 (m, $H^{\beta}{}_{py}$ **free**, $H^{7/6}{}_{pq}$ **25a**, **25b**), 7.20-7.09 (m, $H^{7/6}{}_{pq}$, $H^{10}{}_{pq}$, $H^{11}{}_{pq}$ **25a**, **25b**), 1.30 (s, HCH_3 **25a**, **25b**).

Preparation of **[Pt(pq){(κ*C*:κ*S*-2-SC$_5$H$_4$N-C=CH^{t}Bu}]** (**26**)

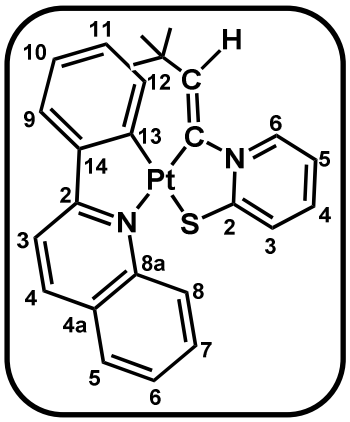

0.023 g (0.208 mmol) of 2-mercaptopyridine was added to an orange solution of [Pt(pq)(μ−κC$^{\alpha}$:η^2-C≡C^{t}Bu)]$_2$ (**16**) (0.100 g, 0.104 mmol) in CH_2Cl_2 (20 mL). After 5 min of stirring the red solution obtained was evaporated to small volume (2 mL) and treated with *n*-hexane (2 mL). The mixture was kept at -30ºC affording red microcrystalline solid of **26** (0.060 g, 49%).

Anal. Calcd for $C_{26}H_{24}N_2PtS$ (591.13): C, 52.78; H, 4.09; N, 4.75. Found: C, 52.39; H, 4.19; N, 4.43.

ESI (+): *m/z* (%) 591 (42) $[M+H]^+$, 702 (100) $[M+SpyH]^+$, 978 (5) $[2M-pq]^+$, 702 (4) $[2M+H]^+$.

IR (KBr) (cm^{-1}): ν(C=C)$_{(C=CHtBu)}$ 1602 (s).

^{1}H NMR (δ, 300.13 MHz, CDCl$_3$): Data for **26$_Z$** : δ 8.63 (d, J = 8.8 Hz, H$^8_{pq}$), 8.32 (d, J_{H-H} = 5.8, H$^3_{Spy}$), 8.24 (d, J_{H-H} = 8.6, H$^{3/4}_{pq}$), 7.93 (d, J_{H-H} = 7.4, J_{Pt-H} = 66.2, H$^{12}_{pq}$),7.90 (d, J_{H-H} = 8.6, H$^{3/4}_{pq}$), 7.78 (d, J_{H-H} = 6.5, H$^7_{pq}$, H$^6_{Spy}$), 7.66 (d, J_{H-H} = 7.3, H$^9_{pq}$), 7.52 (t, J_{H-H} = 7.5, H$^6_{pq}$), 7.47 (d, J_{H-H} = 8.5, H$^5_{pq}$), 7.37 (t, J_{H-H} = 7.3, H$^5_{Spy}$), 7.20 (t, J_{H-H} = 7.2, H$^{11}_{pq}$), 7.10 (t, J_{H-H} = 7.2, H$^{10}_{pq}$), 6.77 (m t, J_{H-H} = 6.4, H$^4_{Spy}$), 5.76 (s, J_{Pt-H} = 106.2, H$_{C=C}$), 1.40 (s, 9H, HCH$_3$).

^{13}C{^{1}H} NMR (δ,100.67 MHz, CDCl$_3$): 171.1 (s, C$^2_{Spy}$), 167.5 (s, C$^2_{pq}$), 154.0 (s, C$^{13}_{pq}$), 150.4 (s, C$^{\alpha}_{C=C}$), 147.0 (s, C$^{8a}_{pq}$), 146.0 (s, C$^{14}_{pq}$), 144.6 (s, J_{Pt-C} = 92.4, C$^{\beta}_{C=C}$), 138.8 (s, C$^4_{pq}$), 137.7 (s, C$^5_{Spy}$), 137.5 (s, C$^3_{Spy}$), 137.1 (s, C$^{12}_{pq}$), 131.1 (s, C$^6_{Spy}$), 130.8 (s, C$^{11}_{pq}$), 129.3 (s, C$^8_{pq}$), 128.5 (s, C$^5_{pq}$), 128.4 (s, C$^7_{pq}$), 128.1 (s, C$^{4a}_{pq}$), 126.6 (s, C$^6_{pq}$), 125.3 (s, C$^9_{pq}$), 122.4 (s, C$^{10}_{pq}$), 116.9 (s, J_{Pt-C} = 22.9, C$^3_{pq}$), 116.6 (s, C$^4_{Spy}$), 32.6 (s, -CH$_3$), 31.2 (s, *C*(CH$_3$)).

Data for 26$_E$ (obtained from the mixture **55:45**, **26$_Z$:26$_E$):** δ 8.74 (d, J = 9.1 Hz, H$^8_{pq}$), 8.24 (d, J_{H-H} = 5.2, H$_{Spy}$), 8.22 (d, J_{H-H} = 8.5, H$^{3/4}_{pq}$) 7.90 (d, J_{H-H} = 8.5, H$^{3/4}_{pq}$), 7.98 (d, J_{H-H} = 7.6, J_{Pt-H} = 55.8, H$^{12}_{pq}$), 7.77 (t, J_{H-H} = 7.6, H$^7_{pq}$, H$_{SPy}$), 7.71 (d, J_{H-H} = 7.6, H$^9_{pq}$),

7.61 (d, $J_{H\text{-}H}$ = 8.3, H^{6}_{pq}), 7.40 (d, $J_{H\text{-}H}$ = 7.5, H^{5}_{pq}), 7.32 (t, $J_{H\text{-}H}$ = 7.3, H_{Spy}); 7.16 (t, $J_{H\text{-}H}$ = 7.4, H^{11}_{pq}), 7.12 (t, $J_{H\text{-}H}$ = 7.2, H^{10}_{pq}), 6.75 (m, $J_{H\text{-}H}$ = 6.6, H_{Spy}), 6.04 (s, $J_{Pt\text{-}H}$ = 58.3, $H_{C=C}$), 1.55 (s, 9H, HCH_3).

Preparation of **[Pt(pq){μ-*Z*-*κC*:*κN*-C=CH(ᵗBu)-4-SC$_5$H$_4$N}]$_2$ (27)**

Complex **27** was prepared as a microcrystaline orange solid following a procedure similar to that described for **7**, starting from [Pt(pq)(μ–κC^{α}:η^2-C≡C^{t}Bu)]$_2$ (**16**) (0.100 g, 0.104 mmol) and 0.023 g (0.208 mmoles) of 4-mercaptopyridine (0.084 g, 68%).

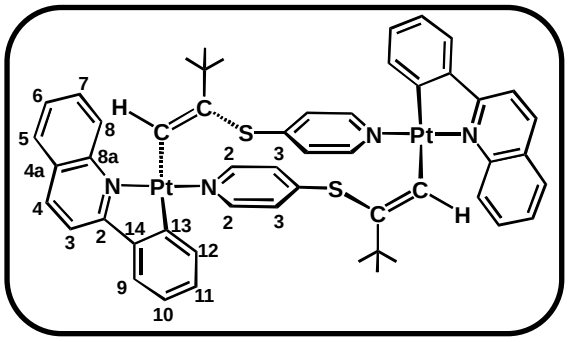

Anal. Calcd for $C_{52}H_{48}N_4Pt_2S_2$ (1182.26): C, 52.78; H, 4.09; N, 4.75. Found: C, 52.46; H, 4.26; N, 4.32.
ESI (+): *m/z* (%) 978 (3) $[M\text{-}pq]^+$, 1183 (100) $[M+H]^+$.

IR (KBr) (cm^{-1}): ν(C=C)$_{(CH=CtBu)}$ 1606 (s).

^{1}H NMR (δ, 300.13 MHz, CDCl$_3$): δ 8.48 (d, J = 6.1 Hz, H$^8{}_{pq}$), 8.23 (d, $J_{H\text{-}H}$ = 8.7, H$^{3/4}{}_{pq}$), 8.09 (d, $J_{H\text{-}H}$ = 6.2, H$^5{}_{pq}$), 7.96 (d, $J_{H\text{-}H}$ = 8.7, H$^{3/4}{}_{pq}$), 7.91 (d, $J_{H\text{-}H}$ = 7.8, H$^2{}_{Spy}$), 7.81 (d, $J_{H\text{-}H}$ = 8.9, H$^{2'}{}_{Spy}$), 7.71 (t, $J_{H\text{-}H}$ = 7.7, H$^{12}{}_{pq}$, H$^{11}{}_{pq}$); 7.34 (t, $J_{H\text{-}H}$ = 7.0, H$^{10}{}_{pq}$); 7.21-7.00 (m, 4H, H$^3{}_{Spy}$, H$^{3'}{}_{Spy}$, H$^9{}_{pq}$, H$^7{}_{pq}$); 6.76 (d, $J_{H\text{-}H}$ = 6.2, H$^6{}_{pq}$); 6.58 (s, $J_{Pt\text{-}H}$ = 143.8, $H_{C=C}$); 1.54 (s, 18H, HCH_3).

The low solubility of this complex precludes its characterization by $^{13}C\{^1H\}$ NMR.

Preparation of **[{Pt(bzq)(C≡CPh)$_2$}{Pb(HBpz$_3$)}]$_2$ (28)**

To a yellow solution of (NBu$_4$)[Pt(bzq)(C≡CPh)$_2$] (0.200 g, 0.244 mmoles) in acetone (15 ml) was added 0.112 g (0.244 mmoles) of [Pb(HBpz$_3$)]Cl and 0.300 g (2.44 mmoles) of NaClO$_4$. After 30 minutes of reaction the observed yellow precipitate was filtered and washed with H$_2$O (5 ml) and EtOH (5 ml) (0.175 g, 72%).

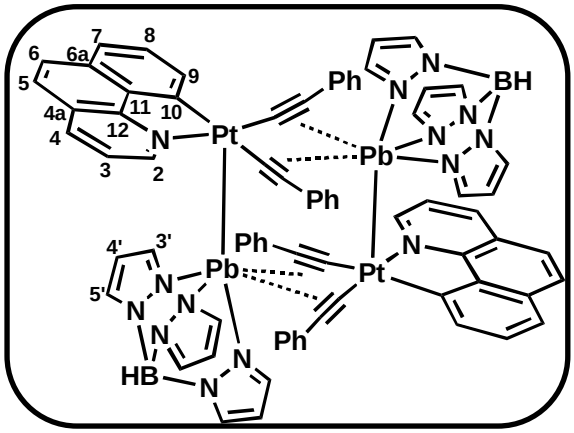

Anal. Calcd for [C$_{38}$H$_{28}$N$_7$BPtPb]$_2$ (1991.58): C, 45.83; H, 2.83; N, 9.85. Found: C, 45.22; H, 2.85; N, 9.50.

MALDI-TOF (+): *m/z* (%): 894 (24) [M/2-C≡CPh]$^+$, 996 (4) [M/2]$^+$, 1257 (20) [Pt$_2$(bzq)$_2$(C≡CPh)$_3$Pb]$^+$, 1416 (100) [M/2+HBpz$_3$Pb]$^+$, 1777 (20) [M- HBpz$_3$Pb]$^+$

IR (nujol) (cm^{-1}): ν (C≡C)$_{st}$ 2094 (s), 2086 (s), 2070 (s), 2060 (s)

Λ$_M$ (CH$_2$Cl$_2$): 0 Ω^{-1} cm^{-2} mol^{-1}

^{1}H NMR (δ, 400.17 MHz, CDCl$_3$): 9.82 (d, $J_{H\text{-}H}$ = 2.6, $J_{Pt\text{-}H}$ = 29.6, H$^2_{bzq}$), 8.60 (s, $J_{Pt\text{-}H}$ = 38.9, H$^9_{bzq}$), 8.15 (d, $J_{H\text{-}H}$ = 6.2, H$^4_{bzq}$), 7.70 (d, $J_{H\text{-}H}$ = 8.8, H$^{5/6}_{bzq}$), 7.59 (m, Ph), 7.56 (m, H$^7_{bzq}$, H$^8_{bzq}$, H$^{5'}_{pz}$), 7.42 (d, $J_{H\text{-}H}$ = 8.8, H$^{5/6}_{bzq}$),7.31 (s, H$^3_{bzq}$), 6.92 (s, H$^{3'}_{pz}$, Ph), 6.68 (s, Ph), 5.92 (s, H$^{4'}_{pz}$).

The low solubility of this complex precludes its characterization by ^{13}C{^{1}H} and ^{195}Pt{^{1}H} NMR.

Preparation of **[{Pt(bzq)(C≡CC$_6$H$_4$OMe-3)$_2$}{Pb(HBpz$_3$)}]$_2$ (29)**

To a yellow solution of (NBu$_4$)[Pt(bzq)(C≡CC$_6$H$_4$OMe-3)$_2$] (0.150 g, 0.171 mmoles) in acetone (15 ml) was added 78 mg (0.171 mmoles) of [Pb(HBpz$_3$)]Cl and 0.209 g (1.71 mmoles) of NaClO$_4$ After 4 h of reaction, the observed yellow precipitate was filtered and washed with H$_2$O (5 ml) y EtOH (5 ml) (0.101 g, 56%).

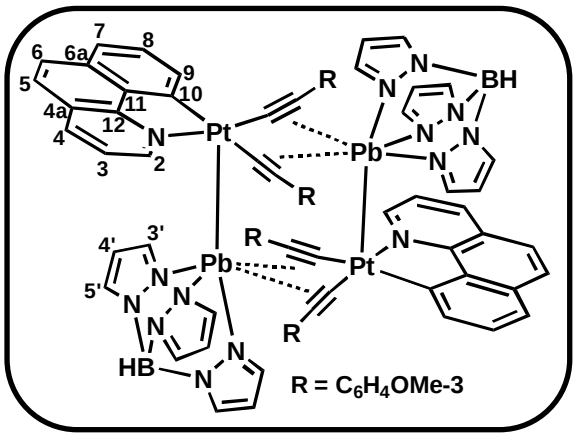

Anal. Calcd for [C$_{40}$H$_{32}$N$_7$O$_2$BPtPb]$_2$ (2111.68): C, 45.50; H, 3.05; N, 9.29. Found: C, 44.92; H, 2.89; N, 9.29.

MALDI-TOF (+): *m/z* (%): 793 (24) [M/2-2C≡CC$_6$H$_4$OMe-3]$^+$, 924 (52) [M/2-C≡CC$_6$H$_4$OMe-3]$^+$, 1056 (14) [M/2]$^+$, 1347 (20) [M/2-C≡CC$_6$H$_4$OMe-3+HBpz$_3$Pb]$^+$, 1477 (100) [M/2+ HBpz$_3$Pb]$^+$, 1899 (20) [M - HBpz$_3$Pb]$^+$.

IR (Nujol) (cm^{-1}): ν (C≡C)$_{st}$ 2085 (m/br), 2060 (m)

Λ$_M$(CH$_2$Cl$_2$): 0 Ω^{-1} cm^{-2} mol^{-1}

^{1}H NMR (δ, 400.17 MHz, CDCl$_3$): 9.80 (d, $J_{H\text{-}H}$ = 5.1, $J_{Pt\text{-}H}$ = 31.2, H^2$_{bzq}$), 8.58 (d, $J_{H\text{-}H}$ = 5.4, $J_{Pt\text{-}H}$ = 38.6, H^9$_{bzq}$), 8.14 (d, $J_{H\text{-}H}$ = 6.9, H^4$_{bzq}$), 7.67 (d, $J_{H\text{-}H}$ = 8.6, H$^{5/6}$$_{bzq}$), 7.58 (m, H^7$_{bzq}$, H^8$_{bzq}$), 7.55 (m, H$^{5'}$$_{pz}$, C$_6H_4$), 7.40 (d, $J_{H\text{-}H}$ = 8.6, H$^{5/6}$$_{bzq}$),7.33 (t, $J_{H\text{-}H}$ = 6.4, H^3$_{bzq}$), 6.93 (m, H$^{3'}$$_{pz}$, C$_6H_4$), 6.64 (d, $J_{H\text{-}H}$ = 7.7, C$_6$H$_4$), 6.55 (d, $J_{H\text{-}H}$ = 8.0, C$_6$H$_4$), 6.50 (d, $J_{H\text{-}H}$ = 7.3, C$_6$H$_4$), 6.02 (s, C$_6$H$_4$), 5.94 (s, H$^{4'}$$_{pz}$), 5.87 (s, C$_6H_4$), 3.35 (s, OMe).

^{13}C{^{1}H} NMR (δ, 75.5 MHz, CDCl$_3$): 159.0 (s, C^{3}C$_6$H$_4$), 158.8 (s, C^{3}C$_6$H$_4$), 150.5 (s, C^2$_{bzq}$), 142.1 (s, C^3$_{pz}$), 136.8 (s, C^4$_{bzq}$), 135.7 (s, C$^{5/6}$$_{bzq}$), 134.9 (s, C^9$_{bzq}$, C^5$_{pz}$), 130.1 (s, C^7$_{bzq}$), 129.5 (s, C$^{5/6}$$_{bzq}$), 128.7 (s, C^{5}C$_6H_4$), 128.5 (s, C^{5}C$_6H_4$), 127.7 (s, C^{1}C$_6H_4$), 126.6 (s, C^{1}C$_6H_4$), 124.9 (s, C^{6}C$_6H_4$), 124.4 (s, C^{6}C$_6H_4$), 122.6 (s, C^3$_{bzq}$), 122.0 (s, C^8$_{bzq}$), 121.1 (s, C^{2}C$_6H_4$), 115.4 (s, C^{2}C$_6H_4$), 114.0 (s, C^{4}C$_6H_4$), 113.9 (s, C^{4}C$_6H_4$), 104.4 (s, C^4$_{pz}$), 54.9 (s, C$_{OMe}$), 54.7 (s, C$_{OMe}$).

^{195}Pt{^{1}H} NMR (δ, 86.0 MHz, CDCl$_3$, 252 K): -3208 (s).

Preparation of (**NBu_4)[{Pt(bzq)(C≡C$C_6H_4CF_3$-4)$_2$}$_2${Pb($HBpz_3$)}] (30)**

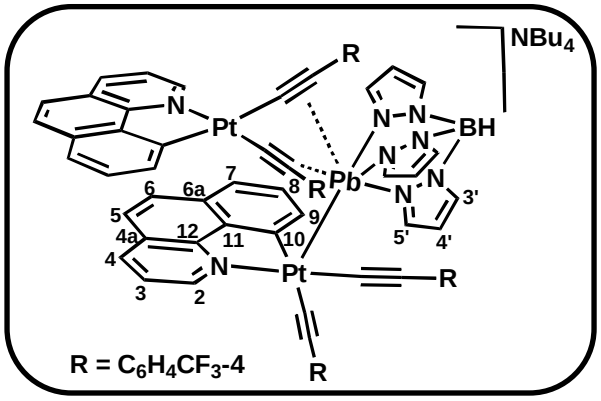

To a yellow solution of (NBu_4)[Pt(bzq)(C≡C$C_6H_4CF_3$-4)$_2$] (0.150 g, 0.157 mmoles) in acetone (15 ml) was added 0.072 g (0.157 mmoles) of [Pb($HBpz_3$)]Cl and 0.193 g (1.57 mmoles) of $NaClO_4$ was added. After 4 h of reaction, a grey precipitate was filtered and the filtrate was evaporated to dryness and the yellow residue treated with H_2O (5 ml) (0.147 g, 90%).

Anal. Calcd for $C_{87}H_{78}N_9F_{12}BPt_2Pb$ (2085.80): C, 50.10; H, 3.77; N, 6.04. Found: C, 49.88; H, 3.67; N, 6.46.

MALDI-TOF (-) *m/z* (%): 1630 (3) $[M\text{-}NBu_4\text{-}HBpz_3]^-$, 1843 (3) $[M\text{-}NBu_4]^-$.

IR (Nujol) (cm^{-1}): ν $(C\equiv C)_{st}$ 2111 (s), 2088 (s), 2070 (s), 2040 (sh)

Λ_M (CH_2Cl_2) = 98 Ω^{-1} cm^{-2} mol^{-1}

^{1}H NMR (δ, 400.17 MHz, $CDCl_3$): 9.67 (d, $J_{H\text{-}H}$ = 3.8, $J_{Pt\text{-}H}$ = 28.7, $H^2{}_{bzq}$), 8.40 (d, $J_{H\text{-}H}$ = 6.9, $J_{Pt\text{-}H}$ = 37.7, $H^9{}_{bzq}$), 7.91 (d, $J_{H\text{-}H}$ = 6.2, $H^4{}_{bzq}$), 7.60 (d, $J_{H\text{-}H}$ = 8.7, $H^{5/6}{}_{bzq}$), 7.54 (m, $H^7{}_{bzq}$, $H^8{}_{bzq}$), 7.48 (m, $H^{5'}{}_{pz}$), 7.24 (d, $J_{H\text{-}H}$ = 8.7, $H^{5/6}{}_{bzq}$), 7.16 (s, $H^3{}_{bzq}$), 7.05 (d, $J_{H\text{-}H}$ = 7.4, C_6H_4), 6.84 (d, $J_{H\text{-}H}$ = 7.4, C_6H_4), 6.83 (s, $H^{3'}{}_{pz}$), 5.80 (s, $H^{4'}{}_{pz}$), 3.20 (m, NCH_2, NBu_4), 1.43 (m, -CH_2-, NBu_4), 1.18 (q, -CH_2-, NBu_4), 0.77 (t, -CH_3, NBu_4).

^{13}C{^{1}H} NMR (δ, 75.5 MHz, $CDCl_3$): 150.2 (s, $C^2{}_{bzq}$), 144.2 (s), 142.0 (s), 136.3 (s), 135.2 (s), 134.8 (s), 133.8 (s), 131.4 (s), 129.8 (s), 129.4 (s), 126.7 (s), 124.6 (s), 124.3 (s), 122.6 (s), 121.5 (s), 121.3 (s), 104.4 (s), 59.1 (s, NCH_2, NBu_4), 24.2 (s, -CH_2-, NBu_4), 19.6 (s, -CH_2-, NBu_4), 13.6 (s, -CH_3, NBu_4). Because of the low resolution of the spectrum can not make a complete assignment

^{19}F NMR (δ, 282.48 MHz, $CDCl_3$): -62.2 (s, CF_3).

Preparation of **[Pt(C_6F_5)(ppy)(dmso)] (32)**

2-Phenylpyridine (0.23 gr, 1.46 mmol) was added to a toluene solution (20 mL) of *cis*-[Pt(C_6F_5)$_2$(dmso)$_2$] (1 g, 1.46 mmol) and the mixture refluxed for 32 h. The resulting yellow-green solution was filtered through celite, the filtrate was evaporated to small volume (~ 2 mL), and treated with *n*-hexane (10 mL) to give **32** as a dark yellow solid (0.85g, 97%).

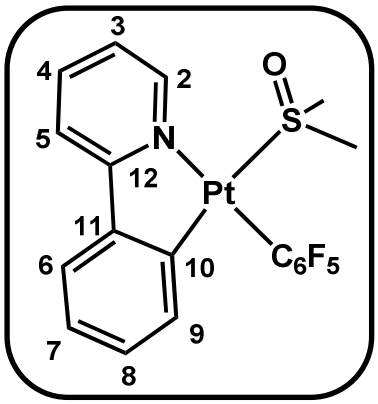

Anal. Calcd for $C_{19}H_{14}F_5NOPtS$: C, 38.39; H, 2.37; N, 2.36; S, 5.39. Found: C, 38.72; H, 2.48; N, 2.34; S, 5.49%.

MALDI-TOF (+): *m/z* (%) 516 $[Pt(C_6F_5)(ppy)]^+$ (19), 594 $[M]^+$ (100).

IR (nujol) (cm^{-1}): $\nu(C_6F_{5\ Xsens})$ 796 (m).

^{1}H NMR (δ, 400.17 MHz, CD_3COCD_3): 9.73 (d, J_{H-H} = 5.6, $^3J_{Pt-H}$ = 21.7, H^2_{ppy}), 8.14 (m, H^4_{ppy}, H^5_{ppy}), 7.76 (d, J_{H-H} = 7.8, H^6_{ppy}), 7.48 (t, J_{H-H} = 6.5, H^3_{ppy}), 7.10 (t, J_{H-H} = 7.5, H^7_{ppy}), 6.96 (t, J_{H-H} = 7.5, H^8_{ppy}), 6.41 (d, J_{H-H} = 7.5, $^3J_{Pt-H}$ = 62.4, H^9_{ppy}), 3.11 (s, $^3J_{Pt-H}$ = 14.9, 6H, $CH_{3\ dmso}$).

^{19}F NMR (δ, 376.5 MHz, 298 K, CD_3COCD_3): -117.5 (d, $^3J_{Pt-F}$ = 494, 2 *o*-F), -163.1 (t, 1 *p*-F), -164.5 (m, 2 *m*-F).

^{13}C{^{1}H} NMR (δ, 100.6 MHz, CD_3COCD_3): 166.8 (s, $^1J_{Pt-C}$ = 81.7, C^{10}_{ppy}), 151.7 (s, C^2_{ppy}), 148.6 (dm, J_{C-F} = 231.2, C_{C6F5}), 147.8 (s, C^{12}_{ppy}), 146.6 (s, C^{11}_{ppy}), 141.0 (s, C^4_{ppy}), 136.8 (s, $^2J_{Pt-C}$ = 109.3, C^9_{ppy}), 130.6 (s, $^3J_{Pt-C}$ = 68.8, C^8_{ppy}), 126.2 (s, C^7_{ppy}), 124.7 (s, $^3J_{Pt-C}$ = 37.4, C^6_{ppy}), 124.1 (s, $^3J_{Pt-C}$ = 17.4, C^3_{ppy}), 120.3 (s, $^3J_{Pt-C}$ = 28.8, C^5_{ppy}), 45.32 (s, $^2J_{Pt-C}$ = 36.3, $CH_{3\ dmso}$).

Preparation of **[{Pt(C_6F_5)(bzq)}$_2$Pb(Spy)$_2$] (33)**

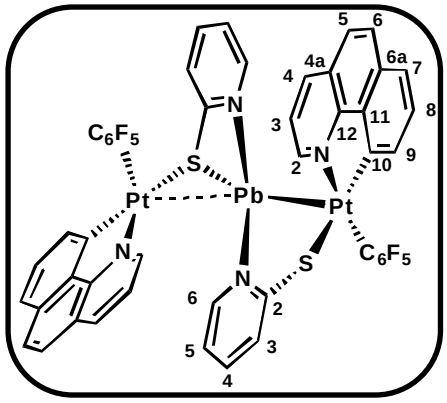

To a suspension of [Pb(Spy)$_2$] (0.0536 g, 0.125 mmol) in CH_2Cl_2 (15 ml) was added 2 equiv of [Pt(C_6F_5)(bzq)(acetone)] (**31**) (0.150 g, 0.250 mmol), and the initial yellow suspension was partially dissolved, giving rise a red solution. The mixture was stirred for 1 hour and filtered through Celite. The red solution was evaporated to small volume (2 ml) and n-hexane was added (5 ml) to give an orange solid identified as **33** (0.157 g, 83% yield).

Anal. Calcd for $C_{48}H_{24}F_{10}N_4PbPt_2S_2$: C, 38.23; H, 1.60; N, 3.71; S, 4.25. Found: C, 38.27; H, 1.57; N, 3.64; S, 4.11%.

MALDI-TOF (+): *m/z* (%) 650 [Pt(bzq)(C_6F_5)(Spy)]$^+$ (22), 857 [Pt(bzq)(C_6F_5)Pb(Spy)]$^+$ (92), 1398 [{Pt(bzq)(C_6F_5)}Pb(Spy)]$^+$ (36), 1508 [M]$^+$ (3).

IR (nujol) (cm^{-1}): ν(C_6F_5 Xsens) 800.

^{1}H NMR (δ, 400.17 MHz, CD_2Cl_2): 9.01 (s br, 1H, H^2_{bzq}), 8.12 (s br, 1H, H^4_{bzq}), 7.80 (d, $J_{H\text{-}H}$ = 8.5, 1H, $H^{5/6}_{bzq}$), 7.66 (d, $J_{H\text{-}H}$ = 7.7, 2H, $H^{5/6}_{bzq}$, H^7_{bzq}), 7.51 (s br, 1H, H^6_{Spy}), 7.39 (t, $J_{H\text{-}H}$ = 7.3, 1H, H^8_{bzq}), 7.30 (s br, 1H, H^3_{bzq}) 7.11 (s, 1H, H^4_{Spy}), 7.00 (s, 1H, H^3_{Spy}), 6.94 (s, 1H, H^9_{bzq}), 6.38 (s br, 1H, H^5_{Spy}). **^{1}H NMR (δ, 400.17 MHz, CD_3COCD_3)**: 8.95 (d, $J_{H\text{-}H}$ = 3.5, $^3J_{Pt\text{-}H}$ = 21.6, H^2_{bzq}), 8.42 (d, $J_{H\text{-}H}$ = 6.8, H^4_{bzq}), 7.88 (d, $J_{H\text{-}H}$ = 8.8, 1H, $H^{5/6}_{bzq}$), 7.70 (m, 2H, $H^{5/6}_{bzq}$, H^7_{bzq}), 7.52 (m, 1H, H^6_{Spy}), 7.48 (m, 1H, H^3_{bzq}), 7.43 (t, $J_{H\text{-}H}$ = 7.6, H^8_{bzq}), 7.31 (t, 1H, $J_{H\text{-}H}$ = 7.2, H^4_{Spy}), 7.09 (m, 2H, H^3_{Spy}, H^9_{bzq}), 6.63 (t, $J_{H\text{-}H}$ = 5.3, 1H, H^5_{Spy}).

^{19}F NMR (δ, 282.4 MHz, 298 K, CD_2Cl_2): -116.5 (m, 2 *o*-F), -162.0 (t, 1 *p*-F), -162.9 (m, 2 *m*-F). **^{19}F NMR (δ, 376.5 MHz, 186 K, CD_2Cl_2):** -116.3 (t, $^3J_{Pt\text{-}F}$ = 405, 2 *o*-F), -123.5 (t, $^3J_{Pt\text{-}F}$ = 303, $J_{Pb\text{-}F}$ = 1564, 2 *o*-F), -163.4 (t, 2 *p*-F), -163.5 (m_{br}, 2 *m*-F), -164.1 (m_{br}, 2 *m*-F). **^{19}F NMR (δ, 282.4 MHz, 298 K, CD_3COCD_3):** -118.8 (dm, $^3J_{Pt\text{-}o\text{-}F}$ = 282, 2 *o*-F), -165.5 (t, 1 *p*-F), -166.0 (m, 2 *m*-F).

$^{13}C\{^{1}H\}$ NMR (δ, 100.6 MHz, CD_3COCD_3): 156.8 (s, C^{10}_{bzq}), 148.7 (s, C^{2}_{bzq}), 146.3 (s, C^{6}_{Spy}), 139.6 (s, C^{4}_{bzq}), 137.6 (s, C^{4}_{Spy}), 135.0 (s, C^{6a}_{bzq}), 134.3 (s, C^{9}_{bzq}), 132.2 (s, C^{3}_{Spy}), 130.6 (s, C^{8}_{bzq}), 130.2 (s, C^{6}_{bzq}), 128.0 (s, C^{4a}_{bzq}), 124.5 (s, C^{5}_{bzq}), 123.7 (s, C^{7}_{bzq}), 123.3 (s, C^{3}_{bzq}), 120.5 (s, C^{5}_{Spy})

Preparation of **[{Pt(C_6F_5)(bzq)}$_2$Pb(μ–SpyCF$_3$-5)$_2$] (34)**

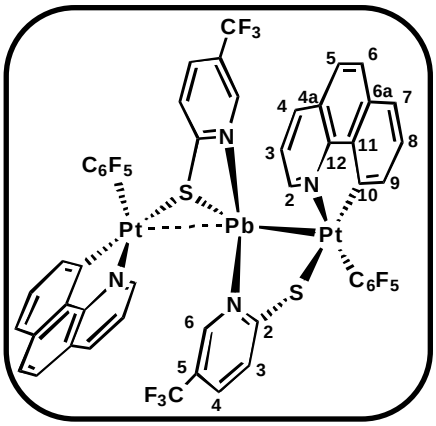

To a yellow suspension of [Pb(SpyCF$_3$-5)$_2$], (0.070 g, 0.125 mmol) in CH_2Cl_2 (15 mL) was added 2 equiv of [Pt(C_6F_5)(bzq)(OCMe$_2$)] (**31**) (0.150 g, 0.250 mmol). The resulting orange solution was stirred for 1h and concentrated to small volume (2 mL) to afford **34** as an orange solid. (0.143 g, 70%).

Anal. Calcd for $C_{50}H_{22}F_{16}N_4PbPt_2S_2$: C, 36.52; H, 1.35; N, 3.41; S, 3.90. Found: C, 36.41; H, 1.36; N, 3.17; S, 4.24%.

MALDI-TOF (+): *m/z* (%) 718 [Pt(C_6F_5)(bzq)(SpyCF$_3$)]$^+$ (2), 925 [Pt(C_6F_5)(bzq)Pb(SpyCF$_3$)]$^+$ (100), 1465 [{Pt(C_6F_5)(bzq)}$_2$Pb(SpyCF$_3$)]$^+$ (3).

IR (nujol) (cm^{-1}): *ν*(C_6F_5 Xsens) 799 (s).

^{1}H NMR (δ, 400.17 MHz, CD_2Cl_2): 9.27 (s$_{br}$, H^2$_{bzq}$), 8.10 (d, J_{H-H} = 7.7, H^4$_{bzq}$), 7.75 (d, J_{H-H} = 8.7, H$^{5/6}$$_{bzq}$), 7.66 (d, J_{H-H} = 7.9, H^7$_{bzq}$), 7.43 (m, H^3$_{bzq}$, H$^{5/6}$$_{bzq}$, H^8$_{bzq,}$ H^6$_{SpyCF3}$), 7.21 (d, J_{H-H} = 7.6, H$^{3/4}$$_{SpyCF3}$), 7.06 (d, J_{H-H} = 7.5, H$^{3/4}$$_{SpyCF3}$), 7.03 (d, J_{H-H} = 7.4, $^3J_{Pt-H}$ = 56.1, H^9$_{bzq}$). **^{1}H NMR (δ, 400.17 MHz, CD_3COCD_3):** 9.25 (d, J_{H-H} = 4.8, $^3J_{Pt-H}$ = 26.5, H^2$_{bzq}$), 8.40 (d, J_{H-H} = 7.5, H^4$_{bzq}$), 7.85 (d, J_{H-H} = 8.7, H$^{5/6}$$_{bzq}$), 7.69 (d, J_{H-H} = 7.9, H^7$_{bzq}$), 7.60 (m, H$^{5/6}$$_{bzq}$, H^3$_{bzq}$), 7.57 (s, H^6$_{SpyCF3}$), 7.50 (d, J = 7.3, H$^{3/4}$$_{SpyCF3}$), 7.41 (t, J = 7.5, H^8$_{bzq}$), 7.21 (d, J = 7.3, H$^{3/4}$$_{SpyCF3}$), 7.03 (d, J_{H-H} = 6.9, $^3J_{Pt-H}$ = 57.5, H^9$_{bzq}$).

^{19}F NMR (δ, 376.5 MHz, 298 K, CD_2Cl_2): - 63.1 (s, CF_3), -115.7 (br, 2 *o*-F), -124.8 (br, 2 *o*-F), -162.7 (t, 2 *p*-F), -164.0 (m$_{br}$, 4 *m*-F). **^{19}F NMR (δ, 376.5 MHz, 186 K, CD_2Cl_2):** -62.8 (s, CF_3), -115.7 (d, $^3J_{Pt-F}$ = 384, 2 *o*-F), -124.6 (d, $^3J_{Pt-F}$ = 289, J_{Pb-F} = 1594, 2 *o*-F), -162.1 (t, 2 *p*-F), -162.8 (m, 2 *m*-F), -163.7 (m, 2 *m*-F). **^{19}F NMR (δ, 376.5 MHz, 298 K, CD_3COCD_3)**: -63.1 (s, CF_3), -118.5 (t, $^2J_{Pt-F}$ = 383, 4 *o*-F), -165.1 (t, 2 *p*-F), -165.8 (m, 4 *m*-F).

The low solubility of this complex precludes its characterization by $^{13}C\{^1H\}$ NMR.

Preparation of **[{Pt(C_6F_5)(ppy)}$_2$Pb(μ–Spy)$_2$] (35)**

To a suspension of [Pb(Spy)$_2$] (0.072 g, 0.168 mmol) in CH_2Cl_2 (15 mL) was added 2 equiv of [Pt(C_6F_5)(ppy)(dmso)] (**32**) (0.200 g, 0.336 mmol), and the initial yellow suspension was partially dissolved, giving rise a red solution. The mixture was stirred for 1 hour and filtered through Celite. The red solution was evaporated to small volume (2 mL) and *n*-hexane was added (5 mL) to give an orange solid identified as **35** (0.176 g, 72%).

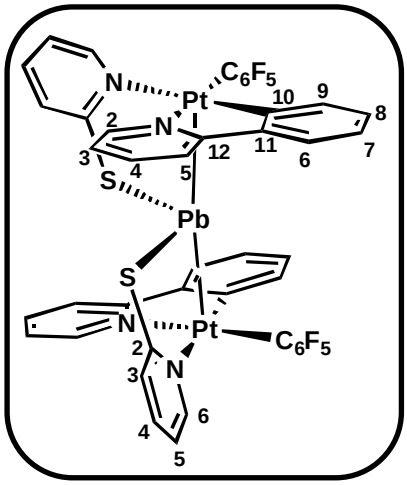

Anal. Calcd for $C_{44}H_{24}F_{10}N_4PbPt_2S_2$: C, 36.19; H, 1.66; N, 3.84; S, 4.39. Found: C, 36.60; H, 1.97; N, 3.38; S, 4.21%.

MALDI-TOF (+): *m/z* (%) 626 [Pt(C_6F_5)(ppy)(Spy)]$^+$ (100), 833 [Pt(C_6F_5)(ppy)Pb(Spy)]$^+$ (39), 1350 [{Pt(C_6F_5)(bzq)}$_2$Pb(Spy)]$^+$ (41).
IR (nujol) (cm^{-1}): ν(C_6F_5 $_{Xsens}$) 799 (vs).

^{1}H NMR (δ, 400.17 MHz, CD_2Cl_2): 8.72 (s_{br}, H^2_{ppy}), 7.78 (s, H^6_{Spy}), 7.63 (m, H^4_{ppy}, H^5_{ppy}), 7.58 (d, J_{H-H} = 7.6, H^6_{ppy}), 7.24 (s_{br}, H^4_{Spy}), 7.15 (t, J_{H-H} = 7.4, H^7_{ppy}), 7.03 (s_{br}, H^3_{Spy}), 7.01 (t, J_{H-H} = 7.2, H^3_{ppy}, H^8_{ppy}), 6.86 (s_{br}, H^5_{Spy},), 6.79 (d, J_{H-H} = 6.8, $^3J_{Pt-H}$ = 54.7, H^9_{ppy}). **^{1}H NMR (δ, 400.17 MHz, CD_3COCD_3):** 8.73 (s_{br}, H^2_{ppy}), 7.94 (s_{br}, H^6_{Spy}), 7.91 (m, H^4_{ppy}, H^5_{ppy}), 7.73 (d, J_{H-H} = 7.5, H^6_{ppy}), 7.41 (t, J_{H-H} = 7.1, H^4_{Spy}), 7.13 (t, J_{H-H} = 7.3, H^7_{ppy}), 7.09 (s_{br}, H^3_{Spy}), 7.07 (m, H^3_{ppy}), 6.99 (t, J_{H-H} = 7.1, H^8_{ppy}), 6.94 (s_{br}, H^5_{Spy},), 6.80 (d, J_{H-H} = 7.2, $^3J_{Pt-H}$ = 59.4, H^9_{ppy}).

^{19}F NMR (δ, 376.5 MHz, 298 K, CD_2Cl_2): -120.0 (m_{br}, 4 *o*-F), -163.8 (t, 2 *p*-F), -164.5 (m, 4 *m*-F). **^{19}F NMR (δ, 376.5 MHz, 186 K, CD_2Cl_2):** -116.1 (d, $^3J_{Pt-F}$ = 404, 2 *o*-F), -123.2 (d, $^3J_{Pt-F}$ = 317, J_{Pb-F} = 1557, 2 *o*-F), -163.1 (t, 2 *p*-F), -163.7 (m, 2 *m*-F), -164.1 (m, 2 *m*-F). **^{19}F NMR (δ, 282.4 MHz, 298 K, CD_3COCD_3):** -117.9 (dm, $^3J_{Pt-F}$ = 408, 4 *o*-F), -164.9 (t, 2 *p*-F), -165.1 (m, 4 *m*-F).

^{13}C{^{1}H} NMR (δ, 100.6 MHz, CD_3COCD_3): 167.7 (s, C^{10}_{ppy}), 149.4 (s, C^2_{ppy}), 146.8 (s, C^6_{Spy}), 140.8 (s, C^5_{ppy}), 138.0 (s, C^4_{Spy}), 137.1 (s, C^9_{ppy}), 132.6 (s, C^3_{Spy}), 131.3 (s, C^8_{ppy}), 125.4 (s, $C^{6/7}_{ppy}$), 125.3 (s, $C^{6/7}_{ppy}$), 124.4 (s, C^3_{ppy}), 121.0 (s, C^5_{Spy}), 120.3 (s, C^4_{ppy}).

Preparation of **[{Pt(C_6F_5)(ppy)}$_2$Pb(μ–SpyCF$_3$-5)$_2$] (36)**.

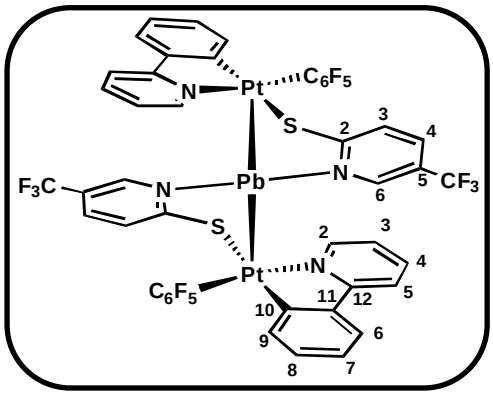

This compound was obtained as a yellow solid (0.221 g, 82%) following a similar procedure to that described for **35** using as starting precursors [Pb(SpyCF$_3$-5)$_2$] (0.0948 g, 0.168 mmol) and [Pt(C_6F_5)(ppy)(dmso)] (**32**) (0.200 g, 0.336 mmol).

Anal. Calcd for $C_{46}H_{22}F_{16}N_4PbPt_2S_2$: C, 34.61; H, 1.39; N, 3.51; S, 4.02. Found: C, 34.59; H, 1.82; N, 3.93; S, 4.43%.

MALDI-TOF (+): *m/z* (%) 695 [Pt(C_6F_5)(ppy)(SpyCF$_3$)]$^+$ (25), 901 [Pt(C_6F_5)(ppy)Pb(SpyCF$_3$)]$^+$ (100), 1418 [{Pt(C_6F_5)(bzq)}$_2$Pb(SpyCF$_3$)]$^+$ (10).

IR (nujol) (cm^{-1}): *ν*(C_6F_5 $_{Xsens}$) 794 (vs).

^{1}H NMR (δ, 400.17 MHz, CD_2Cl_2): 8.93 (s_{br}, H^2_{ppy}), 7.86 (s_{br}, H^6_{SpyCF3}), 7.61 (s_{br}, H^4_{ppy}), 7.47 (s_{br}, H^5_{ppy}, H^6_{ppy}), 7.37 (d, J_{H-H} = 7.9, $H^{3/4}_{Spy}$), 7.15 (m, H^7_{ppy}, $H^{3/4}_{Spy}$), 7.04 (m, H^3_{ppy}, H^8_{ppy}), 6.83 (d, J_{H-H} = 6.7, $^3J_{Pt-H}$ = 60.9, H^9_{ppy}).

^{1}H NMR (δ, 400.17 MHz, CD_3COCD_3): 8.92 (d, J_{H-H} = 4.6, $^3J_{Pt-H}$ = 26.0, H^2_{ppy}), 8.20 (s_{br}, H^6_{SpyCF3}), 7.84 (d, J_{H-H} = 7.8, H^5_{ppy}), 7.81 (t, J_{H-H} = 7.7, H^4_{ppy}), 7.63 (t, J_{H-H} = 8.2, H^6_{ppy}, $H^{3/4}_{Spy}$), 7.30 (d, J_{H-H} = 5.4, $H^{3/4}_{Spy}$), 7.16 (t, J_{H-H} = 5.8, H^3_{ppy}), 7.10 (t, J_{H-H} = 7.2, H^7_{ppy}), 7.01 (t, J_{H-H} = 7.0, H^8_{ppy}), 6.84 (d, J_{H-H} = 7.3, $^3J_{Pt-H}$ = 57.5, H^9_{ppy}).

^{19}F NMR (δ, 376.5 MHz, 298 K, CD_2Cl_2): - 62.8 (s, CF_3), -116.4 (br, 2 *o*-F), -123.7 (br, 2 *o*-F), -162.7 (t, 2 *p*-F), -163.9 (m, 4 *m*-F). **^{19}F NMR (δ, 376.5 MHz, 186 K, CD_2Cl_2):** -62.1 (s, CF_3), -115.9 (d, $^3J_{Pt-F}$ = 387, 2 *o*-F), -123.1 (br, 2 *o*-F), -162.5 (t, 2 *p*-F), -163.0 (m, 2 *m*-F), -164.0 (m, 2 *m*-F). **^{19}F NMR (δ, 376.5 MHz, CD_3COCD_3):** -64.6 (s, CF_3), -117.5 (m, $^3J_{Pt-F}$ = 382, 4 *o*-F), -164.4 (t, 2 *p*-F), -165.0 (m, 4 *m*-F).

^{13}C{^{1}H} NMR (δ, 100.6 MHz, CD_3COCD_3): 171.3 (s_{br}, C^2_{SpyCF3}), 167.4 (s, $^1J_{Pt-C}$ = 76.8, C^{10}_{ppy}), 150.8 (dm, $^1J_{C-F}$ = 235.2, C_{C6F5}), 149.9 (s, C^2_{ppy}), 148.3 (dm, $^1J_{C-F}$ = 232.1, C_{C6F5}), 147.3 (s, $C^{11/12}_{ppy}$), 146.6 (s, $C^{11/12}_{ppy}$) 143.9 (s, C^6_{SpyCF3}), 141.1 (s, C^5_{ppy}), 137.4 (dm, $^1J_{C-F}$ = 247.8, C_{C6F5}), 137.3 (s, $^2J_{Pt-C}$ = 96.6, C^9_{ppy}), 133.7 (s, C^3_{SpyCF3}), 132.4 (s,

C^4_{SpyCF3}), 131.4 (s, $^3J_{Pt-C}$ = 66.8, C^8_{ppy}), 125.7 (s, C^7_{ppy}), 125.3 (s, $^3J_{Pt-C}$ = 37.2, C^6_{ppy}), 124.7 (q, J_{C-F} = 271, C_{CF3}), 124.5 (s, $^3J_{Pt-C}$ = 18.4, C^3_{ppy}), 122.6 (q, $^2J_{C-F}$ = 32.4, C^5_{Spy}), 120.1 (s, $^3J_{Pt-C}$ = 26.7, C^4_{ppy}).

D) X-Ray crystallography

X-RAY CRYSTALLOGRAPHY EXPERIMENTAL DETAILS: CHAPTER 1

Details of the structural analyses for all complexes are summarized in Tables E.1 and E.2. Yellow (**1**, **7**, **8**, **11**) or orange (**3**, **6**, **9**) crystals were obtained by slow diffusion at room temperature of *n*-hexane (**1**, **3**, **11**), EtOH (**6**, **8**, **9**) or *i*-PrOH (**7**) into solutions of the complexes in acetone (**1**), CH_2Cl_2 (**3**, **6**, **11**) or acetonitrile (**7**, **8**, **9**). In all the cases, graphite-monochromatic Mo-K_α radiation was used. For complexes **1** and **11**, X-ray intensity data were collected with an Oxford Diffraction Xcalibur CCD diffractometer, being the diffraction frames integrated and corrected for absorption using the Crysalis RED package.[21] For the rest of derivatives, data collection were performed on a NONIUS-κCCD area-detector diffractometer, and the images were processed using the DENZO and SCALEPACK suite of programs,[5] being the absorption corrected at this point for **7** and **8**. For the rest of crystals, the absorption correction was performed using XABS2[22] (**3, 6**) or MULTI-SCAN[23] (**9**), with the WINGX program suite.[24] The structures were solved by Direct and Patterson Methods using SIR2004[25] (**1**) or DIRDIF96[26] (**3**, **6**, **7**, **8**, **11**) or by Direct Methods using SHELXS-97[27] (**9**), and refined by full-matrix least squares on F^2 with SHELXL-97.[27] All non-hydrogen atoms were assigned anisotropic displacement parameters. For complexes **1**, **7**, **8** and **11**, the correct assignment of the position of the C and N atoms bonded to platinum in the benzoquinolate and 2-phenylpyridinate ligands, and for complexes **7**, **8** and **9**, that of the C and N atoms of the terminal pyrazolate group of the trispyrazolylmethane ligands, was confirmed by examination of the ΔMSDA values for bonds involving these atoms,[28] after refining each case in three different ways (with the identities of the C and N in one position, reversed, and with 50/50 hybrid scattering factor at each of the affected atomic sites). All the hydrogen atoms were constrained to idealized geometries fixing isotropic displacement parameters 1.2 times the U_{iso} value of their attached carbon; except for the methine H20 in the structure of **7**, which was located from difference maps and assigned isotropic parameters. Finally, except for **7** and **8**, the structures show some residual peaks greater than 1 eA^{-3} in the vicinity of the platinum atoms (or the PF_6^- anion for **9**), but with no chemical meaning.

Tabla E.1: Datos cristalográficos y sobre la resolución de los complejos de **1**, **3** y **6**

	1	**3**	**6**
empirical formula	$C_{19}H_{16}BN_5Pt$	$C_{21}H_{18}BN_5Pt$	$C_{22}H_{18}N_5PF_6Pt$
*F*w	520.27	546.30	692.47
T (K)	293(2)	120(1)	171(1)
wavelength (Å)	0.71073	0.71073	0.71073
crystal system	Monoclinic	Monoclinic	Orthorrombic
space group	P2 1/n	P 2 1/n	P 2(1) 2(1) 2(1)
crystal size (mm^3)	0.22 x 0.17 x 0.1	0.375 x 0.375 x 0.225	0.25 x 0.15 x 0.125
A (Å)	13.97810(10)	7.9171(2)	9.0161(2)
B (Å)	7.34350(10)	24.0327(7)	11.3196(3)
c (Å)	16.5901(2)	10.6607(2)	22.2307(5)
α (º)	90	90	90
β (º)	105.469(2)	111.021	90
γ (º)	90	90	90
V ($Å^3$)	1641.25(3)	1893.41(8)	2268.84(9)
Z	4	4	4
D_{calc} (Mg/m^3)	2.106	1.916	2.027
Absorption coeficient (mm^{-1})	8.563	7.427	6.326
F(000)	992	1048	1328
θ range (º)	3.02 to 28.89	1.69 to 26.73	3.56 to 26.37
index ranges	-18≤h≤19, -8≤k≤9, -21≤l≤22	-10≤h≤10, -30≤k≤30, -13≤l≤13	-11≤h≤11, 0≤k≤14, 0≤l≤27
no. of data/restraints/params	3512 / 0 / 243	3990 / 0 / 261	4615 / 0/ 317
GOF of F^2	1.050	1.138	1.041
final R indixes [I› 2σ(*I*)][a]	R1 = 0.0165, wR2 = 0.0421	R1 = 0.0464, wR2 = 0.1183	R1 = 0.0454, wR2 = 0.0767
R indixes (all data)[a]	R1 = 0.0196, wR2 = 0.0426	R1 = 0.0505, wR2 = 0.1225	R1 = 0.0793, wR2 = 0.0886
Largest diff. peak and hole (e A^{-3})	1.746 and -0.805	3.879 and -5287	1.139 and -1.857

Tabla E.2: Datos cristalográficos y sobre la resolución de los complejos de **7**, **8**, **9** y **11**

	7	**8**	**9**	**11**
empirical formula	$C_{23}H_{18}N_7PF_6Pt$	$C_{21}H_{18}N_7PF_6Pt$	$C_{25}H_{20}N_7PF_6Pt$	$C_{32}H_{22}N_6Pt_2$
*F*w	732.50	708.48	758.54	880.74
T (K)	100(1)	173(1)	173(1)	100(1)
wavelength (Å)	0.71073	0.71073	0.71073	0.71073
crystal system	Triclinic	Triclinic	Monoclinic	Monoclinic
space group	P -1	P -1	P 2 1/n	C 2/c
crystal size (mm^3)	0.30x0.15x0.15	0.45x0.25x0.125	0.3x0.225x0.075	0.29x0.16x0.06
A (Å)	7.8450(3)	7.9337(2)	14.9313(3)	C 2/c
B (Å)	9.9470(4)	9.9271(3)	7.8894(2)	22.0174(4)
c (Å)	15.4350(5)	14.9341(5)	23.1851(2)	15.7942(3)
α (º)	77.109(2)	79.9730(10)	90	15.6794(3)
β (º)	78.729(2)	77.165(2)	107.2070(10)	90
γ (º)	83.414(2)	83.888(2)	90	107.581(2)
V ($Å^3$)	1148.27(5)	1126.475(5)	2608.94(10)	90
Z	2	2	4	8
D_{calc} (Mg/m^3)	2.119	2.089	1.931	5197.79(17)
Absorption coeficient (mm^{-1})	6.258	6.376	5.513	10.789
F(000)	704	680	1464	3296
θ range (º)	3.20 to 28.16	3.35 to 28.15	4.11 to 25.68	3.83 to 28.85
index ranges	0≤h≤10, -12≤k≤13, -19≤l≤20	0≤h≤10, -12≤k≤13, -18≤l≤19	-18≤h≤18, -9≤k≤9, -28≤l≤28	-28≤h≤29, -21≤k≤21, -18≤l≤19
no. of data/restraints/params	5478 / 0 / 348	5352 / 0 / 325	4928 / 0 / 361	6079 / 0 / 361
GOF of F^2	1.066	1.049	1.043	1.055
final R indixes [I› 2σ(*I*)][a]	R1 = 0.0181, wR2 = 0.0433	R1 = 0.0252, wR2 = 0.0570	R1 = 0.0567, wR2 = 0.1409	R1 = 0.0201, wR2 = 0.0443
R indixes (all data)[a]	R1 = 0.0195, wR2 = 0.0440	R1 = 0.0295, wR2 = 0.0587	R1 = 0.0758, wR2 = 0.1554	R1 = 0.0256, wR2 = 0.0453
Largest diff. peak and hole (e A^{-3})	0.856 and -1.511	0.978 and -0.932	4.241 and -2.292	1.274 and -0.750

X-RAY CRYSTALLOGRAPHY EXPERIMENTAL DETAILS: CHAPTER 2

Details of the X-ray analyses are summarized in Table E.3. Orange (**14**·CH_2Cl_2, **16**, **17**·$3CH_2Cl_2$) crystals were obtained by slow diffusion at -30ºC (**14**, **17**) or room temperature (**16**) of *n*-hexane into solutions of the complexes in CH_2Cl_2. In all the cases, graphite-monochromatic Mo-K_α radiation was used, X-ray intensity data were collected with a NONIUS-κCCD area-detector diffractometer and images processed using the DENZO and SCALEPACK suite of programs,[29] carrying out the absorption correction at this point for complex **16** and **17**·$3CH_2Cl_2$. For **2**·CH_2Cl_2 the absorption correction was performed using MULTISCAN[23] with the WINGX program suite.[30] The structures were solved by Patterson using SHELXS-97[27] (**16**) or SIR-2004[31] (**14**·CH_2Cl_2 and **17**·$3CH_2Cl_2$), and refined by full-matrix least squares on F^2 with SHELXL-97.[27] All non-hydrogen atoms were assigned anisotropic displacement parameters. All the hydrogen atoms were constrained to idealized geometries fixing isotropic displacement parameters 1.2 times the U_{iso} value of their attached carbon for the aromatic and methylene carbons and 1.5 times for the methyl groups. Complex **14**·CH_2Cl_2, crystallizes in the non-centrosymmetric space group $P2_12_12_1$, with an absolute structure parameter of [0.089(8)]. For **17**·$3CH_2Cl_2$ disordered crystallization molecules of CH_2Cl_2 were observed, and several restrains have been used in order to model positional disorders (**17**·$3CH_2Cl_2$ 0.50/0.50). Finally, structure of **16** shows some residual peaks greater than 1 eA^{-3} in the vicinity of the platinum atoms, but with no chemical meaning.

Table E.3: Crystallographic data for **14**·CH_2Cl_2, **16** and **17**·3 CH_2Cl_2

	14·CH_2Cl_2	**16**	**17**·3 CH_2Cl_2
empirical formula	$C_{59}H_{70}N_2O_3Cl_2Pt$	$C_{42}H_{38}N_2Pt_2$	$C_{51}H_{40}N_2\ Cl_6Pt_2$
*F*w	1121.16	960.92	1283.73
T (K)	173(2)	173(2)	173(2)
wavelength (Å)	0.71073	0.71073	0.71073
crystal system	Orthorhombic	Triclinic	Monoclinic
space group	*P*212121	*P*-1	*P*21/n
crystal size (mm^3)	0.45 x 0.20 x 0.20	0.45 x 0.40 x 0.15	0.30 x 0.20x 0.10
A (Å)	14.5844(2)	10.7312(6)	16.7730(6)
B (Å)	15.9449(3)	11.0656(6)	13.8680(3)
c (Å)	22.7833(5)	16.4790(9)	20.4720(8)
α (º)	90	82.168(3)	90
β (º)	90	74.397(2)	103.4290(10)
γ (º)	90	63.497(2)	90
V ($Å^3$)	5298.18(17)	1686.36(16)	4631.8(3)
Z	4	2	4
D_{calc} (Mg/m^3)	1.406	1.892	1.841
Absorption coeficient (mm^{-1})	2.795	8.319	6.418
F(000)	2296	920	2472
θ range (º)	2.97 to 26.37	2.78 to 25.68	2.59 to 27.46
index ranges	-18≤h≤18, -19≤k≤17, -28≤l≤28	0≤h≤13, -11≤k≤13, -19≤l≤20	0≤h≤21, 0≤k≤17, -26≤l≤25
no. of data/restraints/params	10650/1/586	6384/0/415	10493/2/569
GOF of F^2	0.753	1.102	0.831
final R indixes [I› 2σ(*I*)][a]	R1 = 0.0366, wR2 = 0.1002	R1 = 0.0315, wR2 = 0.0744	R1 = 0.0367, wR2 = 0.0885
R indixes (all data)[a]	R1=0.0416, wR2=0.1089	R1=0.0401, wR2=0.0784	R1=0.0569, wR2=0.1019
Largest diff. peak and hole (e A^{-3})	0.646 and -1.056	1.667 and -1.155	0.849 and -0.754

X-RAY CRYSTALLOGRAPHY EXPERIMENTAL DETAILS: CHAPTER 3

Details of the structural analyses for all complexes are summarized in Table E.4 Orange (**21**, **23**) and orange-red (**26**) crystals were obtained by slow diffusion at room temperature of *n*-hexane into solutions of the complexes in $CHCl_3$ (**21**, **23**) or CH_2Cl_2 (**26**). In all the cases, graphite-monochromatic Mo-K_α radiation was used, X-ray intensity data were collected with a NONIUS-κCCD area-detector diffractometer and images processed using the DENZO and SCALEPACK suite of programs,[5] carrying out the absorption correction at this point. The structures were solved by Direct and Patterson Methods using SIR2004,[25] and refined by full-matrix least squares on F^2 with SHELXL-97.[27] All non-hydrogen atoms were assigned anisotropic displacement parameters. All the hydrogen atoms were constrained to idealized geometries fixing isotropic displacement parameters 1.2 times the U_{iso} value of their attached carbon. Several restrains have been used in order to model positional disorder in one C≡C^{t}Bu groups in **26** (10 restrain 0.70/0.30).Finally, the structures show some residual peaks greater than 1 eA^{-3} in the vicinity of the platinum atoms, but with no chemical meaning.

Table E.4: Some Selected crystal data and Structure Refinement Details for **21**·2$CHCl_3$·C_6H_{14}, **23**·8$CHCl_3$ and **26**

	21·2$CHCl_3$·C_6H_{14}	**23**·4$CHCl_3$	**26**
empirical formula	$C_{60}H_{62}Cl_6N_4Pt_2$	$C_{116}H_{104}Cl_{24}N_8Pt_4$	$C_{26}H_{24}N_2SPt$
*F*w	1442.02	3241.23	591.62
T (K)	173(2)	173(2)	213(1)
wavelength (Å)	0.71073	0.71073	0.71073
crystal system	Triclinic	Triclinic	Monoclinic
space group	P-1	P-1	P 2 1/a
crystal size (mm^3)	0.25 x 0.25 x 0.15	0.4 x 0.2 x 0.1	0.3 x 0.3 x 0.05
A (Å)	13.1180(3)	16.1460(5)	11.079(2)
B (Å)	13.8089(5)	19.1590(6)	11.207(2)
c (Å)	17.1915(6)	23.2760(6)	18.336(4)
α (º)	103.738(2)	69.0100(10)	90
β (º)	94.528(2)	79.852(2)	104.695(15)
γ (º)	103.049(2)	69.8410(10)	90
V ($Å^3$)	2917.89(16)	6299.2(3)	2202.2(7)
Z	2	2	4
D_{calc} (Mg/m^3)	1.641	1.709	1.784
Absorption coeficient (mm^{-1})	5.105	4.986	6.482
F(000)	1416	3152	1152
θ range (º)	1.72 to 25.68	0.94 to 26.37	2.93 to 26.37
index ranges	0≤h≤15, -16≤k≤16, -20≤l≤20	0≤h≤20,-22≤k≤23, -28≤l≤29	0≤h≤13, 0≤k≤13, -22≤l≤22
no. of data/restraints/params	11041/0/631	2571/3/1369	4429/10/265
GOF of F^2	1.059	1.105	1.018
final R indixes [I› 2σ(*I*)][a]	R1 = 0.0334, wR2 = 0.0762	R1 = 0.0577, wR2 = 0.1185	R1 = 0.0504, wR2 = 0.1560
R indixes (all data)[a]	R1 = 0.0415, wR2 = 0.0808	R1 = 0.1064, wR2 = 0.1403	R1 = 0.0714, wR2 = 0.1881
Largest diff. peak and hole (e A^{-3})	3.088 and -1.337	1.588 and -1.067	1.313 and -1.867

X-RAY CRYSTALLOGRAPHY EXPERIMENTAL DETAILS: CHAPTER 4

Details of the structural analyses for all complexes are summarized in Table E.5. Yellow crystals were obtained by slow diffusion at -30ºC (**28**, **30**·2$CHCl_3$) or 4ºC (**29**·CH_2Cl_2) of *n*-hexane into solutions of the complexes in CH_2Cl_2 (**28**, **29**·CH_2Cl_2) or $CHCl_3$ (**30**·2$CHCl_3$). In all the cases, graphite-monochromatic Mo-K_α radiation was used, data collection were performed on a NONIUS-κCCD area-detector diffractometer and the images were processed using the DENZO and SCALEPACK suite of programs.[32] The absorption correction was performed using XABS2[22] (**29**·CH_2Cl_2) or MULTI-SCAN[23] (**28**, **29**·CH_2Cl_2), with the WINGX program suite.[24] The structures were solved by Direct and Patterson Methods using SIR2004[25] (**28**, **30**·$CHCl_3$) or by Patterson Methods using SHELXS-97[27] (**29**·CH_2Cl_2), and refined by full-matrix least squares on F^2 with SHELXL-97.[27] All the hydrogen atoms were constrained to idealized geometries fixing isotropic displacement parameters 1.2 times the U_{iso} value of their attached carbon for the aromatic carbons and 1.5 times for the methyl groups. All the hydrogen atoms were constrained to idealized geometries fixing isotropic displacement parameters 1.2 times the U_{iso} value of their attached carbon. For **30**·2$CHCl_3$, disordered crystallization molecules of $CHCl_3$ were observed and modelled. Finally, the structures show some residual peaks greater than 1 eA^{-3} in the vicinity of the platinum or lead atoms, but with no chemical meaning.

Tabla E.5: Some Selected crystal data and Structure Refinement Details for **28**, **29**·CH_2Cl_2 and **30**·$2CHCl_3$

	28	**29**·CH_2Cl_2	**30**·$2CHCl_3$
empirical formula	$C_{38}H_{28}BN_7PbPt$	$C_{40.50}H_{33}BClN_7O_2PbPt$	$C_{89}H_{79}BCl_6F_{12}N_9PbPt_2$
*F*w	995.76	1098.28	2323.49
T (K)	173(1)	173(2)	173(1)
wavelength (Å)	0.71073	0.71073	0.71073
crystal system	Monoclinic	Triclinic	Triclinic
space group	P 21/n	P -1	P -1
crystal size (mm^3)	0.5 x 0.25 x 0.2	0.45 x 0.25 x 0.2	0.25 x 0.25 x 0.2
A (Å)	12.4886(6)	12.6778(2)	12.7567(3)
B (Å)	16.7105(6)	13.1486(3)	15.2714(4)
c (Å)	15.6547(7)	24.0518(6)	22.8713(4)
α (º)	90	91.8070(10)	87.9010(10)
β (º)	98.1152(19)	101.3530(10)	82.9660(10)
γ (º)	90	106.0210(10)	84.3140(10)
V ($Å^3$)	3234.5	3762.48(14)	4398.97(17)
Z	4	4	2
D_{calc} (Mg/m^3)	2.045	1.939	1.754
Absorption coeficient (mm^{-1})	9.559	8.300	5.340
F(000)	1880	2092	2258
θ range (º)	2.44 to 25.35	0.87 to 27.47	2.27 to 26.37°.
index ranges	-15≤h≤10, -20≤k ≤18, -18≤l≤17	-16≤h≤15, -17≤k≤16, -31≤l≤31	-15≤h≤15, -19≤k≤18, -28≤l≤28
no. of data/restraints/params	5862 / 0 / 433	61590 / 0 / 954	17861 / 12 / 1063
GOF of F^2	1.199	1.036	1.018
final R indixes [I› 2σ(*I*)][a]	R1 = 0.0314, wR2 = 0.0924	R1 = 0.0592, wR2 = 0.1410	R1 = 0.0436, wR2 = 0.1070
R indixes (all data)[a]	R1 = 0.0418, wR2 = 0.1249	R1 = 0.0843, wR2 = 0.1598	R1 = 0.0583, wR2 = 0.1153
Largest diff. peak and hole (e A^{-3})	1.006 and -1.605	1.859 and -2.158	2.097 and -1.576

X-RAY CRYSTALLOGRAPHY EXPERIMENTAL DETAILS: CHAPTER 5

Details Details of the X-ray analyses are summarized in Tables E.6, E.7 and E.8. Suitable monocrystals for X-ray diffraction were obtained as follow: Greenish-yellow (**32**) and orange (**33**·1.5CH_2Cl_2, **33**·1.5acetone, **34**·0.9CH_2Cl_2, [**36(acetone)**]) crystals were obtained by slow diffusion at -30ºC of *n*-hexane into solutions of the complexes in CH_2Cl_2 (**32**, **33**·1.5CH_2Cl_2, **34**·0.9CH_2Cl_2) or acetone (**33**·1.5acetone, [**36(acetone)**]), respectively. Yellow [**34·(acetone)$_{1.5}$**, **36**·4C_6H_6, **36**·4$CHCl_3$)] or orange (**35**·2$CHCl_3$, **36**·2CH_2Cl_2) crystals were obtained by slow evaporation at 4 ºC of the corresponding saturated solutions of the complexes in acetone (**34**), chloroform (**35**), benzene (**36**) or dichloromethane (**36**) or by cooling at -30ºC a saturated solution of complex **36** in chloroform (**36**·4$CHCl_3$). In all the cases, graphite-monochromatic Mo-K_α radiation was used. For **32** and [**36·acetone**], the data were acquired with an Oxford Diffraction Xcalibur CCD diffractometer, and the diffraction frames were integrated and corrected for absorption using the Crysalis RED package.[21] For the rest of the structures, X-ray intensity data were collected with a NONIUS-κCCD area-detector diffractometer and images processed using the DENZO and SCALEPACK suite of programs,[5] carrying out the absorption correction at this point for complex **33**·1.5CH_2Cl_2, **33**·1.5acetone, **34**·0.9CH_2Cl_2, **35**·2$CHCl_3$, **36**·4C_6H_6, **36**·2CH_2Cl_2 and **36**·4$CHCl_3$. For **[34·(acetone)$_{1.5}$]**, the absorption correction was performed using SORTAV.[23] The structures were solved by Direct Methods or Patterson using SHELXS-97[27] (**32**, **33**·1.5CH_2Cl_2, **33**·1.5acetone, **[34·(acetone)$_{1.5}$]**, **35**·2$CHCl_3$ and [**36·acetone**]) or SIR-2004[25] (**34**·0.9CH_2Cl_2 **36**·4$CHCl_3$, **36**·4C_6H_6 and **36**·2CH_2Cl_2), and refined by full-matrix least squares on F^2 with SHELXL-97.[27] All the hydrogen atoms were constrained to idealized geometries fixing isotropic displacement parameters 1.2 times the U_{iso} value of their attached carbon. All the hydrogen atoms were constrained to idealized geometries fixing isotropic displacement parameters 1.2 times the U_{iso} value of their attached carbon for the aromatic and methylene carbons and 1.5 times for the methyl groups. For complex **[34·(acetone)$_{1.5}$]**, which crystallizes in the non-centrosymmetric space group $P2_1$, the crystal chosen for this structural analysis was found to be a meroedric twin, as confirmed by the absolute structure parameter [0.456(6)]. Inspection of the symmetry (using Platon[28a]) does not suggest any obvious spacegroup change. For **34**·0.9CH_2Cl_2 and **36**·2CH_2Cl_2, disordered crystallization molecules of CH_2Cl_2 were

observed, but could not be properly modelled. Both structures were examined with PLATON[28a,33] and SQUEEZE.[28a,34] In the case, of **34**·0.9CH_2Cl_2, it was revealed the presence of two voids of 835 $Å^3$ in the unit cell, containing each of them 135 e^-, which fits well with the presence of 7 molecules of CH_2Cl_2 in the unit cell. Therefore, we have included them in the empirical formula as crystallization solvent (**34**·0.9CH_2Cl_2). In the case, of **36**·2CH_2Cl_2, it was revealed the presence of six voids in the unit cell, containing a total of 490 e^-, which fits well with the presence of 12 molecules of CH_2Cl_2 in the unit cell. Therefore, we have also included them in the empirical formula as crystallization solvent (**36**·2CH_2Cl_2). Several restrains have been used in order to model positional disorders in crystallization solvents (**35**·2$CHCl_3$ 0.70/0.30, 0.60/0.40; **36**·4$CHCl_3$ 0.60/0.40) or in one CF_3 group (**34**·0.9CH_2Cl_2 0.70/0.30; [**34·(acetone)$_{1.5}$**] 0.55/0.45; **36**·4C_6H_6 0.70/0.30; **36**·2CH_2Cl_2 0.50/0.50). Finally, structures of **32**, [**34·(acetone)$_{1.5}$**], **35**·2$CHCl_3$, **36**·2CH_2Cl_2 and **36**·4$CHCl_3$ show some residual peaks greater than 1 eA^{-3} in the vicinity of the platinum atoms or the crystallization solvent, but with no chemical meaning.

Table E.6: Some Selected crystal data and Structure Refinement Details for **33**·1.5CH_2Cl_2, **33**·1.5acetone, **34**·0.9CH_2Cl_2, and [**34·(acetone)$_{1.5}$**]

	33·1.5CH_2Cl_2	**33**·1.5acetone	**34**·0.9CH_2Cl_2	[**34·(acetone)$_{1.5}$**]
empirical formula	$C_{49.5}Cl_3H_{27}F_{10}N_4PbPt_2S_2$	$C_{55.50}H_{39}F_{10}N_4O_{2.50}PbPt_2S_2$	$C_{50.9}H_{23.8}Cl_{11.8}F_{16}N_4PbPt_2S_2$	$C_{54.5}H_{31}F_{16}N_4O_{1.5}PbPt_2S_2$
*F*w	1635.59	1653.40	1720.66	1731.32
T (K)	100(1)	193(1)	173(1)	173(1)
wavelength (Å)	0.71073	0.71073	0.71073	0.71073
crystal system	Triclinic	Triclinic	Monoclinic	Monoclinic
space group	P-1	P-1	*C*2/c	$P2_1$
crystal size (mm^3)	0.38 x 0.23 x 0.12	0.30 x 0.15 x 0.15	0.2 x 0.2 x 0.15	0.35x 0.1x 0.05
A (Å)	12.3991(3)	10.7618(3)	24.4445(7)	12.3543(2)
B (Å)	13.1073(4)	13.8101(5)	19.6760(6)	29.5382(6)
c (Å)	17.2525(6)	19.2886(7);	25.1616(6)	15.3044(3)
α (º)	100.356(3)	106.702(1)	90	90
β (º)	101.793(3)	95.471(2)	118.915(2)	111.1230(10)
γ (º)	111.777(3)	98.767(2)	90	90
V ($Å^3$)	2445.98(13)	2684.20(16)	10593.3(5)	5209.68(17)
Z	2	2	8	4
D_{calc} (Mg/m^3)	2.221	2.046	2. 158	2.207
Absorption coeficient (mm^{-1})	9.467	8.487	8.613	8.765
F(000)	1526	1560	6112	3248
θ range (º)	4.19 to 25.68	1.62 to 26.37	1.92 to 25.68	3.30 to 26.37
index ranges	-15≤h≤14, -15≤k≤15, 0≤l≤21	-13≤h≤13, -17≤k≤16, 0≤l≤24	-29≤h≤26, -0≤k≤23, -0≤l≤30	-15≤h≤15, -36≤k≤36, -19≤l≤19
no. of data/restraints/params	9235/0/620	10937/0/665	9988/6/667	21246/1/1452
GOF of F^2	1.026	1.033	1.058	1.022
final R indixes [I› 2σ(*I*)][a]	R1 = 0.0258, wR2 = 0.0642	R1 = 0.0293, wR2 = 0.0735	R1 = 0.0353, wR2 = 0.0687	R1 = 0.0437, wR2 = 0.0817
R indixes (all data)[a]	R1 = 0.0297, wR2 = 0.0658	R1 = 0.0358, wR2 = 0.0757	R1 = 0.0507, wR2 = 0.0729	R1 = 0.0598, wR2 = 0.0882
Largest diff. peak and hole (e A^{-3})	1.822 and -1.831	1.520 and -1.039	1.007 and -1.162	1.450 and -1.236

Table E.7: Some Selected crystal data and Structure Refinement Details for **32** and **35**·4 $CHCl_3$

	32	**35**·4 $CHCl_3$
empirical formula	$C_{19}H_{14}F_5NOPtS$	$C_{46}H_{26}Cl_6F_{10}N_4PbPt_2S_2$
*F*w	594.46	1698.90
T (K)	100(1)	173(1)
wavelength (Å)	0.71073	0.71073
crystal system	Monoclinic	Triclinic
space group	*C*2/c	*P*-1
crystal size (mm^3)	0.28 x 0.19 x 0.03	0.2 x 0.1 x 0.1
A (Å)	27.1407(5)	12.6330(3)
B (Å)	12.2572(2)	13.0439(5)
c (Å)	11.7974(3)	17.2434(8)
α (º)	90	79.130(2)
β (º)	111.832(2)	85.227(3)
γ (º)	90	61.443(2)
V ($Å^3$)	3643.15(13)	2450.89(16)
Z	8	2
D_{calc} (Mg/m^3)	2.168	2.302
Absorption coeficient (mm^{-1})	7.876	9.610
F(000)	2256	1584
θ range (º)	4.37 to 26.37	2.33 to 27.47
index ranges	-33≤h≤33, -15≤k ≤15, -14≤l≤14	0≤h≤16, -14≤k≤16, -22≤l≤22
no. of data/restraints/params	3710/0/253	11130/0/659
GOF of F^2	1.058	1.029
final R indixes [I› 2σ(*I*)][a]	R1 = 0.0171, wR2 = 0.0393	R1 = 0.0377, wR2 = 0.0814
R indixes (all data)[a]	R1 = 0.0190, wR2 = 0.0403	R1 = 0.0543, wR2 = 0.0900
Largest diff. peak and hole (e A^{-3})	1.191 and -0.470	2.245 and -2.128

Table E.8: Some Selected crystal data and Structure Refinement Details **36**·$4C_6H_6$, **36**·$4CHCl_3$, **[36(acetone)]** and **36**·$2CH_2Cl_2$.

	36·4 C_6H_6	**36**·4 $CHCl_3$	**[36(acetone)]**	**36**·$2CH_2Cl_2$
empirical formula	$C_{70}H_{46}F_{16}N_4Pb_1Pt_2S_2$	$C_{50}H_{26}Cl_{12}F_{16}N_4PbPt_2S_2$	$C_{49}H_{28}F_{16}N_4OPbPt_2S_2$	$C_{48}H_{26}Cl_4F_{16}N_4PbPt_2S_2$
*F*w	1908.60	2073.64	1654.24	1766.05
T (K)	173(2)	173(1)	100(1)	173(1)
wavelength (Å)	0.71073	0.71073	0.71073	0.71073
crystal system	Monoclinic	Monoclinic	Triclinic	Triclinic
space group	*C*2/c	*C*2/c	*P*-1	*P*-1
crystal size (mm^3)	0.3x0.15x0.15	0.4 x 0.3 x 0.1	0.26x 0.22 x 0.1	0.25 x 0.15 x 0.10
A (Å)	25.1644(8)	25.025(3)	11.3814(4)	14.1726(3)
B (Å)	11.8412(4)	12.0740(10)	14.8392(4)	18.0991(4)
c (Å)	21.9793(5)	21.3850(10)	16.1301(4)	28.0328(6)
α (º)	90	90	110.064(3)	91.0050(10)
β (º)	100.719(2)	106.219(12)	106.667(3)	95.8920(10)
γ (º)	90	90	96.519(3)	93.2280(10)
V ($Å^3$)	6435.0(3)	6204.4(9);	2382.43(12)	7139.4(3)
Z	4	2	2	6
D_{calc} (Mg/m^3)	1.970	2.220	2.306	2.464
Absorption coeficient (mm^{-1})	7.105	7.878	9.577	9.581
F(000)	3632	3888	1544	4440
θ range (º)	3.28 to 27.68	3.32 to 26.37	4.16 to 28.88	1.36 to 25.68
index ranges	0≤h≤32, 0≤k≤15, -28≤l≤27	-31≤h≤31, -16≤k≤15, 0≤l≤26	-15≤h≤15, -18≤k≤19, -21≤l≤21	-17≤h≤17, -22≤k≤22, 0 ≤l≤34
no. of data/restraints/params	7408/4/438	6336/1/411	11270/0/676	26434/8/1909
GOF of F^2	1.038	1.035	1.031	1.071
final R indixes [I› 2σ(*I*)][a]	R1 = 0.0240, wR2 = 0.0551	R1 = 0.0320, wR2 = 0.0691	R1 = 0.0202, wR2 = 0.0430	R1 = 0.0431, wR2 = 0.1042
R indixes (all data)[a]	R1 = 0.0296, wR2 = 0.0578	R1 = 0.0459, wR2 = 0.0743	R1 = 0.0238, wR2 = 0.0442	R1 = 0.0674, wR2 = 0.1120
Largest diff. peak and hole (e A^{-3})	0.860 and -1.389	1.070 and –1.763	0.956 and -0.942	2.127 and -1.261

E) References

1. Geary, W. J. *Coord. Chem. Rev.* **1971**, *7*, 81.
2. Frisch, M. J. T., G. W.; Schlegel, H. B.; Scuseria, G. E.; Robb, M. A.; Cheeseman, J. R.; Montgomery Jr, J. A.; Vreven, T.; Kudin, K. N.; Burant, J. C.; Millam, J. M.; Iyengar, S. S.; Tomasi, J.; Farkas, O.; Tomasi, J.; Barone, V.; Mennucci, B.; Cossi, M.; Scalmani, G.; Rega, N.; Petersson, G. A.; Nakatsuji, H.; Hada, M.; Ehara, M.; Toyota, K.; Fukuda, R.; Hasegawa, J.; Ishida, M.; Nakajima, T.; Honda, Y.; Kitao, O.; Nakai, H.; Klene, M.; Li, X.; Knox, J. E.; Hratchian, H. P.; Cross, J. B.; Bakken, V.; Adamo, C.; Jaramillo, J.; Gomperts, R.; Stratman, R. E.; Yazyev, O.; Austin, A. J.; Cammi, R.; Pomelli, C.; Ochterski, J. W.; Ayala, P. Y.; Morokuma, K.; Voth, G. A.; Salvador, P.; Dannenberg, J. J.; Zakrzewski, V. G.; Dapprich, S.; Daniels, A. D.; Strain, M. C.; Farkas, O.; Malick, D. K.; Rabuck, A. D.; Raghavachari, K.; Foresman, J. B.; Ortiz, J. V.; Cui, Q.; Baboul, A. G.; Clifford, S.; Cioslowski, J.; Stefanov, B. B.; Liu, G.; Liashenko, A.; Piskorz, P.; Komaromi, I.; Martin, R. L.; Fox, D. J.; Keith, T.; Al-Laham, M. A.; Peng, C. Y.; Nanayakkara, A.; Challacombe, M.; Gill, P. M. W.; Johnson, B.; Chen, W.; Wong, M. W.; Gonzalez, C.; Pople, J. A; *Gaussian 03, Revision E.01*: Gaussian, Inc., Wallingford CT, 2004.
3. (a) Becke, A. D. *Phys. Rev. A* **1988**, *38*, 3098 ; (b) Lee, C.; Yang, W.; Parr, R. G. *Phys. Rev. B* **1988**, *37*, 785 ; (c) Becke, A. D. *J. Chem. Phys.* **1993**, *98*, 5648.
4. (a) Gorelsky, S. I. *AOMix: Program for Molecular Orbital Analysis; University of Ottawa* **2009**, http://www.sg-chem.net/; (b) Gorelsky, S. I.; Lever, A. B. P. *J. Organomet. Chem.* **2001**, *635*, 187.
5. Otwinowsky, Z.; Minor, W. In *Methods Enzymol.*; Carter Jr., C. V., Sweet, R. M., Eds.; Academic Press: New York, USA, 1997; Vol. 276A, p 307.
6. Mabbott, D. J.; Mann, B. E.; Maitlis, P. M. *J. Chem. Soc., Dalton Trans.* **1977**, 294.
7. Pregosin, P. S.; Wombacher, F.; Albinati, A.; Lianza, F. *J. Organomet. Chem.* **1991**, *418*, 249.
8. Mdleleni, M. M.; Bridgewater, J. S.; Watts, R. J.; Ford, P. C. *Inorg. Chem.* **1995**, *34*, 2334.
9. Trofimenko, S. *J. Am. Chem. Soc.* **1967**, *89*, 3170.

10. Reger, D. L.; Grattan, T. C.; Brown, K. J.; Little, C. A.; Lamba, J. J. S.; Rheingold, A. L.; Sommer, R. D. *J. Organomet. Chem.* **2000**, *607*, 120.
11. Pettinari, C.; Pettinari, R. *Coord. Chem. Rev.* **2005**, *249*, 525.
12. Coe, B. J.; Harries, J. L.; Harris, J. A.; Brunschwig, B. S.; Coles, S. J.; Light, M. E.; Hursthouse, M. B. *Dalton Trans.* **2004**, 2935.
13. Amoroso, A. J.; Cargill Thompson, A. M. W.; Maher, J. P.; McCleverty, J. A.; Ward, M. D. *Inorg. Chem.* **1995**, *34*, 4828.
14. Fernández, S.; Forniés, J.; Gil, B.; Gómez, J.; Lalinde, E. *Dalton Trans.* **2003**, 822.
15. Díez, Á., Tesis Doctoral, Universidad de La Rioja, 2010.
16. Reger, D. L.; Huff, M. F.; Rheingold, A. L.; Haggerty, B. S. *J. Am. Chem. Soc.* **1992**, *114*, 579.
17. Yagyu, T.; Ohashi, J.-I.; Maeda, M. *Organometallics* **2007**, *26*, 2383.
18. Berenguer, J. R.; Lalinde, E.; Moreno, M. T.; Sánchez, S.; Torroba, J. *Inorg. Chem.* **2012**, *51*, 11665.
19. Sousa-Pedrares, A.; Casanova, M. I.; García-Vázquez, J. A.; Durán, M. L.; Romero, J.; Sousa, A.; Silver, J.; Titler, P. J. *Eur. J. Inorg. Chem.* **2003**, 678.
20. Niedermair, F.; Waich, K.; Kappaun, S.; Mayr, T.; Trimmel, G.; Mereiter, K.; Slugovc, C. *Inorg. Chim. Acta* **2007**, *360*, 2767.
21. *CrysAlis; RED. A program for Xcalibur CCD System X-Ray diffraction data reduction* **2005**, Oxford Diffraction LTD.; Oxford.
22. Parkin, S.; Moezzi, B.; Hope, H. *J. Appl. Crystallogr.* **1995**, *28*, 53.
23. Blessing, R. H. *Acta Crystallogr.* **1995**, *A51*, 33.
24. Farrugia, L. J. *J. Appl. Crystallogr.* **1999**, *32*, 837.
25. Burla, M. C.; Caliandro, R.; Camalli, M.; Carrozzini, B.; Cascarano, G. L.; De Caro, L.; Giacovazzo, C.; Polidori, G.; Spagna, R. *J. App. Crystallogr.* **2005**, *38*, 381.
26. Beurskens, P. T.; Beurskens, G.; Bosman, W. P.; de Gelder, R.; Garcia-Granda, S.; Gould, R. O.; Israel, R.; Smits, J. M. M. *DIRDIF96 program system.* **1996**, Crystallography Laboratory.
27. Sheldrick, G. M. *SHELX-97, a program for the refinement of crystal structures* University of Göttingen: Göttingen, Germany, 1997.
28. (a) Speck, A. L. *Acta Crystallogr., Sect. A* **1990**, *A46*, c34; (b) Hirshfeld, F. L. *Acta Crystallogr., Sect. A* **1976**, *32*, 239.

29. Otwinowski, Z.; Minor, W. In *Methods in Enzymology*; Carter, C. V., Jr., Sweet, R. M., Eds.; Academic Press: New York, 1997; Vol. 276A, p 307.
30. Farrugia, L. J. *Appl. Crystallogr.* **1999**, *32*, 837.
31. Burla, M. C.; Caliandro, R.; Camalli, M.; Carrozzini, B.; Cascarano, G. L.; De Caro, L.; Giacovazzo, C.; Polidori, G.; Spagna, R. *J. Appl. Crystallogr.* **2005**, *38*, 381.
32. Otwinosky, Z.; Minor, W. In *Methods Enzymol.*; Carter Jr., C. V., Sweet, R. M., Eds.; Academis Press: New York, 1997; Vol. 276A, p 307.
33. Spek, A. L. *PLATON, A Multipurpose Crystallographic Tool, Utrecht University, Utrecht, The Netherlands* **1998**.
34. Spek, A. L. *SQUEEZE, incorporated into PLATON: A Multipurpose Crystallographic Tool, University of Utrecht, Utrecht, The Netherlands* **2005**.